frontiers | Research Topics

Advancements in understanding and managing preeclampsia: exploring molecular mechanisms, biomarkers, and clinical implications

Edited by
Rajni Kant, Rajesh Kumar Manne and Subhradip Karmakar

Coordinated by
Narasaiah Kovuru

Published in
Frontiers in Cell and Developmental Biology

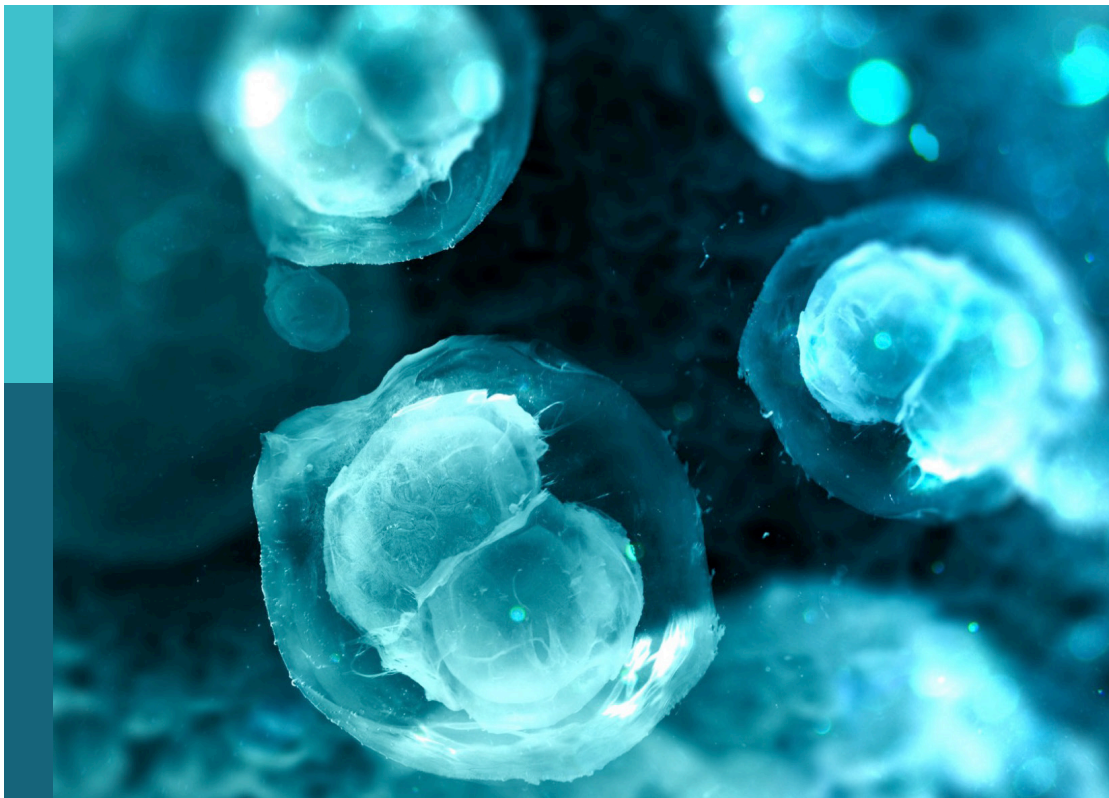

ISSN 1664-8714
ISBN 978-2-8325-7168-2
DOI 10.3389/978-2-8325-7168-2

Generative AI statement
Any alternative text (Alt text) provided alongside figures in the articles in this ebook has been generated by Frontiers with the support of artificial intelligence and reasonable efforts have been made to ensure accuracy, including review by the authors wherever possible. If you identify any issues, please contact us.

About Frontiers

Frontiers is more than just an open access publisher of scholarly articles: it is a pioneering approach to the world of academia, radically improving the way scholarly research is managed. The grand vision of Frontiers is a world where all people have an equal opportunity to seek, share and generate knowledge. Frontiers provides immediate and permanent online open access to all its publications, but this alone is not enough to realize our grand goals.

Frontiers journal series

The Frontiers journal series is a multi-tier and interdisciplinary set of open-access, online journals, promising a paradigm shift from the current review, selection and dissemination processes in academic publishing. All Frontiers journals are driven by researchers for researchers; therefore, they constitute a service to the scholarly community. At the same time, the *Frontiers journal series* operates on a revolutionary invention, the tiered publishing system, initially addressing specific communities of scholars, and gradually climbing up to broader public understanding, thus serving the interests of the lay society, too.

Dedication to quality

Each Frontiers article is a landmark of the highest quality, thanks to genuinely collaborative interactions between authors and review editors, who include some of the world's best academicians. Research must be certified by peers before entering a stream of knowledge that may eventually reach the public - and shape society; therefore, Frontiers only applies the most rigorous and unbiased reviews. Frontiers revolutionizes research publishing by freely delivering the most outstanding research, evaluated with no bias from both the academic and social point of view. By applying the most advanced information technologies, Frontiers is catapulting scholarly publishing into a new generation.

What are Frontiers Research Topics?

Frontiers Research Topics are very popular trademarks of the *Frontiers journals series*: they are collections of at least ten articles, all centered on a particular subject. With their unique mix of varied contributions from Original Research to Review Articles, Frontiers Research Topics unify the most influential researchers, the latest key findings and historical advances in a hot research area.

Find out more on how to host your own Frontiers Research Topic or contribute to one as an author by contacting the Frontiers editorial office: frontiersin.org/about/contact

Advancements in understanding and managing preeclampsia: exploring molecular mechanisms, biomarkers, and clinical implications

Topic editors

Rajni Kant — Kaohsiung Medical University, Taiwan

Rajesh Kumar Manne — Duke University Medical Center, Duke University, United States

Subhradip Karmakar — All India Institute of Medical Sciences, India

Topic coordinator

Narasaiah Kovuru — Children's Hospital of Philadelphia, United States

Citation

Kant, R., Manne, R. K., Karmakar, S., Kovuru, N., eds. (2025). *Advancements in understanding and managing preeclampsia: exploring molecular mechanisms, biomarkers, and clinical implications*. Lausanne: Frontiers Media SA.

doi: 10.3389/978-2-8325-7168-2

Table of contents

frontiers | Frontiers in Cell and Developmental Biology

TYPE Editorial
PUBLISHED 07 November 2025
DOI 10.3389/fcell.2025.1718459

OPEN ACCESS

EDITED AND REVIEWED BY
Abdul Rehman Phull,
Shah Abdul Latif University, Pakistan

*CORRESPONDENCE
Rajesh Kumar Manne,
rajeshkumar.manne@duke.edu
Subhradip Karmakar,
subhradip.k@aiims.edu

RECEIVED 03 October 2025
ACCEPTED 22 October 2025
PUBLISHED 07 November 2025

CITATION
Kant R, Manne RK and Karmakar S (2025) Editorial: Advancements in understanding and managing preeclampsia: exploring molecular mechanisms, biomarkers, and clinical implications.
Front. Cell Dev. Biol. 13:1718459.
doi: 10.3389/fcell.2025.1718459

Editorial: Advancements in understanding and managing preeclampsia: exploring molecular mechanisms, biomarkers, and clinical implications

Rajni Kant[1], Rajesh Kumar Manne[1]* and Subhradip Karmakar[2]*

[1]Department of Pathology, Duke University Medical Center, Duke University School of Medicine, Durham, NC, United States, [2]Department of Biochemistry, All India Institute of Medical Sciences, New Delhi, India

KEYWORDS

preeclampsia, biomarker, metabolic reprograming, placenta, mitochondria

Editorial on the Research Topic
Advancements in understanding and managing preeclampsia: exploring molecular mechanisms, biomarkers, and clinical implications

Introduction

Preeclampsia remains one of the most serious and complex challenges in obstetrics affecting 3%–8% of pregnancies worldwide and standing as a leading cause of maternal and perinatal morbidity and mortality. Despite decades of research, this multisystem disorder, characterized by new-onset hypertension and organ dysfunction after 20 weeks of gestation, remains incompletely understood and inadequately managed. However, recent advances in genomics, metabolomics, and systems biology are revolutionizing our understanding of preeclampsia's molecular underpinnings, offering unprecedented opportunities for precision medicine approaches to prediction, prevention, and treatment. This Research Topic brings together complimentary studies that advance insights into molecular and cellular mechanisms while outlining translational pathways toward improved clinical care, offering a timely and integrated perspective on preeclampsia.

The heterogeneity challenge: recognizing preeclampsia subtypes

A major advancement in preeclampsia research is the recognition that it is not a single disease but a spectrum of clinical and molecular subtypes. Notably, early-onset

preeclampsia (EOP), which develops before 34 weeks of gestation, differs significantly in its underlying pathophysiology from late-onset preeclampsia (LOP), which occurs after 34 weeks. Han et al. illustrated through integrated weighted gene co-expression network analysis that severe and early-onset preeclampsia shows substantial molecular alterations between these subtypes. They found that EOP is associated with pronounced molecular disruptions, including two key gene modules linked to gonadotropin secretion, lipid storage, and chronic inflammation. In contrast, LOP displayed more subtle changes in placental gene expression, primarily involving stress-response pathways. In contrast, late-onset preeclampsia exhibits more nuanced changes in placental gene expression patterns. These distinct molecular signatures unique to each subtype carries significant implications for clinical management. EOP is marked by notable placental dysfunction with irregular trophoblast invasion and poor remodeling of spiral arteries, while LOP more often associated with maternal constitutional factors and cardiovascular risk. Comprehending these unique pathways allows for individualized therapeutic strategies. Importantly, Han et al. pointed out that abnormal placental lipid storage could be a contributing factor to the severity and EOP, emphasizing metabolic dysregulation as a key aspect shared among preeclampsia subtypes.

Metabolic reprogramming: the cellular foundation of disease

Energy metabolism dysregulation has emerged as a central theme in preeclampsia pathogenesis, with mitochondrial dysfunction serving as a critical upstream mediator of disease progression. Li et al. identified multiple energy metabolism-related genes (MMRDEGs) through comprehensive bioinformatics analysis and several energy metabolism-related genes involvement in glycolysis, gluconeogenesis, lipid transport, and glucagon secretion. Among the most consistently dysregulated genes, including CRH (Corticotropin-Releasing Hormone), LEP (Leptin), PDK4 (Pyruvate Dehydrogenase Kinase Isozyme 4), SPP1 (Secreted Phosphoprotein 1), and SST (Somatostatin) demonstrated consistent dysregulation across preeclampsia cohorts, with qRT-PCR validation confirming increased LEP and CRH expression alongside altered SPP1 levels in preeclampsia samples.

Importantly, the identification of mitochondrial energy metabolism-related differentially expressed genes has provided new insights into disease mechanisms. Li et al. established that genes including OCRL, TPI1, GAPDH, and LDHA form diagnostic models with promising predictive performance, predominantly enriched in pyruvate metabolism, glycolysis, and ATP metabolism pathways. This metabolic dysfunction appears to drive oxidative stress and inflammatory responses through immune modulation, with CIBERSORT analysis highlighting significant variations in immune cell composition between preeclampsia and control groups, creating a pathological cascade that culminates in the clinical syndrome of preeclampsia.

Inflammatory networks and immune dysfunction

The inflammatory aspect of preeclampsia encompasses much more than mere maternal immune activation, involving intricate networks of cellular stress responses and immune regulation disorders. Zhao et al. discovered that BNIP3-driven mitophagy is a novel mechanism linking cellular stress intensifies placental damage through activation of the NLRP1 inflammasome. Their study showed that both BNIP3-mediated mitophagy and NLRP1 inflammasome activation occur in mouse models of L-NAME-induced preeclampsia and in human placentas affected by preeclampsia. Notably, knockdown of BNIP3 in JEG3 cells preventing mitophagy and NLRP1 inflammasome activation upon subjected to hypoxia and reoxygenation. This pathway highlights the direct connection between mitochondrial dysfunction and inflammatory responses, with mitochondrial reactive oxygen species (mtROS) acting as a crucial mediator. Zhao et al. illustrated that silencing BNIP3 results in a notable decrease in mitochondrial damage and mtROS production., Furthermore, treatment with the antioxidant MitoTEMPO after BNIP3 silencing led to an even greater reduction in NLRP1 expression. Crucially, BNIP3 knockdown mitigates placental damage in preeclampsia mouse models, establishing a definitive therapeutic target for potential intervention.

Cell-free DNA: a window into placental pathology

Cell-free DNA (cfDNA) analysis represents one of the most clinically promising advancements in preeclampsia research, offering non-invasive insights into placental health and disease progression. In a comprehensive review, Guo et al. outlined the multidimensional roles of cfDNA in preeclampsia. Their review highlighting quantitative alterations in cfDNA, fragmentomic profiles, and placenta-specific methylation patterns such as RASSF1A that demonstrate significant value for early prediction and severity stratification of PE. The mechanistic basis of cfDNA release involves placental hypoxia-induced trophoblast apoptosis, epigenetic dysregulation activating TLR9/NF-κB inflammatory pathways, and oxidative stress-mediated mitochondrial cfDNA fragmentation.

Guo et al. emphasized that integrating cfDNA with complementary biomarkers enhances predictive performance beyond what can be achieved with traditional clinical parameters alone. However, they acknowledged that challenges remain regarding preanalytical variability and dynamic gestational changes, with assay standardization constituting the fundamental translational bottleneck. Their review advocates for advancing fragmentomics-integrated multi-omics frameworks for precision prediction, representing a critical step toward personalized preeclampsia management.

Therapeutic horizons: from bench to bedside

Secondary prevention methods for preeclampsia are progressing beyond the conventional approaches of low-dose aspirin and calcium supplementation. Akbar et al. offered an extensive review

of pharmacological strategies for secondary prevention, showing that low-dose aspirin (LDA) can effectively reduce the incidence of early-onset preeclampsia (EOP) when initiated before 16 weeks of gestation. They noted that calcium supplementation benefits women who have inadequate dietary calcium intake. Concurrently, low molecular weight heparins (LMWH) appear to be promising, albeit with limited use for patients with a history of severe placental vasculopathy. New treatment targets are being explored, including metabolic modulators like metformin, which Akbar et al. suggested may reduce preeclampsia rates due to its anti-inflammatory and vascular benefits, especially in women with significant obesity. Statins, such as pravastatin, have demonstrated positive outcomes in lowering the incidence of preterm preeclampsia and enhancing maternal-fetal health through their multifaceted cardiovascular protective properties. Recognizing oxidative stress as a key pathogenic factor has prompted investigations into targeted antioxidant therapies. Afrose et al. assessed treatments aimed at oxidative stress in *in vitro* models of placental stress, revealing that agents like AD-01 and resveratrol may have therapeutic value by mitigating oxidative stress-related cellular dysfunction. Their research indicated that metformin could alleviate increases in uric acid and malondialdehyde induced by DMOG, Rho-6G, or TNF-α, while AD-01 effectively reduced both markers under various stress situations. These results bolster the advancement of precision medicine strategies aimed at addressing specific molecular pathways based on individual risk factors and disease classifications.

Clinical context: comprehensive outcome assessment

The clinical implications of these molecular discoveries must be understood within the broader context of maternal and fetal outcomes. Ibeh et al. provided valuable insights through their retrospective analysis of 151 pregnant patients with thrombocytopenia, demonstrating that hypertensive disorders in pregnancy (including preeclampsia) are associated with higher neonatal intensive care unit transfer rates and lower birth weights in newborns. Their study revealed that thromboelastography (TEG) parameters correlate with pre-delivery platelet count in moderate and severe thrombocytopenia groups, suggesting that patients with preeclampsia-associated thrombocytopenia may have significant changes in blood coagulation and fibrinolysis systems requiring enhanced monitoring.

Mitochondrial biomarkers in preeclampsia

The identification of mitochondrial and programmed cell death (mtPCD) biomarkers represents a significant advancement in understanding preeclampsia pathogenesis., Moving beyond traditional clinical parameters, these findings reveal fundamental cellular mechanisms driving this devastating pregnancy disorder. Through sophisticated bioinformatics integration of multiple datasets and rigorous experimental validation, Lin et al. have identified four critical genes—*SLC25A5*, *ACSF2*, *MFF*, and *PMAIP1*—that offer both diagnostic precision and mechanistic insights into preeclampsia development, suggesting a coordinated disruption of mitochondrial homeostasis and cellular survival pathways that fundamentally alter placental function. Particularly compelling is the identification of regulatory networks, including the *KCNQ1OT1*/hsa-miR-200b-3p/*ACSF2* axis, which opens new therapeutic intervention strategies. Additionally, drug predictions analysis identified clodronic acid offer immediate translational potential. This mtPCD-focused approach not only enhances our diagnostic capabilities through machine learning-validated biomarker panels but also fundamentally reframes preeclampsia as a disorder of mitochondrial dysfunction and programmed cell death dysregulation, positioning mitochondrial biology as a central therapeutic target for improving maternal and fetal outcomes in this complex pregnancy syndrome.

MicroRNA biomarkers herald a new Era in pregnancy risk prediction

The integration of molecular biomarkers into routine prenatal care represents a paradigm shift toward precision obstetrics, with a microRNA (miRNA) profiling emerging as a potential tool for this transformation. A comprehensive retrospective study using over 600 pregnancies, Hromadnikova et al. has demonstrated that combinations of cardiovascular disease-associated miRNAs with maternal clinical characteristics can achieve remarkable predictive accuracy for adverse pregnancy outcomes. Detection rates exceeding 80% for most complications including preeclampsia (83.33%), HELLP syndrome (92.86%), and gestational diabetes requiring therapy (89.47%). Particularly striking is the 91.67% detection rate for stillbirth using miRNA biomarkers alone, obtained from a simple blood draw between 10–13 weeks of gestation. This approach transcends traditional risk assessment by identifying molecular signatures of cardiovascular dysfunction that underlie many pregnancy complications, enabling early intervention strategies that could fundamentally alter pregnancy trajectories. The cost-effectiveness and accessibility of this miRNA-based approach make it particularly promising for widespread implementation, potentially transforming pregnancy care from reactive management to proactive prevention across diverse healthcare settings.

Challenges and future directions

Despite remarkable progress in understanding preeclampsia's molecular foundations, significant translational challenges persist. The complexity of preeclampsia's pathophysiology, with multiple interacting pathways involving metabolism, immunity, and vascular function, require a systems-level approaches rather than single-target interventions are unlikely to address its multifactorial nature. As emphasized by Guo et al. standardization of analytical platforms, particularly for cfDNA fragmentomics and multi-omics integration, represents a fundamental bottleneck for clinical translation. Additional limitations include the small and non-diverse cohorts in most studies, the lack of longitudinal validation, and practical feasibility Research Topic such as high costs and variability across healthcare systems.

Future research priorities should include the validation of molecular biomarkers in diverse populations, the development of point-of-care diagnostic platforms, and clinical trials of combination therapeutic strategies targeting multiple pathogenic pathways simultaneously. The integration of artificial intelligence (AI) and machine learning approaches with multi-omics data, as demonstrated by Wang et al. offers unprecedented opportunities for developing personalized risk prediction models and treatment algorithms.

Conclusion

The merging of genomics, metabolomics, and systems biology is revolutionizing our comprehension of preeclampsia, changing it from a poorly understood syndrome to a Research Topic of related disorders with specific molecular pathways that can be targeted. Studies such as identifying subtype-specific signatures (Han et al.), illustrating metabolic reprogramming patterns (Li et al.), mapping inflammatory networks (Zhao et al.), and highlighting cfDNA biomarkers (Guo et al.), offers a thorough guide for precision medicine approaches to this complex Research Topic. Future efforts must also focus on addressing global disparities, ensuring that biomarker-based diagnostics and preventive strategies are accessible in low-resource settings, while also recognizing the long-term cardiovascular risks for mothers and developmental consequences for children. As we move closer to applying these findings clinically, our attention must transition from simple descriptive molecular profiling to validating functionality and targeting therapeutics, as demonstrated in the therapeutic studies conducted by Afrose et al. and the extensive prevention strategies proposed by Akbar et al. Mitochondria-based biomarkers by Lin et al. provided a clue for early detection of PE as well as miRNA-based biomarkers by Hromadnikova et al. The primary objective remains evident: to convert preeclampsia, currently a major cause of maternal and perinatal mortality, into a condition that can be prevented and managed through early prediction, targeted prevention, and personalized treatment plans. The way ahead necessitates ongoing interdisciplinary collaboration among basic scientists, clinicians, and translational researchers, along with a sustained commitment to standardization initiatives and clinical validation research. Only through such coordinated efforts can we fully achieve the potential of precision medicine to enhance outcomes for preeclampsia and related complications during pregnancy.

Author contributions

RK: Methodology, Supervision, Writing – original draft, Writing – review and editing, Investigation, Project administration, Validation. RM: Investigation, Writing – review and editing, Methodology. SK: Methodology, Supervision, Writing – original draft, Writing – review and editing, Conceptualization, Data curation, Formal Analysis.

Funding

The author(s) declare that no financial support was received for the research and/or publication of this article.

Conflict of interest

The authors declare that the research was conducted in the absence of any commercial or financial relationships that could be construed as a potential conflict of interest.

Generative AI statement

The author(s) declare that no Generative AI was used in the creation of this manuscript.

Any alternative text (alt text) provided alongside figures in this article has been generated by Frontiers with the support of artificial intelligence and reasonable efforts have been made to ensure accuracy, including review by the authors wherever possible. If you identify any issues, please contact us.

Publisher's note

frontiers | Frontiers in Cell and Developmental Biology

TYPE Original Research
PUBLISHED 04 September 2024
DOI 10.3389/fcell.2024.1461547

OPEN ACCESS

EDITED BY
Rajesh Kumar Manne,
Duke University, United States

REVIEWED BY
Ramesh Butti,
National Centre for Cell Science, India
Ling Bai,
Duke University, United States
Naresh Damuka,
Wake Forest University, United States

*CORRESPONDENCE
Ilona Hromadnikova,
ilona.hromadnikova@lf3.cuni.cz

†These authors have contributed equally to this work

RECEIVED 08 July 2024
ACCEPTED 26 August 2024
PUBLISHED 04 September 2024

CITATION
Hromadnikova I, Kotlabova K and Krofta L (2024) First-trimester predictive models for adverse pregnancy outcomes—a base for implementation of strategies to prevent cardiovascular disease development. *Front. Cell Dev. Biol.* 12:1461547. doi: 10.3389/fcell.2024.1461547

First-trimester predictive models for adverse pregnancy outcomes—a base for implementation of strategies to prevent cardiovascular disease development

Ilona Hromadnikova[1]*†, Katerina Kotlabova[1†] and Ladislav Krofta[2†]

[1]Department of Molecular Biology and Cell Pathology, Third Faculty of Medicine, Charles University, Prague, Czechia, [2]Institute for the Care of the Mother and Child, Third Faculty of Medicine, Charles University, Prague, Czechia

Introduction: This study aimed to establish efficient, cost-effective, and early predictive models for adverse pregnancy outcomes based on the combinations of a minimum number of miRNA biomarkers, whose altered expression was observed in specific pregnancy-related complications and selected maternal clinical characteristics.

Methods: This retrospective study included singleton pregnancies with gestational hypertension (GH, n = 83), preeclampsia (PE, n = 66), HELLP syndrome (n = 14), fetal growth restriction (FGR, n = 82), small for gestational age (SGA, n = 37), gestational diabetes mellitus (GDM, n = 121), preterm birth in the absence of other complications (n = 106), late miscarriage (n = 34), stillbirth (n = 24), and 80 normal term pregnancies. MiRNA gene expression profiling was performed on the whole peripheral venous blood samples collected between 10 and 13 weeks of gestation using real-time reverse transcription polymerase chain reaction (RT-PCR).

Results: Most pregnancies with adverse outcomes were identified using the proposed approach (the combinations of selected miRNAs and appropriate maternal clinical characteristics) (GH, 69.88%; PE, 83.33%; HELLP, 92.86%; FGR, 73.17%; SGA, 81.08%; GDM on therapy, 89.47%; and late miscarriage, 84.85%). In the case of stillbirth, no addition of maternal clinical characteristics to the predictive model was necessary because a high detection rate was achieved by a combination of miRNA biomarkers only [91.67% cases at 10.0% false positive rate (FPR)].

Conclusion: The proposed models based on the combinations of selected cardiovascular disease-associated miRNAs and maternal clinical variables have a high predictive potential for identifying women at increased risk of adverse pregnancy outcomes; this can be incorporated into routine first-trimester screening programs. Preventive programs can be initiated based on these models to lower cardiovascular risk and prevent the development of

metabolic/cardiovascular/cerebrovascular diseases because timely implementation of beneficial lifestyle strategies may reverse the dysregulation of miRNAs maintaining and controlling the cardiovascular system.

KEYWORDS

first-trimester screening, cardiovascular risk, miRNA, predictive models, preventive program, risk factors

1 Introduction

MiRNAs are small non-coding RNAs (18–25 nucleotides) that regulate gene expression at the post-transcriptional level (Lai, 2002; Bartel, 2004). Increased miRNA expression results in the degradation of mRNAs or blockage of translation of potential target genes. Conversely, upregulation of potential target genes results from decreased miRNA levels. An altered miRNA expression profile usually contributes to the pathophysiology of the disease and may be used for the diagnosis and/or the assessment of prognosis of the disease (Piletič and Kunej, 2016; Wang et al., 2016; Condrat et al., 2020).

Recently, we observed an altered expression profile of miRNAs that play a role in homeostasis and maintenance of the cardiovascular system and the pathophysiology of cardiovascular and cerebrovascular diseases in women at risk of adverse pregnancy outcomes (Hromadnikova et al., 2022d; Hromadnikova et al., 2023a). Initially, we proposed early predictive models for gestational hypertension (GH) (Hromadnikova et al., 2022a), preeclampsia (PE) (Hromadnikova et al., 2022a), HELLP syndrome (Hromadnikova et al., 2023a), fetal growth restriction (FGR) (Hromadnikova et al., 2022b), small for gestational age (SGA) (Hromadnikova et al., 2022b), preterm delivery in the absence of other pregnancy-related complications (Hromadnikova et al., 2022c), gestational diabetes mellitus (GDM) (Hromadnikova et al., 2022d), miscarriage or stillbirth (Hromadnikova et al., 2023c) based only on miRNA biomarkers.

Afterwards, we identified multiple independent risk factors predisposing to the development of pregnancy-related complications such as maternal age and body mass index (BMI) at early stages of gestation, nulliparity, confirmed diagnosis of autoimmune disease, infertility treatment using assisted reproductive technology, presence of chronic hypertension, presence of thrombophilia gene mutations, history of pregnancy-related complications (PE, HELLP, SGA, FGR, and preterm birth) in previous pregnancy (ies), history of miscarriage (before 20 gestational weeks), and occurrence of diabetes mellitus in first-degree relatives (Hromadnikova et al., 2024; Hromadnikova et al., 2023a; Hromadnikova et al., 2023b; Hromadnikova et al., 2022e; Hromadnikova et al., 2022d; Hromadnikova et al., 2023c).

Subsequently, we involved these maternal clinical characteristics in miRNA-based predictive models, which increased the detection rate of pregnancies at high risk of adverse pregnancy outcomes (Hromadnikova et al., 2024; Hromadnikova et al., 2023a; Hromadnikova et al., 2023b; Hromadnikova et al., 2022e; Hromadnikova et al., 2022d; Hromadnikova et al., 2023c). In addition, we added first-trimester screening for PE and/or FGR and spontaneous preterm birth, both determined using the FMF algorithm (Tan et al., 2018), to the predictive models for GH, PE, HELLP syndrome, FGR, SGA, and GDM, as these two independent variables slightly increased the detection rates.

Currently, we focused on the development of efficient, cost-effective, early predictive models for identifying adverse pregnancy outcomes based on a selection of six miRNAs (miR-181a-5p, miR-20a-5p, miR-146a-5p, miR-574-3p, miR-1-3p, and miR-16-5p), whose altered expression was a common phenomenon shared between multiple pregnancy-related complications (Table 1). These miRNAs were combined with maternal clinical characteristics previously identified as the risk factors for a complicated gestational course (Table 2).

2 Materials and methods

2.1 Patients cohort

This study included pregnancies diagnosed with gestational hypertension (n = 83), preeclampsia (n = 66), HELLP syndrome (n = 14), fetal growth restriction (n = 82), small for gestational age (n = 37), preterm birth [spontaneous preterm birth (PTB) or preterm prelabor rupture of membranes (PPROM)] in the absence of other pregnancy-related complications (n = 106), gestational diabetes mellitus requiring administration of appropriate therapy (n = 20), late miscarriage (n = 34), and stillbirth (n = 24) together with reference group (normal term pregnancies, n = 80).

2.1.1 Inclusion and exclusion criteria

- Singleton pregnancies of Caucasian descent only undergoing the first-trimester screening at 10–13 weeks of gestation
- Pregnancies with confirmed adverse obstetric outcomes. The diagnoses were assessed using appropriate guidelines (ACOG Committee on Practice Bulletins–Obstetrics, 2002; ACOG Committee on Practice Bulletins—Gynecology, 2018; ACOG Committee on Practice Bulletins–Obstetrics, 2020; American College of Obstetricians and Gynecologists et al., 2020; ACOG Committee on Practice Bulletins–Obstetrics, 2021; American Diabetes Association, 2009; International Association of Diabetes and Pregnancy Study Groups Consensus Panel, 2010; Martin et al., 1991; Martin et al., 2006; Weinstein, 1982; Audibert et al., 1996; Moutquin et al., 1996; Sibai, 2004; Barton and Sibai, 2004; Romero et al., 2006; Goldenberg et al., 2008; Leeners et al., 2011; Malmström and Merken, 2018).
- Only pregnancies with complete medical records that had been followed up and delivered at the Institute for the Care of Mother and Child, Prague, Czech Republic

TABLE 1 MiRNA altered expression profile during early gestational stages - common sign of adverse pregnancy outcomes.

	GH	PE	HELLP	FGR	SGA	Pretem delivery (PPROM or PTB) No other complications	GDM on therapy	Pregnancy loss	
								Late miscarriage	Stillbirth
miR-181a-5p	+	+	+	+	+			+	+
miR-20a-5p		+		+	+		+		+
miR-146a-5p		+	+	+	+	+		+	+
miR-574-3p		+		+					+
miR-1-3p			+		+			+	+
miR-16-5p				+		+		+	+

GH, gestational hypertension; PE, preeclampsia; FGR, fetal growth restriction; SGA, small for gestational age; GDM, gestational diabetes mellitus; PPROM, preterm prelabor rupture of membranes; PTB, spontaneous preterm birth; HELLP, hemolysis, elevated liver enzymes and low platelets syndrome.

TABLE 2 Maternal clinical characteristics representing risk factors for adverse pregnancy outcomes involved in first-trimester predictive models.

Variables involved in prediction models	GH	PE	HELLP	FGR	SGA	Preterm delivery[a]	GDM	Late miscarriage
Maternal age at early gestational stages	+	+	+	+	+	+	++	+
BMI at early gestational stages	+	+	+	+	+	+	++	+
Nulliparity	+	+		+				
Confirmed diagnosis of autoimmune disease	+	+	+	+		+		+
Chronic hypertension in anamnesis				+				
Family history of diabetes mellitus (first-degree relatives only)							+	
Current pregnancy conceived after ART techniques (IVF/ICSI/other)	+	+	+	+	+	+	++	+
Trombophilia gene mutations			+				+	+
History of miscarriage (spontaneous loss of pregnancy before 20 weeks of gestation)							+	+
History of HELLP and/or PE		+	+					
History of SGA or FGR				+				
History of preterm birth						+		
Presence of non-autoimmune hypothyroidism								+
Presence of uterine fibroids or abnormal shaped womb								+
Predictive Model I-Number of Variables	**5**	**6**	**6**	**7**	**3**	**5**	**3**	**8**
Screen-positive for PE and/or FGR by FMF algorithm	+	+	+	+	+	+	+	+
Screen-positive for preterm birth by FMF algorithm	+	+	NA[b]	+	+	+	NA[c]	
Predictive Model II-Number of Variables (Model I + FMF screening results)	**7**	**8**	**7**	**9**	**5**	**7**	**7**	**9**

GH, gestational hypertension; PE, preeclampsia; HELLP, haemolysis, elevated liver enzymes and low platelets syndrome; FGR, fetal growth restriction; SGA, small-for-gestational-age; PTB, spontaneous preterm birth; PPROM, preterm prelabor rupture of membranes; GDM, gestational diabetes mellitus; BMI, body mass index; ART, assisted reproductive technology; IVF, *in vitro* fertilization; ICSI, intracytoplasmic sperm injection; FMF, Fetal Medicine Foundation. Bold values highlight the final number of variables used in Predictive Model I and Predictive Model II.
[a]PPROM, or PTB, with no other complications; NA, not analysed in model.
[b]low number of patients with appropriate data.
[c]no occurrence of preterm birth in this group of pregnancies; ++, maternal clinical variables used in prediction model I for GDM.

- PE: pregnancies with the onset of PE with or without FGR irrespective of the severity of the disease and gestational age of the onset of the disease
- HELLP syndrome: pregnancies with the onset of HELLP syndrome with or without PE with no sign of SGA or FGR

- SGA or FGR: only cases without PE regardless of the gestational age of the onset of the disease
- Preterm birth: PTB or PPROM occurring before 37 gestational weeks in the absence of other pregnancy-related complications (GH, PE, HELLP, FGR, SGA, or GDM)
- GDM: Patients newly diagnosed with diabetes mellitus during early gestation, patients with the occurrence of chronic hypertension, and those ones carrying growth restricted or SGA fetuses, fetuses with anomalies or chromosomal abnormalities were intentionally excluded from the study. Likewise, patients demonstrating concurrently other pregnancy-related complications such as GH, PE, HELLP syndrome, *in utero* infections, PTB, PPROM, fetal demise *in utero* or stillbirth were also excluded from the study.
- Pregnancy losses: late miscarriage occurring between 13 and 20 weeks of gestation or stillbirth occurring after 20 weeks of gestation, both explained and unexplained causes were included in the study
- Selected maternal-age-matched normal term pregnancies
- Selected gestational-age-matched at sampling (weeks) normal term pregnancies

The selection of maternal-age-matched, and gestational-age-matched at sampling (weeks) normal term pregnancies ensured the homogeneity and comparability between the studied groups.

Pilot and validation studies were performed. Sample size calculation was used to calculate the minimal required sample size of subjects for analyses.

All procedures were in accordance with the ethical standards of the responsible committee on human experimentation (institutional and national) and the Helsinki Declaration of 1964 and its later amendments. All the included patients provided informed consent for participation in the study. The Ethics Committee of the Third Faculty of Medicine, Charles University, granted initial approval for this study (Implication of placental-specific miRNAs in maternal circulation for diagnosis and prediction of pregnancy-related complications, date of approval: 7 April 2011). Ongoing approval for the study was obtained from the Ethics Committee of the Third Faculty of Medicine, Charles University (Long-term monitoring of complex cardiovascular profiles in mother, fetus, and offspring descending from pregnancy-related complications, date of approval: 27 March 2014) and the Ethics Committee of the Institute for the Care of the Mother and Child, Charles University (Long-term monitoring of complex cardiovascular profiles in mother, fetus, and offspring descending from pregnancy-related complications, date of approval: 28 May 2015, number of approval: 1/4/2015). Informed consent is a complex process as it involves attaining consent for collecting peripheral blood samples at the beginning of pregnancy. In addition, it also includes gaining consent for collecting peripheral blood samples at the onset of pregnancy-related complications and collecting placental samples during childbirth in case of the onset of pregnancy-related complications.

2.2 Collection and processing of samples

Collection and processing of samples, reverse transcription (RT), and real-time PCR analyses were performed as previously described (Hromadnikova et al., 2022a; Hromadnikova et al., 2022b; Hromadnikova et al., 2022c; Hromadnikova et al., 2022d; Hromadnikova et al., 2022e; Hromadnikova et al., 2023a; Hromadnikova et al., 2023b; Hromadnikova et al., 2023c; Hromadnikova et al., 2024).

Briefly, total RNA enriched for small RNAs was isolated from whole peripheral venous blood (EDTA) using a mirVana miRNA isolation kit (Ambion, Austin, United States of America). mRNAs of miRNAs of interest were reverse transcribed into complementary DNA (cDNA) using miRNA-specific stem loop primers and TaqMan MicroRNA Reverse Transcription Kit (Applied Biosystems, Branchburg, United States of America). Reverse transcription was performed in a total reaction volume of 10 μL.

Subsequently, 3 μL of cDNA was mixed in a total reaction volume of 15 μL with specific primers, TaqMan MGB probes (the components of TaqMan MicroRNA Assays), and the components of the TaqMan Universal PCR Master Mix (Applied Biosystems, Branchburg, United States of America). Real-time RT-qPCR was performed on a 7,500 Real-Time PCR System under standard TaqMan PCR conditions described in the TaqMan guidelines. The miRNA gene expression was determined using the comparative Ct method (Livak and Schmittgen, 2001). The normalization factor (Vandesompele et al., 2002) (geometric mean of Ct values of selected endogenous controls: RNU58A and RNU38B) was used to normalize the miRNA gene expression data.

2.3 Criteria for the MiRNA selection

In total, 29 miRNAs were screened at early stages of gestation in pregnancies at risk of adverse pregnancy outcomes. The set involved the following miRNAs: miR-1-3p, miR-16-5p, miR-17-5p, miR-20a-5p, miR-20b-5p, miR-21-5p, miR-23a-3p, miR-24-3p, miR-26a-5p, miR-29a-3p, miR-92a-3p, miR-100-5p, miR-103a-3p, miR-125b-5p, miR-126-3p, miR-130b-3p, miR-133a-3p, miR-143-3p, miR-145-5p, miR-146a-5p, miR-155-5p, miR-181a-5p, miR-195-5p, miR-199a-5p, miR-210-3p, miR-221-3p, miR-342-3p, miR-499a-5p, and miR-574-3p. Only the most frequently dysregulated miRNAs (miR-181a-5p, miR-20a-5p, miR-146a-5p, miR-574-3p, miR-1-3p, and miR-16-5p) were selected for the cost-effective early predictive models for adverse obstetric outcomes (Table 1; Table 3). Other miRNAs showed either no altered expression or were dysregulated in no more than two pregnancy-related complications.

2.4 Statistical analysis

Predictive models for adverse pregnancy outcomes were constructed using logistic regression and receiver operating characteristic (ROC) curve analyses (MedCalc Software bvba, Ostend, Belgium). ROC curves displayed the areas under the curves (AUC), the cut-off points associated with sensitivities, specificities, positive and negative likelihood ratios (LR+, LR-), and sensitivities at 10.0% false positive rate (FPR) (MedCalc Software bvba, Ostend, Belgium). Initially, all independent variables (selected miRNAs and maternal clinical characteristics) and dependent variables (diagnoses, for example preeclampsia – 1, normal term pregnancies - 0) were entered into the logistic regression models for particular pregnancy-related complications.

TABLE 3 Characteristics of selected MiRNAs.

Assay name (the manufacturer)	Assay ID (the manufacturer)	miRBase ID	NCBI Location Chromosome	Mature miRNA sequence
hsa-miR-1	002222	hsa-miR-1-3p	Chr20: 62554306–62554376 [+]	5′-UGGAAUGUAAAGAAGUAUGUAU-3′
hsa-miR-16	000391	hsa-miR-16-5p	Chr13: 50048973–50049061 [-]	5′-UAGCAGCACGUAAAUAUUGGCG- 3′
hsa-miR-20a	000580	hsa-miR-20a-5p	Chr13: 91351065–91351135 [+]	5′-UAAAGUGCUUAUAGUGCAGGU AG-3′
hsa-miR-146a	000468	hsa-miR-146a-5p	Chr5: 160485352–160485450 [+]	5′-UGAGAACUGAAUUCCAUGGGUU-3′
hsa-miR-181a	000480	hsa-miR-181a-5p	Chr1: 198859044–198859153 [-]	5′-AACAUUCAACGCUGUCGGUGAGU-3′
hsa-miR-574-3p	002349	hsa-miR-574-3p	Chr4: 38868032–38868127 [+]	5′-CACGCUCAUGCACACACCCACA-3′

Subsequent ROC curve analyses were applied (MedCalc Software bvba, Ostend, Belgium), where the predictive probabilities gained from logistic regression analyses were saved and next used as the new variables and the diagnoses (for example preeclampsia – 1, normal term pregnancies - 0) acted as the classification variables in ROC curve analyses.

2.5 Analysis of MiRNA-target interactions

The miRWalk database (http://mirwalk.umm.uni-heidelberg.de/) and disease ontology module (http://mirwalk.umm.uni-heidelberg.de/diseases/) were used to provide information on the predicted and/or validated targets of miRNAs. Pregnancy-related complications, such as preeclampsia, HELLP syndrome, placental insufficiency, and GDM were available in the miRWalk database. The only common targets associated with pregnancy-related complications, cardiovascular risk factors (obesity, hypertension, atherosclerosis, prediabetes syndrome, and diabetes mellitus), and cardiovascular and cerebrovascular diseases (myocardial infarction, cerebral infarction, systolic and diastolic heart failure, and heart, cardiovascular, and cerebrovascular diseases as a whole) were reported.

3 Results

3.1 The cost-effective first-trimester predictive models for adverse pregnancy outcomes

The cost-effective first-trimester predictive models for adverse pregnancy outcomes were based on the combinations of a minimum number of miRNA biomarkers with jointly altered expression during the early gestational stages. In addition, maternal clinical characteristics identified as the risk factors for adverse pregnancy outcomes were added into the predictive models.

Several miRNAs of the six joint miRNAs were dysregulated at the early gestational stages in pregnancies with various adverse pregnancy outcomes (GH: 1 miRNA; PE: 4 miRNAs; HELLP syndrome: 3 miRNAs; FGR: 5 miRNAs; SGA: 4 miRNAs; GDM on therapy: 1 miRNA; late miscarriage: 4 miRNAs; stillbirth: six miRNAs; and preterm delivery in the absence of the above-mentioned pregnancy-related complications: two miRNAs).

The combinations of these miRNAs correctly predicted the occurrence of various adverse pregnancy outcomes in a portion of cases at 10.0% FPR (GH: 22.89% cases; PE: 48.48% cases; HELLP syndrome: 57.14% cases; FGR: 37.80% cases; SGA: 75.68% cases; GDM on therapy: 20.0% cases; late miscarriage: 52.94% cases; stillbirth: 91.67% cases; and preterm delivery in the absence of the above-mentioned pregnancy-related complications: 27.36% cases) (Table 4).

Predictive models based on the combinations of these miRNAs and selected maternal clinical characteristics identified as the risk factors for appropriate adverse pregnancy outcomes in our previous studies showed higher detection rates at 10.0% FPR (GH, 62.65%; PE, 78.79%; HELLP syndrome, 85.71%; FGR, 58.54%; SGA, 70.27%; GDM on therapy, 78.95%; late miscarriage, 84.85%; and preterm delivery in the absence of the above-mentioned pregnancy-related complications, 45.28%) (Hromadnikova et al., 2022d; Hromadnikova et al., 2022e; Hromadnikova et al., 2023a; Hromadnikova et al., 2023b; Hromadnikova et al., 2023c; Hromadnikova et al., 2024) (Table 4). In the case of stillbirth, maternal clinical characteristics need not be added to the predictive model because the detection rate of cases was high only when using a combination of appropriate miRNAs.

More advanced predictive models, which included the results of first-trimester screening for PE and/or FGR and spontaneous preterm birth using the FMF algorithm, increased the detection rates of various adverse pregnancy outcomes at 10.0% FPR (GH: 69.88% cases; PE: 83.33% cases; HELLP syndrome: 92.86% cases; FGR: 73.17% cases; SGA: 81.08% cases; GDM on therapy: 89.47% cases; and preterm delivery in the absence of the above-mentioned pregnancy-related complications: 51.89% cases). In the case of late miscarriage, the detection rate remained the same at a FPR of 10.0% (84.85%) (Table 4).

3.2 Mutual comparison of individual first-trimester predictive models

Only one of six joint miRNAs (miR-181a-5p) was dysregulated at the early gestational stages in pregnancies developing GH. MiR-181a-5p was upregulated in 22.89% of cases with 10.0% FPR (Hromadnikova et al., 2022a). A predictive model based on a

TABLE 4 Predictive models for adverse pregnancy outcomes based on the combinations of MiRNA biomarkers with jointly altered expression during early gestational stages and maternal clinical variables representing risk factors for adverse pregnancy outcomes.

	AUC	95% CI	*p*- value	Sensitivity (At 10% FPR)	Criterion (At 10% FPR)	Youden index J	Youden index associated Criterion	Sensitivity	95%CI	Specificity	95%CI	+LR	95%CI	-LR	95%CI
Predictive Model for GH (Hromadnikova et al. 2024)															
1 miRNA only (miR-181a-5p)	0.649	0.570–0.722	<0.001	22.89%	>0.5216	0.2645	>0.2618	61.45%	50.1–71.9	65.00%	53.5–75.3	1.76	1.2–2.5	0.59	0.4–0.8
1 miRNA +5 maternal clinical characteristics	0.858	0.794–0.907	<0.001	62.65%	>0.6399	0.5577	>0.4314	79.52%	69.2–87.6	76.25%	65.4–85.1	3.35	2.2–5.0	0.27	0.2–0.4
1 miRNA +7 maternal clinical characteristics	0.894	0.837–0.937	<0.001	69.88%	>0.5692	0.6627	>0.6955	66.27%	55.1–76.3	100.0%	95.5–100.0	-	-	0.34	0.2–0.5
Predictive Model for PE															
4 miRNAs only (miR-181a-5p, miR-20a-5p, miR-146a-5p, and miR-574-3p)	0.715	0.634–0.786	<0.001	48.48%	>0.5444	0.3973	>0.5504	48.48%	36.0–61.1	91.25%	82.8–96.4	5.54	2.6–11.7	0.56	0.4–0.7
4 miRNAs +6 maternal clinical characteristics	0.902	0.842–0.945	<0.001	78.79%	>0.4562	0.7004	>0.4657	78.79%	67.0–87.9	91.25%	82.8–96.4	9.00	4.4–18.5	0.23	0.1–0.4
4 miRNAs +8 maternal clinical characteristics	0.934	0.880–0.968	<0.001	83.33%	>0.3707	0.7905	>0.5331	80.30%	68.7–89.1	98.75%	93.2–100.0	64.24	9.1–452.2	0.20	0.1–0.3
Predictive Model for HELLP															
3 miRNAs only (miR-181a-5p, miR-146a-5p, and miR-1-3p)	0.895	0.814–0.949	<0.001	57.14%	>0.1862	0.6446	>0.1161	85.71%	57.2–98.2	78.75%	68.2–87.1	4.03	2.5–6.5	0.18	0.05–0.7
3 miRNAs +6 maternal clinical characteristics	0.970	0.912–0.994	<0.001	85.71%	>0.1106	0.8161	>0.0855	92.86%	66.1–99.8	88.75%	79.7–94.7	8.25	4.4–15.5	0.008	0.01–0.5
3 miRNAs +7 maternal clinical characteristics	0.969	0.911–0.994	<0.001	92.86%	>0.1116	0.8786	>0.1704	92.86%	66.1–99.8	95.00%	87.7–98.6	18.57	7.1–48.8	0.075	0.01–0.5
Predictive Model for FGR															
5 miRNAs only (miR-181a-5p, miR-20a-5p, miR-146a-5p, miR-574-3p, and miR-16-5p)	0.680	0.602–0.751	<0.001	37.80%	>0.6185	0.3409	>0.6919	36.59%	26.2–48.0	97.50%	91.3–99.7	14.63	3.6–59.2	0.65	0.5–0.8
5 miRNAs +7 maternal clinical characteristics	0.815	0.747–0.872	<0.001	58.54%	>0.5995	0.5326	>0.4896	69.51%	58.4–79.2	83.75%	73.8–91.1	4.28	2.5–7.2	0.36	0.3–0.5

(Continued on following page)

10.3389/fcell.2024.1461547

TABLE 4 (*Continued*) Predictive models for adverse pregnancy outcomes based on the combinations of MiRNA biomarkers with jointly altered expression during early gestational stages and maternal clinical variables representing risk factors for adverse pregnancy outcomes.

	AUC	95% CI	*p*- value	Sensitivity (At 10% FPR)	Criterion (At 10% FPR)	Youden index J	Youden index associated Criterion	Sensitivity	95%CI	Specificity	95%CI	+LR	95%CI	-LR	95%CI
5 miRNAs +9 maternal clinical characteristics	0.860	0.797–0.909	<0.001	73.17%	>0.5002	0.6701	>0.6066	69.51%	58.4–79.2	97.50%	91.3–99.7	27.80	7.0–110.1	0.31	0.2–0.4
Predictive Model for SGA (Hromadnikova et al., 2023b)															
4 miRNAs only (miR-181a-5p, miR-20a-5p, miR-146a-5p, and miR-1-3p)	0.868	0.792–0.923	<0.001	75.68%	>0.3664	0.6568	>0.3664	75.68%	58.8–88.2	90.00%	81.2–95.6	7.57	3.8–15.0	0.27	0.2–0.5
4 miRNAs +3 maternal clinical characteristics	0.870	0.795–0.925	<0.001	70.27%	>0.3844	0.6443	>0.3309	75.68%	58.8–88.2	88.75%	79.7–94.7	6.73	3.5–12.8	0.27	0.2–0.5
4 miRNAs +5 maternal clinical characteristics	0.922	0.858–0.964	<0.001	81.08%	>0.3109	0.7253	>0.2844	83.78%	68.0–93.8	88.75%	79.7–94.7	7.45	4.0–14.0	0.18	0.09–0.4
Predictive Model for GDM on therapy															
1 miRNA only (miR-20a-5p)	0.709	0.610–0.796	<0.001	20.00%	>0.2865	0.3625	>0.1343	100.00%	83.2–100.0	36.25%	25.8–47.8	1.57	1.3–1.9	0	-
1 miRNA +3 maternal clinical characteristics	0.949	0.886–0.983	<0.001	78.95%	>0.2605	0.7447	>0.1674	89.47%	66.9–98.7	85.00%	75.3–92.0	5.96	3.5–10.3	0.12	0.03–0.5
1 miRNA +7 maternal clinical characteristics	0.957	0.896–0.987	<0.001	89.47%	>0.2039	0.7947	>0.2039	89.47%	66.9–98.7	90.00%	81.2–95.6	8.95	4.6–17.6	0.12	0.03–0.4
Predictive Model for Late Miscarriage															
4 miRNAs only (miR-181a-5p, miR-146a-5p, miR-16-5p, and miR-1-3p)	0.828	0.746–0.892	<0.001	52.94%	>0.3683	0.5140	>0.2598	67.65%	49.5–82.6	83.75%	73.8–91.1	4.16	2.4–7.2	0.39	0.2–0.6
4 miRNAs +8 maternal clinical characteristics	0.936	0.874–0.973	<0.001	84.85%	>0.2005	0.7807	>0.3892	81.82%	64.5–93.0	96.25%	89.4–99.2	21.82	7.1–67.0	0.19	0.09–0.4
4 miRNAs +9 maternal clinical characteristics	0.935	0.873–0.973	<0.001	84.85%	>0.1967	0.7735	>0.2471	84.85%	68.1–94.9	92.50%	84.4–97.2	11.31	5.2–24.8	0.16	0.07–0.4
Predictive Model for Stillbirth															
6 miRNAs only (miR-181a-5p, miR-20a-5p, miR-146a-5p, miR-574-3p, miR-16-5p, and miR-1-3p)	0.967	0.912–0.992	<0.001	91.67%	>0.0602	0.9167	>0.2737	91.67%%	73.0–99.0	100.00%	95.5–100.0	-	-	0.083	0.02–0.3

(Continued on following page)

10.3389/fcell.2024.1461547

TABLE 4 (*Continued*) Predictive models for adverse pregnancy outcomes based on the combinations of MiRNA biomarkers with jointly altered expression during early gestational stages and maternal clinical variables representing risk factors for adverse pregnancy outcomes.

	AUC	95% CI	*p*- value	Sensitivity (At 10% FPR)	Criterion	Youden index J	Youden index associated Criterion	Sensitivity	95%CI	Specificity	95%CI	+LR	95%CI	-LR	95%CI
Predictive Model for Preterm Delivery (PTB or PPROM) in the Absence of Other Pregnancy-Related Complications															
2 miRNAs only (miR-16-5p and miR-146a-5p)	0.631	0.557–0.700	<0.001	27.36%	>0.6804	0.2212	>0.6570	39.62%	30.3–49.6	82.50%	72.4–90.1	2.26	1.3–3.8	0.73	0.6–0.9
2 miRNAs +5 maternal clinical characteristics	0.740	0.670–0.801	<0.001	45.28%	>0.5930	0.3934	>0.6010	44.34%	34.7–54.3	95.00%	87.7–98.6	8.87	3.3–23.6	0.59	0.5–0.7
2 miRNAs +7 maternal clinical characteristics	0.766	0.698–0.825	<0.001	51.89%	>0.5804	0.4252	>0.5769	53.77%	43.8–63.5	88.75%	79.7–94.7	4.78	2.5–9.1	0.52	0.4–0.6

GH, gestational hypertension; PE, preeclampsia; HELLP, haemolysis, elevated liver enzymes and low platelets syndrome; FGR, fetal growth restriction; SGA, small-for-gestational-age; GDM, gestational diabetes mellitus; PTB, spontaneous preterm birth; PPROM, preterm prelabor rupture of membranes.

combination of the first-trimester expression profile of miR-181a-5p and five maternal clinical characteristics (maternal age and BMI at early gestational stages, nulliparity, confirmed diagnosis of autoimmune disease, and infertility treatment using assisted reproductive technology) reached a detection rate of 62.65% for GH cases at 10.0% FPR (Hromadnikova et al., 2024). A more advanced GH predictive model based on the combination of the first-trimester expression profile of miR-181a-5p and seven maternal clinical characteristics (adding the results gained from the first-trimester screening for PE and/or FGR and spontaneous preterm birth, both using the FMF algorithm) slightly increased the detection rate to 69.88% cases at 10.0% FPR (Hromadnikova et al., 2024). The predictive power for GH can only be improved using this approach.

Previously demonstrated PE predictive models based on the combinations of only six miRNAs (AUC 0.730, $p < 0.001$) (Hromadnikova et al., 2022a) or only eight miRNAs (AUC 0.815, $p < 0.001$) (Hromadnikova, 2023a) reached detection rates of 48.48% and 53.03%, respectively, at 10.0% FPR. Expanding the models based on miRNA expression profiles for the same selected maternal clinical characteristics representing risk factors for PE increased the predictive power significantly: six miRNAs +6 clinical variables (78.79% cases at 10.0% FPR, AUC 0.903, $p < 0.001$), eight miRNAs +6 clinical variables (77.27% cases at 10.0% FPR, AUC 0.931, $p < 0.001$), six miRNAs +8 clinical variables (84.85% cases at 10.0% FPR, AUC 0.939, $p < 0.001$), eight miRNAs +8 clinical variables (84.85% cases at 10.0% FPR, AUC 0.950, $p < 0.001$) (Hromadnikova et al., 2024). The PE predictive model based on four out of six miRNAs common to adverse pregnancy outcomes and the same maternal clinical characteristics (six variables or eight variables) reached a similar detection power (78.79% cases at 10.0% FPR, AUC 0.902, $p < 0.001$; 83.33% cases at 10.0% FPR, AUC 0.934, $p < 0.001$) as the similar models with a higher number of miRNA biomarkers and may be considered as the most cost-effective first-trimester predictive model for PE irrespective of disease severity and time of disease onset.

The HELLP syndrome predictive model previously demonstrated by our group based on the combination of six miRNAs (AUC 0.903, $p < 0.001$) (Hromadnikova et al., 2023a; Hromadnikova, 2022f) reached a detection rate of 78.57% at 10.0% FPR. When this model was expanded for the same selected maternal clinical characteristics representing risk factors for HELLP syndrome, the predictive power significantly increased: six miRNAs +6 clinical variables (85.71% cases at 10.0% FPR, AUC 0.979, $p < 0.001$) and six miRNAs +7 clinical variables (92.86% cases at 10.0% FPR, AUC 0.975, $p < 0.001$) (Hromadnikova et al., 2023a; Hromadnikova, 2022f). The HELLP syndrome predictive model based on three out of six miRNAs common to adverse pregnancy outcomes and the same maternal clinical characteristics (six variables or seven variables) reached similar detection power (85.71% cases at 10.0% FPR, AUC 0.970, $p < 0.001$; 92.86% cases at 10.0% FPR, AUC 0.969, $p < 0.001$) as similar models with six miRNA biomarkers and may be considered the most cost-effective first-trimester predictive model for HELLP syndrome.

Previously demonstrated FGR predictive models by our group based on the combinations of only seven miRNAs (AUC 0.725, $p < 0.001$) (Hromadnikova et al., 2022b) or 10 miRNAs (AUC 0.774, $p < 0.001$) (Hromadnikova, 2023a) reached a detection rate of 42.68%

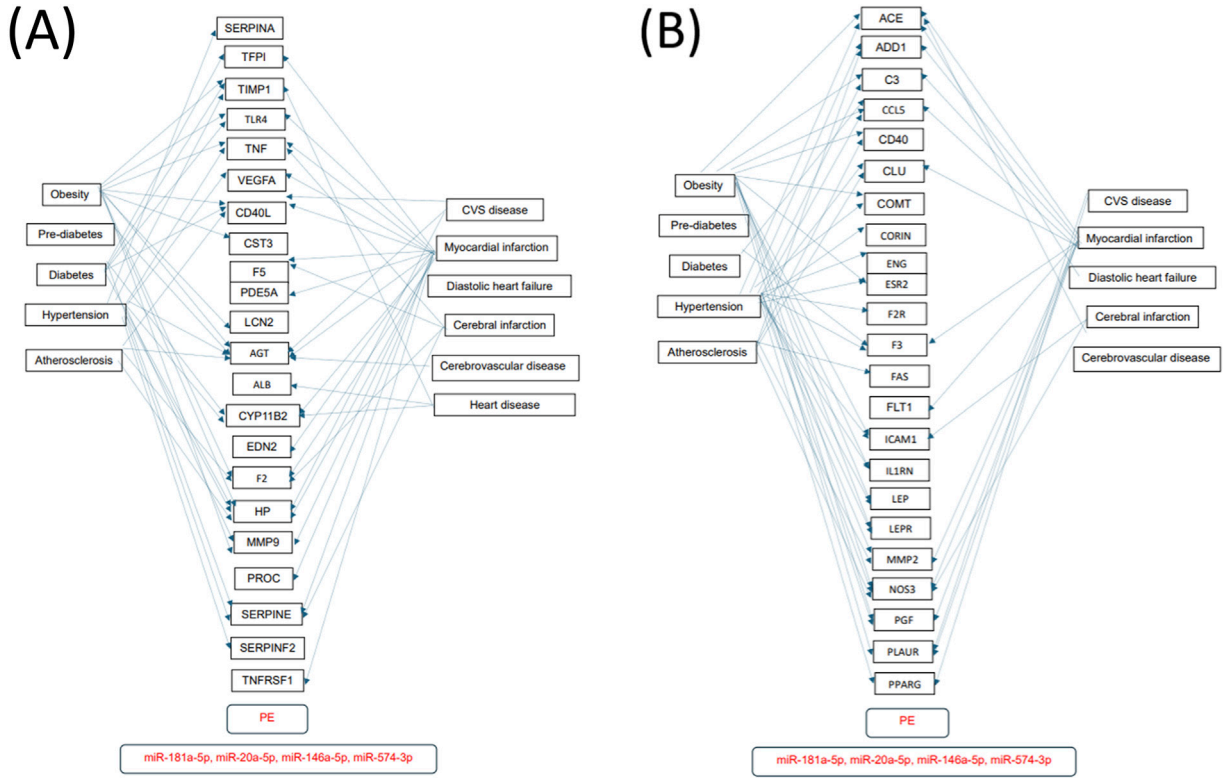

FIGURE 1
MiRNA-target interactions–Common targets of preeclampsia, cardiovascular risk factors, cardiovascular and cerebrovascular diseases. Search for interactions between miR-20a-5p, miR-146a-5p, miR-181a-5p, and miR-574-3p and genes using the miRWalk database and disease ontology module revealed numerous common targets **(A,B)** associated with preeclampsia, cardiovascular risk factors, cardiovascular and cerebrovascular diseases.

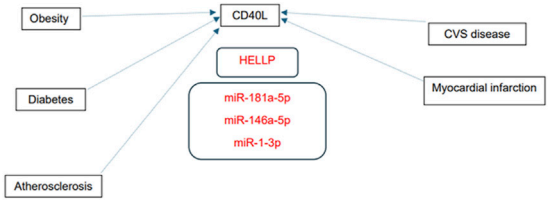

FIGURE 2
MiRNA-target interactions–Common targets of HELLP syndrome, cardiovascular risk factors and cardiovascular diseases. Search for interactions between miR-1-3p, miR-146a-5p, and miR-181a-5p and genes using the miRWalk database and disease ontology module revealed one common target (CD40LG, gene encoding CD40 ligand) associated with HELLP syndrome, cardiovascular risk factors and cardiovascular diseases.

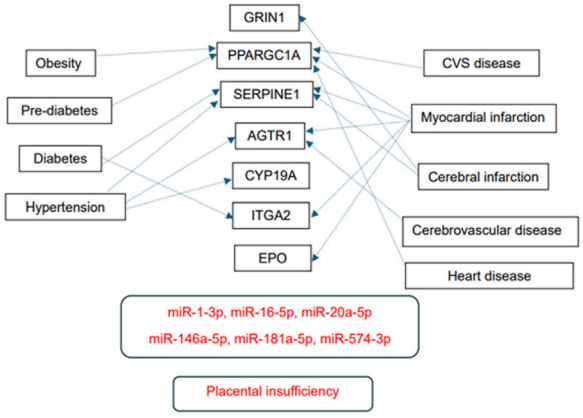

FIGURE 3
MiRNA-target interactions–Common targets of placental insufficiency, cardiovascular risk factors, cardiovascular and cerebrovascular diseases. Search for interactions between miR-1-3p, miR-16-5p, miR-20a-5p, miR-146a-5p, miR-181a-5p, and miR-574-3p and genes using the miRWalk database and disease ontology module revealed several common targets associated with placental insufficiency, cardiovascular risk factors, cardiovascular and cerebrovascular diseases.

cases and 40.24% cases at 10.0% FPR. With the expansion with the same selected maternal clinical characteristics representing risk factors for FGR the models showed significantly increased predictive power: seven miRNAs +7 clinical variables (64.63% cases at 10.0% FPR, AUC 0.840, $p < 0.001$), 10 miRNAs +7 clinical variables (65.85% cases at 10.0% FPR, AUC 0.855, $p < 0.001$), seven miRNAs +9 clinical variables (74.39% cases at 10.0% FPR, AUC 0.887, $p < 0.001$), 10 miRNAs +9 clinical variables (78.05% cases at 10.0% FPR, AUC 0.896, $p < 0.001$) (Hromadnikova et al., 2023b). The FGR predictive models based on five out of six miRNAs common to adverse pregnancy outcomes and the same maternal clinical characteristics (seven variables or

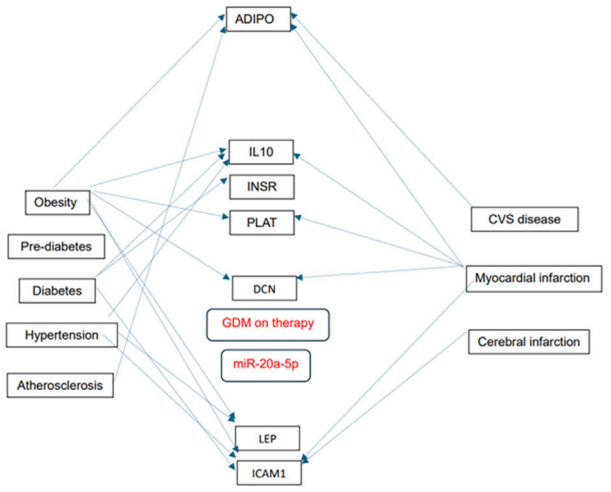

FIGURE 4
MiRNA-target interactions–Common targets of gestational diabetes mellitus, cardiovascular risk factors, cardiovascular and cerebrovascular diseases. Search for interactions between miR-20a-5p and genes using the miRWalk database and disease ontology module revealed several common targets associated with gestational diabetes mellitus, cardiovascular risk factors, cardiovascular and cerebrovascular diseases.

nine variables) reached a slightly lower detection power (58.54% cases at 10.0% FPR, AUC 0.815, $p < 0.001$; 73.17% cases at 10.0% FPR, AUC 0.860, $p < 0.001$) than similar models with a higher number of miRNA biomarkers. However, it may still be considered the most cost-effective first-trimester predictive models for FGR, irrespective of disease severity and time of disease onset.

Similarly, the most cost-effective first-trimester predictive model for SGA, which had already been presented, is based on the combination of four out of six miRNAs common to adverse pregnancy outcomes and five maternal clinical characteristics (81.08% cases at 10.0% FPR, AUC 0.922, $p < 0.001$) (Hromadnikova et al., 2023b). Another SGA predictive model containing eight miRNAs and five maternal clinical characteristics showed a slightly higher detection rate (89.19% cases at 10.0% FPR, AUC 0.956, $p < 0.001$) (Hromadnikova et al., 2023b). The combination of only four miRNAs (75.68% cases at 10.0% FPR, AUC 0.868, $p < 0.001$) (Hromadnikova et al., 2022b) or the combination of only eight miRNAs (83.78% cases at 10.0% FPR, AUC 0.926, $p < 0.001$) (Hromadnikova, 2023a) substantially impacted the SGA detection rate. The implementation of maternal clinical variables slightly increased the SGA detection rate.

A previously demonstrated predictive model for GDM requiring the administration of appropriate therapy by our group based on the combination of only three miRNAs (AUC 0.731, $p < 0.001$) (Hromadnikova et al., 2022d; Hromadnikova 2023b) reached a detection rate of 30.0% cases at 10.0% FPR. When this model was extended to the same selected maternal clinical characteristics representing risk factors for GDM, the predictive power was significantly increased: 3 miRNAs +3 clinical variables (78.95% cases at 10.0% FPR, AUC 0.949, $p < 0.001$) and 3 miRNAs +7 clinical variables (89.47% cases at 10.0% FPR, AUC 0.957, $p < 0.001$) (Hromadnikova et al., 2022d). The predictive model for GDM requiring administration of appropriate therapy based on 1 out of six miRNAs common to adverse pregnancy outcomes and the same maternal clinical characteristics (3 variables or seven variables) reached the same detection power (78.95% cases at 10.0% FPR, AUC 0.949, $p < 0.001$; 89.47% cases at 10.0% FPR, AUC 0.957, $p < 0.001$) as the similar models with a higher number of miRNA biomarkers and may be considered as the most cost-effective first-trimester predictive model for GDM requiring administration of appropriate therapy.

A previously demonstrated predictive model for late miscarriage by our group, based on the combination of only six miRNAs (AUC 0.941, $p < 0.001$) (Hromadnikova et al., 2023c), reached a detection rate of 79.41% at 10.0% FPR. Four of these miRNAs, dysregulated at early gestational stages in pregnancies affected by late miscarriage, were common to adverse pregnancy outcomes. The combination of only these four miRNAs was insufficient to predict the occurrence of late miscarriage (52.94% cases at 10.0% FPR, AUC 0.828, $p < 0.001$). The predictive model based on four miRNAs common to adverse pregnancy outcomes was further expanded to include maternal clinical characteristics (maternal age and BMI at early gestational stages, confirmed diagnosis of autoimmune disease, infertility treatment using assisted reproductive technology, presence of non-autoimmune hypothyroidism, presence of uterine fibroids or abnormal-shaped womb, history of miscarriage(s) in previous gestation(s), and presence of thrombophilia gene mutations) to increase the detection power of late miscarriage. Since the predictive power for late miscarriage significantly increased, this model can also be utilized as a cost-effective model (84.85% cases at 10.0% FPR, AUC 0.936, $p < 0.001$). Alternatively, this model may be extended to the results of first-trimester screening for PE and/or FGR using the FMF algorithm; however, the detection rate of pregnancies with late miscarriage remained the same as that of the model without this variable (84.85% cases at 10.0% FPR, AUC 0.935, $p < 0.001$).

Predictive models based on the combinations of only two miRNAs common to adverse pregnancy outcomes (91.67% cases at 10.0% FPR, AUC 0.951, $p < 0.001$) (Hromadnikova, 2022f; Hromadnikova et al., 2023a) or six miRNAs commonly associated with adverse pregnancy outcomes (91.67% cases at 10.0% FPR, AUC 0.967, $p < 0.001$) were sufficient to predict the later occurrence of stillbirth cost-effectively. Maternal clinical characteristics were not included in the stillbirth predictive models. A previously introduced predictive model for stillbirth based on a combination of 11 dysregulated miRNAs at the early gestational stages achieved a slightly higher detection power (95.83% cases at 10.0% FPR, AUC 0.986, $p < 0.001$) (Hromadnikova, 2022f; Hromadnikova et al., 2023a).

Previously demonstrated predictive models for preterm delivery (PPROM or PTB) in the absence of other pregnancy-related complications by our group, based on the combinations of six miRNAs (AUC 0.812, $p < 0.001$) or 12 miRNAs (AUC 0.818, $p < 0.001$) (Hromadnikova et al., 2022c; Hromadnikova, 2023a), reached a detection rate of 52.83% at 10.0% FPR. Extension of the models based on miRNA expression profiles for the same selected maternal clinical characteristics representing risk factors for preterm delivery in the absence of other pregnancy-related complications increased the predictive power significantly: six miRNAs +5 clinical variables (69.81% cases at 10.0% FPR, AUC 0.874, $p < 0.001$),

12 miRNAs +5 clinical variables (66.98% cases at 10.0% FPR, AUC 0.877, $p < 0.001$), six miRNAs +7 clinical variables (71.70% cases at 10.0% FPR, AUC 0.879, $p < 0.001$), 12 miRNAs +7 clinical variables (73.58% cases at 10.0% FPR, AUC 0.887, $p < 0.001$) (Hromadnikova et al., 2022e). The predictive models based on two out of six miRNAs common to adverse pregnancy outcomes and the same maternal clinical characteristics (five variables or seven variables) reached significantly lower detection power (45.28% cases at 10.0% FPR, AUC 0.740, $p < 0.001$; 51.89% cases at 10.0% FPR, AUC 0.766, $p < 0.001$) and cannot be considered as optimal cost-effective first-trimester predictive models for preterm delivery in the absence of other pregnancy-related complications.

3.3 Analysis of MiRNA-target interactions

Numerous predicted and/or validated targets of miRNAs that predict the occurrence of PE have been associated with cardiovascular risk factors and cardiovascular and cerebrovascular diseases (Figures 1A, B). In case of HELLP syndrome, only one common target (CD40LG, the gene encoding the CD40 ligand) associated with cardiovascular risk factors and cardiovascular diseases was identified (Figure 2). Placental insufficiency, usually manifested clinically as preeclampsia and/or fetal growth restriction, has several common miRNA targets associated with cardiovascular risk factors and cardiovascular and cerebrovascular diseases (Figure 3). MiR-20a-5p, a biomarker used solely to predict the occurrence of GDM requiring appropriate therapy, also showed several common targets associated with cardiovascular risk factors and cardiovascular and cerebrovascular diseases (Figure 4).

4 Discussion

Currently, no first-trimester predictive algorithm for GH, HELLP syndrome, SGA, GDM, late miscarriage, and stillbirth is available. Novel efficient cost-effective modalities for predicting these pregnancy-related complications at the early gestational stages have been proposed. The proposed approach is based on the combinations of selected maternal clinical characteristics and a minimum number of miRNA biomarkers, which play key roles in cardiovascular system maintenance and control and pathogenesis of cardiovascular diseases and whose altered expression was also observed at early gestational stages in pregnancies with adverse outcomes.

At present, the first-trimester algorithm used by the majority of fetal medicine centres developed by the Fetal Medicine Foundation (FMF) calculates the risks for the development of early PE (before 34 gestational weeks) and FGR (before 37 gestational weeks). The risks are calculated on the basis of knowledge of maternal history, BMI, mean arterial blood pressure (MAP), serum levels of pregnancy-associated plasma protein-A (PAPP-A) and placental growth factor (PIGF), and mean uterine artery pulsatility index (UtA-PI) (O´Gorman et al., 2016; O´Gorman et al., 2017; The Fetal Medicine Foundation, 2023; Tan et al., 2018; Mazer Zumaeta et al., 2020). Using the predictive models based on six miRNA biomarkers and selected maternal clinical characteristics, the detection rate of PE increased 2.50 times and the detection rate of FGR 2.61 times when compared with the first-trimester screening for PE and/or FGR using the FMF algorithm. Moreover, using the proposed approach any subtype of PE and FGR regardless of the severity of the disease (mild and severe PE) and time of disease onset can be detected.

In addition, we demonstrated that numerous predicted and/or validated targets of miRNAs used to predict the occurrence of pregnancy-related complications in the first trimester of gestation were associated with several cardiovascular risk factors and cardiovascular and cerebrovascular diseases.

Pregnancy-related complications have been reported to be associated with the increased risk of later development of diabetes mellitus (Ray et al., 2005; Libby et al., 2007; Lykke et al., 2009; Männistö et al., 2013; Thilaganathan, 2016; Thilaganathan, 2017), metabolic syndrome (Yang et al., 2015; Udenze, 2016), hypertension (Bellamy et al., 2007; Craici et al., 2008; Lykke et al., 2009; Männistö et al., 2013; Hypertension in Pregnancy, 2013; Veerbeek et al., 2015; Thilaganathan, 2016; Thilaganathan, 2017), kidney diseases (Männistö et al., 2013), atherosclerosis (Haukkamaa et al., 2009; McDonald et al., 2013), ischemic heart disease (Irgens et al., 2001; Garovic and Hayman, 2007; Bellamy et al., 2007; Craici et al., 2008; Mongraw-Chaffin et al., 2010; Borna et al., 2012; Berks et al., 2013; Männistö et al., 2013), myocardial infarction (Garovic and Hayman, 2007; Mongraw-Chaffin et al., 2010; Männistö et al., 2013; Hypertension in Pregnancy, 2013; Thilaganathan, 2016; Thilaganathan, 2017), heart failure (Männistö et al., 2013; Hypertension in Pregnancy, 2013; Thilaganathan, 2016; Thilaganathan, 2017), stroke (Irgens et al., 2001; Bellamy et al., 2007; Craici et al., 2008; Mongraw-Chaffin et al., 2010; Berks et al., 2013; Männistö et al., 2013; Hypertension in Pregnancy, 2013; Thilaganathan, 2016; Thilaganathan, 2017) and deep venous thrombosis in mothers (Bellamy et al., 2007; Craici et al., 2008; Lykke et al., 2009).

Based on this evidence, we suggest initiating preventive programs for pregnancies at risk of developing pregnancy-related complications as early as possible with the aim of lowering cardiovascular risk and the consequent development of metabolic, cardiovascular, and cerebrovascular diseases. The dysregulation of miRNAs involving in cardiovascular system maintenance and control may still be reversible via the timely implementation of beneficial lifestyle strategies.

Consecutive large-scale retrospective and prospective analyses are needed to verify the reliability of predictive models based on the combinations of the minimum number of miRNA biomarkers common to adverse pregnancy outcomes and maternal clinical characteristics to differentiate between pregnancies with normal and abnormal courses of gestation at early gestational stages. Gynecologists and obstetricians could have a feasible, cost-effective way of identifying pregnancies at risk of adverse pregnancy outcomes at disposal at early gestational stages if satisfactory discrimination power could be achieved.

The dysregulated miRNAs associated with cardiovascular system maintenance and control may be reversed back to normal via the timely implementation of beneficial lifestyle strategies, which may reduce or delay potential cardiovascular risk in mothers.

Data availability statement

The raw data supporting the conclusions of this article will be made available by the authors, without undue reservation.

Ethics statement

The studies involving humans were approved by the Ethics Committee of the Third Faculty of Medicine, Charles University and Ethics Committee of the Institute for the Care of the Mother and Child, Charles University. The studies were conducted in accordance with the local legislation and institutional requirements. The participants provided their written informed consent to participate in this study.

Author contributions

IH: Conceptualization, Data curation, Formal Analysis, Funding acquisition, Methodology, Project administration, Resources, Software, Supervision, Validation, Writing–original draft, Writing–review and editing. KK: Data curation, Formal Analysis, Investigation, Methodology, Software, Validation, Visualization, Writing–review and editing. LK: Conceptualization, Funding acquisition, Project administration, Resources, Software, Supervision, Validation, Writing–review and editing.

Funding

The author(s) declare that financial support was received for the research, authorship, and/or publication of this article. This work was supported by the Charles University Research Program Cooperatio - Mother and Childhood Care (no. 207035) and a research grant SVV (no. 260645).

Acknowledgments

We thank the staff of the Institute for the Care of Mother and Child for their assistance with the collection of the patient biological samples.

Conflict of interest

The authors declare that the research was conducted in the absence of any commercial or financial relationships that could be construed as a potential conflict of interest.

Publisher's note

All claims expressed in this article are solely those of the authors and do not necessarily represent those of their affiliated organizations, or those of the publisher, the editors and the reviewers. Any product that may be evaluated in this article, or claim that may be made by its manufacturer, is not guaranteed or endorsed by the publisher.

References

ACOG Committee on Practice Bulletins—Gynecology (2018). ACOG practice bulletin No. 200: early pregnancy loss. *Obstet. Gynecol.* 132, e197–e207. doi:10.1097/AOG.0000000000002899

ACOG Committee on Practice Bulletins–Obstetrics (2002). ACOG practice bulletin. Diagnosis and management of preeclampsia and eclampsia. Number 33, January 2002. *Obstet. Gynecol.* 99, 159–167. doi:10.1016/s0029-7844(01)01747-1

ACOG Committee on Practice Bulletins–Obstetrics (2020). Gestational hypertension and preeclampsia: ACOG practice bulletin, number 222. *Obstet. Gynecol.* 135, e237–e260. doi:10.1097/AOG.0000000000003891

ACOG Committee on Practice Bulletins—Obstetrics (2021). ACOG practice bulletin, number 227. Fetal growth restriction. *Obstet. Gynecol.* 137, e16–e28. doi:10.1097/AOG.0000000000004251

American College of Obstetricians and Gynecologists; Society for Maternal-Fetal Medicine in collaboration with Metz, T. D., Berry, R. S., Fretts, R. C., Reddy, U. M., et al. (2020). Obstetric Care Consensus #10: management of Stillbirth: (replaces practice bulletin number 102, March 2009). *Am. J. Obstet. Gynecol.* 222, B2–B20. doi:10.1016/j.ajog.2020.01.017

American Diabetes Association (2009). Diagnosis and classification of diabetes mellitus. *Diabetes. Care* 32, S62–S67. doi:10.2337/dc09-S062

Audibert, F., Friedman, S. A., Frangieh, A. Y., and Sibai, B. M. (1996). Clinical utility of strict diagnostic criteria for the HELLP (hemolysis, elevated liver enzymes, and low platelets) syndrome. *Am. J. Obstet. Gynecol.* 175, 460–464. doi:10.1016/s0002-9378(96)70162-x

Bartel, D. P. (2004). MicroRNAs: genomics, biogenesis, mechanism, and function. *Cell* 116, 281–297. doi:10.1016/s0092-8674(04)00045-5

Barton, J. R., and Sibai, B. M. (2004). Diagnosis and management of hemolysis, elevated liver enzymes, and low platelets syndrome. *Clin. Perinatol.* 31, 807–833. doi:10.1016/j.clp.2004.06.008

Bellamy, L., Casas, J. P., Hingorani, A. D., and Williams, D. J. (2007). Pre-eclampsia and risk of cardiovascular disease and cancer in later life: systematic review and meta-analysis. *BMJ* 335, 974. doi:10.1136/bmj.39335.385301.BE

Berks, D., Hoedjes, M., Raat, H., Duvekot, J. J., Steegers, E. A., and Habbema, J. D. (2013). Risk of cardiovascular disease after pre-eclampsia and the effect of lifestyle interventions: a literature-based study. *BJOG* 120, 924–931. doi:10.1111/1471-0528.12191

Borna, S., Neamatipoor, E., and Radman, N. (2012). Risk of coronary artery disease in women with history of pregnancies complicated by preeclampsia and LBW. *J. Matern. Fetal. Neonatal. Med.* 25, 1114–1116. doi:10.3109/14767058.2011.624218

Condrat, C. E., Thompson, D. C., Barbu, M. G., Bugnar, O. L., Boboc, A., Cretoiu, D., et al. (2020). miRNAs as biomarkers in disease: latest findings regarding their role in diagnosis and prognosis. *Cells* 9, 276. doi:10.3390/cells9020276

Craici, I. M., Wagner, S. J., Hayman, S. R., and Garovic, V. D. (2008). Pre-eclamptic pregnancies: an opportunity to identify women at risk for future cardiovascular disease. *Womens. Health. (Lond).* 4, 133–135. doi:10.2217/17455057.4.2.133

Garovic, V. D., and Hayman, S. R. (2007). Hypertension in pregnancy: an emerging risk factor for cardiovascular disease. *Nat. Clin. Pract. Nephrol.* 3, 613–622. doi:10.1038/ncpneph0623

Goldenberg, R. L., Culhane, J. F., Iams, J. D., and Romero, R. (2008). Epidemiology and causes of preterm birth. *Lancet* 371, 75–84. doi:10.1016/S0140-6736(08)60074-4

Haukkamaa, L., Moilanen, L., Kattainen, A., Luoto, R., Kahonen, M., Leinonen, M., et al. (2009). Pre-eclampsia is a risk factor of carotid artery atherosclerosis. *Cerebrovasc. Dis.* 27, 599–607. doi:10.1159/000216834

Hromadnikova, I. (2022f). *Czech national patent application No. PV 2022-505.*

Hromadnikova, I. (2023a). *Czech national patent No. 309639.*

Hromadnikova, I. (2023b). *Czech national patent No. 309886.*

Hromadnikova, I., Kotlabova, K., and Krofta, L. (2022a). Cardiovascular disease-associated microRNA dysregulation during the first trimester of gestation in women with chronic hypertension and normotensive women subsequently developing gestational hypertension or preeclampsia with or without fetal growth restriction. *Biomedicines* 10, 256. doi:10.3390/biomedicines10020256

Hromadnikova, I., Kotlabova, K., and Krofta, L. (2022b). First-trimester screening for fetal growth restriction and small-for-gestational-age pregnancies without preeclampsia using cardiovascular disease-associated microRNA biomarkers. *Biomedicines* 10, 718. doi:10.3390/biomedicines10030718

Hromadnikova, I., Kotlabova, K., and Krofta, L. (2022c). First trimester prediction of preterm delivery in the absence of other pregnancy-related complications using cardiovascular-disease associated microRNA biomarkers. *Int. J. Mol. Sci.* 23, 3951. doi:10.3390/ijms23073951

Hromadnikova, I., Kotlabova, K., and Krofta, L. (2022d). Cardiovascular disease-associated microRNAs as novel biomarkers of first-trimester screening for gestational diabetes mellitus in the absence of other pregnancy-related complications. *Int. J. Mol. Sci.* 23, 10635. doi:10.3390/ijms231810635

Hromadnikova, I., Kotlabova, K., and Krofta, L. (2022e). Novel first-trimester prediction model for any type of preterm birth occurring before 37 gestational

weeks in the absence of other pregnancy-related complications based on cardiovascular disease-associated microRNAs and basic maternal clinical characteristics. *Biomedicines* 10, 2591. doi:10.3390/biomedicines10102591

Hromadnikova, I., Kotlabova, K., and Krofta, L. (2023a). First-trimester screening for HELLP syndrome-Prediction model based on microRNA biomarkers and maternal clinical characteristics. *Int. J. Mol. Sci.* 24, 5177. doi:10.3390/ijms24065177

Hromadnikova, I., Kotlabova, K., and Krofta, L. (2023b). First trimester prediction models for small-for- gestational age and fetal growth restricted fetuses without the presence of preeclampsia. *Mol. Cell. Probes.* 72, 101941. doi:10.1016/j.mcp.2023.101941

Hromadnikova, I., Kotlabova, K., and Krofta, L. (2023c). First-trimester screening for miscarriage or stillbirth-Prediction model based on microRNA biomarkers. *Int. J. Mol. Sci.* 24, 10137. doi:10.3390/ijms241210137

Hromadnikova, I., Kotlabova, K., and Krofta, L. (2024). First trimester prediction model for gestational hypertension and any subtype of preeclampsia based on cardiovascular disease associated microRNAs and maternal clinical characteristics. *Under Rev. Ann. Med.*

Hypertension in pregnancy (2013). Report of the American college of obstetricians and gynecologists' task force on hypertension in pregnancy. *Obstet. Gynecol.* 122, 1122–1131. doi:10.1097/01.AOG.0000437382.03963.88

International Association of Diabetes and Pregnancy Study Groups Consensus Panel, Metzger, B. E., Gabbe, S. G., Persson, B., Buchanan, T. A., Catalano, P. A., Damm, P., et al. (2010). International association of diabetes and pregnancy study groups recommendations on the diagnosis and classification of hyperglycemia in pregnancy. Diabetes. *Care* 33, 676–682. doi:10.2337/dc09-1848

Irgens, H. U., Reisaeter, L., Irgens, L. M., and Lie, R. T. (2001). Long term mortality of mothers and fathers after pre-eclampsia: population based cohort study. *BMJ* 23, 1213–1217. doi:10.1136/bmj.323.7323.1213

Lai, E. C. (2002). Micro RNAs are complementary to 3' UTR sequence motifs that mediate negative post-transcriptional regulation. *Nat. Genet.* 30, 363–364. doi:10.1038/ng865

Leeners, B., Neumaier-Wagner, P. M., Kuse, S., Mütze, S., Rudnik-Schöneborn, S., Zerres, K., et al. (2011). Recurrence risks of hypertensive diseases in pregnancy after HELLP syndrome. *J. Perinat. Med.* 39, 673–678. doi:10.1515/jpm.2011.081

Libby, G., Murphy, D. J., McEwan, N. F., Greene, S. A., Forsyth, J. S., Chien, P. W., et al. (2007). Pre-eclampsia and the later development of type 2 diabetes in mothers and their children: an intergenerational study from the Walker cohort. *Diabetologia* 50, 523–530. doi:10.1007/s00125-006-0558-z

Livak, K. J., and Schmittgen, T. D. (2001). Analysis of relative gene expression data using real-time quantitative PCR and the 2(-Delta Delta C(T)) Method. *Methods* 25, 402–408. doi:10.1006/meth.2001.1262

Lykke, J. A., Langhoff-Roos, J., Sibai, B. M., Funai, E. F., Triche, E. W., and Paidas, M. J. (2009). Hypertensive pregnancy disorders and subsequent cardiovascular morbidity and type 2 diabetes mellitus in the mother. *Hypertension* 53, 944–951. doi:10.1161/HYPERTENSIONAHA.109.130765

Malmström, O., and Morken, N. H. (2018). HELLP syndrome, risk factors in first and second pregnancy: a population-based cohort study. *Acta. Obstet. Gynecol. Scand.* 97, 709–716. doi:10.1111/aogs.13322

Männistö, T., Mendola, P., Vääräsmäki, M., Järvelin, M. R., Hartikainen, A. L., Pouta, A., et al. (2013). Elevated blood pressure in pregnancy and subsequent chronic disease risk. *Circulation* 127, 681–690. doi:10.1161/CIRCULATIONAHA.112.128751

Martin, J. N., Jr., Blake, P. G., Perry, K. G., Jr., McCaul, J. F., Hess, L. W., and Martin, R. W. (1991). The natural history of HELLP syndrome: patterns of disease progression and regression. *Am. J. Obstet. Gynecol.* 164, 1500–1509. doi:10.1016/0002-9378(91)91429-z

Martin, J. N., Jr., Rose, C. H., and Briery, C. M. (2006). Understanding and managing HELLP syndrome: the integral role of aggressive glucocorticoids for mother and child. *Am. J. Obstet. Gynecol.* 195, 914–934. doi:10.1016/j.ajog.2005.08.044

Mazer Zumaeta, A., Wright, A., Syngelaki, A., Maritsa, V. A., Da Silva, A. B., and Nicolaides, K. H. (2020). Screening for pre-eclampsia at 11–13 weeks' gestation: use of pregnancy-associated plasma protein-A, placental growth factor or both. *Ultrasound. Obstet. Gynecol.* 56, 400–407. doi:10.1002/uog.22093

McDonald, S. D., Ray, J., Teo, K., Jung, H., Salehian, O., Yusuf, S., et al. (2013). Measures of cardiovascular risk and subclinical atherosclerosis in a cohort of women with a remote history of preeclampsia. *Atherosclerosis* 229, 234–239. doi:10.1016/j.atherosclerosis.2013.04.020

Mongraw-Chaffin, M. L., Cirillo, P. M., and Cohn, B. A. (2010). Preeclampsia and cardiovascular disease death: prospective evidence from the child health and development studies cohort. *Hypertension* 56, 166–171. doi:10.1161/HYPERTENSIONAHA.110.150078

Moutquin, J. M., Milot Roy, V., and Irion, O. (1996). Preterm prevention: effectivenss of current strategies. *J. Soc. Obstet. Gynaecol. Can.* 18, 571–588. doi:10.1016/S0849-5831(16)30300-7

O'Gorman, N., Wright, D., Poon, L. C., Rolnik, D. L., Syngelaki, A., de Alvarado, M., et al. (2017). Multicenter screening for pre-eclampsia by maternal factors and biomarkers at 11–13 weeks' gestation: comparison with NICE guidelines and ACOG recommendations. *Ultrasound. Obstet. Gynecol.* 49, 756–760. doi:10.1002/uog.17455

O'Gorman, N., Wright, D., Syngelaki, A., Akolekar, R., Wright, A., Poon, L. C., et al. (2016). Competing risks model in screening for preeclampsia by maternal factors and biomarkers at 11–13 weeks gestation. *Am. J. Obstet. Gynecol.* 214, 103.e1–103.e12. doi:10.1016/j.ajog.2015.08.034

Piletič, K., and Kunej, T. (2016). MicroRNA epigenetic signatures in human disease. *Arch. Toxicol.* 90, 2405–2419. doi:10.1007/s00204-016-1815-7

Ray, J. G., Vermeulen, M. J., Schull, M. J., and Redelmeier, D. A. (2005). Cardiovascular health after maternal placental syndromes (CHAMPS): population-based retrospective cohort study. *Lancet* 366, 1797–1803. doi:10.1016/S0140-6736(05)67726-4

Romero, R., Espinoza, J., Kusanovic, J. P., Gotsch, F., Hassan, S., Erez, O., et al. (2006). The preterm parturition syndrome. *BJOG* 113, 17–42. doi:10.1111/j.1471-0528.2006.01120.x

Sibai, B. M. (2004). Imitators of severe pre-eclampsia/eclampsia. *Clin. Perinatol.* 31, 835–852. doi:10.1016/j.clp.2004.06.007

Tan, M. Y., Syngelaki, A., Poon, L. C., Rolnik, D. L., O'Gorman, N., Delgado, J. L., et al. (2018). Screening for pre-eclampsia by maternal factors and biomarkers at 11-13 weeks' gestation. *Obstet. Gynecol.* 52, 186–195. doi:10.1002/uog.19112

The Fetal Medicine Foundation (2023). Stratification of pregnancy management 11–13 Weeks' gestation. Available at: https://courses.fetalmedicine.com/fmf/show/861?locale=en (Accessed February 27, 2023).

Thilaganathan, B. (2016). Association of higher maternal blood pressure with lower infant birthweight: placental cause or cardiovascular effect? *Hypertension* 67, 499–500. doi:10.1161/HYPERTENSIONAHA.115.06880

Thilaganathan, B. (2017). Placental syndromes: getting to the heart of the matter. *Ultrasound. Obstet. Gynecol.* 49, 7–9. doi:10.1002/uog.17378

Udenze, I. C. (2016). Association of pre-eclampsia with metabolic syndrome and increased risk of cardiovascular disease in women: a systemic review. *Niger. J. Clin. Pract.* 19, 431–435. doi:10.4103/1119-3077.180055

Vandesompele, J., De Preter, K., Pattyn, F., Poppe, B., Van Roy, N., De Paepe, A., et al. (2002). Accurate normalization of real-time quantitative RT-PCR data by geometric averaging of multiple internal control genes. *Genome. Biol.* 3, RESEARCH0034. doi:10.1186/gb-2002-3-7-research0034

Veerbeek, J. H., Hermes, W., Breimer, A. Y., van Rijn, B. B., Koenen, S. V., Mol, B. W., et al. (2015). Cardiovascular disease risk factors after early-onset preeclampsia, late-onset preeclampsia, and pregnancy-induced hypertension. *Hypertension* 65, 600–606. doi:10.1161/HYPERTENSIONAHA.114.04850

Wang, J., Chen, J., and Sen, S. (2016). MicroRNA as biomarkers and diagnostics. *J. Cell. Physiol.* 231, 25–30. doi:10.1002/jcp.25056

Weinstein, L. (1982). Syndrome of hemolysis, elevated liver enzymes, and low platelet count: a severe consequence of hypertension in pregnancy. 1982. *Am. J. Obstet. Gynecol.* 193, 859; discussion 860. doi:10.1016/j.ajog.2005.02.113

Yang, J. J., Lee, S. A., Choi, J. Y., Song, M., Han, S., Yoon, H. S., et al. (2015). Subsequent risk of metabolic syndrome in women with a history of preeclampsia: data from the Health Examinees Study. *J. Epidemiol.* 25, 281–288. doi:10.2188/jea.JE20140136

frontiers | Frontiers in Immunology

TYPE Original Research
PUBLISHED 23 January 2025
DOI 10.3389/fimmu.2024.1453633

OPEN ACCESS

EDITED BY
Rajni Kant,
Kaohsiung Medical University, Taiwan

REVIEWED BY
Vasudevarao Penugurti,
Duke University, United States
Lokanatha Oruganti,
Tulane University, United States
Indrasen Magre,
Duke University, United States
Mohammad Anas,
University of Illinois Chicago, United States

*CORRESPONDENCE
FenFang Shen
279560170@qq.com
Rui Li
lr69696@163.com

†These authors have contributed equally to this work

RECEIVED 04 September 2024
ACCEPTED 24 December 2024
PUBLISHED 23 January 2025

CITATION
Lin R, Weng X, Lin L, Hu X, Liu Z, Zheng J, Shen F and Li R (2025) Identification and preliminary validation of biomarkers associated with mitochondrial and programmed cell death in pre-eclampsia. *Front. Immunol.* 15:1453633. doi: 10.3389/fimmu.2024.1453633

Identification and preliminary validation of biomarkers associated with mitochondrial and programmed cell death in pre-eclampsia

Rong Lin[1,2†], XiaoYing Weng[1,2†], Liang Lin[1,2], XuYang Hu[1,2], ZhiYan Liu[1,2], Jing Zheng[1,2], FenFang Shen[1,2*] and Rui Li[1,2*]

[1]Medical Centre of Maternity and Child Health, Shengli Clinical Medical College of Fujian Medical University, Fuzhou, Fujian, China, [2]Fuzhou University Affiliated Provincial Hospital, Fuzhou, Fujian, China

Background: The involvement of mitochondrial and programmed cell death (mtPCD)–related genes in the pathogenesis of pre-eclampsia (PE) remains inadequately characterized.

Methods: This study explores the role of mtPCD genes in PE through bioinformatics and experimental approaches. Differentially expressed mtPCD genes were identified as potential biomarkers from the GSE10588 and GSE98224 datasets and subsequently validated. Hub genes were determined using support vector machine, least absolute shrinkage and selection operator, and Boruta based on consistent expression profiles. Their performance was assessed through nomogram and artificial neural network models. Biomarkers were subjected to localization, functional annotation, regulatory network analysis, and drug prediction. Clinical validation was conducted *via* real-time quantitative polymerase chain reaction (RT-qPCR), immunofluorescence, and Western blot.

Results: Four genes [solute carrier family 25 member 5 (*SLC25A5*), acyl-CoA synthetase family member 2 (*ACSF2*), mitochondrial fission factor (*MFF*), and phorbol-12-myristate-13-acetate–induced protein 1 (*PMAIP1*)] were identified as biomarkers distinguishing PE from normal controls. Functional analysis indicated their involvement in various biological pathways. Immune analysis revealed associations between biomarkers and immune cell activity. A regulatory network was informed by biomarker expression and database predictions, in which *KCNQ1OT1* modulates *ACSF2* expression *via* hsa-miR-200b-3p. Drug predictions, including clodronic acid, were also proposed. Immunofluorescence, RT-qPCR, and Western blot confirmed reduced expression of *SLC25A5, MFF*, and *PMAIP1* in PE, whereas *ACSF2* was significantly upregulated.

Conclusion: These four mtPCD-related biomarkers may play a pivotal role in PE pathogenesis, offering new perspectives on the disease's diagnostic and mechanistic pathways.

KEYWORDS

mitochondrial, programmed cell death, pre-eclampsia, bioinformatics, database

1 Introduction

Pre-eclampsia (PE) is a distinct, progressive multisystem disorder that typically arises after 20 weeks of gestation, characterized by hypertension and proteinuria (1). It can lead to complications such as fetal growth restriction, fetal distress, and preterm birth, with severe cases resulting in stillbirth and neonatal death (2). The global incidence of PE is approximately 5% to 8% (3, 4), causing an estimated 75,000 maternal deaths and 500,000 neonatal deaths annually, making it the second leading cause of maternal mortality. New-onset hypertension is a key diagnostic criterion for PE (5). The condition is classified into early-onset PE, which occurs before 34 weeks of gestation, and late-onset PE, which occurs at or after 34 weeks (6). Although extensive studies have linked PE pathogenesis to placental hypoxia and ischemia, oxidative stress, inflammatory responses, angiogenesis, functional imbalance, and immune dysregulation (7), the exact mechanisms remain incompletely understood. Current management focuses on controlling hypertension and monitoring maternal and fetal health, with the only effective treatment being the termination of pregnancy (8). However, premature termination increases the risks associated with preterm birth, jeopardizing both maternal and fetal health (9). Although soluble fms-like tyrosine kinase 1 (sFlt-1) and placental growth factor (*PlGF*) have been explored as screening markers for PE (10, 11), their predictive value remains suboptimal. The sFlt-1/*PlGF* ratio rises significantly both prior to and during the clinical onset of PE. While its negative predictive value is as high as 99%, its positive predictive value is limited to just 36.7%, indicating its insufficient efficacy in predicting PE onset (12, 13). Furthermore, variability in testing methods across laboratories compromises the reliability and accuracy of the sFlt-1/*PlGF* ratio (14). Differences in detection protocols can introduce measurement biases, affecting the interpretation of the ratio. Moreover, by the time an elevated sFlt-1/*PlGF* ratio is detected, most patients have already developed clinical symptoms of PE, limiting its utility for early prediction and intervention. Given these challenges, there is an urgent need to identify novel biomarkers with high specificity and sensitivity that could not only predict PE but also serve as potential therapeutic targets for early intervention.

Two main forms of cell death—accidental cell death and programmed cell death (PCD)—are recognized. PCD is the primary mode of cell death, a vital physiological process that is tightly regulated by multiple mechanisms and plays a pivotal role in eliminating damaged or unnecessary cells to maintain tissue homeostasis (15). The term "programmed cell death" was coined by Richard Lockshin and Carroll M. Williams in the 1960s (16) and primarily refers to apoptosis, necroptosis, and pyroptosis. Other forms include ferroptosis, cuproptosis, autophagy, endocytosis, disulfidptosis, lysosomal cell death, and cytotoxicity (17). PCD is implicated in numerous diseases, including cancer, cardiovascular disorders, inflammation, and neurodegenerative diseases (18–20). Recent research on the pathogenesis of PE has increasingly focused on trophoblast programmed death. Trophoblast cell necrosis has been shown to reduce cell viability; increase mortality; impair migration, invasion, and tube formation; and promote cell fusion. These alterations disrupt spiral artery remodeling, leading to placental dysfunction and the progression of PE (21). Several studies suggest that trophoblast PCD contributes to placental insufficiency, which, in turn, causes PE (22–25). With advancing research on PCD mechanisms, various drugs targeting these pathways have been clinically developed, demonstrating significant potential in cancer treatment. For instance, Venetoclax (a *BCL-2*–specific inhibitor) and Navitoclax (inhibitors of *BCL-2, BCL-xL*, and *BCL-W*) have shown promise in the treatment of leukemia and lymphoma (26, 27). However, current research on PE prediction and treatment has largely overlooked the detailed exploration of trophoblast PCD. Despite significant progress in understanding related mechanisms in cancer therapy, there remains considerable opportunity for investigation in the context of PE. Thus, a deeper study of PCD may offer new insights and therapeutic strategies for the prediction and treatment of PE.

Since the first description of PCD 60 years ago, numerous studies have confirmed the involvement of mitochondria in PCD, identifying them as key regulators in triggering this process. Mitochondria are ubiquitous, double-membrane-bound organelles that regulate cellular energy production, support cell activities, modulate cellular metabolic pathways, which even mediate cell fate decisions. They can participate directly or indirectly in PCD through various mechanisms and pathways, influencing the onset and progression of numerous human diseases. Mitochondria-related PCD is extensively involved in the pathological progression of diseases across different organ systems (28). An observational study first reported in 1989 found a high prevalence of PE in families with mitochondrial dysfunction (29). Since then, mitochondrial dysfunction in the placenta has been demonstrated in both pregnant women with PE and animal models of the condition (30). Over the past 30 years, compelling evidence has shown that abnormal mitochondrial function is a major contributor to placental dysfunction, and it is well established that PE arises from placental dysfunction, although the exact cause of PE remains unclear. Mitochondrial dysregulation caused by placental hypoxia is typically characterized by increased mitochondrial reactive oxygen species (ROS), mitochondrial fission, mitophagy, and apoptosis, along with reduced release of bioactive factors from the placenta. These alterations lead to placental and vascular endothelial dysfunction, ultimately driving the development of PE (31). Furthermore, oxidative stress is a critical factor in this process. As key organelles are responsible for intracellular energy supply, mitochondria are highly vulnerable to functional damage, which can disrupt energy metabolism (32). In PE, mitochondrial oxidative

Abbreviations: AKI, acute kidney injury; *ACSF2*, acyl-CoA synthetase family member 2; ANN, artificial neural network; BP, Biological Process; *BH3*, *BCL-2* homeodomain 3; CC, Cell Component; DE, differential genes; DEGs, differentially expressed genes; DGI, drug–gene interaction; *DRP 1*, dynein-related protein 1; GO, Gene Ontology; KEGG, Kyoto Encyclopedia of Genes and Genomes; LASSO, least absolute shrinkage and selection operator; *MFF*, mitochondrial fission; MRGs, mitochondrial-related genes; mtPCD, mitochondrial and programmed cell death; PCD, programmed cell death; PCDs, programmed cell death–related genes; PE, pathogenesis of pre-eclampsia; *PlGF*, placental growth factor; PPI, protein–protein interaction; sFlt-1, soluble fms-like tyrosine kinase 1; SVM, support vector machine.

phosphorylation may be impaired, leading to reduced ATP production (33). Additionally, maintaining metabolic turnover balance is essential for immune cell function, and mitochondrial dysfunction can disturb this balance, compromising immune cell activity (34). Mitochondrial dysregulation and dysfunction induced by placental hypoxia and oxidative stress play a pivotal role in the pathogenesis of PE, from impairing placental and vascular endothelial cell function to disrupting immune cell metabolism. These changes highlight the critical need for in-depth research into mitochondria-related mechanisms to fully understand the pathogenesis of PE. Further exploration of the role of mitochondria and PCD in PE is essential to better understand their interaction in disease development, providing vital insights for the development of new therapeutic strategies and diagnostic tools.

In conclusion, PCD and mitochondrial dysfunction play central roles in the pathogenesis of PE. To further investigate the intersection of these two factors, this study explored potential molecular mechanisms associated with PE biomarkers using the Gene Expression Omnibus (GEO) database (GSE10588 and GSE98224). The study assessed the predictive efficacy of these biomarkers for PE and proposed drug predictions, offering new targets and strategies for the diagnosis and treatment of PE. Additionally, real-time quantitative polymerase chain reaction (RT-qPCR) validation was conducted to confirm the findings, reinforcing the significance of the identified biomarkers and their potential roles in PE.

2 Materials and methods

2.1 Data extraction

In this study, the GSE10588 dataset (35) and GSE98224 dataset (36) were retrieved from the GEO database (https://www.ncbi.nlm.nih.gov/geo/). The GSE10588 dataset included 17 placental tissue samples from patients with PE and 26 placental tissue samples from normal individuals, serving as the training set. For validation, the GSE98224 dataset consisted of 30 placental tissue samples from patients with PE and 18 placental tissue samples from normal individuals, acting as the validation set. A total of 1,136 mitochondrial-related genes (MRGs) were obtained from the MitoCarta 3.0 database, and 1,548 programmed cell death–related genes (PCDs) were collected from the literature.

2.2 Identification of DE-mtPCDs

Differentially expressed genes (DEGs) in the GSE10588 dataset were identified using the limma package (37) (v 3.56.2). The criteria for defining DEGs were an adjusted p-value <0.05 and |log2 fold change (log2FC)| >0.5. The DEGs were then intersected with MRGs to obtain differentially expressed MRGs (DE-MRGs). Following this, the DEGs were intersected with PCDs to identify differentially expressed PCDs (DE-PCDs). Finally, the intersection of DE-MRGs and DE-PCDs was used to identify differentially expressed mitochondrial PCD–related genes (DE-mtPCD).

2.3 Functional enrichment analysis of DE-mtPCDs

To explore the potential roles of the DE-mtPCD, functional enrichment analysis was conducted using the ClusterProfiler package (38) (v 4.8.3), which included Gene Ontology (GO) and Kyoto Encyclopedia of Genes and Genomes (KEGG) pathway enrichment analyses. The DE-mtPCDs were subjected to both GO and KEGG analyses, with a filtering criterion of p.adjust <0.05.

2.4 Protein–protein interaction analysis and visualization of DE-mtPCDs

Protein–protein interaction (PPI) analysis was performed on the DE-mtPCD by inputting the genes into the STRING database (https://string-db.org/), using an interaction score threshold of 0.4 to exclude low-confidence interactions. The resulting network was visualized using Cytoscape software (39) (v 3.9.1).

2.5 Identification of hub genes among DE-mtPCDs

To further identify potential hub genes within the DE-mtPCD, three machine learning algorithms were employed: support vector machine (SVM), least absolute shrinkage and selection operator (LASSO), and Boruta. Feature genes were screened using the mlbench package, glmnet package (40) (v 4.1-2), and Boruta package (v 8.0.0), respectively. The intersection of the feature genes identified by all three algorithms was defined as the hub genes.

2.6 Validation and selection of biomarker genes

To validate the ability of the identified hub genes to distinguish between PE and normal samples and to identify suitable biomarkers, a Wilcoxon test was performed to confirm their differential expression in both the GSE10588 and GSE98224 datasets. Genes that exhibited significant and consistent expression patterns in both datasets were considered potential biomarkers.

2.7 Nomogram model construction and performance evaluation

To elucidate the relationship between each biomarker and PE onset, the rms package (v 6.2-0) (41) was used to construct a

Nomogram model based on multivariable logistic regression. Additionally, the diagnostic potential of sFlt-1 and *PlGF* biomarkers, previously confirmed in the literature, was explored by constructing nomogram models for the *PlGF* (PGF) and sFlt-1 (FLT1) genes in the GSE10588 and GSE98224 datasets. Calibration curves were generated to assess the reliability and accuracy of the model predictions. To further verify the model performance, receiver operating characteristic (ROC) curves were plotted using the pROC package (v 1.18.4) (42) for both datasets.

2.8 ANN diagnostic model construction and performance evaluation

To assess whether the biomarkers can distinguish between PE and normal samples in the GSE10588 dataset, an artificial neural network (ANN) diagnostic model based on logistic regression was developed using the neuralnet package (v 1.44.2) (43). ROC curves were subsequently generated on the basis of the predicted results from the GSE10588 dataset to assess diagnostic performance. Additionally, biomarker expression levels from the GSE98224 dataset were input into the trained ANN model, and ROC curves were plotted to evaluate the model's accuracy.

2.9 Biomarker genomic localization analysis

Gene chromosomal localization is essential for understanding gene function, studying genetic diseases, and advancing gene therapy and genomics. The OmicCircos package was used to analyze and visualize the genomic localization of biomarkers on chromosomes.

2.10 Biomarker subcellular localization prediction and analysis

To further investigate the subcellular localization of biomarkers and their relevance to PE pathogenesis, the mRNALocater online tool (http://bio-bigdata.cn/mRNALocater/) was employed to predict the subcellular localization of biomarkers in the GSE10588 dataset. Subcellular localization scores were also calculated for the biomarkers.

2.11 GSVA

To explore the impact of differential biomarker expression on KEGG pathways, the GSE10588 dataset was divided into high- and low-expression groups on the basis of the median expression levels of biomarkers. Gene set variation analysis (GSVA) scores for KEGG pathways were then calculated between the two expression groups using the c2.cp.kegg.v2023.1.Hs.symbols.gmt as a background gene set. Differential signaling pathways were identified on the basis of the criteria $|t| > 2$ and $p < 0.05$ using the limma package (v 3.56.2) (37).

2.12 Immune microenvironment analysis

To analyze the immune microenvironment of PE and normal samples, the Single Sample Gene Set Enrichment Analysis (ssGSEA) algorithm from the GSVA package (v 1.42.0) (44) was used to calculate scores for 28 immune cell compositions based on gene expression profiles from the GSE10588 dataset. Differential analysis using the Wilcoxon test was then performed to identify immune cell types with differential expression. Additionally, Spearman correlation analysis was conducted to explore the relationship between biomarkers and the identified immune cell types.

2.13 Construction of regulatory network

To explore the regulatory mechanisms of the aforementioned biomarkers, miRDB (http://mirdb.org/) and miRTarBase (https://awi.cuhk.edu.cn/~miRTarBase/miRTarBase_2025/php/index.php) databases were employed to predict miRNAs that regulate these biomarkers. In miRDB, miRNAs with a Target score ≥80 were selected, whereas, for miRTarBase, only miRNAs with reported experimental evidence were considered. The overlap between these two sets of miRNAs was determined to identify shared regulatory miRNAs. Subsequently, StarBase (http://starbase.sysu.edu.cn/) and miRNet (https://www.mirnet.ca/) databases were utilized to predict the long non-coding RNAs (lncRNAs) interacting with the shared miRNAs. The intersection of predicted lncRNAs from both databases was used to obtain common lncRNAs. A regulatory network consisting of lncRNAs, miRNAs, and mRNAs was then constructed. Cytoscape software (v 3.9.1) (39) was employed to visualize and analyze the resulting complex biological network.

2.14 Drug prediction

For the identification of potential drugs targeting biomarkers for PE treatment, drug prediction was carried out by integrating results from DrugBank (https://www.drugbank.ca/) and the Drug-Gene Interaction (DGI) database (http://www.dgidb.org/), resulting in a comprehensive list of candidate drugs. The relationships between drugs and biomarkers were represented in a drug-biomarker network, which was also visualized using Cytoscape (v 3.9.1) (39).

2.15 Validation of the biological indicators of the screening

2.15.1 Sample collection

2.15.1.1 Study objects

This research was conducted at the Obstetrics and Gynecology Department of Fujian Provincial Hospital (Jinshan Branch). Ten pregnant women scheduled for delivery were enrolled and classified into two groups: the experimental group, comprising five individuals diagnosed with PE, and the control group, consisting of five women who underwent cesarean deliveries for reasons unrelated to medical complications, such as social considerations or non-vertex fetal presentations (e.g., transverse or breech positions).

2.15.1.2 Specimen collection

Approximately 40 g of placental tissue were collected, with large vessels and connective tissue removed. The tissue was thoroughly washed with 0.9% saline until the wash solution became nearly colorless, then finely minced into 1- to 3-mm pieces, preserved in a sterile isotonic solution, and subsequently frozen at −80°C.

The study adhered to the Declaration of Helsinki and received approval from the Ethics Committee of Fujian Provincial Hospital (protocol code K2023 - 02 - 016, approval date: 22 February 2023). Informed consent was obtained from all participants.

2.15.2 Real-time quantitative polymerase chain reaction

Total RNA was extracted from the placental tissue samples of five control and five patients with PE using TRIzol solution (Ambion, Austin, USA), following the manufacturer's instructions. The RNA concentration was determined using NanoDrop, and complementary DNA (cDNA) was synthesized with the SweScript First Strand cDNA Synthesis Kit (Servicebio, Wuhan, China). The reverse transcription conditions were as follows: primer-template binding at 25°C for 5 min, cDNA synthesis at 50°C for 15 min, and denaturation of the first strand from mRNA at 58°C, followed by storage at 4°C. Primers for RT-qPCR were designed and synthesized (Table 1). Quantitative analysis was performed using the CFX96 real-time quantitative fluorescence PCR machine (BIO-RAD, California, USA). The reaction conditions included an initial denaturation at 95°C for 1 min, followed by 40 cycles of denaturation at 95°C for 20 s, annealing at 55°C for 20 s, and extension at 72°C for 30 s. Amplification and melting curves were generated, and the Cycle threshold (Ct) values were recorded. Glyceraldehyde-3-phosphate dehydrogenase (GAPDH) was used as an internal control, and gene expression levels were calculated using the $2^{-\Delta\Delta Ct}$ method.

2.15.3 Immunofluorescence assay

Tissue samples were fixed in 4% paraformaldehyde and embedded in paraffin. Deparaffinized and rehydrated tissue sections were permeabilized with 0.1% Triton X-100 in Phosphate Buffer Saline (PBS) for 5 min and blocked with 10% goat serum for 1 hour. Antigen retrieval was performed by heating the sections in Ethylenediaminetetraacetic Acid (EDTA)-Tris buffer [50 mM Tris and 1 mM EDTA (pH 9.0)]. After washing, the sections were incubated with primary antibodies overnight at 4°C, followed by incubation with fluorescent secondary antibodies. The slides were mounted with a 4',6-diamidino-2-phenylindole (DAPI)-containing medium and observed under a laser confocal microscope (Olympus Corporation, Japan).

TABLE 1 Related primer sequences.

Primer	Sequences
SLC25A5 F	AGACTGCGTGGTCCGTATTC
SLC25A5 R	TGCCAGATTCCCTGCAAAGT
ACSF2 F	CTGTGAACCCAGCCTACCAG
ACSF2 R	GCTGGGCATTCTCCACTTCT
MFF F	AACCCCTGGCACTGAAAACA
MFF R	TGCCAACTGCTCGGATTTCT
PMAIP1 F	CCAAGCCGGATTTGCGATTG
PMAIP1 R	CTCCTAGAGACAGCCGCCTA
GAPDH F	CGAAGGTGGAGTCAACGGATTT
GAPDH R	ATGGGTGGAATCATATTGGAAC

2.15.4 Western blot assay

Proteins were extracted from tissues of each experimental group. These proteins were then separated using 10% sodium dodecyl sulfate–polyacrylamide gel electrophoresis and subsequently transferred onto a membrane. The membrane was blocked to prevent non-specific binding, followed by incubation with the corresponding primary antibodies against solute carrier family 25 member 5 (*SLC25A5*), acyl-CoA synthetase family member 2 (*ACSF2*), mitochondrial fission factor (*MFF*), and phorbol-12-myristate-13-acetate–induced protein 1 (*PMAIP1*) overnight. After incubation with the primary antibodies, the membrane was incubated with the appropriate secondary antibodies and then exposed to detect the protein bands.

2.16 Statistical analysis

Data were processed and analyzed using R software and GraphPad Prism version 9.0. Differences between groups were assessed using t-tests, the Wilcoxon rank-sum test, and one-way ANOVA, with p-values <0.05 considered statistically significant.

3 Results

3.1 Identification of DEGs and DE-mtPCDs in PE

A total of 1,438 DEGs were identified in the GSE10588 dataset between the PE and normal groups, with 817 genes upregulated and 621 genes downregulated in the PE group (Figures 1A, B). A total of 95 DE-MRGs were identified by intersecting the DEGs with MRGs, of which 42 were upregulated and 53 were downregulated in the PE group. Additionally, 132 DE-PCDs were obtained by intersecting the DEGs with PCDs, with 84 upregulated and 48 downregulated in the PE group. By further intersecting the DE-MRGs with the DE-PCDs, 14 DE-mtPCDs were identified, comprising five upregulated and nine downregulated genes in the PE group (Figures 1C–F).

3.2 Functional and pathway enrichment of DE-mtPCDs in PE

To explore the biological functions and pathways associated with the identified DE-mtPCDs, an enrichment analysis was performed. The analysis revealed 225 enriched GO terms, including 160

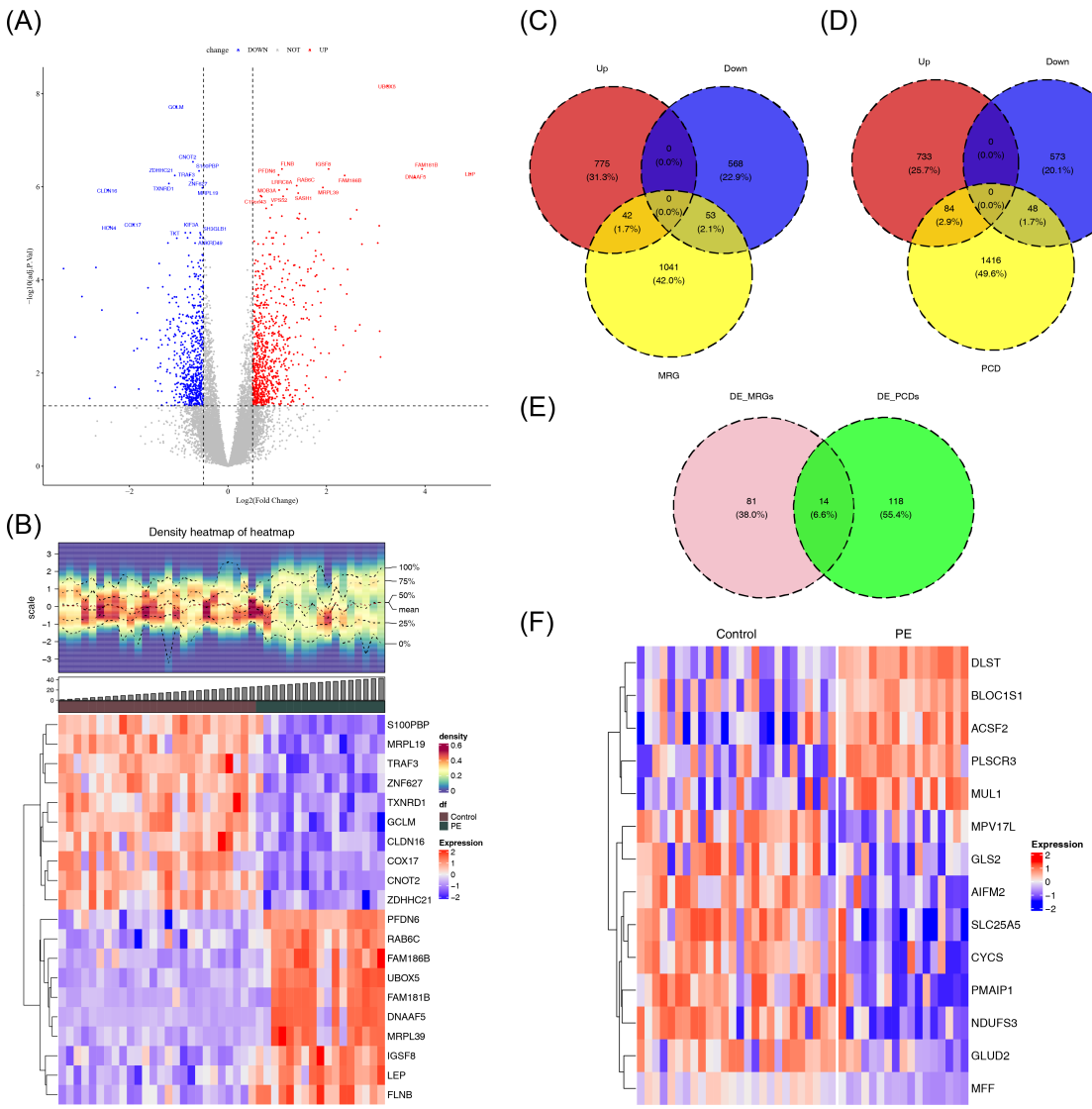

FIGURE 1
Identification of DE-mtPCDs in the GSE10588 dataset. **(A)** Volcano plot of the DEGs, with downregulated genes in blue, upregulated genes in red, and genes with insignificant differences in gray. **(B)** Heatmap of the DEGs, with the upper section displaying the expression density heatmap of differentially expressed genes across samples, showing lines for the five quantiles and mean values, and the lower section indicating high expression in red and low expression in blue. **(C)** Venn diagram of DE-MRGs. **(D)** Venn diagram of DE-PCDs. **(E)** Venn diagram of DE-mtPCDs. **(F)** Heatmap of DE-mtPCDs, with red indicating high expression and blue indicating low expression. DEGs, differentially expressed genes; DE-MRGs, differentially expressed mitochondrial–related genes; DE-PCDs, differentially expressed programmed cell death genes; DE-mtPCDs, differentially expressed mitochondrial and programmed cell death genes.

Biological Process (BP), 24 Cellular Component (CC), and 41 Molecular Function (MF) terms. The BP enrichment analysis indicated that the DE-mtPCDs were significantly enriched in mitochondrial functions and apoptosis-related processes, such as regulation of mitochondrial membrane permeability and apoptotic mitochondrial changes (Figure 2A). The CC analysis showed that the DE-mtPCDs were primarily localized in membrane structures of organelles, including peroxisomes and the mitochondrial inner membrane (Figure 2B). The MF analysis revealed that the DE-mtPCDs predominantly affected oxidative-reduction processes involved in electron transfer activity (Figure 2C). KEGG pathway analysis further indicated enrichment in 23 metabolic pathways, including several apoptosis-related pathways such as the p53 signaling pathway and apoptosis pathway, as well as disease-associated pathways like Huntington's disease and prion diseases (Figure 2D). A PPI network constructed with the 14 DE-mtPCDs, consisting of 11 nodes and 12 edges, revealed multiple interactions among these proteins, including cytochrome c (*CYCS*) with *MFF*, *PMAIP1*, *SLC25A5*, Nicotinamide Adenine Dinucleotide (Reduced) Hydrogen (NADH) dehydrogenase (ubiquinone) Fe-S protein 3 (NDUFS3), and apoptosis-inducing factor mitochondria-associated 2 (AIFM2) (Figure 2E).

3.3 Identification of Hub genes in PE

Based on the 14 DE-mtPCDs, the SVM algorithm was used to screen 14 feature genes (Figure 3A). After 10-fold cross-validation, 10 feature genes were identified in the LASSO regression model, with dihydrolipoamide S-succinyltransferase (*DLST*), *CYCS*, *SLC25A5*, *NDUFS3*, *ACSF2*, *MPV17* mitochondrial inner membrane protein like (*MPV17L*), glutaminase 2 (*GLS2*), *MFF*, *PMAIP1*, and phospholipid scramblase 3 (*PLSCR3*) selected, achieving the lowest error rate at the optimal lambda.best parameter value of 0.01397921 (Figures 3B, C). Additionally, the Boruta algorithm identified 14 feature genes, which scored significantly higher than the maximum Z-score among shadow attributes (median, 2.077892) (Figure 3D). To establish a consensus set of feature genes, the intersection of the feature genes obtained from the three algorithms was taken, resulting in a final set of 10 hub genes. These hub genes included *DLST*, *CYCS*, *SLC25A5*, *NDUFS3*, *ACSF2*, *MPV17L*, *GLS2*, *MFF*, *PMAIP1*, and *PLSCR3* (Figure 3E; Supplementary Table S1).

3.4 Biomarker discovery and localization in PE

To validate the discriminatory ability of the candidate biomarkers in distinguishing PE samples from normal samples and to select suitable genes as biomarkers, the expression of the 10 hub genes was analyzed across two datasets. The final results revealed that 5 of the 10 hub genes showed differential expression between PE and control samples in both datasets. However, the expression trend of *GLS2* was inconsistent across the datasets, leading to its exclusion. Therefore, four genes—*SLC25A5*, *ACSF2*, *MFF*, and *PMAIP1*—were selected for further investigation due to their significant differential expression and consistent trends in both the GSE10588 and GSE98224 datasets. Among these, *SLC25A5*, *MFF*, and *PMAIP1* exhibited low expression in the PE group, whereas *ACSF2* displayed an opposite trend in the two datasets. Thus, these four genes were identified as final biomarkers for PE (Figures 4A, B). To investigate the chromosomal locations of the four biomarkers, the chromosomal positions for each biomarker

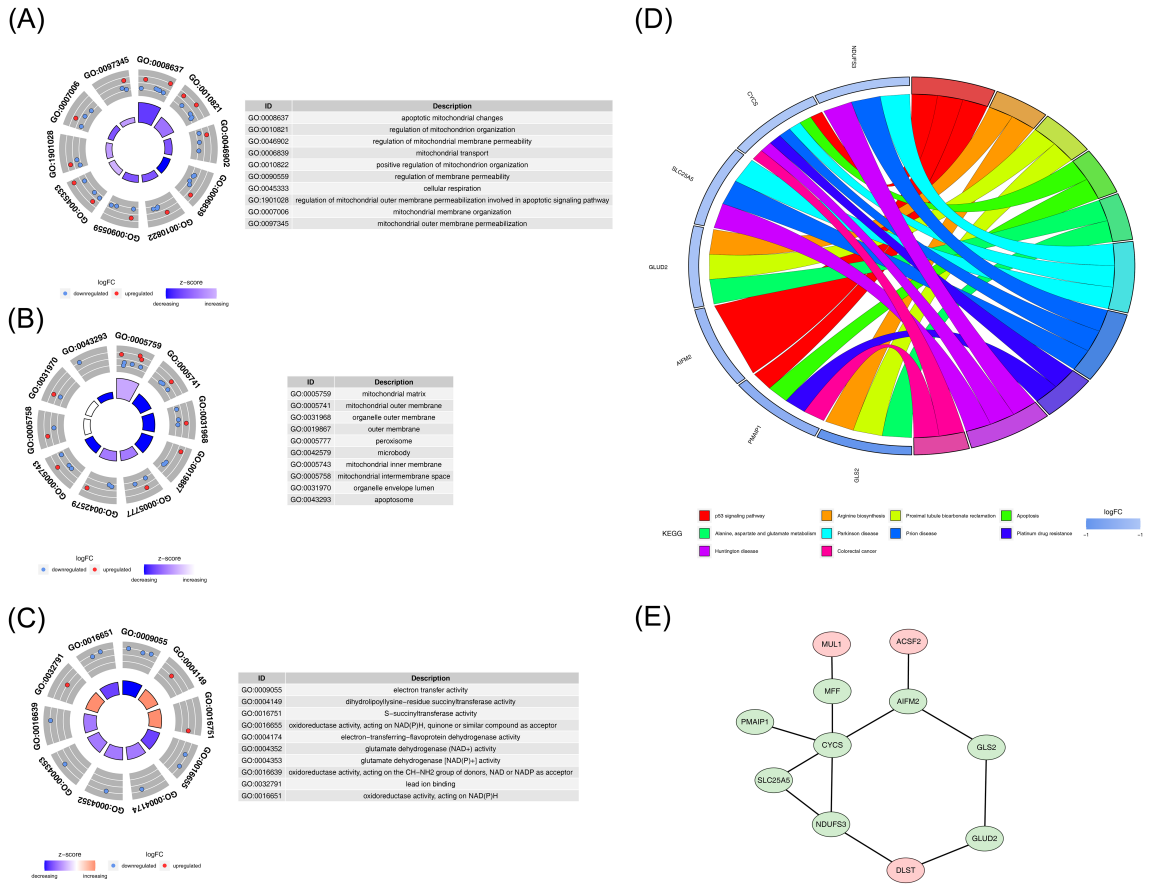

FIGURE 2
Functional enrichment analysis of DE-mtPCDs. **(A)** Enriched GO terms for DE-mtPCDs in Biological Process. **(B)** Cell Component. **(C)** Molecular Function. **(D)** KEGG enrichment results for DE-mtPCDs. **(E)** Protein–protein interaction network of DE-mtPCDs, with gene labels represented by nodes; red indicates upregulated genes, and green indicates downregulated genes; each line represents an interaction between genes. DE-mtPCDs, differentially expressed mitochondrial and programmed cell death genes; KEGG, Kyoto Encyclopedia of Genes and Genomes.

were analyzed. In summary, the analysis revealed that the chromosomal locations of the four biomarkers were also analyzed. The results showed that *SLC25A5* is located on chromosome X, *ACSF2* on chromosome 17, *MFF* on chromosome 2, and *PMAIP1* on chromosome 18 (Figure 4C). Additionally, subcellular localization analysis provided insights into the potential roles of these biomarkers in PE pathogenesis. *ACSF2* and *SLC25A5* were localized to cellular membrane structures, suggesting their involvement in membrane-related processes associated with PE. In contrast, *MFF* and *PMAIP1* were localized to the cell nucleus, indicating their potential involvement in nuclear processes linked to the disease (Figure 4D).

3.5 Identification and characterization of PE biomarkers

To further explore the relationship between each biomarker and the occurrence of PE, a nomogram was constructed on the basis of multiple logistic regression using the rms package in R. The nomogram assigned scores to each biomarker according to its expression level, and the total score was used to predict the probability of a PE diagnosis (Figure 5A). Calibration curve analysis indicated good model calibration, with an average error of 0.039 (Figure 5D). The area under the ROC curve (AUC) for the GSE10588 dataset was greater than 0.7, demonstrating the model's strong discriminatory power (Figures 5G, H). The model robustness was further validated in the GSE98224 dataset, where the ROC curve also showed an AUC greater than 0.7 (Figure 5I). Nomograms were constructed separately for the two datasets (Figures 5B, C), and the calibration curves revealed mean errors of 0.058 and 0.0611, respectively (Figures 5E, F). In the GSE10588 dataset, the AUC value was 0.905 (0.783–1.000) (Figure 5I), and, in the GSE98224 dataset, the AUC value was 0.841 (0.720–0.961) (Figure 5J), indicating the accuracy of the nomogram models. The diagnostic potential of the biomarkers screened in this study was found to be superior to the results of FLT1 and PGF in the training set (AUC = 0.985 vs. AUC = 0.905).

Furthermore, an ANN diagnostic model was constructed on the basis of the biomarker data from the GSE10588 dataset. The weights of the four biomarkers in the ANN model ranged from −1.26 to 0.99, with *SLC25A5* having a weight of −1.26088, *ACSF2* having a weight of 0.98769, *MFF* having a weight of −0.64141, and *PMAIP1* having a weight of −0.85598 (Figure 5K). The ROC curve for the ANN model in the GSE10588 dataset yielded an AUC value of 0.989, indicating the model's accuracy in distinguishing PE from normal samples (Figure 5L). In the GSE98224 dataset, the AUC value was 0.83, further confirming the robustness of the model in predicting PE (Figure 5M).

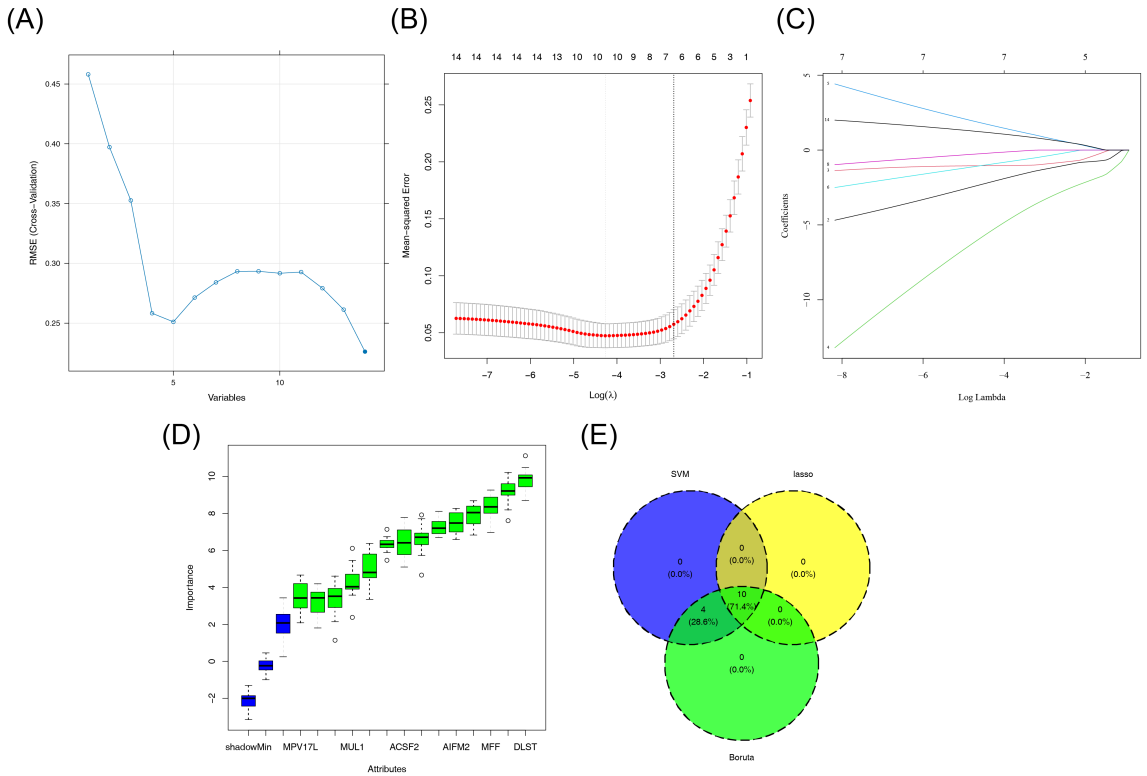

FIGURE 3
Machine learning screening results. **(A)** SVM classification results. **(B, C)** LASSO regression results. **(D)** Boruta algorithm results. **(E)** Venn diagram showing the crossover genes between LASSO, SVM, and Boruta. LASSO, least absolute shrinkage and selection operator; SVM, support vector machine.

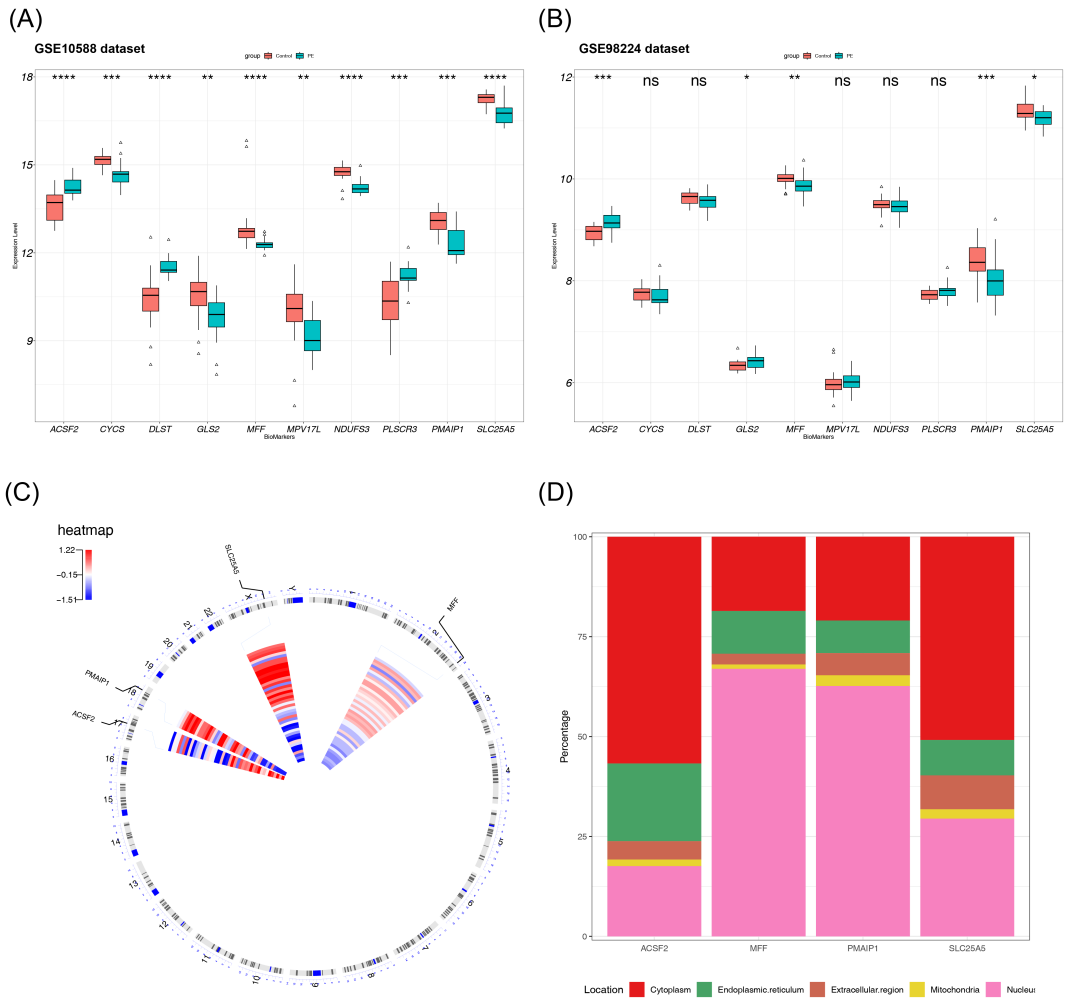

FIGURE 4
Biomarker discovery and localization. **(A)** Expression distribution of 10 candidate biomarkers in the GSE10588 dataset, with differences in expression verified using a rank sum test. **(B)** Expression distribution of 10 candidate biomarkers in the GSE98224 dataset. **(C)** Chromosomal localization of the biomarkers. **(D)** Subcellular structural localization of the biomarkers. NS, non-significant, $p > 0.05$; *$p < 0.05$; **$p < 0.01$; ***$p < 0.001$; ****$p < 0.0001$.

3.6 Impact of differential expression of PE biomarkers on pathways

To further explore the impact of differential expression of biomarkers on KEGG pathways, the four biomarkers *(SLC25A5, ACSF2, MFF*, and *PMAIP1)* were categorized into high- and low-expression groups based on their median expression levels in the GSE10588 dataset. GSVA was conducted using the c2.cp.kegg.v2023.1.Hs.symbols.gmt gene set (containing 186 gene sets in total). The GSVA score for each KEGG pathway was calculated, and differential signaling pathways were screened using a threshold of $|t| > 2$ and $p < 0.05$ *via* the limma package. The analysis revealed five pathways with differential activation in both high- and low-expression groups of the biomarkers: mismatch repair, RNA degradation, Notch signaling pathway, proteasome, and glycosphingolipid biosynthesis globo series (Figures 6A–E; Supplementary Figures S1-S5).

3.7 Differential immune cells in PE samples and controls and their correlations

To analyze immune differences between the PE and normal samples in the GSE10588 dataset, the composition scores of each immune cell type were computed and displayed in a heatmap (Figure 7A). Among the 28 immune cell types analyzed, 11 showed significant differences between the PE and normal groups. Activated dendritic cells, CD56dim natural killer cells, plasmacytoid dendritic cells, and T follicular helper cells had higher scores in the PE group, whereas the other differential immune cells showed the

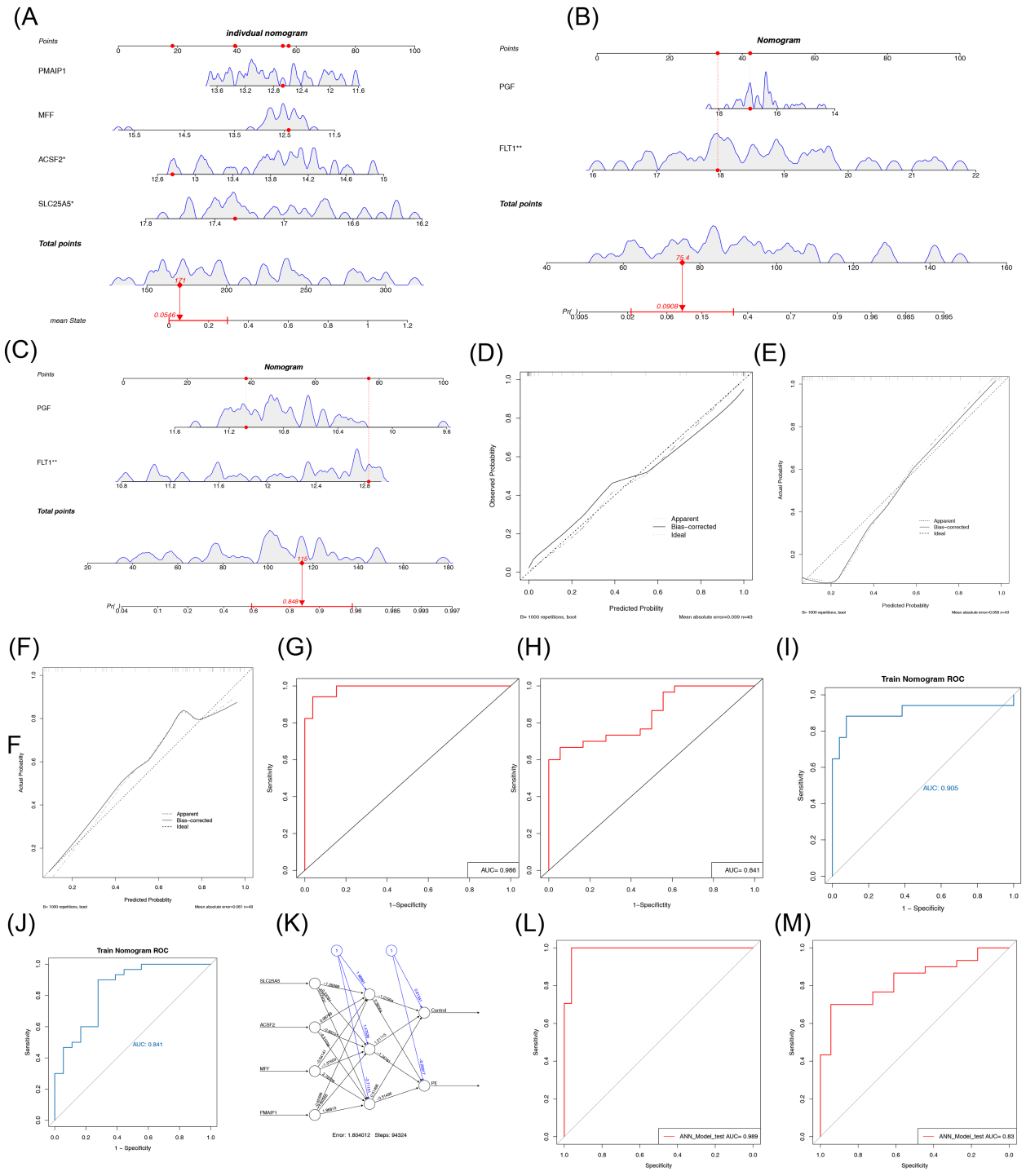

FIGURE 5
Evaluation and validation of the nomogram and artificial neural network diagnostic PE model. **(A)** Nomogram model of biomarkers. **(B)** Calibration curve of the model. **(C, D)** ROC curve of the model in the GSE10588 set and GSE98224 set. **(E)** Nomogram model of FLT1 and PGF in the GSE10588 dataset. **(F)** Calibration curves of FLT1 and PGF diagnostic models in the GSE10588 dataset. **(G)** ROC curves of FLT1 and PGF diagnostic models in the GSE10588 dataset. **(H)** Nomogram model of FLT1 and PGF in the GSE98224 dataset. **(I)** Calibration curves of FLT1 and PGF diagnostic models in the GSE98224 dataset. **(J)** ROC curves of FLT1 and PGF diagnostic models in the GSE98224 dataset. **(K)** Structural diagram of the artificial neural network composed of the five biomarkers. **(L, M)** ROC curve for artificial neural network evaluation in the GSE10588 set and GSE98224 set. PE, pre-eclampsia; ROC, receiver operating characteristic. *p < 0.05, **p < 0.01.

FIGURE 6
GSVA. **(A–D)** KEGG pathways with significant differences between high– and low–biomarker expression groups. Blue represents pathways activated in the high expression group, and green represents pathways activated in the low expression group. **(E)** Venn diagram of KEGG pathways shared by four groups. GSVA, gene set variation analysis; KEGG, Kyoto Encyclopedia of Genes and Genomes.

opposite trend (Figure 7B). Correlation analysis of the differential immune cells revealed that regulatory T cells and effector memory CD8 T cells had the strongest positive correlation (cor = 0.693), whereas activated dendritic cells showed the strongest negative correlation with type 2 T helper cells (cor = –0.322) (Figure 7C). To explore the relationship between biomarkers and differential immune cells, the correlation between the four biomarkers and the 11 differential immune cells was analyzed. Type 2 T helper cells showed significant correlations with all four biomarkers ($|cor| > 0.3$, $p < 0.05$), suggesting that these biomarkers may serve as potential targets for immunotherapy (Figure 7D).

3.8 Regulatory mechanisms and potential drugs for PE

To understand the regulatory mechanisms of the biomarkers, databases were utilized to predict corresponding regulatory factors. The miRDB and miRTarBase databases were used to predict miRNAs targeting the four biomarkers, resulting in 89 and 187 miRNAs, respectively. The intersection of these predictions yielded 25 miRNAs that could potentially regulate the biomarkers (Figure 8A). Using the StarBase and miRNet databases, 122 and 159 lncRNAs were predicted, respectively, based on the 25 miRNAs.

The intersection of these lncRNAs resulted in a final set of 44 lncRNAs (Figure 8B). A lncRNA–miRNA–mRNA regulatory network was then constructed, with *KCNQ1* Opposite Strand/Antisense Transcript 1 (*KCNQ1OT1*) being identified as a regulator of *ACSF2* expression *via* modulation of hsa-miR-200b-3p (Figure 8C). Finally, drug predictions based on the biomarkers were conducted using relevant databases. Potential drug candidates for the treatment of PE included clodronic acid, etidronic acid, glutamic acid, L-glutamine, ammonia, bortezomib, trichostatin A, and butyric acid (Figure 8D).

3.9 Validation of the biological indicators of the screening

3.9.1 Real-time quantitative polymerase chain reaction to verify the expression of biomarkers in PE

Gene expression patterns of *SLC25A5, MFF, PMAIP1*, and *ACSF2* in relation to PE were assessed using clinical RT-qPCR analysis. The results indicated that *SLC25A5, MFF*, and *PMAIP1* were downregulated in the PE group, whereas *ACSF2* was upregulated, reflecting distinct expression profiles for these genes in the context of PE (Figures 9A–D). These results aligned with the data obtained from the dataset.

3.9.2 Immunofluorescence assay to verify the expression of biomarkers in the placenta of normal pregnancy and PE

Immunofluorescence assays were conducted to examine the expression of *SLC25A5, MFF, PMAIP1*, and *ACSF2* in placentas from both PE and normal pregnancies. *SLC25A5* and *MFF* were localized to the cytoplasm and cell membrane of trophoblast cells, whereas *ACSF2* and *PMAIP1* were exclusively present in the cytoplasm. In the PE group, the expression intensity of *SLC25A5*, *MFF*, and *PMAIP1* was notably lower than in the control group, with significantly reduced average optical density values. Conversely, *ACSF2* exhibited enhanced expression and a significantly higher average optical density in the PE group, indicating distinct expression patterns for these genes in the context of PE (Figures 10A, B).

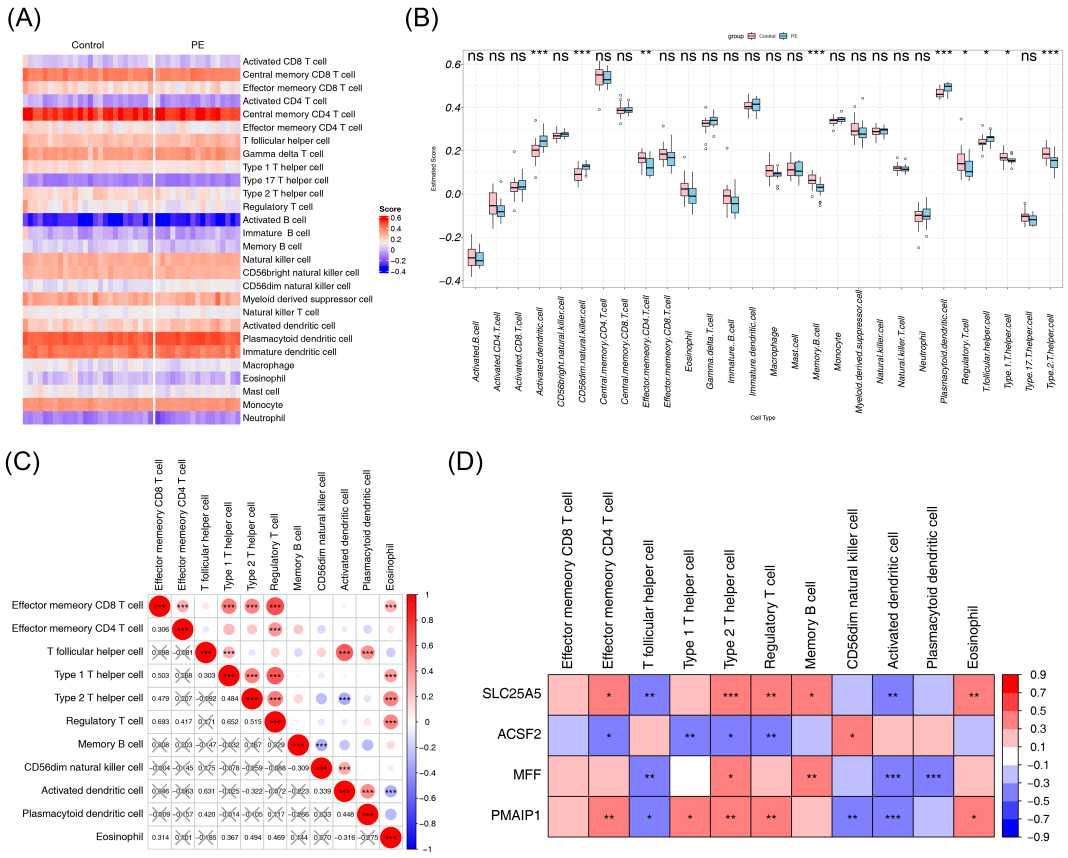

FIGURE 7
Immune infiltration analysis. **(A)** Heatmap of the immune cell composition score for each sample, with red indicating higher scores and blue indicating lower scores. **(B)** Differences in immune cell content between the PE and control groups. **(C)** Correlation heatmap of differential immune cells, with the correlation coefficient in the lower left corner, and X representing p > 0.05. **(D)** Correlation heatmap between biomarkers and differential immune cells. NS, non-significant, p > 0.05; *p < 0.05; **p < 0.01; ***p < 0.001. PE, pre-eclampsia.

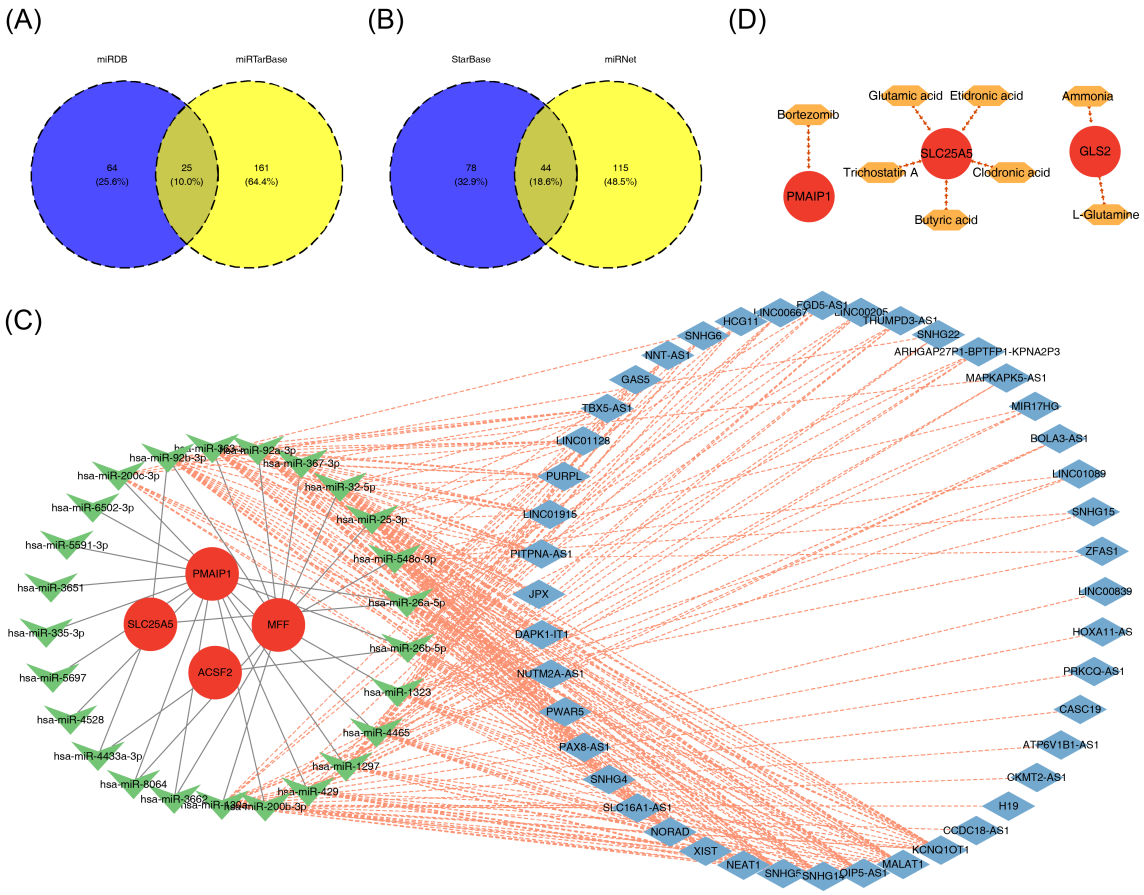

FIGURE 8
The ceRNA regulatory network and drug prediction. **(A, B)** Venn diagrams of shared miRNAs **(A)** and common lncRNAs **(B)** predicted by biomarkers. **(C)** The lncRNA–miRNA–mRNA regulatory network. **(D)** Drug–mRNA network, with red circles indicating biomarkers and orange hexagons indicating drugs. CeRNA, competing endogenous RNAs; miRNA, microRNA; lncRNA, long non-coding RNA.

3.9.3 Western blot to verify the expression of biomarkers in the placenta of normal pregnancy and PE

Western blot analysis confirmed these observations, revealing decreased expression levels of *SLC25A5, MFF*, and *PMAIP1* and an increased expression of *ACSF2* in the PE group compared to that in the control group (Figures 11A, B).

4 Discussion

PE, a pregnancy-specific complication, is a major cause of maternal and fetal morbidity and mortality, contributing to 4.6% of pregnancy-related complications (4). The pathogenesis of PE involves a range of factors, including placental hypoxia and ischemia, oxidative stress, inflammatory response, angiogenesis dysfunction, immune dysregulation, and their complex interactions (7). Among these, impaired trophoblast cell proliferation and abnormal invasion contribute to insufficient spiral artery remodeling, resulting in placental ischemia and hypoxia, which is considered a key pathogenic mechanism (45). Numerous studies have emphasized that PCD plays a critical role in trophoblast damage (46). Mitochondria, as central organelles in PCD, are involved in releasing or recruiting specific cell death promoters (47). Mitochondrial dysfunction, which disrupts intracellular energy metabolism, may trigger inflammation and vascular abnormalities, leading to trophoblast cell death (46). These insights open new avenues for exploring the pathogenesis of PE.

In this study, 1,438 DEGs were identified using bioinformatics, integrating public database data with clinical samples. After intersecting these genes with 1,136 MRGs and 1,548 PCD-related genes, 14 DE-mtPCD genes were obtained. GO and KEGG enrichment analyses of these DE-mtPCD genes revealed functional enrichment related to transmembrane transport, mitochondria, membrane permeability, peroxisome structures, apoptotic complexes, electron transfer, and redox processes. KEGG pathways associated with apoptosis, such as the p53 and apoptosis signaling pathways, were also identified. Previous research has indicated that p53-mediated trophoblast apoptosis is linked to the etiology of PE (48). The apoptosis pathway, which regulates PCD, is a terminal pathway for nearly all cell types.

To identify biomarkers involved in the onset of PE, this study applied three machine learning methods to select 10 key genes. Expression differences of these candidate biomarkers were verified

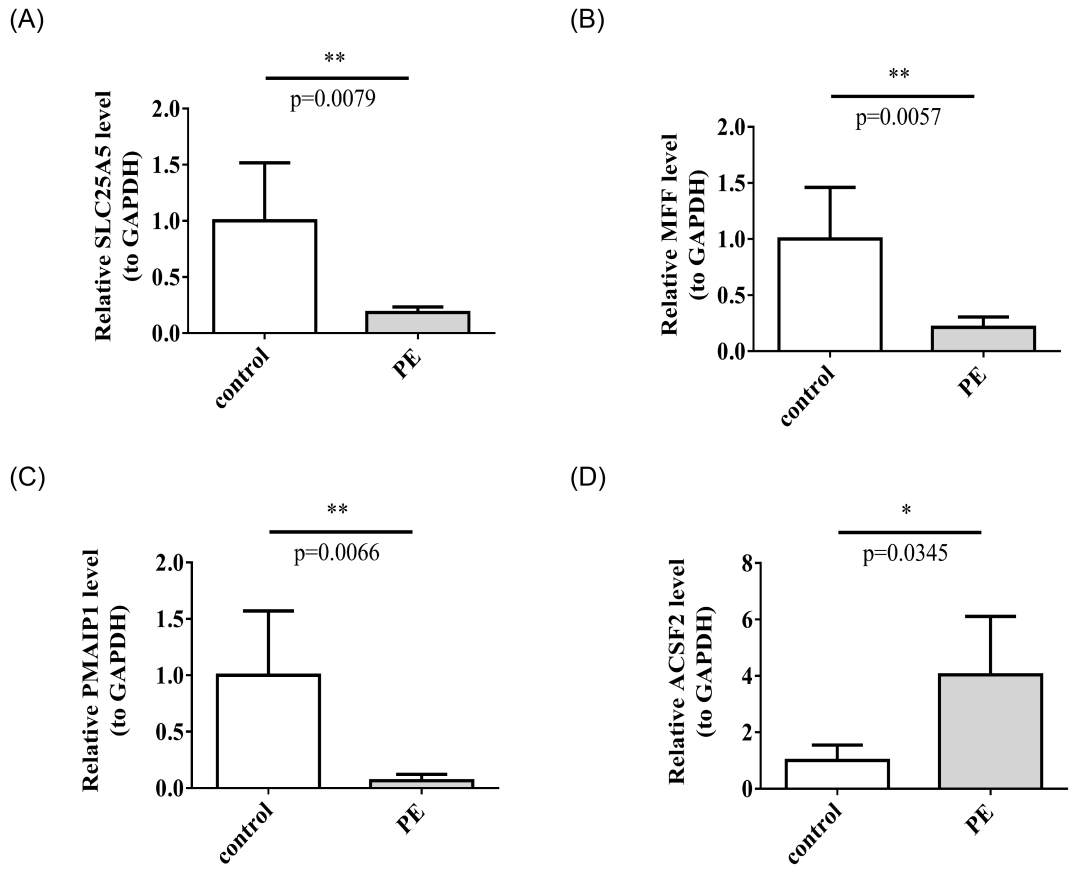

FIGURE 9
The mRNA expression levels of *SLC25A5* **(A)**, *MFF* **(B)**, *PMAIP1* **(C)**, *ACSF2* **(D)**. in control and PE samples by RT-qPCR. RT-qPCR, real-time quantitative polymerase chain reaction. *p < 0.05, **p < 0.01.

in both the training and validation sets, ultimately identifying four genes—*SLC25A5, ACSF2, MFF*, and *PMAIP1*—as potential diagnostic biomarkers for PE. Specifically, *SLC25A5, MFF*, and *PMAIP1* were downregulated in the PE group, whereas *ACSF2* was upregulated across both datasets. *SLC25A5*, known as adenine nucleotide translocator 2, is critical for ATP/ADP exchange and plays a significant role in various diseases. High expression of *SLC25A5* is associated with poor prognosis in MRG studies (48). Furthermore, exposure to perfluorooctane sulfonate has been shown to impair trophoblast migration, invasion, and vascular formation, reducing *SLC25A5* expression in both the placenta and JEG-3 cells. Animal and *in vitro* experiments confirmed that mitochondrial dysfunction mediated by *SLC25A5* in trophoblast cells induces these pathophysiological effects, ultimately leading to PE (49). These observations suggest that *SLC25A5* may contribute to placental dysfunction by affecting mitochondrial function, warranting further investigation.

ACSF2, a member of the acyl-CoA synthetase (*ACS*) family, catalyzes the sulfur esterification of acyl thioesters to form coenzyme A, which plays a central role in cellular lipid metabolism (50). Mitophagy, the selective degradation of damaged mitochondria, is essential for maintaining mitochondrial homeostasis and generating ATP to support various cellular functions (51). Inhibition of *ACSF2* in Human renal cortex proximal convoluted tubule epithelial cells-2 (HK-2) cells has been shown to reduce cellular lipid peroxidation, enhance mitophagy, restore mitochondrial function, and protect against ischemia-reperfusion–induced acute kidney injury (52). In another study, overexpression of *DRAM1* in mice enhanced mitophagy, improved placental mitochondrial function in PE mice, and significantly reduced blood lipid and urinary protein levels (53). These observations suggest that *ACSF2* may alleviate PE symptoms by enhancing mitophagy and improving mitochondrial function, positioning it as a potential therapeutic target for PE. Additionally, *ACSF2* is significantly associated with immune-related pathways such as Toll-like receptor signaling, Nuclear Factor κ-Light-Chain Enhancer of Activated B Cells (NF-κB) signaling, and Nucleotide binding oligomerization domain (NOD)-like receptor signaling (54–56), all of which are implicated in the pathogenesis of PE, further supporting the potential involvement of *ACSF2* in PE onset (57–59). Future experiments are needed to clarify the specific role of *ACSF2* in PE pathogenesis.

MFF, located on the outer mitochondrial membrane, is crucial for activating mitochondrial fission and mediating mitochondrial death. Studies have shown that genetic deletion of *MFF* suppresses pro-inflammatory responses, renal tubular oxidative stress, and renal cell death, significantly mitigating renal failure caused by

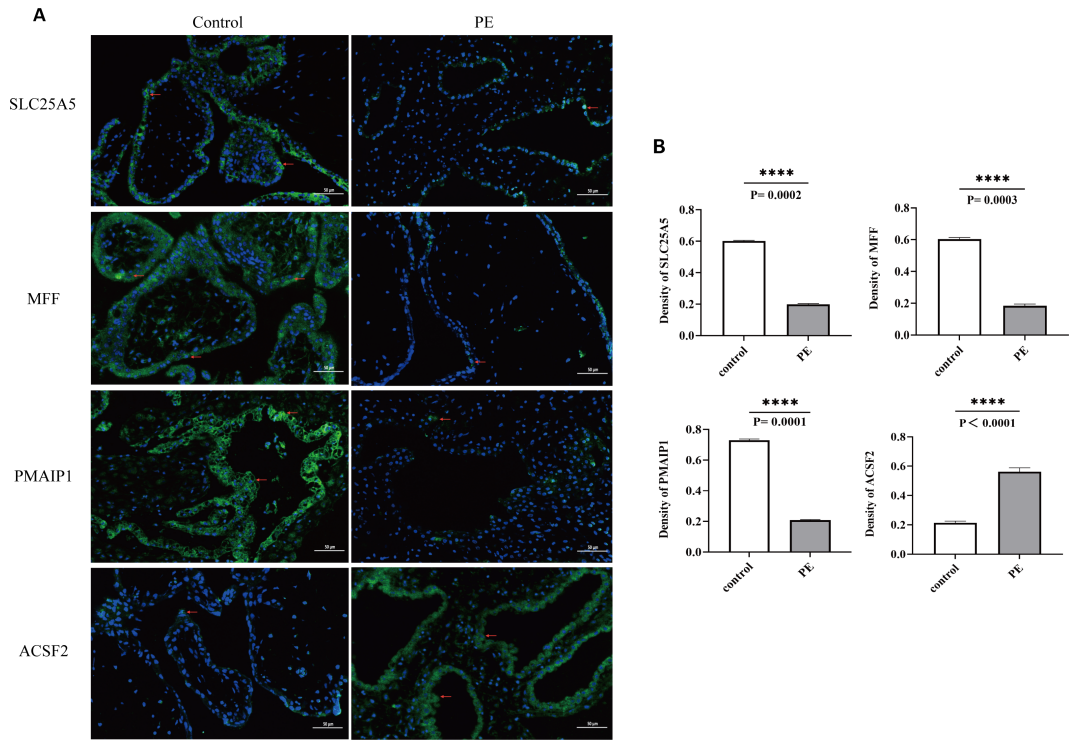

FIGURE 10
(A) Blue indicates the nucleus, green indicates the expressed target protein, and red arrows highlight the target protein expression sites in the cell. **(B)** Optical density analysis of immunofluorescence images for the four biomarkers. The AOD of SLC25A5, MFF, PMAIP1, and ACSF2 was significantly lower than in the control group, whereas ACSF2 showed significantly higher expression than in the control group. ****p < 0.0001; AOD, average optical density.

ischemic acute kidney injury (AKI) (60). *MFF* mediates mitochondrial fission by facilitating the translocation of dynein-related protein 1 (*Drp1*) from the cytosol to mitochondria and negatively regulates calcium (Ca^{2+}) transport from the ER to mitochondria. *MFF* deficiency leads to mitochondrial Ca^{2+} overload, which triggers excessive ROS production, impedes mitochondrial biogenesis, and results in encephalopathy (61).

PMAIP1, a member of the pro-apoptotic *BCL-2* family (specifically the BH3 subfamily), regulates apoptosis and proliferation in various tumor cells (62–64). *PMAIP1* contains a

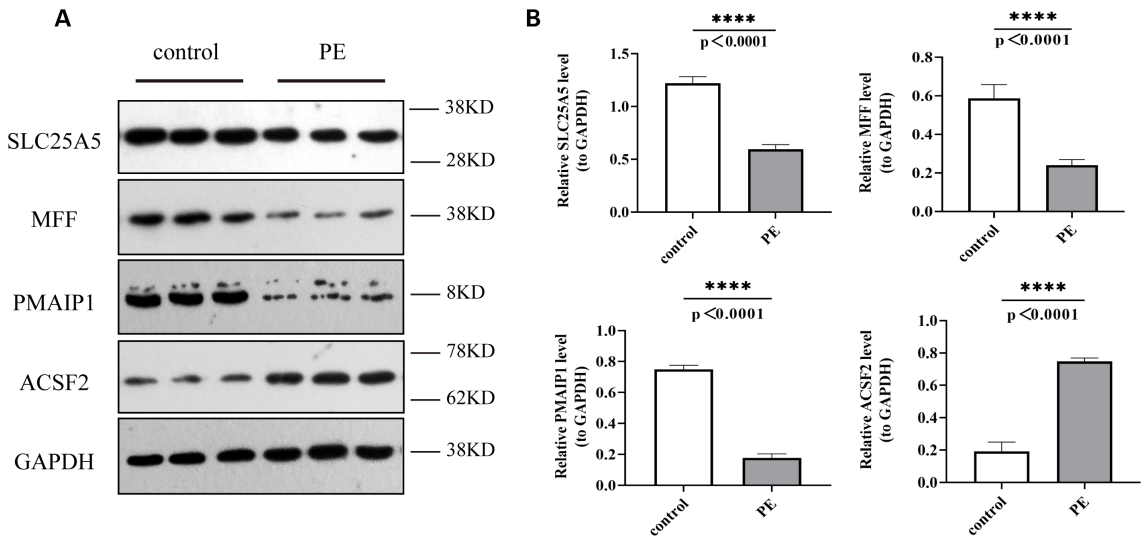

FIGURE 11
Protein expression levels of *SLC25A5, MFF, PMAIP1*, and *ACSF2* in control and PE samples by Western blot. **(A)** Western Blot (WB) results; **(B)** Quantitative analysis of WB results. WB, Western blot. ****p < 0.0001.

binding site for p53, which directly interacts with this site to promote *PMAIP1* transcription and protein expression, mediating apoptosis (65). Although *PMAIP1* is primarily recognized as a mediator of p53-induced apoptosis, it has been found that hypoxia-inducible factor 1α can bind to the hypoxia response element upstream of the PMAIP1 promoter, thereby activating *PMAIP1* transcription and confirming its role in apoptosis through a p53-independent pathway (66).

Although *SLC25A5, ACSF2, MFF*, and *PMAIP1* have not been previously linked to PE, they are known to significantly influence mitochondrial function and tumor cell death. Given the similarities between trophoblast cell invasion and proliferation and tumor cell behavior, it is plausible that these biomarkers may play a role in mediating trophoblast cell death during PE pathogenesis.

Building on the previous results, the gene expression of *SLC25A5, MFF, PMAIP1*, and *ACSF2* was further assessed in placental tissues from both PE and normal pregnancies using RT-qPCR. The findings revealed a reduction in the expression levels of *SLC25A5, MFF*, and *PMAIP1*, whereas *ACSF2* expression was elevated in the PE group. These clinical validation results were consistent with the dataset analysis, suggesting that *SLC25A5, MFF, PMAIP1*, and *ACSF2* could serve as novel potential targets for the prevention and treatment of PE.

Further analyses using a nomogram and ANN demonstrated the strong discriminatory ability of these biomarkers in distinguishing between PE and normal groups, underscoring their potential for effective PE diagnosis. In medical diagnostics, the AUC is a critical metric for evaluating test accuracy, with AUC values approaching 1 indicating greater diagnostic reliability (67). In this study, the AUC for the biomarkers *SLC25A5, MFF, PMAIP1*, and *ACSF2* was 0.986, highlighting their exceptional accuracy in predicting PE. While traditional biomarkers have proven useful in PE diagnosis, the present findings suggest that these novel biomarkers may offer superior diagnostic performance. Clinically, a higher AUC provides substantial benefits by more accurately distinguishing true patients with PE. This approach reduces the misclassification of healthy individuals as patients with PE (false positives) and minimizes missed diagnoses (false negatives), offering a more reliable foundation for early diagnosis, timely intervention, and improved patient outcomes.

Further GSVA identified five pathways that exhibited significant differences between high- and low-expression groups of the four biomarkers, including mismatch repair, RNA degradation, Notch signaling pathway, proteasome, and glycosphingolipid biosynthesis (Globo and Isoglobo Series). Mismatch repair, a critical DNA repair pathway, is involved in mitosis, meiosis, cell apoptosis, immunoglobulin gene rearrangement, and somatic hypermutation. Disruption of this pathway may be central to the PCD observed in PE cells (68). In RNA regulation, RNA degradation, particularly of polyadenylated RNA, occurs rapidly during early apoptosis, potentially serving as a marker of cell death and being associated with mitochondrial release proteins (69). The Notch signaling pathway plays a pivotal role in determining cell fate and regulating cell differentiation, proliferation, and apoptosis through interactions between Notch ligands and receptors (70). This pathway is essential for normal placental and trophoblast development, promoting successful pregnancy (71). Notch1, in particular, is critical for the proliferation and survival of extravillous trophoblast precursors, and defects in trophoblast differentiation are linked to severe pregnancy complications, including PE (72). The proteasome pathway, involved in protein modification and degradation, is also implicated in regulating apoptosis through various signaling pathways, such as the ubiquitin-proteasome and autophagy pathways (73). These pathways are interconnected with apoptosis and have been linked to PE pathogenesis. Therefore, these four biomarkers may contribute to mediating trophoblast apoptosis and the development of PE, although further exploration of the underlying mechanisms is warranted.

Gene regulatory networks are essential for the regulation of gene expression and play a significant role in disease development. lncRNAs and Circular RNAs (circRNAs) can modulate miRNA activity, influencing downstream mRNA expression and impacting conditions such as PE (74). In this study, a database was used to predict corresponding regulatory factors, resulting in the identification of 44 lncRNA–miRNA–mRNA interaction networks, which were visualized. Although no prior studies have documented these specific regulatory networks in PE, they represent an area of considerable potential for further investigation into the regulatory mechanisms underlying PE. Additionally, drug prediction based on these four biomarkers identified potential therapeutic candidates for PE treatment, including glutamic acid and clodronate. These findings offer promising targets for the development of therapeutic strategies for PE.

Extensive research has highlighted the involvement of immune imbalance in the pathophysiology of PE (75, 76). Several bioinformatics analyses have also indicated significant immune infiltration differences between PE and normal controls (77). In this study, immune variations between PE and normal samples were analyzed using the GSE10588 dataset, revealing that 11 immune cell types were significantly different between the two groups. The correlation analysis between these differential immune cells and the four biomarkers demonstrated that type 2 T helper (Th2) cells were significantly associated with all four biomarkers. Specifically, Th2 cells were positively correlated with *SLC25A5, MFF*, and *PMAIP1* and negatively with *ACSF2*. MFF interacts with *Drp1* to initiate mitochondrial division, which may influence the mitochondrial function and survival of Th2 cells (78). As a pro-apoptotic protein, *PMAIP1* (also known as *NOXA*) regulates the survival and function of memory CD4(+) Th1/Th2 cells by binding to anti-apoptotic proteins such as Mcl-1 and *Bcl2A1* (79). *SLC25A5* plays a role in apoptosis regulation by modulating mitochondrial membrane permeability, which could further impact Th2 cell survival (80). Moreover, *ACSF2* may influence the energy metabolism and overall function of Th2 cells by regulating lipid metabolism (52). These findings suggest that these four biomarkers modulate Th2 cell survival, function, and energy metabolism *via* distinct mechanisms, highlighting the potential role of Th2 cells in

regulating the immune response in PE. After placental implantation in normal pregnancy, the early inflammatory Th1 immune response rapidly shifts to a Th2 anti-inflammatory response. Dominant Th2 immunity overcomes Th1 immunity at the placental implantation site, balancing Th1 activity to protect the fetus and support fetal and placental development. However, an enhanced Th2 response during pregnancy can contribute to or exacerbate autoimmune diseases (81). Other studies (82) have reported that, while Th2 cells increase in normal pregnancy circulation, they decrease in pre-eclamptic pregnancies. This dysregulation, often observed in the first month of PE, is accompanied by a rise in circulating and placental $CD4^+$ Th1 cells, elevated pro-inflammatory cytokine levels, increased autoantibody production, and oxidative stress, suggesting that Th2 cells and related pathways may serve as potential targets for immunotherapy.

This study is the first to investigate the association between PE and mtPCD based on public databases. Through bioinformatics analysis, biomarkers of diagnostic value were identified, and related pathway analyses were conducted. However, several limitations must be acknowledged. Firstly, conclusions derived from bioinformatics analysis may be susceptible to bias. Bioinformatics heavily depends on existing databases and algorithms, and factors such as the accuracy, completeness of data sources, and the applicability of algorithms can influence the results. Thus, further clinical validation of the findings is essential. Although verification experiments, including PCR, immunofluorescence, and Western blot, were performed, the experimental validation remains incomplete. Additional experiments, such as Cell Mito stress Seahorse assays and blood analyses, were not conducted. Moreover, the small sample size used for experimental validation limits the representativeness and generalizability of the results. Furthermore, although potential drugs such as clodronic acid, etidronic acid, and glutamic acid were predicted, their effectiveness in PE samples was not evaluated. Finally, although the differential expression of biomarkers has been preliminarily validated, their biological roles in the pathogenesis of PE and their ability to predict disease severity or complications have not been comprehensively explored. This gap in understanding limits the potential for developing effective biomarker-based therapeutic strategies.

To address these limitations, future work will focus on further bioinformatics analyses and clinical validation of targeted experiments. By increasing the sample size and including samples from different races, regions, and lifestyle factors, this study aims to enhance the representativeness and generalizability of the study results. Additionally, experimental validation using blood samples will be incorporated to provide a more comprehensive exploration of the biomarkers' characteristics and effects. Further, the correlation between biomarkers and genes highly expressed in hypertension will be analyzed to assess whether differential expression of biomarkers is influenced by hypertension. Extending the analysis of immune cell populations, particularly Th2 cells, could explore their role in PE. Advanced biotechnologies such as gene editing, cell function assays, and animal model construction could uncover the biological functions of these biomarkers in PE pathogenesis and the efficacy of potential drugs. This approach will provide a comprehensive molecular, cellular, and systemic analysis of the relationship between biomarkers and PE pathogenesis. Moreover, more cases of PE with varying severity and complications will be collected, further evaluating the predictive efficacy of these biomarkers for disease severity and complications by combining expression level data with clinical outcomes.

5 Conclusions

This study is the first to establish a link between mtPCD-related genes and PE. Four biomarkers—*SLC25A5, ACSF2, MFF*, and *PMAIP1*—associated with mtPCD were identified, demonstrating strong diagnostic potential for PE. Furthermore, the study has conducted preliminary investigations into the functional enrichment pathways, lncRNA–miRNA–mRNA regulatory network, immune infiltration, and drug predictions related to these biomarkers, revealing their substantial application potential. These biomarkers may not only serve as novel therapeutic targets, with the development of specific drugs or treatments potentially transforming disease outcomes, but also offer valuable tools for screening and assessing drug efficacy. These findings open new avenues for advancing the diagnosis and treatment of PE.

Data availability statement

The datasets presented in this study can be found in online repositories. The names of the repository/repositories and accession number(s) can be found in the article/Supplementary Material.

Ethics statement

The studies involving humans were approved by Ethics Committee of Fujian Provincial Hospital(protocol code K2023-02-016 and date of approval: 2023-02-22). The studies were conducted in accordance with the local legislation and institutional requirements. The participants provided their written informed consent to participate in this study.

Author contributions

RoL: Formal analysis, Visualization, Writing – original draft. XW: Formal analysis, Visualization, Writing – original draft. LL: Writing – review & editing. XH: Formal analysis, Visualization, Writing – review & editing. ZL: Data curation, Investigation, Writing – review & editing. JZ: Data curation, Investigation, Writing – review & editing. FS: Data curation, Formal analysis, Visualization, Writing – review & editing. RuL: Project administration, Validation, Writing – review & editing.

Funding

The author(s) declare financial support was received for the research, authorship, and/or publication of this article. This work was sponsored by Fujian Provincial Health Technology Project (No. 2020QNB005) and Natural Science Fundation of Fujian Province (No.2024J011012).

Acknowledgments

We thank the entire team and Fujian Provincial Health Technology Project for their support and assistance with this study.

Conflict of interest

The authors declare that the research was conducted in the absence of any commercial or financial relationships that could be construed as a potential conflict of interest.

Publisher's note

All claims expressed in this article are solely those of the authors and do not necessarily represent those of their affiliated organizations, or those of the publisher, the editors and the reviewers. Any product that may be evaluated in this article, or claim that may be made by its manufacturer, is not guaranteed or endorsed by the publisher.

Supplementary material

The Supplementary Material for this article can be found online at: https://www.frontiersin.org/articles/10.3389/fimmu.2024.1453633/full#supplementary-material

SUPPLEMENTARY FIGURE 1
Mismatch repair pathway in DNA repair processes.

SUPPLEMENTARY FIGURE 2
Glycosphingolipid biosynthesis in the globo series pathway.

SUPPLEMENTARY FIGURE 3
The Notch signaling pathway, a key determinant of cell fate.

SUPPLEMENTARY FIGURE 4
The proteasome pathway regulates cell apoptosis.

SUPPLEMENTARY FIGURE 5
RNA degradation pathway modulates RNA expression.

SUPPLEMENTARY TABLE 1
List of KEGG enrichment results.

SUPPLEMENTARY TABLE 2
List of LASSO regression coefficients for the 10 hub genes.

SUPPLEMENTARY TABLE 3
Chromosomal localization of the four biomarkers.

SUPPLEMENTARY TABLE 4
List of regression coefficients.

SUPPLEMENTARY TABLE 5
List of targeted drugs for the biomarkers.

References

1. ACOG practice bulletin no. 202: gestational hypertension and preeclampsia. *Obstet Gynecol.* (2019) 133:1. doi: 10.1097/AOG.0000000000003018

2. Kong B, Ma D, Duan T, Di W, Zhu L, Qi H, et al. *Obstetrics and Gynecology, 10rd.* Beijing: People's Medical Publishing House (2024) p. 87–95.

3. Unger T, Borghi C, Charchar F, Khan NA, Poulter NR, Prabhakaran D, et al. 2020 International Society of Hypertension global hypertension practice guidelines. *J Hypertens.* (2020) 38:982–1004. doi: 10.1097/HJH.0000000000002453

4. Garovic VD, Dechend R, Easterling T, Karumanchi SA, McMurtry Baird S, Magee LA, et al. Hypertension in pregnancy: diagnosis, blood pressure goals, and pharmacotherapy: A scientific statement from the American heart association. *Hypertension.* (2022) 79:e21–41. doi: 10.1161/HYP.0000000000000208

5. Brown MA, Magee LA, Kenny LC, Karumanchi SA, McCarthy FP, Saito S, et al. Hypertensive disorders of pregnancy: ISSHP classification, diagnosis, and management recommendations for international practice. *Hypertension.* (2018) 72:24–43. doi: 10.1161/HYPERTENSIONAHA.117.10803

6. Aneman I, Pienaar D, Suvakov S, Simic TP, Garovic VD, McClements L. Mechanisms of key innate immune cells in early- and late-onset preeclampsia. *Front Immunol.* (2020) 11:1864. doi: 10.3389/fimmu.2020.01864

7. Phipps EA, Thadhani R, Benzing T, Karumanchi SA. Pre-eclampsia: pathogenesis, novel diagnostics and therapies. *Nat Rev Nephrol.* (2019) 15:275–89. doi: 10.1038/s41581-019-0119-6

8. Kelemu T, Erlandsson L, Seifu D, Abebe M, Teklu S, Storry JR, et al. Association of maternal regulatory single nucleotide polymorphic CD99 genotype with preeclampsia in pregnancies carrying male fetuses in Ethiopian women. *Int J Mol Sci.* (2020) 21 (16):5837. doi: 10.3390/ijms21165837

9. Li C, Liu W, Lao Q, Lu H, Zhao Y. Placenta autophagy is closely associated with preeclampsia. *Aging (Albany NY).* (2022) 15:15657–75. doi: 10.18632/aging.204436

10. Correa PJ, Palmeiro Y, Soto MJ, Ugarte C, Illanes SE. Etiopathogenesis, prediction, and prevention of preeclampsia. *Hypertens Pregnancy.* (2016) 35:280–94. doi: 10.1080/10641955.2016.1181180

11. Al-Rubaie Z, Askie LM, Ray JG, Hudson HM, Lord SJ. The performance of risk prediction models for pre-eclampsia using routinely collected maternal characteristics and comparison with models that include specialised tests and with clinical guideline decision rules: a systematic review. *Bjog.* (2016) 123:1441–52. doi: 10.1111/1471-0528.14029

12. Nikuei P, Rajaei M, Roozbeh N, Mohseni F, Poordarvishi F, Azad M, et al. Diagnostic accuracy of sFlt1/PlGF ratio as a marker for preeclampsia. *BMC Pregnancy Childbirth.* (2020) 20:80. doi: 10.1186/s12884-020-2744-2

13. Zeisler H, Llurba E, Chantraine FJ, Vatish M, Staff AC, Sennström M, et al. Soluble fms-like tyrosine kinase-1 to placental growth factor ratio: ruling out pre-eclampsia for up to 4 weeks and value of retesting. *Ultrasound Obstet Gynecol.* (2019) 53:367–75. doi: 10.1002/uog.2019.53.issue-3

14. Izumi S, Iwama N, Metoki H. Prediction of preterm preeclampsia risk in Asians using a simple two-item assessment in early pregnancy. *Hypertens Res.* (2024) 47:1231–4. doi: 10.1038/s41440-024-01590-1

15. Sun Y, Zhong N, Zhu X, Fan Q, Li K, Chen Y, et al. Identification of important genes associated with acute myocardial infarction using multiple cell death patterns. *Cell Signal Dec.* (2023) 112:110921. doi: 10.1016/j.cellsig.2023.110921

16. Lockshin RA, Williams CM. Programmed cell death–I. Cytology of degeneration in the intersegmental muscles of the pernyi silkmoth. *J Insect Physiol.* (1965) 11:123–33. doi: 10.1016/0022-1910(65)90099-5

17. Yuan J. Ofengeim D. A guide to cell death pathways. *Nat Rev Mol Cell Biol.* (2024) 25(5):379–95. doi: 10.1038/s41580-023-00689-6

18. Tao P, Sun J, Wu Z, Wang S, Wang J, Li W, et al. A dominant autoinflammatory disease caused by non-cleavable variants of RIPK1. *Nature.* (2020) 577:109–14. doi: 10.1038/s41586-019-1830-y

19. Liu Y, Li X, Zhou X, Wang J, Ao X. FADD as a key molecular player in cancer progression. *Mol Med.* (2022) 28:132. doi: 10.1186/s10020-022-00560-y

20. Fleming A, Bourdenx M, Fujimaki M, Karabiyik C, Krause GJ, Lopez A, et al. The different autophagy degradation pathways and neurodegeneration. *Neuron.* (2022) 110:935–66. doi: 10.1016/j.neuron.2022.01.017

21. Yu H, Chen L, Du B. Necroptosis in the pathophysiology of preeclampsia. *Cell Cycle*. (2023) 22:1713–25. doi: 10.1080/15384101.2023.2229138

22. Lv Z, Xiong LL, Qin X, Zhang H, Luo X, Peng W, et al. Role of GRK2 in trophoblast necroptosis and spiral artery remodeling: implications for preeclampsia pathogenesis. *Front Cell Dev Biol*. (2021) 9:694261. doi: 10.3389/fcell.2021.694261

23. Yu H, Zhang Y, Liu M, Liao L, Wei X, Zhou R. SIRT3 deficiency affects the migration, invasion, tube formation and necroptosis of trophoblast and is implicated in the pathogenesis of preeclampsia. *Placenta*. (2022) 120:1–9. doi: 10.1016/j.placenta.2022.01.014

24. Zhang J, Huang J, Lin X, Fei K, Xie Y, Peng Q, et al. Phosphoglycerate mutase 5 promotes necroptosis in trophoblast cells through activation of dynamin-related protein 1 in early-onset preeclampsia. *Am J Reprod Immunol*. (2022) 87:e13539. doi: 10.1111/aji.13539

25. Hannan NJ, Beard S, Binder NK, Onda K, Kaitu'u-Lino TJ, Chen Q, et al. Key players of the necroptosis pathway RIPK1 and SIRT2 are altered in placenta from preeclampsia and fetal growth restriction. *Placenta*. (2017) 51:1–9. doi: 10.1016/j.placenta.2017.01.002

26. Brinkmann K, Ng AP, de Graaf CA, Strasser A. What can we learn from mice lacking pro-survival BCL-2 proteins to advance BH3 mimetic drugs for cancer therapy? *Cell Death Differ*. (2022) 29:1079–93. doi: 10.1038/s41418-022-00987-0

27. Smith WM, Reed DR. Targeting apoptosis in ALL. *Curr Hematol Malig Rep*. (2022) 17:53–60. doi: 10.1007/s11899-022-00661-9

28. Nguyen TT, Wei S, Nguyen TH, Jo Y, Zhang Y, Park W, et al. Mitochondria-associated programmed cell death as a therapeutic target for age-related disease. *Exp Mol Med Aug*. (2023) 55:1595–619. doi: 10.1038/s12276-023-01046-5

29. Torbergsen T, Oian P, Mathiesen E, Borud O. Pre-eclampsia–a mitochondrial disease? *Acta Obstet Gynecol Scand*. (1989) 68:145–8. doi: 10.3109/00016348909009902

30. Marín R, Chiarello DI, Abad C, Rojas D, Toledo F, Sobrevia L. Oxidative stress and mitochondrial dysfunction in early-onset and late-onset preeclampsia. *Biochim Biophys Acta Mol Basis Dis*. (2020) 1866:165961. doi: 10.1016/j.bbadis.2020.165961

31. Hu XQ, Zhang L. Mitochondrial dysfunction in the pathogenesis of preeclampsia. *Curr Hypertens Rep*. (2022) 24:157–72. doi: 10.1007/s11906-022-01184-7

32. Wu H, Zhao X, Hochrein SM, Eckstein M, Gubert GF, Knöpper K, et al. Mitochondrial dysfunction promotes the transition of precursor to terminally exhausted T cells through HIF-1α-mediated glycolytic reprogramming. *Nat Commun*. (2023) 14:6858. doi: 10.1038/s41467-023-42634-3

33. Yung HW, Colleoni F, Dommett E, Cindrova-Davies T, Kingdom J, Murray AJ, et al. Noncanonical mitochondrial unfolded protein response impairs placental oxidative phosphorylation in early-onset preeclampsia. *Proc Natl Acad Sci U S A*. (2019) 116:18109–18. doi: 10.1073/pnas.1907548116

34. Li J, Xu P, Chen S. Research progress on mitochondria regulating tumor immunity. *Zhejiang Da Xue Xue Bao Yi Xue Ban*. (2024) 53:1–14. doi: 10.3724/zdxbyxb-2023-0484

35. Sitras V, Paulssen RH, Grønaas H, Leirvik J, Hanssen TA, Vårtun A, et al. Differential placental gene expression in severe preeclampsia. *Placenta*. (2009) 30:424–33. doi: 10.1016/j.placenta.2009.01.012

36. Wilson SL, Leavey K, Cox BJ, Robinson WP. Mining DNA methylation alterations towards a classification of placental pathologies. *Hum Mol Genet*. (2018) 27:135–46. doi: 10.1093/hmg/ddx391

37. Ritchie ME, Phipson B, Wu D, Hu Y, Law CW, Shi W, et al. limma powers differential expression analyses for RNA-sequencing and microarray studies. *Nucleic Acids Res*. (2015) 43:e47. doi: 10.1093/nar/gkv007

38. Wu T, Hu E, Xu S, Chen M, Guo P, Dai Z, et al. clusterProfiler 4.0: A universal enrichment tool for interpreting omics data. *Innovation (Camb)*. (2021) 2:100141. doi: 10.1016/j.xinn.2021.100141

39. Shannon P, Markiel A, Ozier O, Baliga NS, Wang JT, Ramage D, et al. Cytoscape: a software environment for integrated models of biomolecular interaction networks. *Genome Res*. (2003) 13:2498–504. doi: 10.1101/gr.1239303

40. Li Y, Lu F, Yin Y. Applying logistic LASSO regression for the diagnosis of atypical Crohn's disease. *Sci Rep*. (2022) 12:11340. doi: 10.1038/s41598-022-15609-5

41. Sachs MC. plotROC: A tool for plotting ROC curves. *J Stat Softw*. (2017) 79:2. doi: 10.18637/jss.v079.c02

42. Yan P, Ke B, Song J, Fang X. Identification of immune-related molecular clusters and diagnostic markers in chronic kidney disease based on cluster analysis. *Front Genet*. (2023) 14:1111976. doi: 10.3389/fgene.2023.1111976

43. Qing M, Yang D, Shang Q, Li W, Zhou Y, Xu H, et al. Humoral immune disorders affect clinical outcomes of oral lichen planus. *Oral Dis*. (2023) 30(4):2337–46. doi: 10.1111/odi.14667

44. Hänzelmann S, Castelo R, Guinney J. GSVA: gene set variation analysis for microarray and RNA-seq data. *BMC Bioinf*. (2013) 14:7. doi: 10.1186/1471-2105-14-7

45. Staff AC, Fjeldstad HE, Fosheim IK, Moe K, Turowski G, Johnsen GM, et al. Failure of physiological transformation and spiral artery atherosis: their roles in preeclampsia. *Am J Obstet Gynecol*. (2022) 226:S895–s906. doi: 10.1016/j.ajog.2020.09.026

46. Ding Y, Yang X, Han X, Shi M, Sun L, Liu M, et al. Ferroptosis-related gene expression in the pathogenesis of preeclampsia. *Front Genet*. (2022) 13:927869. doi: 10.3389/fgene.2022.927869

47. Vaka R, Deer E, Cunningham M, McMaster KM, Wallace K, Cornelius DC, et al. Characterization of mitochondrial bioenergetics in preeclampsia. *J Clin Med*. (2021) 10 (21):5063. doi: 10.3390/jcm10215063

48. Seneviratne JA, Carter DR, Mittra R, Gifford A, Kim PY, Luo JS, et al. Inhibition of mitochondrial translocase SLC25A5 and histone deacetylation is an effective combination therapy in neuroblastoma. *Int J Cancer*. (2023) 152:1399–413. doi: 10.1002/ijc.v152.7

49. Zhao Y, Zhao H, Xu H, An P, Ma B, Lu H, et al. Perfluorooctane sulfonate exposure induces preeclampsia-like syndromes by damaging trophoblast mitochondria in pregnant mice. *Ecotoxicol Environ Saf*. (2022) 247:114256. doi: 10.1016/j.ecoenv.2022.114256

50. Watkins PA, Maiguel D, Jia Z, Pevsner J. Evidence for 26 distinct acyl-coenzyme A synthetase genes in the human genome. *J Lipid Res*. (2007) 48:2736–50. doi: 10.1194/jlr.M700378-JLR200

51. Zhang W, Chen C, Wang J, Liu L, He Y, Chen Q. Mitophagy in cardiomyocytes and in platelets: A major mechanism of cardioprotection against ischemia/reperfusion injury. *Physiol (Bethesda)*. (2018) 33:86–98. doi: 10.1152/physiol.00030.2017

52. Shi H, Qi H, Xie D, Zhuang J, Qi H, Dai Y, et al. Inhibition of ACSF2 protects against renal ischemia/reperfusion injury via mediating mitophagy in proximal tubular cells. *Free Radic Biol Med*. (2023) 198:68–82. doi: 10.1016/j.freeradbiomed.2023.02.003

53. Chen G, Lin Y, Chen L, Zeng F, Zhang L, Huang Y, et al. Role of DRAM1 in mitophagy contributes to preeclampsia regulation in mice. *Mol Med Rep*. (2020) 22:1847–58. doi: 10.3892/mmr.2020.11269

54. Zhou M, Xu W, Wang J, Yan J, Shi Y, Zhang C, et al. Boosting mTOR-dependent autophagy via upstream TLR4-MyD88-MAPK signalling and downstream NF-κB pathway quenches intestinal inflammation and oxidative stress injury. *EBioMedicine*. (2018) 35:345–60. doi: 10.1016/j.ebiom.2018.08.035

55. Cao H, Liu J, Shen P, Cai J, Han Y, Zhu K, et al. Protective effect of naringin on DSS-induced ulcerative colitis in mice. *J Agric Food Chem*. (2018) 66:13133–40. doi: 10.1021/acs.jafc.8b03942

56. Schmitt H, Ulmschneider J, Billmeier U, Vieth M, Scarozza P, Sonnewald S, et al. The TLR9 agonist cobitolimod induces IL10-producing wound healing macrophages and regulatory T cells in ulcerative colitis. *J Crohns Colitis*. (2020) 14:508–24. doi: 10.1093/ecco-jcc/jjz170

57. Afkham A, Eghbal-Fard S, Heydarlou H, Azizi R, Aghebati-Maleki L, Yousefi M. Toll-like receptors signaling network in pre-eclampsia: An updated review. *J Cell Physiol*. (2019) 234:2229–40. doi: 10.1002/jcp.v234.3

58. Sha H, Ma Y, Tong Y, Zhao J, Qin F. Apocynin inhibits placental TLR4/NF-κB signaling pathway and ameliorates preeclampsia-like symptoms in rats. *Pregnancy Hypertens*. (2020) 22:210–5. doi: 10.1016/j.preghy.2020.10.006

59. Liang Y, Wang P, Shi Y, Cui B, Meng J. Long noncoding RNA maternally expressed gene 3 improves trophoblast dysfunction and inflammation in preeclampsia through the Wnt/β-Catenin/nod-like receptor pyrin domain-containing 3 axis. *Front Mol Biosci*. (2022) 9:1022450. doi: 10.3389/fmolb.2022.1022450

60. Wang J, Zhu P, Toan S, Li R, Ren J, Zhou H. Pum2-Mff axis fine-tunes mitochondrial quality control in acute ischemic kidney injury. *Cell Biol Toxicol Aug*. (2020) 36:365–78. doi: 10.1007/s10565-020-09513-9

61. Sun X, Dong S, Kato H, Kong J, Ito Y, Hirofuji Y, et al. Mitochondrial calcium-triggered oxidative stress and developmental defects in dopaminergic neurons differentiated from deciduous teeth-derived dental pulp stem cells with MFF insufficiency. *Antioxidants (Basel)*. (2022) 11(7):1361. doi: 10.3390/antiox11071361

62. Jin S, Cojocari D, Purkal JJ, Popovic R, Talaty NN, Xiao Y, et al. 5-azacitidine induces NOXA to prime AML cells for venetoclax-mediated apoptosis. *Clin Cancer Res*. (2020) 26:3371–83. doi: 10.1158/1078-0432.CCR-19-1900

63. Zheng YJ, Liang TS, Wang J, Zhao JY, Yang DK, Liu ZS. Silencing lncRNA LOC101928963 inhibits proliferation and promotes apoptosis in spinal cord glioma cells by binding to PMAIP1. *Mol Ther Nucleic Acids*. (2019) 18:485–95. doi: 10.1016/j.omtn.2019.07.026

64. Do H, Kim D, Kang J, Son B, Seo D, Youn H, et al. TFAP2C increases cell proliferation by downregulating GADD45B and PMAIP1 in non-small cell lung cancer cells. *Biol Res*. (2019) 52:35. doi: 10.1186/s40659-019-0244-5

65. Morsi RZ, Hage-Sleiman R, Kobeissy H, Dbaibo G. Noxa: role in cancer pathogenesis and treatment. *Curr Cancer Drug Targets*. (2018) 18:914–28. doi: 10.2174/1568009618666180308105048

66. Isaja L, Mucci S, Vera J, Rodríguez-Varela MS, Marazita M, Morris-Hanon O, et al. Chemical hypoxia induces apoptosis of human pluripotent stem cells by a NOXA-mediated HIF-1α and HIF-2α independent mechanism. *Sci Rep*. (2020) 10:20653. doi: 10.1038/s41598-020-77792-7

67. Metz CE. Basic principles of ROC analysis. *Semin Nucl Med*. (1978) 8:283–98. doi: 10.1016/S0001-2998(78)80014-2

68. Olave MC, Graham RP. Mismatch repair deficiency: The what, how and why it is important. *Genes Chromosomes Cancer*. (2022) 61:314–21. doi: 10.1002/gcc.23015

69. Liu X, Fu R, Pan Y, Meza-Sosa KF, Zhang Z, Lieberman J. PNPT1 release from mitochondria during apoptosis triggers decay of Poly(A) RNAs. *Cell*. (2018) 174:187–201.e112. doi: 10.1016/j.cell.2018.04.017

70. Zhou B, Lin W, Long Y, Yang Y, Zhang H, Wu K, et al. Notch signaling pathway: architecture, disease, and therapeutics. *Signal Transduct Target Ther*. (2022) 7:95. doi: 10.1038/s41392-022-00934-y

71. Haider S, Pollheimer J, Knöfler M. Notch signalling in placental development and gestational diseases. *Placenta*. (2017) 56:65–72. doi: 10.1016/j.placenta.2017.01.117

72. Dietrich B, Haider S, Meinhardt G, Pollheimer J, Knöfler M. WNT and NOTCH signaling in human trophoblast development and differentiation. *Cell Mol Life Sci*. (2022) 79:292. doi: 10.1007/s00018-022-04285-3

73. Jiang TX, Zou JB, Zhu QQ, Liu CH, Wang GF, Du TT, et al. SIP/CacyBP promotes autophagy by regulating levels of BRUCE/Apollon, which stimulates LC3-I degradation. *Proc Natl Acad Sci U S A*. (2019) 116:13404–13. doi: 10.1073/pnas.1901039116

74. Song X, Luo X, Gao Q, Wang Y, Gao Q, Long W. Dysregulation of lncRNAs in placenta and pathogenesis of preeclampsia. *Curr Drug Targets*. (2017) 18:1165–70. doi: 10.2174/1389450118666170404160000

75. Dunk CE, Bucher M, Zhang J, Hayder H, Geraghty DE, Lye SJ, et al. Human leukocyte antigen HLA-C, HLA-G, HLA-F, and HLA-E placental profiles are altered in early severe preeclampsia and preterm birth with chorioamnionitis. *Am J Obstet Gynecol*. (2022) 227:641.e641–641.e613. doi: 10.1016/j.ajog.2022.07.021

76. de Moreuil C, Pan-Petesch B, Trémouilhac C, Dupré PF, Merviel P, Anouilh F, et al. Clinical risk factors for vasculo-placental disorders: results from a prospective case-control study nested in HEMOTHEPP French cohort study. *J Gynecol Obstet Hum Reprod*. (2023) 52:102511. doi: 10.1016/j.jogoh.2022.102511

77. Meng Y, Li C, Liu CX. Immune cell infiltration landscape and immune marker molecular typing in preeclampsia. *Bioengineered*. (2021) 12:540–54. doi: 10.1080/21655979.2021.1875707

78. Li D, Li Y, Pan W, Yang B, Fu C. Role of dynamin-related protein 1-dependent mitochondrial fission in drug-induced toxicity. *Pharmacol Res*. (2024) 206:107250. doi: 10.1016/j.phrs.2024.107250

79. Park J, Han JH, Myung SH, Kang H, Cho JY, Kim TH. A peptide containing Noxa mitochondrial-targeting domain induces cell death via mitochondrial and endoplasmic reticulum disruption. *Biochem Biophys Res Commun*. (2019) 518:80–6. doi: 10.1016/j.bbrc.2019.08.011

80. Gao R, Zhou D, Qiu X, Zhang J, Luo D, Yang X, et al. Cancer therapeutic potential and prognostic value of the SLC25 mitochondrial carrier family: A review. *Cancer Control*. (2024) 31:10732748241287905. doi: 10.1177/10732748241287905

81. Wang W, Sung N, Gilman-Sachs A, Kwak-Kim J. T helper (Th) cell profiles in pregnancy and recurrent pregnancy losses: Th1/Th2/Th9/Th17/Th22/Tfh cells. *Front Immunol*. (2020) 11:2025. doi: 10.3389/fimmu.2020.02025

82. Harmon AC, Cornelius DC, Amaral LM, Faulkner JL, Cunningham MW Jr, Wallace K, et al. The role of inflammation in the pathology of preeclampsia. *Clin Sci (Lond)*. (2016) 130:409–19. doi: 10.1042/CS20150702

frontiers | Frontiers in Immunology

TYPE Original Research
PUBLISHED 04 February 2025
DOI 10.3389/fimmu.2025.1496046

OPEN ACCESS

EDITED BY
Rajesh Kumar Manne,
Duke University, United States

REVIEWED BY
Rajni Kant,
Kaohsiung Medical University, Taiwan
Arun Paripati,
Nationwide Children's Hospital, United States
Lokanatha Oruganti,
Tulane University, United States

*CORRESPONDENCE
Mengjia Peng
pemeji@wmu.edu.cn

RECEIVED 15 September 2024
ACCEPTED 16 January 2025
PUBLISHED 04 February 2025

CITATION
Li R, Zhou C, Ye K, Chen H and Peng M (2025) Identification of genes involved in energy metabolism in preeclampsia and discovery of early biomarkers.
Front. Immunol. 16:1496046.
doi: 10.3389/fimmu.2025.1496046

Identification of genes involved in energy metabolism in preeclampsia and discovery of early biomarkers

Ruohua Li, Cuixia Zhou, Kejun Ye, Haihui Chen and Mengjia Peng*

Department of Gynecology and Obstetrics, The Third Affiliated Hospital of Wenzhou Medical University, Rui'an, China

Background: Preeclampsia is a complex pregnancy condition marked by hypertension and organ dysfunction, posing significant risks to maternal and fetal health. This study investigates the role of energy metabolism-associated genes in preeclampsia development and identifies potential early diagnostic biomarkers.

Methods: Preeclampsia datasets from Gene Expression Omnibus were analyzed for batch correction, normalization, and differential expression. Enrichment analyses using gene ontology, Kyoto Encyclopedia of Genes and Genomes, and gene set enrichment were performed. Protein-protein interaction networks were constructed to identify key genes, and regulatory networks involving transcription factors, miRNAs, and RNA-binding proteins were established. Differential expression was validated with receiver operating characteristic curve analyses, and immune infiltration was assessed.

Results: Six energy metabolism-related genes were identified. Enrichment analyses revealed their involvement in glycolysis, gluconeogenesis, lipid transport, bone remodeling, and glucagon secretion. Key differentially expressed genes included *CRH(Corticotropin-Releasing Hormone)*, *LEP (Leptin)*, *PDK4(Pyruvate Dehydrogenase Kinase Isozyme 4)*, *SPP1(Secreted Phosphoprotein 1)*, *and SST(Somatostatin)*. *PDK4* exhibited moderate accuracy in receiver operating characteristic analysis. Immune infiltration analysis indicated significant differences between preeclampsia and control samples. qRT-PCR confirmed *LEP* and *CRH* increased, while *SPP1* expression in preeclampsia samples.

Conclusion: Dysregulated energy metabolism-related genes may contribute to preeclampsia through metabolic and immune changes. Identifying these genes aids in understanding preeclampsia's molecular basis and early diagnosis. Future studies should validate these markers in larger cohorts and explore targeted treatments.

KEYWORDS

preeclampsia, energy metabolism, gene expression, biomarkers, immune infiltration

1 Introduction

Preeclampsia (PE) is a complex condition that affects various bodily systems and occurs in 2%–8% of pregnancies worldwide. It continues to be a significant cause of maternal and fetal morbidity and mortality (1). It is believed that PE is responsible for approximately 76,000 maternal and 500,000 fetal fatalities annually (2). It is a pregnancy-related disease that usually occurs after 20 weeks of gestation, characterized by high blood pressure and proteinuria. According to the definition of the World Health Organization, PE refers to a pregnant woman with a blood pressure ≥140/90 mmHg in the later stages of pregnancy and urine containing ≥300 milligrams of protein. It poses significant health hazards, including the potential onset of eclampsia, hemolysis, elevated liver enzymes, and low platelet count (HELLP) syndrome, and enduring cardiovascular issues (3). The pathophysiological mechanism of PE is intricate, encompassing various factors such as placental insufficiency, vascular endothelial dysfunction, and immune dysregulation. Research has demonstrated that in a normal pregnancy, the placenta releases specific signaling molecules to facilitate maternal blood vessel dilation and increased blood flow to accommodate the fetal growth requirements. However, in individuals with PE, there is often inhibition of placental development and function, resulting in damage to endothelial cells and a systemic inflammatory response, ultimately leading to elevated blood pressure and other complications (4). Despite advancements in prenatal care, the primary method for diagnosing PE is to monitor blood pressure and protein levels in the urine. The clinical physician also takes into consideration other potential symptoms, such as cephalalgia, visual impairments, epigastric discomfort, and renal function irregularities. The presence of these symptoms is typically associated with the severity of the condition and holds prognostic significance. Treatment includes using antihypertensive drugs to control the mother's blood pressure and early low-dose aspirin and calcium supplements to reduce the risk of developing PE. In severe cases, termination of pregnancy is frequently required; however, this generally results in premature birth. Although these interventions are necessary, treatment options for PE are significantly limited, focusing primarily on symptom management rather than addressing the underlying cause of the condition (5). Current treatments have potential limitations, including side effects from antihypertensive drugs and early delivery-associated risks, emphasizing the importance of improving our understanding of PE management strategies.

The disruption of metabolism and metabolites in PE pathogenesis is becoming an essential component of the disease pathophysiology. Studies have reported that carbohydrate and lipid metabolism abnormalities are essential in the etiology and clinical progression of PE (6, 7). Previous studies have indicated a connection between the diverse expression of energy metabolism-related genes (EMRGs) and the emergence of several pregnancy complications, including gestational diabetes mellitus and fetal obesity. This suggests that these conditions can have a common pathophysiological foundation and can be potential targets for treatment (8). Furthermore, differential expression of EMRGs has been associated with altered mitochondrial function and oxidative stress (9), which are characteristic features of the placental pathology in PE (10). Despite the preceding insights, there are significant gaps in understanding the complex energy metabolic pathways and their interactions in PE pathogenesis.

A comprehensive comprehension of the pathogenesis, biomarkers, and associated complications of PE is imperative for enhancing early diagnosis and treatment efficacy. Our study aimed to identify and analyze EMR differentially expressed genes (DEGs) in PE and determine their functional significance. Using bioinformatics methods, including data collection, differential gene expression analysis, functional pathway enrichment, protein-protein interaction (PPI) network creation, regulatory network visualization, and immune infiltration assessment, we provide a new perspective on molecular alterations in PE. This integrated genomic and bioinformatics approach aims to develop novel diagnostic markers and therapeutic targets, increasing our understanding of the molecular foundation underlying PE and aiding in personalized medical strategies to mitigate its impact on mothers and offspring.

2 Materials and methods

2.1 Data download

The gene expression omnibus (GEO) database (11) (https://www.ncbi.nlm.nih.gov/geo/) provided the PE datasets GSE60438 (12) and GSE75010 (13–18), which were retrieved using the R package "GEOquery". Dataset GSE60438 was derived from *Homo sapiens*, originating from decidua basalis tissue, with chip platforms GPL10558 and GPL6884. Dataset GSE75010 was derived from *Homo sapiens* placental tissues using the chip platform GPL6244. Detailed information is provided in Table 1. Additionally, dataset GSE60438 contained 42 control and 35 PE samples on the GPL10558 platform and 23 control and 25 PE samples on the

TABLE 1 GEO Microarray Chip Information.

	GSE60438	GSE60438	GSE75010
Platform	GPL10558	GPL6884	GPL6244
Species	Homo sapiens	Homo sapiens	Homo sapiens
Tissue	Decidua Basalis	Decidua Basalis	Placenta
Samples in PE group	35	25	80
Samples in Control group	42	23	77
Reference	PMID: 26010865	PMID: 26010865	PMID: 27160201; PMID: 28962696; PMID: 29187609; PMID: 29507646; PMID: 30278173; PMID: 30312585

GEO, Gene Expression Omnibus; PE, Preeclampsia.

GPL6884 platform. Dataset GSE75010 comprised 77 control and 80 PE samples. Following batch correction, the combined data from both GPL platforms in dataset GSE60438 were included in the study, whereas dataset GSE75010 was used as a validation set.

We obtained EMRGs from the GeneCards database (19). The GeneCards database provides extensive provides on genes in the human body. After conducting a search using the term "Energy Metabolism" and filtering for "Protein Coding" and "Relevance Score > 2" EMRGs, 571 EMRGs were obtained. Furthermore, using "Energy Metabolism" as the keyword in PubMed, 8 EMRGs were found in the published literature (20). Following the combination and elimination of duplicates, 573 EMRGs were identified, with detailed information presented in Supplementary Table S1.

The "sva" (21) package in R was used to correct batch effects in data from two GPL platforms (GPL10558 and GPL6884) to obtain the merged GEO dataset (combined datasets). The combined datasets included 65 control and 60 PE samples. Finally, the annotation and standardization of the merged datasets were performed using the R software package "limma" (22). To determine the impact of the batch effect, we performed a principal component analysis (PCA) (23) on the expression matrix before and following its removal.

2.2 Energy metabolism-related differentially expressed genes in PE

The "limma" R package was used to analyze the differences in gene expression between PE and control groups. To identify the DEGs, criteria of |log fold change(logFC)| > 0.5 and a $p < 0.05$ were set. Additionally, genes with a logFC > 0.5 and a $p < 0.05$ were classified as upregulated DEGs. Conversely, genes with a logFC < -0.5 and a $p < 0.05$ were identified as downregulated DEGs. The differential analysis results were depicted using the volcano plot feature provided by the "ggplot2" package in R.

We combined datasets to identify EMRGs that were differentially expressed in association with PE. We determined variance to identify genes exhibiting significant differences (|logFC| > 0.5 and $p < 0.05$). Venn diagrams were used to map the intersection of the DEGs and EMRGs, enabling the identification of EMRDEGs. We generated a heatmap with the R package "pheatmap". Furthermore, we constructed a chromosome localization map using the R package "RCircos" (24).

2.3 Enrichment analysis using gene ontology and the Kyoto encyclopedia of genes and genomes

GO (25) analysis is a widely used methodology for in-depth investigations aimed to improve functionality across multiple dimensions, including biological process (BP), cellular component (CC), and molecular function (MF). The KEGG (26) database is an extensive resource for deciphering the intricate functions and uses of biological systems by connecting genetic information with biochemical pathways and cellular activities. We employed the R package "clusterProfiler" (27) to perform GO and KEGG enrichment analyses on the EMRDEGs. The parameters established for including genes were an adjusted p-value (adj. p) < 0.05 and a false discovery rate (FDR) < 0.05, both of which were considered statistically significant. The Benjamini–Hochberg (BH) procedure was used as a p-value adjustment method.

2.4 Gene set enrichment analysis

GSEA (28) is a statistical technique to determine if predefined gene groups exhibit significant enrichment across various biological conditions. In this study, the genes of combined datasets were first sorted according to logFC values. Then, GSEA was performed on the entire set of genes from the merged datasets, using the "clusterProfiler" package in R. GSEA settings were accessing the "c2.cp.all.v2022.1.Hs.symbols.gmt [All Canonical Pathways] (3050)" gene set from the Molecular Signatures database (29), using 2022 seeds, performing 1000 calculations, with each gene set containing between 10 and 500 genes. The evaluation standards were established as adj. $p < 0.05$ and FDR (q-value) < 0.05 via the BH method for p-value adjustment.

2.5 Analysis of PPI and identification of key genes

The PPI network includes essential proteins involved in numerous biological functions, including signaling pathways, gene expression regulation, metabolism of energy and substances, and cell cycle management. This network is crucial for comprehending protein functionalities, signaling mechanisms, and physiological and pathological functional associations. The search tool for the retrieval of interacting genes/proteins (STRING) database (30) (https://cn.string-db.org/) investigates the connections among identified and anticipated proteins. This study used the STRING database to build a PPI network associated with EMRDEGs, adhering to the criteria of a minimum interaction coefficient exceeding 0.400, which corresponded to a medium confidence level. The associated regions within the PPI network could indicate molecular assemblies with distinct biological roles. Certain genes were identified as key genes within the PPI network as a result of their interactions with other genes.

The GeneMANIA database (31) (https://genemania.org/) was used to predict potential gene functions, evaluate gene lists, and pinpoint genes for further functional analyses. When provided with a list of query genes, GeneMANIA identifies functionally similar genes by analyzing a comprehensive genomics and proteomics dataset. It assigns weights to each functional genomic dataset based on the anticipated value of the query in this process. Besides, GeneMANIA can predict gene functions by identifying genes likely to share tasks with a given query gene based on their interactions. Using the GeneMANIA online website, the PPI network was created to predict genes with functions similar to those of key genes.

2.6 Construction of regulatory network

Gene expression is regulated by transcription factors (TFs) through their interaction with crucial genes during the post-transcriptional phase. We used the ChIPBase database (http://rna.sysu.edu.cn/chipbase/) (32) to obtain data on TFs and determine their control over essential genes. The screening criterion for mRNA-TF interaction pairs was based on the total number of upstream and downstream samples, which was required to be > 5. Finally, the mRNA-TF regulatory network was developed using Cytoscape software.

The role of miRNA in regulation is vital for developmental and evolutionary mechanisms in organisms. Different target genes could be regulated, and several miRNAs could influence a single target gene. To investigate the association between pivotal genes and miRNA, we retrieved the miRNA that interacted with key genes from the encyclopedia of RNA interactomes (ENCORI) database (https://rnasysu.com/encori/) (33). We used a screening threshold of pancancerNum > 5 to select mRNA-miRNA interaction pairs. The interaction network between mRNA and miRNA was illustrated using Cytoscape software.

Furthermore, RNA-binding proteins (RBPs) control gene expression by engaging with crucial mRNAs after transcription. We used the ENCORI database to extract RBP information and analyze their regulation of key mRNAs.The criterion for screening mRNA-RBP interaction pairs was clusterNum >1. Ultimately, Cytoscape software was used to visualize the constructed mRNA-RBP regulatory network.

2.7 Validation of differential gene expression and analysis of key genes using receiver operating characteristic curves

To analyze the variation in key gene expression between the PE and control groups within the combined datasets, we used the Mann–Whitney U test. Comparative maps were constructed based on the expression levels of these essential genes. Subsequently, the R package "pROC" (34) was used to generate the ROC curve for the significant genes. The area under the curve (AUC) evaluated the effectiveness of gene expression in diagnosing PE. The validation process was performed using the GSE75010 dataset.

2.8 Immune infiltration analysis

We measured the proportion of immune cell infiltration using single-sample (ss) GSEA (35). The recognized categories of immune cells comprised activated CD8 + T cells, activated dendritic cells, gamma-delta T cells, natural killer (NK) cells, regulatory T cells (Tregs), and several other human immune cell subtypes. The proportion calculated through ssGSEA was used to illustrate the relative levels of immune cell infiltration in each sample, creating an immune cell infiltration matrix. Then, immune cells indicating significant variations between the two groups were selected for additional analysis, and their relationships were evaluated using the Spearman method. Correlation heatmaps were created with the R package "pheatmap" to demonstrate the correlation between immune cells. The Spearman method determined the relationship between crucial genes and immune cells, with a significance threshold set at $p < 0.05$. Using the R package "ggplot2", a bubble map was drawn to illustrate the connection between essential genes and immune cells. We selected immune cells with top1 positive and top1 negative correlation with key genes and plotted correlation scatter plots using ggplot2.

2.9 Patient and tissue samples

Placenta samples were obtained from 52 pregnant women who underwent cesarean sections at the Third Affiliated Hospital of Wenzhou Medical University. 26 had PE, and 26 were healthy controls matched for gestational age. Each group included 14 term pregnancy and 12 preterm pregnancies. Ethical approval was obtained from the Research Ethics Committee at the Ruian People's Hospital, under approval number YJ2024130. All participants provided written consent. The inclusion criteria for the PE group included blood pressure ≥ 140/90 mmHg and 24-h urinary protein ≥ 0.3 g/24 h after 20 weeks of gestation, age between 20 and 40 years old, and no significant abnormalities during pregnancy. Exclusion criteria included other pregnancy complications such as gestational diabetes mellitus; Prepregnancy comorbidities such as prepregnancy hypertension, prepregnancy diabetes, serious medical and surgical diseases, infectious diseases such as COVID-19, obstetric complications, congenital diseases of the fetus, or the use of drugs that may affect the results of the experiment. After delivery, a tissue sample was extracted from the central region of the placenta and preserved at −80°C for long-term storage.

2.10 Isolation of RNA and analysis using quantitative real-time-polymerase chain reaction

Total RNA was extracted from placental tissue samples using the tissue total RNA isolation kit V2 (Vazyme) according to the manufacturer's instructions. The concentration and purity of the extracted RNA were assessed using a NanoDrop spectrophotometer (Thermo Fisher Scientific). RNA samples with an A260/A280 ratio between 1.8 and 2.0 were considered suitable for further analysis. Subsequently, 1 μg of total RNA was reverse transcribed into complementary DNA (cDNA) using the HiScript III All-in-one RT SuperMix (Vazyme) in a 20 μL reaction volume. The reverse transcription reaction was performed at 25°C for 5 minutes, followed by 50°C for 15 minutes, and terminated by heating at 85°C for 5 minutes. Quantitative real-time PCR (qRT-PCR) was conducted using the CFX Connect real-time PCR system (BioRad, Hercules, CA, USA) with Taq Pro Universal SYBR qPCR Master Mix (Vazyme). Each qRT-PCR reaction was carried out in a 10 μL volume containing 5 μL of SYBR Green Master Mix, 0.5 μL of each forward and reverse primer (10 μM), 1 μL of cDNA template, and 3

μL of nuclease-free water. The thermal cycling conditions were as follows: initial denaturation at 95°C for 30 seconds, followed by 40 cycles of denaturation at 95°C for 10 seconds, annealing at 60°C for 30 seconds, and extension at 72°C for 30 seconds. A melt curve analysis was performed to verify the specificity of the amplification products. The relative expression levels of the key genes were normalized to the expression of the housekeeping gene glyceraldehyde-3-phosphate dehydrogenase (GAPDH) using the $2^{-\Delta\Delta Ct}$ method. All reactions were performed in triplicate, and the average Ct values were used for analysis. The results were expressed as fold changes in gene expression relative to the control group.

2.11 Isolation of protein and analysis using Western Blotting

Tissues were minced and homogenized in RIPA lysis buffer (P0013B, Beyotime) with PMSF (100 mM, ST506, Beyotime), using 150-250 μL of lysis buffer per 20 mg of tissue. The homogenates were centrifuged similarly to obtain the supernatant. Protein concentration was determined using the BCA protein assay kit. Samples were diluted to equal concentrations with RIPA lysis buffer containing PMSF and mixed with 5× protein loading buffer. The samples were denatured by heating at 100°C for 5-10 minutes and then cooled on ice. SDS-PAGE was performed using self-prepared gels by first casting the separating and stacking gels between clean glass plates. The samples were then loaded into the wells formed by the comb in the stacking gel, and electrophoresis was conducted to separate proteins based on their molecular weight. Proteins were transferred to PVDF membranes (ISEQ00010, Millipore) using a wet transfer system (Mini Trans-Blot, BIO-RAD). The membranes were blocked with non-fat milk blocking solution for 1-2 hours at room temperature and incubated overnight at 4°C with primary antibodies diluted in antibody dilution buffer (P0256-500ml, Beyotime). After washing, the membranes were incubated with HRP-conjugated secondary antibodies for 1 hour at room temperature. The protein bands were visualized by using BeyoECL Plus working solution (P0018S, Beyotime) and detected with a chemiluminescence imaging system. The relative expression levels of proteins were analyzed by Image J.

2.12 Statistical analysis

The study used R software (version 4.3.1) for statistical analysis and data handling. The independent student t-test was implemented to assess the statistical significance of normally distributed data and compare continuous variables between two groups unless otherwise specified. For non-normally distributed variables, the Mann–Whitney U or Wilcoxon rank sum test was used to determine differences. Furthermore, the Kruskal–Wallis test was applied to compare outcomes among three or more groups. Spearman's rank correlation was used to determine the correlation coefficients for several molecules without particular specifications. All statistical analyses used two-tailed *p*-values, with a significance level set at $p < 0.05$.

3 Results

3.1 Analytical flow diagram

Figure 1 displays the technical approach of the study, providing a concise overview of the analytical processes used in this study.It begins with the combination of datasets GSE60438 (GPL10558 and GPL6884) and proceeds with the identification of differentially expressed genes (DEGs). Energy metabolism-related genes (EMRGs) are intersected with DEGs to identify energy metabolism-related differentially expressed genes (EMRDEGs). The subsequent enrichment analyses include Gene Set Enrichment Analysis (GSEA), Gene Ontology (GO), and Kyoto Encyclopedia of Genes and Genomes (KEGG) enrichment. A protein-protein interaction (PPI) network is constructed to identify key genes, which are further analyzed for immune infiltration. Key genes are validated using the GSE75010 dataset through the Wilcoxon Rank Sum Test and Receiver Operating Characteristic (ROC) analysis. Finally, regulatory networks involving mRNA-TF, mRNA-miRNA, and mRNA-RBP interactions are constructed to understand the regulatory mechanisms.

3.2 Merging of PE datasets

To eliminate batch effects from the PE datasets GSE60438 (using GPL10558 and GPL6884 platforms), the R package "sva" was used, resulting in combined datasets. Boxplots (Figures 2A, B) were used to compare the expression values of the datasets pre- and post-batch effect removal. Furthermore, a PCA plot (Figures 2C, D) compared the distribution of low-dimensional features in the dataset before and after addressing batch effects. The outcomes from the distribution box plot and PCA plot indicated that the batch effect in the PE dataset samples was significantly reduced after batch correction.

3.3 Genes with altered expression associated with energy metabolism in PE

The data from the combined datasets were separated into PE and control groups. We performed a comparative analysis of gene expression levels between PE and control groups across the combined datasets using the R package "limma". The findings identified 55 genes with differential expression, satisfying the criteria of $|logFC| > 0.5$ and a $p < 0.05$ in the combined datasets. Out of these DEGs, 15 indicated increased expression ($logFC > 0.5$, $p < 0.05$), whereas 40 exhibited decreased expression ($logFC < -0.5$, $p < 0.05$), which was illustrated in the volcano plot analysis of the dataset (Figure 3A).

To identify genes that exhibited differential expression and were associated with energy metabolism, we selected genes with $|logFC| > 0.5$ and a $p < 0.05$ from the overlap of DEGs and EMRGs (Figure 3B). Six EMRDEGs, including *CRH*, *IRX3(Iroquois Homeobox 3)*, *LEP*, *PDK4*,

10.3389/fimmu.2025.1496046

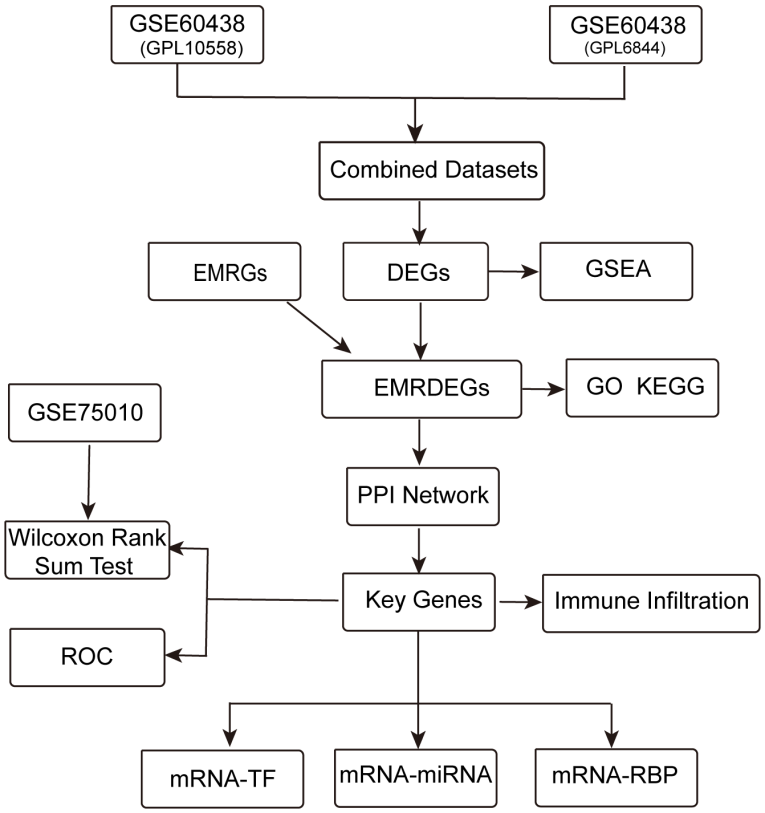

FIGURE 1
Technology roadmap. DEGs, Differentially Expressed Genes; EMRGs, Energy Metabolism-Related Genes. EMRDEGs, Energy Metabolism-Related Differentially Expressed Genes; GO, Gene Ontology; KEGG, Kyoto Encyclopedia of Genes and Genomes; GSEA, Gene Set Enrichment Analysis; ROC, Receiver Operating Characteristic Curve; PPI Network, Protein-protein Interaction Network; TF, Transcription Factor; RBP, RNA-Binding Protein.

SPP1, and *SST*, were identified (Table 2). The variations in the expression of identified EMRDEGs among different sample groups in the combined datasets were investigated through the intersection results. The analysis results were visualized in a heatmap created with the "pheatmap" package in R (Figure 3C). Besides, the R package "RCircos" was used to plot the positions of these six EMRDEGs on human chromosomes and constructed a chromosome localization map (Figure 3D). The mapping revealed that most of these EMRDEGs were located on chromosome 7, particularly *LEP* and *PDK4*.

3.4 Enrichment analysis using GO and KEGG

We employed GO and KEGG enrichment analyses to investigate the association between BP, CC, MF, and biological pathways (KEGG) of six EMRDEGs and PE. The six EMRDEGs underwent GO and KEGG enrichment analyses (Table 3). The results indicated that the six EMRDEGs were primarily involved in several BP, including cell lipid export, regulation of bone remodeling, tissue and bone restructuring, and glucagon release. Furthermore, they were associated with CC, neuronal cell bodies, and MFs related to hormone activity, receptor signaling activation, peptide hormone receptor binding, neuropeptide hormone activity, and other hormone receptor interactions. Additionally, the biological pathway associated with neuroactive ligand-receptor interaction (KEGG) exhibited an increase. The findings from GO and KEGG enrichment analyses were presented using bar graphs (Figure 4A).

Following GO and KEGG enrichment analyses, BP, CC, MF, and biological pathways (KEGG) were schematically presented (Figures 4B–E). The connections display the molecules corresponding to the entries, with annotations for each. The magnitude of the nodes indicates the quantity of molecules present in each record.

3.5 GSEA

We conducted GSEA to determine how gene expression levels across the combined datasets influenced PE and to identify the associated BPs. The relationship between affected CCs and performed MFs is depicted in Figure 5A, with specific results provided in Table 4. The findings indicated that all genes in the combined datasets were significantly enriched in glycolysis and gluconeogenesis (Figure 5B), faerie-mediated Ca^{2+} mobilization (Figure 5C), NK cell-mediated cytotoxicity (Figure 5D), interleukin (IL) 10 signaling (Figure 5E), IL12 pathway (Figure 5F), an overview of proinflammatory and profibrotic mediators (Figure 5G), neutrophil degranulation (Figure 5H), and other biologically related functions and signaling pathways.

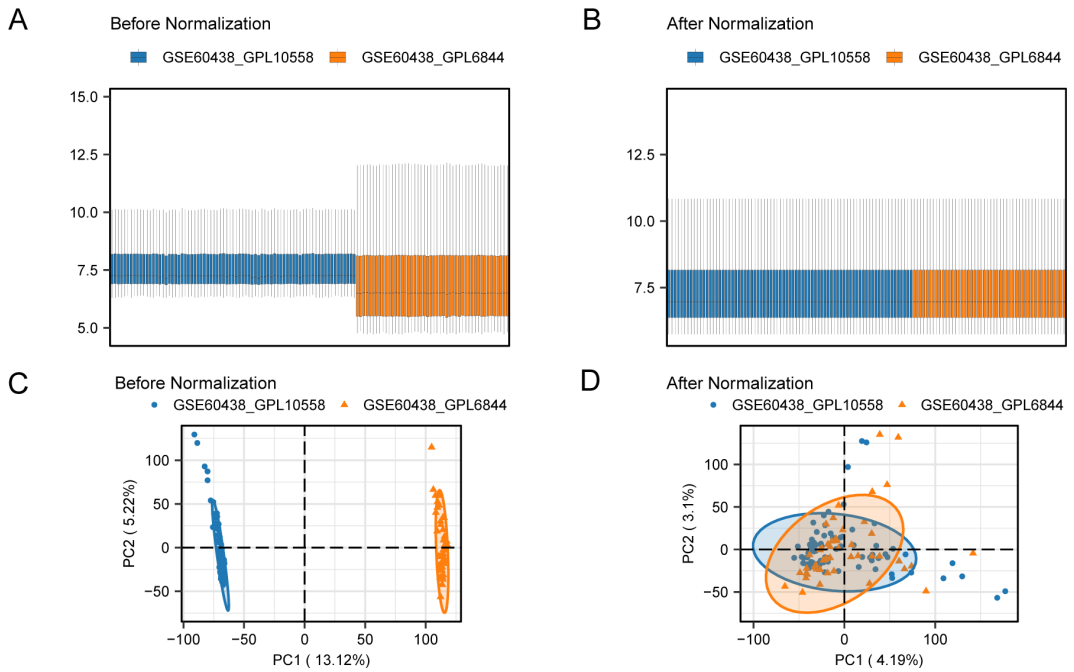

FIGURE 2
Batch effects removal of GSE60438 (GPL10558, GPL6884). **(A)** Boxplots of combined datasets distribution before batch removal. **(B)** Post-batch integrated combined datasets distribution boxplots. **(C)** PCA plot of the datasets before debatching. **(D)** Go to the PCA map of the combined datasets after batch processing. PCA, Principal Component Analysis; PE, Preeclampsia. The PE dataset GSE60438 (GPL10558 platform) is blue, and the PE dataset GSE60438 (GPL6884 platform) is orange.

3.6 PPI network

PPI interaction analysis was performed, and the PPI network of six EMRDEGs was constructed using the STRING database (Figure 6A). The PPI network findings indicated a connection among five EMRDEGs: *CRH*, *LEP*, *PDK4*, *SPP1*, and *SST*. Furthermore, the interaction network of five EMRDEGs and their functionally similar genes (Figure 6B) was predicted and constructed using the GeneMANIA website. The colored lines represent their co-expression and share protein domains and other information. Among them, there were 5 EMRDEGs and 20 functionally similar proteins.

3.7 Construction of regulatory network

We constructed the mRNA-TF regulatory network, which included five key genes (*CRH*, *LEP*, *PDK4*, *SPP1*, and *SST*) and 39 TFs, resulting in 51 mRNA-TF interactions (Figure 7A). Detailed information is provided in Supplementary Table S2. The mRNA-miRNA regulatory network consisted of two key genes (*PDK4* and *SPP1*) and 56 miRNAs, resulting in 59 mRNA-miRNA interactions (Figure 7B). Detailed data is presented in Supplementary Table S3. Our derived mRNA-RBP network included three key genes (*LEP*, *PDK4*, and *SPP1*) and 30 RBP molecules, resulting in 32 mRNA-RBP interactions (Figure 7C). Detailed data is provided be found in Supplementary Table S4.

3.8 Validation of differential gene expression and analysis of key genes using ROC curves

To investigate the key genes (*CRH*, *LEP*, *PDK4*, *SPP1*, and *SST*) across the combined datasets, a comparative analysis was performed through a group comparison (Figure 8A), indicating the outcomes of the differential expression analysis for these five key genes in PE samples compared with control samples from the combined datasets. The findings from the differential analysis (Figure 8A) indicated that two crucial genes (*PDK4* and *SPP1*) exhibited a significant statistical difference ($p < 0.001$) in both PE and control groups across the combined datasets. Furthermore, *SST* demonstrated a statistical significance ($p < 0.01$) across both types of samples. The other two crucial genes (*CRH* and *LEP*) exhibited significant expression in both PE and control groups, with a $p < 0.05$. Moreover, the expression levels of crucial genes in combined datasets were evaluated by creating ROC curves with the "pROC" package in R. The ROC curve (Figures 8B–F) revealed that the expression levels of key genes, including *PDK4* in PE samples, exhibited moderate to high accuracy across different groups (AUC: 0.7–0.9). The expression levels of crucial genes (*CRH*, *LEP*, *SPP1*, and *SST*) in PE samples demonstrated low precision across various groups (AUC: 0.5–0.7). The ROC curves for key genes in dataset GSE75010 (Figures 8G–K) revealed that the expression levels of *CRH* and *LEP* in PE samples demonstrated moderate to high precision among various groups (AUC between 0.7 and 0.9).

10.3389/fimmu.2025.1496046

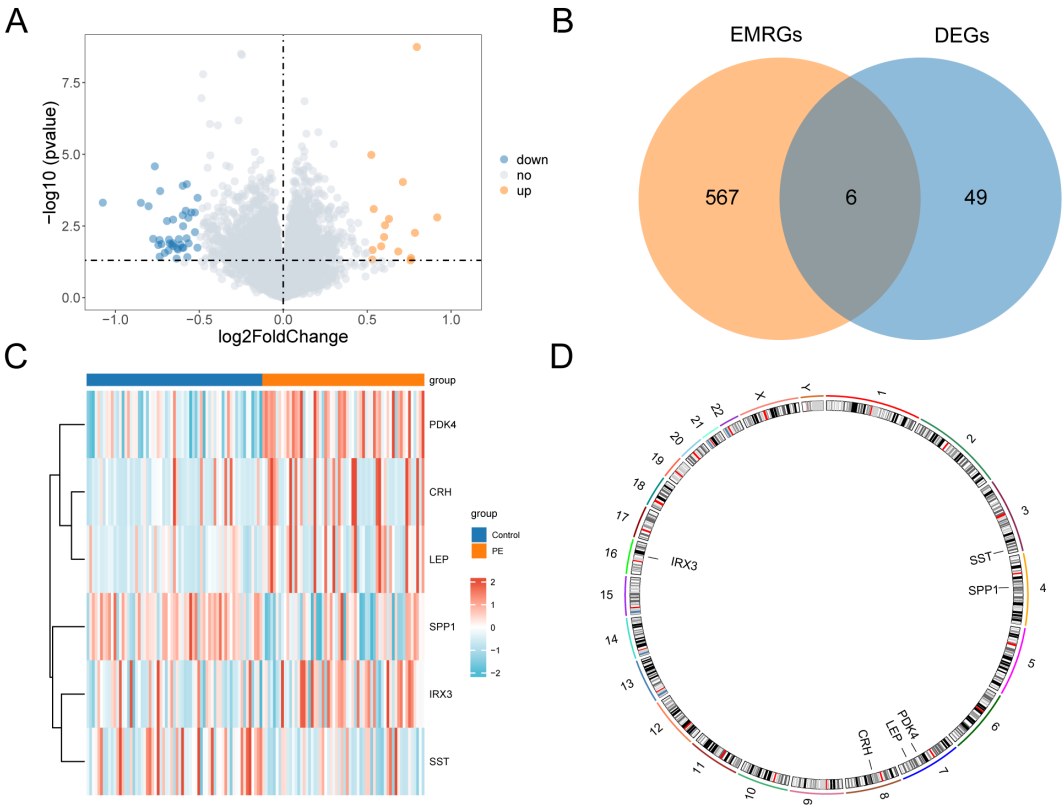

FIGURE 3
Differential gene expression analysis. **(A)** Volcano plot of differentially expressed genes analysis between PE and Control groups in combined datasets. **(B)** DEGs and EMRGs Venn diagram in the combined datasets. **(C)** Heat map of EMRDEGs in the combined datasets. **(D)** Chromosomal mapping of EMRDEGs; DEGs, Differentially Expressed Genes; EMRGs, Energy Metabolism Related Genes; EMRDEGs, Energy Metabolism Related Differentially Expressed Genes. The orange is the PE group, and the blue is the Control group. The red in the heat map represents high expression, and the blue represents low expression.

Conversely, the expression levels of crucial genes (*PDK4*, *SPP1*, and *SST*) in PE samples demonstrated reduced precision across different groups (AUC: 0.5–0.7).

3.9 Immune infiltration analysis

The ssGSEA algorithm evaluated the presence of 28 types of immune cells using expression data from combined datasets. Immune cells were selected with a $p < 0.05$ using a comparative group plot. The differences in immune cell infiltration levels across various groups were observed. The comparative chart (Figure 9A) indicateds that 16 immune cell types, including activated CD4+ T cells, activated CD8+ T cells, activated dendritic cells, CD56bright NK cells, CD56dim NK cells, effector memory CD8+ T cells, eosinophils, gamma-delta T cells, immature B cells, macrophages, myeloid-derived suppressor cells (MDSCs), monocytes, plasmacytoid dendritic cells, Tregs, T follicular helper cells, and type 1 T helper cells, exhibited significant differences between PE and control samples ($p < 0.05$).The correlation results from the combined datasets (Figure 9B) exhibited the abundance of 16 different immune cell infiltrations in the immune infiltration study. The results revealed a significant correlation among immune cells. The correlation between 5 key genes and 16 immune cells was examined and visualized using a correlation bubble diagram (Figure 9C). The results indicated a significant

TABLE 2 Description of EMRDEGs.

ID	Description	logFC	AveExpr	t	*p*-value	B
CRH	Corticotropin Releasing Hormone	0.917196	7.729465	3.229391	0.001586	1.28882
PDK4	Pyruvate Dehydrogenase Kinase 4	0.795918	9.086324	6.492432	1.80 e-09	11.111
SPP1	Secreted Phosphoprotein 1	0.76471	12.14558	4.36649	2.62 e-05	2.371449
SST	Somatostatin	0.56438	7.620709	3.22046	0.001632	1.31405
LEP	Leptin	0.539052	7.895897	3.434848	0.000805	0.69233

EMRDEGs, Energy Metabolism-Related Differentially Expressed Genes.

10.3389/fimmu.2025.1496046

TABLE 3 Results of GO and KEGG enrichment analysis for EMRDEGs.

ONTOLOGY	ID	Description	GeneRatio	BgRatio	*p*-value	p.adjust	q-value
BP	GO: 0031667	response to nutrient levels	4/6	446/18800	4.5143 e-06	0.00037793	0.0001242
BP	GO: 0009991	response to extracellular stimulus	4/6	479/18800	5.9945 e-06	0.00038785	0.00012746
BP	GO: 0140353	lipid export from cell	3/6	43/18800	2.2184 e-07	0.00010706	3.5186 e-05
BP	GO: 0046850	regulation of bone remodeling	3/6	49/18800	3.3095 e-07	0.00010706	3.5186 e-05
BP	GO: 0034103	regulation of tissue remodeling	3/6	86/18800	1.8302 e-06	0.00031735	0.0001043
BP	GO: 0046849	bone remodeling	3/6	88/18800	1.962 e-06	0.00031735	0.0001043
BP	GO: 0032368	regulation of lipid transport	3/6	118/18800	4.7551 e-06	0.00037793	0.0001242
BP	GO: 0046887	positive regulation of hormone secretion	3/6	122/18800	5.2572 e-06	0.00037793	0.0001242
BP	GO: 0007584	response to nutrient	3/6	150/18800	9.7837 e-06	0.00057546	0.00018912
BP	GO: 1905952	regulation of lipid localization	3/6	155/18800	1.0796 e-05	0.00058206	0.00019129
BP	GO: 0048771	tissue remodeling	3/6	174/18800	1.527 e-05	0.00075997	0.00024976
BP	GO: 0007565	female pregnancy	3/6	185/18800	1.8347 e-05	0.00084791	0.00027866
BP	GO: 0070091	glucagon secretion	2/6	10/18800	3.8155 e-06	0.00037793	0.0001242
BP	GO: 0070092	regulation of glucagon secretion	2/6	10/18800	3.8155 e-06	0.00037793	0.0001242
CC	GO: 0043025	neuronal cell body	2/6	482/19594	0.00848281	0.02544843	0.01785855
MF	GO: 0048018	receptor ligand activity	4/6	489/18410	7.0699 e-06	3.2414 e-05	1.3123 e-05
MF	GO: 0030546	signaling receptor activator activity	4/6	496/18410	7.4802 e-06	3.2414 e-05	1.3123 e-05
MF	GO: 0005179	hormone activity	3/6	122/18410	5.5967 e-06	3.2414 e-05	1.3123 e-05
MF	GO: 0051428	peptide hormone receptor binding	1/6	19/18410	0.00617717	0.0200758	0.00812785
MF	GO: 0005184	neuropeptide hormone activity	1/6	30/18410	0.00973887	0.02250149	0.00910992
MF	GO: 0051427	hormone receptor binding	1/6	32/18410	0.0103853	0.02250149	0.00910992
MF	GO: 0050840	extracellular matrix binding	1/6	55/18410	0.01779409	0.03304617	0.01337902
KEGG	hsa04080	Neuroactive ligand-receptor interaction	3/5	362/8164	0.00080884	0.01617674	0.0119197

GO, Gene Ontology; BP, Biological Process; CC, Cellular Component; MF, Molecular Function; KEGG, Kyoto Encyclopedia of Genes and Genomes; EMRDEGs, Energy Metabolism-Related Differentially Expressed Genes.

positive correlation between *SPP1* and Tregs, with an r-value = 0.458 and a $p < 0.05$. The key gene *LEP* exhibited a significantly negative correlation with CD56dim NK cells (r-value = –0.359, $p < 0.05$). Finally, a correlation scatter plot demonstrated the relationship between top1 positive and top1 negative key genes and immune cells (Figures 9D, E).

3.10 Validation of key genes in PE

To determine the mRNA expression levels of five crucial genes in PE, qRT-PCR analysis was performed on 26 patients with PE and 26 placental samples of comparable gestational age. Table 5 presents the primer sequences. The clinical features of the patient are presented in Table 6. The two groups exhibited no significant variances in gestational age and birth weight. The PE group revealed higher systolic and diastolic blood pressure levels than the control group. The results of qRT-PCR indicated that, in contrast to the control group, the expressions of *LEP* and *CRH* in placental samples of PE patients were significantly elevated, while the expression level of *SPP1* was significantly reduced (Figures 10A–E). Through the Western blotting experiment, we further examined the protein expression levels of *LEP*, *CRH*, and *SPP1* (Figures 10F). The findings demonstrated that, compared with the control group, the expression of *LEP* and *CRH* proteins in placental samples of PE patients increased markedly, while the expression level of *SPP1* decreased conspicuously (Figures 10G–I).

4 Discussion

PE is a complicated disorder that impacts around 2%–8% of pregnancies globally and continues to be a major contributor to maternal and perinatal illness and death (36). PE occurs after the 20th week of pregnancy and is characterized by the sudden onset of high blood pressure and protein in the urine. PE can result in serious complications, including eclampsia, HELLP syndrome, and long-term cardiovascular risks for both the mother and child (37). The exact mechanisms underlying PE remain unclear; however, it is hypothesized that irregular placental growth and operation cause

10.3389/fimmu.2025.1496046

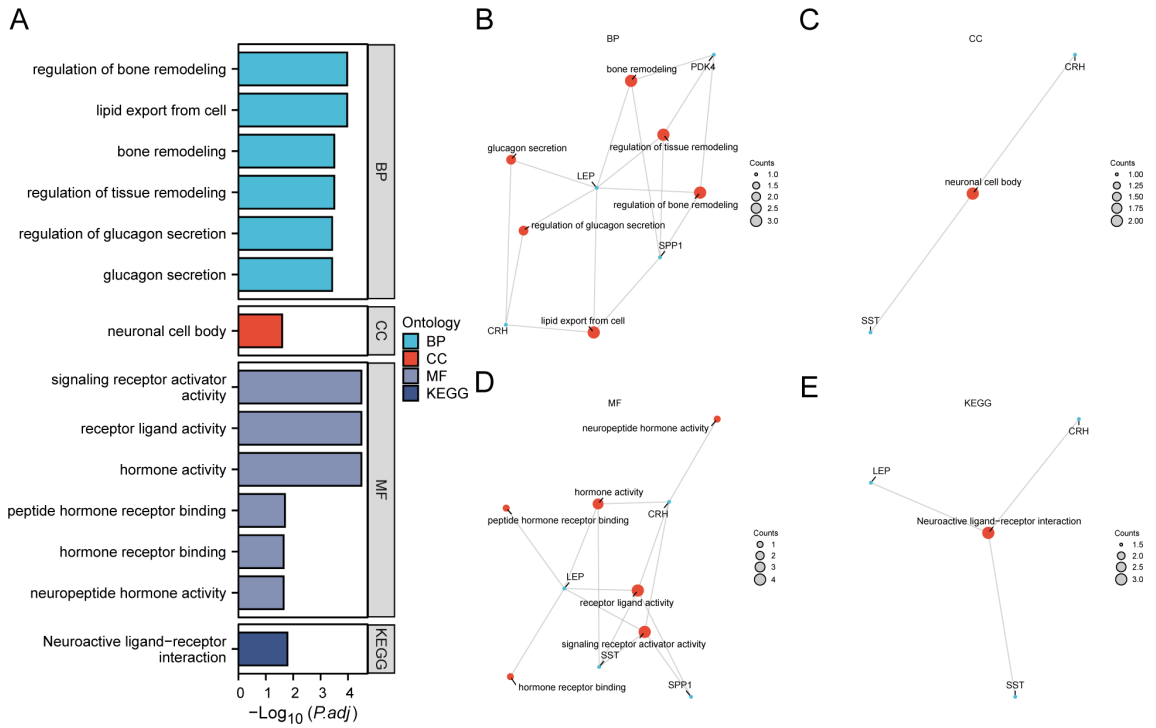

FIGURE 4
GO and KEGG enrichment analysis for EMRDEGs. **(A)** Bar graph of GO and KEGG enrichment analysis results of EMRDEGs: BP, CC, MF, and KEGG. GO terms and KEGG terms are indicated on the ordinate. B-E. GO and KEGG enrichment analysis results of EMRDEGs network diagram exhibiting BP **(B)**, CC **(C)**, MF **(D)**, and KEGG **(E)**. The orange nodes represent items, the blue nodes represent molecules, and the lines represent the relationship between items and molecules. EMRDEGs, Energy Metabolism-Related Differentially Expressed Genes; GO, Gene Ontology; KEGG, Kyoto Encyclopedia of Genes and Genomes; BP, Biological Process; CC, Cellular Component; MF, Molecular Function. The screening criteria for GO and KEGG enrichment analysis were adj. $p < 0.05$, and FDR value (q-value) < 0.05, and the p-value correction method was Benjamini-Hochberg (BH).

widespread inflammation and impairment of endothelial function (38). Current diagnostic approaches for PE primarily depend on blood pressure monitoring and urinalysis for proteinuria. Nevertheless, these methodologies are often nonspecific and can only detect the disease in its advanced stages, which leads to delayed intervention (39). Research into the underlying mechanisms of PE is imperative for the development of predictive biomarkers and effective therapeutic strategies, as it has a substantial health impact on pregnant women and their offspring.

Currently, the diagnosis of PE often relies on multiple biomarkers, with the most common being *soluble vascular endothelial growth factor receptor-1* (*sFlt-1*) and *placental growth factor* (*PlGF*). *sFlt-1* is an anti-angiogenic factor secreted by the placenta, with significantly elevated levels in PE patients, while *PlGF* is a factor that promotes blood vessel formation and generally exhibits decreased levels during PE. Research has demonstrated that the *sFlt-1*/*PlGF* ratio can serve as an effective indicator for assessing both the occurrence and severity of PE (40). By detecting this ratio, clinicians can identify PE at an early stage, thereby providing a foundation for timely intervention. However, despite their potential application in diagnosing PE, *sFlt-1* and *PlGF* possess limited accuracy and specificity. Firstly, these markers' levels are not only influenced by PE but may also be affected by other pregnancy-related factors such as gestational diabetes or placental abruption, leading to false positive or negative results. Furthermore, fluctuations in *sFlt-1* and *PlGF* levels throughout pregnancy may impact measurements at a single time point. Therefore, relying solely on these two biomarkers is insufficient for definitively diagnosing PE; integrating additional biomarkers may enhance diagnostic precision.

New developments in genomics and bioinformatics have created opportunities to understand the molecular foundations of diseases, including PE. By integrating phenotypic data with high-throughput molecular analyses, researchers can reveal novel biomarkers and therapeutic targets that can revolutionize PE management (41). Recent studies have suggested that alterations in EMRGs can contribute to PE pathogenesis by affecting placental function and maternal systemic response (42). This research direction holds the potential to improve our understanding of PE as well as identify novel diagnostic markers that can result in earlier detection and intervention, thereby improving outcomes for mothers and their offspring (43). Significant progress has been achieved; however, there is a crucial lack in our comprehension of the complex molecular mechanisms contributing to PE development. These gaps underscore the necessity for further investigation.

In this study, we have identified six EMRDEGs and observed their differential expression in patients with PE. These genes may reflect the metabolic and immune changes occurring in PE, offering novel diagnostic insights. Our findings underscore the significance of

10.3389/fimmu.2025.1496046

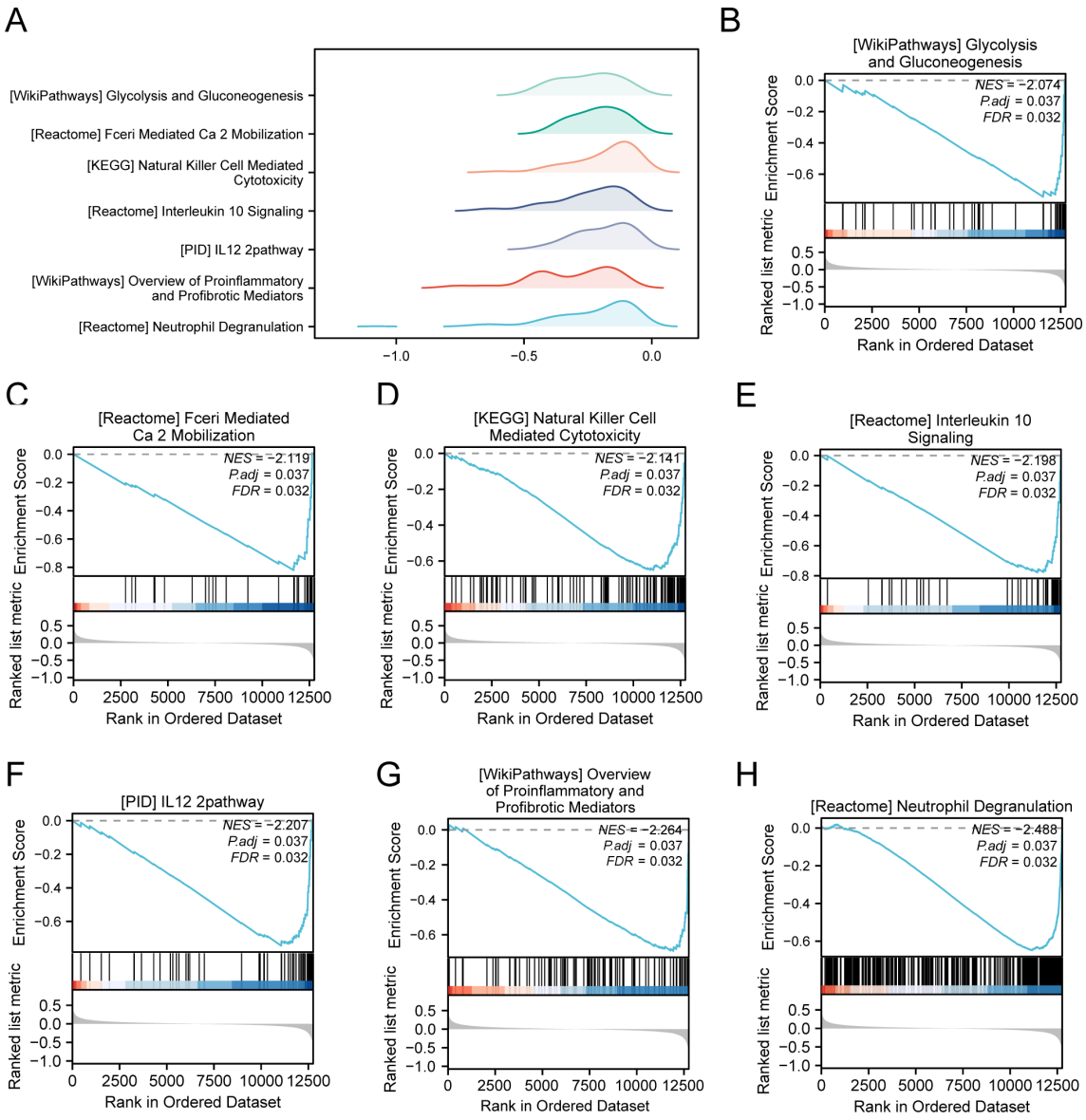

FIGURE 5
GSEA for combined datasets. **(A)** GSEA mountain map presentation of 7 biological functions of the combined datasets. B-h. GSEA revealed that EMRDEGs were significantly enriched in WP_GLYCOLYSIS_AND_GLUCONEOGENESIS **(B)**, REACTOME_FCERI_MEDIATED_CA_2_MOBILIZATION **(C)**, KEGG_NATURAL_KILLER_CELL_MEDIATED_CYTOTOXICITY **(D)**, Reactome_interleukin_10 signaling **(E)**, PID_IL12_2PATHWAY **(F)**, WP_OVERVIEW_OF_PROINFLAMMATORY_AND_PROFIBROTIC_MEDIATORS **(G)**, REACTOME_NEUTROPHIL_DEGRANULATION **(H)**. GSEA, Gene Set Enrichment Analysis; EMRDEGs, Energy Metabolism-Related Differentially Expressed Genes; The screening criteria of GSEA were adj. $p < 0.05$ and FDR value (q-value) < 0.05, and the p-value correction method was Benjamini-Hochberg (BH).

metabolic alterations in the pathogenesis of PE, a facet that has been underappreciated among existing biomarkers such as *sFlt-1* and *PlGF*. Furthermore, variations in EMRDEGs may offer new perspectives into the pathophysiological mechanisms underlying PE and complement ongoing efforts to identify early diagnostic markers.

Our findings indicated a significant upregulation of *LEP* in placental samples from patients with PE, suggesting that dysregulation of the *LEP* gene could contribute to the metabolic disturbances observed in PE. *LEP* emerged as a critical player among the DEGs. *LEP*, an adipose tissue-derived hormone, controls energy equilibrium and metabolic processes (44). Increased *LEP* levels have been associated with insulin resistance and inflammation (45), both of which are pertinent in the context of PE. Additionally, prior research has indicated the effect of *LEP* on regulating vascular function and its potential role in the onset of hypertension, a characteristic feature of PE (46). Consequently, the upregulation of *LEP* in PE can reflect an adaptive response to altered energy metabolism, consistent with our findings.

SPP1 is another key gene that exhibited significant downregulation in our analysis. *SPP1*, an osteopontin, plays a role in multiple biological activities, including cell adhesion, movement, and immune response regulation (47). Its expression is crucial for placental development and function. Its reduced expression in PE could impair trophoblast invasion and placental development,

TABLE 4 Results of GSEA for combined datasets.

ID	Set Size	Enrichment Score	NES	*p*-value	p adjust	q-value
REACTOME_NEUTROPHIL_DEGRANULATION	382	0.64867	2.48836	0.001495	0.036503	0.031576
WP_OVERVIEW_OF_PROINFLAMMATORY_AND_PROFIBROTIC_MEDIATORS	101	0.69267	2.26388	0.001709	0.036503	0.031576
PID_IL12_2PATHWAY	54	0.74499	2.20711	0.001862	0.036503	0.031576
REACTOME_INTERLEUKIN_10_SIGNALING	43	0.77819	2.19766	0.001873	0.036503	0.031576
KEGG_NATURAL_KILLER_CELL_MEDIATED_CYTOTOXICITY	103	0.6511	2.14121	0.001692	0.036503	0.031576
REACTOME_FCERI_MEDIATED_CA_2_MOBILIZATION	29	0.82047	2.11928	0.001946	0.036503	0.031576
WP_GLYCOLYSIS_AND_GLUCONEOGENESIS	40	0.74474	2.07394	0.001905	0.036503	0.031576
PID_IL12_STAT4_PATHWAY	31	0.77487	2.06097	0.001901	0.036503	0.031576
REACTOME_COSTIMULATION_BY_THE_CD28_FAMILY	58	0.65126	1.9598	0.001818	0.036503	0.031576
BIOCARTA_IL17_PATHWAY	13	0.8883	1.95493	0.002066	0.036503	0.031576
PID_IL8_CXCR2_PATHWAY	29	0.75551	1.95148	0.001946	0.036503	0.031576
PID_IL23_PATHWAY	35	0.70314	1.92153	0.001869	0.036503	0.031576
BIOCARTA_NO2IL12_PATHWAY	14	0.85133	1.91891	0.002024	0.036503	0.031576
REACTOME_SIGNALING_BY_INTERLEUKINS	394	0.49928	1.91331	0.001522	0.036503	0.031576
WP_IL1_AND_MEGAKARYOCYTES_IN_OBESITY	22	0.75449	1.86687	0.001931	0.036503	0.031576
REACTOME_MET_PROMOTES_CELL_MOTILITY	40	0.640364	1.8563	0.002096	0.036503	0.031576
REACTOME_GLYCOLYSIS	62	0.60937	1.85012	0.001812	0.036503	0.031576
PID_IL8_CXCR1_PATHWAY	23	0.73136	1.81709	0.001949	0.036503	0.031576
WP_IL3_SIGNALING_PATHWAY	48	0.6214	1.80337	0.001859	0.036503	0.031576
KEGG_FC_EPSILON_RI_SIGNALING_PATHWAY	71	0.57231	1.78336	0.001795	0.036503	0.031576
REACTOME_INTERLEUKIN_4_AND_INTERLEUKIN_13_SIGNALING	97	0.54652	1.77469	0.001721	0.036503	0.031576
REACTOME_GLUCOSE_METABOLISM	81	0.55491	1.7502	0.001808	0.036503	0.031576
WP_IL18_SIGNALING_PATHWAY	234	0.45265	1.64082	0.001616	0.036503	0.031576

GSEA, Gene Set Enrichment Analysis.

resulting in inadequate remodeling of maternal spiral arteries (48), which was validated by our study.

Furthermore, *CRH* was identified as a DEG in our study. *CRH* is an important neuropeptide whose secretion is regulated by a variety of factors, including physiological and environmental stress. Studies have shown that during pregnancy, the synthesis and secretion of *CRH* increases significantly, which is closely related to pregnancy-related physiological changes. In particular, during the second and third trimesters of pregnancy, the level of *CRH* in the maternal blood increases significantly, which may be due to the synthetic effects of the placenta. The placenta regulates the maternal immune response and endocrine system by producing *CRH*, and affects the blood flow and nutrient supply of the placenta, which may lead to placental dysfunction and hypertension [16]. Collectively, these findings improve our understanding of the molecular foundations of PE and open new avenues for targeted interventions to restore normal energy metabolism and placental function.

Our study identified several EMRGs that exhibited differential expression in PE, focusing on their involvement in glycolysis and gluconeogenesis pathways. Glycolysis and gluconeogenesis are critical metabolic pathways that regulate glucose homeostasis, providing energy and metabolic intermediates for various cellular processes. The dysregulation of these pathways can result in altered energy metabolism, a hallmark of PE.

Recent studies have suggested the importance of metabolic alterations in PE pathogenesis, demonstrating a shift towards glycolytic metabolism as a potential disease hallmark. Ackerman et al. observed a glycolytic change of placental tissues from cases of early-onset PE with or without fetal growth restriction, pointing to altered tissue bioenergetics (49). Hu et al. further reinforced the idea by examining exosomal mRNA and lncRNA profiles in cord blood and identifying the involvement of glycolysis and gluconeogenesis in developing PE (50). In line with our GSEA, which identified significant enrichment of the glycolysis and gluconeogenesis pathways in PE, this underscores the critical role of metabolic changes in the pathophysiology of diseases.

Moreover, the differential expression of EMRGs in PE suggested a broader impact on cellular energy metabolism and oxidative stress. Li

10.3389/fimmu.2025.1496046

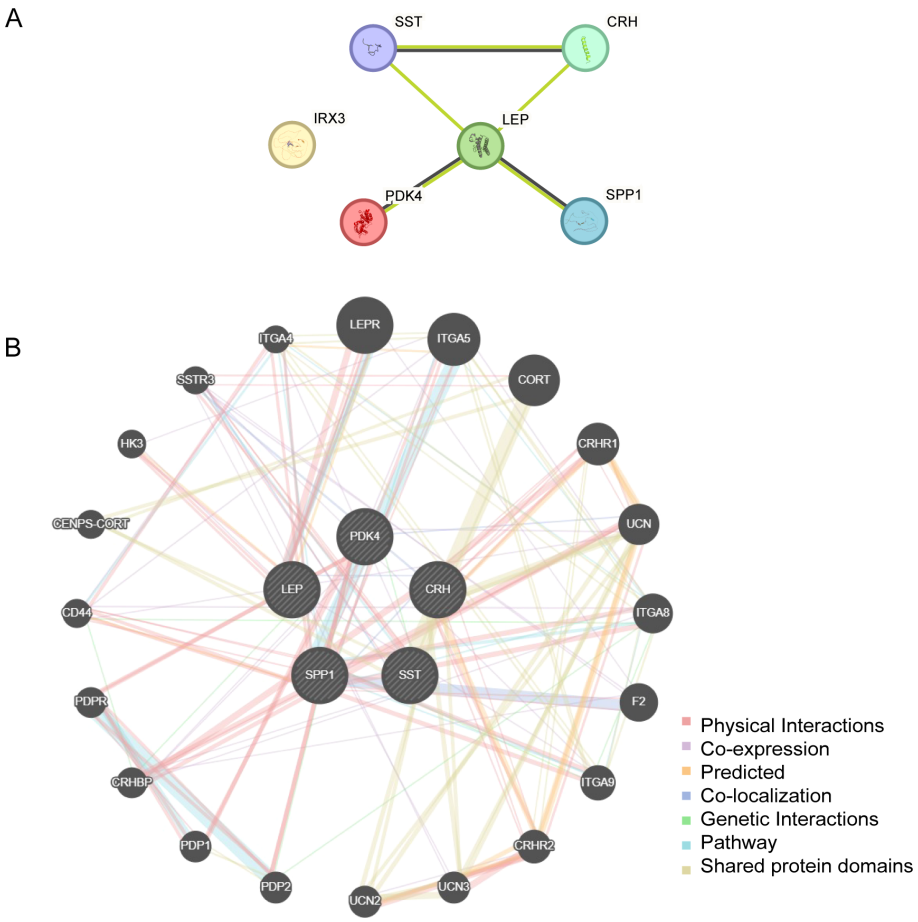

FIGURE 6
PPI network analysis. **(A)** PPI Network of EMRDEGs calculated from the STRING database. **(B)** The GeneMANIA website predicts the interaction network of functionally similar genes of EMRDEGs. The circles in the figure indicate the EMRDEGs and their functionally identical genes, and the corresponding colors of the lines represent the interconnected functions. PPI, Protein-protein Interaction; EMRDEGs, Energy Metabolism-Related Differentially Expressed Genes.

et al. identified key proteins associated with glycolysis/gluconeogenesis and oxidative phosphorylation in syncytiotrophoblast extracellular vesicles from patients with early-onset severe PE, further supporting the role of disrupted energy metabolism in the condition (51). Furthermore,Tong et al. found that genes involved in glycolysis/gluconeogenesis were significantly inhibited in the decidua of severe PE, indicating impaired energy metabolism at the maternal-fetal interface (52).

Meanwhile, GO and KEGG analyses in the study highlighted crucial roles in lipid metabolism, hormone function, and bone remodeling. The varying expression levels of genes, including *CRH*, *LEP*, *PDK4*, *SPP1*, and *SST*, provided evidence for possible biomarkers and treatment targets. The alteration in *LEP* levels, known for regulating energy homeostasis, underscored the complex interplay of metabolic disruptions in PE. Furthermore, creating networks for protein interactions and regulatory frameworks involving TFs, miRNAs, and RBPs provided a deeper insight into the molecular interactions and regulatory processes in PE. The findings highlighted the complexity of gene regulation and the potential for targeted therapeutic interventions.

The immune landscape in PE is characterized by a complex interplay of altered innate and adaptive immune responses, which is crucial for understanding disease pathogenesis. Zhou et al. identified shifts in NK cell gene expression and an increase in Tregs in PE via single-cell RNA sequencing, suggesting a response to counteract the inflammatory state of PE (53). Han et al.'s employed mass cytometry to analyze maternal blood and depicted immune feature shifts that predicted PE, with early pregnancy marked by a proinflammatory response and diminished Treg signaling, highlighting the role of early immune dysregulation in PE (54). Furthermore, Luo et al.focused on the dysfunction of NK cells and macrophages, demonstrating that aberrant human leukocyte antigen (HLA) molecule expression by extravillous trophoblasts could enhance NK cell cytotoxicity, exacerbating placental dysfunction (55). Our research confirmed the preceding findings, revealing significant alterations in different immune cells, including Tregs and CD56dim NK cells, in samples from patients with PE compared to the control group. These findings underscored the importance of immune cells in preserving immune tolerance at the maternal-fetal interface, highlighting the necessity for additional

10.3389/fimmu.2025.1496046

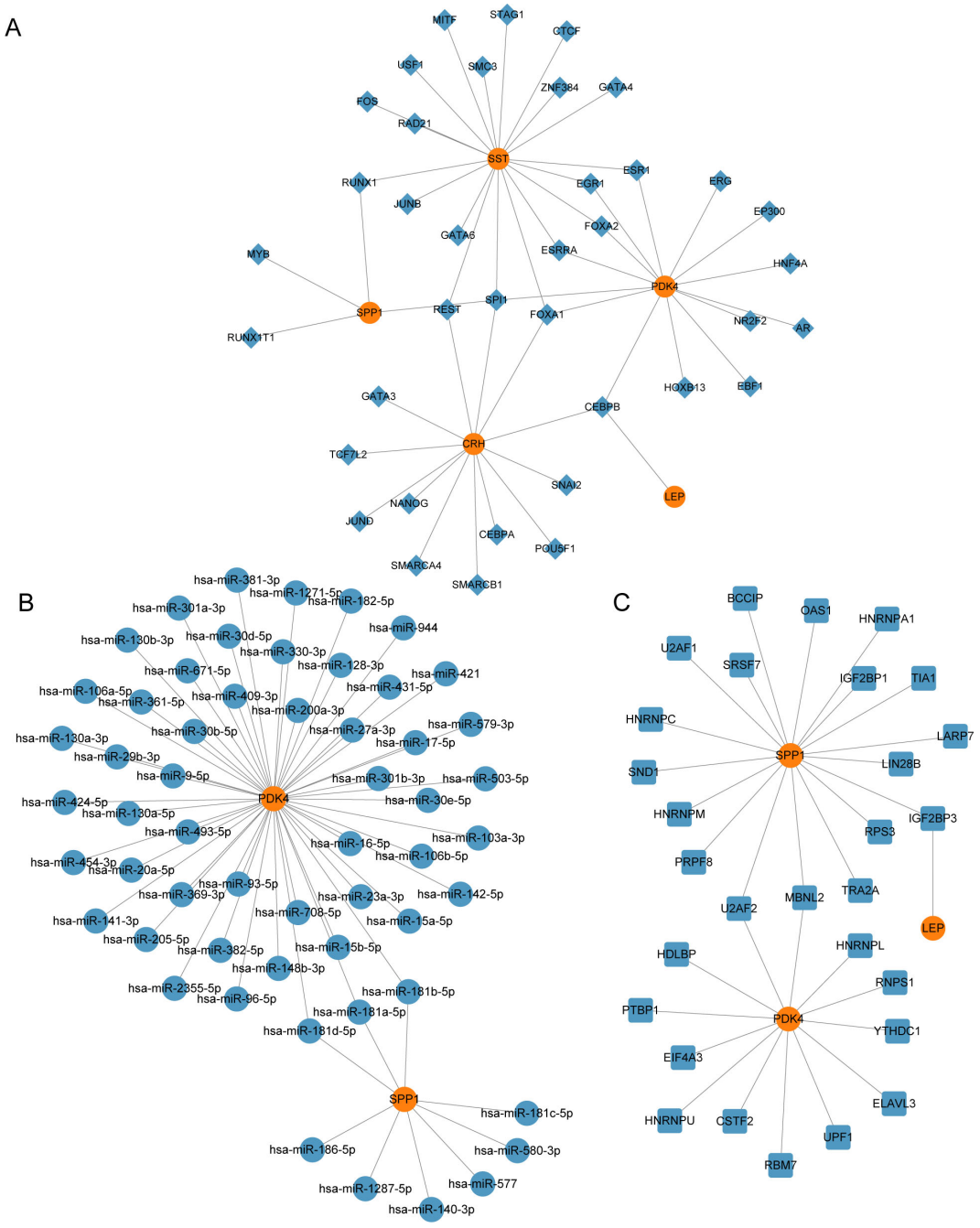

FIGURE 7
Regulatory network of EMRDEGs. **(A)** mRNA-TF Regulatory Network of Key Genes. **(B)** mRNA-miRNA Regulatory Network of Key Genes. **(C)** mRNA-RBP Regulatory Network of Key Genes. EMRDEGs, Energy Metabolism-Related Differentially Expressed Genes; TF, Transcription Factor; RBP, RNA-Binding Protein. Orange is mRNA, blue diamonds are TF, blue circles are miRNA, and blue squares are RBP.

research on how these immune alterations impacted the advancement and detection of the disease.

An imbalance in energy metabolism significantly influences the immune system through various mechanisms, aligning with our findings on the interactions between specific genes and immune cell populations in PE. Firstly, insulin resistance and abnormal lipid metabolism can trigger systemic inflammation, leading to elevated levels of pro-inflammatory cytokines such as TNF-α and IL-6 (56). These cytokines activate immune cells and alter their function and distribution, contributing to the immune dysregulation observed in PE. Secondly, energy metabolism imbalances can directly affect the metabolic pathways of immune cells; for example, changes in glucose metabolism can impact the activity and function of T cells and macrophages (57). Furthermore, metabolic dysregulation can impact the functionality of immune cells such as NK cells and Tregs, resulting in the breakdown of immune tolerance and exacerbation of inflammatory response, thereby further worsening the immune dysfunction observed in PE (58). These mechanisms

10.3389/fimmu.2025.1496046

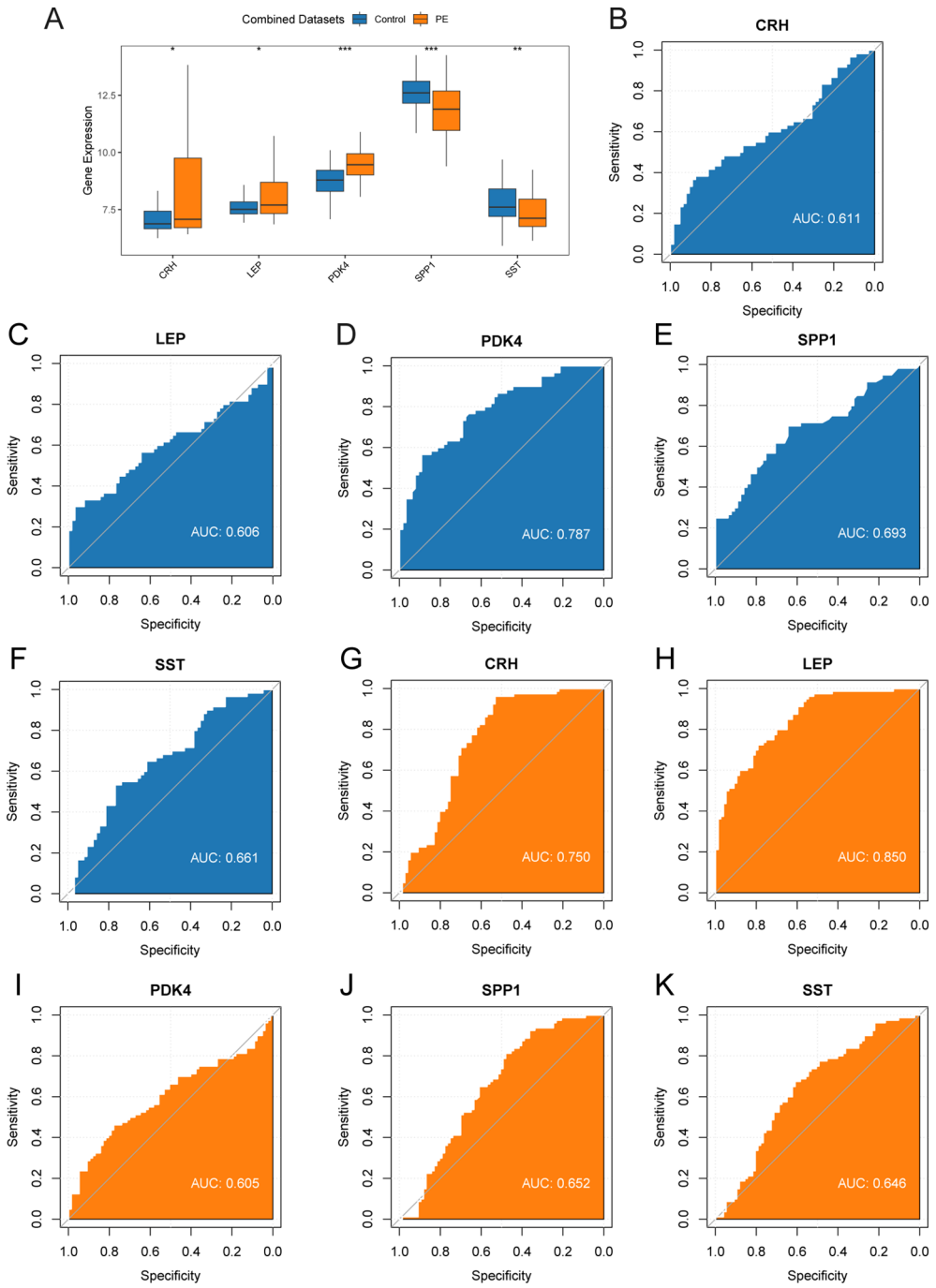

FIGURE 8
Differential expression validation and ROC curve analysis. **(A)** Group comparison plot of Key Genes in PE samples and Control samples of combined datasets. B-F. ROC curves of Key Genes *CRH* **(B)**, *LEP* **(C)**, *PDK4* **(D)**, *SPP1* **(E)**, and *SST* **(F)** in combined datasets. G-K. ROC curves of Key Genes *CRH* **(G)**, *LEP* **(H)**, *PDK4* **(I)**, *SPP1* **(J)**, and *SST* **(K)** in dataset GSE75010. ROC, Receiver Operating Characteristic; AUC, Area Under The Curve. ROC, Receiver Operating Characteristic Curve; TPR, True Positive Rate; FPR, False Positive Rate. * represents *p*-value < 0.05, statistically significant; ** represents *p*-value < 0.01, highly statistically significant; *** represents *p*-value < 0.001 and highly statistically significant. AUC between 0.5-0.7 had low accuracy, and AUC of 0.7-0.9 had moderate accuracy. In the group comparison figure, the PE group is orange, and the Control group is blue.

underscore the intricate relationship between energy metabolism and immune regulation, highlighting the potential of targeting metabolic pathways to modulate immune responses in PE.

Our findings underscored significant interactions between certain genes and specific immune cell populations, offering insights into the intricate immune modulation in PE. Furthermore, we observed a significant positive correlation between *SPP1* and Tregs. The gene *SPP1* is recognized for its involvement in regulating the immune system, promoting blood vessel formation, and modifying tissue structure (59). However, no direct studies have been published on the association between *SPP1* and Tregs in PE, *SPP1* is among the most upregulated genes during

10.3389/fimmu.2025.1496046

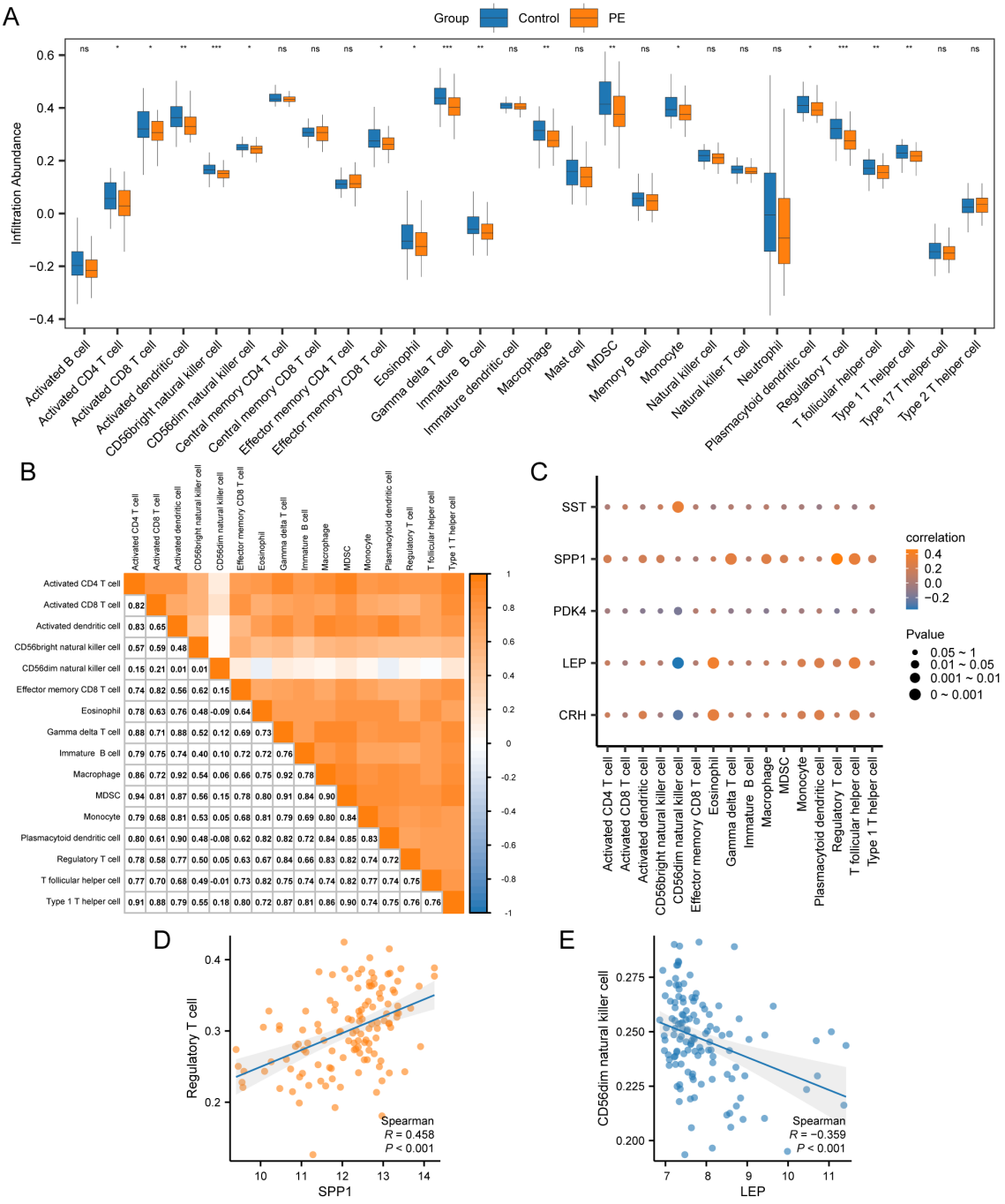

FIGURE 9
Immune infiltration analysis by ssGSEA algorithm. **(A)** Group comparison plot of immune cells in PE and Control samples from the combined datasets. **(B)** Correlation heatmap of immune cell infiltration abundance in the combined datasets. **(C)** Bubble correlation plot between Key Genes and immune cell infiltration abundance in the combined datasets. **(D)** Scatter plot of the correlation between Top1 positively correlated Key Genes and immune cells. **(E)** Scatter plot of correlation between TOP1-negatively correlated Key Genes and immune cells. ssGSEA, single-sample Gene-Set Enrichment Analysis; ns stands for *p*-value ≥ 0.05, not statistically significant; * represents *p*-value < 0.05, statistically significant; ** represents *p*-value < 0.01, highly statistically significant; *** represents *p*-value < 0.001 and highly statistically significant. The absolute value of the correlation coefficient (r-value) below 0.3 was weak or no correlation; between 0.3 and 0.5 was a weak correlation, between 0.5 and 0.8 was a moderate correlation, and above 0.8 was a strong correlation. In the group comparison plot, the PE samples are orange, and the Control samples are blue. In the heat map and correlation map, orange is a positive correlation, blue is a negative correlation, and the depth of color represents the strength of the correlation.

T-cell activation, and it has diverse roles in immune response regulation (60). This relationship suggests that *SPP1* promotes an immunosuppressive environment conducive to fetal tolerance. Additionally, Tregs are known for maintaining immune homeostasis and preventing autoimmunity by suppressing abnormal immune responses. Based on the established mechanisms, we hypothesized that reduced expression of *SPP1* in PE could negatively impact the immunosuppressive environment

TABLE 5 Primer sequences for qRT-PCR.

Gene	Primer sequences (5′-3′)
CRH	GGTCCCTACTCCTACTGCAAC (forward) CCAAGCATTCTCGATAGGCATTC (reverse)
LEP	TGCCTTCCAGAAACGTGATCC (forward) CTCTGTGGAGTAGCCTGAAGC (reverse)
PDK4	GACCCAGTCACCAATCAAAATCT (forward) GGTTCATCAGCATCCGAGTAGA (reverse)
SPP1	CTCCATTGACTCGAACGACTC (forward) CAGGTCTGCGAAACTTCTTAGAT (reverse)
SST	ACCCAACCAGACGGAGAATGA (forward) ACCCAACCAGACGGAGAATGA (reverse)

qRT–PCR, quantitative real–time PCR.

and the expansion and function of Tregs, ultimately affecting overall immune homeostasis and potentially contributing to the pathophysiological processes of PE.

Furthermore, our research exhibited a negative correlation between *LEP* and CD56dim NK cells, highlighting the intricate interplay between the *LEP* gene and specific NK cell subsets. This subset, well-known for its crucial role in regulating maternal-fetal immunity, is influenced by the signaling pathways of *LEP* (61). NK cells are critical in establishing appropriate maternal-fetal immune interactions in early pregnancy, indicating the complex role of *LEP* in regulating adverse immune responses in PE. Increased *LEP* levels, possibly reflective of the inflammatory state and placental insufficiency in PE, may impair the cytolytic function of CD56dim NK cells, hampering their role in placental and fetal development. Moreover, *LEP* emerges as a potentially influential factor in shaping the immune environment in PE, potentially impacting the balance between tolerance and immune activation

TABLE 6 Clinical information of the patients.

Category	PE (n = 26)	Control (n = 26)	*p*-value
Age (years)	31.385 ± 5.93	29.846 ± 4.62	0.302
Gestational age at delivery (weeks)	36.423 ± 2.53	36.423 ± 2.53	1
Systolic blood pressure(mmHg)	155.73 ± 20.36	121.38 ± 6.84	< 0.001
Diastolic blood pressure (mmHg)	93.654 ± 10.88	74.346 ± 4.09	< 0.001
Neonatal birth weight (g)	2713.8 ± 618.71	2934.6 ± 576.38	0.323
1 min Apgar (score)			0.204
10	23 (88.5%)	26 (100%)	
9	2 (7.7%)	0 (0%)	
7	1 (3.8%)	0 (0%)	
5 min Apgar (score)			0.471
10	24 (92.3%)	26 (100%)	
9	2 (7.7%)	0 (0%)	

necessary for a successful pregnancy outcome. In conclusion, the immune system dysfunction observed in PE, which is marked by alterations in the infiltration and activity of immune cells, highlights the significance of immune processes in disease pathophysiology. These findings provided valuable insights into potential therapeutic targets and highlighted the need for further research to develop immune-based interventions for PE.

The potential of biomarkers such as *LEP*, *SPP1*, and *CRH* in predicting the severity or complications of PE is noteworthy. Differential expression analysis from the combined datasets revealed significant differences in the expression of these biomarkers between PE and control groups. This was confirmed by qRT-PCR and Western blot of clinical samples. Additionally, the correlation between key genes and specific immune cells indicates that these biomarkers may modulate immune responses in PE. Given their significant differential expression and association with energy metabolism and immune regulation, these key genes hold promise as biomarkers for predicting PE severity or complications.

The identified biomarkers were compared with established diagnostic markers for PE, such as *sFlt-1* and *PlGF*. The mechanism of *sFlt-1* involves inhibiting normal angiogenesis, leading to placental dysfunction and symptoms like hypertension, while *PlGF* levels typically decrease in PE patients (41). The *sFlt-1*/*PlGF* ratio is widely used for early PE diagnosis due to its high specificity and sensitivity. In contrast, *LEP* is involved in energy balance and metabolic processes, with its upregulation in PE placental samples potentially linked to insulin resistance and inflammation. The increase of CRH level in PE patients may be related to the disturbance of placental energy metabolism, and further aggravate the condition by affecting placental oxidative stress and inflammatory response. *SPP1* downregulation may affect trophoblast invasion and placental development. While *sFlt-1* and *PlGF* are well-established in clinical practice for early identification of high-risk pregnancies, *LEP*, *SPP1*, and *CRH* hold potential as new diagnostic and therapeutic targets. Further research on these new biomarkers could enhance our understanding of PE's underlying mechanisms and improve diagnostic and treatment strategies.

Known treatments for PE, such as antihypertensive drugs, early low-dose aspirin, and calcium supplements, may influence the expression of the identified genes. For instance, antihypertensive drugs have been shown to affect *LEP* expression by improving blood flow and reducing blood pressure (62). Early low-dose aspirin may regulate *LEP* levels by inhibiting platelet activation and associated inflammatory responses, thus improving energy metabolism and balance (63). These therapeutic interventions highlight the potential for targeted treatments to modulate gene expression and improve outcomes for patients with PE.

In light of our findings, exploring therapeutic approaches targeting the identified genes could offer new avenues for PE treatment. For instance, *LEP* 's therapeutic potential could be harnessed through anti-inflammatory drugs. Given the relationship between *LEP* and inflammatory states, certain anti-inflammatory medications, such as non-steroidal anti-inflammatory drugs (NSAIDs), might mitigate the inflammatory response in PE. By reducing *LEP* levels, these drugs could

10.3389/fimmu.2025.1496046

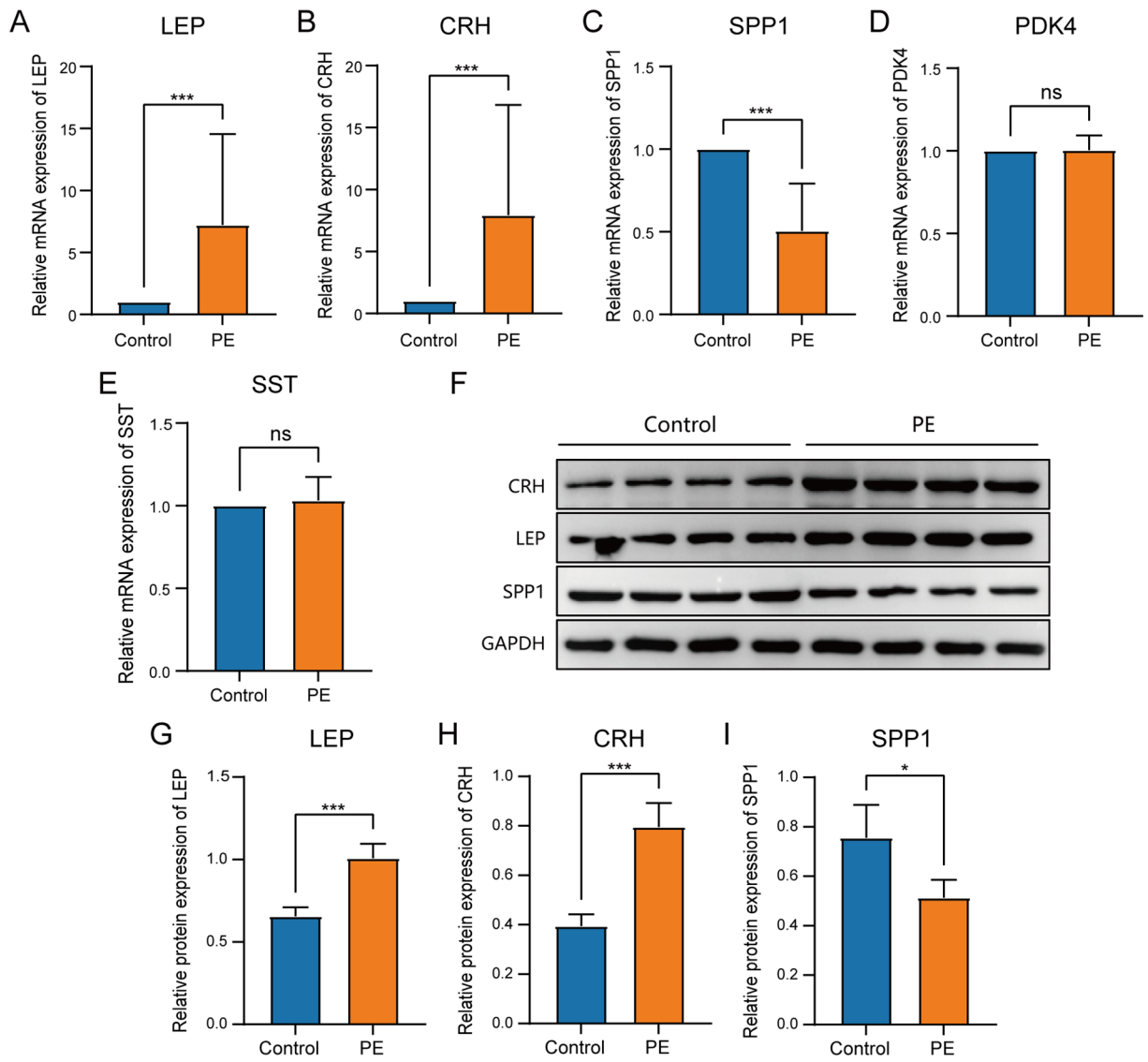

FIGURE 10
Comparison of key genes expression in placental samples of the control group and PE group. The expression bars of *LEP* **(A)**, *CRH* **(B)**, *SPP1* **(C)**, *PDK4* **(D)**, and *SST* **(E)** in the control group and PE group describe the mRNA expression levels of key genes. **(F)**Western blot analysis of *LEP*, *CRH*, *SPP1* protein expression levels in placental samples of preeclampsia group and control group. The expression bars of *LEP* **(G)**, *CRH* **(H)**, and *SPP1* **(I)** in the control group and PE group describe the protein expression levels of key genes.Blue bars representing the control group and orange representing the PE group. ns stands for p-value ≥ 0.05, not statistically significant; * represents p-value < 0.05, statistically significant; *** represents p-value < 0.001 and highly statistically significant.

potentially improve maternal metabolic status and vascular function. Additionally, *SPP1*'s role in placental development and function suggests that therapies promoting *SPP1* expression could be beneficial. Furthermore, *SPP1*'s involvement in immune regulation indicates its potential as an immunomodulatory agent in PE treatment, promoting fetal tolerance and improving pregnancy outcomes.

Translating these findings into clinical practice presents several challenges. One major challenge is the standardization of biomarker assays. To effectively utilize new biomarkers such as *LEP*, *SPP1*, and *CRH* in clinical settings, standardized detection protocols must be established, including standardized detection methods and quality control measures. Additionally, clinical validation and external validation are crucial. Although our study has identified potential biomarkers, their clinical efficacy needs to be confirmed through large-scale clinical validation. This includes addressing challenges related to the scale and representativeness of the study population and the complexity of clinical scenarios.

Despite the comprehensive bioinformatics approach employed, this study has certain limitations. First, the quality and source of the data used can significantly impact the results, as variations in sample collection, processing, and storage conditions across different studies can introduce inconsistencies. Second, integrating multiple datasets from different sources could introduce batch effects despite efforts to correct these effects using computational methods. Such batch effects could still influence the results and

interpretations. Third, the choice of analysis tools and algorithms can affect the outcomes, as different tools and algorithms may yield varying results, introducing bias. Fourth, functional annotation relies on existing databases, which may not be comprehensive or up-to-date, limiting the accuracy and completeness of the functional insights derived. Fifth, the study lacked extensive clinical validation, which was crucial for translating the findings into clinical practice, and the results need to be validated in larger, independent cohorts and through functional experiments to establish their clinical relevance. Additionally, the sample size was relatively small, with only 12 placental samples collected for qRT-PCR validation, which could limit the generalizability of the results. Lastly, the study was not conducted in cells or animals and was not robust enough to be validated in wet laboratory experiments, limiting the ability to confirm the biological significance of the identified genes and pathways.

5 Conclusion

In conclusion, the study effectively detected EMRDEGs in PE by integrating and analyzing various datasets. The functional enrichment studies indicated important BPs and pathways associated with EMRDEGs, offering an understanding of the fundamental mechanisms of PE. Identifying interactions between proteins and regulatory networks, including mRNA-TF, mRNA-miRNA, and mRNA-RBP, highlighted significant genes and their possible regulatory mechanisms. Immune infiltration analysis suggested that specific immune cell types were differentially abundant between PE and control groups and might correlate with key genes. The potential for diagnosis using these important genes was revealed through ROC curves, and their expression was confirmed using qRT-PCR. The results provided a comprehensive insight into the molecular foundation of PE and indicated possible biomarkers and targets for treatment. Future studies should focus on larger sample sizes, wet lab validations, and extensive clinical trials to further substantiate the findings and facilitate their translation into clinical applications.

Data availability statement

The original contributions presented in the study are included in the article/Supplementary Material. Further inquiries can be directed to the corresponding author/s.

Ethics statement

The studies involving humans were approved by the Research Ethics Committee at the Ruian People's Hospital. The studies were conducted in accordance with the local legislation and institutional requirements. The participants provided their written informed consent to participate in this study.

Author contributions

RL: Data curation, Formal Analysis, Writing – original draft. CZ: Investigation, Writing – review & editing. KY: Validation, Writing – review & editing. HC: Visualization, Writing – review & editing. MP: Conceptualization, Methodology, Project administration, Supervision, Writing – review & editing.

Funding

The author(s) declare that financial support was received for the research, authorship, and/or publication of this article. This study was supported by the Wenzhou Basic Research Project (No: Y20240606).

Acknowledgments

We extend our heartfelt thanks to the patients who generously provided placental samples, making this research possible. We would like to acknowledge the use of ChatGPT-4o for language refinement and grammar checking in the preparation of this manuscript. ChatGPT-4o, developed by OpenAI, assisted in enhancing the clarity and coherence of the text.

Conflict of interest

The authors declare that the research was conducted in the absence of any commercial or financial relationships that could be construed as a potential conflict of interest.

Publisher's note

Supplementary material

The Supplementary Material for this article can be found online at: https://www.frontiersin.org/articles/10.3389/fimmu.2025.1496046/full#supplementary-material

SUPPLEMENTARY TABLE 1
EMRGs.

SUPPLEMENTARY TABLE 2
mRNA-TF.

SUPPLEMENTARY TABLE 3
mRNA-miRNA.

SUPPLEMENTARY TABLE 4
mRNA-RPB.

References

1. Gestational hypertension and preeclampsia. *Obstetrics Gynecology*. (2020) 135: e237–e60. doi: 10.1097/AOG.0000000000003891

2. Dimitriadis E, Rolnik DL, Zhou W, Estrada-Gutierrez G, Koga K, Francisco RPV, et al. Pre-eclampsia. *Nat Rev Dis Primers*. (2023) 9:8. doi: 10.1038/s41572-023-00417-6

3. Brown MA, Magee LA, Kenny LC, Karumanchi SA, McCarthy FP, Saito S, et al. Hypertensive disorders of pregnancy. *Hypertension*. (2018) 72:24–43. doi: 10.1161/HYPERTENSIONAHA.117.10803

4. Bertini A, Salas R, Chabert S, Sobrevia L, Pardo F. Using machine learning to predict complications in pregnancy: A systematic review. *Front Bioeng Biotechnol*. (2021) 9:780389. doi: 10.3389/fbioe.2021.780389

5. Chaiworapongsa T, Chaemsaithong P, Yeo L, Romero R. Pre-eclampsia part 1: current understanding of its pathophysiology. *Nat Rev Nephrol*. (2014) 10:466–80. doi: 10.1038/nrneph.2014.102

6. Hu M, Li J, Baker PN, Tong C. Revisiting preeclampsia: A metabolic disorder of the placenta. *FEBS J*. (2022) 289:336–54. doi: 10.1111/febs.15745

7. Aye ILMH, Aiken CE, Charnock-Jones DS, Smith GCS. Placental energy metabolism in health and disease—Significance of development and implications for preeclampsia. *Am J Obstetrics Gynecology*. (2022) 226:S928–S44. doi: 10.1016/j.ajog.2020.11.005

8. Radaelli T, Lepercq J, Varastehpour A, Basu S, Catalano PM, Hauguel-De-Mouzon S. Differential regulation of genes for fetoplacental lipid pathways in pregnancy with gestational and type 1 diabetes mellitus. *Am J Obstetrics Gynecology*. (2009) 201:209.e1–.e10. doi: 10.1016/j.ajog.2009.04.019

9. Wang Y, Fan J, Liu Y, Du J, Liang B, Wang H, et al. Identification and validation of dhcr7 as a diagnostic biomarker involved in the proliferation and mitochondrial function of breast cancer. *Aging*. (2024) 16:5967–86. doi: 10.18632/aging.205683

10. Marín R, Chiarello DI, Abad C, Rojas D, Toledo F, Sobrevia L. Oxidative stress and mitochondrial dysfunction in early-onset and late-onset preeclampsia. *Biochim Biophys Acta (BBA) - Mol Basis Dis*. (2020) 1866. doi: 10.1016/j.bbadis.2020.165961

11. Barrett T, Wilhite SE, Ledoux P, Evangelista C, Kim IF, Tomashevsky M, et al. Ncbi geo: archive for functional genomics data sets–update. *Nucleic Acids Res*. (2013) 41:D991–5. doi: 10.1093/nar/gks1193

12. Yong HE, Melton PE, Johnson MP, Freed KA, Kalionis B, Murthi P, et al. Genome-wide transcriptome directed pathway analysis of maternal pre-eclampsia susceptibility genes. *PloS One*. (2015) 10:e0128230. doi: 10.1371/journal.pone.0128230

13. Leavey K, Benton SJ, Grynspan D, Kingdom JC, Bainbridge SA, Cox BJ. Unsupervised placental gene expression profiling identifies clinically relevant subclasses of human preeclampsia. *Hypertension (Dallas Tex: 1979)*. (2016) 68:137–47. doi: 10.1161/HYPERTENSIONAHA.116.07293

14. Leavey K, Benton SJ, Grynspan D, Bainbridge SA, Morgen EK, Cox BJ. Gene markers of normal villous maturation and their expression in placentas with maturational pathology. *Placenta*. (2017) 58:52–9. doi: 10.1016/j.placenta.2017.08.005

15. Christians JK, Leavey K, Cox BJ. Associations between imprinted gene expression in the placenta, human fetal growth and preeclampsia. *Biol Lett*. (2017) 13:20170643. doi: 10.1098/rsbl.2017.0643

16. Leavey K, Wilson SL, Bainbridge SA, Robinson WP, Cox BJ. Epigenetic regulation of placental gene expression in transcriptional subtypes of preeclampsia. *Clin Epigenet*. (2018) 10:28. doi: 10.1186/s13148-018-0463-6

17. Benton SJ, Leavey K, Grynspan D, Cox BJ, Bainbridge SA. The clinical heterogeneity of preeclampsia is related to both placental gene expression and placental histopathology. *Am J Obstetrics Gynecology*. (2018) 219:604.e1–.e25. doi: 10.1016/j.ajog.2018.09.036

18. Gibbs I, Leavey K, Benton SJ, Grynspan D, Bainbridge SA, Cox BJ. Placental transcriptional and histologic subtypes of normotensive fetal growth restriction are comparable to preeclampsia. *Am J Obstetrics Gynecology*. (2019) 220:110.e1–.e21. doi: 10.1016/j.ajog.2018.10.003

19. Stelzer G, Rosen N, Plaschkes I, Zimmerman S, Twik M, Fishilevich S, et al. The genecards suite: from gene data mining to disease genome sequence analyses. *Curr Protoc Bioinf*. (2016) 54:1.30.1–1.3. doi: 10.1002/cpbi.5

20. Liu H, Zhang J, Wei C, Liu Z, Zhou W, Yang P, et al. Prognostic signature construction of energy metabolism-related genes in pancreatic cancer. *Front Oncol*. (2015) 12:917897. doi: 10.3389/fonc.2022.917897

21. Leek JT, Johnson WE, Parker HS, Jaffe AE, Storey JD. The sva package for removing batch effects and other unwanted variation in high-throughput experiments. *Bioinformatics*. (2012) 28:882–3. doi: 10.1093/bioinformatics/bts034

22. Ritchie ME, Phipson B, Wu D, Hu Y, Law CW, Shi W, et al. Limma powers differential expression analyses for rna-sequencing and microarray studies. *Front Oncol*. (2015) 43:e47–e. doi: 10.1093/nar/gkv007

23. Yeung KY, Ruzzo WL. Principal component analysis for clustering gene expression data. *Bioinformatics*. (2001) 17(9):763–74. doi: 10.1093/bioinformatics/17.9.763

24. Zhang H, Meltzer P, Davis S, Benton SJ, Leavey K, Grynspan D, et al. Rcircos: an R package for circos 2d track plots. *BMC Bioinf*. (2013) 14:244. doi: 10.1186/1471-2105-14-244

25. Mi H, Muruganujan A, Ebert D, Huang X, Thomas PD. Panther version 14: more genomes, a new panther go-slim and improvements in enrichment analysis tools. *Nucleic Acids Res*. (2019) 47:D419–D26. doi: 10.1093/nar/gky1038

26. Kanehisa M, Goto S. Kegg: kyoto encyclopedia of genes and genomes. *Nucleic Acids Res*. (2000) 28:27–30. doi: 10.1093/nar/28.1.27

27. Yu G, Wang L-G, Han Y, He Q-Y. Clusterprofiler: an R package for comparing biological themes among gene clusters. *Omics: A J Integr Biol*. (2012) 16:284–7. doi: 10.1089/omi.2011.0118

28. Hänzelmann S, Castelo R, Guinney J, Subramanian A, Tamayo P, Mootha VK, et al. Gene set enrichment analysis: A knowledge-based approach for interpreting genome-wide expression profiles. *Proc Natl Acad Sci*. (2005) 102:15545–50. doi: 10.1073/pnas.0506580102

29. Liberzon A, Subramanian A, Pinchback R, Thorvaldsdóttir H, Tamayo P, Mesirov JP. Molecular signatures database (Msigdb) 3.0. *Bioinf (Oxford England)*. (2011) 27:1739–40. doi: 10.1093/bioinformatics/btr260

30. Szklarczyk D, Gable AL, Lyon D, Junge A, Wyder S, Huerta-Cepas J, et al. String V11: protein-protein association networks with increased coverage, supporting functional discovery in genome-wide experimental datasets. *Nucleic Acids Res*. (2019) 47:D607–D13. doi: 10.1093/nar/gky1131

31. Franz M, Rodriguez H, Lopes C, Zuberi K, Montojo J, Bader GD, et al. Genemania update 2018. *Nucleic Acids Res*. (2018) 46:W60–W4. doi: 10.1093/nar/gky311

32. Zhou K-R, Liu S, Sun W-J, Zheng L-L, Zhou H, Yang J-H, et al. Chipbase V2.0: decoding transcriptional regulatory networks of non-coding rnas and protein-coding genes from chip-seq data. *Nucleic Acids Res*. (2017) 45:D43–50. doi: 10.1093/nar/gkw965

33. Li J-H, Liu S, Zhou H, Qu L-H, Yang J-H. Starbase V2.0: decoding mirna-cerna, mirna-ncrna and protein–rna interaction networks from large-scale clip-seq data. *Nucleic Acids Res*. (2014) 42:D92–7. doi: 10.1093/nar/gkt1248

34. Robin X, Turck N, Hainard A, Tiberti N, Lisacek F, Sanchez J-C, et al. Proc: an open-source package for R and S+ to analyze and compare roc curves. *BMC Bioinf*. (2011) 12:77. doi: 10.1186/1471-2105-12-77

35. Xiao B, Liu L, Li A, Xiang C, Wang P, Li H, et al. Identification and verification of immune-related gene prognostic signature based on ssgsea for osteosarcoma. *Front Oncol*. (2020) 10:607622. doi: 10.3389/fonc.2020.607622

36. Hansson SR, Nääv Å, Erlandsson L. Oxidative stress in preeclampsia and the role of free fetal hemoglobin. *Front Physiol*. (2015) 5:516. doi: 10.3389/fphys.2014.00516

37. Darby M, Martin JN, LaMarca B. A complicated role for the renin–angiotensin system during pregnancy: highlighting the importance of drug discovery. *Expert Opin Drug Saf*. (2013) 12:857–64. doi: 10.1517/14740338.2013.823945

38. Wenger NK, Arnold A, Bairey Merz CN, Cooper-DeHoff RM, Ferdinand KC, Fleg JL, et al. Hypertension across a Woman's life cycle. *J Am Coll Cardiol*. (2018) 71:1797–813. doi: 10.1016/j.jacc.2018.02.033

39. Al-Jameil N, Aziz Khan F, Fareed Khan M, Tabassum H. A brief overview of preeclampsia. *J Clin Med Res*. (2013) 6:1–7. doi: 10.4021/jocmr1682w

40. Fox R, Kitt J, Leeson P, Aye CYL, Lewandowski AJ. Preeclampsia: risk factors, diagnosis, management, and the cardiovascular impact on the offspring. *J Clin Med*. (2019) 8. doi: 10.3390/jcm8101625

41. Levine RJ, Maynard SE, Qian C, Lim K-H, England LJ, Yu KF, et al. Circulating angiogenic factors and the risk of preeclampsia. *New Engl J Med*. (2004) 350:672–83. doi: 10.1056/NEJMoa031884

42. Austdal M, Tangerås L, Skråstad R, Salvesen K, Austgulen R, Iversen A-C, et al. First trimester urine and serum metabolomics for prediction of preeclampsia and gestational hypertension: A prospective screening study. *Int J Mol Sci*. (2015) 16:21520–38. doi: 10.3390/ijms160921520

43. Myatt L, Roberts JM. Preeclampsia: syndrome or disease? *Curr Hypertension Rep*. (2015) 17:83. doi: 10.1007/s11906-015-0595-4

44. Colleluori G, Galli C, Severi I, Perugini J, Giordano A. Early life stress, brain development, and obesity risk: is oxytocin the missing link? *Cells*. (2022) 11:623. doi: 10.3390/cells11040623

45. Boiko AS, Mednova IA, Kornetova EG, Goncharova AA, Semke AV, Bokhan NA, et al. Metabolic hormones in schizophrenia patients with antipsychotic-induced metabolic syndrome. *J Personalized Med*. (2022) 12:1655. doi: 10.3390/jpm12101655

46. Alston MC, Redman LM, Sones JL. An overview of obesity, cholesterol, and systemic inflammation in preeclampsia. *Nutrients*. (2022) 14:2087. doi: 10.3390/nu14102087

47. Sheibani N, Morrison ME, Gurel Z, Park S, Sorenson CM. Bim deficiency differentially impacts the function of kidney endothelial and epithelial cells through modulation of their local microenvironment. *Am J Physiology-Renal Physiol*. (2012) 302:F809–F19. doi: 10.1152/ajprenal.00498.2011

48. Bazer FW, Wu G, Johnson GA, Kim J, Song G. Uterine histotroph and conceptus development: select nutrients and secreted phosphoprotein 1 affect mechanistic target of rapamycin cell signaling in ewes1. *Biol Reprod*. (2011) 85:1094–107. doi: 10.1095/biolreprod.111.094722

49. Ackerman WE, Buhimschi CS, Brown TL, Zhao G, Summerfield TL, Buhimschi IA. Transcriptomics-based subphenotyping of the human placenta enabled by weighted correlation network analysis in early-onset preeclampsia with and without fetal growth restriction. *Hypertension*. (2023) 80:1363–74. doi: 10.1161/HYPERTENSIONAHA.122.20807

50. Maynard SE, Min J-Y, Merchan J, Lim K-H, Li J, Mondal S, et al. Excess placental soluble fms-like tyrosine kinase 1 (Sflt1) may contribute to endothelial dysfunction, hypertension, and proteinuria in preeclampsia. *J Clin Invest*. (2003) 111:649–58. doi: 10.1172/jci17189

51. Li H, Han L, Yang Z, Huang W, Zhang X, Gu Y, et al. Differential proteomic analysis of syncytiotrophoblast extracellular vesicles from early-onset severe preeclampsia, using 8-plex itraq labeling coupled with 2d nano lc-ms/ms. *Cell Physiol Biochem*. (2015) 36:1116–30. doi: 10.1159/000430283

52. Tong J, Zhao W, Lv H, Li WP, Chen ZJ, Zhang C. Transcriptomic profiling in human decidua of severe preeclampsia detected by rna sequencing. *J Cell Biochem*. (2018) 119:607–15. doi: 10.1002/jcb.26221

53. Zhou W, Chen Y, Zheng Y, Bai Y, Yin J, Wu X-X, et al. Characterizing immune variation and diagnostic indicators of preeclampsia by single-cell rna sequencing and machine learning. *Commun Biol*. (2024) 7:32. doi: 10.1038/s42003-023-05669-2

54. Han X, Ghaemi MS, Ando K, Peterson LS, Ganio EA, Tsai AS, et al. Differential dynamics of the maternal immune system in healthy pregnancy and preeclampsia. *Front Immunol*. (2022) 10:1305. doi: 10.3389/fimmu.2019.01305

55. Luo F, Yue J, Li L, Mei J, Liu X, Huang Y. Narrative review of the relationship between the maternal-fetal interface immune tolerance and the onset of preeclampsia. *Ann Trans Med*. (2022) 10:713–. doi: 10.21037/atm-22-2287

56. Hu X, Zhou J, Song SS, Kong W, Shi YC, Chen LL, et al. Tlr4/ap-1-targeted anti-inflammatory intervention attenuates insulin sensitivity and liver steatosis. *Mediators Inflammation*. (2020) 2020:2960517. doi: 10.1155/2020/2960517

57. Marko AJ, Miller RA, Kelman A, Frauwirth KA. Induction of glucose metabolism in stimulated T lymphocytes is regulated by mitogen-activated protein kinase signaling. *PloS One*. (2010) 5:e15425. doi: 10.1371/journal.pone.0015425

58. Maya J. Surveying the metabolic and dysfunctional profiles of T cells and nk cells in myalgic encephalomyelitis/chronic fatigue syndrome. *Int J Mol Sci*. (2023) 24. doi: 10.3390/ijms241511937

59. Liu Y, Ye G, Dong B, Huang L, Zhang C, Sheng Y, et al. A pan-cancer analysis of the oncogenic role of secreted phosphoprotein 1 (Spp1) in human cancers. *Ann Trans Med*. (2022) 10:279–. doi: 10.21037/atm-22-829

60. Rittling SR, Singh R. Osteopontin in immune-mediated diseases. *Biol Reprod*. (2015) 94:1638–45. doi: 10.1177/0022034515605270

61. Pérez-Pérez A, Vilariño-García T, Fernández-Riejos P, Martín-González J, Segura-Egea JJ, Sánchez-Margalet V. Role of leptin as a link between metabolism and the immune system. *Biol Reprod*. (2017) 35:71–84. doi: 10.1016/j.cytogfr.2017.03.001

62. Seth R, Knight WD, Overton JM. Combined amylin-leptin treatment lowers blood pressure and adiposity in lean and obese rats. *Int J Obes (Lond)*. (2011) 35:1183–92. doi: 10.1038/ijo.2010.262

63. Kurylowicz A, Kozniewski K. Anti-inflammatory strategies targeting metaflammation in type 2 diabetes. *Molecules*. (2020) 25. doi: 10.3390/molecules25092224

frontiers | Frontiers in Cell and Developmental Biology

TYPE Review
PUBLISHED 07 February 2025
DOI 10.3389/fcell.2025.1520218

OPEN ACCESS

EDITED BY
Subhradip Karmakar,
All India Institute of Medical Sciences, India

REVIEWED BY
Arun Paripati,
Nationwide Children's Hospital, United States
Lokanatha Oruganti,
Tulane University, United States

*CORRESPONDENCE
Muhammad Ilham Aldika Akbar,
muhammad-i-a-a@fk.unair.ac.id

RECEIVED 30 October 2024
ACCEPTED 23 January 2025
PUBLISHED 07 February 2025

CITATION
Aldika Akbar MI, Rosaudyn R, Gumilar KE, Shanmugalingam R and Dekker G (2025) Secondary prevention of preeclampsia. *Front. Cell Dev. Biol.* 13:1520218. doi: 10.3389/fcell.2025.1520218

Secondary prevention of preeclampsia

Muhammad Ilham Aldika Akbar[1,2]*, Roudhona Rosaudyn[3], Khanisyah Erza Gumilar[2,4], Renuka Shanmugalingam[5] and Gustaaf Dekker[1,6]

[1]Department Obstetrics and Gynecology, Faculty of Medicine, Universitas Airlangga, Surabaya, Indonesia, [2]Department Obstetrics and Gynecology, Universitas Airlangga Hospital, Surabaya, Indonesia, [3]Department Obstetrics and Gynecology, Dr. Soetomo General Academic Hospital, Surabaya, Indonesia, [4]Graduate Institute of Biomedical Science, China Medical University, Taichung, Taiwan, [5]Department of Renal Medicineand, Liverpool Hospital, Sydney, NSW, Australia, [6]Department Obstetrics and Gynecology, Lyell McEwin Hospital, University of Adelaide, Adelaide, SA, Australia

Preventing preeclampsia (PE) is crucial for the wellbeing of the mother, fetus, and the neonate with three levels: primary, secondary, and tertiary. Secondary prevention involves pharmacological therapies aimed at stopping the disease's progression before clinical signs. The predominant approach currently employed is the daily administration of low dose Aspirin and calcium. PE is a multifaceted illness characterized by syncytiotrophoblast (STB) stress, leading to endothelial dysfunction and systemic inflammation. Various subtypes of PE, in particular early-onset PE (EOP) and late-onset PE (LOP), have different pathophysiological pathways leading to STB stress and also different perinatal outcomes. Low-dose Aspirin (LDA) has been shown to be beneficial in lowering the occurrence of EOP, especially when started before 16 weeks of pregnancy. Calcium supplementation is advantageous for women with poor dietary calcium intake, reducing endothelium activation and hypertension. Low molecular weight heparins (LMWH), have pleiotropic effects, besides their anticoagulant effects, LMWH have significant anti-inflammatory effects, and have a potential restricted use in patients with history of prior severe placental vasculopathy with or without the maternal preeclamptic syndrome. Pravastatin and other statins have shown positive results in lowering preterm PE and improving outcomes for both the mother and baby. Proton pump inhibitors (PPIs) have shown potential in lowering soluble FMS-like tyrosine kinase-1 (sFlt-1) levels and enhancing endothelial function, but clinical trials have been inconsistent. Metformin, primarily used for improving insulin sensitivity, has potential advantages in decreasing PE incidence due to its anti-inflammatory and vascular properties, particularly in morbidly obese women. Nitric oxide (NO) donors and L-arginine have been shown to effectively reduce vascular resistance and improving blood flow to placenta, potentially reducing PE risk. In conclusion, various pharmacological treatments have the potential to prevent secondary PE, but their effectiveness depends on underlying risk factors and intervention time. Further research is needed to determine the optimal (combination) of method(s) for the individual patient with her individual risk profile.

KEYWORDS

preeclampsia, high risk pregnancy, prevention, maternal death, maternal health

Introduction

Prevention of PE would represent a breakthrough in medicine. The general term prevention has 3 different connotations: primary, secondary, or tertiary. Primary prevention means avoiding occurrence of a disease. For PE this would be restricted to public health education efforts to reduce the rate of obesity and recommendations on having longer periods of sexual relationships prior to conceiving (Dekker and Robillard, 2021; Robillard et al., 2019). Secondary prevention in the context of PE implies breaking off the disease process before emergence of clinically recognizable disease–the focus of this review. Tertiary prevention means prevention of complications caused by the disease process, and is thus more or less synonymous with treatment (Dekker and Sibai, 2001).

The focus of this review is on secondary, primarily pharmacological, prevention of preeclampsia. Starting with a discussion on LDA going back to the mid-1980s, calcium supplementation starting in the 1990s, and followed by more recent preventative attempts like pravastatin, metformin, LMWH, PPI's, and NO donors/L-arginine. Since secondary prevention typically targets one or more of the important pathogenetic/pathophysiologic pathways this review will start with a short summary of current understanding of this heterogeneous syndrome.

Preeclampsia: a heterogeneous syndrome

Over many years, the late, Prof Chris Redman, one of the most influential PE researchers, has stressed the importance of not approaching PE as a single disease entity but as a heterogeneous syndrome (Redman, 2014). It is now abundantly clear that different pathways lead to the final common pathway of STB stress. The STB being a syncytium, cannot repair itself and ages (senescence) quite in contrast with, for example, liver parenchymal cells. "Premature aging," an intrinsically inflammatory process, and the STB stress result, amongst other factors, in positive stress signals like increase sFlt-1and sEng and a negative stress signal (decrease PLGF) accompanied by degrees of systemic inflammation (Redman et al., 2022). The imbalance between PLGF and sFlt-1 appears to be one of the leading causes of the well-known endothelial cell disease with a drop in NO synthesis and the well known prostacyclin (PGI2) and Thromboxane A2 (TXA2) imbalance. STB stress (danger signal) will trigger oxidative stress, and the inflammatory cascade leading to an imbalance between pro-inflammatory and anti-inflammatory Th1 cells. Excessive production of pro-inflammatory cytokines, such as IL-6 and TNFα, further, affects the endothelium, not only by decreasing release of aforementioned vasodilators (PGI2 and NO) but also by the increased expression of endothelial cell adhesion molecules like immunoglobulin-like adhesion molecules, integrins, cadherins and selectins. Endothelial dysfunction and the systemic inflammation lead to vasoconstriction, platelet aggregation (TXA2), and increased vascular permeability. (Phipps et al., 2016; Maynard et al., 2005; Young et al., 2010; Matsubara et al., 2015; Anto et al., 2018; Dekker and Sibai, 1998).

The heterogeneity of the syndrome is based on the different pathways leading to STB stress. In the classic type of PE, so called early-onset PE (EOP) (PE leading to mostly iatrogenic preterm birth <34 weeks), STB stress is caused by superficial cytotrophoblast (CTB) invasion in the about 100 spiral arteries. This superficial CTB invasion leads to poorly modified spiral arteries and subsequently pulsatile high velocity damaging bloods flows in the intervillous space. Ongoing lack of spiral artery modification later leads to intermittent ischemia/reperfusion and oxidative stress adversely affecting the STB. The currently much more common phenotype of PE, is late-onset PE (LOP), i.e., PE leading to birth after 34 weeks (Staff and Redman, 2018a; Redman, 2017). Typically, in disease close to term there is no problem with original placentation, the STB stress more relates to chronic cardiometabolic conditions also associated with systemic inflammation (Chris Redman introduced the term "metaflammation") (Roberts et al., 2017). EOP is typically associated with abnormal uterine artery Doppler flow patterns, fetal growth restriction (FGR), and adverse consequences for both the mother and the newborn. While LOP patients typically have normal uterine artery Doppler flow patterns and more favourable perinatal outcomes, patients still may experience major maternal morbidity if not recognised and appropriately managed the risk of maternal death (Valensise et al., 2008) (Staff and Redman, 2018b).

Secondary prevention of preeclampsia

Low-dose aspirin (LDA)

With the discovery that there was an imbalance between TXA2 and PGI2 in PE, it was reasonable to evaluate whether LDA would be effective for PE prevention. Aspirin, a non-selective COX inhibitor, at a low dose reduces TXA2 levels without reducing PGI2 levels due to the first pass effect (liver de-acetylates aspirin for 90%–95%) and the fact that platelets being without a nucleus cannot resynthesize COX (Ahn and Hwang, 2023). It is important to note that although Aspirin is a non-selective COX inhibitor, the dose of Aspirin may affect the effect on COX1 vs. COX2. Platelet inactivation occurs by inhibiting both COX-1 and COX-2, which in turn inhibits the production of TXA2. COX-1 is an enzyme that is present in all tissues at all times, whereas COX-2 is only produced in reaction to reactive oxygen species, cytokines, endotoxins, or growth factors during inflammatory circumstances (Faki and Er, 2021). The COX enzyme catalyzes the conversion of arachidonic acid into prostaglandin H2 (PGH2). PGH2 can then be further transformed into TXA2, PGI2 or PGE2, or other prostaglandins depending on the cell type and tissue (Mangana et al., 2021). TXA2 participates in platelet aggregation, vasoconstriction, and as a stimulant for smooth muscle cell growth. Conversely, PGI2 exhibits the contrary effect to TXA2 (Anto et al., 2018). When administered in low dosages, Aspirin specifically inhibits the activity of COX-1. However, when given in high doses (not applicable in the obstetric preventative context), aspirin inhibits the actions of both COX-1 and COX-2 (Shanmugalingam et al., 2019a).

The first double blind randomized clinical trial was published in 1986 by Wallenburg and Dekker (Dekker, 1989; Wallenburg et al., 1986). A large group of low-risk nulliparous pregnant women had an

angiotensin II infusion test; 46 normotensive women at 28 weeks' gestation were judged to be at risk for PE by increased blood pressure response to infused angiotensin II. Twelve of 23 women taking placebo developed PE, whereas only 2 of 21 women on 60 mg of Aspirin developed PE (83% decrease). Just prior to this double blind RCT, Beaufils et al. published a study in a group of just 102 patients with a historical risk of PE and/or FGR. In this unblinded study, patients were randomly allocated to receive 300 mg dipyridamole plus 150 mg of Aspirin; in the treatment group no cases of preeclampsia vs. 6 (8.5%) in the no-treatment group (Beaufils et al., 1985). It is not clear why 150 mg was chosen–but this study is still of historical interest, since the 150 mg was also used in the more recent ASPRE trial (Rolnik et al., 2017).

The following convoluted road that led to the current ongoing use of LDA in the prevention of PE is detailed in an elegant review by Scott Walsh and Jerome Strauss (Walsh and Strauss, 2021). A plethora of clinical trials followed, reporting varying degrees of effectiveness of LDA treatment. Two large multicenter intent-to-treat studies were conducted in nulliparous pregnant women given 60 mg/day of aspirin by the NICHD Maternal-Fetal Medicine Unit Network and the Collaborative Low-dose Aspirin Study in Pregnancy (CLASP) trials (Sibai et al., 1993; CLASP: a randomised trial of, 1994). Only modest decreases in the incidence of PE were found. The MFM Unit Network study reported no improvement in perinatal morbidity and a possible increased risk of placental abruption. Interest in LDA declined after the MFM Network Unit and CLASP studies due to the existing concerns about placental abruption and the small beneficial effects of LDA.

Real interest in LDA re-emerged by the re-analysis of all RCT by Roberge showing a massive reduction in the PE rate (OR 0.47) with LDA of at least 100 mg (virtually all these studies used 100 mg) started prior to 16 weeks's gestation (Roberge et al., 2018). Finally, the ASPRE study by Rolnik et al., studying the effect of 150 mg of Aspirin (the old Beaufils dose) in patients with a high risk first trimester screen for PE as introduced by Kypros Nicolaides (Rolnik et al., 2017), demonstrated that LDA at a dosage of 150 mg per day from 11 to 14 weeks of pregnancy until 36 weeks can decrease the likelihood of developing PE. In the LDA group, only 1.6% of patients experienced preterm PE, compared to 4.3% in placebo group (62% reduction). There were no significant differences in terms of maternal complications during pregnancy or adverse impacts on the fetus as compared to the placebo group (Rolnik et al., 2017). Interestingly, in a *post hoc* analysis of the ASPRE trial, Poon et al. demonstrated that 150 mg of Aspirin does not prevent superimposed PE in patients with chronic hypertension, but may reduce "placental" preterm birth (Poon et al., 2017). A Cochrane review of 77 studies demonstrated that LDA decreased the likelihood of preterm birth decreased by 9% and fetal death by 15%. The efficacy of LDA is contingent upon the adherence of patients to the prescribed medication regimen, which has a success rate ranging from 76% to 90% in the prevention of PE (Rolnik et al., 2017; Brownfoot and Rolnik, 2024; Chang et al., 2023a). It is important to acknowledge that in wealthy nations where aneuploidy screening is standard, the FMF screening algorithm may prove cost-effective; however, this algorithm may not be universally applicable, especially in poor and resource-limited countries, due to its expensive costs and the requisite expertise and manpower needed to conduct high-quality uterine artery Doppler assessments around 12 weeks of gestation (Poon and Nicolaides, 2014). Moreover, in these contexts, the availability of serum indicators such as PAPP-A and PlGF may be significantly limited.

The dose of LDA is still a major controversial topic, it is important to note that in the Roberge et al. systematic review, the OR for developing PE was also 0.47 – virtually all the studies in this review used 100 mg of aspirin, i.e., similar efficacy as in the ASPRE trial (Roberge et al., 2018). Recent meta-analysis and pharmacokinetic studies, however, continue to contribute towards a growing body of evidence that favours the use of 150 mg daily (Ghesquiere et al., 2023; Shanmugalingam et al., 2019b) Nevertheless, current RCTs comparing the efficacy and side effect of various doses of Aspirin will provide better clarity on the optimal dose of aspirin in preventing PE (Brito et al., 2019; Sinha et al., 2023).

Research over the past decade has shown that the effect of LDA involves much more than just correcting the PGI2/TXA2 imbalance. The fact that LDA only prevents EOP and has no effect on LOP clearly indicates the importance of LDA affecting placentation/TB function. The mechanism of COX-2 inhibition can improve the RAAS, ROS/NOS pathways, restore the angiogenesis balance, vascular function, and generate the substance 15-epi-Lipoxin A4, which possesses potent anti-inflammatory characteristics (Shanmugalingam et al., 2020). All of these effects may contribute via different pathways in the prevention of PE (Figure 1) (Shanmugalingam et al., 2020; Mirabito Colafella et al., 2020).

LDA is considered to be efficacious in preventing PE when administered at a dosage of ≥100 mg (preferably 150 mg), taken at night, and initiated before the 16th week of pregnancy and continued until the 36th week of pregnancy or until delivery (Brownfoot and Rolnik, 2024; Shen et al., 2021). ACOG, ISSHP, FIGO, SOMANZ, and NICE advise administering LDA to pregnant women who are at a high risk of developing PE, however, the recommended doses and time of initiation differs among these guidelines (Chang et al., 2023b; Bokuda and Ichihara, 2023) (Table 1).

Calcium and vitamin D

Oral calcium supplementation is recommended as an additional preventative intervention in women with inadequate dietary calcium intake (<1 g/day) (Magee et al., 2022; Hofmeyr et al., 2019) Calcium minimises endothelial cell activation through anti-inflammatory cytokines and upregulation of NO (Cabral-Pacheco et al., 2020; López-Jaramillo et al., 1995). Hypocalcemia can lead to activation of parathyroid glands, which in turn promotes the secretion of renin. Elevated intracellular calcium levels will induce vasoconstriction (Figure 2) (van Gelder et al., 2022). A Cochrane study demonstrated evidence from 27 randomized controlled trials supporting the efficacy of calcium supplementation in preventing PE and preterm birth. Additionally, calcium supplement reduce the risk of maternal mortality and significant complications associated with high blood pressure during pregnancy (Hofmeyr et al., 2018). This is specifically intended for women who are following low calcium diets (Hofmeyr et al., 2018). This discovery is supported by the World Health Organization (WHO), which demonstrated that

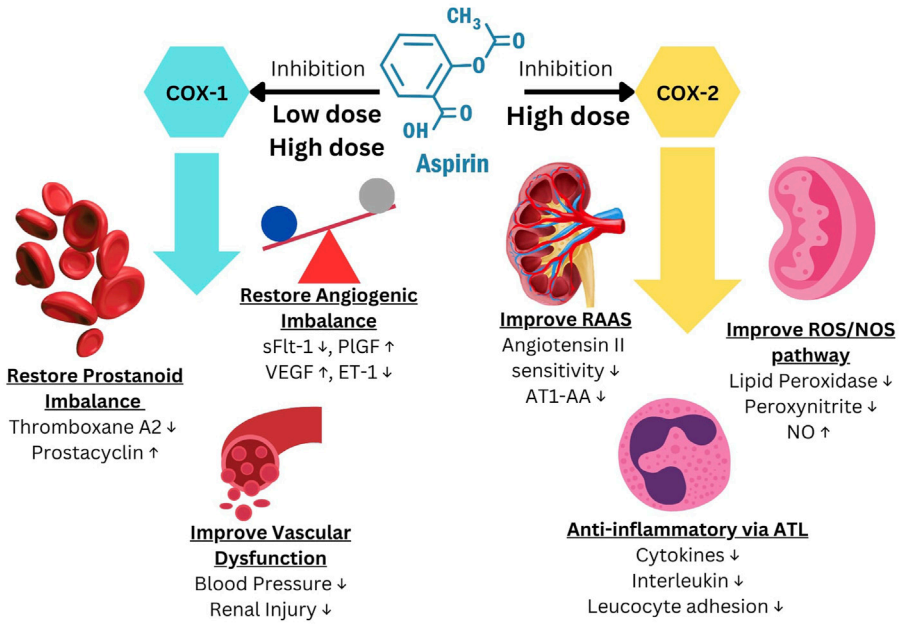

FIGURE 1
Aspirin mechanism of action to prevent Preeclampsia. Modified from Shanmugalingam et al. (2020), Mirabito Colafella et al. (2020).

TABLE 1 Comparison of recommendations on the use of aspirin in prevention of preeclampsia.

Organization	Indication	Timing	Dose
ACOG 2018	- Recommended for high risk pregnant women - Recommended for women with ≥1 moderate risk factors	Start from 12 to 28 weeks gestation (best at < 16 weeks), continued until delivery	81 mg/day
ISSHP 2018	- Recommended for high risk pregnant women	Start from <20 weeks gestation (best at < 16 weeks)	75–162 mg/day
NICE 2019	- Recommended for high risk pregnant women - Recommended for women with ≥1 moderate risk factors	Start from ≥12 weeks gestation, continued until delivery	75–150 mg/day
FIGO 2019	- Recommended for high risk pregnant women	Start from 11 to 14 weeks, and continued until 36 weeks, delivery, or onset of preeclampsia	150 mg/day
SOMANZ 2023	- Recommended for high risk pregnant women	Start prior of 16 weeks, and stop between 34 weeks until delivery, based on individualised judgement	150 mg/day
POGI 2016	- Recommended for high risk pregnant women	Start from <20 weeks gestation	75 mg/day

administering calcium to pregnant women in regions with calcium deficiency can effectively lower the risk of hypertension during pregnancy. According to a review by Brownfoot et a administering calcium has limited impact on reducing the likelihood of PE but it plays a crucial role in mitigating severe consequences associated with PE, such as eclampsia, severe gestational hypertension, and neonatal mortality (Brownfoot and Rolnik, 2024).

Nonetheless, Brownfoot's perspective has faced numerous challenges from different studies. Two systematic reviews report that calcium supplementation, as compared to a placebo, resulted in a 51%–55% decrease in the development of preeclampsia (Hofmeyr et al., 2018; Woo Kinshella et al., 2022). The advantages of supplementing remain consistent regardless of the dosage, risk of preeclampsia, time of calcium delivery, or co-interventions, particularly vitamin D. Nevertheless, the efficacy of calcium is restricted in people with inadequate initial calcium consumption. Administering calcium was linked to a slight 0.2% increase in the probability of developing HELLP syndrome, but it also resulted in a 1.0% decrease in the occurrence of death or severe maternal morbidity. While calcium does not definitively decrease the occurrence of preterm PE, it does lower the prevalence of preterm birth and infants with low birth weight (Woo Kinshella et al., 2022). A recent meta-analysis, which included 26 randomized controlled trials with a total of 20,038 participants, revealed that the administration of calcium resulted in a 49% reduction in the risk of PE and a 30% reduction in the risk of gestational hypertension when compared to a placebo. In addition, there was a propensity to decrease the occurrence of preterm labour, labour induction, small for gestational age, low birth weight infants, perinatal mortality, and maternal mortality in the group that received calcium supplementation (Jaiswal et al., 2024).

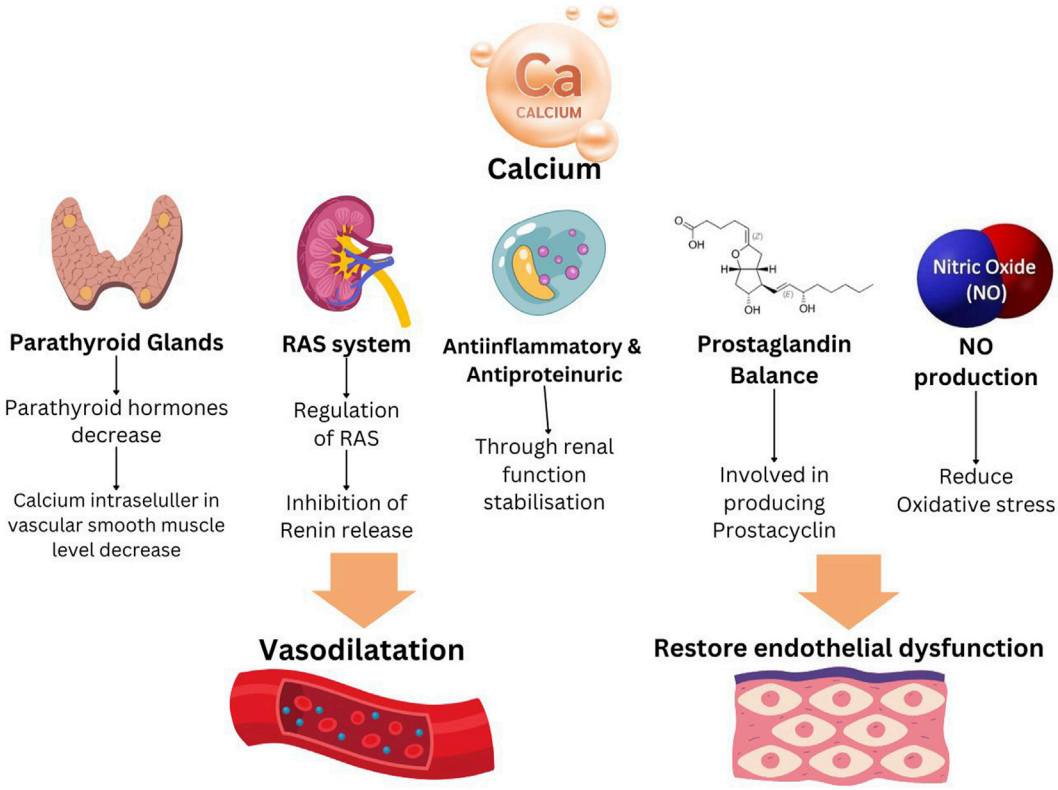

FIGURE 2
Mechanism of action of calcium in preeclampsia prevention.

Administering low doses of calcium, either alone or in combination with other nutrients, has been shown in multiple studies to decrease the occurrence of preeclampsia. Research indicates that the administration of high doses of calcium can effectively lower the likelihood of elevated blood pressure. Overall, calcium administration generally lowers the incidence of PE. However, this impact is most significant in pregnant women who have a poor intake of calcium. Pregnant women who have a low intake of calcium (<800 mg/day) are urged to consume either calcium replacement (<1 g elemental calcium/day) or calcium supplementation (1.5–2 g elemental calcium/day) in order to decrease the likelihood of developing preeclampsia (Poon et al., 2019).

New evidence indicates that the dosage of calcium does not impact its efficacy in preventing PE. Kinshella et al. performed a network meta-analysis (NMA) to assess the efficacy of low dose (<1 g/day) and high dose (>1 g/day) calcium supplementation in the prevention of PE. The evaluation of calcium dose by the NMA included 25 trials with a total of 15,038 participants. In contrast, the meta-analysis included 30 trials with a total of 20,445 women. Calcium supplementation at both high and low doses effectively reduced PE, with a relative risk (RR) of 0.49 and 95% confidence intervals (CI) of 0.36–0.66 and 0.49%, 95% CI 0.36–0.65, respectively. According to the NMA, there was no clear difference in the impact of high-dose calcium compared to low-dose calcium (RR 0.79%, 95% CI 0.43–1.40). The Cochrane research also endorses the use of either high or low doses of calcium to prevent PE. Nevertheless, the administration of a low dosage of calcium did not exhibit a distinct impact on preterm birth, stillbirth, or mortality prior to departure from the hospital (Hofmeyr et al., 2018). Calcium was found to be similarly effective regardless of the risk of PE in early pregnancy, the simultaneous use of vitamin D, or the date of calcium initiation (Woo Kinshella et al., 2022).

In conclusion, the WHO (2018) recommends for daily oral calcium supplementation at a dosage of 1.5–2 g (elemental calcium) in populations with insufficient dietary calcium consumption to mitigate the risk of PE, irrespective of individual preeclampsia risk factors (WHO, 2018). The most recent recommendations (2020) propose for calcium supplementation prior to pregnancy (preconception) to reduce the risk of PE, but within the context of scientific research (WHO) (WHO, 2024). A 2019 multicountry trial (n = 1355) compared 500 mg calcium or placebo daily from enrolment before pregnancy to 20 weeks of gestation, then 1.5 g calcium/day in both groups. The intervention did not reduce PE overall, but participants with compliance of more than 80% from the last prepregnancy visit to 20 weeks had a statistically significant effect (RR = 0.66, 95% CI: 0.44–0.98; P = 0.037). This is the basis of WHO's latest recommendations (Hofmeyr et al., 2019). The summarized recommendation for calcium supplementation during pregnancy to prevent preeclampsia is presented in Table 2.

PE has been linked to hypovitaminosis D (Bodnar et al., 2007; Ilham et al., 2019). Multiple hypotheses propose a relationship between vitamin D levels and the development of PE. Among these are vitamin D's functions in the modulation of pro-inflammatory responses and the reduction of oxidative stress in PE, the promotion of angiogenesis through VEGF and gene

TABLE 2 Calcium suplementation during pregnancy to prevent preeclampsia.

Mechanisms of action	- Vasodilators caused by - Inhibition release of renin from parathyroid glands - Reduce intracelullar calcium level in vascular smooth muscle - Upregulations of NO - Anti-inflammatory properties - Inhibiton of endothelial activation (López-Jaramillo et al., 1995; van Gelder et al., 2022; Omotayo et al., 2016)
Target population	Pregnant women with low dietary calcium consumption (<800 mg/day) (WHO, 2018; Omotayo et al., 2016)
Calcium type	Calcium carbonate (Omotayo et al., 2016)
Doses	- WHO recommends 1.5–2 g daily (WHO, 2018) - Some evidence suggest dose less than 1 g/day (low dose) may be beneficial (Omotayo et al., 2016)
Timing	Start as early as possible in pregnancy, limited evidence suggest to start before pregnancy (pre-conception) (Hofmeyr et al., 2019; Poon et al., 2019)

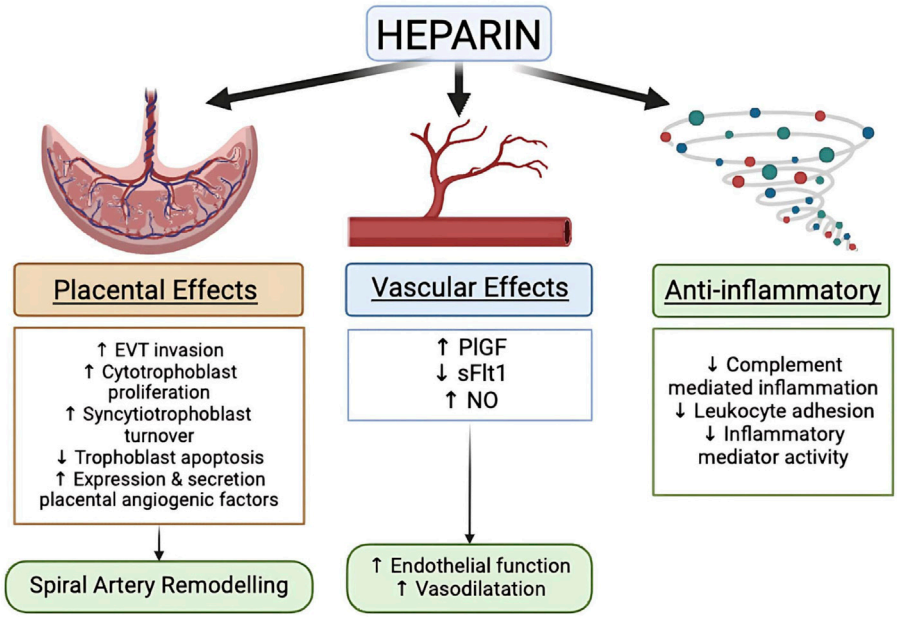

FIGURE 3
Heparin mechanism on the prevention of PE [modified from Wat et al. (2018a)].

modulation, and the reduction of blood pressure through the renin-angiotensin system (RAS) (Purswani et al., 2017). Nevertheless, the findings of numerous studies demonstrate contradictory outcomes for the efficacy of vitamin D in avoiding preeclampsia. The updated systematic review in Cochrane (2024) indicated that among eight studies, vitamin D supplementation compared to placebo for the prevention of PE demonstrated uncertain evidence (Palacios et al., 2019). In other systematic review by Purswani JM et al., showed that the evidence of the role of vitamin D in preventing PE is inconsistent (Purswani et al., 2017). These conclussion was taken mostly from observational study and only two RCT involved in this review. In a 50-year-old controlled experiment with 5,644 women, Olsen and Secher demonstrated a 31.5% reduction in the incidence of preeclampsia following multivitamin and mineral supplementation. This study wasn't focused just on vitamin D as a preventive measure for PE, but rather included multivitamin and mineral supplements (Olsen and Secher, 1990). However in Alimoradi's metanalysis including 19 studies, it was shown that the supplementation of vitamin D reduce the risk of PE for 39% (RR: 0.61; 95% CI: 0.47–0.78; $p = 0.27$) (Alimoradi et al., 2024). This was supported by AlSubai's metanalysis including 10 RCT and 24 observational studies with the same result (OR: 0.50; 95% CI: 0.4–0.63; $p = 0.00001$) (AlSubai et al., 2023). In summary, the evidence regarding the utilization of vitamin D as a preventive measure for PE remains inconclusive. Nonetheless, there exists a certain potential in utilizing these agents for the prevention of PE, particularly within populations deficient in vitamin D.

Low molecular weight heparin (LMWH)

Already in 1976, Bonnar and Redman contemplated whether or not there could be a place for heparin in the prevention of PE. Now 50 years later and after many trials, the role of LMWH in the

prevention of PE still is still a topic of debate (Bonnar et al., 1976). Although heparin and the various LMWH's are primarily known as anticoagulant agents, as a group they clearly also possess many anticoagulant-independent properties that may be relevant in the prevention of PE, including effects on placental, vascular and inflammatory function (Figure 3) (Wat et al., 2018a). A meta-analysis by Roberge et al. on 8 studies found that combined LMWH and LDA therapy is superior to LDA alone in preventing recurrent PE (relative risk [RR] 0.54, 95% CI 0.31–0.92) and SGA births (RR 0.54, 95% CI 0.32–0.91) (Roberge et al., 2016). A separate meta-analysis conducted by Rodger et al. also showed that LMWH–the most commonly prescribed heparin derivative, including dalteparin, enoxaparin, and nadroparin are effective in augmenting the preventive efficacy of aspirin as compared with LDA alone (14% *versus* 27%) (Rodger et al., 2016). However, LMWH alone does not appear to significantly reduce the rates of PE or SGA births, suggesting that is has synergistic effects with aspirin (Singh et al., 2024). Despite these promising findings, several recent large multicentre trials, such as the EPPI, HEPEPE and TIPPS trials, did not find similar beneficial effects of LMWH therapy for PE prevention.

The New Zealand (NZ) non blinded trial (EPPI) by Groom et al. examined the use of 40 mg of enoxaparin in 155 high-risk women; concerns about this trial would be that it included patients with BMI's > 40. Also, the subgroup of patients with prior preterm PE (<36 weeks) was only 30 *versus* 38. Regarding the dose, we clearly miss good data on pharmacokinetics of LMWH in very obese pregnant women, also as addressed earlier, we still don't know exactly what the main beneficial effect is of LMWH (Groom et al., 2016). The French study by Haddad et al. (HEPEPE) looked at placenta-mediated pregnancy complications. In an open label multicentre trial 124 patients received 100 mg of enoxaparin plus 100 mg of aspirin *versus* only aspirin. The rate of placenta-mediated complications was only modestly but not significantly reduced in the LMWH group 34.4% compared with 41% (relative risk 0.84, 95% CI 0.61–1.16, P = 0.29). This is an important study using a more adequate dose of enoxaparin. However, it should be noted that only 4 *versus* 7 patients had a history of early-onset PE, close to 50% in both groups were included for prior fetal losses <22 weeks (Haddad et al., 2016).

Furthermore, the use of LMWH for the prevention of PE carries more potential risk than the use LDA, such as bleeding and heparin-induced thrombocytopenia, although such risks were demonstrated to be minimal in recent randomized clinical trials (Arepally, 2017; Zullino et al., 2021). One of the primary limitations of these large trials is the inclusion of all patients with the preeclamptic syndrome with out consideration of the underlying etiology, thereby diluting the potential efficacy of LMWH therapy, which may benefit only a subset of patients. Therefore, further investigation is justified to evaluate the therapeutic potential of LMWH for the prevention of PE (McLaughlin et al., 2018).

A classic example is the very large well conduced multicentre TIPPS trial by Rodgers et al.; a trial that took 12 years to complete and eventually included 143 "high risk" patients receiving dalteparin and 141 placebo on top of LDA (Rodger, 2014). This ambitious study, where we can only admire the stamina of the researchers, tried to look at "everything," prevention of venous thrombo-embolism, pregnancy loss and placenta-mediated complications. The TIPPS study did not show any benefit. But the authors failed to emphasize that close to 90% of patients were included for just having a simple thrombophilia like factor V, prothrombin gene or protein S deficiency. Clearly just having one of these thrombophilia does not require prophylactic treatment with LMWH (and importantly this was confirmed by the TIPPS study). Only 20 *versus* 25 had a history of PE (gestational age not even provided), as such the TIPPS study was very much underpowered to address the prevention of preterm PE (Rodger, 2014).

The most recent systematic review by Lemini et al. included 15 studies (also the aforementioned study by Haddad et al. and even the TIPPS study), with a total of 2795 participants. In high-risk women, treatment with LMWH in addition to LDA was associated with a reduction in the rate of PE, (OR 0.62; 95%: 0.43–0.90; P¼.010); SGA (OR 0.61; 95% CI 0.44–0.85) and perinatal death (OR 0.49; 95% CI 0.25–0.94). The authors of this review do emphasize their concerns about methodological quality of the studies ranged from moderate to very low owing to concerns about the risk of bias (double blinding not possible), type of patients included (e.g., TIPPS) and the variable dose of LMWH (Cruz-Lemini et al., 2022).

In summary, just having a thrombophilia does not warrant the use of prophylactic LMWH. The benefits of LMWH (similar to LDA) are clearly pleiotropic, and much more than just antithrombotic (Wat et al., 2018b). LMWH should not be used as a routine in the prevention of PE, but their use in combination with LDA has a defined place in preventing recurrent placental mediated complications (with or without PE) particular in the group of patients with documented prior placental vasculopathy.

Pravastatin

Statins are commonly utilized to reduce cholesterol levels and manage cardiovascular risks. Statins function as inhibitors of the enzyme HMG-CoA reductase, which is responsible for the production of 3-hydroxy-methylglutaryl coenzyme A (HMG-CoA)(ref). Statins are gaining prominence in studies as a potential preventive agent for PE. Laboratory studies, involving molecular analysis, animals, and preclinical research, have shown that statins have beneficial effects on many pathways involved in the development of PE (Katsi et al., 2017; Ramma and Ahmed, 2014; Ilham Aldika Akbar, 2021). The pleiotropic potentially beneficial effects of pravastatin in preventing PE are presented in Figure 4.

Pravastatin has been found to reverse angiogenic imbalance and placental hypoxia, characterized by elevated sFlt-1 expression, in experimental mice with preeclampsia (Ahmed and Ramma, 2015). The cause of this effect is believed to be the activation of the heme oxygenase 1/carbon monoxide (HO-1/CO) pathway. The treatment of statins in both *in vivo* and *in vitro* experiments resulted in an increase in the expression and transcription of HO-1 in endothelial cells, vascular smooth muscle, and other cells. HO-1 is a crucial antioxidant protein that plays a significant role in the process of converting heme into biliverdin, resulting in the release of carbon monoxide (CO) and ferrous ions (Fe^{2+}) (Saad et al., 2014). Activation of this pathway suppresses the secretion of sFlt-1 and sEng from endothelial and placental cells, and is believed to promote the synthesis of VEGF and P1GF. In the end, the production of ET-1

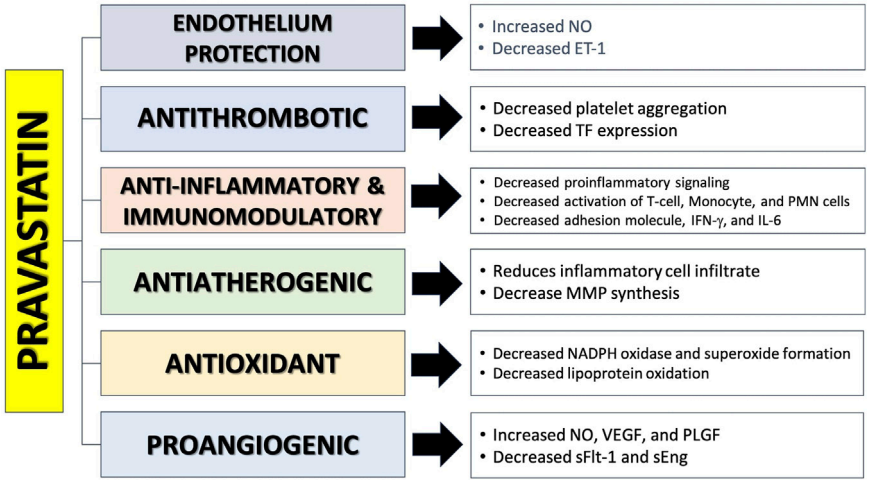

FIGURE 4
The mechanism of action of pravastatin in preventing preeclampsia (Katsi et al., 2017; Ramma and Ahmed, 2014; Vahedian-Azimi et al., 2021; Girardi, 2017; Tong et al., 2022a; Mészáros et al., 2023a; Akbar et al., 2021a; Akbar et al., 2024).

will decrease and the levels of NO will increase as a result of decreased oxidative stress in endothelial cells (Akbar et al., 2021a; Saad et al., 2014; Akbar et al., 2022). Brownfoot et al. reported that pravastatin has the potential to decrease the release of sFlt-1 from isolated cytotrophoblast cells and human umbilical vein endothelial cells (HUVEC) acquired from preeclamptic patients (Brownfoot et al., 2015; Brownfoot et al., 2016a). Pravastatin is also able to reduce the expression of VCAM-1 and ET-1 and reduce leukocyte adhesion to endothelial cells. During a trial investigation with HUVEC, pravastatin had the least harmful effect when compared to simvastatin and rosuvastatin. All three statins shown efficacy in lowering ET-1 and sFLt-1, which are crucial variables contributing to endothelial dysfunction, during this experiment. High doses of simvastatin and rosuvastatin exhibit harmful effects on endothelial cells (Rodger, 2014; Cruz-Lemini et al., 2022).

Additional preclinical studies also suggested that pravastatin may have a preventive effect on PE due to its positive impact on maternal and placental blood vessels (Tong et al., 2022b). Costantine et al. conducted a small pilot randomized controlled trial (RCT) focussed on pharmacokinetics and side effects with a sample size of 20, and found a lower (non-significant) rate of PE in the pravastatin group (0 *versus* 4). Importantly, cord blood profiles were not different and pravastatin levels in cord blood were below detection level. Administration of pravastatin also improved the patient's angiogenic profile by reducing levels of sFlt-1 and sEng, and boosting levels of PIGF (Costantine et al., 2016). The first sizeable (unblinded) multicenter RCT was conducted by Akbar et al. In this multicentre trial high risk patients with an estimated risk of 40% for developing PE were receiving LDA vs. LDA plus 20 mg bd pravastatin. In the Surabaya arm of this Indonesian INOVASIA study various PE biomarkers and cytokines were also examined. The biomarkers can be divided based on their action in the pathogenesis of PE: the anti-angiogenic factors (driving the development of PE), i.e., sFlt-1, sEng, sFlt-1/PlGF ratio, IL-6, and ET-1; and the pro-angiogenic factors (reducing PE risk), i.e., PlGF, VEGF, and NO (Akbar et al., 2021a). Pravastatin demonstrated the ability to stabilize fluctuations in levels of sFlt-1, PlGF, sFlt-1/PlGF ratio, and sEng when compared to the control group (Akbar et al., 2021b). The control group had a noteworthy rise in sFlt-1, sFLt-1/PlGF ratio, sEng, and PlGF, indicating alterations in the development of PE. In addition, Akbar et al. study shown that the administration of Pravastatin not only enhanced NO levels but also decreased IL-6 and ET-1 levels (Akbar et al., 2021a). Figure 5 provides an overview of all effects of pravastatin on the various biomarkers changes on Pravastatin administration based on INOVASIA study.

The overall results of the Indonesian multicentre RCT included 87 women in the treatment group and 86 women in the control group. The use of pravastatin greatly decreases the occurrence of preterm PE (odds ratio = 0.034; 95% CI0.2–0.91) and (mostly iatrogenic) premature birth (OR 0.340; 95% CI0.165–0.7). There was no effect on the overall PE rate, but because of the beneficial effects of pravastatin on preterm PE, administration of pravastatin also improved perinatal outcomes, such as increased Apgar scores and reduced incidence of low birth weight infants. Furthermore, there were no cases of congenital anomalies observed in the infants of mothers who were administered pravastatin (Akbar et al., 2022).

A recent systematic analysis conducted by Akbar et al. has shown that Pravastatin is linked to a decreased likelihood of PE (OR: 0.51; 95% CI: 0.29–0.90), preterm PE (OR: 0.034; 95% CI: 0.202–0.905), and preterm birth (OR: 0.31; 95% CI: 0.16–0.58). Pravastatin had no effect on the likelihood of developing PE with severe characteristics and having a small size for gestational age. Pregnant women who were administered pravastatin experienced improved perinatal outcomes, including mean higher birthweight, better Apgar scores, reduced NICU admission rates, shorter length of stay, and lower incidence of respiratory distress syndrome (Akbar et al., 2024). The findings of these studies suggest that Pravastatin has potential as a preventive treatment for PE, particularly preterm PE, as well as (iatrogenic) preterm labour. Additional long term follow up research is required to repeat these findings in different populations with particular focus on neurodevelopment milestones in pravastatin exposed infants.

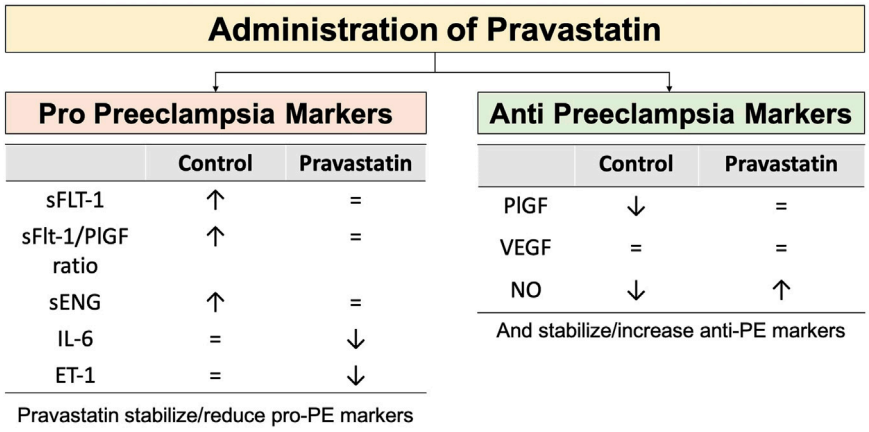

FIGURE 5
The effect of administration of Pravastatin in serum biomarkers changes in high risk PE pregnant women *versus* control. Pravastatin has the ability to stabilize or decrease the levels of pro-PE markers. In the control group, there is an observed increase in the levels of pro-PE markers. Pravastatin has the effect of stabilizing or increasing the levels of anti-PE markers. In the control group, there is a considerable fall in the levels of anti-PE markers. Pravastatin protects against alterations in biomarkers that contribute to the development of PE (Akbar et al., 2021a; Akbar et al., 2021b). Notes: ↑: increase level, ↓: decrease level, = : no significant changes.

Metformin

Metformin is a drug to increase insulin sensitivity and reduce blood glucose levels. Metformin is commonly used as a treatment for Polycystic Ovary Syndrome (PCOS) and gestational diabetes mellitus during pregnancy. Experimental studies have demonstrated that Metformin exerts an influence on many parameters that contribute to the reduction of PE risk in animal models. Metformin is believed to inhibit nuclear factor kappa B (NF-kB) by activating the AMPK pathway, which leads to a decrease in the production of pro-inflammatory substances such IL-1B, IL-6, TNFα, IL-8, and IL-2. Additionally, metformin increases the activity of eNOS, which promotes the release of nitric oxide (NO) and prostaglandin E2 (PGE2). Another study shown that metformin effectively suppressed the activity of VCAM1 and ICAM1 within endothelial cells, leading to enhanced vascularization. Additionally, metformin increased the levels of matrix metalloproteinase 2 (MMP-2) and vascular endothelial growth factor (VEGF) (Brownfoot et al., 2016b; Poniedziałek-Czajkowska et al., 2021). In human studies, metformin has been found to decrease protein and gene expression from inflammatory endothelium cells, as well as VCAM-1, in individuals with diabetes mellitus and impaired glucose tolerance. In another research study, metformin was found to decrease the levels of sFlt-1 and sEng in human tissue, most likely by inhibiting the mitochondrial transport chain. This chain was found to be more active in placentas affected by preterm PE. Metformin has the ability to decrease endothelial dysfunction and enhance angiogenesis (Brownfoot et al., 2016b). The mechanism of action by which metformin prevents PE is displayed in Figure 6.

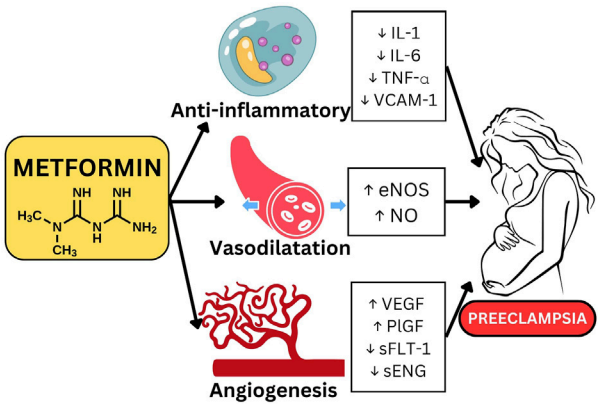

FIGURE 6
Metformin mechanism of action in reducing Preeclampsia risk.

The impact of metformin on the probability of developing PE varies across studies, maybe due to variations in dosage (ranging from 500 to 3,000 mg/day), the presence of different underlying conditions (such as obesity, PCOS, gestational diabetic mellitus, or type 2 DM), or differences in the timing of medication starting (ranging from 6 to 36 weeks). Metformin has a notable impact on reducing the occurrence of PE in pregnant women who have morbid obesity. However, in pregnancies complicated by gestational diabetes mellitus, multiple studies have found no statistically significant difference in the occurrence of PE between the group receiving metformin and the control group. The metformin group did not experience a reduction in the risk of PE or gestational hypertension, indicating the ineffectiveness of metformin in this regard (Poniedziałek-Czajkowska et al., 2021). The EMPOWAR research was a clinical experiment that assessed the impact of providing metformin to pregnant obese women. The trial was randomized, double-blind, and placebo-controlled. The experimental cohort received a daily dosage of metformin ranging from 500 to 2,500 mg, starting at 12 weeks of age and continuing until delivery. No significant difference in the occurrence of PE was seen between the groups receiving metformin and placebo (Chiswick et al., 2015).

The meta-analysis conducted by Alqudah A et al. included 5 randomized controlled trials (RCTs) that compared metformin

with placebo. The study indicated no significant difference in the risk of PE between the two groups RR = 0.86 (95% CI 0.33–2.26), p-value of 0.76. However, positive outcomes were observed in terms of lower maternal weight gain and a reduced risk of PE when compared to the insulin group (McDougall et al., 2022). Kalafat et al. conducted a meta-analysis of 15 randomized controlled trials (RCTs) and discovered that in women with gestational diabetes, the use of metformin was linked to a lower risk of pregnancy-induced hypertension compared to insulin. Additionally, there was a slightly lower risk of PE, but this reduction was not statistically significant. In obese women, the usage of metformin was found to have a minimal effect on reducing the incidence of PE, when compared to a placebo (Kalafat et al., 2018). In metaanalysis involving 35 studies, Metformin was associated with lower gestational weight gain (1.57 kg ± 0.60 kg; I_2 = 86%, $p < 0.0001$) and likelihood of PE (OR 0.69, 95% CI 0.50–0.95; I_2 = 55%, $p = 0.02$) compared to placebo (Tarry-Adkins et al., 2021). In another study, Metformin was reported to reduce the risk of abortion, preterm PE, preterm labor, and gestational HT (He et al., 2023).

Multiple studies have identified an increased risk of harm to the unborn child when metformin is used during pregnancy. Studies also indicate a correlation between the consumption of metformin during pregnancy and the occurrence of a small for gestational age fetus. The reason for this is believed to be that metformin influences the availability of nutrients and the growth of the fetus by inhibiting mitochondrial complex I. The fetus may experience cardiometabolic issues as a result of an imbalance between folic acid and vitamin B12. Therefore, it is advisable to take these B vitamins in conjunction with metformin administration (Verma and Mehendale, 2022). It should be note that the FDA categorizes Metformin as safe (category B) for pregnant women (Mészáros et al., 2023a). (Akbar et al., 2021b).

Proton pump inhibitor

Proton Pump Inhibitors (PPIs) hinder the activity of the hydrogen-potassium-ATPase pump located in the parietal cells lining the stomach, resulting in a decrease in the production of gastric acid. PPIs are often prescribed medications for the treatment of gastric reflux disease. PPI have been deemed safe for use by pregnant women according to a meta-analysis study (Matok et al., 2012). The impact of PPI on the prevention or treatment of PE is currently under investigation (Hastie et al., 2019). Experimental investigations have shown that PPIs have the ability to decrease sFlt-1 levels in animals (Gu et al., 2022). Onda et al. reported that the administration of PPI can decrease the production of sFlt-1 and sEng in several types of cells, including primary trophoblast cells, normal and preeclamptic placental cells, HUVECs, and primary uterine microvascular cells. Esomeprazole, the most powerful PPI, exerts a vasodilatory impact on blood vessels and reduces blood pressure by affecting endothelial cells (Onda et al., 2017). The study conducted by Saleh et al. shown a correlation between the use of PPI and a reduction in blood sFlt-1 levels in pregnant women who had or were suspected to have PE. In addition, PPI can also decrease the levels of endoglin and ET-1 (Saleh et al., 2017). Administration of PPI has the ability to decrease the production of certain pro-inflammatory cytokines, including IL-1b, IL-6, IL-10, and CC-motif chemokine ligand (CCL) (Onda et al., 2017). The mechanism of action of PPI to prevent preeclampsia is illustrated in Figure 7.

A cohort study conducted in South Korea found no evidence to suggest that the use of PPIsr educes the incidence of PE in pregnant women. Nevertheless, in this investigation, the dosage administered was equivalent to the therapeutic dosage prescribed for gastrointestinal issues. The precise dosage required for the prevention of PE remains uncertain (Choi and Shin, 2021). These findings are in line with the meta-analysis of Hussain et al., that the use of PPIs in pregnancy actually increases the risk of PE at any gestational age, even though the risk is very small or trivial (Hussain et al., 2022). The study conducted by van Gelder et al. concluded that administering PPI does not decrease the likelihood of developing LOP. In fact, the risk of developing this condition actually increases when PPI are used between the 17th and 33rd weeks of gestation (van Gelder et al., 2022). In another cohort study, PPIs were associated with the incidence of PE in term pregnancies. On the other hand, it was found that there was a reduced risk of PE with complications of preterm birth or with complications of birth weight that was not appropriate for the gestational age. It can be concluded that PPIs have the theoretical potential to prevent EOP (Hastie et al., 2019), currently preventative trials using PPI's are in progress. (Poniedziałek-Czajkowska et al., 2021; Chiswick et al., 2015)

Multiple studies have confirmed the safety of using PPI during pregnancy, making them a common prescription for managing gastrointestinal issues in pregnant women. Numerous studies have shown that PPIs are safe for the fetus, and newborn, i.e., no congenital anomalies, normal birthweight distribution, and no adverse effect on Apgar scores (Chiswick et al., 2015; McDougall et al., 2022)

Nitric-oxide donor (NO)

Nitric oxide (NO), originally identified as the endothelium-derived relaxing factor, is the main vasodilatory substance produced by the endothelium in response to chemical and mechanical stimuli. Nitric oxide is a signalling chemical that is created by a group of enzymes called nitric oxide synthases (NOS), which are dependent on calcium and calmodulin (Förstermann and Sessa, 2011). These enzymes produce nitric oxide from L-arginine. In this context, endothelial NOS is the most significant. Nitric oxide triggers the relaxation of vascular smooth muscle cells by inducing soluble guanylate cyclase (sGC). This process triggers an increase in the levels of cyclic guanosine 3′,5′-monophosphate (cGMP) inside the cells and activates protein kinases that are dependent on cGMP. PE-related endothelial dysfunction is characterized by a reduced availability of NO. Therefore, it is postulated that this will lead to an elevation in blood pressure due to the imbalance between the vasodilator and vasoconstrictor effects on the smooth muscle of the blood vessels. Nitric oxide exerts substantial inhibitory effects on platelet aggregation and activation through processes that are dependent on both cGMP and independent of it. NO also hampers the growth of vascular smooth muscle cells and the stimulation of inflammatory cells, among other tasks. Moreover,

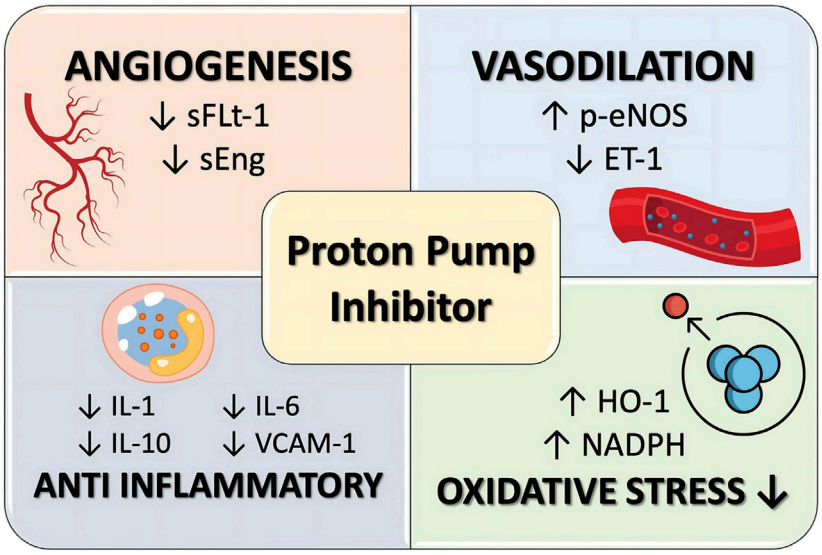

FIGURE 7
PPI mechanism of action in preeclampsia prevention.

the process of S-nitrosylation, in which proteins are modified by the addition of NO, has the capability to control their activity, hence potentially impacting biological processes. Pregnant women with normotension display significant alterations in the placental S-nitroso-proteome compared to those without high blood pressure during pregnancy (Johal et al., 2014).

A systematic review of the Cochrane database, encompassing six studies, revealed a lack of conclusive evidence on the efficacy of NO donors and precursors in preventing PE or its sequelae (Meher and Duley, 2007). The review's conclusions are mostly constrained by the insufficient sample size. The comparison of NO donor or its precursor (L-arginine) with placebo or no intervention was conducted in four studies. The available information is inadequate to establish definitive conclusions regarding the effectiveness of nitric oxide donors and precursors in preventing pre-eclampsia or its associated problems. The relative risk (RR) is 0.83 with a 95% confidence interval (CI) of 0.49–1.41. Adverse effects that occur following the administration of NO donor supplements, such as isosorbide mononitrate, may include intense headaches that are significant enough to lead to discontinuation of the treatment. Recent research indicates that isosorbide mononitrate and L-arginine have equivalent (lack of) efficacy in preventing PE (Dymara-Konopka and Laskowska, 2019). Currently, there is very limited information about the preventive effectiveness of these drugs in women who are at risk of developing pre-eclampsia.

L-arginine

L-Arginine is a semi-essential amino acid that serves as a precursor to NO through the NOS enzymatic pathway. L-arginine is the primary precursor of NO during pregnancy, which is crucial for maintaining a sufficient blood supply to the placenta. Various studies yielded divergent results concerning alterations in L-arginine levels in PE (Wardhana et al., 2021). According to the research conducted by Tashie et al., which corresponds with other prior studies, women with PE had elevated levels of ADMA, which led to reduced levels of NO due to the inhibition of eNOS. ADMA functions as a competitive inhibitor of eNOS activity. The bioavailability of L-arginine plays a crucial role in determining the production of NO in the body. Optimal synthesis of nitric oxide (NO) occurs at physiological levels of L-arginine. The study found that the levels of L-arginine were within the normal range, however in the group with PE, the levels were comparatively elevated compared to the placebo group. This is believed to be caused by a malfunction in the transportation of L-arginine through the y + transport system or by an increase in ADMA, which hinders the uptake of L-arginine by cells through the y + transport system by acting as a competitive inhibitor (Tashie et al., 2020). These findings contrast with numerous studies that have found a decline in L-arginine levels in women with PE compared to women with normal blood pressure (Dymara-Konopka and Laskowska, 2019; Wardhana et al., 2021). The reduction in L-arginine levels is also observed in cases of severe PE (Wahyuningsih et al., 2021). The reduction of L-arginine levels, acting as a competitive inhibitor of ADMA, will lead to the impairment of NO signalling in PE (Dymara-Konopka and Laskowska, 2019).

Supplementation of L-arginine in combination with vitamins C and E prior to 24 weeks of pregnancy shown a notable decrease in the occurrence of PE as compared to the group that received a placebo (Vadillo-Ortega et al., 2011). Supplementing pregnant women with chronic HT with L-arginine can decrease the necessity for HT medications, but it does not decrease the occurrence of superimposed PE (Dymara-Konopka and Laskowska, 2019). Administering L-arginine has been shown to decrease the occurrence of PE by 74% in the study conducted by

TABLE 3 Meta-analysis studies the effect of L-Arginine suplementation on pregnancy.

No	Authors (year)	Number of study and participants	Methods	Results
1	Chen et al. (2016)	9 trials (576 participants)	L-arginine vs. placebo	- Increase fetal birth weight - Increase gestational age on delivery - Decrease newborn RDS rates - Decrease newborn ICH - Decrease pulpability index on Umbilical Artery
2	Sagadevan et al. (2021)	7 studies (524 participants)	L-arginine vs. placebo	- Decrease PE risk (OR: 0.38; 95% CI: 0.25–0.58) - Decrease blood pressure (both systolic and diastolic) - No effect on gestational age, latency periods, and neonatal outcomes (birth weight and Apgar scores)
3	Goto (2021b)	10 studies	L-arginine vs. placebo	- Decrease pretem birth and FGR risk - Decrease newborn RDS rate - Increase fetal birth weight and gestational age on delivery - Increase newborn Apgar score - No effect on miscarriage, infection, ICH, admission to NICU, and cesarean section rates

Camarena Pulido et al. (2016). These findings align with the study conducted by Nadia Taj et al., which also reported an efficacy rate of 92.3% (Taj et al., 2022). Ortega et al. conducted a RCT to compare the effects of administering food supplements including L-arginine and antioxidant vitamins with a placebo in preventing PE in high-risk groups. The occurrence of PE was notably lower in the treatment group as compared to the placebo group, with an absolute risk reduction of 0.17 (95% CI = 0.12–0.21; $p < 0.001$). Additionally, administering L-arginine in combination with antioxidant vitamins demonstrated a more effective preventive impact compared to administering antioxidant vitamins alone. The absolute risk decrease was 0.09 (95% CI 0.05–0.14, $p = 0.004$) (Vadillo-Ortega et al., 2011). A meta-analysis of 10 trials indicated that oral L-arginine supplementation was associated with a decreased risk of neonates with fetal growth restriction, preterm labor, and respiratory distress syndrome. (Goto, 2021a). Multiple studies have revealed variations in the recommended safe amount and duration of arginine supplementation for pregnant women. However, one observational study concluded that a daily dose of 30 g of arginine for a period of 90 days is considered safe during pregnancy. Nevertheless, other studies have demonstrated favorable consequences on pregnancy results through the utilization of oral arginine supplementation at low dosages (3–7 g/day) for an extended duration (Weckman et al., 2019). Table 3 displays three recent meta-analyses regarding the efficacy of L-arginine in preventing PE.

Future direction

Currently, only aspirin and calcium (particularly in populations with deficient calcium levels) are considered approved medications for the secondary prevention of preeclampsia. Other medications shown promise efficacy in the prevention of preeclampsia include statins and L-arginine (Akbar et al., 2024; Akbar et al., 2022). Additional medicines that have inconsistent effects include Vitamin D, metformin, proton pump inhibitors, LMWH, and NO-donors. Extensive investigations are still required to ascertain the efficacy of these medications in preventing preeclampsia. Furthermore, additional agents with the potential for preventing preeclampsia are under investigation, including immunomodulators and anti-inflammatory agents (Tacrolimus, Eculizumab, Sulfasalazine, Etanercept, Hydroxychloroquine), micronutrients (Vitamin C, Vitamin E, DHA, Folic acid, Zinc, etc.), antioxidants (Sofalcone and Resveratrol), hormones (Melatonin), Sildenafil Citrate, and herbal extracts (Nigella sativa) (Brownfoot and Rolnik, 2024; Mészáros et al., 2023b; Rahma et al., 2017; Sakowicz et al., 2023; de Alwis et al., 2020).

Conclusion

Several pharmacological therapies demonstrate promise efficacy as preventative medicines for PE. LDA and calcium supplementation clearly represent the pivotal methods to reduce the rate of PE. Recent multicentre studies using pravastatin look very promising. Additional preventative medications, such as Metformin, LMWH, NO-donor, and L-Arginine, may be effective for particular patients with specific risk profiles (morbid obesity, placental thrombosis, etc.). Further research is required to arrive at a more individualized preventative approach for individual women with individual risk profiles and particularly also regarding timing of intervention, dose used and long-term safety.

Author contributions

MA: Conceptualization, Formal Analysis, Methodology, Resources, Software, Validation, Visualization, Writing–original draft, Writing–review and editing. RR: Conceptualization, Data curation, Investigation, Software, Writing–original draft, Writing–review and editing. KG: Formal Analysis, Project administration, Resources, Validation, Visualization, Writing–original draft, Writing–review and editing. RS: Conceptualization, Investigation, Methodology, Resources, Supervision, Validation, Writing–original draft, Writing–review and editing. GD: Conceptualization, Data curation, Formal

Analysis, Investigation, Methodology, Project administration, Supervision, Writing–original draft, Writing–review and editing.

Funding

The author(s) declare that no financial support was received for the research, authorship, and/or publication of this article.

Conflict of interest

The authors declare that the research was conducted in the absence of any commercial or financial relationships that could be construed as a potential conflict of interest.

Generative AI statement

The author(s) declare that Generative AI was used in the creation of this manuscript. We use Quillbot to do grammar checking and paraphrasing.

Publisher's note

All claims expressed in this article are solely those of the authors and do not necessarily represent those of their affiliated organizations, or those of the publisher, the editors and the reviewers. Any product that may be evaluated in this article, or claim that may be made by its manufacturer, is not guaranteed or endorsed by the publisher.

References

Ahmed, A., and Ramma, W. (2015). Unravelling the theories of pre-eclampsia: are the protective pathways the new paradigm? *Br. J. Pharmacol.* 172, 1574–1586. doi:10.1111/bph.12977

Ahn, T. G., and Hwang, J. Y. (2023). Preeclampsia and aspirin. *Obstet. Gynecol. Sci.* 66, 120–132. doi:10.5468/OGS.22261

Akbar, M. I. A., Azis, M. A., Riu, D. S., Wawengkang, E., Ernawati, E., Bachnas, M. A., et al. (2022). INOVASIA study: a multicenter randomized clinical trial of pravastatin to prevent preeclampsia in high-risk patients. *Am. J. Perinatol.* 41, 1203–1211. doi:10.1055/a-1798-1925

Akbar, M. I. A., Wungu, C. D. K., and Dekker, G. (2024). Role of pravastatin in the prevention of preeclampsia: a systematic review and meta-analysis of randomized-controlled trials. *J. Pharm. Pharmacogn. Res.* 12, 573–585. doi:10.56499/jppres23.1791_12.3.573

Akbar, M. I. A., Yosediputra, A., Pratama, R. E., Fadhilah, N. L., Sulistyowati, S., Amani, F. Z., et al. (2021a). Pravastatin suppresses inflammatory cytokines and endothelial activation in patients at risk of developing preeclampsia: INOVASIA study. *J. Maternal-Fetal Neonatal Med.* 35, 5375–5382. doi:10.1080/14767058.2021.1879785

Akbar, M. I. A., Yosediputra, A., Pratama, R. E., Fadhilah, N. L., Sulistyowati, S., Amani, F. Z., et al. (2021b). INOVASIA study: a randomized open controlled trial to evaluate pravastatin to prevent preeclampsia and its effects on sFlt1/PlGF levels. *Am. J. Perinatol.* 41, 300–309. doi:10.1055/a-1673-5603

Alimoradi, Z., Kazemi, F., Tiznobeik, A., Griffiths, M. D., Masoumi, S. Z., and Aghababaei, S. (2024). The effect of vitamin D supplementation in pregnancy on the incidence of preeclampsia: a systematic review and meta-analysis. *Eur. J. Integr. Med.* 66, 102343. doi:10.1016/J.EUJIM.2024.102343

AlSubai, A., Baqai, M. H., Agha, H., Shankarlal, N., Javaid, S. S., Jesrani, E. K., et al. (2023). Vitamin D and preeclampsia: a systematic review and meta-analysis. *SAGE Open Med.* 11, 20503121231212093. doi:10.1177/20503121231212093

Anto, E. O., Roberts, P., Turpin, C. A., and Wang, W. (2018). Oxidative stress as a key signaling pathway in placental angiogenesis changes oxidative stress as a key signaling pathway in placental angiogenesis changes in preeclampsia: updates in pathogenesis, novel biomarkers and therapeutics. *Curr. Pharmacogenomics Person. Med.* 16, 1–15. doi:10.2174/1875692117666181207120011

Arepally, G. M. (2017). Heparin-induced thrombocytopenia. *Blood* 129, 2864–2872. doi:10.1182/BLOOD-2016-11-709873

Beaufils, M., Donsimoni, R., Uzan, S., and Colau, J. C. (1985). Prevention of pre-eclampsia by early antiplatelet therapy. *Lancet* 1, 840–842. doi:10.1016/S0140-6736(85)92207-X

Bodnar, L. M., Catov, J. M., Simhan, H. N., Holick, M. F., Powers, R. W., and Roberts, J. M. (2007). Maternal vitamin D deficiency increases the risk of preeclampsia. *J. Clin. Endocrinol. Metab.* 92, 3517–3522. doi:10.1210/JC.2007-0718

Bokuda, K., and Ichihara, A. (2023). Preeclampsia up to date—what's going on? *Hypertens. Res.* 46, 1900–1907. doi:10.1038/s41440-023-01323-w

Bonnar, J., Redman, C. W., and Denson, K. W. (1976). The role of coagulation and fibrinolysis in preeclampsia. *Perspect. Nephrol. Hypertens.* 5, 85–93. Available at: https://europepmc.org/article/med/1005056 (Accessed July 29, 2024).

Brito, M. E., Ferreira, L. C., Cruz, J., Oliveira, N., Nemescu, D., Calomfirescu, M., et al. (2019). OP08.05: aspirin 100mg versus 150mg in pregnancy at high risk for pre-eclampsia. *Ultrasound Obstetrics and Gynecol.* 54, 109. doi:10.1002/UOG.20722

Brownfoot, F., and Rolnik, D. L. (2024). Prevention of preeclampsia. *Best. Pract. Res. Clin. Obstet. Gynaecol.* 93, 102481. doi:10.1016/J.BPOBGYN.2024.102481

Brownfoot, F. C., Hastie, R., Hannan, N. J., Cannon, P., Tuohey, L., Parry, L. J., et al. (2016b). Metformin as a prevention and treatment for preeclampsia: effects on soluble fms-like tyrosine kinase 1 and soluble endoglin secretion and endothelial dysfunction. *Am. J. Obstet. Gynecol.* 214, 356.e1–356. doi:10.1016/j.ajog.2015.12.019

Brownfoot, F. C., Tong, S., Hannan, N. J., Binder, N. K., Walker, S. P., Cannon, P., et al. (2015). Effects of pravastatin on human placenta, endothelium, and women with severe preeclampsia. *Hypertension* 66, 687–697. doi:10.1161/HYPERTENSIONAHA.115.05445

Brownfoot, F. C., Tong, S., Hannan, N. J., Hastie, R., Cannon, P., and Kaitu'u-Lino, T. J. (2016a). Effects of simvastatin, rosuvastatin and pravastatin on soluble fms-like tyrosine kinase 1 (sFlt-1) and soluble endoglin (sENG) secretion from human umbilical vein endothelial cells, primary trophoblast cells and placenta. *BMC Pregnancy Childbirth* 16, 117. doi:10.1186/s12884-016-0902-3

Cabral-Pacheco, G. A., Garza-Veloz, I., La Rosa, C. C. D., Ramirez-Acuña, J. M., Perez-Romero, B. A., Guerrero-Rodriguez, J. F., et al. (2020). The roles of matrix metalloproteinases and their inhibitors in human diseases. *Int. J. Mol. Sci.* 21, 1–53. doi:10.3390/IJMS21249739

Camarena Pulido, E. E., García Benavides, L., Panduro Barón, J. G., Pascoe Gonzalez, S., Madrigal Saray, A. J., García Padilla, F. E., et al. (2016). Efficacy of L-arginine for preventing preeclampsia in high-risk pregnancies: a double-blind, randomized, clinical trial. *Hypertens. Pregnancy* 35, 217–225. doi:10.3109/10641955.2015.1137586

Chang, K. J., Seow, K. M., and Chen, K. H. (2023a). Preeclampsia: recent advances in predicting, preventing, and managing the maternal and fetal life-threatening condition. *Int. J. Environ. Res. Public Health* 20, 2994. doi:10.3390/IJERPH20042994

Chang, K. J., Seow, K. M., and Chen, K. H. (2023b). Preeclampsia: recent advances in predicting, preventing, and managing the maternal and fetal life-threatening condition. *Int. J. Environ. Res. Public Health* 20, 2994. doi:10.3390/ijerph20042994

Chen, J., Gong, X., Chen, P., Luo, K., and Zhang, X. (2016). Effect of L-arginine and sildenafil citrate on intrauterine growth restriction fetuses: a meta-analysis. *BMC Pregnancy Childbirth* 16, 225. doi:10.1186/S12884-016-1009-6

Chiswick, C., Reynolds, R. M., Denison, F., Drake, A. J., Forbes, S., Newby, D. E., et al. (2015). Effect of metformin on maternal and fetal outcomes in obese pregnant women (EMPOWaR): a randomised, double-blind, placebo-controlled trial. *Lancet Diabetes Endocrinol.* 3, 778–786. doi:10.1016/S2213-8587(15)00219-3

Choi, Y. J., and Shin, S. (2021). Aspirin prophylaxis during pregnancy: a systematic review and meta-analysis. *Am. J. Prev. Med.* 61, e31–e45. doi:10.1016/J.AMEPRE.2021.01.032

CLASP: a randomised trial of low-dose aspirin for the prevention and treatment of pre-eclampsia among 9364 pregnant women, *Lancet* 343 (1994). 619–629. doi:10.1016/S0140-6736(94)92633-6

Costantine, M. M., Cleary, K., Hebert, M. F., Ahmed, M. S., Brown, L. M., Ren, Z., et al. (2016). Safety and pharmacokinetics of pravastatin used for the prevention of preeclampsia in high-risk pregnant women: a pilot randomized controlled trial. *Am. J. Obstet. Gynecol.* 214, 720.e1–720.e17. doi:10.1016/j.ajog.2015.12.038

Cruz-Lemini, M., Vázquez, J. C., Ullmo, J., and Llurba, E. (2022). Low-molecular-weight heparin for prevention of preeclampsia and other placenta-mediated complications: a systematic review and meta-analysis. *Am. J. Obstet. Gynecol.* 226, S1126–S1144.e17. doi:10.1016/j.ajog.2020.11.006

de Alwis, N., Binder, N. K., Beard, S., Kaitu'u-Lino, T. J., Tong, S., Brownfoot, F., et al. (2020). Novel approaches to combat preeclampsia: from new drugs to innovative delivery. *Placenta* 102, 10–16. doi:10.1016/J.PLACENTA.2020.08.022

Dekker, G., and Sibai, B. (2001). Primary, secondary, and tertiary prevention of pre-eclampsia. *Lancet* 357, 209–215. doi:10.1016/S0140-6736(00)03599-6

Dekker, G. A. (1989). *Prediction and prevention of pregnancy-induced hypertensive disorders: a clinical and pathophysiologic study*. Rotterdam: Erasmus University. Available at: http://hdl.handle.net/1765/50999 (Accessed July 15, 2024).

Dekker, G. A., and Robillard, P. Y. (2021)., Preeclampsiaan immune disease? An epidemiologic narrative, *Open Explor.* 1, 325–340. doi:10.37349/EI.2021.00022

Dekker, G. A., and Sibai, B. M. (1998). Etiology and pathogenesis of preeclampsia: current concepts. *Am. J. Obstet. Gynecol.* 179, 1359–1375. doi:10.1016/S0002-9378(98)70160-7

Dymara-Konopka, W., and Laskowska, M. (2019). The role of Nitric Oxide, ADMA, and Homocysteine in the etiopathogenesis of preeclampsia—review. *Int. J. Mol. Sci.* 20, 2757. doi:10.3390/ijms20112757

Faki, Y., and Er, A. (2021). Different chemical structures and physiological/pathological roles of cyclooxygenases. *Rambam Maimonides Med. J.* 12, e0003. doi:10.5041/RMMJ.10426

Förstermann, U., and Sessa, W. C. (2011). Nitric oxide synthases: regulation and function. *Eur. Heart J.* 33, 829–837. doi:10.1093/EURHEARTJ/EHR304

Ghesquiere, L., Guerby, P., Marchant, I., Kumar, N., Zare, M., Foisy, M. A., et al. (2023). Comparing aspirin 75 to 81 mg vs 150 to 162 mg for prevention of preterm preeclampsia: systematic review and meta-analysis. *Am. J. Obstet. Gynecol.* MFM 5, 101000. doi:10.1016/J.AJOGMF.2023.101000

Girardi, G. (2017). Pravastatin to treat and prevent preeclampsia. Preclinical and clinical studies. *J. Reprod. Immunol.* 124, 15–20. doi:10.1016/j.jri.2017.09.009

Goto, E. (2021a). Effects of prenatal oral l-arginine on birth outcomes: a meta-analysis. *Sci. Rep.* 11, 22748. doi:10.1038/s41598-021-02182-6

Goto, E. (2021b). Effects of prenatal oral L-arginine on birth outcomes: a meta-analysis. *Sci. Rep.* 11, 22748. doi:10.1038/S41598-021-02182-6

Groom, K. M., McCowan, L. M., Mackay, L. K., Lee, A. C., Said, J. M., Kane, S. C., et al. (2016). Enoxaparin for the prevention of preeclampsia and intrauterine growth restriction in women with a prior history - an open-label randomised trial (the EPPI trial): study protocol. *BMC Pregnancy Childbirth* 16, 367–7. doi:10.1186/s12884-016-1162-y

Gu, S., Zhou, C., Pei, J., Wu, Y., Wan, S., Zhao, X., et al. (2022). Esomeprazole inhibits hypoxia/endothelial dysfunction–induced autophagy in preeclampsia. *Cell. Tissue Res.* 388, 181–194. doi:10.1007/s00441-022-03587-z

Haddad, B., Winer, N., Chitrit, Y., Houfflin-Debarge, V., Chauleur, C., Bages, K., et al. (2016). Enoxaparin and aspirin compared with aspirin alone to prevent placenta-mediated pregnancy complications: a randomized controlled trial. *Obstetrics Gynecol.* 128, 1053–1063. doi:10.1097/AOG.0000000000001673

Hastie, R., Bergman, L., Cluver, C. A., Wikman, A., Hannan, N. J., Walker, S. P., et al. (2019). Proton pump inhibitors and preeclampsia risk among 157 720 women: a Swedish population register-based cohort study. *Hypertension* 73, 1097–1103. doi:10.1161/HYPERTENSIONAHA.118.12547

He, L., Wu, X., Zhan, F., Li, X., and Wu, J. (2023). Protective role of metformin in preeclampsia via the regulation of NF-κB/sFlt-1 and Nrf2/HO-1 signaling pathways by activating AMPK. *Placenta* 143, 91–99. doi:10.1016/j.placenta.2023.10.003

Hofmeyr, G. J., Betrán, A. P., Singata-Madliki, M., Cormick, G., Munjanja, S. P., Fawcus, S., et al. (2019). Prepregnancy and early pregnancy calcium supplementation among women at high risk of pre-eclampsia: a multicentre, double-blind, randomised, placebo-controlled trial. *Lancet* 393, 330–339. doi:10.1016/S0140-6736(18)31818-X

Hofmeyr, G. J., Lawrie, T. A., Atallah, Á. N., and Torloni, M. R. (2018). Calcium supplementation during pregnancy for preventing hypertensive disorders and related problems. *Cochrane Database Syst. Rev.* 2018. doi:10.1002/14651858.cd001059.pub5

Hussain, S., Singh, A., Antony, B., Klugarová, J., Murad, M. H., Jayraj, A. S., et al. (2022). Proton pump inhibitors use and risk of preeclampsia: a meta-analysis. *J. Clin. Med.* 11, 4675. doi:10.3390/jcm11164675

Ilham, M., Akbar, A., Alkaff, F. F., Adrian, A., Harsono, H., Nugraha, R. A., et al. (2019). Serum calcium and 25-hydroxy vitamin D level in normal and early onset pre-eclamptic pregnant women: a study from Indonesia. *J. Clin. Diagnostic Res.* 13, 4–7. doi:10.7860/JCDR/2019/39924.12667

Ilham Aldika Akbar, M. (2021). SY6-2. Possible role of statin to prevent preeclampsia. *Pregnancy Hypertens.* 25, e9. doi:10.1016/J.PREGHY.2021.07.275

Jaiswal, V., Joshi, A., Jha, M., Hanif, M., Arora, A., Gupta, S., et al. (2024). Association between calcium supplementation and gestational hypertension, and preeclampsia: a Meta-analysis of 26 randomized controlled trials. *Curr. Probl. Cardiol.* 49, 102217. doi:10.1016/J.CPCARDIOL.2023.102217

Johal, T., Lees, C. C., Everett, T. R., and Wilkinson, I. B. (2014). The nitric oxide pathway and possible therapeutic options in pre-eclampsia. *Br. J. Clin. Pharmacol.* 78, 244–257. doi:10.1111/BCP.12301

Kalafat, E., Sukur, Y. E., Abdi, A., Thilaganathan, B., and Khalil, A. (2018). Metformin for prevention of hypertensive disorders of pregnancy in women with gestational diabetes or obesity: systematic review and meta-analysis of randomized trials. *Ultrasound Obstet. Gynecol.* 52, 706–714. doi:10.1002/UOG.19084

Katsi, V., Georgountzos, G., Kallistratos, M. S., Zerdes, I., Makris, T., Manolis, A. J., et al. (2017). The role of statins in prevention of preeclampsia: a promise for the future? *Front. Pharmacol.* 8, 247–256. doi:10.3389/fphar.2017.00247

López-Jaramillo, P., Terán, E., and Moncada, S. (1995). Calcium supplementation prevents pregnancy-induced hypertension by increasing the production of vascular nitric oxide. *Med. Hypotheses* 45, 68–72. doi:10.1016/0306-9877(95)90205-8

Magee, L. A., Brown, M. A., Hall, D. R., Gupte, S., Hennessy, A., Karumanchi, S. A., et al. (2022). The 2021 International Society for the Study of Hypertension in Pregnancy classification, diagnosis and management recommendations for international practice. *Pregnancy Hypertens.* 27, 148–169. doi:10.1016/j.preghy.2021.09.008

Mangana, C., Lorigo, M., and Cairrao, E. (2021). Implications of endothelial cell-mediated dysfunctions in vasomotor tone regulation, *Biologics*, Vol. 1, Pages 231–251. doi:10.3390/BIOLOGICS1020015

Matok, I., Levy, A., Wiznitzer, A., Uziel, E., Koren, G., and Gorodischer, R. (2012). The safety of fetal exposure to proton-pump inhibitors during pregnancy. *Dig. Dis. Sci.* 57, 699–705. doi:10.1007/S10620-011-1940-3

Matsubara, K., Higaki, T., Matsubara, Y., and Nawa, A. (2015). Nitric oxide and reactive oxygen species in the pathogenesis of preeclampsia. *Int. J. Mol. Sci.* 16, 4600–4614. doi:10.3390/ijms16034600

Maynard, S. E., Venkatesha, S., Thadhani, R., and Karumanchi, S. A. (2005). Soluble Fms-like tyrosine kinase 1 and endothelial dysfunction in the pathogenesis of preeclampsia. *Pediatr. Res.* 57, 1R–7R. doi:10.1203/01.PDR.0000159567.85157.B7

McDougall, A. R. A., Hastie, R., Goldstein, M., Tuttle, A., Tong, S., Ammerdorffer, A., et al. (2022). Systematic evaluation of the pre-eclampsia drugs, dietary supplements and biologicals pipeline using target product profiles. *BMC Med.* 20, 393. doi:10.1186/s12916-022-02582-z

McLaughlin, K., Scholten, R. R., Parker, J. D., Ferrazzi, E., and Kingdom, J. C. P. (2018). Low molecular weight heparin for the prevention of severe preeclampsia: where next? *Br. J. Clin. Pharmacol.* 84, 673–678. doi:10.1111/BCP.13483

Meher, S., and Duley, L. (2007). Nitric oxide for preventing pre-eclampsia and its complications. *Cochrane Database Syst. Rev.* 2007, CD006490. doi:10.1002/14651858.CD006490

Mészáros, B., Kukor, Z., and Valent, S. (2023b). Recent advances in the prevention and screening of preeclampsia, *J. Clin. Med.* 12, Page 6020–6112. doi:10.3390/JCM12186020

Mészáros, B., Veres, D. S., Nagyistók, L., Somogyi, A., Rosta, K., Herold, Z., et al. (2023a). Pravastatin in preeclampsia: a meta-analysis and systematic review. *Front. Med. (Lausanne)* 9. doi:10.3389/fmed.2022.1076372

Mirabito Colafella, K. M., Neuman, R. I., Visser, W., Danser, A. H. J., and Versmissen, J. (2020). Aspirin for the prevention and treatment of pre-eclampsia: a matter of COX-1 and/or COX-2 inhibition? *Basic Clin. Pharmacol. Toxicol.* 127, 132–141. doi:10.1111/BCPT.13308

Olsen, S. F., and Secher, N. J. (1990). A possible preventive effect of low-dose fish oil on early delivery and pre-eclampsia: indications from a 50-year-old controlled trial. *Br. J. Nutr.* 64, 599–609. doi:10.1079/BJN19900063

Omotayo, M. O., Dickin, K. L., O'Brien, K. O., Neufeld, L. M., De Regil, L. M., and Stoltzfus, R. J. (2016). Calcium supplementation to prevent preeclampsia: translating guidelines into practice in low-income countries. *Adv. Nutr.* 7, 275–278. doi:10.3945/AN.115.010736

Onda, K., Tong, S., Beard, S., Binder, N., Muto, M., Senadheera, S. N., et al. (2017). Proton pump inhibitors decrease soluble fms-like tyrosine kinase-1 and soluble endoglin secretion, decrease hypertension, and rescue endothelial dysfunction. *Hypertension* 69, 457–468. doi:10.1161/HYPERTENSIONAHA.116.08408

Palacios, C., Kostiuk, L. K., and Peña-Rosas, J. P. (2019). Vitamin D supplementation for women during pregnancy. *Cochrane Database Syst. Rev.* 2019. doi:10.1002/14651858.CD008873

Phipps, E., Prasanna, D., Brima, W., and Jim, B. (2016). Preeclampsia: updates in pathogenesis, definitions, and guidelines. *Clin. J. Am. Soc. Nephrol.* 11, 1102–1113. doi:10.2215/CJN.12081115

Poniedziałek-Czajkowska, E., Mierzyński, R., Leszczyńska-Gorzelak, B., and Dłuski, D. (2021). Prevention of hypertensive disorders of pregnancy—is there a place for metformin? *J. Clin. Med.* 10, 2805. doi:10.3390/jcm10132805

Poon, L. C., and Nicolaides, K. H. (2014). First-trimester maternal factors and biomarker screening for preeclampsia. *Prenat. Diagn* 34, 618–627. doi:10.1002/pd.4397

Poon, L. C., Shennan, A., Hyett, J. A., Kapur, A., Hadar, E., Divakar, H., et al. (2019). The International Federation of Gynecology and Obstetrics (FIGO) initiative on pre-eclampsia: a pragmatic guide for first-trimester screening and prevention. *Int. J. Gynecol. and Obstetrics* 145, 1–33. doi:10.1002/ijgo.12802

Poon, L. C., Wright, D., Rolnik, D. L., Syngelaki, A., Delgado, J. L., Tsokaki, T., et al. (2017). Aspirin for Evidence-Based Preeclampsia Prevention trial: effect of aspirin in prevention of preterm preeclampsia in subgroups of women according to their characteristics and medical and obstetrical history. *Am. J. Obstet. Gynecol.* 217, 585.e1–585. doi:10.1016/j.ajog.2017.07.038

Purswani, J. M., Gala, P., Dwarkanath, P., Larkin, H. M., Kurpad, A., and Mehta, S. (2017). The role of vitamin D in pre-eclampsia: a systematic review. *BMC Pregnancy Childbirth* 17, 231–315. doi:10.1186/s12884-017-1408-3

Rahma, H., Indrawan, I. W. A., Nooryanto, M., and Keman, K. (2017). Effect of a black cumin (Nigella sativa) ethanol extract on placental angiotensin II type 1-receptor autoantibody (AT1-AA) serum levels and endothelin-1 (ET-1) expression in a preeclampsia mouse model. *J. Taibah Univ. Med. Sci.* 12, 528–533. doi:10.1016/J.JTUMED.2017.06.002

Ramma, W., and Ahmed, A. (2014). Therapeutic potential of statins and the induction of heme oxygenase-1 in preeclampsia. *J. Reprod. Immunol.* 101–102, 153–160. doi:10.1016/j.jri.2013.12.120

Redman, C. (2014). Pre-eclampsia: a complex and variable disease. *Pregnancy Hypertens.* 4, 241–242. doi:10.1016/J.PREGHY.2014.04.009

Redman, C. W. (2017). Early and late onset preeclampsia: two sides of the same coin. *Int. J. Women's Cardiovasc. Health* 7, 58. doi:10.1016/j.preghy.2016.10.011

Redman, C. W. G., Staff, A. C., and Roberts, J. M. (2022). Syncytiotrophoblast stress in preeclampsia: the convergence point for multiple pathways. *Am. J. Obstet. Gynecol.* 226, S907–S927. doi:10.1016/J.AJOG.2020.09.047

Roberge, S., Bujold, E., and Nicolaides, K. H. (2018). Aspirin for the prevention of preterm and term preeclampsia: systematic review and metaanalysis. *Am. J. Obstet. Gynecol.* 218, 287–293. doi:10.1016/j.ajog.2017.11.561

Roberge, S., Demers, S., Nicolaides, K. H., Bureau, M., Côté, S., and Bujold, E. (2016). Prevention of pre-eclampsia by low-molecular-weight heparin in addition to aspirin: a meta-analysis. *Ultrasound Obstet. Gynecol.* 47, 548–553. doi:10.1002/UOG.15789

Roberts, J. M., Redman, C. W. G., and Collaboration, the G. P. (2017). Global Pregnancy Collaboration symposium: prepregnancy and very early pregnancy antecedents of adverse pregnancy outcomes: overview and recommendations. *Placenta* 60, 103–109. doi:10.1016/J.PLACENTA.2017.07.012

Robillard, P. Y., Dekker, G., Scioscia, M., Bonsante, F., Iacobelli, S., Boukerrou, M., et al. (2019). Increased BMI has a linear association with late-onset preeclampsia: a population-based study. *PLoS One* 14, e0223888. doi:10.1371/JOURNAL.PONE.0223888

Rodger, M. (2014). Pregnancy and venous thromboembolism: "TIPPS" for risk stratification. *Hematol. Am. Soc. Hematol. Educ. Program* 2014, 387–392. doi:10.1182/ASHEDUCATION-2014.1.387

Rodger, M. A., Gris, J. C., de Vries, J. I. P., Martinelli, I., Rey, É., Schleussner, E., et al. (2016). Low-molecular-weight heparin and recurrent placenta-mediated pregnancy complications: a meta-analysis of individual patient data from randomised controlled trials. *Lancet* 388, 2629–2641. doi:10.1016/S0140-6736(16)31139-4

Rolnik, D. L., Wright, D., Poon, L. C., O'Gorman, N., Syngelaki, A., de Paco Matallana, C., et al. (2017). Aspirin versus placebo in pregnancies at high risk for preterm preeclampsia. *N. Engl. J. Med.* 377, 613–622. doi:10.1056/NEJMoa1704559

Saad, A. F., Kechichian, T., Yin, H., Sbrana, E., Longo, M., Wen, M., et al. (2014). Effects of pravastatin on angiogenic and placental hypoxic imbalance in a mouse model of preeclampsia. *Reprod. Sci.* 21, 138–145. doi:10.1177/1933719113492207

Sagadevan, S., Sri Hari, O., Sirajudeen, M. J., Ramalingam, G., and Basutkar, R. S. (2021). Effects of L-arginine on preeclampsia risks and maternal and neonatal outcomes: a systematic review and meta-analysis. *Asian Pac. J. Reproduction* 10, 241–251. doi:10.4103/2305-0500.331261

Sakowicz, A., Bralewska, M., Rybak-Krzyszkowska, M., Grzesiak, M., and Pietrucha, T. (2023). New ideas for the prevention and treatment of preeclampsia and their molecular inspirations, *Int. J. Mol. Sci.* 24, 12100. doi:10.3390/IJMS241512100

Saleh, L., Samantar, R., Garrelds, I. M., Van Den Meiracker, A. H., Visser, W., and Danser, A. H. J. (2017). Low soluble fms-like tyrosine kinase-1, endoglin, and endothelin-1 levels in women with confirmed or suspected preeclampsia using proton pump inhibitors. *Hypertension* 70, 594–600. doi:10.1161/HYPERTENSIONAHA.117.09741

Shanmugalingam, R., Hennessy, A., and Makris, A. (2019a). Aspirin in the prevention of preeclampsia: the conundrum of how, who and when. *J. Hum. Hypertens.* 33, 1–9. doi:10.1038/s41371-018-0113-7

Shanmugalingam, R., Wang, X. S., Motum, P., Fulcher, I., Lee, G., Kumar, R., et al. (2020). The 15-epilipoxin-A4 pathway with prophylactic aspirin in preventing preeclampsia: a longitudinal cohort study. *J. Clin. Endocrinol. Metab.* 105, dgaa642–e4822. doi:10.1210/CLINEM/DGAA642

Shanmugalingam, R., Wang, X. S., Münch, G., Fulcher, I., Lee, G., Chau, K., et al. (2019b). A pharmacokinetic assessment of optimal dosing, preparation, and chronotherapy of aspirin in pregnancy. *Am. J. Obstet. Gynecol.* 221, 255.e1–255. doi:10.1016/J.AJOG.2019.04.027

Shen, L., Martinez-Portilla, R. J., Rolnik, D. L., and Poon, L. C. (2021). ASPRE trial: risk factors for development of preterm pre-eclampsia despite aspirin prophylaxis. *Ultrasound Obstetrics Gynecol.* 58, 546–552. doi:10.1002/UOG.23668

Sibai, B. M., Caritis, S. N., Thom, E., Klebanoff, M., McNellis, D., Rocco, L., et al. (1993). Prevention of preeclampsia with low-dose aspirin in healthy, nulliparous pregnant women. The national Institute of child health and human development network of maternal-fetal medicine units. *N. Engl. J. Med.* 329, 1213–1218. doi:10.1056/NEJM199310213291701

Singh, K. K., Gupta, A., Forstner, D., Guettler, J., Ahrens, M. S., Prakasan Sheeja, A., et al. (2024). LMWH prevents thromboinflammation in the placenta via HBEGF-AKT signaling. *Blood Adv.* 8, 4756–4766. doi:10.1182/BLOODADVANCES.2023011895

Sinha, N., Singh, S., Agarwal, M., Manjhi, P. K., Kumar, R., Singh, S. K., et al. (2023). A randomized controlled study comparing the efficacy of 75mg versus 150mg aspirin for the prevention of preeclampsia in high-risk pregnant women. *Cureus* 15, e39752. doi:10.7759/CUREUS.39752

Staff, A. C., and Redman, C. W. G. (2018a). "The differences between early- and late-onset pre-eclampsia," in *Preeclampsia*, 157–172. doi:10.1007/978-981-10-5891-2_10

Staff, A. C., and Redman, C. W. G. (2018b). The differences between early- and late-onset pre-eclampsia, 157–172. doi:10.1007/978-981-10-5891-2_10

Taj, N., Sajid, A., Rasheed, T., Naz, A., Javed, S., and Munir, M. (2022). Role of l-arginine in the prevention of pre eclampsia in high-risk pregnancies. *Prof. Med. J.* 29, 62–66. doi:10.29309/TPMJ/2022.29.01.5613

Tarry-Adkins, J. L., Ozanne, S. E., and Aiken, C. E. (2021). Impact of metformin treatment during pregnancy on maternal outcomes: a systematic review/meta-analysis, *Sci. Rep.* 11:1 11 9240–9313. doi:10.1038/s41598-021-88650-5

Tashie, W., Fondjo, L. A., Owiredu, W. K. B. A., Ephraim, R. K. D., Asare, L., Adu-Gyamfi, E. A., et al. (2020). Altered bioavailability of nitric oxide and L-arginine is a key determinant of endothelial dysfunction in preeclampsia. *Biomed. Res. Int.* 2020, 3251956. doi:10.1155/2020/3251956

Tong, S., Kaitu'u-Lino, T. J., Hastie, R., Brownfoot, F., Cluver, C., and Hannan, N. (2022a). Pravastatin, proton-pump inhibitors, metformin, micronutrients, and biologics: new horizons for the prevention or treatment of preeclampsia. *Am. J. Obstet. Gynecol.* 226, S1157–S1170. doi:10.1016/J.AJOG.2020.09.014

Tong, S., Kaitu'u-Lino, T. J., Hastie, R., Brownfoot, F., Cluver, C., and Hannan, N. (2022b). Pravastatin, proton-pump inhibitors, metformin, micronutrients, and biologics: new horizons for the prevention or treatment of preeclampsia. *Am. J. Obstet. Gynecol.* 226, S1157–S1170. doi:10.1016/j.ajog.2020.09.014

Vadillo-Ortega, F., Perichart-Perera, O., Espino, S., Avila-Vergara, M. A., Ibarra, I., Ahued, R., et al. (2011). Effect of supplementation during pregnancy with L-arginine and antioxidant vitamins in medical food on pre-eclampsia in high risk population: randomised controlled trial. *BMJ* 342, d2901. doi:10.1136/BMJ.D2901

Vahedian-Azimi, A., Karimi, L., Reiner, Ž., Makvandi, S., and Sahebkar, A. (2021). Effects of statins on preeclampsia: a systematic review. *Pregnancy Hypertens.* 23, 123–130. doi:10.1016/j.preghy.2020.11.014

Valensise, H., Vasapollo, B., Gagliardi, G., and Novelli, G. P. (2008). Early and Late preeclampsia: two different maternal hemodynamic states in the latent phase of the disease. *Hypertension* 52, 873–880. doi:10.1161/HYPERTENSIONAHA.108.117358

van Gelder, M. M. H. J., Beekers, P., van Rijt-Weetink, Y. R. J., van Drongelen, J., Roeleveld, N., and Smits, L. J. M. (2022). Associations between late-onset preeclampsia and the use of calcium-based antacids and proton pump inhibitors during pregnancy: a prospective cohort study. *Clin. Epidemiol.* 14, 1229–1240. doi:10.2147/CLEP.S382303

Verma, V., and Mehendale, A. M. (2022). A review on the use of metformin in pregnancy and its associated fetal outcomes. *Cureus* 14, e30039. doi:10.7759/cureus.30039

Wahyuningsih, D., Usman, A. N., and Prihantono, (2021). Analysis of serum levels L-arginine and 25-hydroxyvitamin D as a predictor of survival of severe preeclampsia mothers. *Gac. Sanit.* 35, S224–S226. doi:10.1016/j.gaceta.2021.10.026

Wallenburg, H. C. S., Makovitz, J. W., Dekker, G. A., and Rotmans, P. (1986). Low-dose aspirin prevents pregnancy-induced hypertension and pre-eclampsia in angiotensin-sensitive primigravida. *Lancet* 1, 1–3. doi:10.1016/S0140-6736(86)91891-X

Walsh, S. W., and Strauss, J. F. (2021). The road to low-dose aspirin therapy for the prevention of preeclampsia began with the placenta. *Int. J. Mol. Sci.* 22, 6985. doi:10.3390/IJMS22136985

Wardhana, M. P., Wicaksono, B., Aditiawarman, W., Ardian, M., Cahyani, M. D., and Rahmatyah, R. (2021). L-arginine protective effect on systemic blood pressure and placental expression of endoglin, transforming growth factor-β1 in the preeclampsia mice model. *Int. J. Women's Health Reproduction Sci.* 9, 29–34. doi:10.15296/ijwhr.2021.06

Wat, J. M., Audette, M. C., and Kingdom, J. C. (2018a). Molecular actions of heparin and their implications in preventing pre-eclampsia. *J. Thrombosis Haemostasis* 16, 1510–1522. doi:10.1111/JTH.14191

Wat, J. M., Audette, M. C., and Kingdom, J. C. (2018b). Molecular actions of heparin and their implications in preventing pre-eclampsia. *J. Thromb. Haemost.* 16, 1510–1522. doi:10.1111/JTH.14191

Weckman, A. M., McDonald, C. R., Baxter, J. A. B., Fawzi, W. W., Conroy, A. L., and Kain, K. C. (2019). Perspective: L-arginine and L-citrulline supplementation in pregnancy: a potential strategy to improve birth outcomes in low-resource settings. *Adv. Nutr.* 10, 765–777. doi:10.1093/advances/nmz015

WHO (2018). WHO recommendation: calcium supplementation during pregnancy for the prevention of pre-eclampsia and its complications - PubMed. Available at: https://pubmed.ncbi.nlm.nih.gov/30629391/(Accessed October 30, 2024).

WHO (2024). WHO recommendation on calcium supplementation before pregnancy for the prevention of pre-eclampsia and its complications. Available at: https://www.who.int/publications/i/item/9789240003118 (Accessed October 30, 2024).

Woo Kinshella, M. L., Sarr, C., Sandhu, A., Bone, J. N., Vidler, M., Moore, S. E., et al. (2022). Calcium for pre-eclampsia prevention: a systematic review and network meta-analysis to guide personalised antenatal care. *BJOG* 129, 1833–1843. doi:10.1111/1471-0528.17222

Young, B. C., Levine, R. J., and Karumanchi, S. A. (2010). Pathogenesis of preeclampsia. *Annu. Rev. Pathol.* 5, 173–192. doi:10.1146/annurev-pathol-121808-102149

Zullino, S., Clemenza, S., Mecacci, F., and Petraglia, F. (2021). Low molecular weight heparins (LMWH) and implications along pregnancy: a focus on the placenta, *Reprod. Sci.* 29:1414–1423. doi:10.1007/S43032-021-00678-0

frontiers | Frontiers in Cell and Developmental Biology

TYPE Original Research
PUBLISHED 28 February 2025
DOI 10.3389/fcell.2025.1539496

OPEN ACCESS

EDITED BY
Rajni Kant,
Kaohsiung Medical University, Taiwan

REVIEWED BY
Zhaowei Tu,
Third Affiliated Hospital of Guangzhou Medical University, China
Arun Paripati,
Nationwide Children's Hospital, United States

*CORRESPONDENCE
Lana McClements,
lana.mcclements@uts.edu.au

RECEIVED 04 December 2024
ACCEPTED 20 January 2025
PUBLISHED 28 February 2025

CITATION
Afrose D, Johansen MD, Nikolic V, Karadzov Orlic N, Mikovic Z, Stefanovic M, Cakic Z, Hansbro PM and McClements L (2025) Evaluating oxidative stress targeting treatments in *in vitro* models of placental stress relevant to preeclampsia.
Front. Cell Dev. Biol. 13:1539496.
doi: 10.3389/fcell.2025.1539496

Evaluating oxidative stress targeting treatments in *in vitro* models of placental stress relevant to preeclampsia

Dinara Afrose[1], Matt D. Johansen[1,2], Valentina Nikolic[3], Natasa Karadzov Orlic[4,5], Zeljko Mikovic[4,5], Milan Stefanovic[6,7], Zoran Cakic[8], Philip M. Hansbro[1,2] and Lana McClements[1,9]*

[1]School of Life Sciences, Faculty of Science, University of Technology Sydney, Sydney, NSW, Australia, [2]Centre for Inflammation, Centenary Institute and University of Technology Sydney, Sydney, NSW, Australia, [3]Department of Pharmacology with Toxicology, Faculty of Medicine, University of Nis, Nis, Serbia, [4]Department of Gynaecology and Obstetrics, Narodni Front, Belgrade, Serbia, [5]Faculty of Medicine, University of Belgrade, Belgrade, Serbia, [6]Department of Gynaecology and Obstetrics, Clinical Centre Nis, Nis, Serbia, [7]Department of Gynaecology and Obstetrics, Faculty of Medicine, University of Nis, Nis, Serbia, [8]Department of Gynaecology and Obstetrics, General Hospital of Leskovac, Leskovac, Serbia, [9]Institute for Biomedical Materials and Devices, Faculty of Science, University of Technology Sydney, Sydney, NSW, Australia

Background: Preeclampsia is a complex pregnancy disorder characterized by the new onset of hypertension and organ dysfunction, often leading to significant maternal and fetal morbidity and mortality. Placental dysfunction is a hallmark feature of preeclampsia, which is often caused by inappropriate trophoblast cell function in association with oxidative stress, inflammation and/or pathological hypoxia. This study explores the role of oxidative stress in trophoblast cell-based models mimicking the preeclamptic placenta and evaluates potential therapeutic strategies targeting these mechanisms.

Methods: Uric acid (UA) and malondialdehyde (MDA) concentrations were measured in human plasma from women with preeclampsia (n = 24) or normotensive controls (n = 14) using colorimetric assays. Custom-made first trimester trophoblast cell line, ACH-3P, was exposed to various preeclampsia-like stimuli including hypoxia mimetic (dimethyloxalylglycine or DMOG, 1 mM), inflammation (tumour necrosis factor or TNF-α, 10 ng/mL) or mitochondria dysfunction agent, (Rhodamine-6G or Rho-6G, 1 μg/mL), ± aspirin (0.5 mM), metformin (0.5 mM), AD-01 (100 nM) or resveratrol (15 μM), for 48 h. Following treatments, UA/MDA, proliferation (MTT), wound scratch and cytometric bead, assays, were performed.

Results: Overall, MDA plasma concentration was increased in the preeclampsia group compared to healthy controls ($p < 0.001$) whereas UA showed a trend towards an increase ($p = 0.06$); when adjusted for differences in gestational age at blood sampling, MDA remained ($p < 0.001$) whereas UA became ($p = 0.03$) significantly correlated with preeclampsia. Our 2D first trimester trophoblast cell-based *in vitro* model of placental stress as observed in preeclampsia, mimicked the increase in UA concentration following treatment with DMOG ($p < 0.0001$), TNF-α ($p < 0.05$) or Rho-6G ($p < 0.001$) whereas MDA cell concentration increased only in the presence of DMOG ($p < 0.0001$) or Rho-6G ($p < 0.001$). Metformin was able to abrogate DMOG- ($p < 0.01$), Rho-6G- ($p < 0.0001$) or TNF-α- ($p < 0.01$) induced increase in UA, or DMOG- ($p < 0.0001$) or TNF-α- ($p < 0.05$)

induced increase in MDA. AD-01 abrogated UA or MDA increase in the presence of TNF-α ($p < 0.001$) or Rho-6G ($p < 0.001$)/DMOG ($p < 0.0001$), respectively. The preeclampsia-like stimuli also mimicked adverse impact on trophoblast cell proliferation, migration and inflammation, most of which were restored with either aspirin, metformin, resveratrol, or AD-01 ($p < 0.05$).

Conclusion: Our 2D *in vitro* models recapitulate the response of the first trimester trophoblast cells to preeclampsia-like stresses, modelling inappropriate placental development, and demonstrate therapeutic potential of repurposed treatments.

KEYWORDS

oxidative stress, preeclampsia, trophoblast cells, placenta, resveratrol, pregnancy, aspirin, metformin

Background

Preeclampsia is a pregnancy-related multiorgan disorder characterized by high blood pressure (BP > 140/90), proteinuria or organ dysfunction including placenta and can be classified into an early-onset (diagnosed <34-week gestation), late-onset (diagnosed ≥34 weeks) or *postpartum* phenotype (Dimitriadis et al., 2023) (Brownfoot and Rolnik, 2024) (Steegers et al., 2010). However, the evolving understanding of preeclampsia as a heterogeneous hypertensive disorder of pregnancy led to the ACOG's hypertension 2019 task force revising the definition of preeclampsia to include the presence of other features including elevated liver enzymes, low platelet count, headache, with or without proteinuria (ACOG, 2019). Globally, preeclampsia is the leading cause of morbidity and mortality among pregnant women and their offspring. It can lead to severe pregnancy complications including eclampsia, Haemolysis, Elevated Liver Enzymes and Low Platelets (HELLP) syndrome, preterm birth, and even death if it is not detected and managed in a timely manner. Long-term, both the mothers and their offspring are at an increased risk of developing cardiovascular and metabolic disorders, later in life (Rana et al., 2019; Sibai et al., 2005; Matthys et al., 2004; Tranquilli et al., 2014; Lopez-Jaramillo et al., 2018). Research indicates that maternal mortality related to preeclampsia is disproportionately higher in low-income and lower socioeconomic countries. Currently, preeclampsia has limited monitoring options, with the only definitive treatment being the delivery of the placenta and baby, often preterm and associated with significant complications (Dimitriadis et al., 2023; Ives et al., 2020). Although the exact etiology of preeclampsia remains unclear, it is often associated with placental dysfunction or cardiovascular maladaptation, leading to excessive oxidative stress, inflammation, endothelial dysfunction, and an antiangiogenic environment (Jung et al., 2022; Bokuda and Ichihara, 2023).

In the early stages of physiological pregnancy, trophoblast cells invade the decidualized endometrial lining of the uterus and remodel the spiral uterine arteries (SUA), ensuring a stable connection between the placenta and maternal circulation. An invasive subtype of extravillous trophoblasts (EVTs) invades the SUA within the decidua in a tightly regulated process, replacing

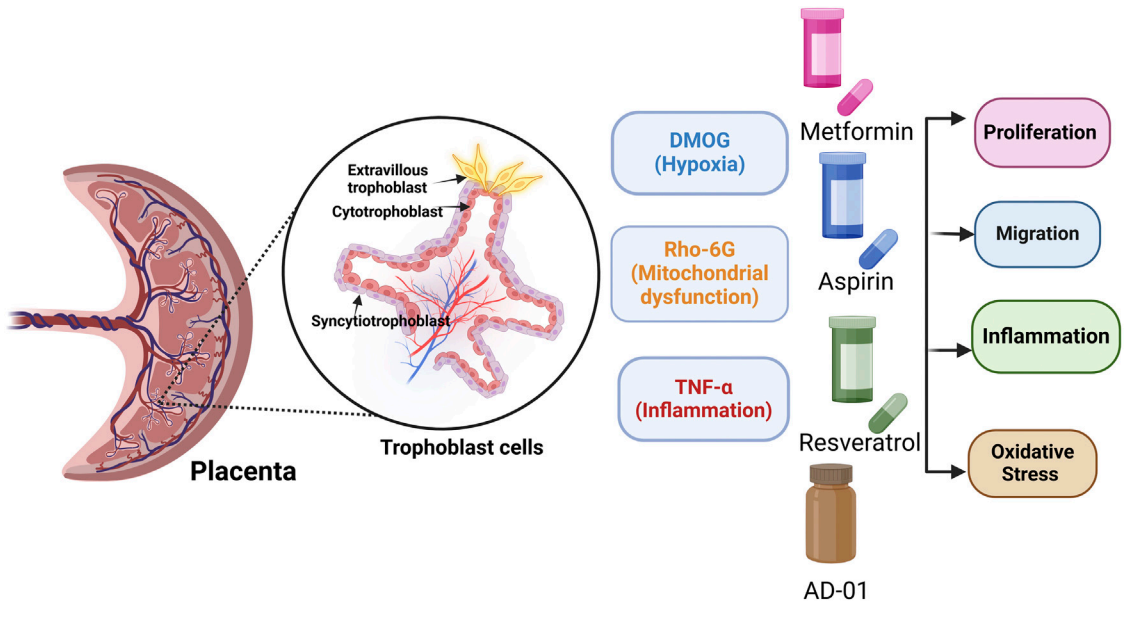

GRAPHICAL ABSTRACT

endothelial and muscle layers, thereby reducing vessel resistance and ensuring uninterrupted blood flow to the fetus (Ridder et al., 2019; Pollheimer et al., 2018). However, in some forms of preeclampsia, the extent and depth of remodeling are less extensive than in a normal pregnancy. Following compromised placentation, impaired SUA remodeling can trigger a cascade of events (Burton et al., 2019). For instance, placental ischemia and inflammation lead to the upregulation of anti-angiogenic proteins, including soluble fms-like tyrosine kinase-1 (sFlt-1), soluble endoglin (sEng) and FK506 binding protein-like (FKBPL), (Todd et al., 2021; Agarwal and Karumanchi, 2011), as well as oxidative stress biomarkers, including uric acid (UA) and malondialdehyde (MDA) (Afrose et al., 2022; Sudjai and Satho, 2022; Khaliq et al., 2018; Yoneyama et al., 2002; Rani et al., 2010). The angiogenic imbalance in association with mitochondrial dysfunction and oxidative stress can ultimately lead to organ damage. Preeclampsia is associated with an exacerbated inflammatory response that may lead to a release of pro-inflammatory cytokines, including TNF-α, interleukin-6 (IL-6), interleukin-8 (IL-8), and interleukin-1 beta (IL-1β). A dysregulated immune response observed in preeclampsia leads to endothelial activation, oxidative stress, and the release of factors that perpetuate the inflammatory reaction (Maynard and Karumanchi, 2011; Martínez-Varea et al., 2014; Geldenhuys et al., 2018)

Even though there is no definitive treatment for preeclampsia, several preventative measures are utilized including lifestyle modifications, exercise, and adequate rest (Bezerra Maia e Holanda Moura S et al., 2012; Davenport et al., 2018). Low-dose aspirin (100–162 mg/day) has been established as an effective prophylactic or preventative treatment for preterm preeclampsia (delivery prior to 37 weeks of gestation), when prescribed prior to 16 weeks of gestation (Rolnik et al., 2017; Bujold et al., 2010; Duley et al., 2007). Several newly emerging treatments for preeclampsia are currently being investigated, through repurposing, including metformin and resveratrol. Metformin is a hypoglycaemic agent with pleiotropic properties, which, in a recent randomised controlled trial in South Africa, showed the ability to extend gestation period in early-onset preeclampsia by an average of 7 days (Alqudah et al., 2018; Cluver et al., 2021; Nafisa et al., 2018). Meta-analyses of studies on high-risk, insulin-resistant women demonstrated that metformin use before or during pregnancy is associated with reduced gestational weight gain and a lower risk of preeclampsia compared to insulin therapy alone (Alqudah et al., 2018). Metformin can improve endothelial function and vasculature while reducing the secretion of sFlt-1 and sEng from human placental tissues, potentially through inhibiting the mitochondrial electron transport chain, further supporting its therapeutic potential in preeclampsia (Brownfoot et al., 2016). Resveratrol is a naturally occurring compound, found in grape skin with anti-inflammatory and antioxidatant properties, and a therapeutic potential in cancer, inflammatory lesions, diabetes mellitus, and cardiovascular disease (Zou et al., 2014) (Lacerda et al., 2023; Singh et al., 2019). A recent study demonstrated that resveratrol improves metabolic health in pregnant individuals and their offspring, and was deemed safe in pregnancy at certain doses (Ramli et al., 2023). Resveratrol appears to enhance the invasive capacity of human trophoblasts by promoting the epithelial-mesenchymal transition (EMT) process, potentially through targeting the Wnt/β-catenin signalling pathway, therefore suggesting that it could be a promising treatment for prevention of preeclampsia (Zou et al., 2019). FKBPL has emerged as a new predictive and diagnostic biomarker and a therapeutic target of preeclampsia (Masoumeh Ghorbanpour et al., 2023; Ghorbanpour et al., 2023; McNally et al., 2021; Todd et al., 2021). FKBPL-based therapeutic peptide mimetic, AD-01 (preclinical peptide candidate), has showed a potent anti-angiogenic and anti-cancer stem cell effects in cancer via CD44 and DLL4 (Yakkundi et al., 2013; McClements et al., 2013; Annett et al., 2020). More recently, AD-01 has also demonstrated an anti-inflammatory utility through the inhibition of NF-kB signalling in association with improved vascular dysfunction (Annett et al., 2021). In cardiovascular disease context, AD-01 was able to restore angiotensin-II-induced cardiac hypertrophy via negative regulation of FKBPL, which could make it useful for preeclampsia treatment although its safety in pregnancy is unknown (Chhor et al., 2023).

In this study, we aimed to design a range of the first trimester trophoblast cell-based *in vitro* models emulating placental stresses preceding preeclampsia to elucidate the impact of individual pathogenic mechanisms and potential therapeutics for preeclampsia prevention. We showed that in our low-cost, representative and reproducible 2D *in vitro* models, we can mimic oxidative stress (increased UA and MDA), impaired trophoblast proliferation and migration, and inflammation, typical for inappropriate placentation leading to preeclampsia. Our comprehensive evaluation of potential treatments shows, for the first time, that through repurposing metformin, resveratrol and AD-01, we can restore the negative impact of preeclampsia-like stresses on trophoblast function, oxidative stress and inflammation.

Methods

Human sample collection

Human plasma samples were collected as part of a multicentre study including three hospitals in Serbia. A total of 38 blood samples were used from participants with preeclampsia (n = 24) or healthy controls (n = 14) of matched age, body mass index (BMI) and blood glucose levels. The samples were collected prior to delivery as previously described (Ghorbanpour et al., 2023). Plasma was isolated from blood samples collected using ethylenediaminetetraacetic acid (EDTA) tubes, by centrifugation at 3,000 g for 10 min at 4°C. To preserve the samples, plasma-containing tubes were stored at −80°C. Preeclampsia was defined in accordance with the ACOG 2019 guidelines, ensuring robust sample characterisation (ACOG, 2019). Clinical characteristics of maternal age, gestational age at sampling/delivery, maternal BMI, systolic blood pressure (sBP), diastolic blood pressure (dBP), blood glucose and concentrations of UA and MDA are presented in Table 1.

Cell culture

Professor Gernot Desoye (Graz Medical University, Austria) generously donated the ACH-3Ps first trimester trophoblast cell line, which was established in 2007 (Hiden et al., 2007). ACH-3Ps were

TABLE 1 Clinical characteristics of normotensive pregnancies and pregnancies with established preeclampsia.

	Control (n = 14)	Preeclampsia (n = 24)	P value
Age (years)	31.14 ± 4.17	33.83 ± 6.58	0.181
Gestational age at delivery (weeks)	39.49 ± 0.82	32.88 ± 3.59	**<0.0001**
BMI (kg/m^2)	25.67 ± 5.72	27.38 ± 4.43	0.313
sBP (mmHg)	115 ± 6.50	155.1 ± 24.13	**<0.0001**
dBP (mmHg)	73.57 ± 7.45	102.8 ± 9.88	**<0.0001**
Blood Glucose (mmol/L)	4.43 ± 0.83	4.38 ± 0.88	0.871
UA (nmol/μL)	33.55 ± 7.87	40.13 ± 10.88	0.06
MDA (μmol/mL)	6.72 ± 0.86	12.27 ± 1.28	**<0.0001**

All clinical characteristics are given as mean ± SD., Bold indicates statistical significance ($p < 0.0001$). Key: BMI, body mass index; sBP, systolic blood pressure; dBP, diastolic blood pressure; UA, uric acid; MDA, malondialdehyde.

immortalized by fusing primary first trimester trophoblast cells from a 12-week gestation placenta with choriocarcinoma cell line, AC1-1 (Hiden et al., 2007). Ham's F12 nutrient mix (Gibco; Thermo Fisher Scientific, cat. 11765062) was used for the ACH-3P cell culture, supplemented with 10% fetal bovine serum (FBS; Gibco; Thermo Fisher Scientific, cat. 10099141) and 1% penicillin-streptomycin (P/S; Gibco; Thermo Fisher Scientific, cat. 15140-122). A selection medium containing azaserine (5.7 M, Sigma-Aldrich) and hypoxanthine (100 M, Sigma-Aldrich) was applied to cells every two to five cell passages. A humidified atmosphere was used to incubate the cells at 37°C, 5% CO_2 and the cultures were routinely tested for the presence of *Mycoplasma*. The cells were dissociated with Accutase (Sigma-Aldrich, cat. A6964) and experiments were conducted at passages P15-25.

Cell stimuli and treatments

ACH-3Ps were seeded at various seeding densities in different size well plates for various sets of experiments (MTT assay, wound-scratch assay, cytometric bead assay (CBA) assay, UA assay and MDA assay) and incubated in a humidified environment at 37°C and 5% CO_2. After attaching, cells were serum starved overnight by using serum reduced medium with Ham's F12 containing 1% FBS, 1% P/S prior to treatments. The following day, cells were treated with stimuli as previously described including 1 mM DMOG (Sigma-Aldrich, United States, cat. D3695) (Nevo et al., 2006; Zippusch et al., 2021) to mimic hypoxic, 10 ng/mL TNF-α (Sigma-Aldrich, United States, cat. T6674) (Brownfoot et al., 2020; Wang et al., 2020) to mimic inflammatory condition, or 1 μg/mL Rho-6G (Sigma-Aldrich, United States, cat. R4127) (Dutra Silva et al., 2021; Gear, 1974) to mimic mitochondrial dysfunction ± metformin (Cluver et al., 2021; Nafisa et al., 2018; Han et al., 2015) (0.5 mM, Sigma-Aldrich, United States, cat. PHR1084), or ± AD-01 (McClements et al., 2013; McClements et al., 2019) (100 nM, MedChemExpress, United Kingdom, cat. HY-P2284), or ± aspirin (Bujold et al., 2010; Panagodage et al., 2016) (0.5 mM, Sigma-Aldrich, United States, cat. PHR1003), or ± resveratrol (Viana-Mattioli et al., 2020; Cluver et al., 2018; Ding et al., 2017) (15 μM, Sigma-Aldrich, United States, cat. R5010), for 48 h with untreated cells being used as a control. Drug dosages were optimized initially and chosen according to the concentrations reflective of human doses for aspirin and metformin following absorption, metabolism, distribution or plasma levels (Gong et al., 2012; Angiolillo et al., 2022).

ACH-3P cell lysates extraction for UA and MDA assays

ACH-3Ps cells were seeded to achieve a total of 3×10^6 cells per condition and incubated in a humidified environment at 37°C and 5% CO_2 for 6 h. Cells were then starved overnight in serum reduced Ham's F12 media containing 1% FBS, 1% P/S prior to adding the treatments. Following the addition of the treatments, cells were washed with cold Phosphate Buffer Saline (PBS) (2 mL) and homogenized with 100 μL UA assay buffer (Abcam, Australia, cat. ab65344). Samples were centrifuged at 14,000 rpm for 2 min at 4°C using a cold microcentrifuge to remove any insoluble material. The supernatant was collected and stored at - 80°C for downstream analysis. For the MDA assay, the same procedure was followed except that before extracting MDA, MDA lysis solution (Abcam, Australia, cat. ab118970) was prepared by mixing 300 μL of MDA lysis buffer with 3 μL Butylated Hydroxytoluene (BHT) (1:100). The purpose of using BHT was to stop further sample peroxidation during sample processing. Cells were homogenised properly until the shiny ring containing the nuclei was removed. Samples were centrifuged at 13,000 rpm for 10 min at 4°C to remove any insoluble material. The supernatant was collected and stored at - 80°C for downstream analysis.

UA and MDA assay

Plasma from women with normotensive pregnancies or preeclampsia and cell lysates from treated ACH-3Ps were used to determine the concentration of UA and MDA. UA assay kit (Abcam, Australia, cat. ab65344) and MDA assay kit (Abcam, Australia, cat. ab118970) were used according to the manufacturer's instructions. Optical density was measured for both analytes (UA and MDA) in plasma and ACH-3Ps cell lysate, samples using a Spark 10 M plate reader (Tecan, Switzerland) at optical density (OD) of 570 nm. The four-parameter logistic (4 PL) curve regression model was used to

10.3389/fcell.2025.1539496

determine concentration values of each sample from the sigmoidal standard curve for both assays (UA and MDA).

MTT assay

An MTT assay was performed using Thiazolyl Blue Tetrazolium Bromide dye (Sigma Aldrich) according to the manufacturer's instructions. MTT assay is a well-established, cost-effective, and widely used method for assessing cell proliferation and viability. The ACH-3P cells were seeded at a concentration of 15,000 cells/well in triplicate wells of a 96-well plate. Cells were serum starved in serum reduced medium (Ham's F12 containing 1% FBS, 1% P/S) overnight. Cells were then incubated in 210 µL medium spiked with PBS or hypoxic stimuli, 1 mM DMOG, mitochondrial dysfunctional stimuli 1 µg/mL Rho-6G or TNF-α (10 ng/ml) ± metformin (0.5 mM) or aspirin (0.5 mM) ± AD-01 (100 nM) ± resveratrol (15 µM) for 24 h, 48 h or 72 h prior to the addition of MTT dye. Next, 20 µL of the MTT reagent was added to each well, and the plates were incubated for 2 h at 37°C. The MTT reagent was then removed, and the resulting formazan crystals were solubilized in 200 µL of dimethylsulfoxide (DMSO; Sigma-Aldrich). The plates were shaken for 10 min to ensure complete solubilization of the crystals. Absorbance was measured at 565 nm using the Tecan Infinite M Plex plate reader (Tecan Life Sciences) and a well containing DMSO was used as a blank.

Wound scratch assay

ACH-3Ps cells were seeded in 24-well plates at a concentration of 400,000 cells per well. Cells were incubated in serum reduced medium as described above overnight prior to the addition of treatments. The following day, a single vertical scratch using a P200 tip from the top to the bottom of each well was applied, before washing the cells twice with 200 µL PBS and replacing the starvation media with Ham's F12 containing 10% FBS, 1% P/S. Next, treatments were added to include PBS as a control group or hypoxic stimuli (1 mM DMOG) ± metformin (0.5 mM or 1.0 mM or 5.0 mM) or ± aspirin (0.1 mM or 0.5 mM) or ± AD-01 (100 nM). Images of each well were taken using the Evos FL Live Cell imaging system (BioScience) and two × 10 objective images were acquired from each well at 0 h, 24 h and 48 h respectively. A wound area was measured, and a percentage of wound closure was calculated using ImageJ. Experiments were conducted in duplicates, and results are expressed as the mean percentage of wound closure ± standard error.

Cytometric bead assay (CBA)

ACH-3Ps cells were seeded onto 24-well plates at the density of 500,000 cells/well before being serum-arrested in their respective medium containing 1% FBS and 1% P/S, overnight. The following day, cells were treated with hypoxic stimuli, 1 mM DMOG, as

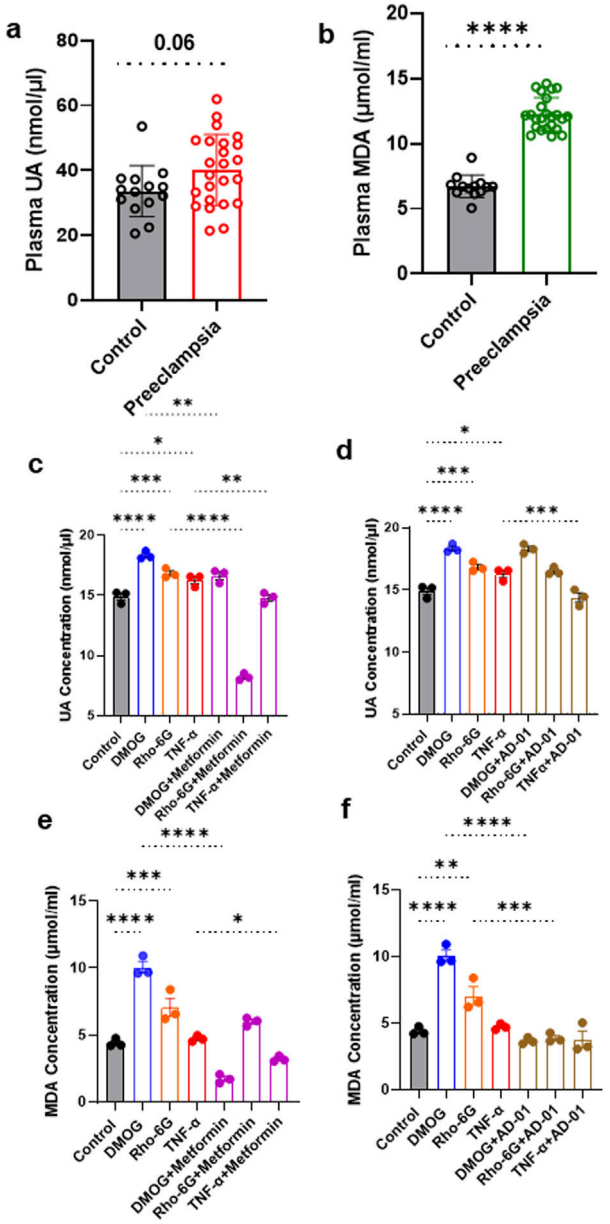

FIGURE 1
UA and MDA are increased in plasma from women with preeclampsia and cell lysates from 2D first trimester trophoblast *in vitro* models of preeclampsia. **(A, B)** UA and MDA concentrations were measured in plasma samples from individuals with preeclampsia or normotensive controls. Absorbances were recorded at 570 nm. **(C)** Metformin or **(D)** AD-01 treatment abrogated the increase in UA and MDA under certain preeclampsia-like conditions. ACH-3P cells were exposed to (DMOG, 1 mM) or (Rho-6G, 1 µg/mL) or (TNF-α, 10 ng/mL) to mimic hypoxia or mitochondrial dysfunction or inflammatory condition, respectively, and treated with metformin (0.5 mM), or AD-01 (100 nM), for 48 h. Untreated cells were used as controls. **(C, D)** UA and **(E, F)** MDA concentration was measured in ACH-3P cell lysates following the addition of treatments. **(A, B)** The data was plotted as mean ± SD; $n \geq 13$; unpaired student's t test; **(C–F)** The data was analyzed by one-way analysis of variance (ANOVA) with Sidak's post-hoc test; and expressed as mean ± SEM; $n = 3$; *$p < 0.05$, **$p < 0.01$, ***$p < 0.001$, ****$p < 0.0001$.

described above or mitochondrial dysfunctional stimuli, 1 μg/mL Rho-6G, ± metformin (0.5 mM) or ± AD-01 (100 nM), for 48 h with untreated cells being used as a control. The supernatant was collected and stored for measuring inflammatory cytokines (Human IFN-α, IL-1β, IL-6, IL-8, IL-10) at - 80°C.

Inflammatory cytokines from ACH-3Ps cells supernatant were quantified using the CBA according to the manufacturer's instructions (Becton Dickinson, United States). A standard curve was generated using the standards provided for each analyte. In a 96-well plate, 10 μL of each sample was added to each well, followed by incubation with 1 μL of capture beads for each analyte (1 h, room temperature, in the dark). For each analyte captured, 1 μL of detection bead was added to each well, followed by room temperature (RT) incubation (2 h, in the dark). A solution of 8% paraformaldehyde was then used to fix the samples overnight (4% final solution). In order to examine the samples, a BD LSR Fortessa equipped with a High-Throughput Sampler (HTS) plate reader was used. FCAP Array software was used to facilitate the analysis of CBA Human Inflammatory Cytokines Kit data of standards and samples.

Statistical analysis

The results of human sample quantifications were presented as mean ± SD, whereas the results of quantitative *in vitro* experiments were presented as mean ± SEM. Normality testing was performed using a Shapiro–Wilk test followed by two-tailed unpaired t-test, or one-way ANOVA with post-hoc multiple comparison tests. For non-normally distributed data, Mann–Whitney or Kruskal–Wallis were used. Statistical analysis was performed using Graph-Pad Prism (version 9.4.0 software, United States) and p value <0.05 was considered statistically significant. An unpaired t-test was used to determine differences between normotensive pregnancy and preeclampsia groups. SPSS software (IBM SPSS Statistics, 29.0.2.0, United States) was used to perform correlations between preeclampsia and UA or MDA plasma concentration using Pearson's correlation and partial correlation controlling for differences in gestational age (GA).

Results

UA and MDA are increased in preeclampsia plasma samples and in the *in vitro* models of preeclamptic placenta

Given UA and MDA are the most reliable oxidative stress biomarkers in preeclampsia that are detectable in plasma and highly secreted by placental cells (Afrose et al., 2022; Khaliq et al., 2018; Rani et al., 2010; Masoura et al., 2015), we quantified these biomarkers in both patient samples and *in vitro* trophoblast models of preeclamptic placenta to validate the model. Based on the clinical characteristics of our patient cohort, as expected, blood pressure was higher and gestational age at delivery lower in the preeclampsia group compared to normotensive controls. The groups were matched for maternal age, BMI and blood glucose levels (Table 1). UA concentrations showed a trend towards an increase in individuals with preeclampsia compared to healthy controls (Control 33.55 ± 7.87 nmol/μL vs. Preeclampsia 40.13 ± 10.88 nmol/μL, p = 0.06; Figure 1A; Table 1).

Although no significant correlation was observed between plasma UA and preeclampsia (r = 0.315, p = 0.06, Table 2), this became statistically significant after adjusting for gestational age as a confounding factor (r = 0.366, p = 0.03, Table 2).

Plasma MDA concentration was significantly increased in the individuals with preeclampsia compared to healthy controls (Control 6.72 ± 0.86 μmol/mL vs. Preeclampsia 12.27 ± 1.28 μmol/mL, p < 0.0001; Figure 1B; Table 3). Furthermore, there was a significant positive correlation between plasma MDA and preeclampsia (r = 0.924, p < 0.001), even when adjusted for differences in gestational age (r = 0.867, p < 0.001; Table 3).

In 2D *in vitro* trophoblast cell models of preeclampsia, UA was increased in response to all three stimuli (hypoxia mimetic, mitochondrial dysfunction, and inflammation) in comparison to control, at 48 h (Control 14.89 ± 0.30 nmol/μL vs. DMOG 18.32 ± 0.19 nmol/μL vs. Rho-6G 16.82 ± 0.22 nmol/μL vs. TNF-α 16.26 ± 0.29 nmol/μL, p < 0.0001; Figure 1C). Here, we tested only metformin and AD-01, given resveratrol is a well-known antioxidant agent (Zou et al., 2014; Lacerda et al., 2023) and aspirin is already used clinically for prevention of preeclampsia and has demonstrated anti-oxidant properties (Rolnik et al., 2017; Bujold et al., 2010; Duley et al., 2007). This increase in UA concentration was abrogated by metformin (0.5 mM) treatment in response to all three stimuli (DMOG 18.32 ± 0.19 nmol/μL vs. DMOG + Metformin 16.63 ± 0.31 nmol/μL, p < 0.01; Rho-6G 16.82 ± 0.22 nmol/μL vs. Rho-6G + Metformin 8.23 ± 0.16 nmol/μL, p < 0.0001; TNF-α 16.26 ± 0.29 nmol/μL vs. TNF-α+Metformin 14.79 ± 0.26 nmol/μL, p < 0.01; Figure 1C). However, only inflammation-induced higher UA concentration was abrogated by AD-01 (100 mM) treatment (TNF-α 16.26 ± 0.29 nmol/μL vs. TNF-α+AD-01 14.37 ± 0.38 nmol/μL, p < 0.001; Figure 1D).

Similarly, a significant increase in MDA concentration was demonstrated in ACH-3P cell lysate in response to hypoxia mimetic and mitochondrial dysfunctional stimuli in comparison to control (Control 4.41 ± 0.18 μmol/mL vs. DMOG 10.07 ± 0.42 μmol/mL vs. Rho-6G 7.06 ± 0.67 μmol/mL, p < 0.0001; Figure 1E) but inflammation did not have any effect on MDA cell concentration (Control 4.41 ± 0.18 μmol/mL vs. TNF-α 4.73 ± 0.13 μmol/mL, p = 0.985; Figure 1E). Higher MDA concentration in the presence of hypoxia mimetic was abrogated by metformin treatment (DMOG 10.07 ± 0.42 μmol/mL vs. DMOG + Metformin 1.72 ± 0.19 μmol/mL, p < 0.0001; Figure 1E). Surprisingly, even though MDA concentration was not significantly increased by inflammatory stimuli (TNF-α) compared to control, it was reduced when metformin treatment was added (TNF-α 4.72 ± 0.13 μmol/mL vs. TNF-α+Metformin 3.20 ± 0.12 μmol/mL, p < 0.05; Figure 1E). We also found that mitochondrial dysfunction induced by Rho-6G led to an increase in MDA concentration (p < 0.001), which was not abrogated by metformin treatment (p > 0.05; Figure 1E). The increase in MDA concentration driven by hypoxia mimetic or mitochondrial dysfunction was abrogated by AD-01 (100 nM) treatment at 48 h (DMOG 10.07 ± 0.42 μmol/mL vs. DMOG + AD-01 3.66 ± 0.14 μmol/mL, p < 0.0001; Rho-6G 7.06 ± 0.67 μmol/mL vs. Rho-6G + AD-01 3.89 ± 0.19 μmol/mL, p < 0.001; Figure 1F), unlike inflammation-induced oxidative stress (p > 0.05; Figure 1F).

TABLE 2 Adjusted correlations for differences in gestational age between plasma samples from pregnant women with preeclampsia or normotensive pregnancies for UA.

Plasma samples	UA	
	Pearson correlation	Correlation adjusted for GA
PE	r = 0.315	r = 0.366
	P = 0.061	***p = 0.030**

Bold and * indicates statistical significance ($p < 0.05$). Key: UA, Uric acid; PE, preeclampsia; GA, gestational age.

TABLE 3 Adjusted correlations for differences in gestational age between plasma samples from pregnant women with preeclampsia or normotensive pregnancies for MDA.

Plasma samples	MDA	
	Pearson correlation	Correlation adjusted for GA
PE	r = 0.924	r = 0.867
	****p < 0.001**	****p < 0.001**

Bold and ** indicates statistical significance ($p < 0.001$). Key: MDA, Malondialdehyde; PE, preeclampsia; GA, gestational age.

This suggests a differential mechanism for AD-01 in the presence of different types of placental stresses.

Trophoblast proliferation is restored by metformin, aspirin or AD-01 treatment in the presence of hypoxia mimetic or oxidative stress, whereas resveratrol only restores hypoxia-induced inhibition of cell proliferation

Trophoblast proliferation in early gestation appears to be impaired in pregnancies that proceed to develop preeclampsia (Farah et al., 2020). Here, we investigated the ability of metformin, aspirin, AD-01 and resveratrol to restore proliferation or viability of trophoblast cells (ACH-3Ps) under hypoxia-like (DMOG) and mitochondrial dysfunction (Rho-6G) stresses (Figures 2A–D). As part of optimization, we conducted a time-course to include 24 h, 48 h and 72 h long treatments with preeclampsia-like stimuli ± treatments (Supplementary Figures S1–S3). We determined that 48 h-long treatments produced the most suitable response and were taken forward (Figure 2). Indeed, both DMOG and Rho-6G reduced the metabolic activity and proliferation of ACH-3Ps cells by ~ 70% ($p < 0.0001$) and ~ 60% ($p < 0.0001$), compared to the control, respectively. Metformin, aspirin, AD-01 and resveratrol rescued hypoxia-induced cell damage (DMOG 26.63% ± 3.58% vs. DMOG + Metformin 45.92% ± 4.02%, $p < 0.001$; Figure 2A), (DMOG 23.25% ± 0.93% vs. DMOG + Aspirin 45.70% ± 2.41%, $p < 0.01$; Figure 2B), (DMOG 32.91% ± 4.87% vs. DMOG + AD-01 47.40% ± 2.81%, $p < 0.05$; Figure 2C), and (DMOG 28.90% ± 1.02% vs. DMOG + Resveratrol 41.67% ± 2.93%, $p < 0.05$; Figure 2D). Similarly, metformin, aspirin and AD-01 restored cell proliferation following induction of mitochondrial dysfunction (Rho-6G 42.44% ± 0.74% vs. Rho-6G + Metformin 56.11% ± 1.30%, $p < 0.01$; Figure 2A), (Rho-6G 32.94% ± 3.91% vs. Rho-6G + Aspirin 61.34% ± 6.85%, $p < 0.01$; Figure 2B), (Rho-6G 31.97% ± 1.16% vs. Rho-6G + AD-01 57.28% ± 3.20%, $p < 0.001$; Figure 2C), whereas resveratrol was not able to rescue ACH-3Ps cell proliferation in these preeclampsia-like conditions (Rho-6G 50.16% ± 3.33% vs. Rho-6G + Resveratrol 43.22% ± 2.57%, $p > 0.05$; Figure 2D). Interestingly, whilst aspirin ($p < 0.01$; Figure 2B) and metformin ($p < 0.05$; Figure 2A) seem to modestly impair trophoblast proliferation under physiological conditions (PBS), AD-01 did not have this effect but shows improved cell proliferation ($p < 0.01$; Figure 2C).

Hypoxia mimetic inhibits trophoblast cell migration while metformin, aspirin, and AD-01 restore it

The root cause of preeclampsia is aberrant placentation, which often involves impaired migration of trophoblasts and remodeling of SUA, in the presence of extended periods of hypoxia (McNally et al., 2017). Therefore, to assess the impact of pathological hypoxia, and evaluate potential treatments (metformin, aspirin and AD-01) for preeclampsia prevention, a wound scratch assay was conducted. The effect of resveratrol was not tested here because of its high toxicity on trophoblast proliferation/survival and inconsistent restorative cell proliferation effects in DMOG- or Rho-G-treated trophoblasts (Figure 2D). Trophoblast cell migration was quantified using ImageJ software in order to calculate the percentage wound closure following 24 h or 48 h treatment (Figure 3A). There was no significant reduction in trophoblast cell migration as a result of HIF-1α activation by DMOG treatment at 24 h although there was a downward trend (Figures 3A, B). Metformin at one dose only (1.0 mM) was able to improve trophoblast migration compared to hypoxia/DMOG at 24 h time point (DMOG 18.87% ± 4.22% vs. DMOG + Metformin (1.0 mM) 43.46% ± 7.46%, $p < 0.05$; Figure 3B). However, at 48 h, DMOG treatment induced statistically significant reduction in trophoblast migration (Control 52.81% ± 5.47% vs. DMOG 31.09% ± 2.66%, $p < 0.05$; Figure 3C), which was restored by metformin treatment back to the

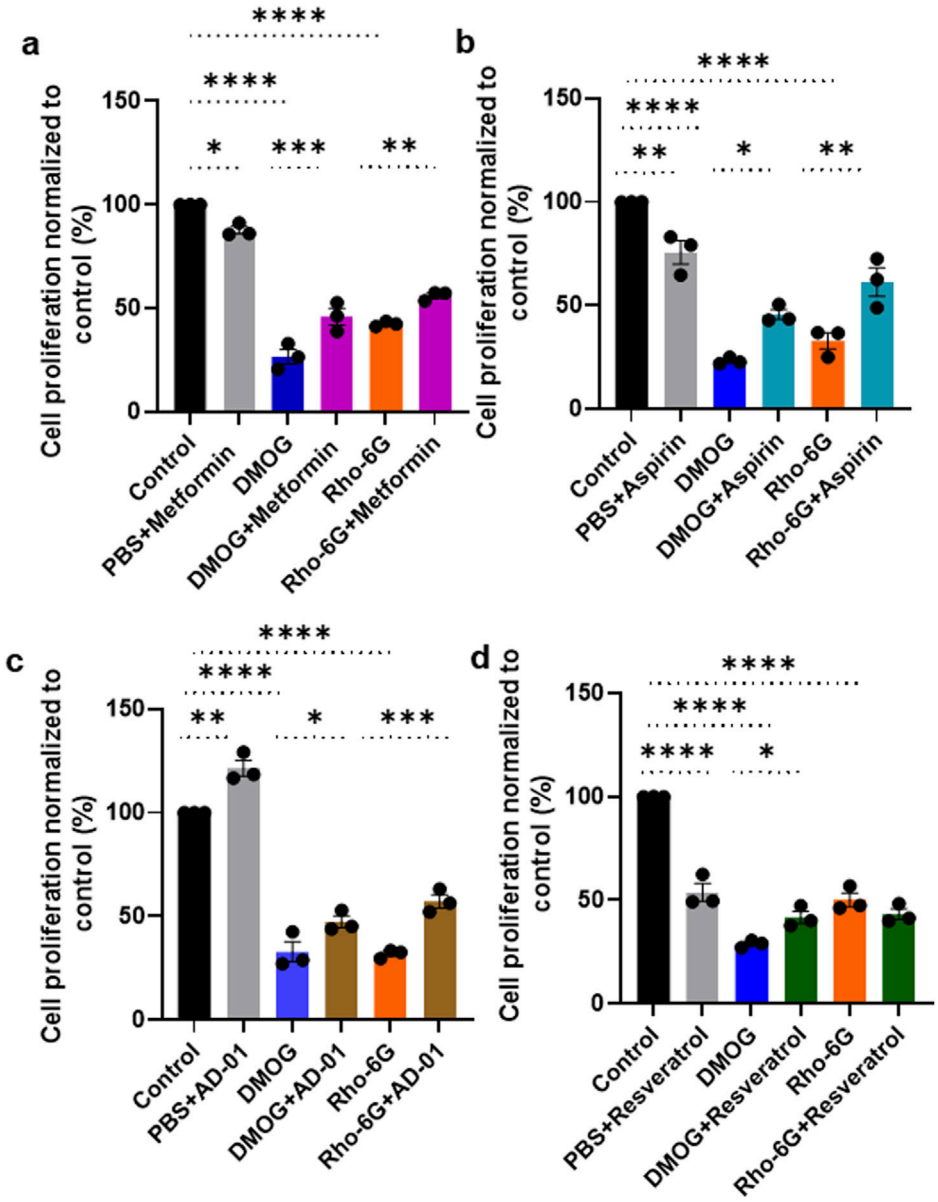

FIGURE 2
Metformin, aspirin and AD-01 improve cell proliferation in the presence of hypoxia and oxidative stress, whereas resveratrol only improves cell proliferation in hypoxic conditions. ACH-3P cells were treated with DMOG (1 mM) or Rho-6G (1 μg/mL) to emulate hypoxia or oxidative stress, respectively, ± **(A–D)** PBS ± **(A)** metformin (0.5 mM), or **(B)** aspirin (0.5 mM), or **(C)** AD-01 (100 nM) or **(D)** resveratrol (15 μM) for 48 h. MTT assay was performed as per manufacturer's instructions and absorbance recorded at 565 nm. Data was analyzed by one-way ANOVA with Sidak's post-hoc test; and expressed as mean ± SEM; n = 3; *p < 0.05; **p < 0.01; **p < 0.001; ****p < 0.0001.

control levels at two different concentrations (0.5 mM and 1.0 mM) (DMOG 31.09% ± 2.66%, vs. DMOG + Metformin (0.5 mM) 62.58% ± 4.25%, $p < 0.01$; vs. DMOG ± Metformin (1.0 mM) 52.14% ± 5.83%, $p < 0.05$; Figure 3C). At both time points, aspirin had the same effect only at one concentration (0.5 mM) that improved trophoblast migration at 24 h (DMOG 18.87% ± 4.22% vs. DMOG + Aspirin 54.05% ± 1.11%, $p < 0.001$; Figure 3D) and 48 h (DMOG 31.09% ± 2.66% vs. DMOG + Aspirin 66.67% ± 3.51%, $p < 0.001$; Figure 3E), compared to DMOG.

Given that metformin and aspirin have already been tested for the treatment or prevention of preeclampsia in humans, respectively (Cluver et al., 2021; Duley et al., 2019), we also wanted to explore novel treatments including FKBPL-based peptide mimetic, AD-01. Following 24 h treatment with DMOG, a similar trend in reduction of trophoblast cell migration was observed, which was not restored by AD-01 at this time point (Control 46.93% ± 8.24% vs. DMOG 22.34% ± 7.25%, $p = 0.07$; Figure 3F). However, there was statistically significant reduction in trophoblast migration induced by hypoxia at 48 h (Control 70.84% ± 3.49% vs. DMOG 43.39% ± 1.24%, $p < 0.001$; Figure 3G), which was improved with AD-01 treatment (100 nM) (DMOG 43.39% ± 1.24% vs. DMOG + AD-01 55.72% ± 1.03%, $p < 0.05$; Figure 3G).

10.3389/fcell.2025.1539496

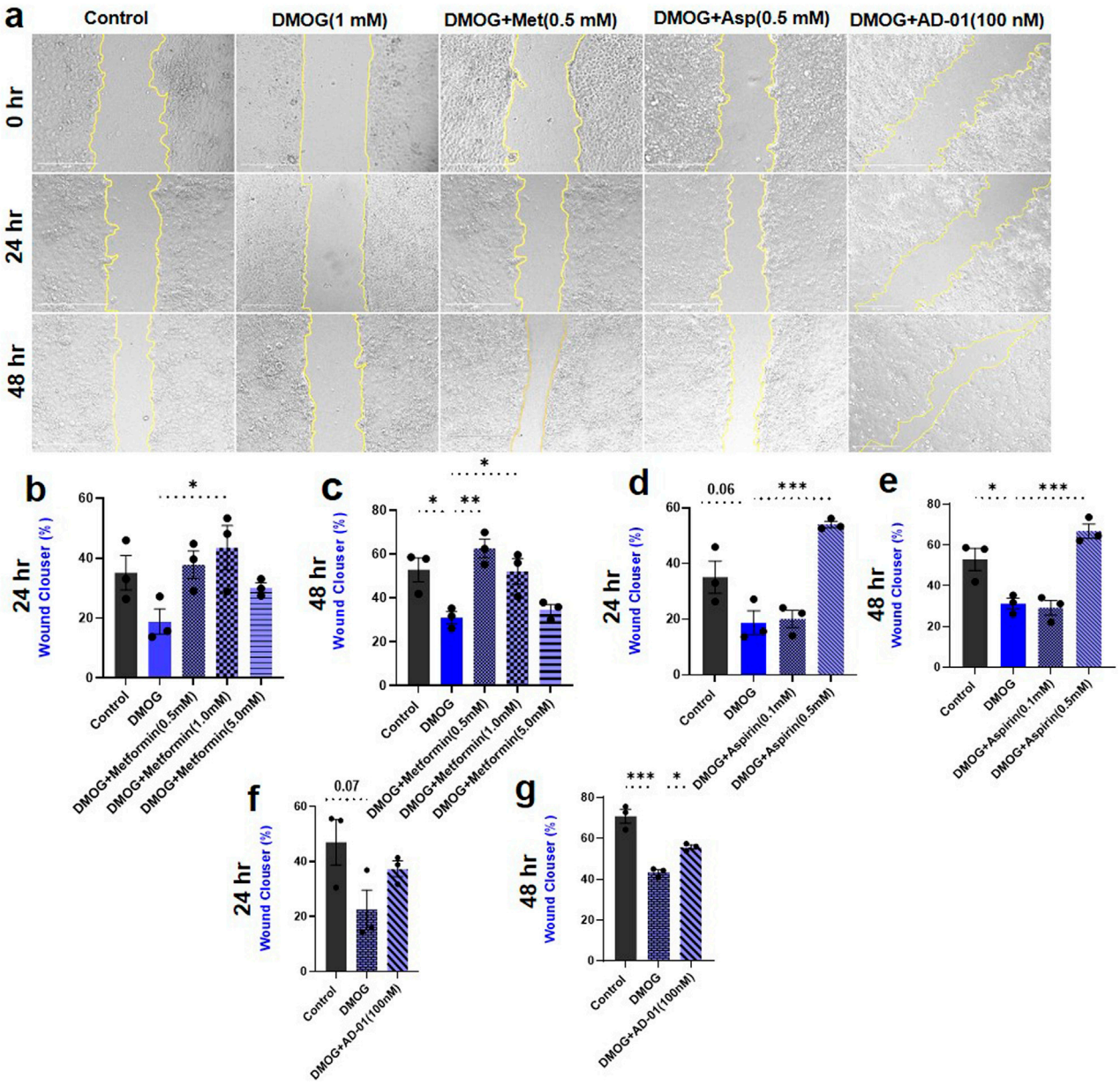

FIGURE 3
Hypoxia reduced trophoblast cell migration only at 48 h time point, and metformin, aspirin, AD-01 restore it to normal. **(A)** Representative images of the wound scratch assay with ACH-3P cells, following treatment with DMOG (1 mM) to mimic hypoxia, and metformin (Met) (0.5 mM), aspirin (asp) (0.5 mM), or AD-01 concentration (100 nM) at t = 0 h, t = 24 h and t = 48 h after wound scratch. Untreated cells were used as controls. The scale bar indicates 400 μm. **(B, C)** Percentage area of wound closure from 0 h to 24 h and 0 h to 48 h following treatment with various metformin doses (0.5 mM, 1 mM and 5 mM) under hypoxia. **(D, E).** Percentage area of wound closure from 0 h to 24 h and 0 h to 48 h following treatment with two different doses of aspirin (0.5 mM, 0.1 mM) under hypoxia. **(F, G)** Percentage area of wound closure from 0 h to 24 h and 0 h to 48 h following treatment with AD-01 (100 nM) under hypoxia. The data is analyzed by one-way ANOVA with Sidak's post hoc test and expressed as mean ± SEM; n = 3; ***p < 0.05, **p < 0.01, ***p < 0.001.

Mitochondrial dysfunction increases pro-inflammatory cytokine levels, which could be potentially abrogated by metformin

The imbalance between pro-inflammatory and anti-inflammatory cytokines in preeclampsia promotes inflammation and oxidative stress, contributing to the development of endothelial dysfunction, hypertension, and potentially organ damage. (Martínez-Varea et al., 2014; Geldenhuys et al., 2018). In this inflammatory and oxidative stress environment, the anti-inflammatory cytokine, IL-10, fails to effectively counteract pro-inflammatory cytokines, which contributes to the progression of the disease (Szarka et al., 2010; Afshari et al., 2005; Udenze et al., 2015). In our *in vitro* first trimester trophoblast cell model of placental stress in preeclampsia, we wanted to determine the inflammatory

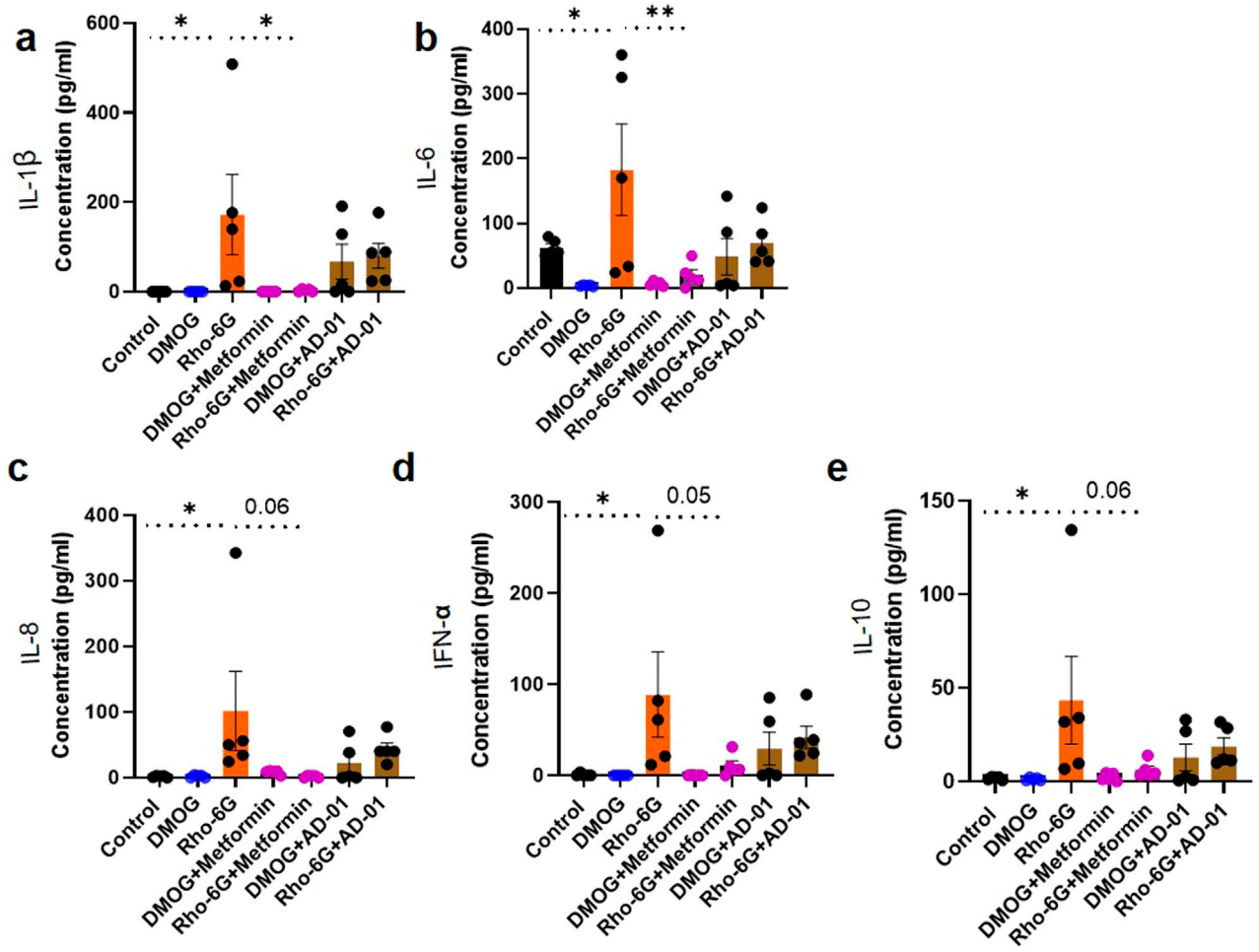

FIGURE 4
Pro-inflammatory cytokines were increased following induction of mitochondrial dysfunction and metformin showed some potential at abrogating this increase in the first trimester trophoblast cells. **(A–E)** ACH-3P cells were treated with DMOG (1 mM) or Rho-6G (1 μg/mL) to mimic hypoxia, or mitochondrial dysfunction, respectively, ± metformin (0.5 mM), or AD-01 (100 nM), for 48 h. Cell supernatants were collected to determine **(A–D)** the pro-inflammatory (IL-1β, IL-6, IL-8, IFN-α) and **(E)** anti-inflammatory cytokine (IL-10) concentrations by Cytometric Bead Array. Untreated cells were used as control groups. Pro-inflammatory cytokines **(A)** IL-1β, **(B)** IL-6, **(C)** IL-8, **(D)** IFN-α levels were increased following mitochondrial dysfunction induction and IL-1β and IL-6 increase was abrogated by metformin treatment in ACH-3Ps. **(E)** Anti-inflammatory IL-10 cytokine was also increased in the presence of mitochondrial dysfunction, which was borderline reduced with metformin. The data was analyzed by one-way analysis of variance (ANOVA) with Sidak's post-hoc test and expressed as mean ± SEM; n = 5; *p < 0.05; **p < 0.01.

mechanism of hypoxia mimetic or mitochondrial dysfunction with or without metformin or AD-01. Resveratrol was not included here due to its toxic effects on trophoblast proliferation demonstrated in Figure 2D and aspirin is a well-known anti-inflammatory agent. Pro-inflammatory cytokine concentrations of IL-1β (Control 0.00 ± 0.00 pg/mL vs. Rho-6G 172.3 ± 89.92 pg/mL, $p < 0.05$, Figure 4A), IL-6 (Control 62.66 ± 5.59 pg/mL vs. Rho-6G 182.7 ± 70.63 pg/mL, $p < 0.05$, Figure 4B), IL-8 (Control 1.99 ± 0.70 pg/mL vs. Rho-6G 101.8 ± 60.49 pg/mL, $p < 0.05$, Figure 4C), IFN-α (Control 0.74 ± 0.74 pg/mL vs. Rho-6G 88.98 ± 46.76 pg/mL, $p < 0.05$, Figure 4D) were increased significantly following treatment with mitochondrial dysfunction agent, Rho-6G. Metformin showed some potential at abrogating the increase in IL-1β (Rho-6G 172.3 ± 89.92 pg/mL vs. Rho-6G + Metformin 2.93 ± 1.28 pg/mL, $p < 0.05$, Figure 4A) and IL-6 (Rho-6G 182.7 ± 70.63 pg/mL vs. Rho-6G + Metformin 20.09 ± 8.34 pg/mL, $p < 0.01$, Figure 4B). Borderline significance was observed in relation to the metformin-mediated reduction of IL-8 (Rho-6G 101.8 ± 60.49 pg/mL vs. Rho-6G + Metformin 8.57 ± 1.51 pg/mL, $p = 0.06$, Figure 4C) and IFN-α (Rho-6G 88.98 ± 46.76 pg/mL vs. Rho-6G + Metformin 10.70 ± 5.38 pg/mL, $p = 0.05$, Figure 4D) in the presence of mitochondrial dysfunction. On the other hand, anti-inflammatory cytokine, IL-10 was also increased as a result of mitochondrial dysfunction and metformin (0.5 mM) treatment borderline normalized its concentration (Control 1.80 ± 0.34 pg/mL vs. Rho-6G 43.44 ± 23.46 pg/mL, $p < 0.05$; Rho-6G 43.44 ± 23.46 pg/mL vs. Rho-6G + Metformin 6.32 ± 1.97 pg/mL , $p = 0.06$, Figure 4E).

In this experiment, although AD-01 showed a trend towards a reduction in pro-inflammatory cytokines (IL-1β, IL-6, IL-8, IFN-α) and IL-10, this was not statistically significant. Interestingly, pro-inflammatory cytokines were not increased in DMOG/hypoxic condition.

Discussion

Preeclampsia is an understudied cardiovascular disorder of pregnancy, however despite some progress, no definitive treatment options currently exist. Several factors have contributed to this, including difficulties in obtaining human samples of the early placenta and the lack of biologically relevant model systems of this disease. In order to develop better monitoring and preventative strategies for pregnant individuals and their offspring at risk of or affected by preeclampsia, reliable and representative models of the early placenta are necessary that recapitulate multifactorial nature of the disease (Ghorbanpour et al., 2023). The root cause of preeclampsia is inappropriate placentation, often related to oxidative stress, aberrant angiogenesis, and/or inflammation (Burton et al., 2019). Our recent meta-analysis based on nine clinical studies identified the three most reliable oxidative stress-related diagnostic biomarkers for preeclampsia including Ischemia-Modified Albumin (IMA), UA, and MDA (Afrose et al., 2022). In this study, we confirmed the increased concentration of UA and MDA in human plasma samples from individuals with preeclampsia, compared to healthy controls. Then, we developed *in vitro* first trimester trophoblast cell models of placental stress preceding preeclampsia that are reflective of three different aspects of its pathogenesis: hypoxia, inflammation and mitochondrial dysfunction (Palei et al., 2013). Using these models, we tested a number of clinically available and novel therapeutics for preeclampsia including aspirin, metformin, resveratrol and FKBPL-based therapeutic peptide mimetic, AD-01 (Cluver et al., 2019; Bujold et al., 2010; Caldeira-Dias et al., 2019; Ghorbanpour et al., 2024). We showed that (i) metformin, and AD-01 can abrogate upregulation of UA and MDA due to preeclampsia-like placental stresses, (ii) metformin, aspirin and AD-01 can improve impaired cell proliferation and migration due to hypoxia-like and mitochondrial dysfunction placental stresses, and (iii) metformin mitigates certain aspects of heightened inflammation as a result of mitochondrial dysfunction. Overall, metformin showed the most promising therapeutic effect across all types of placental stresses and assays. Surprisingly, based on our proliferation or viability assay, all drugs (aspirin, metformin and resveratrol) except AD-01 in physiological conditions had a negative impact on trophoblast proliferation measured by the metabolic activity, suggesting a good safety profile of AD-01, which needs to be investigated further in *in vivo* studies. This was an unexpected result for metformin, aspirin and resveratrol, which are clinically utilized or trialled for preeclampsia prevention/treatment and are deemed safe to use in pregnancy. Nevertheless, their mechanism of action related to trophoblast cells specifically is still not well-understood, which this study elucidated further. Our findings suggest that the inhibitory effects of aspirin, metformin, or resveratrol on trophoblast proliferation might be context-dependent, reflecting their ability to modulate stress-induced cellular responses rather than direct cytotoxicity.

Here we introduce, for the first time, a simple cell model mimicking specific placental stresses preceding preeclampsia using a custom-made first trimester trophoblast cell line that closely resembles primary trophoblasts (Hiden et al., 2007). In our *in vitro* models, preeclampsia-related stresses including hypoxia, inflammation and mitochondria dysfunction were individually mimicked, enabling the evaluation of therapeutic potential of treatments for each aspect of the disease's pathogenesis, paving the way for personalized medicine in preeclampsia. Nevertheless, in the future, various combinations of these placental stresses can be used concurrently.

In this study, we measured UA and MDA oxidative stress markers intracellularly in ACH-3P trophoblast cells, given their strong association with preeclampsia as demonstrated in our previously published meta-analysis, and their role in the pathogenesis of preeclampsia (Afrose et al., 2022; Masoura et al., 2015; Khaliq et al., 2018; Yoneyama et al., 2002; Rani et al., 2010). UA is produced in the liver through purine metabolism and nutritional sources. Preeclampsia is directly associated with placental ischemia and oxidative stress, which can trigger or activate the release of xanthine oxidase enzyme (Myatt and Cui, 2004). UA is formed when adenosine triphosphate is cleaved into adenosine xanthine by xanthine oxidase (Uaa et al., 2017). Many studies have demonstrated that serum UA levels increase with preeclampsia severity, and that UA may play an important role in the pathogenesis of preeclampsia (Sudjai and Satho, 2022; Masoura et al., 2015; Khaliq et al., 2018). Here, we confirmed that following the diagnosis of preeclampsia, UA plasma concentration was increased albeit borderline significant, and this was also reflected in our 2D first trimester trophoblast cell- based *in vitro* models of placental stress in preeclampsia. Significant positive correlation was demonstrated between UA and preeclampsia when adjusted for differences in gestational age at sample collection. In our trophoblast *in vitro* models, UA was increased as a result of all stress stimuli (hypoxic mimetic, inflammation and mitochondrial dysfunction).

More prominent than UA, plasma MDA was significantly higher in preeclampsia compared to healthy controls. However, this was reflected in some of our *in vitro* models where hypoxia or mitochondrial dysfunction was induced, but not in the presence of inflammation. As a three-carbon aldehyde, MDA produces free radicals, which can damage cell membranes and are correlated with the severity of the disease (Sim et al., 2003). A common form of oxidative stress, called uncontrolled lipid peroxidation, can contribute to pregnancy complications, including preeclampsia (Rani et al., 2010; Ferreira et al., 2020). Numerous previous studies have indicated that MDA is elevated in various diseases, including pregnancy-induced hypertension and preeclampsia (Rani et al., 2010; Adiga et al., 2007; Ferreira et al., 2020). Given that in preeclampsia, there is an imbalance between free radicals and antioxidants that results in oxidative stress and, consequently, increased levels of lipid peroxide (Rani et al., 2010), MDA as a biomarker and a therapeutic target shows promise towards clinical translation.

Even though primary human cytotrophoblasts or trophoblast stem cells are the gold standard as *in vitro* placental models, these cells undergo rapid changes once they are cultured, are highly variable between individuals, and do not proliferate, hence have limited utility for drug screening. Although immortalized cell lines are generally considered less representative of the human placenta, they are readily available and can be expanded to meet the requirements of large-scale applications with good reproducibility (Zhao et al., 2021). Previous work has shown that ACH-3Ps contain both cytotrophoblasts that express integrin α6β4 and HLA-G-

positive extravillous trophoblasts (EVTs) expressing integrin α5β1, and matrix metalloproteinases, MMP2 and MMP9, unlike other cell lines including HTR-8/SVneo (Hiden et al., 2007). While ACH-3Ps are not able to undergo syncytialization in 2D culture, the syncytiotrophoblast marker, β-human chorionic gonadotropin (β-hCG), was detectable using pregnancy test in our ACH-3Ps cell culture *in vitro*. The karyotyping of this cell line revealed a male gender, and transcriptomic analysis confirmed a close alignment between the gene expression profiles of ACH-3Ps and their primary trophoblast cell origin. In a microfluidic device, ACH-3P cells were shown to contain both HLA-G- and EpCAM- positive extravillous and villous first trimester trophoblast subpopulation, respectively, which are vital for the development of the placenta (Ghorbanpour et al., 2023). ACH-3Ps are also highly proliferative, enabling large-scale production, which was necessary for quantifying UA and MDA in cell lysates. Therefore, we were able to generate 2D *in vitro* models of placental stress often observed in preeclampsia that were reproducible, low-risk, and low-cost by using this cell line.

Although the pathogenesis of preeclampsia is still poorly understood, the root cause is inappropriate remodelling of the SUA, likely caused by inadequate trophoblast cell function. Subsequently, chronic placental hypoxia follows, leading to restrictive supply of oxygen and nutrients to the fetus (McNally et al., 2017). This can lead to inflammation, mitochondrial dysfunction and oxidative stress within the placental cells, particularly trophoblast cells. Mitochondrial dysfunction in preeclampsia or other obstetrics complications such as gestational diabetes mellitus can lead to impaired energy production and an increased generation of ROS, which in turn leads to endothelial dysfunction, another hallmark feature of preeclampsia (Ferreira et al., 2020; Fisher et al., 2021). In fact, mitochondrial dysfunction is a major source of intracellular and extracellular oxidative stress, as demonstrated within placental tissues from women with preeclampsia (Han et al., 2020; Lian et al., 2022).

In our *in vitro* first trimester trophoblast model of placental stress, we induced hypoxia chemically by DMOG, an activator of HIF-1α and an inhibitor of prolyl-hydroxylases (Nevo et al., 2006; Zippusch et al., 2021; Sasagawa et al., 2021; Zhao et al., 2021). Mitochondrial dysfunction leading to oxidative stress was induced by Rho-6G, a lipophilic dye and a potent inhibitor of oxidative phosphorylation (Dutra Silva et al., 2021; Gear, 1974). TNF-α is a key proinflammatory cytokine involved in preeclampsia pathogenesis (Ghorbanpour et al., 2023), and its effects on trophoblast cells are directly relevant to understanding the interplay between inflammation and oxidative stress in this condition. Inflammation is a key driver of oxidative stress in preeclampsia, as highlighted in our recent review (Afrose et al., 2025), where we discussed how inflammatory processes exacerbate reactive oxygen species (ROS) production, contributing to the oxidative stress observed in this condition. We used these cell-based models to test a number of potential therapeutics for preeclampsia including (i) a well-established preventative treatment for preterm preeclampsia, aspirin (ACOG, 2019), (ii) a hypoglycaemic agent, metformin, emerging as a promising treatment of preeclampsia (Alqudah et al., 2018; Cluver et al., 2021; Decui et al., 2021), (iii) naturally occurring compound-derived drug, resveratrol (Shi et al., 2023), and (iv) a newly developed compound, AD-01, which is a based on an anti-angiogenic protein, FKBPL (McClements et al., 2013). These drugs are known to have pleiotropic effects, including anti-inflammatory, antioxidant, and/or angiogenesis-related properties, which are relevant to preeclampsia. The dosages of the drugs used in this study were representative of the plasma levels following drug absorption, metabolism, and distribution in humans (Angiolillo et al., 2022; Sheleme, 2021; LaMoia and Shulman, 2021; Seidler et al., 2018; Kemper et al., 2022; Singh et al., 2019; Arif and Aggarwal, 2023; Mather et al., 2021). Based on the cell proliferation or viability assay results, metformin, aspirin, resveratrol, or AD-01 may be useful for prevention of preeclampsia by reversing HIF-1α or oxidative stress-induced first trimester trophoblast cell damage. We found a significant reduction in trophoblast cell migration caused by hypoxia mimetic at 48 h.

Immune dysregulation is another major aspect of preeclampsia pathogenesis. The imbalance of pro-inflammatory and anti-inflammatory factors plays a crucial role in preeclampsia development and progression (Rana et al., 2019; Bisson et al., 2023; Weel et al., 2016; Peixoto et al., 2016). We demonstrated, in this study, that pro-inflammatory cytokines (IL-1β, IL-6, IL-8, IFN-α) levels were increased by oxidative stress and abrogated by metformin treatment only. Surprisingly, hypoxia mimetic did not affect pro-inflammatory cytokines levels. We also observed opposite trends in anti-inflammatory cytokine, IL-10, concentration in these experiments. Previous research has shown that IL-10 is downregulated in preeclampsia (Murray et al., 2022; Michalczyk et al., 2020). The increased production of IL-10 could be interpreted as a compensatory mechanism that mitigates the heightened inflammatory response in trophoblast cells by hypoxia (Opichka et al., 2021; Aneman et al., 2020). Further studies are needed to uncover this interaction in the context of preeclampsia.

While the effects and mechanisms of both placental stresses in preeclampsia and treatments should also be investigated in other placental cell types, including endothelial and immune cells, our 2D *in vitro* trophoblast cell model demonstrates value in studying the complex multifactorial pathophysiology of preeclampsia. A key limitation of our study is the use of a single trophoblast cell line (ACH-3P), which may not fully capture the complexity of preeclampsia pathophysiology. In support of this study findings, our previous work demonstrated that AD-01 effectively restores endothelial function and integrity following DMOG treatment, by regulating FKBPL and HIF-1α expression (Ghorbanpour et al., 2024). Given that DMOG is extensively known as HIF-1α mimic, we did not measure HIF-1α expression in trophoblast cells, however we demonstrated increased expression of oxidative stress biomarkers, UA and MDA, which are the most relevant to preeclampsia, in DMOG-treated trophoblasts. Future studies should measure the concentrations of well-known biomarkers of angiogenic imbalance in preeclampsia, sFlt-1 and PlGF (Dimitriadis et al., 2023) to further understand the mechanisms of these potential therapeutics in the context of specific preeclampsia-like stresses in our first trimester trophoblast *in vitro* models. This *in vitro* model can be improved by using primary first trimester trophoblast cells to further our understanding of these specific pathological mechanisms and therapeutic approaches, in preeclampsia. Our

in vitro models can be used for high-throughput screening of potential therapeutics for preeclampsia to develop personalized treatments and gain a deeper understanding of the pathogenesis of this complex disease.

Conclusion

In this study, we developed a simple, low-cost and reproducible 2D *in vitro* model of placental stresses preceding preeclampsia using the custom-made immortalized first trimester trophoblast cell line, ACH-3Ps, which closely resembles primary trophoblasts and contains all three trophoblast subtypes includes cytotrophoblasts, EVTs and syncytiotrophoblasts. All of these trophoblast subtypes are crucial for placental development and growth. We developed this model to mimic the features of hypoxia, mitochondrial dysfunction and inflammation of the preeclamptic placenta. Additionally, we explored therapeutic strategies that can abrogate these pathogenic mechanisms and potentially prevent the development of preeclampsia. We showed that metformin, aspirin, resveratrol and AD-01 show promise as treatments for preeclampsia, capable of abrogating hypoxia-, inflammation- or mitochondrial dysfunction-induced first trimester trophoblast cell damage. Metformin appears to be the most effective across different placental stresses typical of preeclampsia and can improve trophoblast proliferation and migration, as well as reduce oxidative stress and inflammation. This is the first study to report the therapeutic potential of the FKBPL-based therapeutic peptide, AD-01, which appears to be less toxic compared to other treatments tested in physiological conditions, in terms of trophoblast proliferation. However, metformin, aspirin and resveratrol have been extensively tested *in vivo* and in human studies including pregnancy, whereas FKBPL-based therapeutic peptides (AD-01 and ALM201) have only been tested in the context of cancer (El Helali et al., 2022). Future studies should test AD-01 in preclinical pregnancy models to determine its safety and efficacy including the impact on fetal health.

Data availability statement

The original contributions presented in the study are included in the article/Supplementary Material, further inquiries can be directed to the corresponding author.

Ethics statement

The study was approved by the University of Technology Sydney (UTS) Human Research Ethics Executive Review Committee and local hospital ethics committees. The study were conducted in accordance with the local legislation and institutional requirements. The participants provided their written informed consent to participate in this study.

Author contributions

DA: Data curation, Formal Analysis, Investigation, Methodology, Visualization, Writing–original draft. MJ: Data curation, Formal Analysis, Investigation, Visualization, Writing–review and editing. VN: Formal Analysis, Investigation, Methodology, Project administration, Resources, Writing–review and editing. NO: Data curation, Investigation, Methodology, Project administration, Resources, Writing–review and editing. ZM: Data curation, Investigation, Methodology, Project administration, Resources, Writing–review and editing. MS: Data curation, Investigation, Methodology, Project administration, Resources, Writing–review and editing. ZC: Data curation, Investigation, Methodology, Project administration, Resources, Writing–review and editing. PH: Project administration, Resources, Supervision, Writing–review and editing. LM: Conceptualization, Formal Analysis, Funding acquisition, Project administration, Resources, Supervision, Validation, Writing–review and editing.

Funding

The author(s) declare that financial support was received for the research, authorship, and/or publication of this article. This research was supported by an Australian Government Research Training Program (RTP) Stipend and RTP Fee-Offset Scholarship through the University of Technology Sydney and Future Leader Fellowship Level 1 from the National Heart Foundation of Australia (LM, 106628).

Acknowledgments

We thank the participants for taking part in this study and all healthcare staff for helping with the recruitment of the participants. The authors would like to acknowledge the use of BioRender for the creation of the schematics used in figures.

Conflict of interest

LM is an inventor on FKBPL-related patents for prediction and diagnosis of preeclampsia.

The remaining authors declare that the research was conducted in the absence of any commercial or financial relationships that could be construed as a potential conflict of interest.

Generative AI statement

The author(s) declare that no Generative AI was used in the creation of this manuscript.

Publisher's note

Supplementary material

The Supplementary Material for this article can be found online at: https://www.frontiersin.org/articles/10.3389/fcell.2025.1539496/full#supplementary-material

SUPPLEMENTARY FIGURE S1
Time course optimisation related to the effects of aspirin in the presence of preeclampsia-like stimuli on trophoblast cell proliferation. ACH-3Ps cells were treated with DMOG (1 mM), TNF-α (10 ng/mL) or Rho-6G (1 μg/mL) to emulate hypoxia, inflammation or oxidative stress, ± aspirin (0.5 mM) respectively for (A) 24 h or (B) 72 h. MTT assay was performed as per manufacturer's instructions and absorbance recorded at 565 nm minus absorbance at 650 nm. Data analyzed by one-way ANOVA Šídák's multiple comparisons test; and expressed as mean ± SEM; n = 3; ****p < 0.0001.

SUPPLEMENTARY FIGURE S2
Time course optimisation related to the effects of metformin in the presence of preeclampsia-like stimuli on trophoblast cell proliferation. ACH-3Ps cells were treated with DMOG (1 mM), TNF-α (10 ng/mL) or Rho-6G (1 μg/mL) to emulate hypoxia, inflammation or oxidative stress, ± metformin (0.5 mM) respectively for (A) 24 h or (B) 72 h. MTT assay was performed as per manufacturer's instructions and absorbance recorded at 565 nm minus absorbance at 650 nm. Data analyzed by one-way ANOVA Šídák's multiple comparisons test; and expressed as mean ± SEM; n = 3; *p < 0.05; **p < 0.01; **p < 0.001; ****p < 0.0001.

SUPPLEMENTARY FIGURE S3
Time course optimisation related to the effects of resveratrol in the presence of preeclampsia-like stimuli on trophoblast cell proliferation. ACH-3Ps cells were treated with DMOG (1 mM), TNF-α (10 ng/mL) or Rho-6G (1 μg/mL) to emulate hypoxia, inflammation or oxidative stress, ± resveratrol (10 μM) respectively for (A) 24 h or (B) 72 h. MTT assay was performed as per manufacturer's instructions and absorbance recorded at 565 nm minus absorbance at 650 nm. Data analyzed by one-way ANOVA Šídák's multiple comparisons test; and expressed as mean ± SEM; n = 3; *p < 0.05; **p < 0.01; **p < 0.001; ****p < 0.0001.

References

ACOG (2019). *Obstet. Gynecol.* 133 (1), 1. doi:10.1097/AOG.0000000000003018

Adiga, U., D'souza, V., Kamath, A., and Mangalore, N. (2007). Antioxidant activity and lipid peroxidation in preeclampsia. *J. Chin. Med. Assoc.* 70 (10), 435–438. doi:10.1016/S1726-4901(08)70034-0

Afrose, D., Alfonso-Sánchez, S., and McClements, L. (2025). Targeting oxidative stress in preeclampsia. *Hypertens. Pregnancy* 44 (1), 2445556. doi:10.1080/10641955.2024.2445556

Afrose, D., Chen, H., Ranashinghe, A., Liu, C. chi, Henessy, A., Hansbro, P. M., et al. (2022). The diagnostic potential of oxidative stress biomarkers for preeclampsia: systematic review and meta-analysis. *Biol. Sex. Differ.* 13 (1), 26. doi:10.1186/s13293-022-00436-0

Afshari, J. T., Ghomian, N., Shameli, A., Shakeri, M., Fahmidehkar, M., Mahajer, E., et al. (2005). Determination of interleukin-6 and tumor necrosis factor-alpha concentrations in Iranian-khorasanian patients with preeclampsia. *BMC Pregnancy Childbirth* 5 (1), 14. doi:10.1186/1471-2393-5-14

Agarwal, I., and Karumanchi, S. A. (2011). Preeclampsia and the anti-angiogenic state. *Pregnancy Hypertens An Int J Women's Cardiovasc Heal* 1 (1), 17–21. doi:10.1016/j.preghy.2010.10.007

Alqudah, A., McKinley, M. C., McNally, R., Graham, U., Watson, C. J., Lyons, T. J., et al. (2018). Risk of pre-eclampsia in women taking metformin: a systematic review and meta-analysis. *Diabet. Med.* 35 (2), 160–172. doi:10.1111/dme.13523

Aneman, I., Pienaar, D., Suvakov, S., Simic, T. P., Garovic, V. D., and McClements, L. (2020). Mechanisms of key innate immune cells in early- and late-onset preeclampsia. *Front. Immunol.* 11, 1864. doi:10.3389/fimmu.2020.01864

Angiolillo, D. J., Prats, J., Deliargyris, E. N., Schneider, D. J., Scheiman, J., Kimmelstiel, C., et al. (2022). Pharmacokinetic and pharmacodynamic profile of a novel phospholipid aspirin formulation. *Clin. Pharmacokinet.* 61 (4), 465–479. doi:10.1007/s40262-021-01090-2

Annett, S., Moore, G., Short, A., Marshall, A., McCrudden, C., Yakkundi, A., et al. (2020). FKBPL-based peptide, ALM201, targets angiogenesis and cancer stem cells in ovarian cancer. *Br. J. Cancer* 122 (3), 361–371. doi:10.1038/s41416-019-0649-5

Annett, S. L., Spence, S., Garciarena, C., Campbell, C., Dennehy, M., Drakeford, C., et al. (2021). The immunophilin protein FKBPL and its peptide derivatives are novel regulators of vascular integrity and inflammation via nf-κb signaling. *bioRxiv 2021.02.24.431422*. doi:10.1101/2021.02.24.431422

Arif, H., and Aggarwal, S. (2023). "Salicylic acid (aspirin)," in *StatPearls* (Treasure Island, FL: StatPearls).

Bambrana, V., Dayanand, C. D., and Kotur, P. (2017). Relationship between xanthine oxidase, ischemia modified albumin, nitric oxide with antioxidants in non pregnants, pre and post-delivery of normal pregnants and preeclampsia. *Indian J. Clin. Biochem.* 32 (2), 171–178. doi:10.1007/s12291-016-0599-0

Bezerra Maia e Holanda Moura S, Marques Lopes, L., Murthi, P., and da Silva Costa, F. (2012). Prevention of preeclampsia. *J. Pregnancy* 2012, 1–9. doi:10.1155/2012/435090

Bisson, C., Dautel, S., Patel, E., Suresh, S., Dauer, P., and Rana, S. (2023). Preeclampsia pathophysiology and adverse outcomes during pregnancy and postpartum. *Front. Med.* 10, 10. doi:10.3389/fmed.2023.1144170

Bokuda, K., and Ichihara, A. (2023). Preeclampsia up to date—what's going on? *Hypertens. Res.* 46 (8), 1900–1907. doi:10.1038/s41440-023-01323-w

Brownfoot, F., and Rolnik, D. L. (2024). Prevention of preeclampsia. *Best. Pract. Res. Clin. Obstet. Gynaecol.* 93, 102481. doi:10.1016/j.bpobgyn.2024.102481

Brownfoot, F. C., Hastie, R., Hannan, N. J., Cannon, P., Nguyen, T. V., Tuohey, L., et al. (2020). Combining metformin and sulfasalazine additively reduces the secretion of antiangiogenic factors from the placenta: implications for the treatment of preeclampsia. *Placenta* 95, 78–83. doi:10.1016/j.placenta.2020.04.010

Brownfoot, F. C., Hastie, R., Hannan, N. J., Cannon, P., Tuohey, L., Parry, L. J., et al. (2016). Metformin as a prevention and treatment for preeclampsia: effects on soluble fms-like tyrosine kinase 1 and soluble endoglin secretion and endothelial dysfunction. *Am. J. Obstet. Gynecol.* 214 (3), 356.e1–356.e15. doi:10.1016/j.ajog.2015.12.019

Bujold, E., Roberge, S., Lacasse, Y., Bureau, M., Audibert, F., Marcoux, S., et al. (2010). Prevention of preeclampsia and intrauterine growth restriction with aspirin started in early pregnancy: a meta-analysis. *Obstet. Gynecol.* 116 (2), 402–414. doi:10.1097/AOG.0b013e3181e9322a

Burton, G. J., Redman, C. W., Roberts, J. M., and Moffett, A. (2019). Pre-eclampsia: pathophysiology and clinical implications. *BMJ* 15, l2381. doi:10.1136/bmj.l2381

Caldeira-Dias, M., Montenegro, M. F., Bettiol, H., Barbieri, M. A., Cardoso, V. C., Cavalli, R. C., et al. (2019). Resveratrol improves endothelial cell markers impaired by plasma incubation from women who subsequently develop preeclampsia. *Hypertens. Res.* 42 (8), 1166–1174. doi:10.1038/s41440-019-0243-5

Chhor, M., Chen, H., Jerotić, D., Tešić, M., Nikolić, V. N., Pavlović, M., et al. (2023). FK506-Binding protein like (FKBPL) has an important role in Heart failure with preserved ejection fraction pathogenesis with potential diagnostic utility. *Biomolecules* 13 (2), 395. doi:10.3390/biom13020395

Cluver, C., Walker, S. P., Mol, B. W., Hall, D., Hiscock, R., Brownfoot, F. C., et al. (2019). A double blind, randomised, placebo-controlled trial to evaluate the efficacy of metformin to treat preterm pre-eclampsia (PI2 Trial): study protocol. *BMJ Open* 9 (4), e025809. doi:10.1136/bmjopen-2018-025809

Cluver, C. A., Hannan, N. J., van Papendorp, E., Hiscock, R., Beard, S., Mol, B. W., et al. (2018). Esomeprazole to treat women with preterm preeclampsia: a randomized placebo controlled trial. *Am. J. Obstet. Gynecol.* 219 (4), 388.e1–388.e17. doi:10.1016/j.ajog.2018.07.019

Cluver, C. A., Hiscock, R., Decloedt, E. H., Hall, D. R., Schell, S., Mol, B. W., et al. (2021). Use of metformin to prolong gestation in preterm pre-eclampsia: randomised, double blind, placebo controlled trial. *BMJ* 374, n2103. doi:10.1136/bmj.n2103

Davenport, M. H., Ruchat, S. M., Poitras, V. J., Jaramillo Garcia, A., Gray, C. E., Barrowman, N., et al. (2018). Prenatal exercise for the prevention of gestational diabetes mellitus and hypertensive disorders of pregnancy: a systematic review and meta-analysis. *Br. J. Sports Med.* 52 (21), 1367–1375. doi:10.1136/bjsports-2018-099355

Decui, C. X. Z., XX, Zhou, X., and Xu, X. (2021). The role of metformin in treating preeclampsia. *MedNexus* 3, 203–207. doi:10.1097/fm9.0000000000000086

Dimitriadis, E., Rolnik, D. L., Zhou, W., Estrada-Gutierrez, G., Koga, K., Francisco, R. P. V., et al. (2023). Pre-eclampsia. *Nat. Rev. Dis. Prim.* 9 (1), 8. doi:10.1038/s41572-023-00417-6

Ding, J., Kang, Y., Fan, Y., and Chen, Q. (2017). Efficacy of resveratrol to supplement oral nifedipine treatment in pregnancy-induced preeclampsia. *Endocr. Connect.* 6 (8), 595–600. doi:10.1530/EC-17-0130

Duley, L., Henderson-Smart, D. J., Meher, S., and King, J. F. (2007). Antiplatelet agents for preventing pre-eclampsia and its complications. *Cochrane Database Syst. Rev.*, CD004659. doi:10.1002/14651858.CD004659.pub2

Duley, L., Meher, S., Hunter, K. E., Seidler, A. L., and Askie, L. M. (2019). Antiplatelet agents for preventing pre-eclampsia and its complications. *Cochrane Database Syst. Rev.* 2019 (10). doi:10.1002/14651858.CD004659.pub3

Dutra Silva, J., Su, Y., Calfee, C. S., Delucchi, K. L., Weiss, D., McAuley, D. F., et al. (2021). Mesenchymal stromal cell extracellular vesicles rescue mitochondrial dysfunction and improve barrier integrity in clinically relevant models of ARDS. *Eur. Respir. J.* 58 (1), 2002978. doi:10.1183/13993003.02978-2020

El Helali, A., Plummer, R., Jayson, G. C., Coyle, V. M., Drew, Y., Mescallado, N., et al. (2022). A first-in-human Phase I dose-escalation trial of the novel therapeutic peptide, ALM201, demonstrates a favourable safety profile in unselected patients with ovarian cancer and other advanced solid tumours. *Br. J. Cancer* 127 (1), 92–101. doi:10.1038/s41416-022-01780-z

Farah, O., Nguyen, C., Tekkatte, C., and Parast, M. M. (2020). Trophoblast lineage-specific differentiation and associated alterations in preeclampsia and fetal growth restriction. *Placenta* 102, 4–9. doi:10.1016/j.placenta.2020.02.007

Ferreira, R. C., Fragoso, M. B. T., Bueno, N. B., Goulart, M. O. F., and de Oliveira, A. C. M. (2020). Oxidative stress markers in preeclamptic placentas: a systematic review with meta-analysis. *Placenta* 99, 89–100. doi:10.1016/j.placenta.2020.07.023

Fisher, J. J., Vanderpeet, C. L., Bartho, L. A., McKeating, D. R., Cuffe, J. S. M., Holland, O. J., et al. (2021). Mitochondrial dysfunction in placental trophoblast cells experiencing gestational diabetes mellitus. *J. Physiol.* 599 (4), 1291–1305. doi:10.1113/JP280593

Gear, A. R. (1974). Rhodamine 6G. *J. Biol. Chem.* 249 (11), 3628–3637. doi:10.1016/s0021-9258(19)42620-3

Geldenhuys, J., Rossouw, T. M., Lombaard, H. A., Ehlers, M. M., and Kock, M. M. (2018). Disruption in the regulation of immune responses in the placental subtype of preeclampsia. *Front. Immunol.* 9, 1659. doi:10.3389/fimmu.2018.01659

Ghorbanpour, S., Cartland, S. P., Chen, H., Seth, S., Ecker, R. C., Richards, C., et al. (2024). The FKBPL-based therapeutic peptide, AD-01, protects the endothelium from hypoxia-induced damage by stabilizing hypoxia inducible factor-α and inflammation.

Ghorbanpour, S. M., Richards, C., Pienaar, D., Sesperez, K., Aboulkheyr, Es. H., Nikolic, V. N., et al. (2023). A placenta-on-a-chip model to determine the regulation of FKBPL and galectin-3 in preeclampsia. *Cell Mol. Life Sci.* 80 (2), 44. doi:10.1007/s00018-022-04648-w

Gong, L., Goswami, S., Giacomini, K. M., Altman, R. B., and Klein, T. E. (2012). Metformin pathways: pharmacokinetics and pharmacodynamics. *Pharmacogenet Genomics.* 22 (11), 820–827. doi:10.1097/FPC.0b013e3283559b22

Han, C., Huang, P., Lyu, M., and Dong, J. (2020). Oxidative stress and preeclampsia-associated prothrombotic state. *Antioxidants* 9 (11), 1139. doi:10.3390/antiox9111139

Han, C. S., Herrin, M. A., Pitruzzello, M. C., Mulla, M. J., Werner, E. F., Pettker, C. M., et al. (2015). Glucose and metformin modulate human first trimester trophoblast function: a model and potential therapy for diabetes-associated uteroplacental insufficiency. *Am. J. Reprod. Immunol.* 73 (4), 362–371. doi:10.1111/aji.12339

Hiden, U., Bilban, M., Knöfler, M., and Desoye, G. (2007). Kisspeptins and the placenta: regulation of trophoblast invasion. *Rev. Endocr. Metab. Disord.* 8 (1), 31–39. doi:10.1007/s11154-007-9030-8

Ives, C. W., Sinkey, R., Rajapreyar, I., Tita, A. T. N., and Oparil, S. (2020). Preeclampsia-pathophysiology and clinical presentations: JACC state-of-the-art review. *J. Am. Coll. Cardiol.* 76 (14), 1690–1702. doi:10.1016/j.jacc.2020.08.014

Jung, E., Romero, R., Yeo, L., Gomez-Lopez, N., Chaemsaithong, P., Jaovisidha, A., et al. (2022). The etiology of preeclampsia. *Am. J. Obstet. Gynecol.* 226 (2), S844–S866. doi:10.1016/j.ajog.2021.11.1356

Kemper, C., Behnam, D., Brothers, S., Wahlestedt, C., Volmar, C. H., Bennett, D., et al. (2022). Safety and pharmacokinetics of a highly bioavailable resveratrol preparation (JOTROL TM). *AAPS Open* 8 (1), 11. doi:10.1186/s41120-022-00058-1

Khaliq, O. P., Konoshita, T., Moodley, J., and Naicker, T. (2018). The role of uric acid in preeclampsia: is uric acid a causative factor or a sign of preeclampsia? *Curr. Hypertens. Rep.* 20 (9), 80. doi:10.1007/s11906-018-0878-7

Lacerda, D. C., Costa, P. C. T., de Oliveira, Y., and de Brito, A. J. L. (2023). The effect of resveratrol in cardio-metabolic disorders during pregnancy and offspring outcomes: a review. *J. Dev. Orig. Health Dis.* 14 (1), 3–14. doi:10.1017/S2040174422000332

LaMoia, T. E., and Shulman, G. I. (2021). Cellular and molecular mechanisms of metformin action. *Endocr. Rev.* 42 (1), 77–96. doi:10.1210/endrev/bnaa023

Lian, R., Zhu, B. S., and Zeng, X. (2022). An update review of the pathogenesis hypothesis in preeclampsia. *Clin. Exp. Obstet. Gynecol.* 49 (8), 170. doi:10.31083/j.ceog4908170

Lopez-Jaramillo, P., Barajas, J., Rueda-Quijano, S. M., Lopez-Lopez, C., and Felix, C. (2018). Obesity and preeclampsia: common pathophysiological mechanisms. *Front. Physiol.* 9, 9. doi:10.3389/fphys.2018.01838

Martínez-Varea, A., Pellicer, B., Perales-Marín, A., and Pellicer, A. (2014). Relationship between maternal immunological response during pregnancy and onset of preeclampsia. *J. Immunol. Res.* 2014, 210241–210315. doi:10.1155/2014/210241

Masoumeh Ghorbanpour, S., Wen, S., Kaitu'u-Lino, T. J., Hannan, N. J., Jin, D., and McClements, L. (2023). Quantitative point of care tests for timely diagnosis of early-onset preeclampsia with high sensitivity and specificity. *Angew. Chem. Int.* 62 (26), e202301193. doi:10.1002/anie.202301193

Masoura, S., Makedou, K., Theodoridis, T., Kourtis, A., Zepiridis, L., and Athanasiadis, A. (2015). The involvement of uric acid in the pathogenesis of preeclampsia. *Curr. Hypertens. Rev.* 11 (2), 110–115. doi:10.2174/1573402111666150529130703

Mather, A. R., Dom, A. M., and Thorburg, L. L. (2021). Low-dose aspirin in pregnancy: who? when? how much? and why? *Curr. Opin. Obstet. Gynecol.* 33 (2), 65–71. doi:10.1097/GCO.0000000000000694

Matthys, L. A., Coppage, K. H., Lambers, D. S., Barton, J. R., and Sibai, B. M. (2004). Delayed postpartum preeclampsia: an experience of 151 cases. *Am. J. Obstet. Gynecol.* 190 (5), 1464–1466. doi:10.1016/j.ajog.2004.02.037

Maynard, S. E., and Karumanchi, S. A. (2011). Angiogenic factors and preeclampsia. *Semin. Nephrol.* 31 (1), 33–46. doi:10.1016/j.semnephrol.2010.10.004

McClements, L., Annett, S., Yakkundi, A., O'Rourke, M., Valentine, A., Moustafa, N., et al. (2019). FKBPL and its peptide derivatives inhibit endocrine therapy resistant cancer stem cells and breast cancer metastasis by downregulating DLL4 and Notch4. *BMC Cancer* 19 (1), 351. doi:10.1186/s12885-019-5500-0

McClements, L., Yakkundi, A., Papaspyropoulos, A., Harrison, H., Ablett, M. P., Jithesh, P. V., et al. (2013). Targeting treatment-resistant breast cancer stem cells with FKBPL and its peptide derivative, AD-01, via the CD44 pathway. *Clin. Cancer Res.* 19 (14), 3881–3893. doi:10.1158/1078-0432.CCR-13-0595

McNally, R., Alqudah, A., McErlean, E. M., Rennie, C., Morshed, N., Short, A., et al. (2021). Non-viral gene delivery utilizing RALA modulates sFlt-1 secretion, important for preeclampsia. *Nanomedicine.* 16 (22), 1999–2012. doi:10.2217/nnm-2021-0180

McNally, R., Alqudah, A., Obradovic, D., and McClements, L. (2017). Elucidating the pathogenesis of pre-eclampsia using *in vitro* models of spiral uterine artery remodelling. *Curr. Hypertens. Rep.* 19 (11), 93. doi:10.1007/s11906-017-0786-2

Michalczyk, M., Celewicz, A., Celewicz, M., Woźniakowska-Gondek, P., and Rzepka, R. (2020). The role of inflammation in the pathogenesis of preeclampsia. *Mediat. Inflamm.* 2020, 1–9. doi:10.1155/2020/3864941

Murray, E. J., Gumusoglu, S. B., Santillan, D. A., and Santillan, M. K. (2022). Manipulating CD4+ T cell pathways to prevent preeclampsia. *Front. Bioeng. Biotechnol.* 9, 811417. doi:10.3389/fbioe.2021.811417

Myatt, L., and Cui, X. (2004). Oxidative stress in the placenta. *Histochem Cell Biol.* 122 (4), 369–382. doi:10.1007/s00418-004-0677-x

Nafisa, A., Gray, S. G., Cao, Y., Wang, T., Xu, S., Wattoo, F. H., et al. (2018). Endothelial function and dysfunction: impact of metformin. *Pharmacol. Ther.* 192, 150–162. doi:10.1016/j.pharmthera.2018.07.007

Nevo, O., Soleymanlou, N., Wu, Y., Xu, J., Kingdom, J., Many, A., et al. (2006). Increased expression of sFlt-1 in *in vivo* and *in vitro* models of human placental hypoxia is mediated by HIF-1. *Am. J. Physiol. Integr. Comp. Physiol.* 291 (4), R1085–R1093. doi:10.1152/ajpregu.00794.2005

Onovughakpo-Sakpa, E., Onyeneke, C., Ayinbuomwan, E., and Atoe, K. (2021). Antioxidant and malondialdehyde status in preeclampsia. *Niger. J. Exp. Clin. Biosci.* 9 (2), 110–116. doi:10.4103/njecp.njecp_6_21

Opichka, M. A., Rappelt, M. W., Gutterman, D. D., Grobe, J. L., and McIntosh, J. J. (2021). Vascular dysfunction in preeclampsia. *Cells* 10 (11), 3055. doi:10.3390/cells10113055

Palei, A. C., Spradley, F. T., Warrington, J. P., George, E. M., and Granger, J. P. (2013). Pathophysiology of hypertension in pre-eclampsia: a lesson in integrative physiology. *Acta Physiol.* 208 (3), 224–233. doi:10.1111/apha.12106

Panagodage, S., Yong, H. E. J., Da Silva Costa, F., Borg, A. J., Kalionis, B., Brennecke, S. P., et al. (2016). Low-dose acetylsalicylic acid treatment modulates the production of cytokines and improves trophoblast function in an *in vitro* model of early-onset preeclampsia. *Am. J. Pathol.* 186 (12), 3217–3224. doi:10.1016/j.ajpath.2016.08.010

Peixoto, A. B., Araujo Júnior, E., Ribeiro, J. U., Rodrigues, D. B. R., Castro, E. C. C., Caldas, TMRC, et al. (2016). Evaluation of inflammatory mediators in the deciduas of pregnant women with pre-eclampsia/eclampsia. *J. Matern. Neonatal Med.* 29 (1), 75–79. doi:10.3109/14767058.2014.987117

Pollheimer, J., Vondra, S., Baltayeva, J., Beristain, A. G., and Knöfler, M. (2018). Regulation of placental extravillous trophoblasts by the maternal uterine environment. *Front. Immunol.* 9, 2597. doi:10.3389/fimmu.2018.02597

Ramli, I., Posadino, A. M., Giordo, R., Fenu, G., Fardoun, M., Iratni, R., et al. (2023). Effect of resveratrol on pregnancy, prenatal complications and pregnancy-associated structure alterations. *Antioxidants* 12 (2), 341. doi:10.3390/antiox12020341

Rana, S., Lemoine, E., Granger, J. P., and Karumanchi, S. A. (2019). Preeclampsia: pathophysiology, challenges, and perspectives. *Circ. Res.* 124 (7), 1094–1112. doi:10.1161/CIRCRESAHA.118.313276

Rani, N., Dhingra, R., Arya, D. S., Kalaivani, M., Bhatla, N., and Kumar, R. (2010). Role of oxidative stress markers and antioxidants in the placenta of preeclamptic patients. *J. Obstet. Gynaecol. Res.* 36 (6), 1189–1194. doi:10.1111/j.1447-0756.2010.01303.x

Ridder, A., Giorgione, V., Khalil, A., and Thilaganathan, B. (2019). Preeclampsia: the relationship between uterine artery blood flow and trophoblast function. *Int. J. Mol. Sci.* 20 (13), 3263. doi:10.3390/ijms20133263

Rolnik, D. L., Wright, D., Poon, L. C., O'Gorman, N., Syngelaki, A., de Paco, M. C., et al. (2017). Aspirin versus placebo in pregnancies at high risk for preterm preeclampsia. *N. Engl. J. Med.* 377 (7), 613–622. doi:10.1056/NEJMoa1704559

Sasagawa, T., Nagamatsu, T., Yanagisawa, M., Fujii, T., and Shibuya, M. (2021). Hypoxia-inducible factor-1β is essential for upregulation of the hypoxia-induced *FLT1* gene in placental trophoblasts. *Mol. Hum. Reprod.* 27 (12), gaab065. doi:10.1093/molehr/gaab065

Seidler, A. L., Askie, L., and Ray, J. G. (2018). Optimal aspirin dosing for preeclampsia prevention. *Am. J. Obstet. Gynecol.* 219 (1), 117–118. doi:10.1016/j.ajog.2018.03.018

Sheleme, T. (2021). "Clinical pharmacokinetics of metformin," in *Metformin - pharmacology and drug interactions* (IntechOpen).

Shi, J., Wang, J., Jia, N., and Sun, Q. (2023). A network pharmacology study on mechanism of resveratrol in treating preeclampsia via regulation of AGE-RAGE and HIF-1 signalling pathways. *Front. Endocrinol. (Lausanne)* 13, 1044775. doi:10.3389/fendo.2022.1044775

Sibai, B., Dekker, G., and Kupferminc, M. (2005). Pre-eclampsia. *Lancet.* 365 (9461), 785–799. doi:10.1016/S0140-6736(05)17987-2

Sim, A. S., Salonikas, C., Naidoo, D., and Wilcken, D. E. L. (2003). Improved method for plasma malondialdehyde measurement by high-performance liquid chromatography using methyl malondialdehyde as an internal standard. *J. Chromatogr. B* 785 (2), 337–344. doi:10.1016/s1570-0232(02)00956-x

Singh, A. P., Singh, R., Verma, S. S., Rai, V., Kaschula, C. H., Maiti, P., et al. (2019). Health benefits of resveratrol: evidence from clinical studies. *Med. Res. Rev.* 39 (5), 1851–1891. doi:10.1002/med.21565

Steegers, E. A., von Dadelszen, P., Duvekot, J. J., and Pijnenborg, R. (2010). Pre-eclampsia. *Lancet.* 376 (9741), 631–644. doi:10.1016/S0140-6736(10)60279-6

Sudjai, D., and Satho, P. (2022). Relationship between maternal serum uric acid level and preeclampsia with or without severe features. *J. Obstet. Gynaecol. (Lahore).* 42 (7), 2704–2708. doi:10.1080/01443615.2022.2099254

Szarka, A., Rigó, J., Lázár, L., Bekő, G., and Molvarec, A. (2010). Circulating cytokines, chemokines and adhesion molecules in normal pregnancy and preeclampsia determined by multiplex suspension array. *BMC Immunol.* 11 (1), 59. doi:10.1186/1471-2172-11-59

Todd, N., McNally, R., Alqudah, A., Jerotic, D., Suvakov, S., Obradovic, D., et al. (2021). Role of A Novel angiogenesis FKBPL-CD44 pathway in preeclampsia risk stratification and mesenchymal stem cell treatment. *J. Clin. Endocrinol. Metab.* 106 (1), 26–41. doi:10.1210/clinem/dgaa403

Tranquilli, A. L., Dekker, G., Magee, L., Roberts, J., Sibai, B. M., Steyn, W., et al. (2014). The classification, diagnosis and management of the hypertensive disorders of pregnancy: a revised statement from the ISSHP. *Pregnancy Hypertens An Int J Women's Cardiovasc Heal* 4 (2), 97–104. doi:10.1016/j.preghy.2014.02.001

Uaa, S.El D., Salem, M. M., and Abdulazim, D. O. (2017). Uric acid in the pathogenesis of metabolic, renal, and cardiovascular diseases: a review. *J. Adv. Res.* 8 (5), 537–548. doi:10.1016/j.jare.2016.11.004

Udenze, I., Cana and, C. C. M., Awolola, N., and Makwe, C. C. (2015). The role of cytokines as inflammatory mediators in preeclampsia. *Pan Afr. Med. J.* 20 (219), 219. doi:10.11604/pamj.2015.20.219.5317

Viana-Mattioli, S., Cinegaglia, N., Bertozzi-Matheus, M., Bueno-Pereira, T. O., Caldeira-Dias, M., Cavalli, R. C., et al. (2020). SIRT1-dependent effects of resveratrol and grape juice in an *in vitro* model of preeclampsia. *Biomed. Pharmacother.* 131, 110659. doi:10.1016/j.biopha.2020.110659

Wang, Z., Zibrila, A. I., Liu, S., Zhao, G., Li, Y., Xu, J., et al. (2020). Acetylcholine ameliorated TNF-α-induced primary trophoblast malfunction via muscarinic receptors. *Biol. Reprod.* 103 (6), 1238–1248. doi:10.1093/biolre/ioaa158

Weel, I. C., Baergen, R. N., Romão-Veiga, M., Borges, V. T., Ribeiro, V. R., Witkin, S. S., et al. (2016). Association between placental lesions, cytokines and angiogenic factors in pregnant women with preeclampsia. *PLoS One* 11 (6), e0157584. doi:10.1371/journal.pone.0157584

Yakkundi, A., McCallum, L., O'Kane, A., Dyer, H., Worthington, J., McKeen, H. D., et al. (2013). The anti-migratory effects of FKBPL and its peptide derivative, AD-01: regulation of CD44 and the cytoskeletal pathway. *PLoS One* 8 (2), e55075. doi:10.1371/journal.pone.0055075

Yoneyama, Y., Sawa, R., Suzuki, S., Doi, D., Yoneyama, K., Otsubo, Y., et al. (2002). Relationship between plasma malondialdehyde levels and adenosine deaminase activities in preeclampsia. *Clin. Chim. Acta* 322 (1–2), 169–173. doi:10.1016/s0009-8981(02)00175-4

Zhao, J., Chow, R. P., McLeese, R. H., Hookham, M. B., Lyons, T. J., and Yu, J. Y. (2021). Modelling preeclampsia: a comparative analysis of the common human trophoblast cell lines. *FASEB BioAdvances* 3 (1), 23–35. doi:10.1096/fba.2020-00057

Zippusch, S., Besecke, K. F. W., Helms, F., Klingenberg, M., Lyons, A., Behrens, P., et al. (2021). Chemically induced hypoxia by dimethyloxalylglycine (DMOG)-loaded nanoporous silica nanoparticles supports endothelial tube formation by sustained VEGF release from adipose tissue-derived stem cells. *Regen. Biomater.* 8 (5), rbab039. doi:10.1093/rb/rbab039

Zou, Y., Li, S., Wu, D., Xu, Y., Wang, S., Jiang, Y., et al. (2019). Resveratrol promotes trophoblast invasion in pre-eclampsia by inducing epithelial-mesenchymal transition. *J. Cell Mol. Med.* 23 (4), 2702–2710. doi:10.1111/jcmm.14175

Zou, Y., Zuo, Q., Huang, S., Yu, X., Jiang, Z., Zou, S., et al. (2014). Resveratrol inhibits trophoblast apoptosis through oxidative stress in preeclampsia-model rats. *Molecules* 19 (12), 20570–20579. doi:10.3390/molecules191220570

frontiers | Frontiers in Immunology

TYPE Original Research
PUBLISHED 02 April 2025
DOI 10.3389/fimmu.2025.1530015

OPEN ACCESS

EDITED BY
Rajni Kant,
Kaohsiung Medical University, Taiwan

REVIEWED BY
Yanwen Chen,
University of Pittsburgh, United States
Arun Paripati,
Nationwide Children's Hospital, United States
Mohammad Anas,
University of Illinois Chicago, United States

*CORRESPONDENCE
Anna Li
lan52999@126.com
Meihua Zhang
meihua2013@163.com

†These authors have contributed equally to this work

RECEIVED 18 November 2024
ACCEPTED 17 March 2025
PUBLISHED 02 April 2025

CITATION
Zhao M, Yang Z, Kang Y, Fang Z, Zhang C, Wang C, Zhou M, Guo J, Li A and Zhang M (2025) BNIP3-mediated mitophagy aggravates placental injury in preeclampsia via NLRP1 inflammasome.
Front. Immunol. 16:1530015.
doi: 10.3389/fimmu.2025.1530015

BNIP3-mediated mitophagy aggravates placental injury in preeclampsia via NLRP1 inflammasome

Man Zhao†, Zexin Yang†, Yan Kang, Zhenya Fang, Changqing Zhang, Chunying Wang, Meijuan Zhou, Junjun Guo, Anna Li* and Meihua Zhang*

Key Laboratory of Maternal & Fetal Medicine of National Health Commission of China, Shandong Provincial Maternal and Child Health Care Hospital Affiliated to Qingdao University, Jinan, China

Introduction: Preeclampsia (PE) is a hypertensive disorder of pregnancy characterized by pronounced placental oxidative stress and inflammatory damage. However, the contribution of mitophagy to inflammation-induced placental injury in PE remains unclear.

Methods: Human placenta samples were collected from 15 normal pregnant women and 15 preeclampsia pregnant women. Protein expression was analyzed by western blotting, while immunofluorescence staining was employed to localize inflammatory mediators. Mitochondrial reactive oxygen species were quantified using MitoSOX. The concentrations of pro-inflammatory cytokines were quantified using ELISA, and ultrastructural alterations were evaluated by transmission electron microscopy. To investigate molecular mechanisms in vivo, a PE mouse model was established via daily subcutaneous administration of L-NAME, followed by tail vein delivery of AAV9 carrying shRNA for targeted gene knockdown.

Results: In this study, we demonstrate that BNIP3-mediated mitophagy and NLRP1 inflammasome activation occur in an L-NAME-induced PE mouse model and human PE placenta. The results also indicate that knockdown of BNIP3 abolishes mitophagy and NLRP1 inflammasome activation in JEG3 cells in H/R condition, suggesting a positive regulatory role for the BNIP3 in controlling mitophagy and NLRP1-dependent inflammation. Furthermore, silencing BNIP3 leads to a significant reduction in mitochondrial damage and mtROS production. Treatment with MitoTEMPO after BNIP3 silencing further decreases the expression of NLRP1, while overexpression of NLRP1 nullifies the impact of BNIP3 knockdown. Additionally, knockdown of BNIP3 alleviates placental injury in the PE mouse model.

Discussion: These findings reveal a novel mechanism through which BNIP3-mediated mitophagy exacerbates H/R-induced placental injury by inducing mtROS production and activating the NLRP1 inflammasome in PE.

KEYWORDS

preeclampsia, trophoblast, mitophagy, BNIP3, NLRP1

1 Introduction

Preeclampsia (PE), characterized by hypertensive disorders during pregnancy, is a significant contributor to maternal and fetal morbidity and mortality, affecting around 5% to 7% of all pregnant women globally each year (1). Formally defined as the new onset of hypertension accompanied by new-onset proteinuria, PE is often accompanied by other clinical symptoms such as pulmonary edema, liver injury, thrombocytopenia, renal insufficiency, brain dysfunction or visual disturbances (2). Due to the limited understanding of the etiology of PE, there is a scarcity of effective preventive and treatment strategies (3). At the forefront of the maternal-fetal interface, placental insufficiency caused by inadequate remodeling of the maternal vasculature perfusing the intervillous space plays a pivotal role in the development of this syndrome (4). Furthermore, oxidative stress injury in trophoblasts plays a significant role in placental physiology and trophoblast dysfunction (5, 6). Oxidative damage resulting from placental ischemia and hypoxia triggers inflammation and apoptosis (6, 7). Inflammasomes serve as the primary source of inflammatory cytokine release. Nod-like receptor (NLR) family member pyrin domain containing 1 (NLRP1) is an intracellular multimeric protein complex that initiates inflammatory responses through its association with Caspase-1 and ASC (apoptosis-associated speck-like protein containing a CARD) (8).

The NLRP1 inflammasome is an intracellular multimeric protein complex that initiates inflammatory responses and cell death, including pyroptosis and apoptosis, by activating its effector Caspase-1 (9). Numerous studies have demonstrated an upregulation of NLRP1 and Caspase-1 in the placenta of preeclampsia, suggesting that the NLRP1 inflammasome mediates inflammatory responses and contributes to placental injury in preeclampsia (10–12).

Recent studies have demonstrated that mitochondria play a pivotal role in the activation of inflammasomes (13–15). As the primary site of ROS production, mitochondrial homeostasis is intricately linked to inflammasome activation. Mitophagy, a form of selective autophagy, functions to eliminate damaged mitochondria, thus preventing the excessive accumulation of dysfunctional mitochondria, reducing excess ROS, and maintaining normal cellular function.

Mitophagy primarily operates through two mechanisms: the canonical PINK1-PARKIN pathway, which does not involve receptors, and the non-canonical pathway mediated by receptors (16). Under hypoxic conditions, the process is mainly regulated by the interaction between BCL-2 and adenovirus E1B 19-kDa-interacting protein 3 (BNIP3) or its homolog, BNIP3-like (BNIP3L), which directly bind to LC3B to facilitate mitophagy. Notably, BNIP3 has been identified as a crucial component in this process, with HIF-1α serving as an upstream regulator of BNIP3 (17).

Our previous research has demonstrated that excessive BNIP3-mediated mitophagy can induce apoptosis of trophoblasts in the placenta in cases of preeclampsia (PE) (18). While studies have suggested a connection between mitophagy and inflammation triggered by the NLRP3 inflammasome (13), the impact of BNIP3-driven mitophagy on the activation of the NLRP1 inflammasome remains unclear. Therefore, this study aims to clarify the role of BNIP3 in mitophagy and its influence on the activation of the NLRP1 inflammasome in PE.

2 Materials and methods

2.1 Participants and samples

The study was approved by the Ethical Committee of Shandong Provincial Maternal and Child Health Care Hospital, Affiliated to Qingdao University. Placental tissue samples were collected from 15 pregnant women treated at the hospital between January 2022 and March 2024, all of whom provided informed consent. The definition of preeclampsia (PE) followed guidelines established by the American College of Obstetricians and Gynecologists. In summary, patients exhibited systolic blood pressure exceeding 160 mmHg or diastolic blood pressure exceeding 110 mmHg on at least two occasions, along with significant proteinuria (>2 g per 24 hours or R3+ on dipstick testing in two random urine samples collected at intervals of >4 hours), occurring after 20 weeks of gestation, with no preexisting or chronic hypertension. The sample utilized in this study consists of patients with early-onset PE, defined as the onset of clinical signs occurring before the 34th week (40). Women in the normotensive, normal pregnancy group experienced no complications during pregnancy and delivered healthy neonates at term. The exclusion criteria for the study included transient hypertension during pregnancy, multiple pregnancies, intrauterine fetal death, pregnancies resulting from fertility treatment, fetal chromosomal or congenital abnormalities, gestational diabetes, cardiovascular and immune diseases, and renal disease. Each placental sample was collected within one hour of cesarean section and either snap-frozen in liquid nitrogen for further use or fixed in paraformaldehyde for subsequent paraffin embedding. The clinical characteristics of the enrolled pregnant women are presented in Supporting Information (Supplementary Table S1).

2.2 Cell culture and treatment

The JEG-3 human choriocarcinoma cell line was obtained from the American Type Culture Collection. These cells were cultured in Dulbecco's Modified Eagle's Medium (DMEM) (Hyclone), supplemented with 10% fetal bovine serum (FBS) (GIBCO, New Zealand) and 1% penicillin-streptomycin (Solarbio, China). The cells were maintained in a 5% CO2 incubator at 37°C. Lentiviruses packaging BNIP3 short hairpin RNAs (shRNAs) were synthesized by Shanghai GenePharma Co., Ltd. (Shanghai, China), with the specific shRNA sequence being 5'-GCTAAACCTGAAGAGTGATAT-3'.

2.3 Immunoblotting

Total proteins were extracted from the cultured cells or placental tissues using radioimmunoprecipitation assay (RIPA)

lysis buffer and quantified with a BCA kit (Solarbio, Beijing, China). Forty micrograms (40 μg) of protein from each sample were separated by sodium dodecyl sulfate-polyacrylamide gel electrophoresis (SDS-PAGE) and subsequently electrotransferred onto polyvinylidene fluoride (PVDF) membranes (Millipore, Buckinghamshire, UK). The membranes were incubated with the specified antibodies, followed by horseradish peroxidase (HRP)-conjugated secondary antibodies. An enhanced chemiluminescence detection kit (Amersham LifeScience, Buckinghamshire, United Kingdom) was employed to visualize the protein bands. The expression of target proteins was quantified by normalization to β-actin levels.

The following antibodies were purchased: LC3A/B(12741) from Cell Signaling Technology (USA), HIF-1 alpha (340462), BNIP3 (381756), IL1-bata (516288), TOMM20(R25952), Cleaved-Caspase1(341030) from ZEN-BIOSCIENCE(China), NLRP1 (A16212) from Abclonal (China) β-Actin (6600901) from Proteintech (China), and horseradish peroxidase-labeled goat-anti-mouse immunoglobulin G (GB23301) and horseradish peroxidase-labeled goat-anti-rabbit immunoglobulin G (GB23303) from Servicebio (China).

2.4 Immunofluorescence

Paraffin-embedded tissue sections were deparaffinized and rehydrated, followed by antigen retrieval using 0.1% Triton X-100 and sodium citrate. After blocking with 5% goat serum, the slides were incubated with primary antibodies overnight at 4°C in the dark. The primary antibodies used were BNIP3(381756), IL1-bata (516288) (ZEN-BIOSCIENCE, Chengdu, China); IL-18(10663-1-Ap); IL-6 (DF6087, affinity, China); CK7(AB9021, Abcam, USA). Subsequently, the slides were washed and then incubated with a fluorescein-coupled secondary antibody mixture in the dark for 60 minutes at room temperature (1:300 dilution for 1 hour). Nuclei were labeled with DAPI for 10 minutes. The sections were then washed in 1X PBS (3 x 10 minutes), dehydrated in ascending concentrations of ethanol, and sealed with an antifade mounting medium. Visualization was performed using a fluorescence microscope (Olympus, Tokyo, Japan).

2.5 Analysis of mitochondrial reactive oxygen species

MitoSOX™ Red Mitochondrial Superoxide Indicator (M36008, Invitrogen) was utilized for the detection of mitochondrial ROS production. Cells were seeded in 96-well plates and then incubated with MitoSOX (5 μM) and Hoechst (5 μl/ml, MedChemExpress, HY-15631) for 1 hour at 37°C, as previously described. Positive staining was observed and the fluorescence intensity was analyzed using the ImageXpress® Micro Confocal System (Molecular Devices, USA).

2.6 Transmission electron microscopy

The fresh placenta was dissected into 1 mm^3 pieces and then immersed in 2.5% glutaraldehyde for fixation, followed by postfixation with 1% OsO4 for 2 hours. Subsequent steps including dehydration, embedding, polymerization, and lead citrate staining were carried out by a professional service provider (Servicebio, Wuhan, China), following established protocols (18). The embedded samples were sectioned into slices of 60–80 nm thickness and examined using a Hitachi H-7650 transmission electron microscope.

2.7 Staining of the mitochondria

Mitochondria, lysosomes, and nuclei were labeled with 50 nM Mito-Tracker Green (Beyotime, C1048), 50 nM Lyso-Tracker Red (Beyotime, C1049), and 5 μg/mL Hoechst (Beyotime, C1027), respectively, following the manufacturer's instructions. The images were captured using the Confocal Microscopy (Nikon AX, Japan).

2.8 Establishment of preeclampsia mouse model

A preeclamptic mouse model was created using a modified method as previously described. This involved 10-week-old ICR mice, both male and female, obtained from Shandong University's Laboratory Animal Center. The mice were housed in a controlled environment with a 12-hour light/dark cycle at temperatures ranging from 18°C to 22°C, and provided ad libitum access to food and water. Mating was initiated by pairing female mice with male mice at a ratio of 2:1, with the presence of a mating plug designated as gestation day (GD) 0.5.

The mice were divided into two cohorts. In the first cohort consisted of two groups, pregnant mice were randomly allocated into two distinct groups: a control group (Con, n = 6) which was administered 100ul saline solution via subcutaneous injections from GD 9.5 to GD 18.5; an L-NAME group (n = 6) which was administered L-NAME via subcutaneous injections at a dose of 125 mg/kg/day from GD 9.5 to GD 18.5. The relevant data was presented in Supplementary Figure S1.

In second cohort, pregnant mice were randomly allocated into four distinct groups: a control group (Con, n = 6) which was injected with 100 μL of the corresponding vector control (AAV9-GFP-vector, n=6) in the tail vein; a BNIP3 knockdown group (sh-BNIP3, n = 6) which was injected with 100 μL of knockdown BNIP3 type 9 adeno-associated virus (AAV9-GFP-sh-BNIP3; synthesized by WZbio); an L-NAME group (L-NAME-Con, n = 6) which was treated with L-NAME and AAV9-GFP-vector; an L-NAME plus BNIP3 knockdown group (L-NAME-sh-BNIP3, n = 6) which was treated with L-NAME and AAV9-GFP-sh-BNIP3. The control

groups underwent injections of a saline solution in volumes that were equivalent to those administered to the experimental groups, and these injections were administered via the identical routes and during the corresponding timeframes, ensuring a rigorous and balanced comparison. The maternal systolic and diastolic blood pressures were meticulously recorded on GD 14.5 and 17.5 utilizing tail-cuff plethysmography in conjunction with the advanced BP-2010A Blood Pressure Analysis System. Subsequently, on GD 17.5, comprehensive 24-hour urine samples were gathered for the quantification of protein levels, employing the precise BCA assay. The outcomes of these assessments are visually presented in Supplementary Figure S2 for detailed analysis. Upon completion of the study period, specifically on GD 18.5, the mice were humanely euthanized through cervical dislocation, adhering to the highest ethical standards. Following this, vital data including placental weights, the total number of fetuses, and individual fetal weights were meticulously compiled and documented. The procured placental tissues were then carefully preserved for subsequent scientific investigations; some were stored at -80°C for molecular and biochemical analyses, while others were fixed in 4% paraformaldehyde for histological and immunohistochemical studies. The protocol for these animal experiments received approval from the Ethical Committee of the Maternal and Child Health Care Hospital of Shandong Province, associated with Qingdao University.

2.9 Enzyme-linked immunosorbent assay

The concentration of the pro-inflammatory cytokine IL-1β within the cell culture supernatant was quantitatively assessed employing the Human IL-1β Enzyme-Linked Immunosorbent Assay (ELISA) Kit (EK0392, BOSTER, China), adhering strictly to the manufacturer's recommended protocol. Similarly, for the evaluation of IL-6 levels, the IL-6 ELISA Kit (EK0411, BOSTER, China) was utilized following the same rigorous methodological guidelines.

2.10 Statistical analysis

Statistical evaluations were conducted utilizing the latest GraphPad Prism software, version 9.0, from GraphPad Software in La Jolla, California. For qualitative datasets, including immunoblots and photographic imagery, a minimum of three independent experimental replications were analyzed and presented as mean values, accompanied by the standard deviation of the mean (SD), to ensure reliability and precision. To discern significant differences between two groups, the Student's t-test was strategically employed. When assessing variations among three or more groups, a comprehensive approach involving one-way ANOVA was utilized, followed by Tukey's multiple comparisons test. A statistically significant difference was defined as the follows: *p<0.05, **p<0.01, ***p<0.001, **** p<0.0001.

3 Results

3.1 BNIP3-mediated mitophagy and NLRP1 inflammasome were induced on the placenta of PE

Our previous research has shown that excessive activation of mitophagy plays a significant role in causing placental damage in preeclampsia (PE). In order to further investigate the relationship between mitophagy and inflammation, we established a PE-like mouse model through L-NAME injection. Compared to the control group, the expression of HIF-1α, BNIP3, and the ratio of LC3II to LC3I was significantly increased, while the expression of TOMM20 was decreased in the PE-like mouse model (Figures 1A, B). The protein levels of NLRP1, Cleaved-Caspase-1, and IL-1β are indicative of NLRP1 inflammasome activation. Western blot analysis revealed a notable increase in the expression of NLRP1, Cleaved-Caspase-1, and IL-1β in the L-NAME group (Figures 1C, D). Additionally, electron microscopy showed mitochondrial ultrastructural changes with swollen mitochondria and cracked cristae accompanied by autophagosome formation in the L-NAME group (Figure 1E). Immunofluorescence staining of placental tissue demonstrated an upregulation in proinflammatory cytokines such as IL-1β, IL-6 and IL-18 in the PE-like group (Figures 1F-H). These findings indicate that both mitophagy and NLRP1 inflammation are activated within the placenta of PE mice.

To validate these findings, we analyzed placenta samples from normal pregnant women (NP) and women with PE. Consistent with the mouse model, the expression of HIF-1α, BNIP3, and the ratio of LC3II to LC3I were significantly increased in PE placentas compared to NP samples, while the expression of TOMM20 was decreased (Figures 2A, B). Similarly, immunofluorescence analysis revealed elevated BNIP3 expression in trophoblasts through costaining of BNIP3 and CK7 in PE placentas (Figure 2C). The heightened expression of NLRP1, Cleaved-Caspase-1, and IL-1β correlated with NLRP1 inflammasome activation as shown by western blot analysis (Figures 2A, B). Furthermore, immunofluorescence analysis demonstrated increased levels of IL-1β, IL-6 and IL-18 to assess proinflammatory cytokine expression in PE placentas (Figures 2D-F). These results confirm that mitophagy is activated in PE placentas *in vivo* along with NLRP1 inflammation activation.

3.2 Hypoxia-induced activation of BNIP3-mediated mitophagy and NLRP1 inflammasome in trophoblast cells

Following this, JEG3 cells were subjected to H/R conditions *in vitro* to simulate the hypoxic environment in PE placenta. In order to investigate the activation of BNIP3-dependent mitophagy induced by hypoxia, JEG3 cells were cultured under H/R conditions. Western blot analysis revealed that H/R treatment led

10.3389/fimmu.2025.1530015

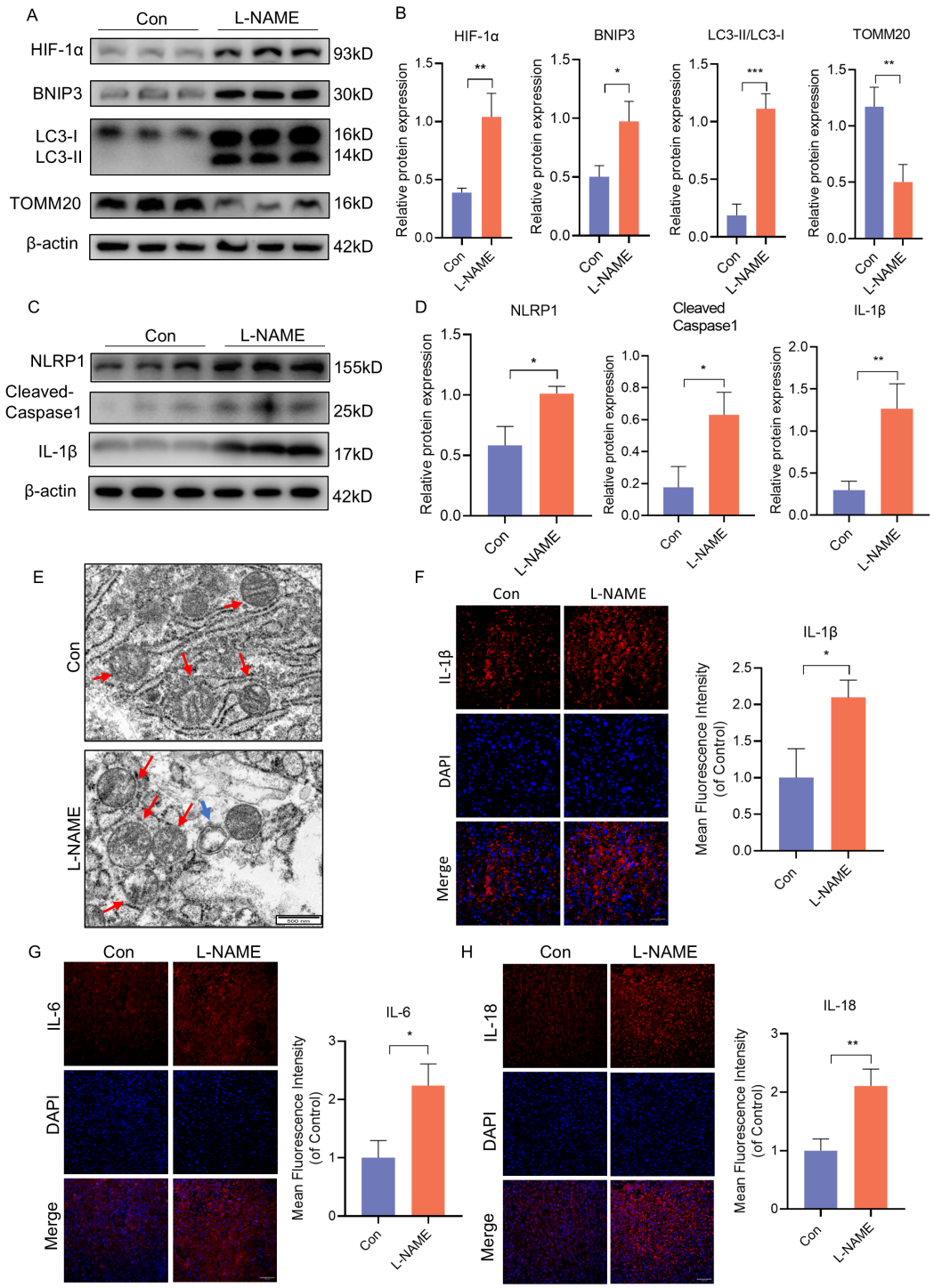

FIGURE 1
BNIP3 mediated mitophagy and NLRP1 inflammasome were activated in PE-like mice. ICR mice were injected with L-NAME or vehicle. **(A, B)** Results of WB and quantification showing the expression of HIF-1α, BNIP3, the ratio of LC3II/LC3Iand TOMM20 that in the placenta of PE-like mice. **(C, D)** Results and quantification of WB showing the expression of NLRP1, Cleaved-Caspase1 and IL-1β that in the placenta of PE-like mice. **(E)** Representative images of placenta in different groups by transmission electron microscopy. The red arrow indicated mitochondria, the blue triangle indicated autophagosome. Scale bar: 500nm. **(F-H)** Representative images of immunofluorescence labelling IL-1β, IL-6 and IL-18 in placenta of Con and L-NAME groups. The data are shown as mean ± SD and analyzed by Student's t-test based on at least three independent experiments. *p < 0.05, **p < 0.01, ***p < 0.001.

10.3389/fimmu.2025.1530015

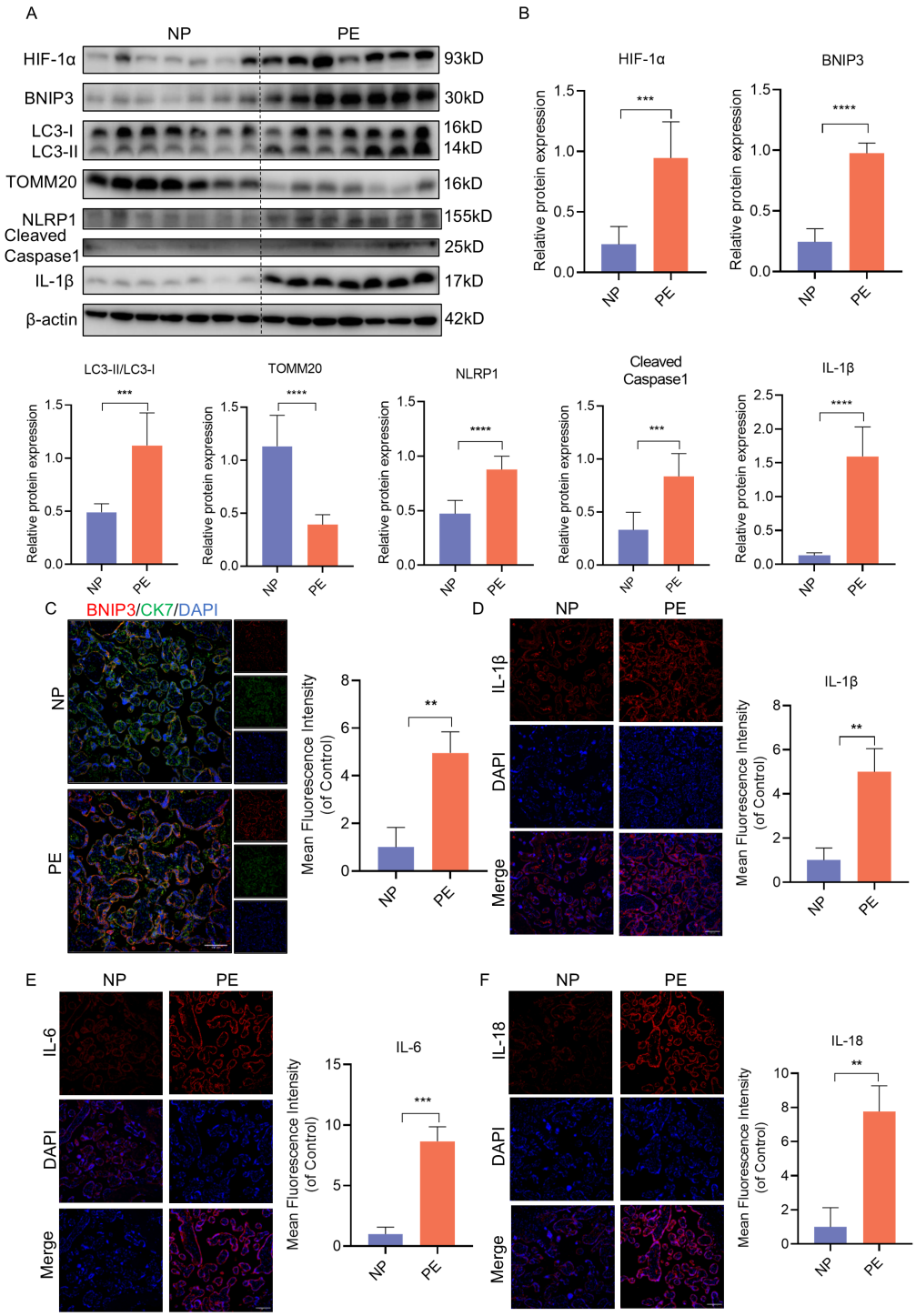

FIGURE 2
HIF-1α-BNIP3-dependent mitophagy and activation of the NLRP1 inflammasome were associated with PE. **(A, B)** WB analysis and quantification showing the expression of HIF-1α, BNIP3, the ratio of LC3II/LC3I, TOMM20, NLRP1, Cleaved-caspase1, IL-1β that in the villi of healthy pregnant women and pregnant women with PE. **(C)** Representative images of immunofluorescence double-labelling CK-7 and BNIP3 of mice in Con and L-NAME group. **(D–F)** Representative images of immunofluorescence labelling IL-1β, IL-6 and IL-18 in placenta of Con and L-NAME groups. The data are shown as mean ± SD and analyzed by Student's t-test based on at least three independent experiments. **p < 0.01, ***p < 0.001, ****p < 0.0001.

to a decrease in TOMM20 expression and an increase in HIF-1α and BNIP3 expression, as well as an elevation in the ratio of LC3II/LC3I within the group (Figures 3A, B). Additionally, Mito-Tracker and Lyso-Tracker were used to label mitochondria and lysosomes respectively. It was observed that JEG3 cells treated with H/R exhibited a significant increase in co-localization of Mito-Tracker Green and Lyso-Tracker Red, indicating a notable enhancement in mitophagy following H/R treatment (Figure 3C). Subsequently,

10.3389/fimmu.2025.1530015

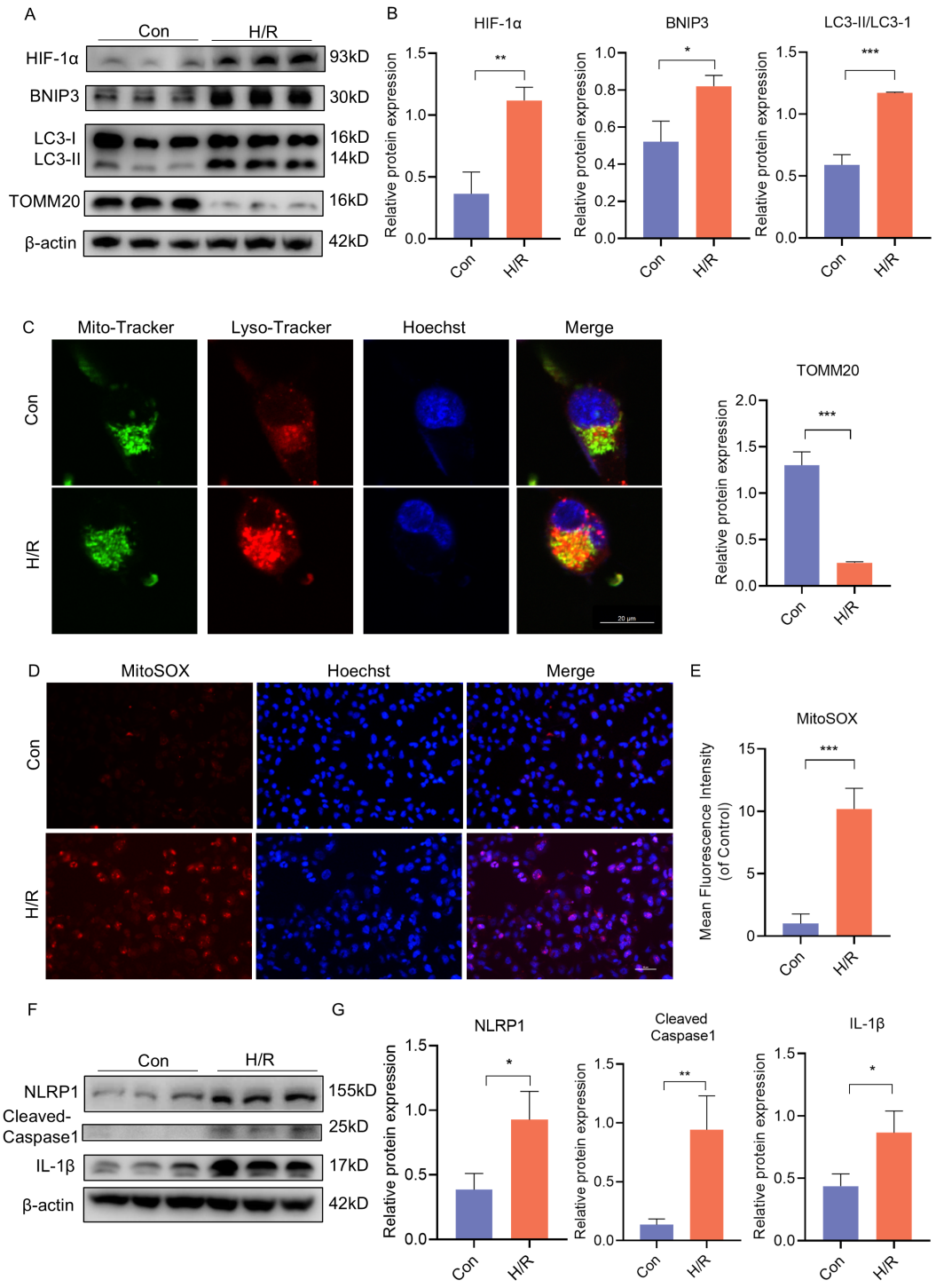

FIGURE 3
H/R activated BNIP3-mediated mitophagy, the ROS production and the NLRP1 inflammasome in JEG3 cells. JEG3 was used with a hypoxia and reoxygenation (H/R) stimulus to mimic PE-like injury *in vitro*. **(A, B)** Western blotting and corresponding semiquantification were performed to analyze the expression of HIF-1α, BNIP3, the ratio of LC3II/LC3I, TOMM20 in JEG3 cells treated in H/R condition. **(C)** Representative images of fluorescence double labelling mitochondrial (Mito-Tracker) and lysosome (Lyso-Tracker) marker. Scale bar: 20 μm. **(D, E)** MitoSOX was used to detect the mitochondrial ROS and analyzed by confocal microscopy (n = 3). Scale bar, 50 μm. **(F, G)** Western blotting and corresponding semiquantification were performed to analyze the expression of NLRP1, Cleaved-Caspase1 and IL-1β in JEG3 cells treated in H/R condition. The data are shown as mean ± SD and analyzed by Student's t-test based on at least three independent experiments. *p < 0.05, **p < 0.01, ***p < 0.001.

mitochondrial function was assessed by quantifying mitochondrial ROS (mtROS) production using MitoSOX, a fluorogenic dye specifically targeting mitochondria for measuring their superoxide anion generation. Analysis of fluorescence intensity demonstrated significantly higher mtROS generation in the H/R group compared to the control (Figures 3D, E). Furthermore, H/R-treated JEG3 cells also resulted in activation of the NLRP1 pathway as evidenced by elevated protein expression of NLRP1, Cleaved-Caspase1, and IL-1β (Figures 3F, G). These findings indicate that not only mitophagy but also NLRP1-mediated inflammation was activated in response to H/R treatment.

3.3 BNIP3 deficiency reduced mitophagy, mitochondrial ROS production, and the induction of NLRP1 inflammasome activation in H/R-induced trophoblasts

To further elucidate the impact of BNIP3 on H/R injury, our focus was on mitophagy. We utilized shRNA to knock down BNIP3 in JEG3 cells and investigate its role in H/R-induced JEG3 cells. After silencing the BNIP3 gene, JEG3 cells were exposed to hypoxia for 24 hours. The successful inhibition of BNIP3 expression by shRNA transfection was confirmed through immunoblot analysis. Western blot analysis showed a significant decrease in BNIP3 protein expression levels in the sh-BNIP3 and sh-BNIP3+H/R groups (Figures 4A, B). Furthermore, colocalization of Mito-Tracker and Lyso-Tracker demonstrated a reduction in mitophagosome formation after BNIP3 knockdown (Figure 4C). Interestingly, H/R injury led to excessive ROS production in JEG3 cells as evidenced by MitoSOX staining; however, this effect was reduced upon BNIP3 knockdown (Figures 4D, E). These findings suggest that under H/R conditions, BNIP3-mediated mitophagy and mitochondrial ROS production are activated but suppressed when BNIP3 is silenced.

In order to explore the influence of BNIP3 and mtROS on NLRP1 inflammasome activation, we treated the cells with Mito-Tempo (MT) alongside intervention targeting BNIP3. Both interventions resulted in decreased NLRP1, Cleaved-Caspase1, and IL-1β expression (Figures 4F, G), indicating that both BNlP3-mediated mitophagy and mtROS play a role in regulating NLRP1 inflammasome activation.

3.4 Activation of the NLRP1 inflammasome partially attenuates the protective effect of BNIP3 silencing against hypoxia injury in JEG3 cells

To further investigate the relationship between BNIP3-mediated mitophagy and the NLRP1 inflammasome, JEG3 cells were treated with MDP (NLRP1 targeted activator) after BNIP3 knockdown to induce NLRP1 inflammasome activation prior to exposure to H/R conditions (Figures 5A, B). The reduction in NLRP1 inflammasome activation observed with BNIP3 silencing was reversed by MDP treatment, as demonstrated by Western blot analysis. To validate the regulatory role of BNIP3 in NLRP1 inflammasome activation, NLRP1 was overexpressed using a plasmid. Consistent with MDP treatment, the overexpression of NLRP1 counteracted the inhibitory effect of BNIP3 on NLRP1 inflammasome activation (Figures 5C, D). Additionally, ELISA assays were used to analyze and compare the levels of IL-1β and IL-6 in the cell supernatant among the four groups, confirming a decrease in inflammatory factors in the sh-BNIP3 group. Furthermore, overexpression of NLRP1 nullified the impact of BNIP3 knockdown (Figure 5E). These findings suggest that BNIP3-mediated mitophagy induces NLRP1 inflammasome activation.

3.5 Deficiency of BNIP3 resulted in decreased mitophagy, reduced activation of the NLRP1 inflammasome, and dysfunction of the placenta with PE

The knockdown of BNIP3 using AAV9-sh-BNIP3 adeno-associated virus in a PE-like mouse model was employed to validate our hypothesis regarding the role of increased BNIP3 levels and its contribution to PE. We observed that the weight of placentas and fetuses in the L-NAME group was significantly lower than that in the control group (Figures 6A-C). Conversely, downregulation of BNIP3 reversed this trend, leading to a rebound in the weight of placentas and fetuses in the L-NAME +AAV9-sh-BNIP3 group. Furthermore, transmission electron microscopy (TEM) images revealed an improvement in mitochondrial ultrastructure as a result of BNIP3 downregulation. The stage of mitophagy, specifically mitophagosome formation, was identified in the placenta of the L-NAME group (Figure 6D). To confirm the inhibitory effect of AAV9-sh-BNIP3, we analyzed BNIP3 levels in the placentas from four groups of pregnant mice (Figures 6E, F). Our findings demonstrated a significantly lower expression of BNIP3 in the AAV9-sh-BNIP3 groups compared to the AAV9-vector groups. Western blot analysis also revealed an increase in TOMM20 expression in the L-NAME+AAV-sh-BNIP3 group compared to the L-NAME group. Additionally, the ratio of LC3II to LC3I was significantly reduced in the L-NAME+AAV-sh-BNIP3 placenta (Figures 6E, F). We assessed the levels of NLRP1, Cleaved-Caspase-1, and IL-1β in the placentas of these four groups. The results indicated that knockdown BNIP3 with AAV9-sh-BNIP3 counteracted the inductive effect of L-NAME on NLRP1 inflammasome activation. Furthermore, immunofluorescence analysis of IL-1β and CK7 was performed to assess proinflammatory cytokine expression in trophoblasts, which were decreased in AAV9-sh-BNIP3+L-NAME placentas (Figure 6G). These observations were consistent with findings from JEG3 cells, inhibiting mitophagy by downregulating BNIP3 expression ultimately improved placental function by relieving NLRP1-inflammasome activation in PE. An integrative schematic model delineating the hypothesized signaling pathways was constructed based on our findings (Figure 7).

10.3389/fimmu.2025.1530015

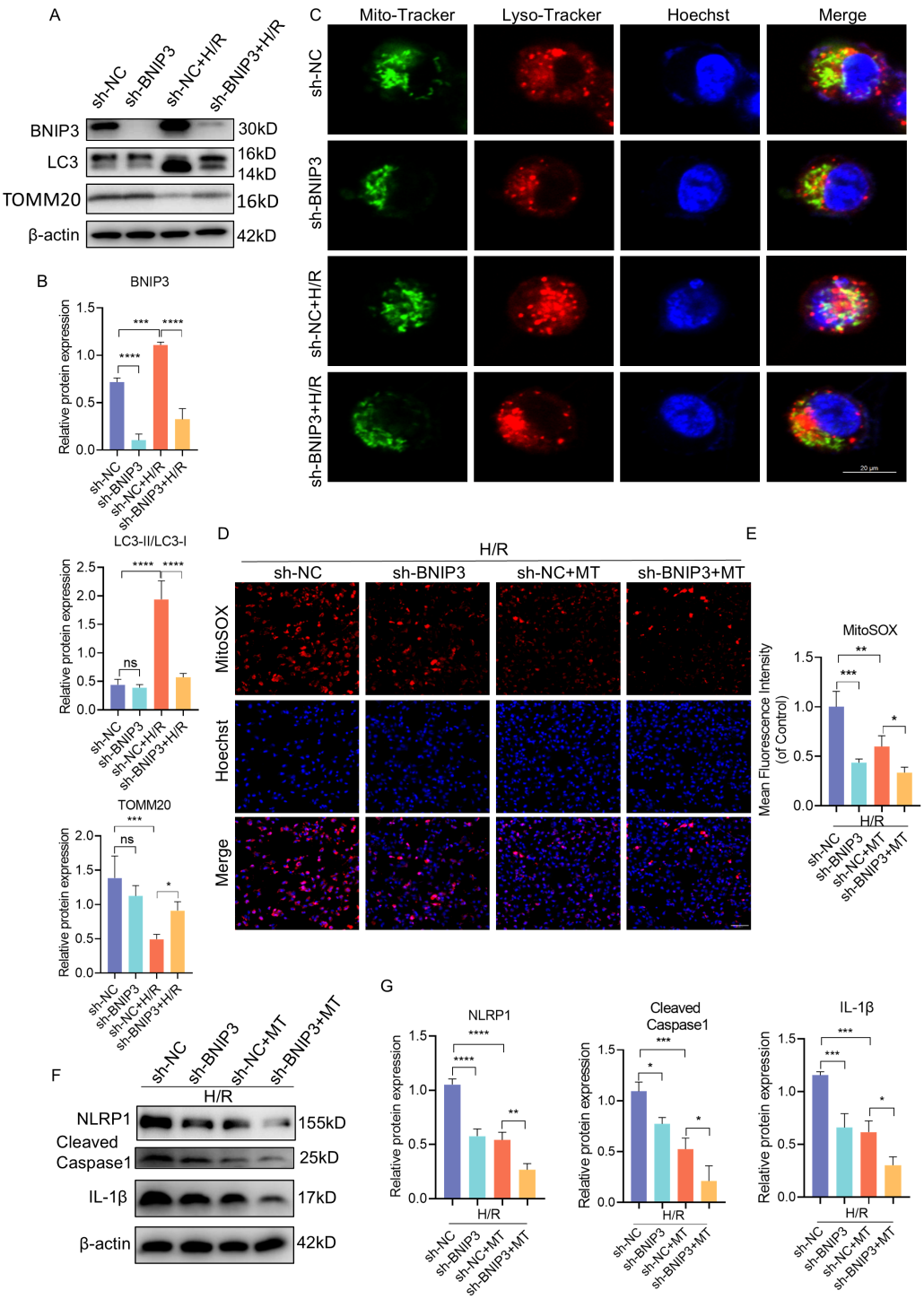

FIGURE 4
BNIP3 silencing alleviated mitophagy, ROS production and NLRP1 inflammasome activation. ShRNA against BNIP3 and sh-NC were transfected into JEG3 cells. **(A, B)** The alteration of BNIP3, LC3II/LC3Iand TOMM20 was detected by Western blotting. **(C)** Representative images of immunofluorescence double labelling mitochondrial (Mito-Tracker) and lysosome (Lyso-Tracker) marker. Scale bar: 20 μm. **(D, E)** MitoSOX was used to detect the mitochondrial ROS and analyzed by confocal microscopy (n = 3). Scale bar, 100 μm. **(F, G)** Western blotting and corresponding semiquantification were performed to analyze the expression of NLRP1, Cleaved-Caspase1 and IL-1β. The data are shown as mean ± SD and analyzed by one-way ANOVA test followed by Tukey–Kramer multiple comparison test based on at least three independent experiments. *p < 0.05, **p < 0.01, ***p < 0.001, ****p < 0.0001. ns: not significant.

10.3389/fimmu.2025.1530015

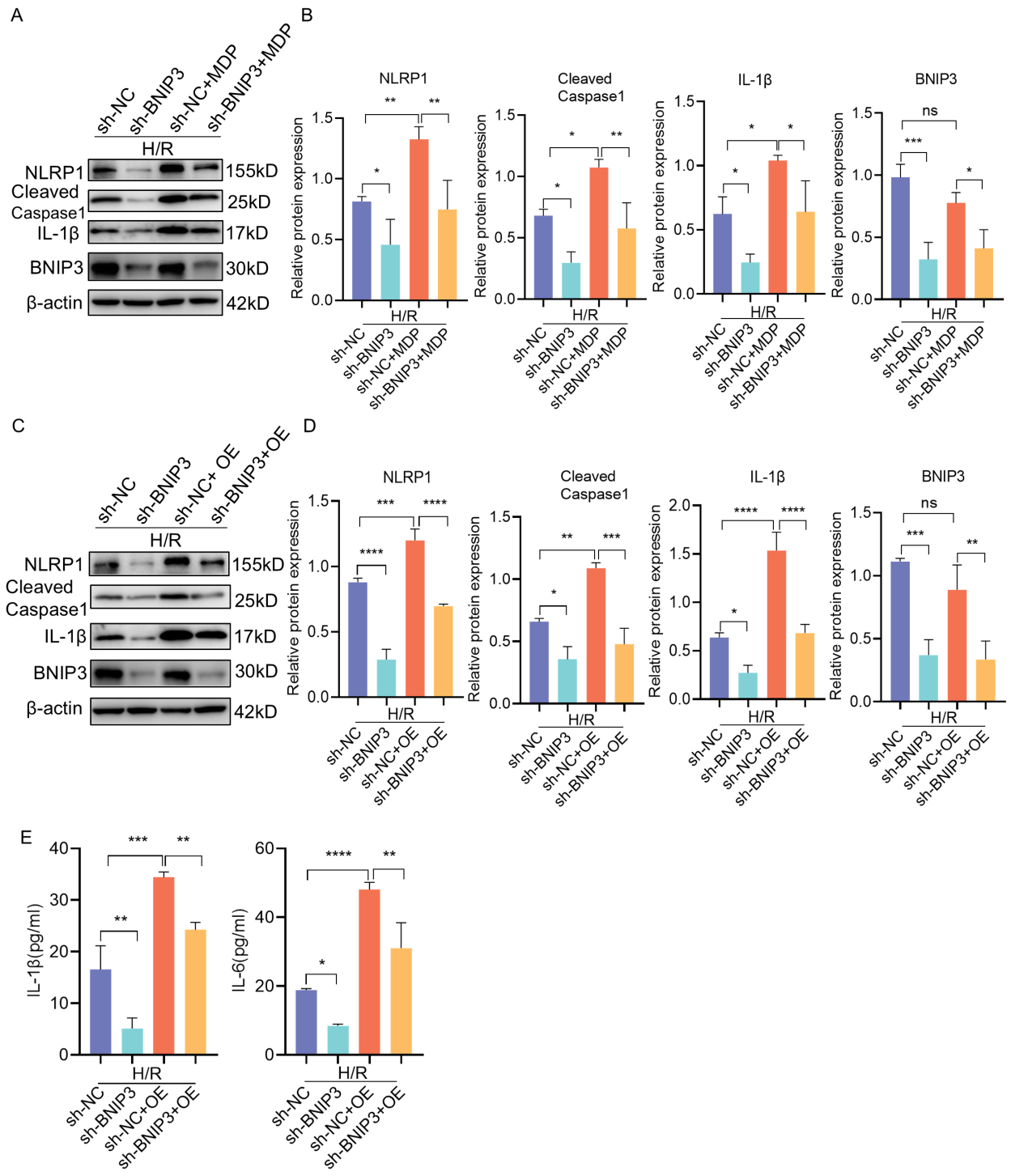

FIGURE 5
BNIP3 mediated NLRP1 inflammasome activation induced by H/R. **(A, B)** JEG3 cells knockdown BNIP3 were treated with MDP (NLRP1 targeted activator), Western blotting and corresponding semiquantification were performed to analyze the expression of NLRP1, Cleaved-Caspase1, IL-1β and BNIP3. **(C, D)** JEG3 cells were transfected with both shRNA targeted BNIP3 and NLRP1 overexpression plasmid. Western blotting and corresponding semiquantification were performed to analyze the expression of NLRP1, Cleaved-Caspase1, IL-1β and BNIP3. **(E)** ELISA assay was used to detected the IL-1β and IL-6 expression in supernant of cell in the four groups. The data are shown as mean ± SD and analyzed by one-way ANOVA test followed by Tukey–Kramer multiple comparison test based on at least three independent experiments. *p < 0.05, **p < 0.01, ***p < 0.001, ****p < 0.0001. ns: not significant.

10.3389/fimmu.2025.1530015

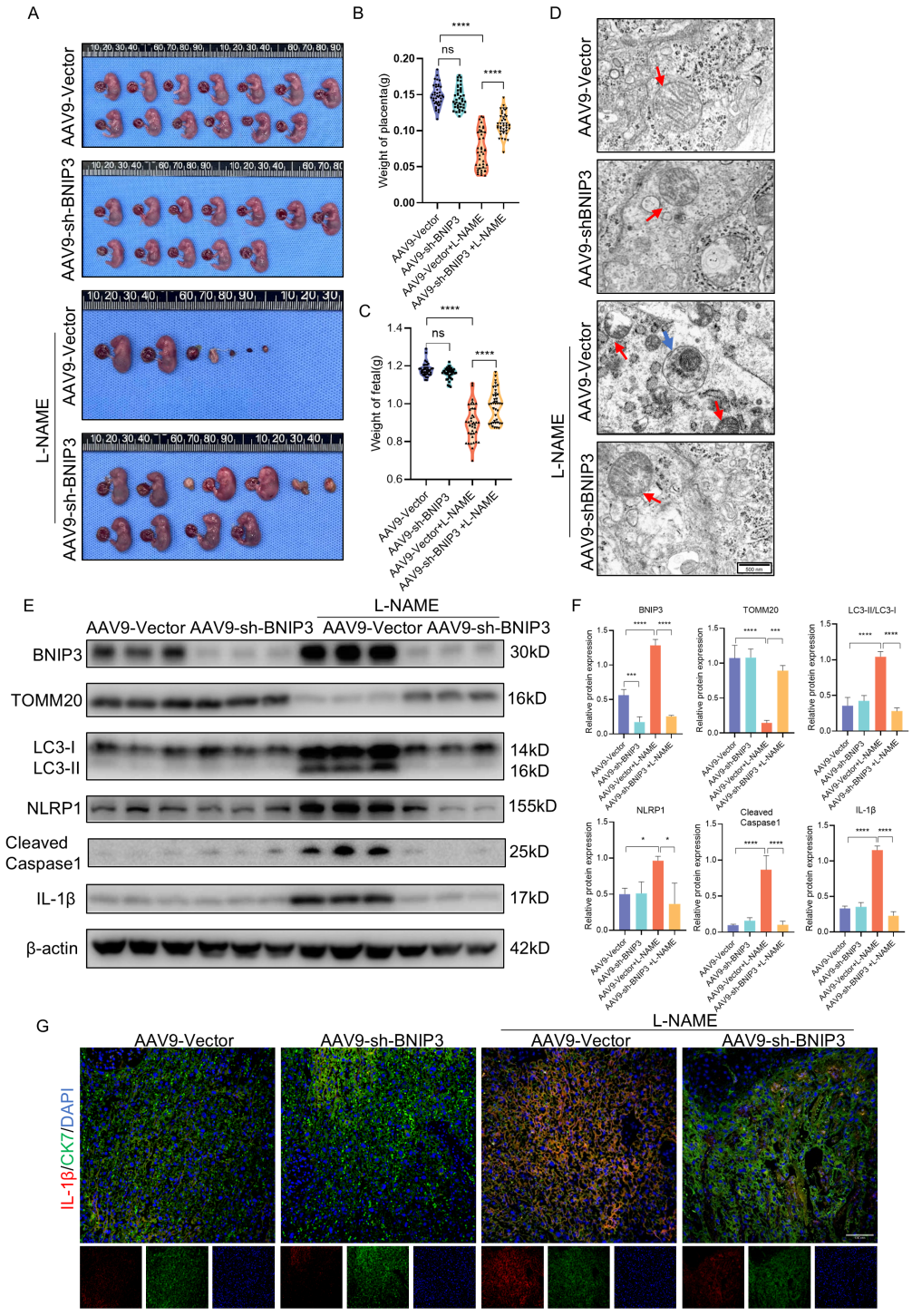

FIGURE 6
BNIP3 deficiency blocked NLRP1 inflammasome activation and mitigated placental injury of PE. **(A-C)** Representative images of the gestational day (GD)18.5 fetuses of the AAV9-Vector group (n = 6) and AAV9-shBNIP3 group (n = 6), L-NAME+ AAV9-Vector group (n = 6) and L-NAME+AAV9-shBNIP3 group (n = 6), and statistics of weight of placentas and fetuses. **(D)** Representative images of placenta in different groups by transmission electron microscopy. **(E, F)** Western blotting and corresponding semiquantification were performed to analyze the expression of BNIP3, TOMM20, the ratio of LC3II/LC3I, NLRP1, Cleaved-Caspase1 and IL-1β. **(G)** Representative images of immunofluorescence labelling IL-1β and CK7 in placentas of different groups. The data are shown as mean ± SD and analyzed by one-way ANOVA test followed by Tukey–Kramer multiple comparison test based on at least three independent experiments. *p < 0.05, ***p < 0.001, ****p < 0.0001. ns: not significant.

10.3389/fimmu.2025.1530015

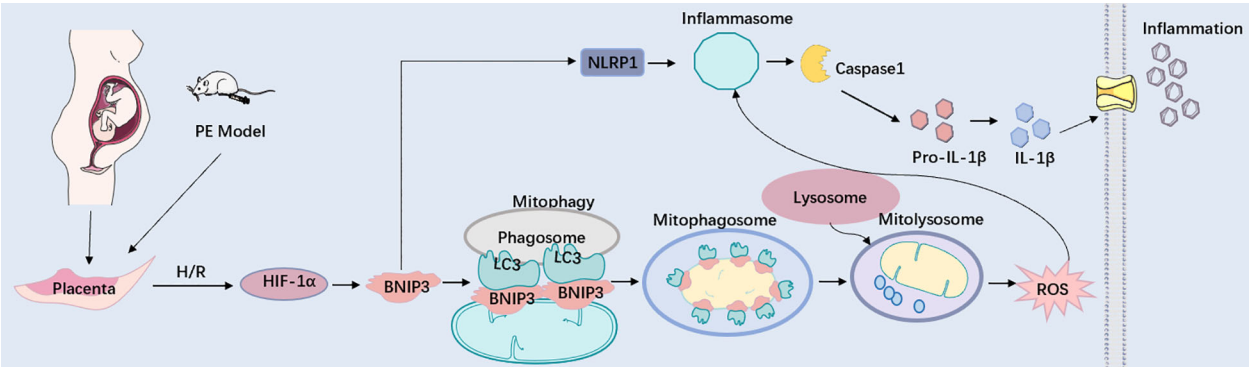

FIGURE 7
BNIP3 upregulation in trophoblasts aggravates placental injury of PE via activating mitophagy and NLRP1-inflammasome. Working model depicting the BNIP3-mediated mitophagy and NLRP1-associated inflammation in trophoblasts during PE. Under pathologically H/R conditions that mimic PE, BNIP3 is activated, subsequently enhancing downstream mitophagy and ROS production. Moreover, BNIP3 promotes the activation of NLRP1, resulting in an increased release of inflammatory mediators and exacerbating placental damage associated with PE both *in vivo* and *in vitro*. Under pathologically H/R conditions that replicate PE, BNIP3 is activated, which subsequently enhances downstream mitophagy and ROS production. Furthermore, BNIP3 facilitates the activation of NLRP1, leading to an increased release of Inflammatory factors and aggravating placental damage of PE *in vivo* and *in vitro*.

4 Discussion

The present study demonstrates the significance of the HIF-1α-BNIP3 pathway in activating the NLRP1 inflammasome under hypoxic conditions, particularly in relation to placental damage caused by hypoxia. Our findings indicate that HIF-1α and BNIP3, as well as its mediated mitophagy, are upregulated in the placentas of pregnant women with preeclampsia (PE), as well as in a PE-like mouse model. Consistent with these results, BNIP3-mediated mitophagy is activated in trophoblasts under hypoxia/reoxygenation (H/R) conditions *in vitro*. Furthermore, we observed activation of the NLRP1 inflammasome pathway and an increase in mitochondrial reactive oxygen species (mtROS) production under these conditions. Additionally, our study reveals that deficiency of BNIP3 rescues both mitophagy activation and NLRP1 inflammasome activation induced by hypoxia both *in vitro* and *in vivo*. These findings provide further evidence for the relationship between BNIP3-mediated mitophagy and the NLRP1 inflammasome, highlighting their role in the development of PE.

The placenta is essential for facilitating communication between the mother and the fetus, ensuring maternal well-being and normal fetal development (19). Various pathological factors, such as hypoxia, inflammation, and metabolic abnormalities, are closely linked to preeclampsia in a multifaceted manner. Within the placenta, trophoblasts subjected to oxidative stress damage due to hypoxia play a pivotal role in the pathogenesis of preeclampsia (4, 6). Additionally, mitochondrial damage characterized by structural breakdown and excessive mitophagy induced by hypoxia is intricately associated with placental dysfunction. Previous research findings, including our own published studies, indicate that mitophagy contributes to placental injury caused by hypoxia in preeclampsia (18, 20). It has been suggested that BNIP3-mediated mitophagy may have a more significant impact than PINK/PARKIN-mediated mitophagy due to its heightened sensitivity to hypoxic environments. Numerous studies have suggested that mitophagy plays a protective role in certain hypoxic tissue injuries. However, our previous research has shown that inhibiting BNIP3-mediated mitophagy reduced trophoblast apoptosis and placenta injury in a PE-like mouse model (18). In this study, we further demonstrate that BNIP3-mediated mitophagy is activated under hypoxic/reoxygenation (H/R) conditions both *in vitro* and in the placenta of PE models. Additionally, the absence of BNIP3 results in decreased accumulation of mitochondrial ROS and inflammatory responses in the placenta of PE-like mice. These conflicting findings indicate that the functions of BNIP3 in mitochondrial regulation may depend on different cellular environments.

Accumulating evidence has demonstrated the critical role of inflammation and oxidative stress, particularly NLRPs, in the pathogenesis of PE (6, 21). The NLRP1 signaling pathway acts as a central component in innate immunity, regulating inflammatory responses and coordinating the host's defense mechanisms against pathogens (22). This pathway has attracted significant attention due to its pivotal involvement in various inflammatory disorders and infectious diseases. NLRP1 serves as a key sensor for danger signals and microbial components, initiating the assembly of the inflammasome complex, which subsequently activates Caspase-1. This activation leads to the production and release of pro-inflammatory cytokines, specifically interleukin-1β (IL-1β) and interleukin-18 (IL-18) (23). Dysregulation of NLRP1 signaling has been implicated in the pathogenesis of numerous diseases, including autoimmune disorders, metabolic syndromes, and neurodegenerative conditions (24–28). However, its physiological functions and implications in obstetric complications remain unclear. Limited research has been conducted on the impact of

hypoxia on NLRP1 activation. However, existing studies have indicated that NLRP1 interacts with HIF-1α under hypoxic conditions in various tissues, such as microvascular endothelium (29), neurons (30), liver (31), and myocardium (32), thereby facilitating ASC-Caspase-1-IL-1β signaling cascades. Nonetheless, other regulatory mechanisms under hypoxic conditions require further investigation. Our study demonstrates that the expression level of NLRP1 is upregulated in human trophoblasts in placenta samples from preeclampsia patients compared to normal pregnant women. This upregulation is associated with hypoxia and its related oxidative stress. Furthermore, our findings suggest that BNIP3-mediated mitophagy plays a significant role in regulating the NLRP1 inflammasome.

Previous research has suggested that mitophagy plays a critical role in the activation of the NLRP3 inflammasome. It has been documented that HIF-1α-BNIP3-mediated mitophagy mitigates renal fibrosis by inhibiting the activation of the NLRP3 inflammasome, and BNIP3-mediated mitophagy also exerts a protective effect on neuroinflammation by suppressing the assembly of the NLRP3 inflammasome (33, 34). The role of BNIP3 in regulating the NLRP1-Caspase1 signaling pathway has not previously been reported. In our current study, we observed that hypoxia-induced activation of BNIP3-mediated mitophagy triggers the NLRP1-Caspase1 pathway. Knockdown of BNIP3 reduced both NLRP1 and Caspase1 expression, as well as inflammatory cytokine release, which was reversed by overexpression of NLRP1. Furthermore, we demonstrated that trophoblast inflammation was attenuated by reducing mitochondrial ROS production with MitoTEMPO, a mitochondria-targeted superoxide dismutase mimetic. Consistent with our findings, several studies have unequivocally shown that ROS directly triggers the activation of NLRP1 in various conditions such as age-related neuronal damage, BAP-induced lung epithelial injury, and H_2O_2-induced neuronal damage (35–37). Furthermore, the ablation of BNIP3 ameliorated placental inflammatory injury in PE-like mice. However, multiple studies have demonstrated that mitophagy suppresses inflammation, including NLRP3 inflammasome-mediated pyroptosis in rheumatoid arthritis, aging muscle, and chronic alcohol exposure-induced cognitive impairment (34, 38, 39). These findings appear to contradict our results, possibly due to the diverse interaction patterns between mitophagy and inflammation at different stages. These data indicate that NLRP1 is downstream of the regulatory pathway of BNIP3-mediated mitophagy and the ROS it generates. The hypoxia/reoxygenation condition leads to excessive activation of mitophagy, which significantly contributes to mitochondrial damage and subsequent ROS production, exacerbating their harmful effects. In conclusion, placental hypoxia induces the upregulation of BNIP3, leading to enhanced mitophagy and ROS production. Subsequently, this activates NLRP1-inflammasome production, resulting in the release of inflammatory factors and subsequent placental inflammatory damage. The study further elucidates the role of BNIP3 in inflammation in preeclampsia (PE) and proposes that BNIP3 could potentially serve as a target for the treatment of pregnancy-related diseases manifesting as placental inflammation, such as PE.

Data availability statement

The original contributions presented in the study are included in the article/Supplementary Material. Further inquiries can be directed to the corresponding authors.

Ethics statement

The studies involving humans were approved by Ethical Committee of Maternal and Child Health Care Hospital of Shandong Province, affiliated to Qingdao University. The studies were conducted in accordance with the local legislation and institutional requirements. The human samples used in this study were acquired from primarily isolated as part of your previous study for which ethical approval was obtained. Written informed consent for participation was not required from the participants or the participants' legal guardians/next of kin in accordance with the national legislation and institutional requirements. The animal study was approved by Ethical Committee of Maternal and Child Health Care Hospital of Shandong Province, affiliated to Qingdao University. The study was conducted in accordance with the local legislation and institutional requirements.

Author contributions

MZ: Data curation, Project administration, Writing – review & editing. ZY: Project administration, Writing – review & editing. YK: Resources, Writing – review & editing. ZF: Resources, Writing – review & editing. CZ: Investigation, Writing – review & editing. CW: Investigation, Writing – review & editing. MJZ: Investigation, Writing – review & editing. JG: Methodology, Writing – review & editing. AL: Funding acquisition, Writing – original draft. MHZ: Conceptualization, Writing – review & editing.

Funding

The author(s) declare that financial support was received for the research and/or publication of this article. National Natural Science Foundation of China (No. 82101778); Special Scientific Research Fund Project of Shandong Provincial Maternal and Child Health Care Hospital (No. YJKY2022-031); Special Scientific Research Projects in the Field of Maternal-Fetal Medicine (No. 2023CAMCHS003A04); the Natural Science Foundation of Shandong Province (No. ZR2021MH262).

Conflict of interest

The authors declare that the research was conducted in the absence of any commercial or financial relationships that could be construed as a potential conflict of interest.

Generative AI statement

The author(s) declare that no Generative AI was used in the creation of this manuscript.

Publisher's note

Supplementary material

The Supplementary Material for this article can be found online at: https://www.frontiersin.org/articles/10.3389/fimmu.2025.1530015/full#supplementary-material

References

1. Ives CW, Sinkey R, Rajapreyar I, Tita ATN, Oparil S. Preeclampsia-pathophysiology and clinical presentations: JACC state-of-the-art review. *J Am Coll Cardiol*. (2020) 76:1690–702. doi: 10.1016/j.jacc.2020.08.014

2. Raymond D, Peterson E. A critical review of early-onset and late-onset preeclampsia. *Obstet Gynecol Surv*. (2011) 66:497–506. doi: 10.1097/OGX.0b013e3182331028

3. Rana S, Lemoine E, Granger JP, Karumanchi SA. Preeclampsia: pathophysiology, challenges, and perspectives. *Circ Res*. (2019) 124:1094–112. doi: 10.1161/CIRCRESAHA.118.313276

4. Lawless L, Qin Y, Xie L, Zhang K. Trophoblast differentiation: mechanisms and implications for pregnancy complications. *Nutrients*. (2023) 15. doi: 10.3390/nu15163564

5. Yang Y, Xu P, Zhu F, Liao J, Wu Y, Hu M, et al. The potent antioxidant MitoQ protects against preeclampsia during late gestation but increases the risk of preeclampsia when administered in early pregnancy. *Antioxid Redox Signal*. (2021) 34:118–36. doi: 10.1089/ars.2019.7891

6. Guerby P, Tasta O, Swiader A, Pont F, Bujold E, Parant O, et al. Role of oxidative stress in the dysfunction of the placental endothelial nitric oxide synthase in preeclampsia. *Redox Biol*. (2021) 40:101861. doi: 10.1016/j.redox.2021.101861

7. Zavatta A, Parisi F, Mandò C, Scaccabarozzi C, Savasi VM, Cetin I. Role of inflammaging on the reproductive function and pregnancy. *Clin Rev Allergy Immunol*. (2023) 64:145–60. doi: 10.1007/s12016-021-08907-9

8. Taabazuing CY, Griswold AR, Bachovchin DA. The NLRP1 and CARD8 inflammasomes. *Immunol Rev*. (2020) 297:13–25. doi: 10.1111/imr.v297.1

9. Zhang Z, Shibata T, Fujimura A, Kitaura J, Miyake K, Ohto U, et al. Structural basis for thioredoxin-mediated suppression of NLRP1 inflammasome. *Nature*. (2023) 622:188–94. doi: 10.1038/s41586-023-06532-4

10. Matias ML, Romao-Veiga M, Ribeiro VR, Nunes PR, Gomes VJ, Devides AC, et al. Progesterone and vitamin D downregulate the activation of the NLRP1/NLRP3 inflammasomes and TLR4-MyD88-NF-κB pathway in monocytes from pregnant women with preeclampsia. *J Reprod Immunol*. (2021) 144:103286. doi: 10.1016/j.jri.2021.103286

11. Matias ML, Gomes VJ, Romao-Veiga M, Ribeiro VR, Nunes PR, Romagnoli GG, et al. Silibinin downregulates the NF-κB pathway and NLRP1/NLRP3 inflammasomes in monocytes from pregnant women with preeclampsia. *Molecules*. (2019) 24. doi: 10.3390/molecules24081548

12. Nunes PR, Romao-Veiga M, Ribeiro VR, de Oliveira LRC, de Carvalho Depra I, de Oliveira LG, et al. Inflammasomes in placental explants of women with preeclampsia cultured with monosodium urate may be modulated by vitamin D. *Hypertens Pregnancy*. (2022) 41:139–48. doi: 10.1080/10641955.2022.2063330

13. Lin Q, Li S, Jiang N, Jin H, Shao X, Zhu X, et al. Inhibiting NLRP3 inflammasome attenuates apoptosis in contrast-induced acute kidney injury through the upregulation of HIF1A and BNIP3-mediated mitophagy. *Autophagy*. (2021) 17:2975–90. doi: 10.1080/15548627.2020.1848971

14. Han X, Xu T, Fang Q, Zhang H, Yue L, Hu G, et al. Quercetin hinders microglial activation to alleviate neurotoxicity via the interplay between NLRP3 inflammasome and mitophagy. *Redox Biol*. (2021) 44:102010. doi: 10.1016/j.redox.2021.102010

15. Ko MS, Yun JY, Baek IJ, Jang JE, Hwang JJ, Lee SE, et al. Mitophagy deficiency increases NLRP3 to induce brown fat dysfunction in mice. *Autophagy*. (2021) 17:1205–21. doi: 10.1080/15548627.2020.1753002

16. Chen Y, Dorn GW 2nd. PINK1-phosphorylated mitofusin 2 is a Parkin receptor for culling damaged mitochondria. *Science*. (2013) 340:471–5. doi: 10.1126/science.1231031

17. He YL, Li J, Gong SH, Cheng X, Zhao M, Cao Y, et al. BNIP3 phosphorylation by JNK1/2 promotes mitophagy via enhancing its stability under hypoxia. *Cell Death Dis*. (2022) 13:966. doi: 10.1038/s41419-022-05418-z

18. Li A, Zhao M, Yang Z, Fang Z, Qi W, Zhang C, et al. 6-Gingerol alleviates placental injury in preeclampsia by inhibiting oxidative stress via BNIP3/LC3 signaling-mediated trophoblast mitophagy. *Front Pharmacol*. (2023) 14:1243734. doi: 10.3389/fphar.2023.1243734

19. Shao X, Yu W, Yang Y, Wang F, Yu X, Wu H, et al. The mystery of the life tree: the placentas†. *Biol Reprod*. (2022) 107:301–16. doi: 10.1093/biolre/ioac095

20. Sun Y, Lv D, Xie Y, Xu H, Li X, Li F, et al. PINK1-mediated mitophagy induction protects against preeclampsia by decreasing ROS and trophoblast pyroptosis. *Placenta*. (2023) 143:1–11. doi: 10.1016/j.placenta.2023.09.010

21. Shirasuna K, Karasawa T, Takahashi M. Role of the NLRP3 inflammasome in preeclampsia. *Front Endocrinol (Lausanne)*. (2020) 11:80. doi: 10.3389/fendo.2020.00080

22. Robinson KS, Toh GA, Rozario P, Chua R, Bauernfried S, Sun Z, et al. ZAKα-driven ribotoxic stress response activates the human NLRP1 inflammasome. *Science*. (2022) 377:328–35. doi: 10.1126/science.abl6324

23. Jenster LM, Lange KE, Normann S, vom Hemdt A, Wuerth JD, Schiffelers LDJ, et al. P38 kinases mediate NLRP1 inflammasome activation after ribotoxic stress response and virus infection. *J Exp Med*. (2023) 220. doi: 10.1084/jem.20220837

24. Song AQ, Gao B, Fan JJ, Zhu YJ, Zhou J, Wang YL, et al. NLRP1 inflammasome contributes to chronic stress-induced depressive-like behaviors in mice. *J Neuroinflamm*. (2020) 17:178. doi: 10.1186/s12974-020-01848-8

25. Burian M, Schmidt MF, Yazdi AS. The NLRP1 inflammasome in skin diseases. *Front Immunol*. (2023) 14:1111611. doi: 10.3389/fimmu.2023.1111611

26. Mi L, Min X, Chai Y, Zhang J, Chen X. NLRP1 inflammasomes: A potential target for the treatment of several types of brain injury. *Front Immunol*. (2022) 13:863774. doi: 10.3389/fimmu.2022.863774

27. Yu CH, Moecking J, Geyer M, Masters SL. Mechanisms of NLRP1-mediated autoinflammatory disease in humans and mice. *J Mol Biol*. (2018) 430:142–52. doi: 10.1016/j.jmb.2017.07.012

28. Yap JKY, Pickard BS, Chan EWL, Gan SY. The role of neuronal NLRP1 inflammasome in Alzheimer's disease: bringing neurons into the neuroinflammation game. *Mol Neurobiol*. (2019) 56:7741–53. doi: 10.1007/s12035-019-1638-7

29. Jung E, Kim YE, Jeon HS, Yoo M, Kim M, Kim YM, et al. Chronic hypoxia of endothelial cells boosts HIF-1α-NLRP1 circuit in Alzheimer's disease. *Free Radic Biol Med*. (2023) 204:385–93. doi: 10.1016/j.freeradbiomed.2023.05.011

30. Huang J, Lu W, Doycheva DM, Gamdzyk M, Hu X, Liu R, et al. IRE1α inhibition attenuates neuronal pyroptosis via miR-125/NLRP1 pathway in a neonatal hypoxic-ischemic encephalopathy rat model. *J Neuroinflamm*. (2020) 17:152. doi: 10.1186/s12974-020-01796-3

31. Yu X, Sun M, Wang J, Zhang S. Chronic intermittent hypoxia activates NLRP1 inflammasome and causes liver injury. *Xi Bao Yu Fen Zi Mian Yi Xue Za Zhi*. (2024) 40:327–32.

32. Cao L, Chen Y, Zhang Z, Li Y, Zhao P. Endoplasmic reticulum stress-induced NLRP1 inflammasome activation contributes to myocardial ischemia/reperfusion injury. *Shock*. (2019) 51:511–8. doi: 10.1097/SHK.0000000000001175

33. Fu ZJ, Wang ZY, Xu L, Chen XH, Li XX, Liao WT, et al. HIF-1α-BNIP3-mediated mitophagy in tubular cells protects against renal ischemia/reperfusion injury. *Redox Biol*. (2020) 36:101671. doi: 10.1016/j.redox.2020.101671

34. Lin X, Wang H, Zou L, Yang B, Chen W, Rong X, et al. The NRF2 activator RTA-408 ameliorates chronic alcohol exposure-induced cognitive impairment and NLRP3 inflammasome activation by modulating impaired mitophagy initiation. *Free Radic Biol Med*. (2024) 220:15–27. doi: 10.1016/j.freeradbiomed.2024.04.236

35. Xu T, Sun L, Shen X, Chen Y, Yin Y, Zhang J, et al. NADPH oxidase 2-mediated NLRP1 inflammasome activation involves in neuronal senescence in hippocampal neurons *in vitro*. *Int Immunopharmacol*. (2019) 69:60–70. doi: 10.1016/j.intimp.2019.01.025

36. Kohno R, Nagata Y, Ishihara T, Amma C, Inomata Y, Seto T, et al. Benzo[a] pyrene induces NLRP1 expression and promotes prolonged inflammasome signaling. *Front Immunol.* (2023) 14:1154857. doi: 10.3389/fimmu.2023.1154857

37. Xu TZ, Shen XY, Sun LL, Chen YL, Zhang BQ, Huang DK, et al. Ginsenoside Rg1 protects against H2O2–induced neuronal damage due to inhibition of the NLRP1 inflammasome signalling pathway in hippocampal neurons *in vitro*. *Int J Mol Med.* (2019) 43:717–26.

38. Hong Z, Wang H, Zhang T, Xu L, Zhai Y, Zhang X, et al. The HIF-1/BNIP3 pathway mediates mitophagy to inhibit the pyroptosis of fibroblast-like synoviocytes in rheumatoid arthritis. *Int Immunopharmacol.* (2024) 127:111378. doi: 10.1016/j.intimp.2023.111378

39. Irazoki A, Martinez-Vicente M, Aparicio P, Aris C, Alibakhshi E, Rubio-Valera M, et al. Coordination of mitochondrial and lysosomal homeostasis mitigates inflammation and muscle atrophy during aging. *Aging Cell.* (2022) 21:e13583. doi: 10.1111/acel.13583

40. Kucukgoz Gulec U, Ozgunen FT, Buyukkurt S, Guzel AB, Urunsak IF, Demir SC, et al. Comparison of clinical and laboratory findings in early- and late-onset preeclampsia. *J Matern Fetal Neonatal Med.* (2013) 26:1228–33. doi: 10.3109/14767058.2013.776533

frontiers | Frontiers in Immunology

TYPE Original Research
PUBLISHED 02 July 2025
DOI 10.3389/fimmu.2025.1571795

OPEN ACCESS

EDITED BY
Subhradip Karmakar,
All India Institute of Medical Sciences, India

REVIEWED BY
Juan Caballero,
Max Planck Institute for Immunobiology and Epigenetics, Germany
Umida Ganieva,
Rosalind Franklin University of Medicine and Science, United States

*CORRESPONDENCE
Mengjia Peng
pemeji@wmu.edu.cn

RECEIVED 06 February 2025
ACCEPTED 14 June 2025
PUBLISHED 02 July 2025

CITATION
Wang Q, Li X, Ye W, Lin L, Ye K and Peng M (2025) Prediction and immune landscape study of potentially key autophagy-related biomarkers in preeclampsia with gestational diabetes mellitus.
Front. Immunol. 16:1571795.
doi: 10.3389/fimmu.2025.1571795

Prediction and immune landscape study of potentially key autophagy-related biomarkers in preeclampsia with gestational diabetes mellitus

Qin Wang[1], Xiaoqi Li[2], Wen Ye[3], Lin Lin[4], Kejun Ye[4] and Mengjia Peng[4*]

[1]Department of Geriatric Integrative, Second Affiliated Hospital of Xinjiang Medical University, Urumqi, Xinjiang, China, [2]The Second Affiliated Hospital of Xinjiang Medical University, The Second Clinical Medical College, Xinjiang Medical University, Urumqi, Xinjiang, China, [3]Nephrology Department, Second Affiliated Hospital of Xinjiang Medical University, Xinjiang, Urumqi, China, [4]Wenzhou Key Laboratory for the Diagnosis and Prevention of Diabetic Complications, Department of Gynecology and Obstetrics, The Third Affiliated Hospital of Wenzhou Medical University (Ruian People's Hospital), Rui'an, Zhejiang, China

Introduction: Gestational diabetes mellitus (GDM) and preeclampsia are prevalent pregnancy complications that threaten maternal and infant health while imposing substantial socioeconomic burdens. Although several interventions exist, shortcomings in individualized treatment and other limitations necessitate urgent in-depth research. This study aimed to examine alterations in autophagy-related gene expression in preeclampsia combined with GDM.

Methods: We conducted bioinformatics analyses including gene expression profiling, weighted gene co-expression network analysis (WGCNA), gene ontology (GO) and KEGG enrichment analyses, machine learning modeling, immune infiltration analyses, and single-cell RNA sequencing. Differentially expressed autophagy-related genes linked to preeclampsia with GDM were identified. Expression levels of four key genes were validated in placental samples using reverse transcription quantitative polymerase chain reaction (RT-qPCR).

Results: Our findings identified potential biomarkers and molecular mechanisms underlying preeclampsia with GDM. Single-cell analysis corroborated these results, revealing distinct autophagy-related gene signatures and enhancing understanding of the pathophysiology.

Discussion: This study elucidates molecular mechanisms connecting GDM and preeclampsia, identifies novel biomarkers and therapeutic targets, and provides a valuable reference for future research and clinical applications. The integration of multi-omics approaches advances precision medicine strategies for these comorbid conditions.

KEYWORDS

preeclampsia, gestational diabetes mellitus, autophagy, gene expression, omnibus, single-cell RNA

1 Introduction

Preeclampsia (PE) and gestational diabetes mellitus (GDM) represent two major pregnancy complications that have the potential to affect maternal and foetal health. PE affects 2-8% of pregnancies globally, whereas GDM occurs in approximately 1.8-20.3% of pregnancies (1, 2). These conditions pose an immediate risk to the mother and foetus, and have long-term health consequences (3, 4). PE is a significant pregnancy complication characterised by high blood pressure and proteinuria after 20 weeks of gestation (5). GDM is characterised by glucose intolerance that occurs or is diagnosed for the first time during pregnancy, leading to hyperglycaemia and associated metabolic disorders (6). The potentially severe consequences of these disorders underscore the importance of identifying reliable biomarkers for early diagnosis and intervention.

Emerging evidence suggests that PE and GDM share common pathophysiological mechanisms, including endothelial dysfunction, inflammation, and metabolic dysregulation (7). GDM in late pregnancy increases the risk of developing PE, and patients with PE tend to have features of GDM, suggesting that the underlying biological pathways may overlap (8, 9). A number of large-scale cohort studies conducted among different populations have confirmed this association. For instance, a Latin American and Caribbean cohort demonstrated that GDM significantly elevates PE risk (RR: 1.93; 95% CI: 1.66–2.25) (10). Similarly, Swedish and Chinese cohorts revealed that GDM increases the likelihood of severe PE (Sweden: OR 2.29, 95% CI 1.88–2.80; China: OR 2.13, 95% CI 1.58–2.87) (11).

Autophagy, a cellular self-degradation process that supplies degradation products, is crucial for cellular homeostasis and linked to the pathogenesis of PE and GDM (12). In PE, abnormal autophagy can lead to an increased stress response and apoptosis of placental cells, resulting in placental dysfunction and impaired foetal growth and development (13). Autophagy may influence the onset and development of GDM by regulating the stress response and metabolic state of placental cells (13). Although extensive research has been conducted, the precise function of autophagy in PE and GDM remains unclear, necessitating additional studies to clarify its mechanism of action and therapeutic potential.

Previous studies have emphasised the significance of autophagy and immune cell infiltration in PE and GDM. The infiltration of immune cells into the placenta contributes significantly to the progression of these diseases (14–16). Autophagy regulates immune responses and inflammation, which are key components of the pathophysiology of PE and GDM (17). Interactions between autophagy-related genes (ARGs) and immune cell infiltration in these diseases remain underexplored and require comprehensive research.

This study used bioinformatics to identify differentially expressed autophagy-related genes (DE-AGs) in PE with GDM. We conducted differential expression and weighted gene co-expression network analysis (WGCNA) to identify DE-AGs in conjunction with autophagy-associated genes. We examined the biological functions and pathways of these DE-AGs using functional enrichment analysis, constructed protein-protein interaction (PPI) networks, and identified key genes using various machine learning techniques. Receiver operating characteristic (ROC) curves were used to assess the diagnostic potential of DE-AGs, and immune cell infiltration was evaluated to understand their immune efficacy. Finally, single-cell RNA sequencing data were analysed to determine the distribution of DE-AGs and different cell types in PE and GDM placental tissues. Our study comprehensively analysed the molecular mechanisms of PE complicating GDM and highlighted the roles of ARGs in these disorders. The identification of DE-AGs and their associated pathways provides potential biomarkers for early diagnosis and identification of therapeutic targets in PE and GDM.

2 Materials and methods

2.1 Data gathering and preparation

Gene expression profiles related to GDM and PE were obtained from the NCBI Gene Expression Omnibus (GEO) database (https://www.ncbi.nlm.nih.gov/geo/). Using the R package 'GEOquery' (v2.64.2) (18), data related to 'preeclampsia' and 'gestational diabetes mellitus' were retrieved from the GEO database. Five datasets were obtained from the GEO database: GSE103552, GSE75010, GSE24129, GSE154414, and GSE30186. The GSE75010 dataset comprises 80 patients with PE and 77 controls, the GSE24129 dataset contains eight patients with PE and eight control cases, the GSE30186 dataset contains six patients with PE and six control cases, the GSE154414 dataset contains four patients with GDM and four control cases, and the GSE103552 dataset includes ten patients with GDM and eight controls, and the GSE173193 dataset includes two placenta samples from PE, GDM and the control group respectively. We performed preprocessing on each dataset, employing the "leave-one-out" method to retain only the first occurrence of duplicate gene names in each dataset, the gene expression levels for all genes in each dataset were log-transformed to ensure that the gene expression values within each dataset had the same distribution. Next, we removed the batch effects between GSE75010 and GSE24129 using the normalizeBetweenArrays function from the "limma" (v3.52.2) package, enabling comparability of expression levels between the two datasets, and subsequently merged GSE75010 and GSE24129. Principal component analysis (PCA) was conducted on the normalised dataset, and box plots along with PCA plots were created using the 'ggplot2' R package (v3.3.6) (19) to visualise sample distribution and clustering.

2.2 Identification of differentially expressed genes

DEGs were identified by extracting samples from the GSE103552 and Merged_Dataset_GSE75010_GSE24129 datasets

and conducting differential analysis using the R package 'limma'(v3.60.4) (20). To ensure higher sensitivity in detecting differentially expressed genes, we established a more permissive fold change threshold to capture a broader range of potential variations.DEGs were identified in the two datasets using the criteria |log2 fold change (log2 FC)| > 0 and $p < 0.05$ (21, 22), followed by de-duplication of the results (23). Volcano maps were created with the R package 'ggplot2', while heat maps utilised the R package 'ComplexHeatmap' (v2.13.1) (24).

2.3 WGCNA

The raw gene expression data were preprocessed using the R package 'WGCNA' (v1.72-5) (25), and The distances between samples were calculated using the dist function, with the default metric being Euclidean distance. Subsequently, the pickSoftThreshold function was used to select the optimal soft threshold. Dynamic modules were identified using the cutreeDynamic function, with each module containing at least 50 genes (26). A dynamic dendrogram was drawn using the plotDendroAndColors function to show the associations and differences between different modules.

Topological Overlap Matrix (TOM) was calculated by the TOMsimilarity function to quantify gene co-expression similarity. Module eigengenes (MEs) were extracted for Pearson correlation analysis with clinical traits. Statistical significance was evaluated using Student's asymptotic P-value (corPvalueStudent function), and results were visualized through a labeledHeatmap displaying correlation coefficients and P-values.

Based on the visualization results of the module clustering, we defined a cutting height: MEDissThres. Subsequently, by calling the mergeCloseModules function, we merged similar gene modules based on this cutting height, producing merged module colors and new module eigengenes (MEs). This simplification of the module structure enhances the biological significance of the analysis and facilitates subsequent functional enrichment and network analysis.

Modules significantly associated with preeclampsia (PE) were prioritized based on P-value ranking. Genes within PE-related modules were extracted for subsequent functional enrichment and regulatory network analyses.

2.4 Screening of ARGs

ARGs were sourced from four complementary databases: GeneCards (https://www.genecards.org/): A comprehensive repository integrating gene annotations from >150 biomedical resources; Human Autophagy Database (http://www.autophagy.lu/): A manually curated knowledgebase specializing in autophagy pathways and regulators; HAMdb (http://hamdb.scbdd.com/home/index/): A disease-focused platform linking autophagy genes to pathological mechanisms; MSigDB (https://www.gsea-msigdb.org/) (version: MSigDB 2023.2.Hs): A functional genomics resource providing hallmark gene sets for pathway enrichment. These genes were then intersected with DEGs and WGCNA modules and analysed to identify the DE-AGs in PE with GDM. Finally, the genes were visualized using the R package 'VennDiagram'(v1.7.3).

2.5 Enrichment analysis of DE-AGs was conducted using Gene Ontology and the Kyoto Encyclopedia of Genes and Genomes

We performed GO enrichment analysis on the DE-AGs in *Homo sapiens*, systematically evaluating three functional categories: biological processes (BP), cellular components (CC), and molecular functions (MF). KEGG pathway analysis was concurrently conducted (27–29). Gene identifiers were standardized using the R package 'org.Hs.eg.db'(v3.19.1), followed by functional enrichment analysis with 'clusterProfiler' (v4.12.6) (30). To quantify directional enrichment patterns, z-scores were calculated for each term using 'GOplot' (v1.0.2) (31), enabling quantitative assessment of biological pathway activation states. Terms with $p < 0.05$ and false discovery rate (FDR) < 0.2 were considered statistically significant (32). Results were filtered for both statistical significance and biological relevance, with final visualizations were generated.

2.6 PPI network

We utilized the STRING database (https://string-db.org/) (version:12.0) (33) to analyze protein–protein interactions among DE-AGs. The combined interaction confidence score (joint score) greater than 0.4 was selected as the medium confidence interaction threshold, and the interaction node data from STRING were imported into Cytoscape (v3.9.1) for PPI network analysis (34). Hub genes were systematically identified through the CytoHubba plugin by applying four complementary algorithms: Maximum Clique Centrality (MCC), Degree, Edge Percolated Component (EPC), and Density of Maximum Neighborhood Component (DMNC). The top 15 genes from each algorithm were cross-compared, and consensus hub genes were defined as those overlapping across all four methods. This integrative approach was visualized through a Venn diagram, highlighting genes consistently prioritized by multiple centrality metrics (35).

2.7 Identification of PE with GDM-related DE-AGs using machine learning

This study employed three machine learning models: least absolute shrinkage and selection operator (LASSO), support vector machine (SVM), and random forest (RF). The R package 'DALEX' (v2.4.3) was used to interpret these models and visualize residual distributions and feature significance. Hyperparameter

optimization was systematically performed using the R package 'caret' (v6.0-94) through grid search across predefined parameter spaces. All models were evaluated via 10-fold cross-validation, with final parameters retained after validation.

Subsequently, the R package 'pROC' (36) was utilized to plot the area under the receiver operating characteristic (ROC) curve (AUC). Feature screening was then performed using LASSO, RF, and SVM methods. The intersection of features derived from these complementary algorithms was prioritized to mitigate model-specific biases. This integrative approach enhanced biomarker discovery reliability, as consensus genes were more likely to reflect biologically stable signatures in gestational diabetes mellitus (GDM) pathogenesis.

For LASSO analysis, we employed the R package 'glmnet' (v4.1.7) to screen coefficients. This involved analyzing cleaned data, extracting lambda values, likelihood values, L1 regularization values, and classification error rates. The results were visualized as described previously (37).

The SVM-based recursive feature elimination (SVM-RFE) (38) technique was implemented using the R package 'e1071' (v1.7-13) (39, 40). By incorporating a feature ranking process into the outer layer of cross-validation (41), we achieved an unbiased estimate of the generalization error.

In the RF algorithm, gene importance rankings were obtained using the average reduction in the Gini index as the indicator (42). The intersection of results from LASSO, SVM-RFE, and RF identified PE with GDM-related DE-AGs. These consensus genes were visualized using UpSet plots to demonstrate multi-algorithm superiority over single-method outputs. These consensus genes were visualized using UpSet plots to demonstrate the advantages of multiple algorithms over single-method outputs.

We employed the Spearman correlation method to evaluate relationships between four DE-AGs. Correlation heatmaps generated with the R package 'corrplot' (v0.92) illustrated gene associations and interactions. The non-parametric Spearman approach was chosen instead of Pearson correlation to account for potential nonlinear relationships and reduce sensitivity to expression value outliers. This strategy was critical for identifying robust co-expression patterns in heterogeneous clinical samples.

2.8 Examination of differential expression PE with GDM-related DE-AGs

We investigated the differences in the expression of PE with GDM-related DE-AGs between the experimental and control groups. Using Shapiro-Wilk tests for normality assessment (α=0.05) and F-tests for variance homogeneity, we selected appropriate statistical comparisons: independent t-tests for parametric data with equal variance ($p>0.05$) and Welch's t-tests for unequal variance ($p<0.05$). Integrated visualizations combining scatter plots (showing individual data points), box plots (depicting quartiles), and violin plots (illustrating probability density) to comprehensively present distribution characteristics. Statistical significance thresholds were maintained as: ns $p\geq0.05$; *$p<0.05$; **$p<0.01$; ***$p<0.001$, with detailed annotation in figure captions.

2.9 ROC analysis of PE with GDM-related DE-AGs

The ROC curves for the GSE103552, Merged_Data set_GSE75010_GSE24129, GSE154414, and GSE30186 datasets were analysed using the R package 'pROC' (V1.18.0) to evaluate sensitivity and specificity. The accuracy of genes for diagnosing PE with GDM was assessed by predicting ROC-related information at specific cutoff values, quantified as the AUC. Genes with an AUC > 0.6 were visualized (43).

2.10 Exploration of the biological functions and signalling pathways of PE with GDM-related DE-AGs

We used the R package 'clusterProfiler'(v4.12.6) to conduct gene set enrichment analysis (GSEA) (44) to identify pathways significantly linked to PE with GDM-related DE-AGs. Species: *Homo sapiens*; reference gene set: c2.cp.all.v2022.1.Hs.symbols.gmt; reference gene set source R package: msigdbr (v7.5.1); ID-converted R package: org.Hs.eg.db. The results of the enrichment analyses were filtered according to the following criteria: normalised enrichment score $|NES| > 1$, FDR < 0.25, $p.adj < 0.05$.

2.11 Methods for evaluation of immune cell infiltration

The infiltration frequency of immune cells in placental tissues was analyzed and compared between the normal group (placental tissues from healthy individuals) and the disease group (placental tissues from patients with specific conditions) using single-sample Gene Set Enrichment Analysis (ssGSEA) (45) implemented via the R package "GSVA". We selected ssGSEA for its ability to provide a robust assessment of immune cell infiltration based on gene expression profiles, enabling evaluation of individual sample enrichment scores. Enrichment scores for each immune cell class were calculated using class-specific gene sets: LM22 (46), allowing assessment of immune cell infiltration in each sample. Comparisons were made between the clinically defined immune cell infiltration patterns of the two groups. Additionally, Spearman's statistical method was used to analyze: pairwise correlations between different immune cell subtypes, and pairwise correlations between DE-AGs and immune cell proportions. The analysis results were visualized as group comparison plots, lollipop plots, and Plotted correlation scatter plots, along with data analysis and visualization of network diagrams using the R package "linkET" (v0.0.7.4), thereby enabling a more intuitive demonstration of the immune infiltration patterns associated with DE-AGs.

2.12 Single-cell data pre-processing and clustering annotation

High-throughput sequencing data from the single-cell dataset GSE173193 (47, 48) were obtained from the GEO database. We screened eligible samples, including two placental tissue samples from patients with gestational diabetes, two placental tissue samples from patients with pre-eclampsia, and two placental tissue samples from normal controls. The R package 'Seurat' (v5.1.0) (49) was used for data analysis. First, the relative proportions of mitochondrial, ribosomal, and erythrocyte genes were calculated using the Seurat function PercentageFeatureSet. Data quality was ensured by applying the following criteria: cells must express over 500 genes, genes should be present in more than three cells (prevents low-abundance artifact retention), mitochondrial gene expression must be below 25% (excludes apoptotic cells per 10x Genomics standards), ribosomal gene expression must be above 3% (ensures active translation while filtering empty droplets), and haemoglobin gene expression must be less than 1% (removes erythrocyte contamination in non-hematopoietic tissues). The dataset was normalised using the NormalizeData function, and 2000 highly variable genes were identified using the FindVariableFeatures function (50). The data were then scale-normalised using the ScaleData function. Highly variable genes were used as input features for PCA, and the RunPCA function was used to perform PCA analysis on the normalised data. To eliminate the batch effect, based on inspection of the PCA elbow plot (Supplementary Figure 3.) which revealed that the first 15 principal components captured the majority of variance while minimizing noise from additional dimensions, the Harmony algorithm (51) from the R package 'harmony' (v1.2.0) was used to select these dimensions for single-cell RNA sequencing data integration. Batch-corrected single-cell RNA sequencing data were visualised using the t-distributed stochastic neighbour embedding (t-SNE) method (52). Initially, cell-cell relationships were established using neighbourhood maps. Subsequently, clustering analysis was performed using the FindClusters function at a resolution of 0.3 to distinguish various cell populations, with these clustering results serving as the basis for further analyses. We manually annotated the data by integrating established lineage markers and consulting the human placental cell atlas available on the CellMarker website (http://xteam.xbio.top/CellMarker/)(version: CellMarker 1.0) to ensure annotation accuracy and reliability (53)("Marker genes can be found in Supplementary File 1"). DEGs in each cell cluster were identified using the Wilcoxon rank sum test via Seurat's FindMarkers function, with criteria of p_val < 0.05 and abs (avg_log2 FC) > 0.5.

2.13 Cell-cell communication

We employed the R package 'CellChat' (v1.6.1) (54) to analyse potential cell-cell interactions. In the present study, we focused on the extravillous trophoblast (EVT) cell population. First, PE samples were extracted, and 3000 cells were randomly selected to create CellChat objects. We then used the 'human' related data from the CellChatDB database (http://www.cellchat.org/). The 'secretion signalling' subset was prioritized for analyzing ligand-receptor interactions due to its critical involvement in cell-cell communication mechanisms essential for EVT cell function, particularly in placental development and crosstalk with the maternal immune system. This subset specifically encapsulates core ligand-receptor pairs that drive these biological processes. Overexpressed ligand-receptor pairs in CellChat objects were identified using the identifyOverExpressedGenes and identifyOverExpressedInteractions functions and mapped to PPI networks using the R package 'CellChat'. The probability of intercellular communication was calculated using the computeCommunProb function, excluding communication between cell populations involving fewer than three cells. Finally, the probability of communication for specific pathways was refined using the computeCommunProbPathway function. The number and strength of intercellular interactions were visualised using the netVisual_circle function, and chord plots were used to show the expression of vascular endothelial growth factor (VEGF), insulin-like growth factor (IGF), epidermal growth factor (EGF), and macrophage migration inhibitory factor (MIF) in PE. The interactions involving VEGF, IGF, EGF, and MIF reveal critical insights into EVT cell regulatory mechanisms. For instance, VEGF is essential for angiogenesis, which is indispensable for placental development. IGF and EGF mediate cellular proliferation and differentiation, while MIF modulates immune responses. The ligand-receptor pairs involved in intercellular communication when EVT cells acted as signal senders and receivers were visualised using netVisual_bubble plots. All visualized communication probability results were subjected to significance screening using a threshold of ($p < 0.05$). Network centrality analysis was performed using the netAnalysis_computeCentrality function (55) and visualised as a heatmap. GDM samples were extracted, and the above process was repeated.

2.14 Pseudo-temporal analysis

We then performed a pseudotemporal analysis of the EVT cell population. The R package 'monocle' (v2.32.0) (56) was utilised for unsupervised pseudo-temporal analysis. The EVT cell clusters from the GDM and PE samples underwent further clustering analysis to identify significantly different cell clusters between the diseased and healthy samples. Then, using the gene-cell matrix at the original unique molecular identifier count scale derived from the Seurat-processed data as input, a cellular dataset containing the expression matrix, phenotypic data, and feature data was constructed using the newCellDataSet function with the parameter expressionFamily = negbinomial.size. Next, the discrete nature of the scale factors and gene expression between cells was corrected using the estimateSizeFactors and estimateDispersions functions. Dimensionality reduction was conducted using the DDRTree method (max_components set to 2), followed by cell sorting and visualisation using the plot_cell_trajectory function. DDRTree effectively captures the

intrinsic structure of data, demonstrating particular suitability for single-cell RNA sequencing datasets. Specifically designed to handle complex trajectories and model branching structures, this method proves critical for pseudotime analysis of EVT cell populations. Compared to alternative dimensionality reduction techniques like PCA or t-SNE, DDRTree's superiority lies in its capacity to preserve biologically meaningful relationships while maintaining cellular lineage associations. This capability enables accurate reconstruction of developmental trajectories, which is fundamentally important for delineating EVT cell dynamics in both physiological and pathological contexts (57). Scatter plots, violin plots, and proposed time trajectory plots were then used to display the potential marker genes screened in the bulk RNA analysis and visualised using functions inside the R package "monocle". Pseudo-temporal highly variant genes were filtered by 'qval < 1e-50', 'mean_expression ≥ 1 & dispersion_empirical ≥ 3 * dispersion_fit', and the differentialGeneTest function was used to analyse the expression changes of these genes in pseudo-time (The threshold of qval < 1e-50 ensures that only genes with highly significant differential expression in pseudotime are included. This threshold minimizes the risk of false positives and ensures that the identified genes are robustly associated with the temporal dynamics of EVT cells. The choice of this threshold is consistent with standard practices in single-cell RNA-seq analysis). Finally, the plot_pseudotime_heatmap function was used to cluster and visualise the screened genes according to their expression patterns. We conducted KEGG enrichment analyses for each gene cluster individually using the R packages 'clusterProfiler' and 'org.Hs.eg.db'. The KEGG enrichment analysis revealed several biological pathways significantly associated with the gene clusters identified in our study. These pathways provide a deeper understanding of the underlying molecular mechanisms and highlight potential therapeutic intervention targets.

2.15 Patient and tissue samples

Twelve placental samples were collected from women who delivered at the Third Affiliated Hospital of Wenzhou Medical University. Six of the women had PE with GDM, whereas the remaining six were healthy controls at the same gestational week of delivery. To avoid the potential effects of uterine contractions on placental metabolism during labour, all women underwent elective caesarean section for clinical reasons that did not affect placental metabolism or perfusion. All women were aged 20–40 years, had singleton pregnancies, and underwent regular obstetric examinations with complete clinical data. The Research Ethics Committee of Ruian People's Hospital approved this study (approval number YJ2024114), and all participating mothers provided written informed consent. The inclusion criteria for the PE with GDM group were: (1) blood pressure of at least 140/90 mmHg with 24-hour urine protein levels of 0.3 g or more after 20 weeks' gestation; (2) a 75 g oral glucose tolerance test conducted between 24 and 28 weeks' gestation showing fasting glucose ≥5.1 mmol/L or 1-hour postprandial glucose ≥10.0 mmol/L or 2-hour postprandial glucose ≥8.5 mmol/L. The inclusion criteria for the control group were as follows: no abnormalities in blood pressure, glucose monitoring, oral glucose tolerance test, or routine urine tests. The exclusion criteria were as follows: (1) Mothers who had severe heart, liver, or kidney disease during pregnancy; preexisting hypertension, diabetes, or other serious medical or surgical conditions; or severe obstetric complications or foetal congenital diseases, including abnormal amniotic fluid volume, placenta previa, placental abruption, intrauterine distress, or foetal congenital heart disease during pregnancy or at the time of delivery; (2) those who did not undergo regular and periodic obstetric examinations; and (3) pregnant women with a history of drug, alcohol, or drug addiction or who use drugs that affect the experimental results during pregnancy and delivery. Under strictly sterile conditions, within 15 minutes after delivery, a professional doctor takes placental tissue of $1cm^3$ from the central part, avoiding the umbilical cord insertion point and the infarcted area. The extracted placental tissues were washed with blood in 0.9% normal saline and transferred to a refrigerator at -80°C for long-term storage.

2.16 Reverse transcription quantitative polymerase chain reaction

RNA was extracted using the Tissue Total RNA Isolation Kit V2 (Vazyme), followed by cDNA synthesis using HiScript III All-in-one RT SuperMix (Vazyme). RT-qPCR was performed on a CFX Connect Real-Time PCR System (Bio-Rad, Hercules, CA, USA) using Taq Pro Universal SYBR qPCR Master Mix (Vazyme). The $2^{-\Delta\Delta Ct}$ method was employed to quantify relative gene expression, using GAPDH as the reference gene.

2.17 Statistical analysis

R software (v4.4.1) was used for data processing and analysis. Unless otherwise stated, we used the independent Student's t-test to evaluate the statistical significance of normally distributed variables when comparing two continuous groups. We used the Mann–Whitney U-Test (Wilcoxon rank-sum test) to assess differences in non-normally distributed variables. The Kruskal–Wallis test was used to compare three or more groups. Spearman's correlation analysis was used to calculate the correlation coefficients between different molecules. P-values were reported as two-tailed, with statistical significance set at $p < 0.05$.

3 Results

3.1 Differential expression analysis of PE with GDM

The GSE103552 and Merged_Dataset_GSE75010_GSE24129 datasets were normalised separately. PCA was conducted, and both datasets showed more significant clustering results. In the GSE103552 dataset, PC1 was 20.6% and PC2 was 12.4% (Figure 1A), whereas in the Merged_Dataset_GSE75010_GSE24129 dataset, PC1 was 16.9% and PC2 was 7% (Figure 1B), indicating a significant difference between the groups. Volcano plot analysis of the GSE103552

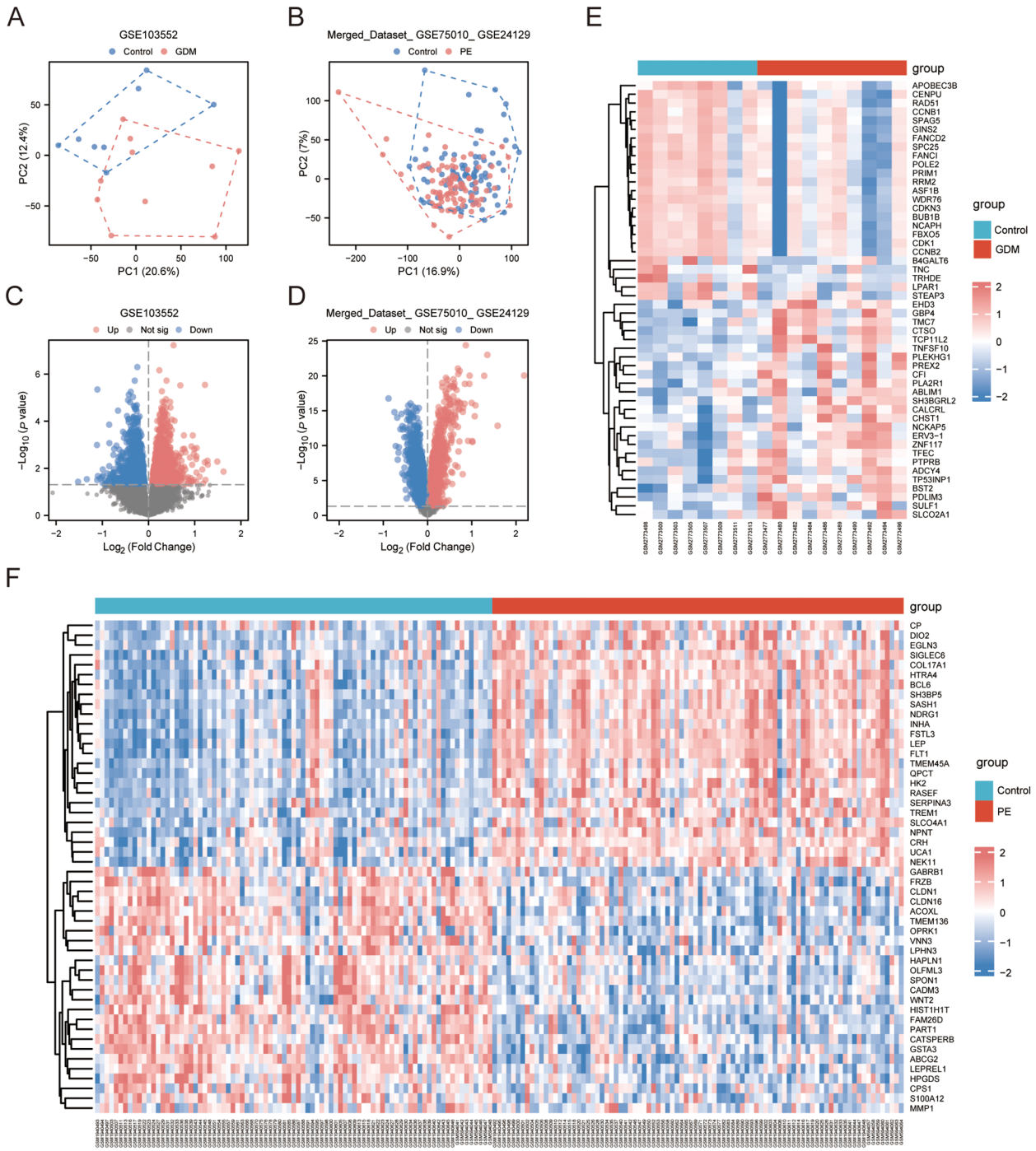

FIGURE 1
DEGs. **(A, B)** PCA of GSE103552 and Merged_Dataset_GSE75010_GSE24129 dataset. **(C, D)** Volcano plots of DEGs in GSE103552 and Merged_Dataset_GSE75010_GSE24129 datasets, |log2 FC| > 0, $p < 0.05$. **(E, F)** Expression heatmap of top 25 up- and downregulated genes in GSE103552 and Merged_Dataset_GSE75010_GSE24129 datasets. DEG, differentially expressed gene; PCA, principal component analysis.

dataset, using a screening threshold of |log2 FC| > 0 and $p < 0.05$, identified 2767 DEGs, with 1261 upregulated and 1506 downregulated (Figure 1C). In the Merged_Dataset_GSE75010_GSE24129 dataset, application of the same screening threshold revealed 6523 DEGs, with 3437 upregulated and 3086 downregulated (Figure 1D). The heat maps show the top 25 upregulated and downregulated genes in both datasets (Figures 1E– F).

3.2 WGCNA

Using 88 PE samples and 85 control samples from the Merged_Dataset_GSE75010_GSE24129 dataset, the top 25% of genes with the largest fluctuations were selected for WGCNA, based on the standard deviation order. Next, the pickSoftThreshold function was constructed based on the scale-free R^2, and the scale-free

power of different soft thresholds was evaluated for scale-free scale fit indices and average connectivity (Figure 2A). In this study, $\beta = 5$ and scale-free $R^2 = 0.8$ were chosen as soft threshold powers. A minimum of 50 genes per module was established, with hierarchical clustering via the cutreeDynamic function used to assign genes to the modules. These modules were depicted as a dynamic shear dendrogram, and the module labels were subsequently converted to colour labels for heat map visualisation. Feature genes from each module underwent secondary hierarchical clustering, leading to the merging of highly similar modules into a new module, followed by redrawing of the heatmap (Figure 2B). Hierarchical clustering trees were drawn to show the clustering results of the feature genes of the modules (Figure 2C), and correlation heatmaps were drawn to show the correlations between the different modules (Figure 2D). We then identified 12 modules and calculated and visualised the correlations and p-values between the different modules and traits (Figure 2E). Finally, the genes in the MEturquoise module were selected as alternative genes.

3.3 Screening of co-expressed DEGs and results of GO and KEGG enrichment analysis

The DEGs, genes in the MEturquoise module in WGCNA, were crossed with 8299 extracted ARGs, and the Venn diagram showed that 48 DE-AGs were obtained (Figure 2F). The 48 DE-AGs were analysed for GO and KEGG enrichment, with 438 BPs, 47 CCs, 56 MFs, and 39 KEGGs. These were then ranked from lowest to highest FDR and visualised (Figure 2G). DEGs were significantly enriched in GO terms related to female gonad development, development of primary female sexual characteristics, glycogen biosynthesis, glucan biosynthesis, phosphatidylinositol 3-kinase binding, calcium-dependent protein binding, phosphatidylinositol 3-kinase regulatory subunit binding, insulin receptor substrate binding, etc. (Figure 2H). KEGG enrichment analysis revealed that DE-AGs were associated with pathways such as insulin resistance, type II diabetes mellitus, insulin signalling, regulation of lipolysis in adipocytes, cortisol synthesis and secretion, lipid and atherosclerosis, IL-17 signalling pathway, aldosterone synthesis and secretion, NF-kappa B signalling pathway, Toll-like receptor (TLR) signalling pathway, etc. (Figure 2I). Insulin resistance in GDM impairs glucose metabolism, raising blood glucose levels and triggering metabolic disturbances that can lead to preeclampsia through endothelial dysfunction and inflammation. Factors like lipolysis regulation and cortisol may worsen insulin resistance, linking obesity and stress to GDM and preeclampsia risk. The IL-17 pathway affects vascular health, while lipid metabolism and atherosclerosis connect dyslipidemia to cardiovascular issues in GDM, increasing preeclampsia risk. These pathways illustrate the complex relationship between metabolic dysregulation, inflammation, and vascular health in pregnant women with GDM.

3.4 PPI network

A PPI network of the 48 DE-AGs was constructed using the STRING database (Figure 3A). The top 15 hub genes were identified using the MCC, Degree, EPC, and DMNC algorithms with the CytoHubba plugin. These genes were further refined to 15 DE-AGs by overlapping the results of the four algorithms (Figure 3B).

3.5 Construction and screening of multiple machine learning models for PE with GDM-related DE-AGs

We developed machine learning models, including LASSO, SVM, and RF, utilising the expression features of 48 DE-AGs. All three models showed a low root mean square of residuals (Figures 3C, D). ROC analysis indicated AUC values of 0.834, 0.900, and 0.906 for the LASSO, SVM-RFE, and RF models, respectively (Figure 3E). We employed the LASSO, SVM-RFE, and RF methods to collectively identify hub genes for detecting GDM alongside PE-related DE-AG biomarkers. Using LASSO, 15 variables were screened: *BTG2*, *S100A6*, *PLEKHA1*, *SCARB1*, *COASY*, *DCXR*, *DNM2*, *RHOB*, *SLC23A2*, *SH3BP5*, *RELL1*, *KIAA0319*, *INHBA*, *PLEKHA2*, and *GLA* (Figures 3F–G). Thirty-eight significant variables were obtained by SVM-RFE, including *SH3BP5*, *ERO1L*, *TET3*, *SCARB1*, *INHBA*, *PLEKHA2*, *SOD1*, *EAF1*, *UBE2Q2*, *TRPV6*, *DNM2*, *SLC20A1*, *BTG2*, *ASAH1*, *PPP1R3B*, *PIK3R1*, *GSTA3*, *LYN*, *SLC23A2*, *S100A6*, *ANXA4*, *VTCN1*, *XPO6*, *RAPH1*, *TRAK2*, *FRMD4B*, *GLA*, *RHOB*, *KIAA0319*, *TRAF3*, *TMEM106C*, *DDIT4L*, *PLEKHA1*, *VWA5A*, *RELL1*, *CDC42BPA*, *COASY*, and *NT5E* (Figure 3H). The top 20 features in terms of importance were obtained using the RF model with the average Gini index reduction as an indicator, including *PLEKHA2*, *ERO1L*, *SH3BP5*, *TRPV6*, *DNM2*, *TET3*, *SLC20A1*, *SCARB1*, *INHBA*, *SLC23A2*, *SOD1*, *PIK3R1*, *BTG2*, *COASY*, *S100A6*, *TRAF3*, *ASAH1*, *EAF1*, *UBE2Q2*, and *RAPH1* (Figure 3I). The results obtained using the three machine learning methods and the 15 key genes obtained by the MCC, Degree, EPC, and DMNC algorithms were considered as intersections to obtain four GDM-merged PE-related DE-AGs: *BTG2*, *S100A6*, *SCARB1*, and *INHBA* (Figure 3J). Spearman's correlations between the four biomarkers and their significance were calculated, and correlation heatmaps were generated (Figure 3K).

3.6 Analysis of expression differences and screening identification

Merged_Dataset_GSE75010_GSE24129 was used as the training set to analyse the expression of the four PE with GDM-related DE-AGs. The results showed that the expression of *BTG2* was lower in the PE group than in the control group (Figure 4A), whereas the expression levels of *S100A6*, *SCARB1*, and *INHBA* were higher in the PE group than in the control group (Figures 4B–D).

10.3389/fimmu.2025.1571795

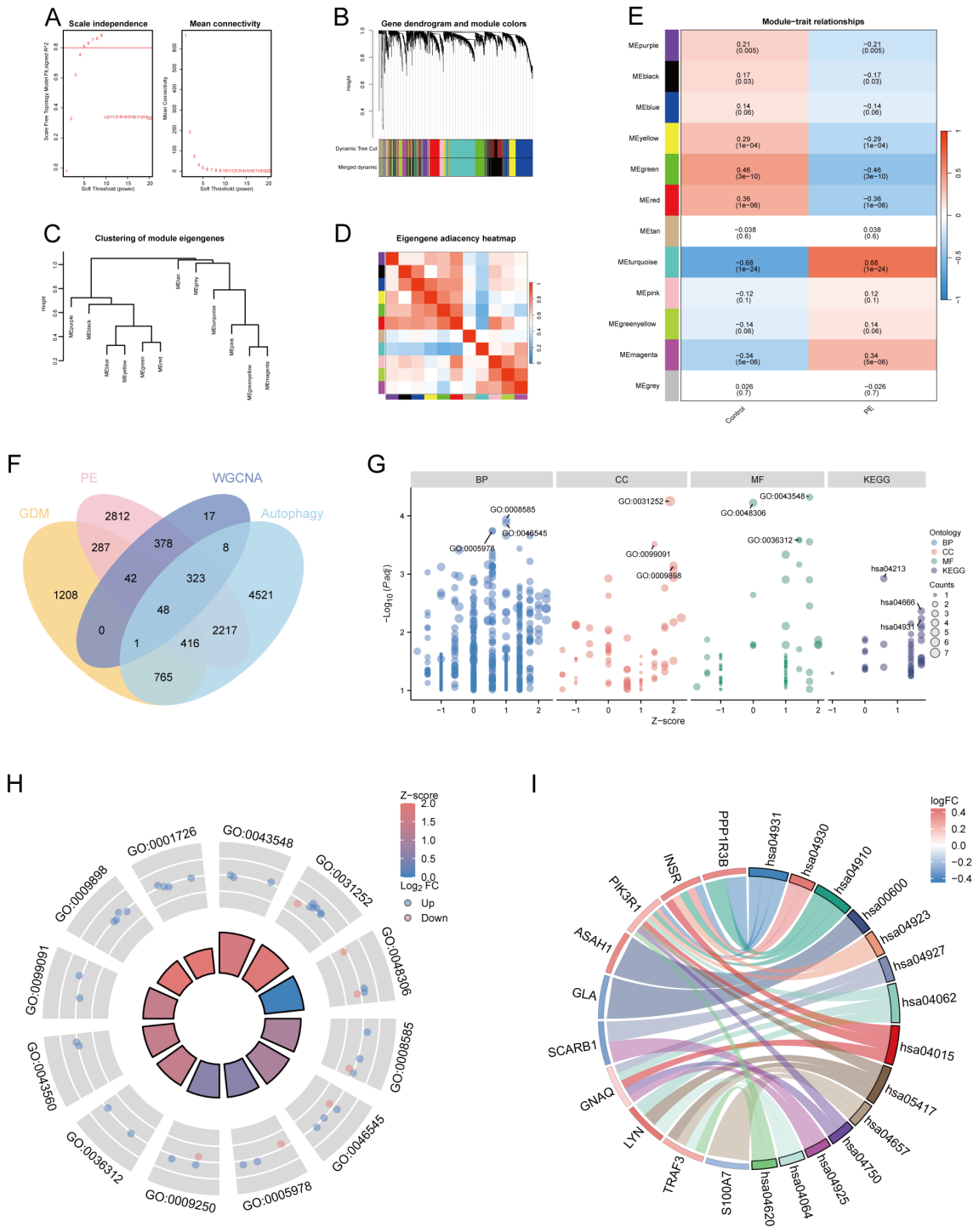

FIGURE 2
WGCNA and functional enrichment analysis of 48 DE-AGs. **(A)** Analysis of scale-free fit index and average connectivity across various soft thresholds. **(B)** Gene clustering tree integrated into a hierarchical clustering heatmap. **(C)** Module feature gene clustering tree. **(D)** Module correlation heatmap. **(E)** Gene-feature correlation heatmap. WGCNA, weighted gene co-expression network analysis. **(F)** Venn diagram plots illustrating the overlap of co-expressed genes among DEGs, MEturquoise module genes in WGCNA, and ARGs. **(G)** Enrichment analysis was conducted using GO and KEGG. GO analysis included BP, CC, and MF. **(H)** Enrichment results of 12 GO entries. **(I)** Enrichment analysis of 14 key KEGG pathways. DE-AG, differentially expressed autophagy-related gene; DEG, differentially expressed gene; WGNCA, weighted gene co-expression network analysis; ARG, autophagy-related gene; GO, Gene Ontology; KEGG, Kyoto Encyclopedia of Genes and Genomes; BP, biological processes; CC, cellular component; MF, molecular function.

10.3389/fimmu.2025.1571795

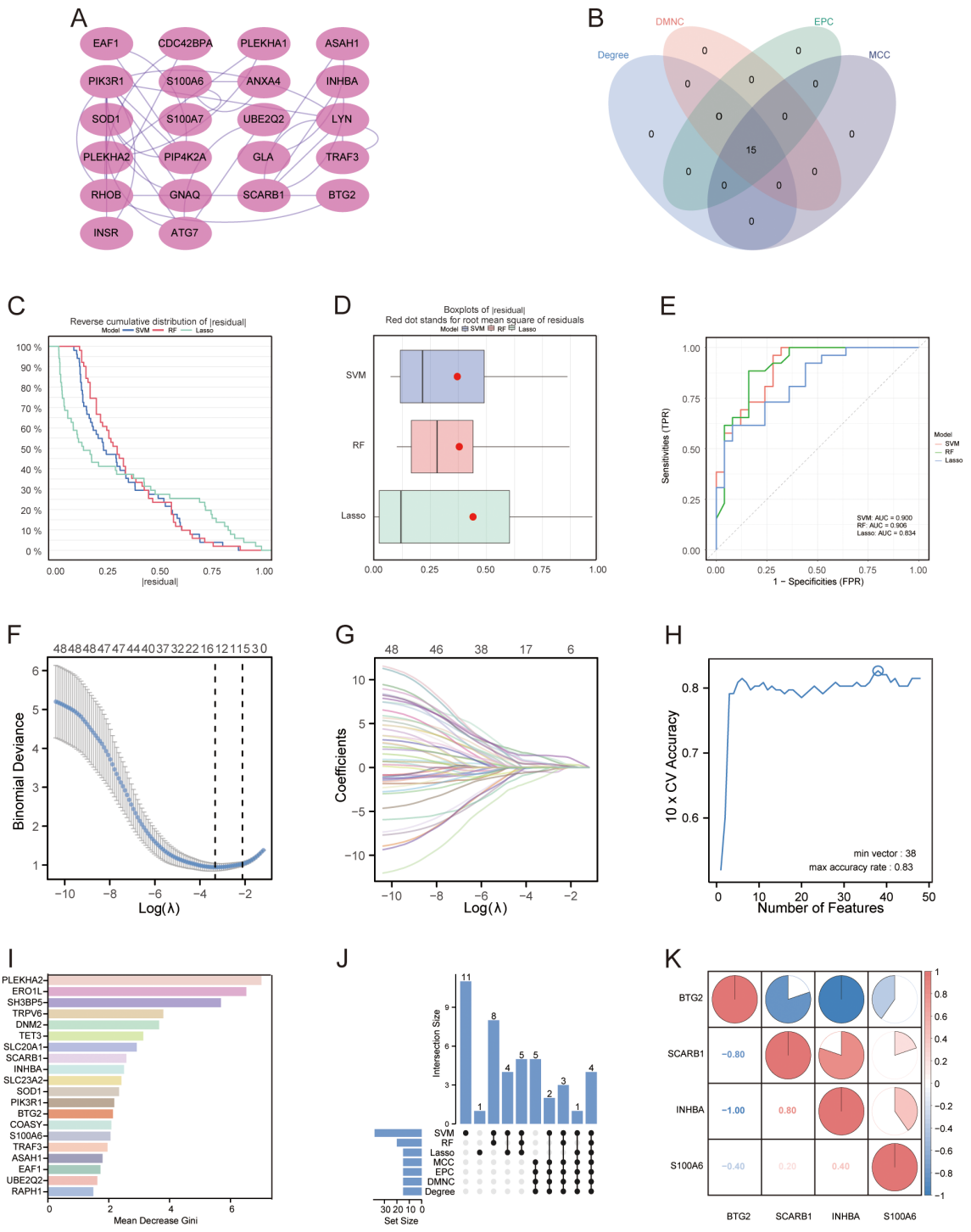

FIGURE 3
PPI networks and machine learning. **(A)** PPI network. Proteins are represented as nodes, and their interactions are depicted as edges. Shading of the node colour indicates the importance of the corresponding protein in the network. **(B)** Venn diagram illustrating the gene count overlap among MCC, Degree, EPC, and DMNC algorithms. **(C, D)** Root mean square of residuals for three machine learning models: LASSO, SVM-RFE, and RF. **(E)** ROC curves of the three machine learning models. **(F)** Cross-validation for parameter selection in LASSO regression. **(G)** LASSO regression for 48 DE-AGs. **(H)** Tenfold cross-validation with SVM-RFE used to identify the optimal feature subset. **(I)** RF algorithm for ranking feature importance based on average Gini index reduction. **(J)** Upset diagram plots illustrating the gene counts across LASSO, SVM, RF, MCC, Degree, EPC, and DMNC methods. **(K)** Correlation heatmap: used to identify correlations between four GDM with PE-related DE-AGs. PPI, protein-protein interaction; LASSO, least absolute shrinkage and selection operator; SVM-RFE, support vector machine-based recursive feature elimination, RF, random forest; GDM, gestational diabetes mellitus; PE, preeclampsia.

The diagnostic performances of the four genes were evaluated using ROC curves. Analysis of the GSE103552 dataset revealed that *BTG2*, *S100A6*, *SCARB1*, and *INHBA* each achieved an AUC exceeding 0.7, indicating a high predictive accuracy (Figures 4E–H). In Merged_Dataset_GSE75010_GSE24129, the AUCs of *BTG2*, *S100A6*, *SCARB1*, and *INHBA* were higher than 0.7, and their predictive ability was highly accurate (Figures 4I–L). External validation utilised the GSE154414 and GSE30186 datasets with diagnostic models assessed via ROC curves. The analysis of independent external datasets GSE154414 and GSE30186 validated the significant diagnostic value of *BTG2*, *S100A6*, *SCARB1*, and *INHBA*, each demonstrating AUCs exceeding 0.6, which aligned with the predicted outcomes (Figures 4M–T). Subsequently, GO and KEGG enrichment analyses were conducted (Figures 5A, B). In the KEGG enrichment analysis, *SCARB1* was mainly enriched in ovarian steroidogenesis, cortisol synthesis and secretion, and aldosterone synthesis and secretion (Figure 5B). In GSEA, *S100A6* and *INHBA* were mainly enriched in NABA_MATRISOME and NABA_MATRISOME_ASSOCIATED (Figures 5C, D). *INHBA* was predominantly associated with KEGG_CYTOKINE_CYTOKINE_RECEPTOR_INTERACTION and REACTOME_PEPTIDE_HORMONE_METABOLISM (Figures 5E, F).

3.7 Immune cell infiltration and functional analysis

A comparative analysis of immune cell infiltration revealed elevated levels of B cells, cytotoxic cells, dendritic cells, mast cells, NK CD56dim cells, plasmacytoid dendritic cells, T cells, T follicular helper cells, Th17 cells, Th2 cells, and regulatory T cells in the PE group. The levels of activated dendritic cells, CD8+ T cells, immature dendritic cells, macrophages, neutrophils, NK CD56bright cells, NK cells, T helper cells, central memory T cells, effector memory T cells, γδT cells, and Th1 cells decreased (Figure 6A). The correlation coefficient indicates the relationship between two variables: positive for direct correlation and negative for inverse correlation. The absolute value signifies the correlation's strength, with 0.3-0.5 as weak, 0.5-0.8 as moderate, and 0.8–1 as strong. A *p*-value less than 0.05 denotes statistical significance. In PE cases, the correlation lollipop plots indicated that the four DE-AGs exhibited varying degrees of correlation with multiple immune cell types (Figures 6B–E). The expression of *BTG2* was positively correlated with the infiltration levels of Th1 and T cells (Figure 6B), with correlation coefficients (R) of 0.433 and 0.367, respectively (Supplementary Figures 3A, B); while Th2 cell infiltration levels showed a negative correlation with *BTG2* expression (Figure 6B), with a correlation coefficient (R) of -0.303 (Supplementary Figure 3C). The expression of *S100A6* was positively correlated with the infiltration levels of NK and CD8+ T cells (Figure 6C), with correlation coefficients (R) of 0.373 and 0.365, respectively (Supplementary Figures 3E, F). The expression of *S100A6* was inversely associated with T helper and Th1 cells (Figure 6C), with correlation coefficients (R) of -0.428 and -0.336, respectively (Supplementary Figures 3D, G). The expression of *SCARB1* was positively correlated with the infiltration levels of NK cells and Th17 cells (Figure 6D), with a correlation coefficient R of 0.543 and 0.315 (Supplementary Figures 3H, M). The expression of *SCARB1* was inversely associated with the infiltration levels of macrophages, γδT cells, T helper cells, and T cells (Figure 6D), with correlation coefficients (R) of -0.438, -0.429, -0.411, and -0.320 (Supplementary Figures 3I–L), respectively. A negative correlation was observed between *INHBA* expression and the infiltration levels of Th1 and T cells (Figure 6E), with correlation coefficients (R) of -0.508 and -0.438, respectively (Supplementary Figures 3N, O). There was also a correlation between different types of immune cells (Supplementary Figure 3P).

3.8 Single-cell data pre-processing and clustering annotation

We conducted an extensive single-cell RNA sequencing analysis on the GSE173193 dataset. At a resolution of 0.3, 19 distinct cell clusters were identified (Figure 7A). Bubble plots further showed the expression of signature genes in different cell clusters (Figure 7B). Our analysis identified 11 cell populations: B cells (marker genes were *CD79A*, *CD79B*, *CD19*, *FCER2*), decidual cells (marker genes were *DDK1*, *IGFBP1*, *PRL*), EVT (marker genes were *HLA-G*, *PAPPA2*), granulocyte cells (marker genes *FCGR3B*, *CXCL8*, *MNDA*, *SELL*), macrophages (marker genes *AIF1*, *CD14*, *CD163*, *CD209*, *CD53*, *CSF1R*), monocytes (marker genes *CD14*, *CD300E*, *CD244*, *HLA-DRA*, *CLEC12A*, *FCN1*), myelocytes (marker genes *TCN1*, *CEACAM8*, *S100A8*, *MMP8*, *DEFA4*, *CAMP*), syncytiotrophoblast (SCT, marker genes *CGA*, *CYP19A1*, *GH2*), T/NK cells (marker genes are *CD3G*, *GZMA*, *CD3D*, *TRBC2*, *GIMAP2*, *XCL2*, *GZMK*, *IFNG*, *CCL5*, *SAMD3*), villous cytotrophoblast (VCT, marker gene is *PARP1*), and venous endothelial cells (VECs, marker genes are *CD34*, *CDH5*, *ICAM1*, *PLVAP*). Subsequently, we applied t-SNE for visualisation (Figure 7C). Based on the criteria of |avg_log2 FC|>0 and p_val<0.05, we identified significant differential genes in GDM and PE samples compared with those in normal control samples using the FindMarkers function and presented these differential genes using multi-group volcano plots (Figures 7D, E). Notably, the potential marker genes for GDM versus PE identified in the bulk RNA analysis also showed significant differences in some cell populations in single-cell differential analysis. A significant difference in EVT distribution was observed between the control and disease groups (Figures 7F–G). Therefore, we selected EVT for further in-depth analysis.

3.9 Cell-cell communication

We analysed the cell-cell communication networks between different cell populations in GDM and PE samples using the R package 'CellChat'. Circle plots show the number of interactions and their strength between cell populations in GDM (Figures 8A, B) and PE

10.3389/fimmu.2025.1571795

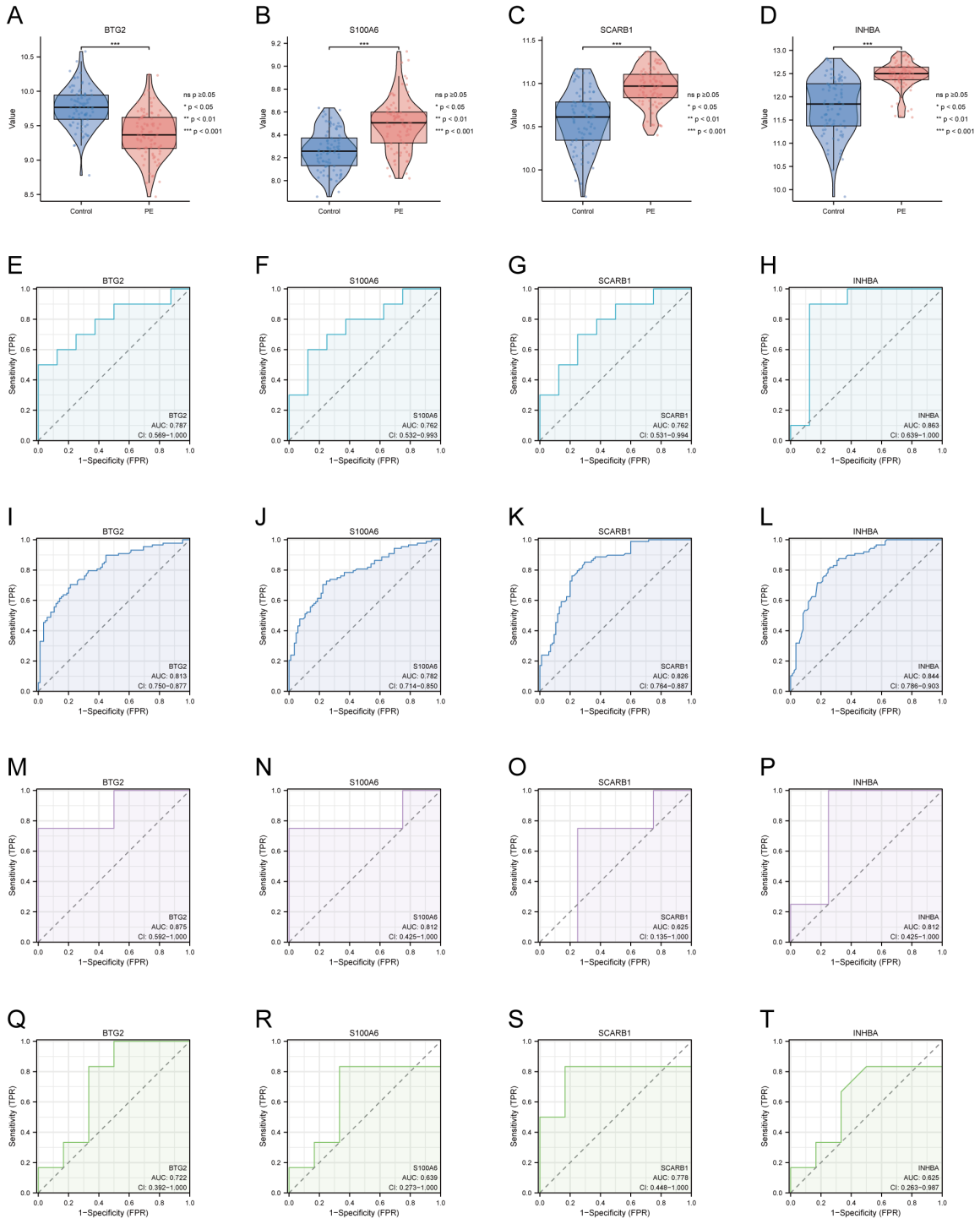

FIGURE 4
Expression of four DE-AGs and ROC validation. **(A–D)** Expression of four DE-AGs: *BTG2* **(A)**, *S100A6* **(B)**, *SCARB1* **(C)**, and *INHBA* **(D)**. **(E–H)** ROC curves for the training set GSE103552. AUC>0.700 for four DE-AGs (*BTG2*, *S100A6*, *SCARB1*, and *INHBA*). *BTG2* **(E)**, *S100A6* **(F)**, *SCARB1* **(G)**, and *INHBA* **(H)**. **(I–L)** ROC curves for the Merged_Dataset_GSE75010_GSE24129 training set. AUC>0.700 for four DE-AGs (*BTG2*, *S100A6*, *SCARB1*, and *INHBA*). *BTG2* **(I)**, *S100A6* **(J)**, *SCARB1* **(K)**, and *INHBA* **(L)**. **(M-P)** ROC curves for validation set GSE15441. AUC>0.600 for four DE-AGs (*BTG2*, *S100A6*, *SCARB1*, and *INHBA*). *BTG2* **(M)**, *S100A6* **(N)**, *SCARB1* **(O)**, and *INHBA* **(P)**. **(F–T)** ROC curves for validation set GSE30186. Note: AUC>0.600 for four DE-AGs (*BTG2*, *S100A6*, *SCARB1*, and *INHBA*). *BTG2* **(Q)**, *S100A6* **(R)**, *SCARB1* **(S)**, and *INHBA* **(T)**. DE-AG, differentially expressed autophagy-related gene; ROC, receiver operating characteristic; AUC, area under the curve; TPR, true positive rate; FPR, false positive rate. Significance levels are denoted as follows: ns $p \geq 0.05$; *$p < 0.05$; **$p < 0.01$; ***$p < 0.001$.

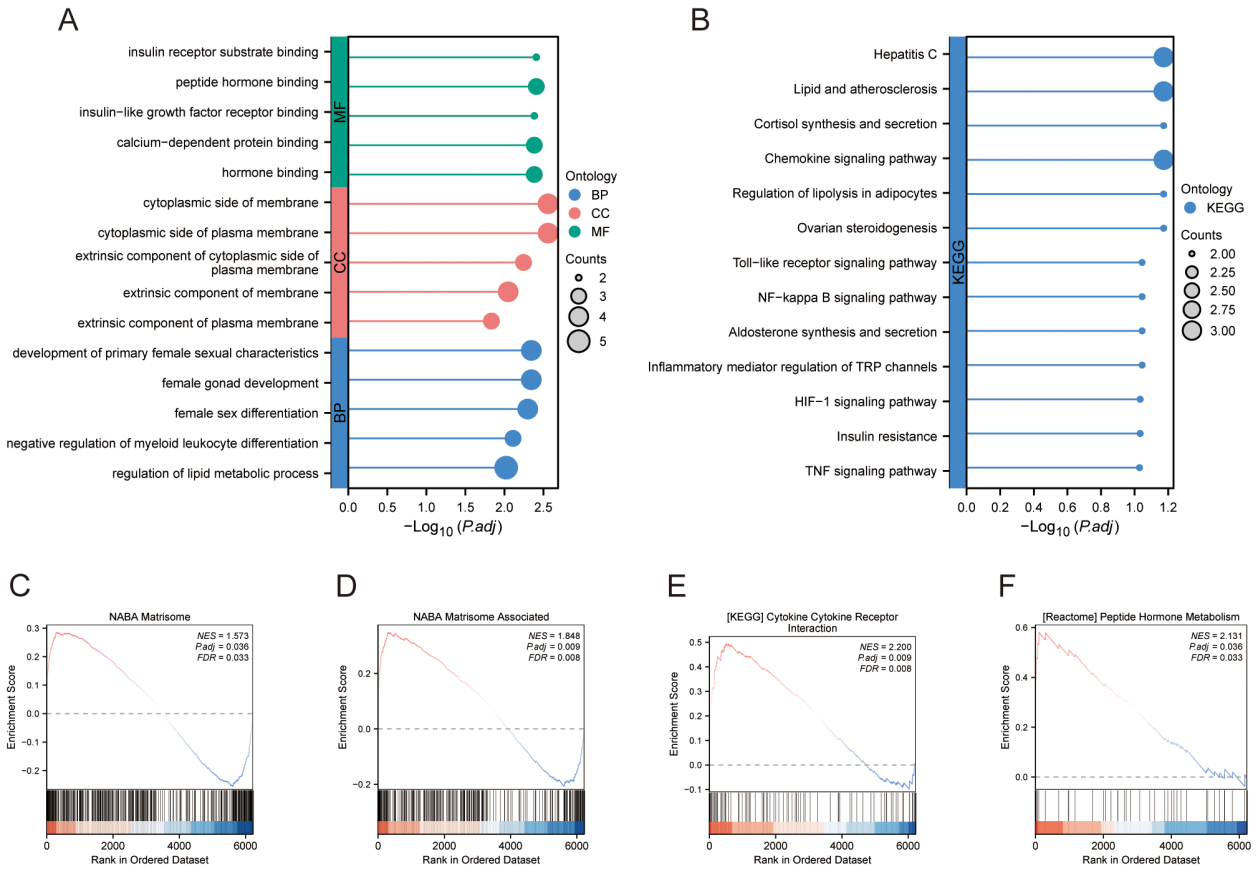

FIGURE 5
Enrichment analysis. **(A)** GO enrichment analysis. **(B)** KEGG enrichment analysis. **(C–F)** GSEA. GO, Gene Ontology; KEGG, Kyoto Encyclopedia of Genes and Genomes; GSEA, gene set enrichment analysis.

(Figures 9A, B). In GDM, chord plots showed communication with other cells through the VEGF (Figures 8C, D), IGF (Figures 8E, F), EGF (Figures 8G, H), and MIF (Figures 8I, J) pathways when EVT acted as a signal sender and receiver. We also visualised communication with other cells via the VEGF (Figures 9C, D), IGF (Figures 9E, F), EGF (Figures 9G, H), and MIF (Figures 9I, J) pathways when EVT acted as a signal transmitter and receiver in PE. The bubble diagrams show the ligand-receptor pairs involved in the communication of EVT cells as signal senders and receivers with other cells in GDM (Figures 8K, L) and PE (Figures 9K, L). As a signal transmitter, EVT communicated with SCT, VCT, decidual cells, and EVT itself via the VEGF pathway in both GDM and PE (Figures 8C, 9C). EVT, as a signal receiver, communicated with macrophages, monocytes, SCT, VCT, B cells, and decidual cells via the VEGF pathway (Figures 8D, 9D). As a signal sender, EVT did not communicate with other cells via the IGF pathway in either GDM or PE (Figures 8E, 9E). EVT as a signal receiver generated communication with macrophages and decidual cells via IGF in GDM, but not with others via the IGF pathway in PE (Figures 8F, 9F). As a signal emitter, EVT did not generate communication with other cells via the EGF pathway in either GDM or PE (Figures 8G, 9G). As a signal receiver, EVT communicated with macrophages, monocytes, and decidual cells via EGF in both GDM and PE (Figures 8H, 9H). As a signal transmitter, EVT communicated with macrophages in both GDM and PE, monocytes, T/NK cells, VECs, and B cells through the MIF pathway in both GDM and PE cells (Figures 8I, 9I). EVT, as a signal receiver, communicated with cells other than myeloid cells through the MIF pathway in GDM but not in PE (Figures 8J, 9J). We then performed a network centrality analysis of cellular communication in the GDM and PE samples, revealing the possible roles of EVT cell populations in the VEGF, IGF, EGF, and MIF pathways in cellular communication in GDM (Supplementary Figures 5A–D) and PE (Supplementary Figures 5G–I). We then comprehensively analysed the roles that different cell populations may play in the overall communication network in GDM (Supplementary Figures 5E, F) and PE (Supplementary Figures 5J, K).

3.10 Proposed temporal trajectory analysis

We further extracted EVT cells from the GDM and PE samples and applied the standard SeuratV5 procedure. In the GDM samples, EVT cells were reclustered into 14 subpopulations (Figure 10A). Scaled bar graphs were plotted to visualise the distinct subpopulations between the GDM group and healthy controls (Figure 10B). In the PE samples, EVT cells were reclustered into 10 subpopulations (Figure 10C), and scaled bar graphs were used to

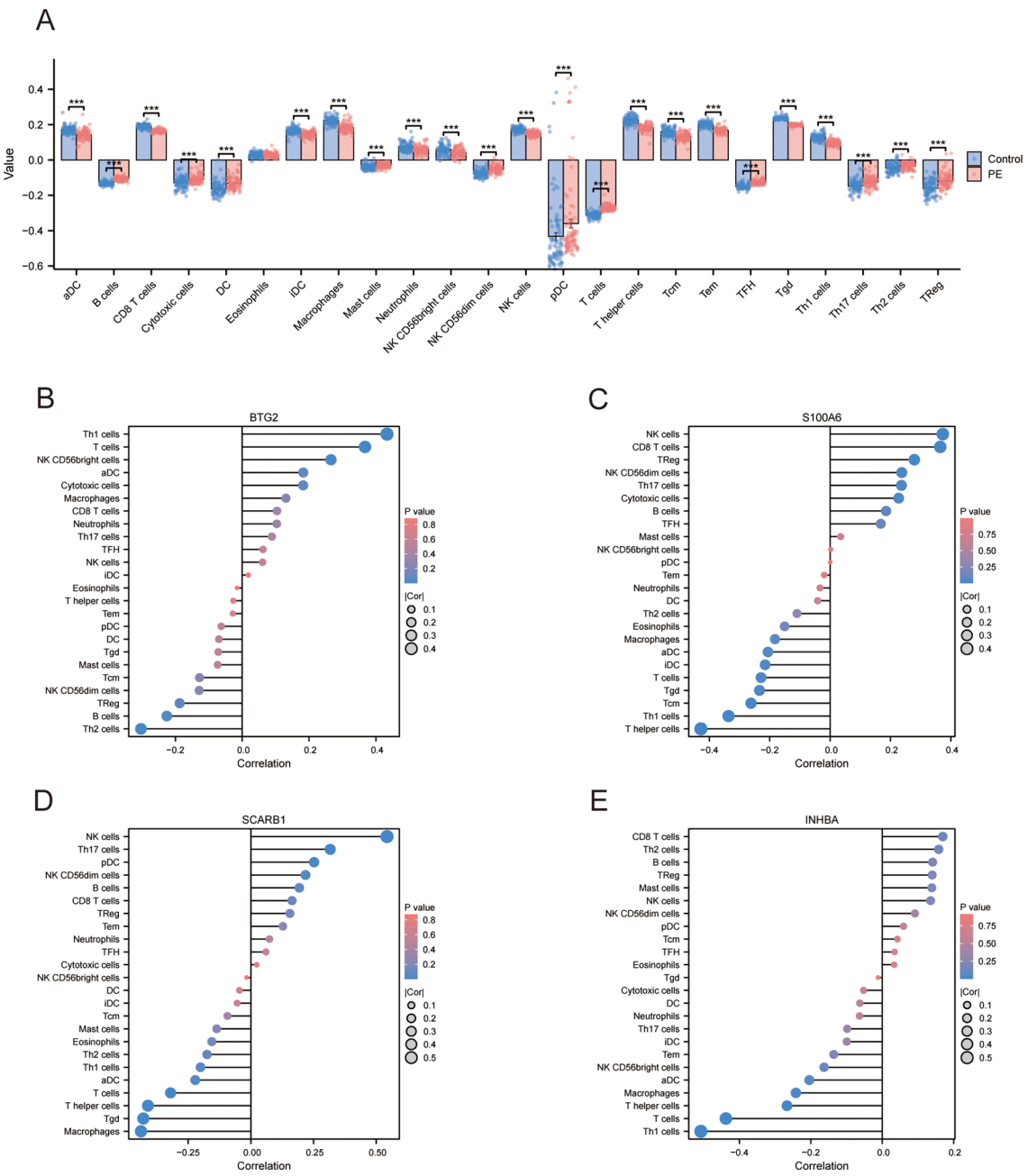

FIGURE 6
Assessment of immune cell infiltration. **(A)** Subgroup comparison plot illustrating immune cell infiltration differences between the two groups determined using the ssGSEA algorithm. Significance level is denoted as follows: *** $p < 0.001$. **(B)** Lollipop plot showing the correlation between *BTG2* and immune cells. **(C)** Lollipop plot illustrating the correlation between *S100A6* and immune cells. **(D)** Lollipop plot illustrating the correlation between *SCARB1* and immune cells. **(E)** Lollipop plot showing the correlation between *INHBA* and immune cells. ssGSEA, single sample gene set enrichment analysis.

visualise significant differences in the subpopulations between the PE group and healthy controls (Figure 10D). Subpopulations 1, 6, and 10 were selected from the GDM samples, and subpopulations 0, 1, and 2 were selected from the PE samples for subsequent analyses. We analysed the proposed time-series trajectories for selected EVT subpopulations in the GDM and PE samples. In the GDM samples, the entire trajectory was divided into three phases (Figure 11A). Figure 11B shows the direction of cell differentiation. The cell density maps along the time axis further demonstrate the distribution and dynamics of EVT during the proposed time course (Figure 11C). We examined the expression changes of four potential biomarkers, *BTG2*, *INHBA*, *S100A6* and *SCARB1*, during the mimetic process and found that *BTG2*, *INHBA*, and *SCARB1* showed large fluctuations during the mimetic process (Figures 11D–F), indicating that these factors could play a crucial role in EVT cell development. We analysed the expression patterns of significantly DEGs in EVT during mimicry and categorised them into four distinct clusters (Figure 11G). We conducted KEGG

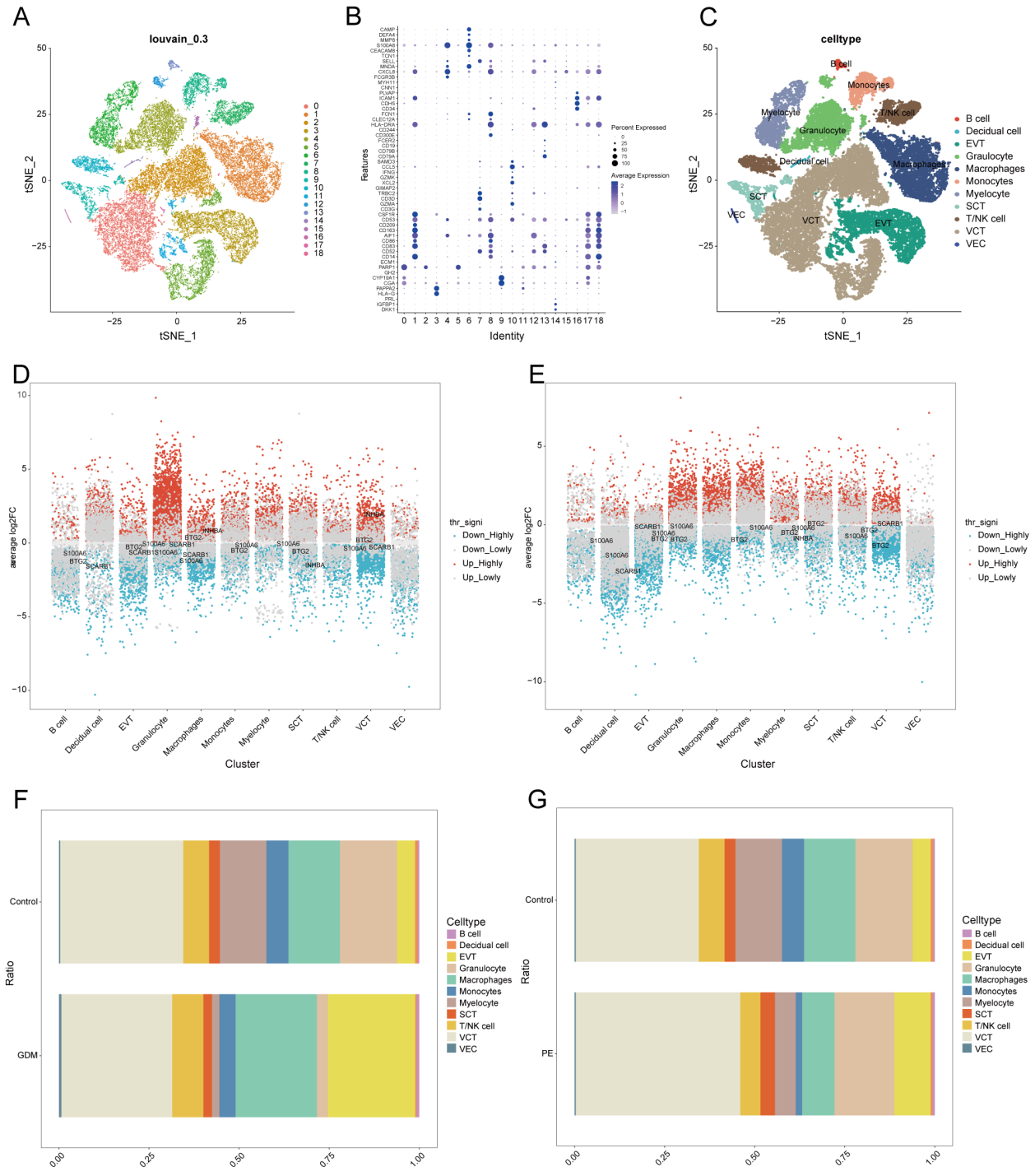

FIGURE 7
Single-cell sample clustering annotation and difference analysis. **(A)** t-SNE plot showing cell clustering results at 0.3 resolution. **(B)** Bubble plots showing marker gene expression in different clusters. **(C)** t-SNE plot after annotation. **(D, E)** Multi-subgroup volcano plots showing differential genes in GDM and PE samples, respectively. **(F, G)** Scale bar plots showing the difference in the proportion of each cell between groups in GDM and PE. t-SNE, t-distributed stochastic neighbour embedding; GDM, gestational diabetes mellitus; PE, preeclampsia.

enrichment analysis on the significantly DEGs, applying thresholds of *p.adj*<0.05 and qvalue<0.25. This analysis identified 33 enriched pathways, the top 30 of which were visualised using a lollipop plot (Figure 12A). For the PE samples, the entire trajectory was divided into five stages (Figure 13A), and Figure 13B shows the direction of cell differentiation. Cell density maps along the time axis further demonstrated the distribution and dynamics of EVT during the mimetic process (Figure 13C). We examined the expression changes of four potential biomarkers, *BTG2*, *INHBA*, *S100A6*, and *SCARB1*, during the mimetic process and found that *BTG2*, *INHBA*,

10.3389/fimmu.2025.1571795

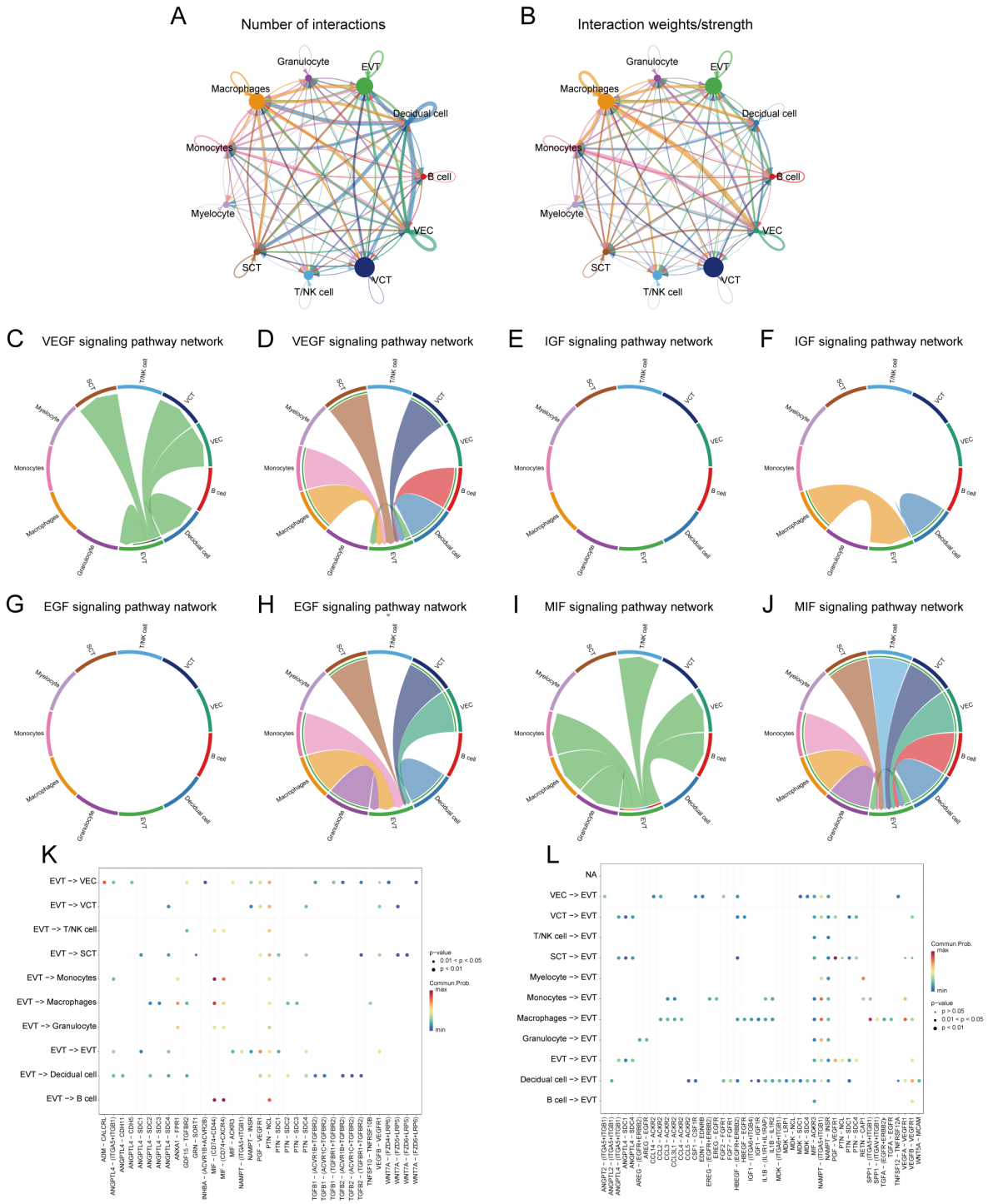

FIGURE 8
Analysis of cellular communication in GDM single-cell samples. **(A, B)** The number of interactions between cell populations and their strength in GDM samples. **(C, D)** Communication between EVT as a signal sender or receiver and other cell populations via the VEGF signalling pathway in GDM samples. **(E, F)** Communication of EVT as a signal sender and receiver via the IGF pathway with other cell populations in GDM samples. **(G, H)** Communication between GDM samples in which EVT acts as a signal sender to or receiver from other cell populations via the EGF pathway. **(I, J)** Communication between GDM samples in which EVT acts as a signal sender/receiver to or from other cell populations via the MIF pathway. **(K, L)** Ligand-receptor pairs are involved in generating communication of EVT cells as signal senders and receivers with other cells in GDM samples. GDM, gestational diabetes mellitus; EVT, extravillous trophoblast; IGF, insulin-like growth hormone; VEGF, vascular endothelial growth factor; EGF, epidermal growth factor; MIF, macrophage migration inhibitory factor.

10.3389/fimmu.2025.1571795

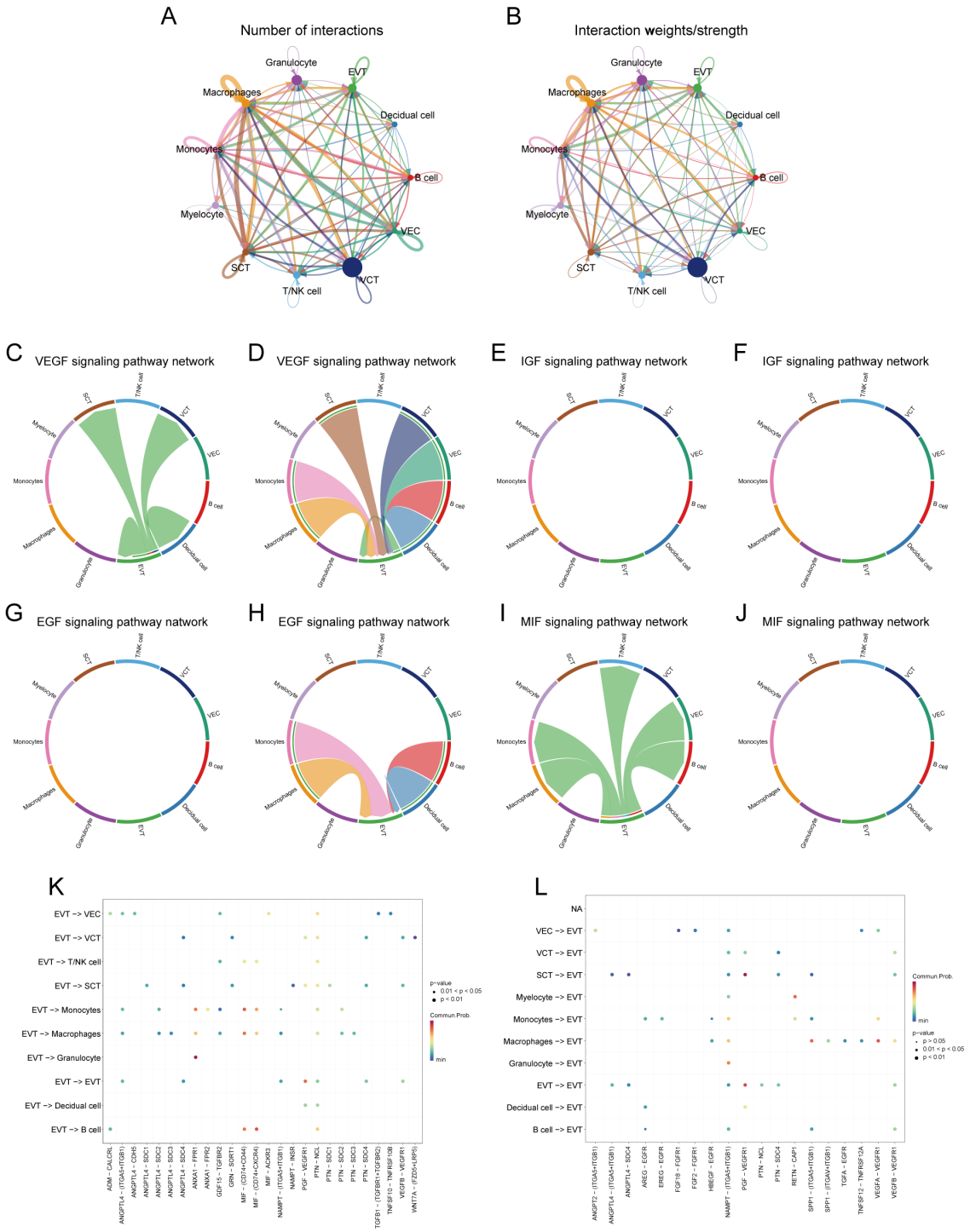

FIGURE 9
Analysis of cellular communication in PE single-cell samples. **(A, B)** Number of interactions between cell populations and their strength in PE samples. **(C, D)** Communication between EVT as a signal sender or receiver and other cell populations through the VEGF signalling pathway in PE samples. **(E, F)** Communication of EVT as a signal sender and receiver via the IGF pathway with other cell populations in PE samples. **(G, H)** Communication between PE samples in which EVT acts as a signal sender to or receiver from other cell populations via the EGF pathway. **(I, J)** Communication between PE samples in which EVT acts as a signal sender/receiver to or from other cell populations via the MIF pathway. **(K, L)** Ligand-receptor pairs are involved in the generation of communication of EVT cells as signal senders or signal receivers with other cells in PE samples. PE, preeclampsia; EVT, extravillous trophoblast; VEGF, vascular endothelial growth factor; IGF, insulin-like growth hormone; EGF, epidermal growth factor; MIF, macrophage migration inhibitory factor.

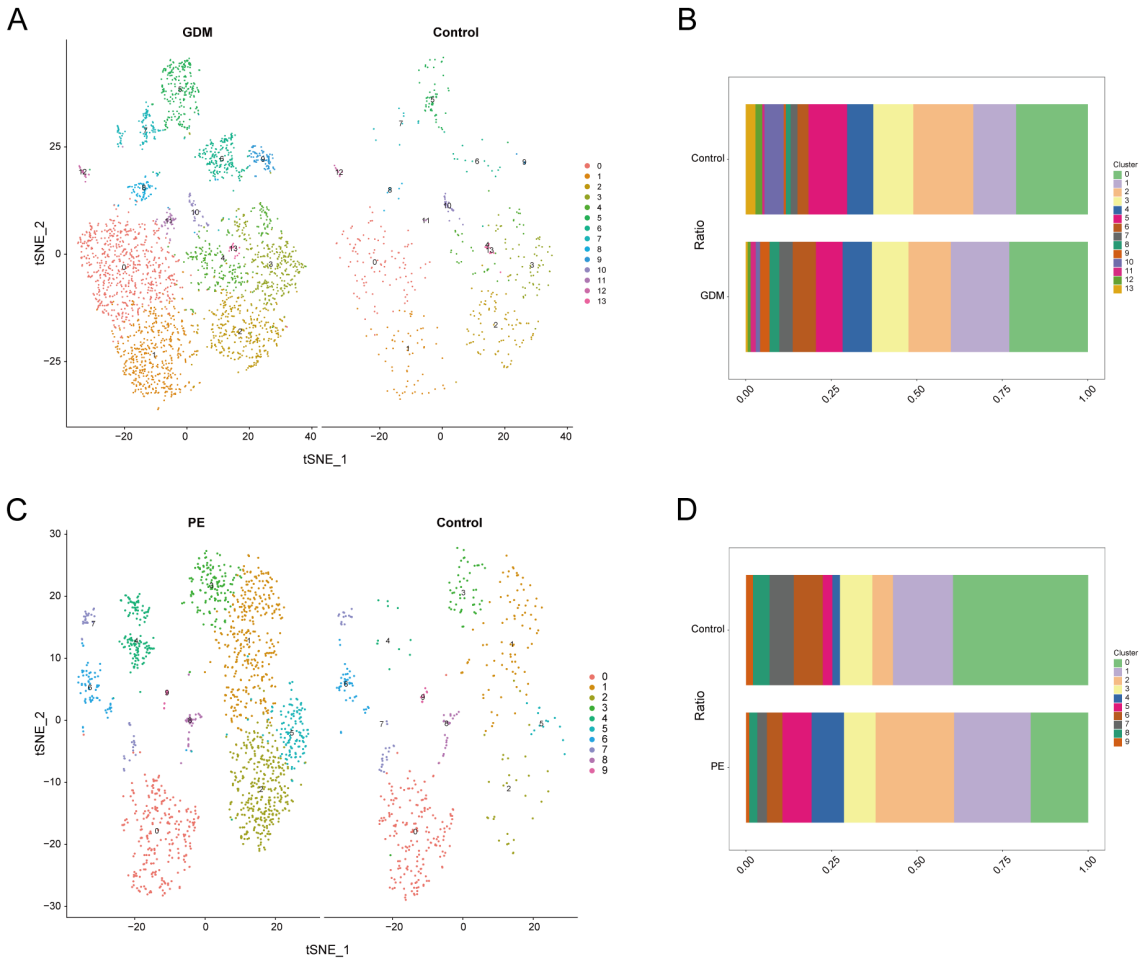

FIGURE 10
Clustering analysis of EVT cell population subpopulations. **(A)** EVT subpopulations of GDM samples. **(B)** Histogram showing the proportion of each EVT subpopulation in GDM samples. **(C)** EVT subpopulations of PE samples. **(D)** Histogram showing the proportion of each EVT subpopulation in PE samples. EVT, extravillous trophoblast; GDM, gestational diabetes mellitus; PE, preeclampsia.

and *SCARB1* showed large fluctuations during the mimetic process (Figures 13D–F), suggesting that they may be important factors during EVT cell development. We analysed the expression patterns of significantly DEGs in EVT during mimicry, categorising these genes into four distinct clusters (Figure 13G). We conducted KEGG enrichment analysis on significantly DEGs, identifying 13 pathways with *p.adj*<0.05 and qvalue<0.25, which were visualised using a lollipop graph (Figure 12B).

3.11 Validation of key genes in PE with GDM

We used RT-qPCR to determine the expression levels of the four key genes in placental samples. The analysis included six samples of PE with GDM and six control samples. Refer to Supplementary Table S1 for the primer sequences. RT-qPCR analysis revealed significantly reduced *BTG2* expression in placental samples from patients with PE and GDM (Figure 14A), and the expression levels of *S100A6*, *SCARB1*, and *INHBA* (Figures 14B–D) were significantly higher in placental samples from patients with PE complicated by GDM than in those from the control group. The significance levels are denoted as follows: $^{**}p < 0.01$, $^{***}p < 0.001$.

4 Discussion

Through comprehensive bioinformatics analysis combining differential expression, WGCNA, and machine learning approaches (LASSO, SVM-RFE, RF), we identified 48 autophagy-related genes (DE-AGs) associated with PE and GDM. Subsequent PPI network analysis and hub gene screening revealed four key candidates: *BTG2* (downregulated), *S100A6*, *SCARB1*, and *INHBA* (all upregulated) in PE with GDM patients compared to controls. While these genes have established roles in other pathologies - *BTG2* in cell cycle regulation (58), *S100A6* in inflammation (59), *SCARB1* in lipid metabolism (60), and *INHBA* in reproductive biology (61) - their specific functions in PE and GDM remain

10.3389/fimmu.2025.1571795

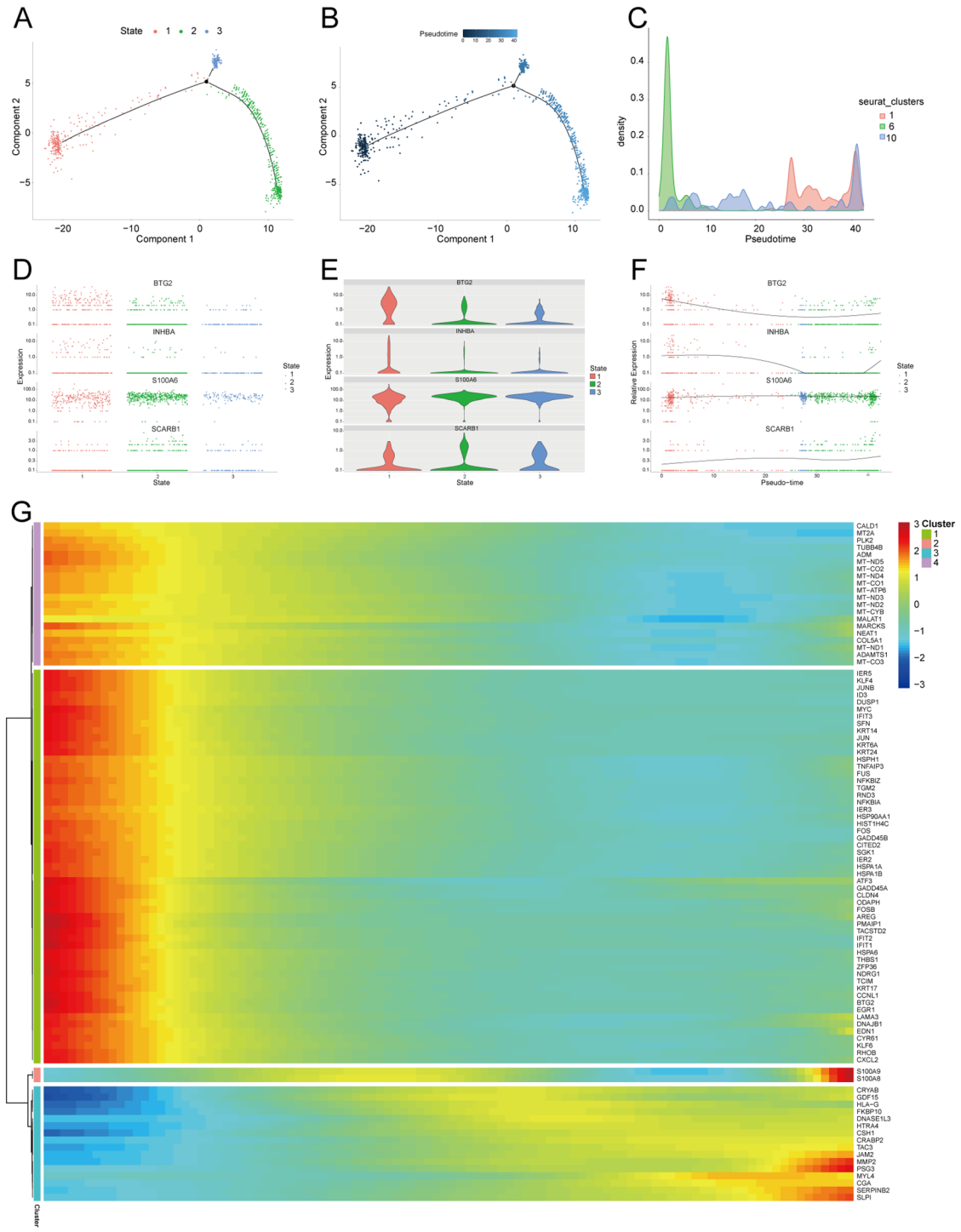

FIGURE 11
Proposed temporal analysis of GDM single-cell samples. **(A)** Three stages of EVT in GDM samples in the proposed temporal trajectory analysis. **(B)** The direction of differentiation and evolution of EVT in GDM samples in the proposed temporal trajectory analysis. **(C)** Cell density plots of EVT in GDM samples along the time axis. **(D, E, F)** Fluctuation of expression of potential biomarkers during EVT mimetic time course in GDM samples. **(G)** Heatmap illustrating expression patterns of significantly DEGs in EVT from GDM samples. GDM, gestational diabetes mellitus; EVT, extravillous trophoblast; DEG, differentially expressed gene.

poorly characterized. This knowledge gap underscores the need for further investigation into these potential biomarkers and their shared molecular mechanisms to improve clinical management of these pregnancy complications.

GO and KEGG analyses of DE-AGs revealed significant enrichment of DE-AGs in autophagy-related pathways including PI3K binding, insulin signaling, NF-kappa B signalling, and TLR signaling. The PI3K pathway serves as a central regulator of cell

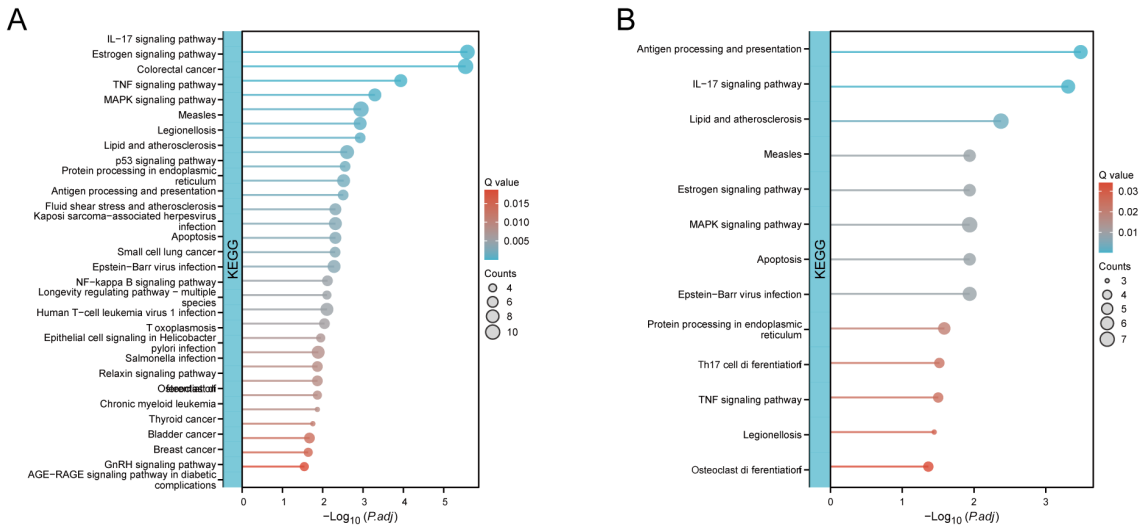

FIGURE 12
KEGG enrichment analysis of significantly DEGs. **(A)** KEGG enrichment analysis conducted on significantly DEGs in GDM samples with EVT during mimicry. **(B)** KEGG enrichment analysis conducted on significantly DEGs in PE samples with EVT during mimicry. KEGG, Kyoto Encyclopedia of Genes and Genomes; DEG, differentially expressed gene; GDM, gestational diabetes mellitus; EVT, extravillous trophoblast; PE, preeclampsia.

growth and metabolism (62), with its activation promoting autophagosome formation (63). Insulin signaling mediates glucose homeostasis (64), while PI3K-dependent Akt phosphorylation activates downstream effectors including NF-κB, a key mediator of inflammatory responses implicated in chronic diseases (65). These pathways exhibit complex cross-regulation - PI3K/Akt activation can suppress NF-κB to enhance autophagy (66), while NF-κB may reciprocally modulate PI3K/Akt activity (67). TLRs initiate immune responses through pathogen recognition and subsequently regulate autophagy via NF-κB and PI3K/Akt/mTOR pathways (68). Notably, our identified DE-AGs functionally intersect with these pathways: *BTG2* modulates both insulin signaling and NF-κB-mediated inflammation (69, 70); *S100A6* participates in TLR signaling (71) *SCARB1* activates PI3K/Akt; and *INHBA* regulates NF-κB-dependent cellular processes (72). These findings position these genes as potential key regulators in PE and GDM pathogenesis through their involvement in these critical pathways.

Enrichment analyses revealed other notable BPs and signalling pathways, including the development of primary female sexual characteristics, glycogen biosynthesis, glucan biosynthesis, calcium-dependent protein binding, and insulin receptor substrate binding. These pathways may contribute significantly to the pathophysiology of PE in GDM. For example, the enrichment of pathways such as insulin resistance and type II diabetes mellitus suggests a key role of metabolic dysregulation in the disease, whereas the enrichment of pathways such as lipid and atherosclerosis emphasises the impact of abnormal lipid metabolism on the development of the disease. Enrichment of the IL-17 signalling pathway, along with aldosterone and cortisol synthesis and secretion, underscores the significance of inflammatory response and endocrine regulation in PE with GDM.

This study utilised ssGSEA to evaluate the variations in immune cell infiltration between patients with PE and normal controls. A significant increase in the infiltration of B cells, cytotoxic cells, dendritic cells, mast cells, NK CD56dim cells, plasmacytoid dendritic cells, T cells, follicular helper T cells, Th17 cells, Th2 cells, and regulatory T cells was observed in the PE group. The infiltration levels of various immune cells, including activated dendritic cells, CD8+ T cells, immature dendritic cells, macrophages, neutrophils, NK CD56bright cells, NK cells, T helper cells, central memory T cells, effector memory T cells, γδT cells, and Th17 cells, were significantly reduced. PE is widely believed to be associated with placental abnormalities resulting in insufficient uterine placental blood flow and subsequent maternal endothelial dysfunction. Endothelial dysfunction is thought to be caused by an imbalance between pro-and antiangiogenic factors, oxidative stress, and excessive inflammatory response (73). Our study confirmed that significant alterations occurred in the immune microenvironment of patients with PE, highlighting the crucial role of the immune system and immune cell-mediated inflammation in the progression of PE (74).

Immune infiltration analyses revealed significant correlations between the four key DE-AGs (*BTG2*, *S100A6*, *SCARB1*, and *INHBA*) and the infiltration levels of several immune cells. *BTG2* expression was positively correlated with Th1 and T cell infiltration but negatively correlated with Th2 cell infiltration. *S100A6* expression positively correlated with NK and CD8+ T cell infiltration and negatively correlated with helper T and Th1 cell infiltration. *SCARB1* expression was positively correlated with macrophage, γδ T cell, helper T cell, and T cell infiltration. *INHBA* expression was negatively correlated with Th1 and T cell infiltration. These findings underscore the significant role of immune cell infiltration in the pathophysiology of PE and

10.3389/fimmu.2025.1571795

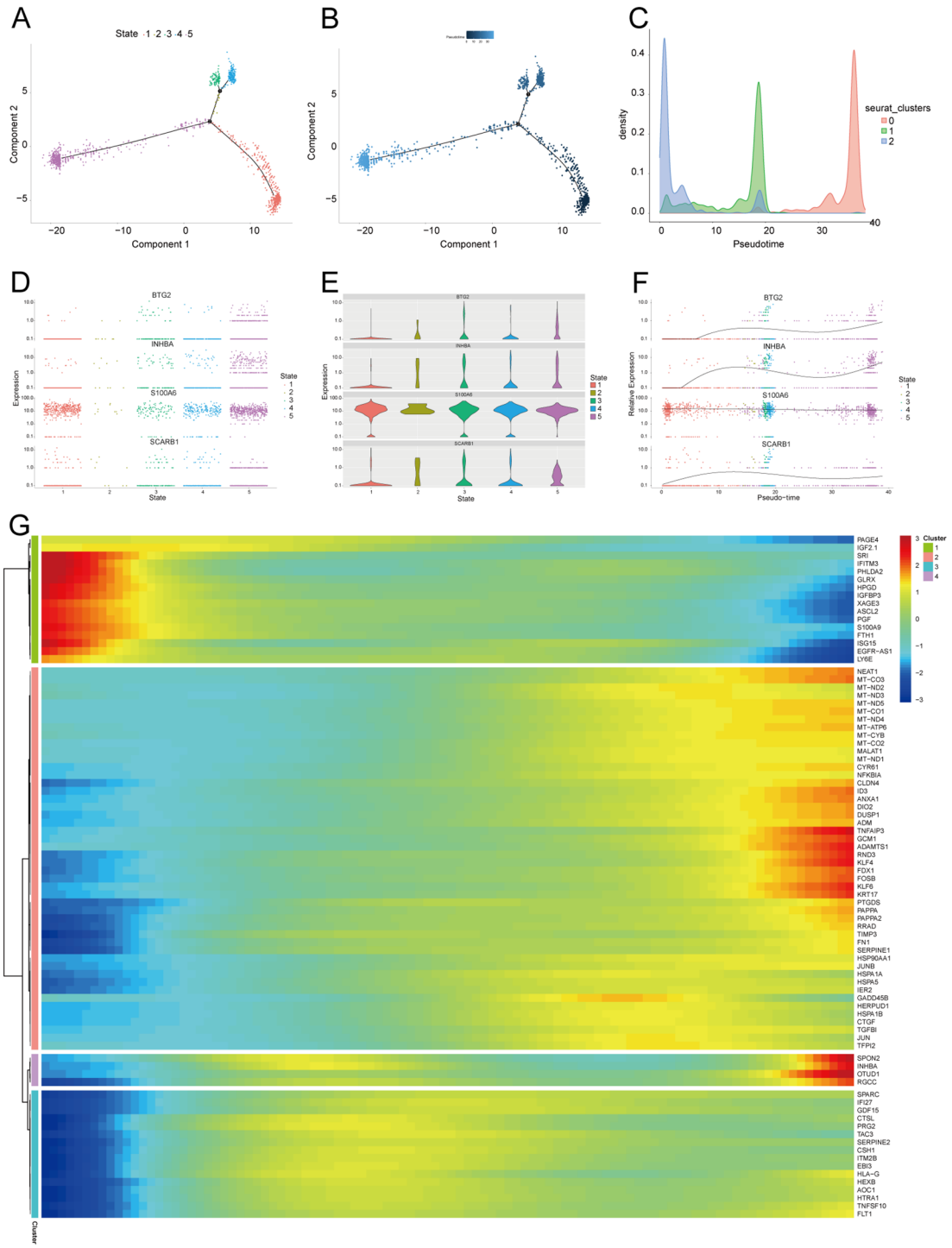

FIGURE 13
Proposed temporal analysis of PE single-cell samples. **(A)** Five stages of EVT in PE samples in the proposed temporal trajectory analysis. **(B)** Direction of differentiation and evolution of EVT in PE samples in the proposed temporal trajectory analysis. **(C)** Cell density plots of EVT in PE samples along the time axis. **(D-G)** Fluctuation of expression of potential biomarkers in PE samples of EVT during the proposed time course. Heatmap illustrating expression patterns of significantly DEGs in EVT from PE samples. PE, preeclampsia; EVT, extravillous trophoblast.

indicate that these key genes may affect the disease by altering the immune microenvironment.

Our study examined the expression patterns and biological roles of four DE-AGs in individual placental cells. Conventional RNA-seq transcriptomic data pose challenges in characterising the heterogeneity of different cell types within the placenta of patients with PE and GDM, and healthy individuals. Technological advancements have led to the development of high-throughput sequencing methods such as scRNA-seq, which offer transcriptomic insights at the cellular level. Based on the scRNA-seq data, we

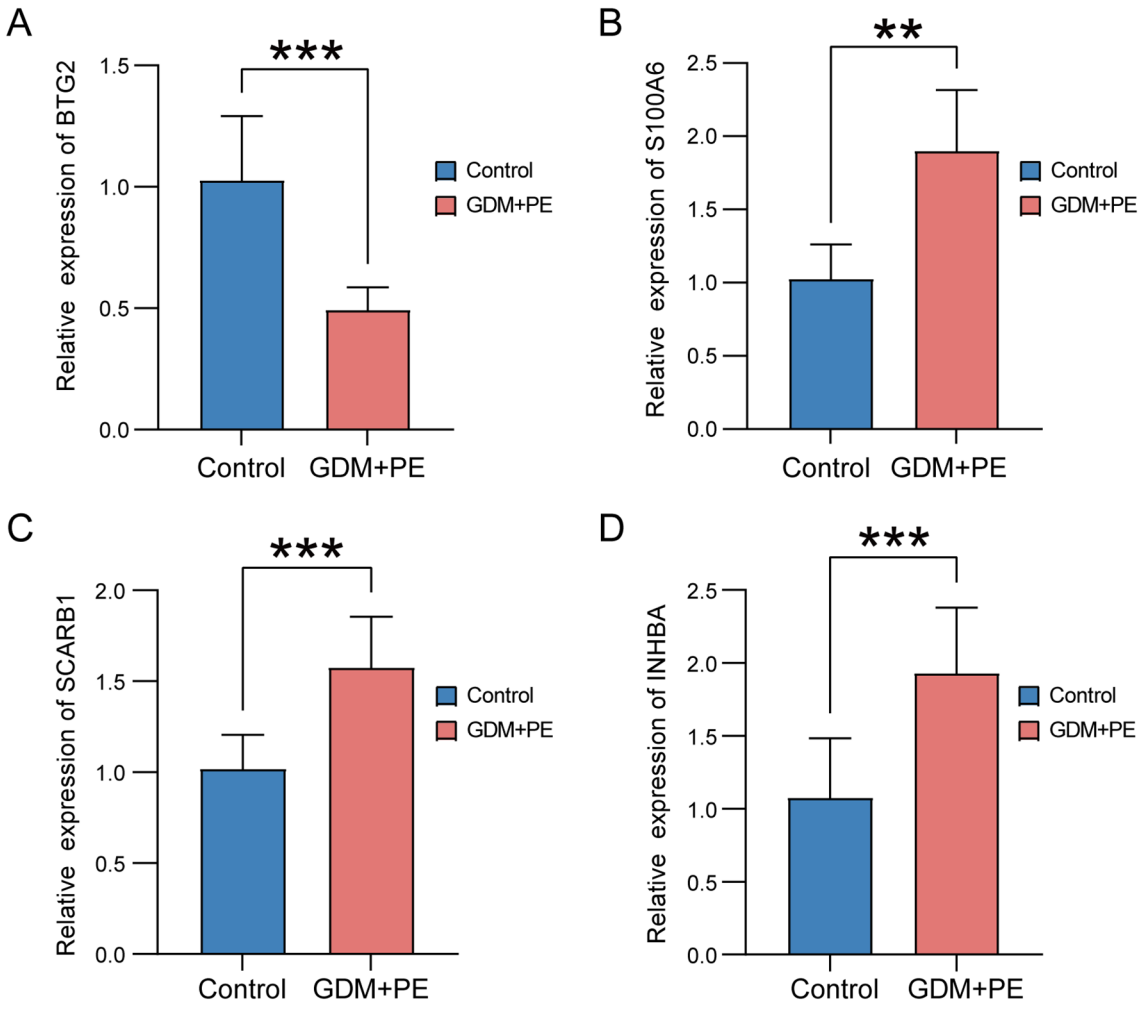

FIGURE 14
Expression of key genes in placental samples from control versus PE with GDM groups. Expression bars depict the levels of key genes *BTG2* **(A)**, *S100A6* **(B)**, *SCARB1* **(C)**, and *INHBA* **(D)** in both control and PE with GDM groups. Significance levels are denoted as follows: $^{**}p < 0.01$; $^{***}p < 0.001$. PE, preeclampsia; GDM, gestational diabetes mellitus.

annotated and identified 11 cellular isoforms. The results showed that *BTG2*, *S100A6*, *SCARB1*, and *INHBA* exhibited specific expression patterns in different cell types within the placenta.

BTG2 exhibited notable differential expression in EVT, which aligned with the trends observed in the bulk RNA analysis. Further refinement of the EVT cell subtypes revealed that *BTG2* was predominantly expressed in specific EVT subpopulations in the placentas of patients with PE and GDM. Functional module scoring and enrichment analysis indicated that EVT subpopulations exhibited elevated autophagic activity and secretion of proinflammatory mediators. GSEA revealed that in patients with GDM and PE, these subpopulations activated pathways related to pro-inflammation and autophagy, influencing cell survival and metabolism regulation.

Intercellular communication analyses revealed that EVT acts as both a signal transmitter and receiver in PE and GDM, communicating with various cells through the VEGF pathway. VEGF is crucial in pregnancy, significantly influencing maternal and foetal health by enhancing placental angiogenesis and improving nutrient and oxygen delivery to both the mother and foetus. Autophagy is crucial for regulating the VEGF pathway. For example, VEGF promotes autophagy by activating adenylate-activated protein kinase, which promotes endothelial cell survival and function. In a hypoxic environment, the upregulation of VEGF expression not only promotes angiogenesis, but also attenuates cellular damage through the autophagy pathway. By analysing the cellular communication of GDM samples, we found that there was intercellular communication between EVT and VECs, and the EVT acted as a signal transmitter to associate with the VEC; however, we did not find the same communication process in PE samples. Compared with EVT in GDM, EVT changed their communication pattern with VEC in PE, and in PE EVT only acted as a signal receiver to associate with VECs, which are not present in GDM, and two diametrically opposed modes of communication between EVTs and VECs were seen in both diseases. Physiological invasion and vascular remodelling of EVT and other BPs are critical for placental health in pregnant mice (13) and this process is influenced by autophagy regulation, which when impaired leads to placental dysplasia under physiological hypoxia in early

pregnancy (75), which further supports the results of our analyses. Our study showed that EVT interacts with macrophages through the VEGF, EGF, and MIF pathways in both PE and GDM, indicating potential immune factor interference in their development. Additionally, macrophage infiltration was observed in PE samples, with significant differences in infiltration proportions between the groups, further implying the influence of immune cells in the progression of PE and GDM. Related studies have confirmed that meconium macrophages can promote the remodelling of uterine spiral arteries through the production of angiogenic factors (76), and the dysregulation of macrophage polarisation may lead to insufficient remodelling of the uterus and insufficient invasion of trophoblast cells, which may trigger a series of pregnancy complications, such as spontaneous abortion, preterm delivery, and PE (77). Therefore, the immune-inflammatory response and related mechanisms in PE with GDM are of great value to be investigated.

Temporal trajectory analysis indicated that three DE-AGs—*BTG2*, *INHBA*, and *SCARB1*— showed notable changes in expression during the mimetic process of EVT in PE combined with GDM. This suggests that they have crucial roles and physiological significance in EVT development. *BTG2*, an anti-proliferative factor involved in cell cycle regulation and apoptosis, may reflect the dynamic changes in EVT cell proliferation and apoptosis in GDM and PE (58, 78). *INHBA* plays a crucial role in cell proliferation, differentiation, and autophagy regulation, and its expression levels indicate its importance in the modulation of EVT cell function (79). Moreover, through the mimetic trajectory, we found the key nodes of EVT in GDM and PE during the mimetic process and performed BEAM analysis on them respectively, finding that *BTG2* was the core gene at the branch in GDM, whereas *INHBA* was the core gene at the branch in PE, which further illustrated the core roles of *BTG2* and *INHBA* in PE merged with GDM. KEGG enrichment analysis of genes with significant differential expression at the branches revealed enrichment in lipid and atherosclerosis and NF-kappa B and TNF signalling pathways in GDM cases. In PE cases, genes were enriched in the lipid atherosclerosis and TNF signalling pathways. Additionally, four DE-AGs (*BTG2*, *INHBA*, *SCARB1*, and *S100A6*) were enriched in these pathways in bulk RNA samples, suggesting a potential link to the underlying mechanism of PE combined with GDM. Dyslipidaemia during pregnancy has been linked to both gestational hypertension and chronic hypertension postpartum (80). Additionally, histone deacetylase influences cytokine expression via NF-κB and HIF-1α pathways, potentially contributing to pregnancy-related disorders like PE (81).

This study has some limitations. First, this study focused solely on mRNA levels, necessitating further research to explore the protein-level alterations of DE-AGs in PE with GDM and their functional implications. Second, the single-cell sequencing component was constrained by a relatively small sample size (n=6), which may limit the generalizability of cell-type-specific immune infiltration patterns. The relatively small clinical sample size may also limit the universality of the results. These methodological boundaries highlight the need for expanded multi-omics validation cohorts in subsequent research. The validation of DE-AGs at the protein level is essential to confirm their functional role in PE combined with GDM. Validation at the protein level may provide insights into the post-transcriptional regulation of these genes and their interactions with other proteins and signalling pathways. Future studies should focus on validating the expression and function of DE-AGs at the protein level using techniques, such as western blotting, immunohistochemistry, and mass spectrometry. Longitudinal studies with larger sample sizes are required to determine the clinical relevance of these findings. Larger sample sizes will provide greater statistical power and allow the identification of other DE-AGs that may be involved in PE associated with GDM, and longitudinal studies will help elucidate temporal changes in DE-AG expression and its relationship to disease progression. These studies will also provide insight into the potential use of DE-AGs as predictive biomarkers for the development of PE with GDM.

5 Conclusion

In summary, our analysis identified key ARGs involved in the pathogenesis of PE with GDM. These findings offer insights into the molecular mechanisms underlying these diseases and help identify potential therapeutic targets. Future research should aim to validate these targets and investigate their clinical applicability in enhancing pregnancy outcomes in patients with PE combined with GDM.

Data availability statement

Publicly available datasets were analyzed in this study. This data can be found here: https://www.ncbi.nlm.nih.gov/geo/.

Ethics statement

The studies involving humans were approved by Research Ethics Committee of the Ruian People's Hospital. The studies were conducted in accordance with the local legislation and institutional requirements. The participants provided their written informed consent to participate in this study.

Author contributions

QW: Data curation, Formal Analysis, Project administration, Software, Writing – original draft. XL: Formal Analysis, Investigation, Methodology, Supervision, Writing – review & editing. WY: Formal Analysis, Validation, Writing – review & editing. LL: Visualization, Writing – review & editing. KY: Investigation, Writing – review & editing. MP: Conceptualization, Funding acquisition, Resources, Writing – review & editing.

Funding

The author(s) declare that financial support was received for the research and/or publication of this article. This study was supported

by the Wenzhou Basic Research Project (No: Y20240606), Xinjiang Uygur Autonomous Region health care research project (BL202436). This study was also supported by the Natural Science Foundation of Xinjiang Uygur Autonomous Region (2022D01C500), Xinjiang Key Laboratory of Neurological Disorder Research (XJDX1711-2253), the Xinjiang Key Laboratory of Neurological Disorder Research.

Acknowledgments

We extend our heartfelt thanks to the patients who generously provided placental samples, making this research possible.

Conflict of interest

The authors declare that the research was conducted in the absence of any commercial or financial relationships that could be construed as a potential conflict of interest.

Generative AI statement

The author(s) declare that no Generative AI was used in the creation of this manuscript.

Publisher's note

Supplementary material

The Supplementary Material for this article can be found online at: https://www.frontiersin.org/articles/10.3389/fimmu.2025.1571795/full#supplementary-material

SUPPLEMENTARY FIGURE 1
Boxplots of the five datasets after cleaning. **(A)** GSE103552. **(B)** GSE30186. **(C)** GSE24129. **(D)** GSE154414. **(E)** GSE75010.

SUPPLEMENTARY FIGURE 2
PCAplots of the five datasets after cleaning. **(A)** GSE103552. **(B)** GSE30186. **(C)** GSE24129. **(D)** GSE154414. **(E)** GSE75010.

SUPPLEMENTARY FIGURE 3
Scatterplot with correlation network heatmap. Scatterplot showing the correlation between *BTG2* **(A–C)**, *S100A6* **(D–G)**, *SCARB1* **(H–M)**, and *INHBA* **(N, O)** and immune cells. **(P)** Heatmap of the correlation network of 24 immune cells.

SUPPLEMENTARY FIGURE 4
Elbow plot for PCA dimensions selection during Harmony normalization.

SUPPLEMENTARY FIGURE 5
(A–D) Network centrality analysis of four signalling pathways (VEGF, IGF, EGF and MIF) in GDM samples. **(E, F)** Possible roles of different cell populations in the overall communication network in GDM samples. **(G–I)** Network centrality analysis of three signalling pathways (VEGF, EGF and MIF) in PE samples. **(J, K)** Possible roles of different cell populations in the overall communication network in PE samples.GDM, gestational diabetes mellitus; PE, preeclampsia; VEGF, vascular endothelial growth factor; IGF, insulin-like growth hormone; MIF, macrophage migration inhibitory factor.

References

1. Gestational hypertension and preeclampsia: ACOG practice bulletin, number 222. *Obstet Gynecol*. (2020) 135:e237–60. doi: 10.1097/AOG.0000000000003891

2. McIntyre HD, Catalano P, Zhang C, Desoye G, Mathiesen ER, Damm P. Gestational diabetes mellitus. *Nat Rev Dis Primers*. (2019) 5:47. doi: 10.1038/s41572-019-0098-8

3. Bi S, Zhang L, Huang L, Li Y, Liang Y, Huang M, et al. Long-term effects of preeclampsia on metabolic and biochemical outcomes in offspring: What can be expected from a meta-analysis? *Obes Rev*. (2022) 23:e13411. doi: 10.1111/obr.13411

4. Damm P, Houshmand-Oeregaard A, Kelstrup L, Lauenborg J, Mathiesen ER, Clausen TD. Gestational diabetes mellitus and long-term consequences for mother and offspring: a view from Denmark. *Diabetologia*. (2016) 59:1396–9. doi: 10.1007/s00125-016-3985-5

5. Wu P, Green M, Myers JE. Hypertensive disorders of pregnancy. *BMJ*. (2023) 381: e071653. doi: 10.1136/bmj-2022-071653

6. de Mendonca E, Fragoso MBT, de Oliveira JM, Xavier JA, Goulart MOF, de Oliveira ACM. Gestational diabetes mellitus: the crosslink among inflammation, nitroxidative stress, intestinal microbiota and alternative therapies. *Antioxidants (Basel)*. (2022) 11:129. doi: 10.3390/antiox11010129

7. McElwain CJ, Tuboly E, McCarthy FP, McCarthy CM. Mechanisms of endothelial dysfunction in pre-eclampsia and gestational diabetes mellitus: windows into future cardiometabolic health? *Front Endocrinol (Lausanne)*. (2020) 11:655. doi: 10.3389/fendo.2020.00655

8. Zhang X, Xiao Y. The association between trimester-specific weight gain and severe preeclampsia/adverse perinatal outcome in gestational diabetes mellitus complicated by preeclampsia: A retrospective case study. *Diabetes Ther*. (2019) 10:725–34. doi: 10.1007/s13300-019-0589-3

9. Weissgerber TL, Mudd LM. Preeclampsia and diabetes. *Curr Diabetes Rep*. (2015) 15:9. doi: 10.1007/s11892-015-0579-4

10. Conde-Agudelo A, Belizan JM. Risk factors for pre-eclampsia in a large cohort of Latin American and Caribbean women. *BJOG*. (2000) 107:75–83. doi: 10.1111/j.1471-0528.2000.tb11582.x.

11. Yang Y, Le Ray I, Zhu J, Zhang J, Hua J, Reilly M. Preeclampsia prevalence, risk factors, and pregnancy outcomes in Sweden and China. *JAMA Netw Open*. (2021) 4: e218401. doi: 10.1001/jamanetworkopen.2021.8401

12. Ichimiya T, Yamakawa T, Hirano T, Yokoyama Y, Hayashi Y, Hirayama D, et al. Autophagy and autophagy-related diseases: A review. *Int J Mol Sci*. (2020) 21:8974. doi: 10.3390/ijms21238974

13. Nakashima A, Tsuda S, Kusabiraki T, Aoki A, Ushijima A, Shima T, et al. Current understanding of autophagy in pregnancy. *Int J Mol Sci*. (2019) 20:2342. doi: 10.3390/ijms20092342

14. Piccinni MP, Robertson SA, Saito S. Editorial: adaptive immunity in pregnancy. *Front Immunol*. (2021) 12:770242. doi: 10.3389/fimmu.2021.770242

15. Luo F, Yue J, Li L, Mei J, Liu X, Huang Y. Narrative review of the relationship between the maternal-fetal interface immune tolerance and the onset of preeclampsia. *Ann Transl Med*. (2022) 10:713. doi: 10.21037/atm-22-2287

16. De Luccia TPB, Pendeloski KPT, Ono E, Mattar R, Pares DBS, Yazaki Sun S, et al. Unveiling the pathophysiology of gestational diabetes: Studies on local and peripheral immune cells. *Scand J Immunol*. (2020) 91:e12860. doi: 10.1111/sji.12860

17. Cui B, Lin H, Yu J, Yu J, Hu Z. Autophagy and the immune response. *Adv Exp Med Biol*. (2019) 1206:595–634. doi: 10.1007/978-981-15-0602-4_27

18. Davis S, Meltzer PS. GEOquery: a bridge between the gene expression omnibus (GEO) and bioConductor. *Bioinformatics*. (2007) 23:1846–7. doi: 10.1093/bioinformatics/btm254

19. Ito K, Murphy D. Application of ggplot2 to pharmacometric graphics. *CPT Pharmacometrics Syst Pharmacol*. (2013) 2:e79. doi: 10.1038/psp.2013.56

20. Ritchie ME, Phipson B, Wu D, Hu Y, Law CW, Shi W, et al. limma powers differential expression analyses for RNA-sequencing and microarray studies. *Nucleic Acids Res*. (2015) 43:e47. doi: 10.1093/nar/gkv007

21. Ye K, Han X, Tian M, Liu L, Gao X, Xia Q, et al. Analysis of human brain RNA-seq data reveals combined effects of 4 types of RNA modifications and 18 types of programmed cell death on Alzheimer's disease. *J Transl Med*. (2025) 23:396. doi: 10.1186/s12967-025-06324-6

22. Zhang X, Shi X, Zhang X, Zhang Y, Yu S, Zhang Y, et al. Repositioning fluphenazine as a cuproptosis-dependent anti-breast cancer drug candidate based on TCGA database. *BioMed Pharmacother*. (2024) 178:117293. doi: 10.1016/j.biopha.2024.117293

23. Ritchie ME, Phipson B, Wu D, Hu Y, Law CW, Shi W, et al. limma powers differential expression analyses for RNA-sequencing and microarray studies. *Nucleic Acids Res*. (2015) 43:e47. doi 10.1093/nar/gkv007

24. Gu Z, Eils R, Schlesner M. Complex heatmaps reveal patterns and correlations in multidimensional genomic data. *Bioinformatics*. (2016) 32:2847–9. doi: 10.1093/bioinformatics/btw313

25. Langfelder P, Horvath S. WGCNA: an R package for weighted correlation network analysis. *BMC Bioinf*. (2008) 9:559. doi: 10.1186/1471-2105-9-559

26. Luo Y, Zhang L, Zhao T. Identification and analysis of cellular senescence-associated signatures in diabetic kidney disease by integrated bioinformatics analysis and machine learning. *Front Endocrinol (Lausanne)*. (2023) 14:1193228. doi: 10.3389/fendo.2023.1193228

27. Kanehisa M, Goto S. KEGG: kyoto encyclopedia of genes and genomes. *Nucleic Acids Res*. (2000) 28:27–30. doi: 10.1093/nar/28.1.27

28. Kanehisa M. Toward understanding the origin and evolution of cellular organisms. *Protein Sci*. (2019) 28:1947–51. doi: 10.1002/pro.3715

29. Kanehisa M, Furumichi M, Sato Y, Kawashima M, Ishiguro-Watanabe M. KEGG for taxonomy-based analysis of pathways and genomes. *Nucleic Acids Res*. (2023) 51:D587–92. doi: 10.1093/nar/gkac963

30. Yu G, Wang LG, Han Y, He QY. clusterProfiler: an R package for comparing biological themes among gene clusters. *OMICS*. (2012) 16:284–7. doi: 10.1089/omi.2011.0118

31. Walter W, Sanchez-Cabo F, Ricote M. GOplot: an R package for visually combining expression data with functional analysis. *Bioinformatics*. (2015) 31:2912–4. doi: 10.1093/bioinformatics/btv300

32. Huang da W, Sherman BT, Lempicki RA. Bioinformatics enrichment tools: paths toward the comprehensive functional analysis of large gene lists. *Nucleic Acids Res*. (2009) 37:1–13. doi: 10.1093/nar/gkn923

33. Szklarczyk D, Gable AL, Nastou KC, Lyon D, Kirsch R, Pyysalo S, et al. The STRING database in 2021: customizable protein-protein networks, and functional characterization of user-uploaded gene/measurement sets. *Nucleic Acids Res*. (2021) 49:D605–12. doi: 10.1093/nar/gkaa1074

34. Smoot ME, Ono K, Ruscheinski J, Wang PL, Ideker T. Cytoscape 2.8: new features for data integration and network visualization. *Bioinformatics*. (2011) 27:431–2. doi: 10.1093/bioinformatics/btq675

35. Chin CH, Chen SH, Wu HH, Ho CW, Ko MT, Lin CY. cytoHubba: identifying hub objects and sub-networks from complex interactome. *BMC Syst Biol*. (2014) 8 Suppl 4:S11. doi: 10.1186/1752-0509-8-S4-S11

36. Robin X, Turck N, Hainard A, Tiberti N, Lisacek F, Sanchez JC, et al. pROC: an open-source package for R and S+ to analyze and compare ROC curves. *BMC Bioinf*. (2011) 12:77. doi: 10.1186/1471-2105-12-77

37. Balasescu E, Ion DA, Cioplea M, Zurac S. Caspases, cell death and diabetic nephropathy. *Rom J Intern Med*. (2015) 53:296–303. doi: 10.1515/rjim-2015-0038

38. Yang F, Mao KZ. Robust feature selection for microarray data based on multicriterion fusion. *IEEE/ACM Trans Comput Biol Bioinform*. (2011) 8:1080–92. doi: 10.1109/TCBB.2010.103

39. Guyon I, Weston J, Barnhill S, Vapnik V. Gene selection for cancer classification using support vector machines. *Mach Learn*. (2002) 46:389–422. doi: 10.1023/A:1012487302797

40. Pandey VK, Mathur A, Kakkar P. Emerging role of Unfolded Protein Response (UPR) mediated proteotoxic apoptosis in diabetes. *Life Sci*. (2019) 216:246–58. doi: 10.1016/j.lfs.2018.11.041

41. Ambroise C, McLachlan GJ. Selection bias in gene extraction on the basis of microarray gene-expression data. *Proc Natl Acad Sci U.S.A*. (2002) 99:6562–6. doi: 10.1073/pnas.102102699

42. Musolf AM, Holzinger ER, Malley JD, Bailey-Wilson JE. What makes a good prediction? Feature importance and beginning to open the black box of machine learning in genetics. *Hum Genet*. (2022) 141:1515–28. doi: 10.1007/s00439-021-02402-z

43. Li S, Li M, Wu J, Li Y, Han J, Cao W, et al. Development and validation of a routine blood parameters-based model for screening the occurrence of retinal detachment in high myopia in the context of PPPM. *EPMA J*. (2023) 14:219–33. doi: 10.1007/s13167-023-00319-3

44. Subramanian A, Tamayo P, Mootha VK, Mukherjee S, Ebert BL, Gillette MA, et al. Gene set enrichment analysis: a knowledge-based approach for interpreting genome-wide expression profiles. *Proc Natl Acad Sci U.S.A*. (2005) 102:15545–50. doi: 10.1073/pnas.0506580102

45. Chen Y, Feng Y, Yan F, Zhao Y, Zhao H, Guo Y. A novel immune-related gene signature to identify the tumor microenvironment and prognose disease among patients with oral squamous cell carcinoma patients using ssGSEA: A bioinformatics and biological validation study. *Front Immunol*. (2022) 13:922195. doi: 10.3389/fimmu.2022.922195

46. Bindea G, Mlecnik B, Tosolini M, Kirilovsky A, Waldner M, Obenauf AC, et al. Spatiotemporal dynamics of intratumoral immune cells reveal the immune landscape in human cancer. *Immunity*. (2013) 39:782–95. doi: 10.1016/j.immuni.2013.10.003

47. Yang Y, Guo F, Peng Y, Chen R, Zhou W, Wang H, et al. Transcriptomic profiling of human placenta in gestational diabetes mellitus at the single-cell level. *Front Endocrinol (Lausanne)*. (2021) 12:679582. doi: 10.3389/fendo.2021.679582

48. Zhang B, Zhang F, Lu F, Wang J, Zhou W, Wang H, et al. Reduced cell invasion may be a characteristic of placental defects in pregnant women of advanced maternal age at single-cell level. *J Zhejiang Univ Sci B*. (2022) 23:747–59. doi: 10.1631/jzus.B2101024

49. Stuart T, Butler A, Hoffman P, Hafemeister C, Papalexi E, Mauck WM 3rd, et al. Comprehensive integration of single-cell data. *Cell*. (2019) 177:1888–1902 e21. doi: 10.1016/j.cell.2019.05.031

50. Becker WR, Nevins SA, Chen DC, Chiu R, Horning AM, Guha TK, et al. Single-cell analyses define a continuum of cell state and composition changes in the Malignant transformation of polyps to colorectal cancer. *Nat Genet*. (2022) 54:985–95. doi: 10.1038/s41588-022-01088-x

51. Korsunsky I, Millard N, Fan J, Slowikowski K, Zhang F, Wei K, et al. Fast, sensitive and accurate integration of single-cell data with Harmony. *Nat Methods*. (2019) 16:1289–96. doi: 10.1038/s41592-019-0619-0

52. Pu W, Shi X, Yu P, Zhang M, Liu Z, Tan L, et al. Single-cell transcriptomic analysis of the tumor ecosystems underlying initiation and progression of papillary thyroid carcinoma. *Nat Commun*. (2021) 12:6058. doi: 10.1038/s41467-021-26343-3

53. Ramachandran P, Dobie R, Wilson-Kanamori JR, Dora EF, Henderson BEP, Luu NT, et al. Resolving the fibrotic niche of human liver cirrhosis at single-cell level. *Nature*. (2019) 575:512–8. doi: 10.1038/s41586-019-1631-3

54. Jin S, Guerrero-Juarez CF, Zhang L, Chang I, Ramos R, Kuan CH, et al. Inference and analysis of cell-cell communication using CellChat. *Nat Commun*. (2021) 12:1088. doi: 10.1038/s41467-021-21246-9

55. Hou J, Yang Y, Han X. Machine learning and single-cell analysis identify molecular features of IPF-associated fibroblast subtypes and their implications on IPF prognosis. *Int J Mol Sci*. (2023) 25:94. doi: 10.3390/ijms25010094

56. Qiu X, Hill A, Packer J, Lin D, Ma YA, Trapnell C. Single-cell mRNA quantification and differential analysis with Census. *Nat Methods*. (2017) 14:309–15. doi: 10.1038/nmeth.4150

57. Zhang W, Zhang J, Jiao D, Tang Q, Gao X, Li Z, et al. Single-cell RNA sequencing reveals a unique fibroblastic subset and immune disorder in lichen sclerosus urethral stricture. *J Inflammation Res*. (2024) 17:5327–46. doi: 10.2147/JIR.S466317

58. Wang J, Li H, Wang L, Zhang J, Li M, Qiao L, et al. Transcriptomic analyses reveal B-cell translocation gene 2 as a potential therapeutic target in ovarian cancer. *Front Oncol*. (2021) 11:681250. doi: 10.3389/fonc.2021.681250

59. Zhang XF, Ma JX, Wang YL, Ma XL. Calcyclin (S100A6) attenuates inflammatory response and mediates apoptosis of chondrocytes in osteoarthritis via the PI3K/AKT pathway. *Orthop Surg*. (2021) 13:1094–101. doi: 10.1111/os.12990

60. Liu J, Gillard BK, Yelamanchili D, Gotto AM Jr., Rosales C, Pownall HJ. High free cholesterol bioavailability drives the tissue pathologies in scarb1(-/-) mice. *Arterioscler Thromb Vasc Biol*. (2021) 41:e453–67. doi: 10.1161/ATVBAHA.121.316535

61. Han Y, Jiang T, Shi J, Liu A, Liu L. Review: Role and regulatory mechanism of inhibin in animal reproductive system. *Theriogenology*. (2023) 202:10–20. doi: 10.1016/j.theriogenology.2023.02.016

62. Mao B, Yuan W, Wu F, Yan Y, Wang B. Autophagy in hepatic ischemia-reperfusion injury. *Cell Death Discov*. (2023) 9:115. doi: 10.1038/s41420-023-01387-0

63. Birgisdottir AB, Mouilleron S, Bhujabal Z, Wirth M, Sjottem E, Evjen G, et al. Members of the autophagy class III phosphatidylinositol 3-kinase complex I interact with GABARAP and GABARAPL1 via LIR motifs. *Autophagy*. (2019) 15:1333–55. doi: 10.1080/15548627.2019.1581009

64. Sheibani M, Jalali-Farahani F, Zarghami R, Sadrai S. Insulin signaling pathway model in adipocyte cells. *Curr Pharm Des*. (2023) 29:37–47. doi: 10.2174/1381612829666221214122802

65. Benchoula K, Parhar IS, Wong EH. The crosstalk of hedgehog, PI3K and Wnt pathways in diabetes. *Arch Biochem Biophys*. (2021) 698:108743. doi: 10.1016/j.abb.2020.108743

66. Hong JM, Moon JH, Oh YM, Park SY. Calcineurin, calcium-dependent serine-threonine phosphatase activation by prion peptide 106–126 enhances nuclear factor-kappaB-linked proinflammatory response through autophagy pathway. *ACS Chem Neurosci*. (2021) 12:3277–83. doi: 10.1021/acschemneuro.1c00453

67. Liu J, Zhu Q, Pan Y, Hao S, Wang Z, Cui C, et al. Electroacupuncture alleviates intrauterine adhesion through regulating autophagy in rats. *Mol Hum Reprod*. (2023) 29:gaad037. doi: 10.1093/molehr/gaad037

68. White J, Suklabaidya S, Vo MT, Choi YB, Harhaj EW. Multifaceted roles of TAX1BP1 in autophagy. *Autophagy*. (2023) 19:44–53. doi: 10.1080/15548627.2022.2070331

69. Pan B, Teng Y, Wang R, Chen D, Chen H. Deciphering the molecular nexus of BTG2 in periodontitis and diabetic kidney disease. *BMC Med Genomics*. (2024) 17:152. doi: 10.1186/s12920-024-01915-6

70. Liu Y, Zou H, Xie Q, Zou L, Kong R, Mao B. Ribonucleic acid-binding protein CPSF6 promotes glycolysis and suppresses apoptosis in hepatocellular carcinoma cells by inhibiting the BTG2 expression. *BioMed Eng Online*. (2021) 20:67. doi: 10.1186/s12938-021-00903-6

71. Durham KK, Kluck G, Mak KC, Deng YD, Trigatti BL. Treatment with apolipoprotein A1 protects mice against doxorubicin-induced cardiotoxicity in a scavenger receptor class B, type I-dependent manner. *Am J Physiol Heart Circ Physiol*. (2019) 316:H1447–57. doi: 10.1152/ajpheart.00432.2018

72. Zhang Y, Yan S, Li Y, Zhang J, Luo Y, Li P, et al. Inhibin betaA is an independent prognostic factor that promotes invasion via Hippo signaling in non–small cell lung cancer. *Mol Med Rep*. (2021) 24:789. doi: 10.3892/mmr.2021.12429

73. Bakrania BA, Spradley FT, Drummond HA, LaMarca B, Ryan MJ, Granger JP. Preeclampsia: linking placental ischemia with maternal endothelial and vascular dysfunction. *Compr Physiol*. (2020) 11:1315–49. doi: 10.1002/j.2040-4603.2021.tb00148.x

74. Rambaldi MP, Weiner E, Mecacci F, Bar J, Petraglia F. Immunomodulation and preeclampsia. *Best Pract Res Clin Obstet Gynaecol*. (2019) 60:87–96. doi: 10.1016/j.bpobgyn.2019.06.005

75. Nakashima A, Yamanaka-Tatematsu M, Fujita N, Koizumi K, Shima T, Yoshida T, et al. Impaired autophagy by soluble endoglin, under physiological hypoxia in early pregnant period, is involved in poor placentation in preeclampsia. *Autophagy*. (2013) 9:303–16. doi: 10.4161/auto.22927

76. Lash GE, Pitman H, Morgan HL, Innes BA, Agwu CN, Bulmer JN. Decidual macrophages: key regulators of vascular remodeling in human pregnancy. *J Leukoc Biol*. (2016) 100:315–25. doi: 10.1189/jlb.1A0815-351R

77. Deer E, Herrock O, Campbell N, Cornelius D, Fitzgerald S, Amaral LM, et al. The role of immune cells and mediators in preeclampsia. *Nat Rev Nephrol*. (2023) 19:257–70. doi: 10.1038/s41581-022-00670-0

78. Zheng Z, Li Y, Lu X, Zhang J, Liu Q, Zhou D, et al. A novel mTOR-associated gene signature for predicting prognosis and evaluating tumor immune microenvironment in lung adenocarcinoma. *Comput Biol Med*. (2022) 145:105394. doi: 10.1016/j.compbiomed.2022.105394

79. Zhou L, Ji S, Xue R, Tian Z, Wei M, Yuan X, et al. Comparative analysis of Scarb1 and Cd36 in grass carp (Ctenopharyngodon idellus): Implications for DHA uptake. *Comp Biochem Physiol B Biochem Mol Biol*. (2025) 275:111025. doi: 10.1016/j.cbpb.2024.111025

80. Mulder J, Kusters DM, Roeters van Lennep JE, Hutten BA. Lipid metabolism during pregnancy: consequences for mother and child. *Curr Opin Lipidol*. (2024) 35:133–40. doi: 10.1097/MOL.0000000000000927

81. Munro SK, Balakrishnan B, Lissaman AC, Gujral P, Ponnampalam AP. Cytokines and pregnancy: Potential regulation by histone deacetylases. *Mol Reprod Dev*. (2021) 88:321–37. doi: 10.1002/mrd.23430

frontiers | Frontiers in Immunology

TYPE Original Research
PUBLISHED 17 July 2025
DOI 10.3389/fimmu.2025.1595706

OPEN ACCESS

EDITED BY
Rajni Kant,
Kaohsiung Medical University, Taiwan

REVIEWED BY
Panicos Shangaris,
King's College London, United Kingdom
Ling Bai,
Duke University, United States
Lokanatha Oruganti,
Tulane University, United States

*CORRESPONDENCE
Shuping Zhao
zhaosp66@126.com

RECEIVED 18 March 2025
ACCEPTED 24 June 2025
PUBLISHED 17 July 2025

CITATION
Li C, Liu F, Li C, Zhao X, Lv Q, Jiang A and Zhao S (2025) Multiple analytical perspectives of mitochondrial genes in the context of preeclampsia: potential diagnostic markers. *Front. Immunol.* 16:1595706. doi: 10.3389/fimmu.2025.1595706

Multiple analytical perspectives of mitochondrial genes in the context of preeclampsia: potential diagnostic markers

Can Li[1,2], Fang Liu[3], Chao Li[2], Xiangzhong Zhao[4], Qiulan Lv[4], Aiping Jiang[2] and Shuping Zhao[1*]

[1]Department of Obstetrics and Gynecology, Qingdao Women and Children's Hospital, Shandong University, Jinan, Shandong, China, [2]Department of Obstetrics and Gynecology, The Affiliated Hospital of Qingdao University, Qingdao, Shandong, China, [3]Department of Obstetrics and Gynecology, Dazhou Dachuan District People's Hospital (Dazhou Third People's Hospital), Dazhou, Sichuan, China, [4]Department of Medical Research Center, The Affiliated Hospital of Qingdao University, Qingdao, Shandong, China

Preeclampsia(PE) is closely linked to adverse maternal and fetal outcomes. Given the pivotal roles of mitochondria in various human diseases and the limited research on their involvement in PE, this study identified biomarkers linked to mitochondrial metabolism in PE and their roles in its pathogenesis. Data from three datasets were integrated using the ComBat algorithm to mitigate batch effects. Differential expression analysis identified genes differentially expressed between PE cases and Control group. Cross-referencing these genes with mitochondrial energy metabolism-related genes (MMRGs) isolated mitochondrial energy metabolism-related differentially expressed genes (MMRDEGs). GO and KEGG analysis were performed to elucidate the functions of the MMRDEGs. A diagnostic model using Random Forest and logistic regression was validated by ROC curve analysis. mRNA expressions of *OCRL*, *TPI1*, *GAPDH*, and *LDHA* were quantified via qPCR. Immune characteristics were explored, and PPI, mRNA-miRNA, mRNA-TF and mRNA-RBP interaction networks were constructed. AlphaFold analyzed protein structures of *OCRL, TPI1, GAPDH*, and *LDHA*. A total of 1073 DEGs and 24 MMRDEGs were identified. *OCRL, TPI1, GAPDH*, and *LDHA* formed the diagnostic model, which were predominantly enriched in pyruvate metabolism, glycolysis, and ATP metabolism pathways. CIBERSORT highlighted immune cell composition variations between PE and Control groups. *OCRL, TPI1, GAPDH*, and *LDHA* exhibited increased mRNA expression levels in preeclamptic placentas. Therefore, MMRDEGs may play a critical role in the mechanism of oxidative stress and inflammatory response in PE by mediating metabolic regulation and immune modulation, potentially serving as diagnostic biomarkers associated with mitochondrial metabolism in preeclampsia.

KEYWORDS

preeclampsia, mitochondria-related genes, diagnostic model, machine learning, immune cells infiltration

1 Introduction

Preeclampsia (PE) is a pregnancy-related multisystem syndrome that occurs at or after 20 week of gestation, characterized by elevated blood pressure (systolic blood pressure ≥140 mmHg and/or diastolic blood pressure ≥90 mmHg) and proteinuria (≥300 mg/24h). This condition can lead to multiple organ dysfunctions, including hematological abnormalities, hepatic impairment, and renal insufficiency. In severe cases, it may also compromise pulmonary function, retinal health, and the integrity of the central nervous system (1–4). PE is one of the leading causes of maternal mortality globally, with an estimated prevalence of approximately 10% (5). Its pathogenesis is closely associated with placental vascular insufficiency, endothelial dysfunction, heightened inflammatory responses, immune imbalance, and systemic small-vessel spasms (6–8). Currently, the management of PE primarily relies on blood pressure control and timely pregnancy termination (9, 10). However, the limited availability of preventive and intervention strategies leads to a high incidence of iatrogenic preterm birth, thus increasing the risk of adverse perinatal outcomes. Therefore, an in-depth exploration of the pathogenesis of PE is essential for reducing its incidence and improving prognostic outcomes.

Mitochondria play a pivotal role in cellular bio-oxidation and energy metabolism, being involved in a range of physiological processes including biosynthesis and signal transduction (11, 12). Therefore, mitochondrial dysfunction disrupts these processes, resulting in elevated generation of reactive oxygen species (ROS) and enhanced apoptosis (13–15). As a critical organ for maternal-fetal material exchange, synthesis, defense, and immunity, the placenta exhibits a high demand for energy, primarily supplied by ATP generated by mitochondria (16, 17). If mitochondrial function diminished, ATP synthesis will consequently decrease, thereby impairing placental function and increasing the risk of complications such as preeclampsia (PE), gestational diabetes mellitus(GDM), and fetal growth restriction(FGR) (18, 19). Numerous studies have demonstrated that elevated levels of oxidative stress in patients with PE contribute to the promotion of inflammatory responses and mitochondrial dysfunction (20, 21). Research further suggests that mitochondrial dysfunction plays a critical role in both the onset and progression of PE. For instance, Long et al. (22)reported that mitochondrial damage leads to trophoblast dysfunction, which in turn contributes to the pathogenesis of PE. These findings suggest that targeting mitochondrial repair could represent a promising therapeutic strategy for managing this condition. In addition, several mitochondria-associated genes, such as *CPOX*, *DEGS1*, and *SH3BP5*, have been validated to possess significant diagnostic value for PE (18). Mitochondria harbor an independent genome distinct from nuclear DNA (23), and alterations in the expression of specific mitochondrial genes have been identified as being closely linked to the diagnosis and treatment of PE (24, 25). In recent years, accumulating evidence has demonstrated that immune cell infiltration is a critical factor in the pathogenesis of various diseases, including PE, preterm birth, GDM, and osteoarthritis (26–28).

Owing to the multifaceted nature of PE, there has been relatively limited progress in its prediction and prevention (29). Given the pivotal role of mitochondrial energy metabolism in various diseases, further exploration into the mechanisms of mitochondrial energy metabolism in PE carries significant clinical implications. This study is expected to offer a theoretical basis and innovative perspectives for the early diagnosis and therapeutic intervention of PE. In this study, we aimed to utilize machine learning techniques to construct an innovative diagnostic model for PE and investigate the association between key differentially expressed genes (DEGs) and immune infiltration. Additionally, we validated the expression levels of these DEGs in placental tissues from PE patients, thereby highlighting their potential significance in the pathophysiological mechanisms underlying PE.

2 Materials and methodologies

2.1 Sample collection

In this research, 20 PE placental tissues, among which 12 cases with severe features, were collected following cesarean sections, with diagnosis conforming to the guidelines established by the Task Force on Hypertension in Pregnancy. Correspondingly, control placental tissues (n=20), matched for age and body mass index (BMI), were also obtained. All placental tissues were sourced from pregnant women who delivered at the Affiliated Hospital of Qingdao University. Because gestational diabetes mellitus (GDM) is associated with an increased incidence of PE (30), exclusion criteria for the research were as follows: twin or multiple pregnancies; fetal structural abnormalities or chromosomal anomalies; the presence of comorbidities or complications including GDM, pre-pregnancy diabetes mellitus, chronic hypertension, cardiac, renal, or liver diseases, infectious diseases, or autoimmune disorders; history of blood transfusion, organ transplantation, or immunotherapy; and any history of smoking, alcohol consumption, or substance abuse. Basic clinical data were collected for this study, encompassing age, BMI, gestational week at delivery, parity, systolic and diastolic blood pressure, newborn weight, and one-minute Apgar score. A sample of maternal placental tissue, approximately 1 cm in diameter, was collected within ten minutes of placental delivery, specifically avoiding areas with infarcts or calcification. These samples were then placed in freezing tubes containing RNA preservation solution and kept at -80°C for subsequent analysis using RT-qPCR. All the participants of the study provided a written informed consent. The investigation was approved by the Ethics Committee of the Affiliated Hospital of Qingdao University (Approval No: QYFY WZLL 28705). It was carried out in rigorous adherence to the guidelines established by the committee.

2.2 Data download

The expression profile datasets GSE24129 (31), GSE30186 (32), GSE54618 (33) and GSE75010 (34) of patients with PE were obtained from GEO database (35) utilizing the GEOquery package (36). The GSE24129 dataset included 16 placental samples, evenly distributed between 8 PE cases and 8 Control group. The GSE30186 dataset comprised 12 placental samples, with an equal number of PE cases and Control group. The GSE54618 dataset consisted of 17 placental samples, including 5 from PE cases and 12 from Control group. Lastly, the GSE75010 dataset contained 80 PE cases and 77 Control group. The dataset GSE24129 and GSE75010 utilized the GPL6244 [HuGene-1_0-st-v1] Affymetrix Human Gene 1.0 ST Array [transcript (gene) version]. For the datasets GSE30186 and GSE54618, the associated platform was the GPL10558 Illumina HumanHT-12 V4.0 expression beadchip. The microarray GPL platform files facilitated related annotation for the probe names across these datasets. Specific information for each dataset is depicted in Supplementary Table 1. Utilizing "mitochondrial energy metabolism" as the search keyword and focusing solely on protein-coding genes, we extracted 219 MMRGs from the datebase of GeneCards (https://www.genecards.org/),which offers extensive data on the human genes (37). Additionally, we derived 188 MMRGs from the published literature (38). By integrating these datasets and removing duplicates, we compiled a consolidated list of 384 MMRGs. The specific names of these genes are listed in Supplementary Table 2.

2.3 Preprocessing the datasets and differential expression analysis

We integrated the GSE24129, GSE30186 and GSE54618 datasets and then eliminated batch effects by applying the ComBat algorithm from the R package (39), followed by normalization using the normalize Between Arrays function. Thus, the Combined dataset (including 19 PE cases and 26 Control group) was obtained. Subsequently, we obtained DEGs by utilizing R's limma package to carry out a differential analysis of the expression of all genes among the PE and the control cohort samples of the combined dataset. To make sure to capture all changes in expression levels, whether up-regulated or down-regulated, we made a screening standard of $p < 0.05$ plus $|\text{logFC}| > 0$ to further study the DEGs (40). The findings of variance analysis through the R package ggplot2 map volcano to display. Then, we took MMRGs and DEGs intersection to obtain the MMRDEGs.

2.4 GO and KEGG analysis

The GO (41) approach is frequently employed in large-scale functional enrichment investigations for the purpose of categorizing genes into groups that are associated with biological process (BP), molecular function (MF), and cellular component (CC). The KEGG (42) serves as a crucial repository for genomic information, diseases, drug-related data and biological pathways. We conducted GO and KEGG annotation analyses of MMRDEGs by employing the R package clusterProfiler (43). We set a marked threshold ($p < 0.05$) for pathway selection, ensuring that only statistically significant pathways were considered in our analysis.

2.5 GSEA and GSVA analysis

GSEA (44) is a widely utilized method for assessing variations in pathway activity and biological process involvement across different sample groups within an expression dataset. In this research, we initially carried out a differential gene expression analysis between various groups (PE/Control and High/Low Risk score) within the combined dataset. Subsequently, genes were categorized into two cohorts based on their logFC values: those with positive and those with negative logFC. For the enrichment analysis of these categorized genes, we utilized the clusterProfiler package. The GSEA configuration for this analysis utilized the following specifications: a seed of 2022, 1000 permutations, and a gene set size ranging from a minimum of 10 to a maximum of 500 genes. We retrieved the gene set "c2.Cp.All.V2022.1.Hs.Symbols.GMT [All Canonical Pathways]" containing 3050 entries from the Molecular Signatures Database (MSigDB) (45). Pathways which got a significant enrichment level ($p < 0.05$) were deemed markedly enriched.

GSVA (46) was designed to assess gene set enrichment within microarray and nuclear transcriptome data. This technique enables the conversion from diverse samples into a sample-specific gene expression matrix and can evaluate the pathway enrichment across multiple specimens. In this study, we also employed the gene set used earlier when GSEA analysis was performed. GSVA was carried out on gene expression matrices derived from distinct groups (PE/Control or High/Low Risk score) within the Combined dataset, utilizing this reference gene set. The analysis revealed functional disparities in enriched pathways between sample cohorts within the Combined dataset. Pathways with a significance level ($p < 0.05$) were further scrutinized; specifically, we selected and examined the 10 pathways exhibiting both the largest and smallest log fold change (logFC).

2.6 Construct MMRDEGs diagnostic model

The RandomForest (RF) (47) technique is a collective learning approach that integrates numerous decision tree models. It belongs to the bagging (bootstrap aggregation) ensemble algorithm, which consists of multiple algorithms. RF is a commonly used approach for model building. By constructing multiple decision trees, the prediction results of each tree in the forest are aggregated using a voting method to obtain the final prediction result for a given sample. In this study, we utilized the MMRDEGs expression levels in the Combined dataset's expression matrix to build a model using

the RandomForest package with parameter set.seed (2023) and ntree = 1000.

$$I(X = xi) = -log_2 p(x_i)$$

We conducted a logistic regression analysis on MMRDEGs to construct a Logistic diagnostic model of the Combined dataset. Moreover, we employed the Logistic regression to analyze the association of the independent variables and dependent variables, when considering dependent variables as binary variables(PE cases and Control group). $p < 0.05$ was a significance level as criteria for identifying MMRDEGs and constructing the Logistic diagnostic model. The molecular expressions of MMRDEGs incorporated in this logistic regression model were visualized through Forest Plot.

Furthermore, we conducted the Least Absolute Shrinkage and Selection Operator (LASSO, the seed number is 2022) by R package glmnet (48) to process the MMRDEGs, which were screened out by utilizing our logistic regression model, to obtain the Logistic-LASSO regression model. LASSO regression analysis reduces overfitting incorporating a penalization factor (lambda × absolute value of slope), thereby improving its capacity for generalization while maintaining interpretability. The results obtained from LASSO analysis were depicted through variable trajectory plot techniques and diagnostic model plot.

$$\text{risk}Score = \sum_i Coefficient\ (hub\ gene_i) * mRNA\ Expression\ (hub\ gene_i)$$

Subsequently, we identified the common MMRDEGs by intersecting the MMRDEGs derived from both the RF model and the Logistic-LASSO regression model, which were then visualized using a Venn diagram. The expression levels of the common MMRDEGs in the Combined dataset were combined with the coefficients of these genes in the regression model of Logistic-LASSO to establish an MMRDEGs diagnostic model and to calculate corresponding Risk-scores. A Nomogram (49), a visual depiction of interrelations among several independent variables on a rectangular plane-coordinate system, was constructed based on the gene expression levels derived from the MMRDEGs diagnostic model generated through Logistic LASSO regression analysis in the Combined dataset. To examine the precision and distinguishing capability of our MMRDEGs diagnostic models, Decision Curve Analysis (DCA) (50), a straightforward approach for appraising molecular markers, diagnostic tests and clinical prediction models, was performed using the ggDCA R package.

2.7 Analysis of the infiltration of immune cells

The relative abundance of a variety of immune cell infiltrates within every sample was quantified utilizing the single-sample gene-set enrichment analysis (ssGSEA) algorithm. The method facilitated to label various immune cell types. For instance, regulatory T cells, $CD8^+$ T cells, dendritic cells and macrophages. We represented the relative abundance of each immune cell type across the samples by enrichment scores, which were calculated utilizing ssGSEA methodology (51, 52). Using the ssGSEA algorithm from the GSVA R package (version 1.46.0), we calculated the enrichment scores of groups within high and low risk cohorts according to the MMRDEGs diagnostic model from the Combined dataset. These scores depicted the extent of immune cell infiltrations in individual specimen, thereby illustrating disparities of the abundance of immune cell infiltration among the different (High and Low) risk cohorts through box plots. Additionally, we examined the correlation of immune cell abundances among the high and low risk cohorts utilizing scatter plots. The association among immune cells and commonly altered MMRDEGs across these groups was analyzed using the Spearman statistical method and depicted in correlation dot plots, increasing our understandings of the immune landscape in relation to preeclampsia risk stratification.

CIBERSORT (53) is a kind of immune infiltration algorithm, that deconvoluted transcriptome expression matrices based on linear support vector regression, to assess the abundance and composition of immune cells within different samples. For this analysis, we input the expression matrix data of samples of the High and the Low risk groups defined by the MMRDEGs diagnostic model in the Combined dataset to CIBERSORT. Using the feature gene matrix of LM22, we refined the results by retaining solely those data points with immune cell enrichment scores >0, thus obtaining and visualizing the comprehensive findings of the immune cell infiltration abundance matrix. Those disparities in immune cell infiltration between the high risk and low risk cohorts were depicted utilizing stacked bar charts. We employed the Spearman statistical method to analyze the correlations among immune cells within the Combined dataset and utilized the R package ggplot2 to visualize the results. Moreover, the interactions among immune cells and commonly altered MMRDEGs were depicted using correlation dot plots, providing insights into the immune dynamics associated with different risk stratifications in PE.

2.8 PPI network and mRNA-RBP, mRNA-TF, mRNA-Drug interaction network

The protein-protein interaction (PPI) network consists of individual proteins that engage with one another. In this study, we constructed the common MMRDEGs PPI network(minimum required interaction score: low confidence (0.150)) using the database of STRING (54). The network was visualized using Cytoscape, which allowed us to identify densely interconnected clusters within the PPI network. These clusters potentially signify molecular assemblies with unique biological roles, offering insights into the molecular mechanisms underlying PE.

ENCORI database (55) (https://starbase.sysu.edu.cn/) facilitates the exploration of interactions among various RNA types, including microRNAs-ncRNA, microRNAs-mRNA, ncRNA-RNA, and RNA-RNA, as well as interactions among RNA-binding proteins (RBPs) and ncRNAs or mRNAs. These interactions are curated utilizing degradome sequencing data and CLIP-seq, supporting comprehensive visual tools of investigating miRNA targets. In our study, we utilized the ENCORI database to forecast RBPs

interacting with the commonly altered MMRDEGs. We established "pancancerNum> 27" as the threshold for selecting significant interactions. and the mRNA-RBP interaction network was rendered utilizing Cytoscape.

HTFtarget database (56) (http://bioinfo.life.hust.edu.cn/hTFtarget) integrates human transcription factors (TFs) and their corresponding control targets data. The CHIPBase database (https://rna.sysu.edu.cn/chipbase/) predicted transcriptional regulatory relationships among millions of TFs and genes. Utilizing both HTFtarget databases and CHIPBase, the TFs that link to common MMRDEGs were identified. We applied the screening criteria of having an upstream and downstream sample count greater than zero. Subsequently, the mRNA-TF interactive network was rendered visually utilizing Cytoscape software.

2.9 RT-qPCR

Placental tissues were lysed using FreeZol reagent (Vazyme, R711) following the manufacturer's instructions. RNA concentration and purity were measured using a spectrophotometer. The isolated RNA was reverse transcribed into cDNA with a reverse transcription kit (Agbio, AG11705). Real-time polymerase chain reaction (qPCR) was then performed using the SYBR Green Pre-Mix Pro Taq HS qPCR Kit (Agbio, AG11701). Relative gene expression levels were normalized to *β-actin* and calculated using the $2^{\wedge(-\Delta\Delta Ct)}$ method. The Supplementary Table 3 lists the primer sequences of mRNAs and internal control.

2.10 Statistical analysis

The entirety of data manipulation and statistical evaluation in this investigation was executed utilizing R software (Release 4.1.2). The independent Student's t-test was used to compare continuous variables (fit normal distribution). We employed the Mann-Whitney U test (Wilcoxon rank sum test) for variables lacking normally distributed. Use Spearman correlation analysis to computer the findings unless otherwise specified. The p-values for statistical tests are two-tailed, and a threshold of 0.05 is deemed indicative of statistically meaningful results.

3 Results

3.1 Dataset processing

According to the technical roadmap of this experiment (Figure 1), we first combined the three datasets (GSE24129, GSE30186, and GSE54618), then batched the data using the ComBat function from R's sva package, and then utilized the Normalize Between Arrays function of the limma package to perform standardization procedures. The dataset of 19 PE cases and 26 Control group, that was combined, was obtained.

The before and after data processing boxplots and PCA plots of the combined dataset, according to the sample source, were showed in the Supplementary Figures 1A–D, respectively. The findings demonstrated that the expression profiles of samples from the Combined dataset exhibited a high degree of consistency, indicating successful removal of batch effects through data processing. The Combined dataset utilized for subsequent analyses represented the batch effect-corrected and normalized data.

We further utilized the limma package to standardize the GSE75010 dataset and compared the pre- and post-processing states of the dataset using boxplots (Supplementary Figures 1E, F). The boxplot analysis demonstrated that the expression levels of samples in the GSE75010 dataset became significantly more consistent after data processing.

3.2 Combined dataset differential expression analysis of PE and control groups

The placenta serves as a critical organ facilitating material transport between mother and fetus, performing multiple functions during pregnancy such as immune protection, endocrine regulation, and serving as a conduit for nutrient and oxygen delivery. Its condition is closely associated with the health of both mother and child during gestation. Torbergsen T et al. first described a high incidence of preeclampsia in a family with mitochondrial disorder (57). Recent research into the mechanisms underlying preeclampsia has revealed mitochondrial dysfunction in both patients with preeclampsia and animal models (58).

We utilized limma package to explore the Combined dataset of PE cases and Control group. And we got 1073 differentially expressed genes using the threshold of $|\log FC| > 0$ and $p < 0.05$, including 603 highly expressed genes in PE cases(the Control group of samples low expressed, logFC is positive, raised genes), and 470 genes low expressed in PE cases(the Control group of samples increased, logFC is negative, cut genes). And then, we presented the outcomes of differential expression analysis between the two groups in the Combined dataset using the volcano plot (Figure 2A). We then intersected these 1073 differently expressed genes (DEGs) with 384 mitochondrial energy metabolism-related genes (MMRGs). And then, 24 mitochondrial energy metabolism-related differentially expressed genes (MMRDEGs) were identified. The 24 MMRDEGs were *ACSL3*, *ALDH16A1*, *ALDH1A3*, *ALDH4A1*, *ATG7*, *BTD*, *FBXL4*, *FOXO1*, *GAPDH*, *GLS*, *HK2*, *KCNJ2*, *LDHA*, *MFN2*, *NDUFS6*, *OCRL*, *PC*, *PGK1*, *PPARG*, *RARS2*, *SOD1*, *TPI1*, *VDAC1*, *XBP1* (Figure 2B).

We also generated a comparative map to analyze the differential expression of 24 MMRDEGs between the two cohorts (Figure 2C). The analysis suggested that 16 MMRDEGs exhibited significant differences, with *ALDH16A1*, *ALDH4A1*, *ATG7*, *GLS* and *SOD1* significantly down-regulated while *ALDH1A3*, *BTD*, *FOXO1*, *GAPDH*, *HK2*, *KCNJ2*, *LDHA*, *OCRL*, *PGK1*, *TPI1*, and *VDAC1* significantly up-regulated.

Then, we drew a simple numerical heat map derived from the expression matrix of these 16 MMRDEGs above (Figure 2D), and

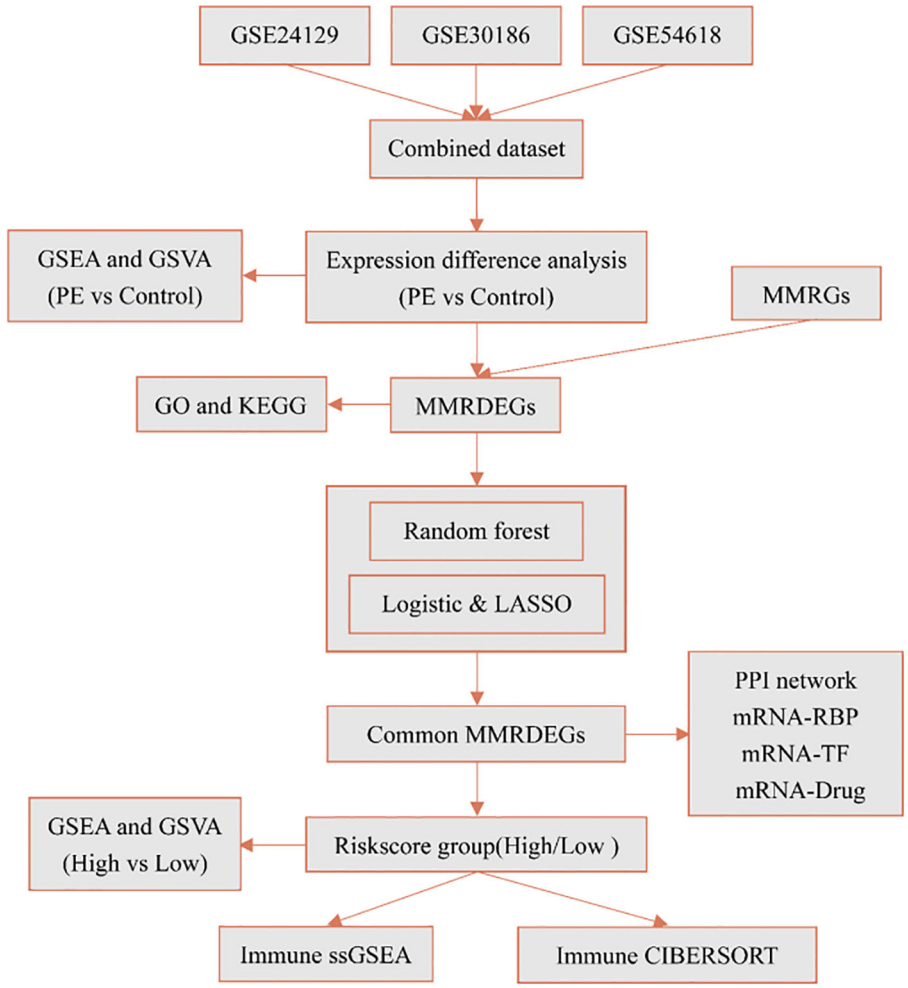

FIGURE 1
Technology roadmap. PE, Preeclampsia; GSEA, Gene Set Enrichment Analysis; GSVA, Gene Set Variation Analysis; MMRGs, Mitochondrial energy metabolism-related genes; MMRDEGs, Mitochondrial energy metabolism related differentially expressed genes; GO, Gene Ontology; KEGG, Kyoto Encyclopedia of Genes and Genomes; LASSO, Least absolute shrinkage and selection operator; RBP, RNA binding protein; TF, Transcription factors; ssGSEA, single-sample gene-set enrichment analysis.

the visualization revealed substantial disparities in the expression patterns of the 16 MMRDEGs between the two sample groups. Additionally, we annotated the positions of these 16 MMRDEGs and draw a chromosome localization map (Figure 2E) by employing the RCircos package, from which the specific distribution of the 16 MMRDEGs on each chromosome can be obtained.

3.3 The GO and the KEGG analysis of MMRDEGs

The biological processes (BP), molecular functions (MF), cellular components (CC), relationships between biological pathways, pathway enrichment analysis using the Kyoto Encyclopedia of Genes and Genomes (KEGG), and gene function enrichment analysis based on Gene Oncology (GO) were carried out to analyze the 16 MMRDEGs. Pathways that below the *P* threshold of 0.05, were considered to be statistically significant. The outcomes showed that the 16 MMRDEGs main enriched in those BPs, such as pyruvate metabolic process, glycolytic process, ATP generation from ADP, generation of precursor metabolites and energy, ATP metabolic process. And in the CCs of the mitochondrial matrix. It was enriched in acting on the aldehyde or oxo group of donors, oxidoreductase activity, NAD or NADP as acceptor, aldehyde dehydrogenase (NAD+) activity, aldehyde dehydrogenase [NAD(P)+] activity, protein phosphatase binding, oxidoreductase activity, acting on the CH-NH group of donors, NAD or NADP as acceptor and other MFs (Figure 3A). It was also enriched in Glycolysis/Gluconeogenesis, HIF-1 signaling pathway, Carbon metabolism, Alanine, aspartate, glutamate metabolism, Inositol phosphate metabolism (Figure 3B) and other KEGG pathways (Supplementary Table 4). In addition, the enrichment consequences of the BP pathways (Figure 3C), CC pathways (Figure 3D), MF pathways (Figure 3E), and KEGG pathways (Figure 3F) of GO analysis were presented utilizing ring network diagrams.

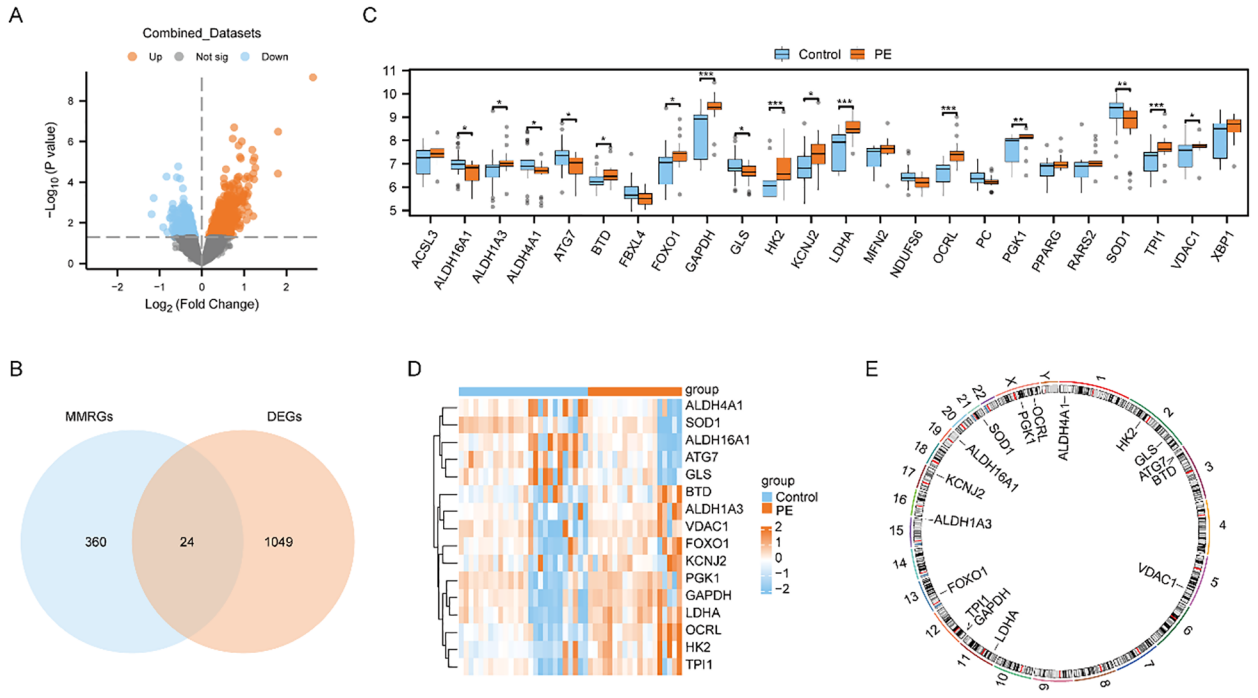

FIGURE 2
Differential expression analysis and correlation analysis of MMRDEGs. **(A)** Volcano plot presentation of the results of differential analysis between PE cases and Control group in Combined datasets. **(B)** Venn diagram of DEGs between PE cases and Control group and MMRGs in Combined datasets. **(C)** Group comparison plot of MMRDEGs between PE cases and Control group in Combined datasets. **(D)** Simplified numerical heatmap of MMRDEGs in Combined datasets. **(E)** Chromosomal mapping of MMRDEGs. The symbol ns was equivalent to $p \geq 0.05$, which was not statistically significant. The symbol * is equivalent to $p < 0.05$, which is statistically significant; The symbol ** is equivalent to $p < 0.01$, which is highly statistically significant; The symbol *** is equivalent to $p < 0.001$ and highly statistically significant. PE, Preeclampsia; DEGs, differentially expressed genes; MMRGs, Mitochondrial energy metabolism related genes; MMRDEGs, Mitochondrial energy metabolism related differentially expressed genes.

We utilized the Pathview R package for pathway mapping to illustrate the KEGG enrichment results of Glycolysis/Gluconeogenesis (Supplementary Figure 2A), Carbon metabolism (Supplementary Figure 2B), Alanine, aspartate and glutamate metabolism (Supplementary Figure 2C), Inositol phosphate metabolism (Supplementary Figure 2D), and HIF-1 signaling pathway (Supplementary Figure 2E).

3.4 GSEA enrichment analysis and GSVA analysis of the control and the PE groups based on the Combined dataset

To appraise the influence of gene expression levels of genes from PE and Control groups of Combined dataset on PE, we examined the relationships between the expression levels of all genes in different groups (PE/Control) of the Combined dataset and the BPs, CCs, and MFs they played, by employing the Gene Set Enrichment Analysis (GSEA). $p < 0.05$ was set as the significant enrichment criterion. The results demonstrated a significant enrichment of genes from different (PE/Control) groups in the Combined dataset, specifically in the vascular smooth muscle contraction pathway (Figure 4B), IL9 signaling pathway (Figure 4C), Notch signaling pathway (Figure 4D), IL2 signaling pathway (Figure 4E), IL6/7 signaling pathway (Figure 4F), cell surface interactions at the vascular wall (Figure 4G), and other pathways (Supplementary Table 5). In addition, the outcomes of GSEA analyzing genes between distinct cohorts (PE/Control) of the Combined dataset were depicted by mountain plot (Figure 4A).

To investigate the distinctions between disease and controls from the Combined dataset, we then performed Gene Set Variation Analysis (GSVA). From the pathways with $p < 0.05$, we identified 10 pathways with the highest and lowest logFC for further examination (Supplementary Table 6), respectively.

The results of GSVA analysis on all the genes of the Combined dataset revealed significant differences among PE and Control groups. Specifically, IKEDA Mir133 targets DN, hyaluronan biosynthesis and export, RHOT1 GTPASE cycle, neurofascin interactions, Irinotecan pathway, Aflatoxin B1 metabolism, Sulindac metabolic pathway, weber methylated LCN in SPERM DN, Tomlins metastasis upregulation of steroid biosynthesis. Additionally, activated NTRK2 signals through FYN and PI3K pathways were observed along with NTRK2 activation of RAC1. Furthermore, HIF1A and PPARG were found to regulate glycolysis. Calvet Rinotecan sensitive vs resistant upregulation was also identified as well as Korkola choriocarcinoma involvement. Lastly erythrocytes demonstrated oxygen uptake and carbon dioxide release while Tesar Alk targeted human es 4D and 5D DN along

10.3389/fimmu.2025.1595706

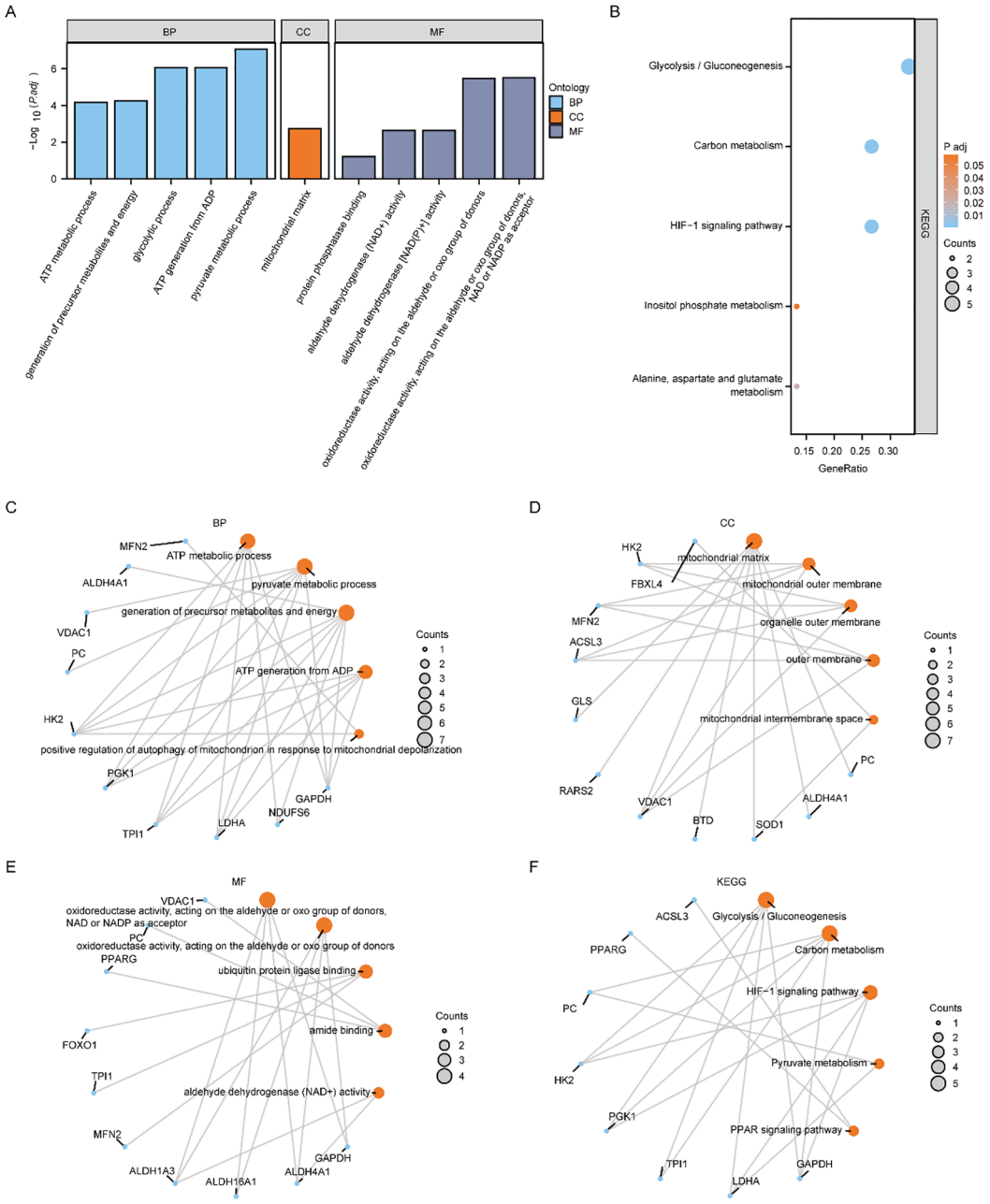

FIGURE 3
Functional enrichment analysis (GO) and pathway enrichment (KEGG) analysis of MMRDEGs. **(A)** Bar graph showing the GO enrichment analysis results of MMRDEGs. **(B)** Bubble plot display of KEGG pathway enrichment analysis results of MMRDEGs. **(C–F)** Loop network diagram of BP pathway **(C)**, CC pathway **(D)**, MF pathway **(E)** and KEGG pathway **(F)** in MMRDEGs enrichment analysis results. In the bar graph **(A)**, the abscissa is the GO terms, and the height of the bar indicates the Padj value of GO terms. In the network diagram **(C–F)**, blue dots represent specific genes, and orange dots represent specific pathways. MMRDEGs, Mitochondrial energy metabolism related differentially expressed genes; GO, Gene Ontology; BP, biological process; CC, cellular component; MF, molecular function; KEGG, Kyoto Encyclopedia of Genes and Genomes; The screening criterion for GO/KEGG enrichment items was $p < 0.05$.

with JAK targeting mouse es D4 DN. Utilizing the outcomes derived from GSVA, we carried out a differential expression analysis of 20 pathways among PE and control cohorts of the Combined dataset. Subsequently, we created a heatmap illustrating the particular differential analysis outcomes (Supplementary Figure 3A) employing the R package. Furthermore, we assessed the extent of group divergence for these 20 pathways across various cohorts from the Combined dataset, utilizing the Mann-Whitney U test, and we use a group comparison plot to illustrate the outcomes (Supplementary Figure 3B). The findings demonstrated marked differences in pathway expression among disease control cohorts within the Combined dataset.

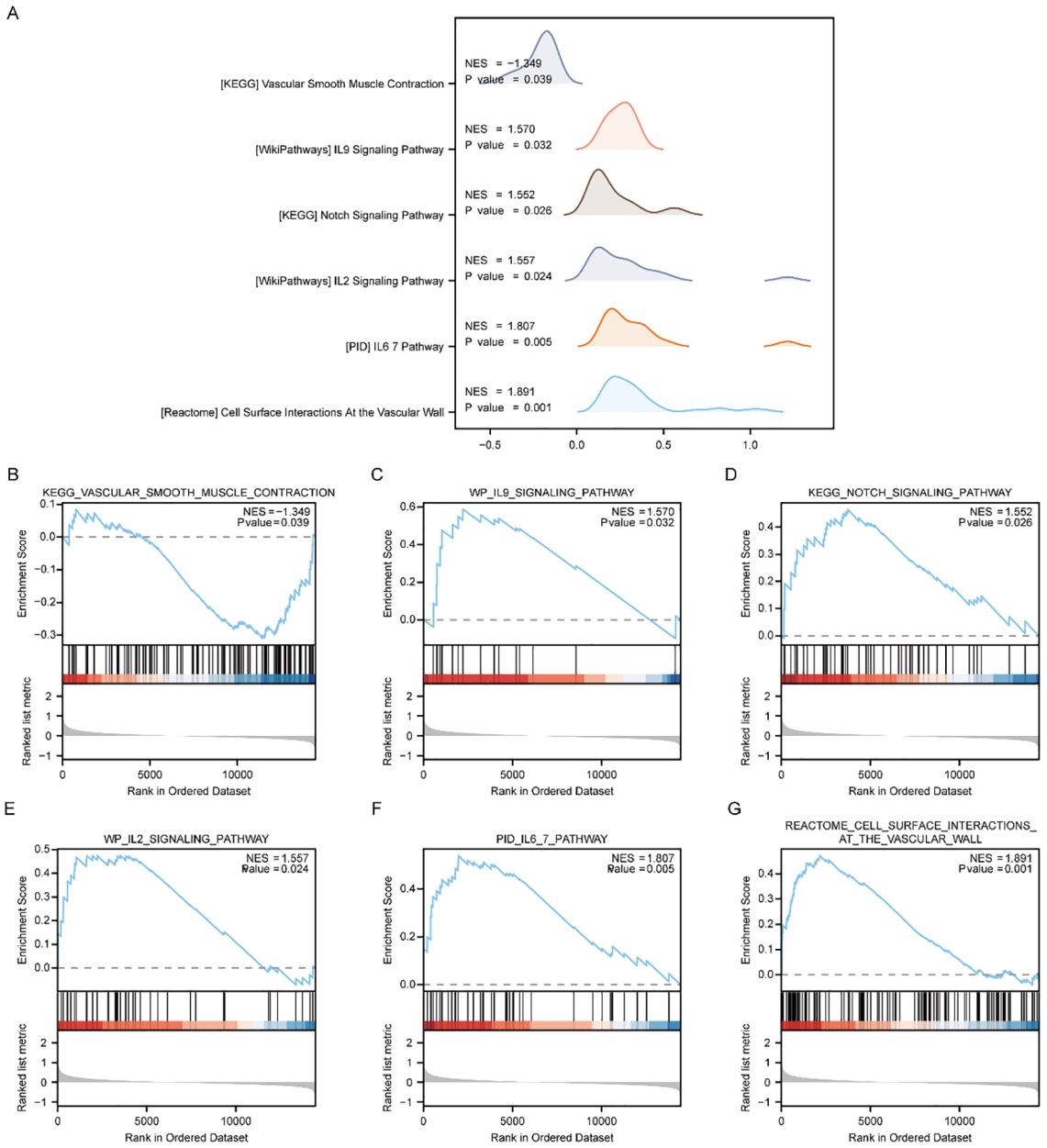

FIGURE 4
GSEA enrichment analysis between PE cases and Control group in Combined dataset. **(A)** Six main biological characteristics of GSEA enrichment analysis of genes between different groups (PE/Control) of Combined dataset. **(B–G)** Genes in Combined dataset were significantly enriched in KEGG vascular smooth muscle contraction **(B)**, IL9 signaling pathway **(C)**, KEGG NOTCH signaling pathway **(D)**, IL2 signaling pathway **(E)**, IL6/7 pathway **(F)**, Cell surface interactions at the vascular wall **(G)**. PE, Preeclampsia; GSEA, Gene Set Enrichment Analysis. The significant enrichment screening criterion for GSEA enrichment analysis was $p < 0.05$.

3.5 Construction of MMRDEGs diagnostic model

Based on the Combined dataset, we examined the expression levels of the 16 MMRDEGs using Random Forest algorithm (RF) to evaluate the values in diagnosis of the 16 MMRDEGs (Figure 5A). IncNodePurity (Increase in NodePurity) indicates the enhancement in node purity. The higher the node purity, the less impurities it contains (that is, the smaller the Gini coefficient). We applied an IncNodePurity threshold of > 0.5 to filter the specific analysis outcomes. The findings (Figure 5B) revealed that 7 diagnostic markers were obtained by RF algorithm. They are: *OCRL*, *GAPDH*, *TPI1*, *LDHA*, *SOD1*, *HK2* and *PGK1*.

Logistic regression was performed utilizing the expression levels of 16 MMRDEGs in the Combined dataset, with the screening criterion of $p< 0.05$ (Figure 5C). The Logistic regression model included a total of 8 MMRDEGs (*ALDH16A1*, *ATG7*, *BTD*, *GAPDH*, *HK2*, *LDHA*, *OCRL* and *TPI1*), and the diagnostic model was developed by the expression relative quantities of the 8 genes in the combined dataset (the expression levels were evaluated

10.3389/fimmu.2025.1595706

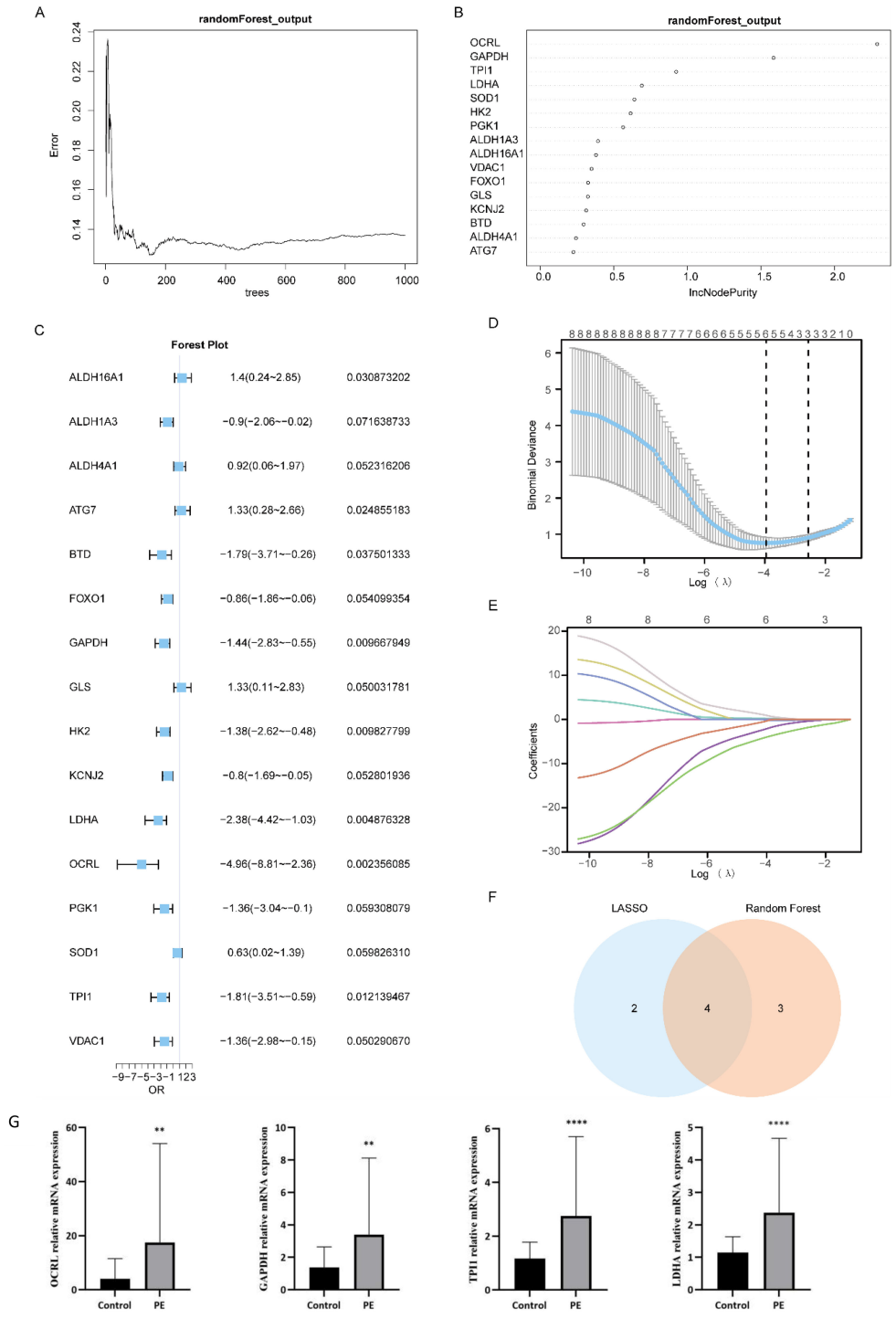

FIGURE 5
Construction of MMRDEGs diagnostic model. **(A)** Plot of model training error of RF algorithm. **(B)** IncNodePurity presentation of MMRDEGs in the RF model (in descending order of IncNodePurity). **(C)** Forest Plot of Logistic regression model for MMRDEGs. **(D)** Diagnostic model plot of LASSO regression model. **(E)** Variable trajectory plot of LASSO regression model. **(F)** Venn diagram of MMRDEGs in LASSO regression model and MMRDEGs in RF model. **(G)** The mRNA expressions of *OCRL*, *GAPDH*, *TPI1* and *LDHA* of placental tissues in the PE cases and Control group. The symbol ** is equivalent to $p < 0.01$, which is highly statistically significant; The symbol **** is equivalent to $p < 0.0001$ and is highly statistically significant. PE, Preeclampsia; MMRDEGs, Mitochondrial energy metabolism related differentially expressed genes; LASSO, Least Absolute Shrinkage and Selection Operator; Common MMRDEGs, Common Mitochondrial energy metabolism related differentially expressed genes.

by Least Absolute Shrinkage and Selection Operator (LASSO) analysis). And the findings of the LASSO analysis were illustrated via the LASSO regression model diagram (Figure 5D) and the LASSO variable trajectory plot (Figure 5E). The findings indicated that the diagnostic model comprised 6 MMRDEGs, which were: *ALDH16A1*, *ATG7*, *GAPDH*, *LDHA*, *OCRL* and *TPI1*.

Then we interposed the MMRDEGs from the RF model and the MMRDEGs from the Logistic-LASSO regression model (Figure 5F), and 4 Common MMRDEGs ($p < 0.05$) were obtained, which were *OCRL*, *GAPDH*, *TPI1* and *LDHA*.

Next, we examined the differential expression of the 4 Common MMRDEGs in the placental tissues of preeclamptic and normal mothers using RT-qPCR. The demographic characteristics of the PE patients are presented in Supplementary Table 7. The findings indicated that the mRNA expressions of the 4 common genes were notably elevated in the placental tissues of the PE cases relative to the Control group ($p < 0.05$, Figure 5G). These four Common MMRDEGs (*OCRL, GAPDH, TPI1, and LDHA*) were identified for the first time in a study of PE. This novel discovery offers fresh insights into the role of mitochondrial metabolism in preeclampsia and may establish a foundation for the development of future biomarkers and therapeutic targets.

And then, utilizing the expression level of the four Common MMRDEGs in Combined dataset and corresponding coefficients established by applying LASSO analysis, we obtained the MMRDEGs diagnostic model of 4 Common MMRDEGs.

$$\begin{aligned}\text{Risk Score} &= 41.58006654 + OCRL\star - 3.921473316 + GAPDH\star \\ &\quad - 2.021501079 + TPI1\star - 0.275314264 + LDHA\star \\ &\quad - 0.08998086\end{aligned}$$

The diagnostic model for MMRDEGs included four Common MMRDEGs. We used combined logistic regression analysis to process the dataset's expression levels to construct a logistic regression model for MMRDEGs. Additionally, we generated a nomogram depicting the impact of these four common MMRDEGs on the logistic regression model (Figure 6A). Our findings revealed that among all variables, *OCRL* exhibited notably superior effectiveness within the MMRDEGs logistic regression model.

The diagnostic model's clinical value was appraised through decision curve analysis (DCA), and the findings were presented in Figure 6B. In the DCA graph, a model's line consistently surpasses those of "All negative" and "All positive" within a specific range, greater net benefits can be obtained, indicating a stronger model performance. Our findings demonstrate that our constructed model exhibits considerable accuracy in diagnosing PE.

To further substantiate the value of the MMRDEGs diagnostic model, we drew ROC curves utilizing the Risk Scores of the diagnostic model of MMRDEGs and the information for grouping (PE/Control) of the Combined dataset and displayed the outcomes (Figure 6C). The MMRDEGs diagnostic model exhibited substantial precision in the diagnosis of the two groups (PE/Control) (AUC = 0.970, CI=0.930-1.000, Figure 6C).

We further validated the diagnostic performance of the MMRDEGs diagnostic model using the GSE75010 dataset. Specifically, we calculated the risk scores by applying the formula derived from the MMRDEGs diagnostic model and the gene expression profiles in GSE75010. Subsequently, we incorporated the grouping information to construct the ROC curve. The results indicated that the MMRDEGs diagnostic model exhibited satisfactory accuracy in distinguishing the PE and Control groups within the GSE75010 dataset (AUC = 0.877, CI 0.823-0.932, Figure 6D).

We also performed functional similarity analysis for four Common MMRDEGs and displayed them using a boxplot. We calculated the semantic similarity of sets of GO terms, GO terms, gene products and gene clusters through the R package GOSemSim. Similarity analysis was performed only on genes that were annotated to pathways in MF, BP, and CC. Finally, functional similarity analysis results between four Common MMRDEGs were obtained and visualized by Boxplot (Figure 6E). The findings indicated that LDHA exhibited the greatest functional similarity score in comparison to other Common MMRDEGs (the X-axis of D graph is the similarity score, with higher values indicating increased functional similarity to other genes).

3.6 GSEA and GSVA based on Combined dataset between the Low and the High-Risk cohorts

Initially, we categorized those disease samples from the Combined dataset into the Low-Risk Score group and the High-Risk Score group utilizing the median Risk-Score of the previous MMRDEGs diagnostic model and performed a differential analysis between the two groups utilizing the limma package (Figure 7A). Based on the results of the differential analysis, we conducted GSEA to explore the relationship among the MFs, the CCs, the BPs and the expression of all genes involved between the different groups (Low/High Risk-Score group) in the Combined dataset, using the threshold of $p < 0.05$ for enrichment selection. The findings demonstrated a significant enrichment of genes linked to the citric acid TCA cycle and respiratory electron transport (Figure 7C), IL5 signaling pathway (Figure 7D), IL7 signaling pathway (Figure 7E), IL6 signaling pathway (Figure 7F), energy metabolism (Figure 7G), electron transport chain Oxphos system in mitochondria (Figure 7H) as well as other pathways, indicating their association with High and Low Risk cohorts (Supplementary Table 8). Furthermore, the GSEA outcomes of genes among the High Risk-Score cohort and the Low Risk-Score cohort in the Combined dataset were presented by mountain plot (Figure 7B).

To investigate the disparities among the High Risk-Score cohort and the Low Risk-Score cohort in the Combined dataset, we subsequently conducted GSVA. From the pathways with a $p < 0.05$, we identified 10 pathways with the highest and lowest logFC for further analysis (refer to Supplementary Table 9 for detailed information), respectively. The GSVA results of all genes revealed significant differences in 20 pathways among the High and Low Risk-Score cohorts in the Combined dataset. These pathways include defective *CSF2RB* causes *SMDP5, IPS LCP* with

10.3389/fimmu.2025.1595706

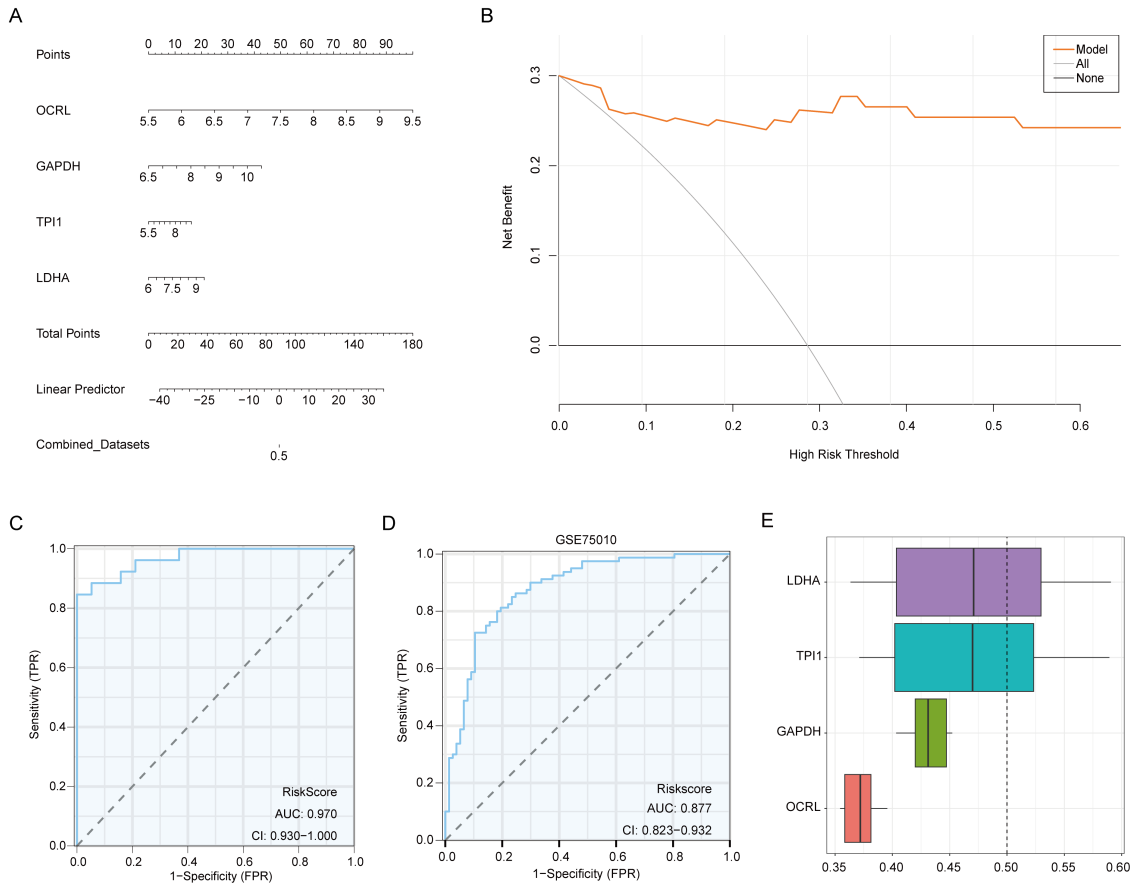

FIGURE 6
Validation of the MMRDEGs diagnostic model. **(A)** Nomogram of Common MMRDEGs in MMRDEGs Logistic regression model. **(B)** Decision curve in Logistic regression model of MMRDEGs. **(C)** ROC curve of MMRDEGs diagnostic model in Combined dataset. **(D)** ROC curve of MMRDEGs diagnostic model in GSE75010. **(E)** Functional similarity analysis results among Common MMRDEGs. ROC, receiver operating characteristic curve; AUC, Area Under the Curve, MMRDEGs, Mitochondrial energy metabolism related differentially expressed genes; Common MMRDEGs, Common Mitochondrial energy metabolism related differentially expressed genes; DCA, Decision Curve Analysis. The closer the AUC in the ROC curve is to 1, the better the diagnostic effect is. When AUC was between 0.5 and 0.7, the accuracy was low. When AUC was 0.7-0.9, it had a certain accuracy. AUC > 0.9 had high accuracy.

H3K4ME3 and *H3K27ME3*, Korkola choriocarcinoma *DN*, *FGFR3B* ligand binding and activation, Aml methylation Cluster *7 DN*, Turashvili breast carcinoma Ductal vs Lobular *DN*, *FTO* obesity variant mechanism, miscellaneous substrates, *PEPI* pathway, *ES LCP* with *H3K4ME3* and *H3K27ME3* angiogenic targets of *VHL HIF2A* up regulation Biocarta Myosin pathway *OPN* targets Cluster 3 *Myc* targets *DN CTNNB1* pathway and proliferation mesothelioma survival up schavolt targets of *TP53* and *TP63 MAPK11* targets Pujana breast cancer with *BRCA1* mutated *DN* regulation of *PTEN* localization. According to the GSVA outcomes, we analyzed the differential expression of 20 pathways among the Low-Risk cohort and the High-Risk cohort in the Combined dataset, and the specific differential analysis findings (Supplementary Figure 4A) was showed as a heatmap by the R package. Furthermore, we employed the Mann-Whitney U test to examine the group distinction level of 20 pathways between diverse cohorts in the Combined dataset and displayed the findings by group comparison plot (Supplementary Figure 4B). The findings suggested that all the expressions of the 20 pathways were markedly different among the Low-Risk cohort and High-Risk cohort in the Combined dataset ($p<0.05$).

3.7 Analysis of differences in ssGSEA immune characteristics among the Low and High-Risk groups in the Combined dataset

We categorized PE samples in the Combined dataset into the Low Risk-Score and the High Risk-Score cohorts by the median Risk-Score of the MMRDEGs diagnostic model.

To study the difference of immune infiltration between the Low/High Risk-Score groups of the Combined dataset, we applied ssGSEA algorithm to computer the abundance of 28 immune cell infiltration in the two risk-score sample groups. And then, we used Mann-Whitney U test to analyze the differences of the two abundances of the Low and High Risk-Score groups, using group comparison plot to exhibit the results (Figure 8A). The findings

10.3389/fimmu.2025.1595706

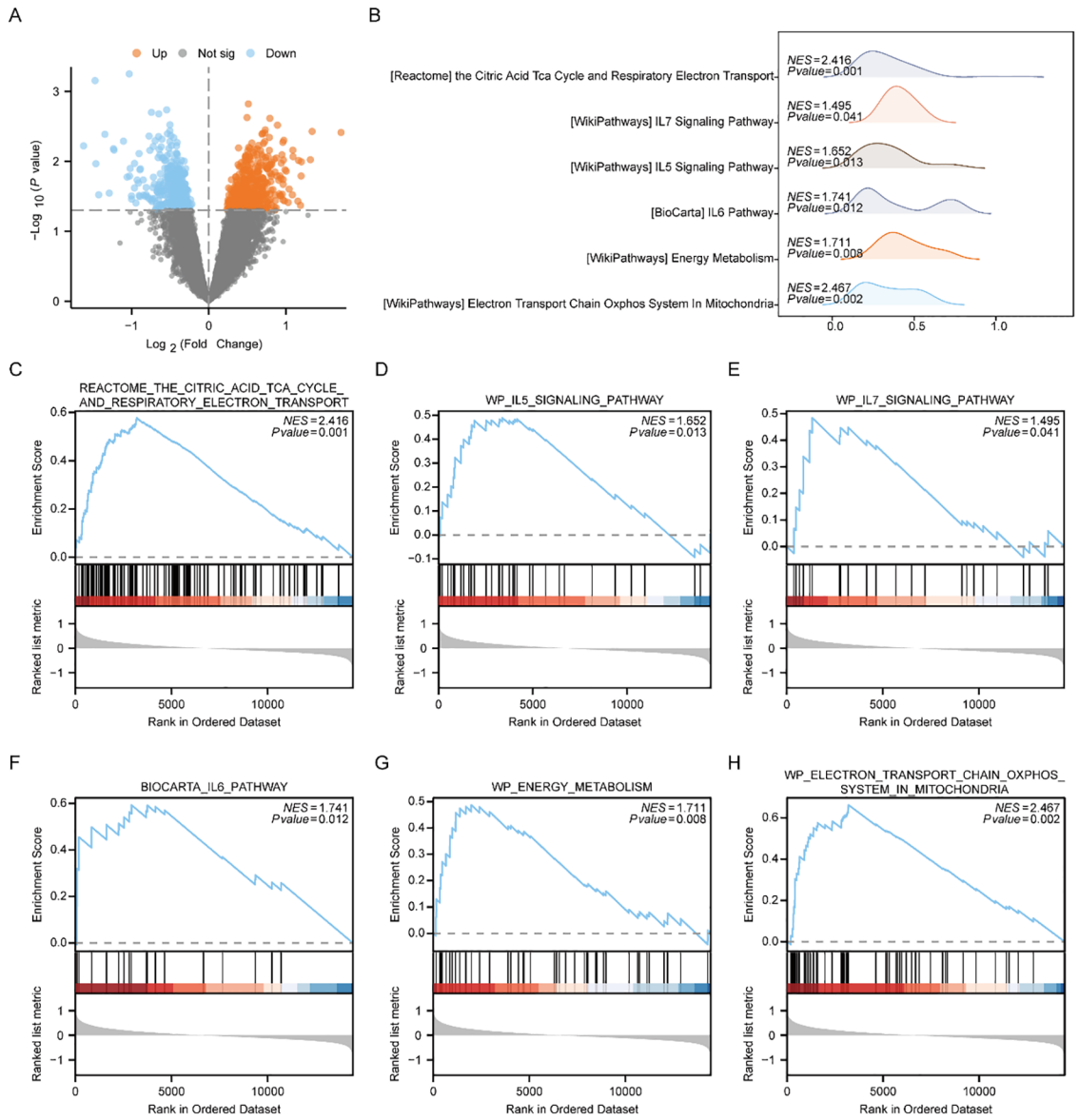

FIGURE 7
GSEA enrichment analysis between high and low risk-score groups of Combined dataset. **(A)** Volcano plot of gene difference analysis between High and Low Risk-score groups in Combined dataset. **(B)** Mountain plot display of six main biological characteristics of GSEA enrichment analysis results. C-H. Genes significantly enriched in the citric acid TCA cycle and respiratory electron transport between the High and Low Risk-score groups of Combined dataset **(C)**, IL7 signaling pathway **(D)**, IL5 signaling pathway **(E)**, IL6 pathway **(F)**, energy metabolism **(G)**, electron transport chain Oxphos system in mitochondria **(H)**. PE, Preeclampsia; GSEA, Gene Set Enrichment Analysis. The significant enrichment screening criterion for GSEA enrichment analysis was $p < 0.05$.

suggested that there were two immune cells, namely Neutrophil and Plasmacytoid Dendritic cell, showing statistically differences in the abundance between the Low and High Risk-Score groups ($p < 0.05$).

We plotted the correlation scatter plots showing the relationship among Neutrophil and Plasmacytoid Dendritic cells in the Low-Risk cohort (Figure 8B) and the High-Risk cohort (Figure 8C) from the Combined dataset. The outcomes showed that, in the Low Risk-Score group, there was a marked inverse association among Neutrophil and Plasmacytoid Dendritic cells (Figure 8B, R = -0.709, p = 0.028). However, there was no association between the two immune cells in the High Risk-Score group (Figure 8C).

We used Spearman's statistical algorithm to calculate the association between the infiltrating abundances of the Neutrophil, Plasmacytoid Dendritic cells in the Low and High Risk-Score cohorts, and the expression of the four Common MMRDEGs in the Combined dataset data group (Figures 8D, E). The findings suggested that Neutrophil was positively correlated with the four Common MMRDEGs in the Low Risk-Score cohort of the Combined dataset (Figure 8D), moreover Neutrophil and *OCRL*

10.3389/fimmu.2025.1595706

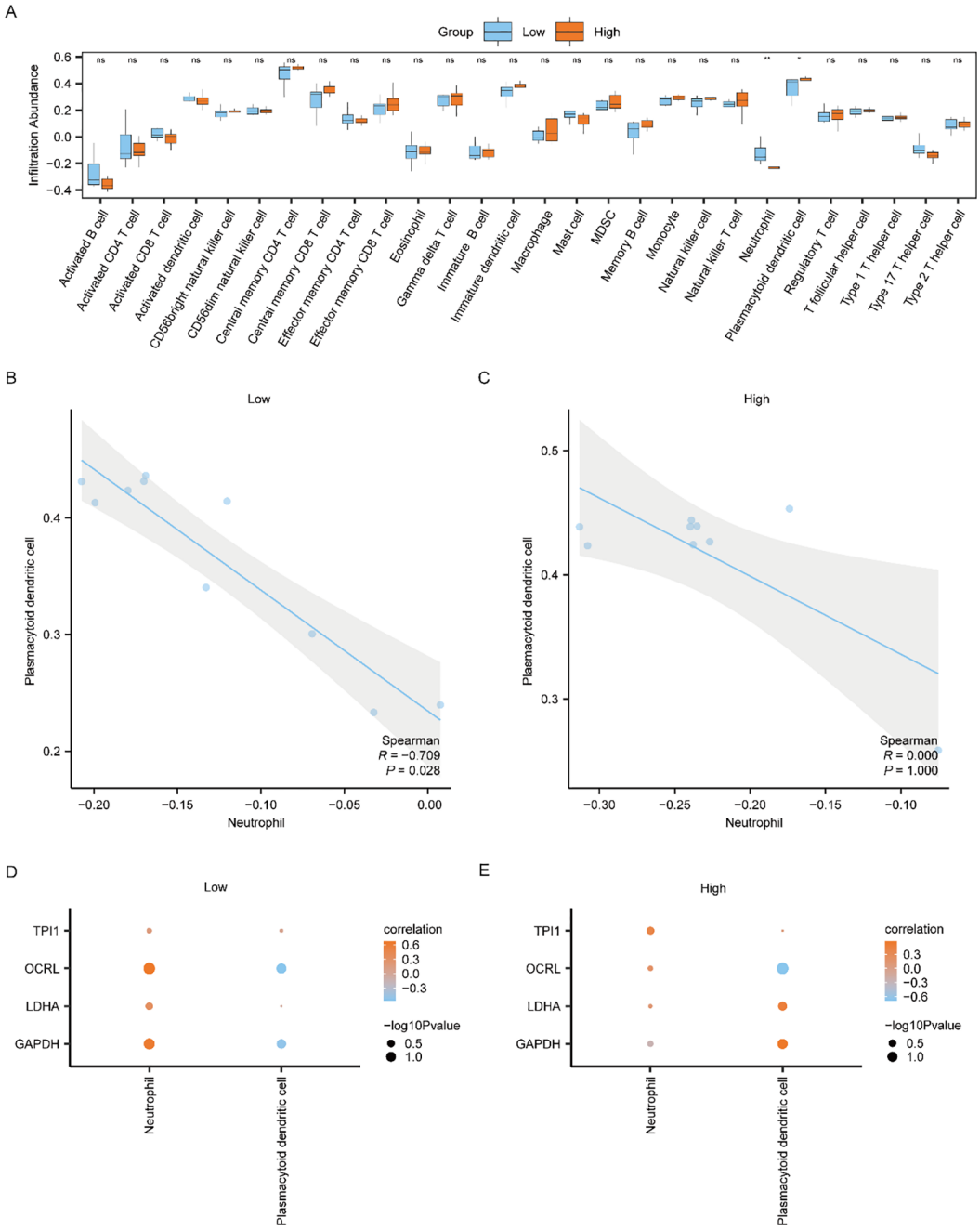

FIGURE 8
Differential analysis of ssGSEA immune characteristics between high and low risk-score groups in Combined dataset data. **(A)** The group comparison of ssGSEA immune infiltration analysis between the Low/High Risk-score groups of Combined dataset data. **(B, C)** Scatter plot of correlation between Neutrophil and Plasmacytoid dendritic cell of cell infiltration abundance in the Low Risk-score group **(B)** and High Risk-score group **(C)** of Combined dataset. **(D, E)** Dot plot of correlation between immune cells and Common MMRDEGs in the Low Risk-score group **(D)** and High Risk-score group **(E)** of Combined dataset. ssGSEA, single-sample gene-set enrichment Analysis; Common MMRDEGs, Common Mitochondrial energy metabolism related differentially expressed genes; PE, preeclampsia. The symbol ns is equivalent to $p \geq 0.05$ and not statistically significant; The symbol * is equivalent to $p < 0.05$, which is statistically significant; The symbol ** is equivalent to $p < 0.01$, which is highly statistically significant; The absolute value of the correlation coefficient in the scatter plot of correlation was more than 0.8, indicating a strong correlation. Moderate correlation was defined as an absolute value between 0.5 and 0.8. 0.3-0.5 is weak correlation; Values below 0.3 are considered weak or uncorrelated.

had the strongest association. In the High Risk-Score cohort of the Combined dataset data, Plasmacytoid Dendritic cells had the strongest correlation with *OCRL* (Figure 8E).

3.8 Cell-type Identification by Estimating Relative Subsets of RNA Transcripts (CIBERSORT) immunosignature comparative analysis among Low Risk-Score and High Risk-Score groups from the Combined dataset

The CIBERSORT method was utilized to estimate the abundance of 22 immune cell infiltrations in both the Low and High Score cohorts. A stacked bar chart was employed to graphically depict the distribution of immune cells across the dataset samples (Supplementary Figure 5A). There were 22 immune cells with non-zero infiltration abundances within the Combined dataset according to the results.

We used Spearman's statistical algorithm to assess the relationships among the 22 immune cells (Supplementary Figure 5B), and the findings suggested that the number of positive and negative associations between the 22 immune cells was basically equal, among which Mast cells activated and B cells memory had the strongest correlation.

We subsequently computed the association among immune cells and the four Common MMRDEGs using Spearman's statistical algorithm (Supplementary Figure 5C). The results showed that T cells CD4 memory activated, Dendritic cells resting, and T cells gamma delta were moderately positively correlated with the four Common MMRDEGs in the Combined dataset. Among all the associations examined, the most pronounced relationship was detected among naïve B cells and *GAPDH*.

3.9 PPI network and mRNA-RBP, mRNA-Drug and mRNA-TF interaction network were constructed

Since these four Common MMRDEGs (*OCRL, GAPDH, TPI1, LDHA*) are the most potentially valuable biomarker genes identified during model construction, they are suspected to play a crucial role in related disease processes. Therefore, conducting an in-depth study on their interactions can aid in understanding their biological mechanisms and clinical applications. Therefore, we utilized the STRING database (PPI network, minimum required interaction score: low confidence (0.150)) to perform the PPI analysis of the 4 Common MMRDEGs (treated as hub genes) and visualized by Cytoscape software (Figure 9A).

And then, we utilized the ENCORI database to forecast RNA binding proteins (RBPs) that interacted with four Common MMRDEGs and subsequently visualized the mRNA-RBP interaction network by Cytoscape software (Figure 9B). The mRNA-RBP interaction network, in which green quadrilateral blocks presenting RBPs and the blue quadrilateral blocks presenting mRNAs, was composed of 4 Common MMRDEGs (*OCRL*, *GAPDH*, *TPI1* and *LDHA*) and 51 RBP molecules, which constituted 58 pairs of mRNA-RBP interaction relationships. The specific mRNA-RBP interaction relationships are depicted in Supplementary Table 10.

We utilized the CHIPBase database (version 3.0) and hTFtarget database to identify transcription factors (TFs) that bound to the four Common MMRDEGs. Then we screened by "Number of samples found (downstream)>0" and "Number of samples found (upstream) >0", and finally got 3 Common MMRDEGs (*OCRL*, *GAPDH*, *TPI1*) and 39 pairs of interaction data of 29 TFs were graphically represented utilizing Cytoscape software (Figure 9C). In the mRNA-TF interaction network, those blue quadrilateral blocks represent mRNAs, and the green quadrilateral blocks are TFs. The detailed mRNA-TF interactions are depicted in the Supplementary Table 11.

We employed the Comparative Toxicogenomics Database (CTD) to identify small molecule compounds or potential drugs that interact with four commonly observed MMRDEGs. The selection criterion for mRNA-Drugs interaction pairs was set as "Reference Count" > 1. To render the mRNA-Drug interaction network (Figure 9D), we employed Cytoscape software. Within the mRNA-Drugs interaction network, the blue quadrilateral blocks signify mRNAs, while the green quadrilateral blocks denote drugs. Our analysis revealed that our mRNA-Drugs interaction network consisted of three common MMRDEGs (*OCRL, LDHA*, and *TPI1*) and twenty-four drug molecules, forming thirty mRNA-Drugs interaction associations. Detailed information regarding these specific interactions can be found in Supplementary Table 12.

The AlphaFold Protein Structure Database (https://www.alphafold.ebi.ac.uk/) encompasses approximately 350,000 protein structure predictions generated by the AlphaFold AI system. This comprehensive database includes predictions for humans and 20 widely studied model organisms in biological research, such as E. coli, Drosophila, zebrafish, and mice. Remarkably, AlphaFold has successfully predicted the structures of 98.5% of human proteins within the human proteome. By combining AlphaFold's structural prediction, we can more comprehensively construct and understand complex interaction networks, revealing the important roles of these genes in cellular metabolic regulation. This, in turn, provides a molecular basis for exploring the mechanisms of related diseases. To investigate the protein structures of four common MMRDEGs, we leveraged the resources provided by the AlphaFold website and presented our findings in Figures 10A–D.

4 Discussion

PE is a prevalent and severe complication of pregnancy, posing a substantial threat to both maternal and infant health. Its prognosis is intricately linked to maternal and infant outcomes. The primary clinical manifestations include hypertension, proteinuria, as well as liver and kidney impairment (59). Currently, the precise pathogenesis of PE remains incompletely elucidated. Study indicates that mitochondrial dysfunction is a pivotal factor in the

10.3389/fimmu.2025.1595706

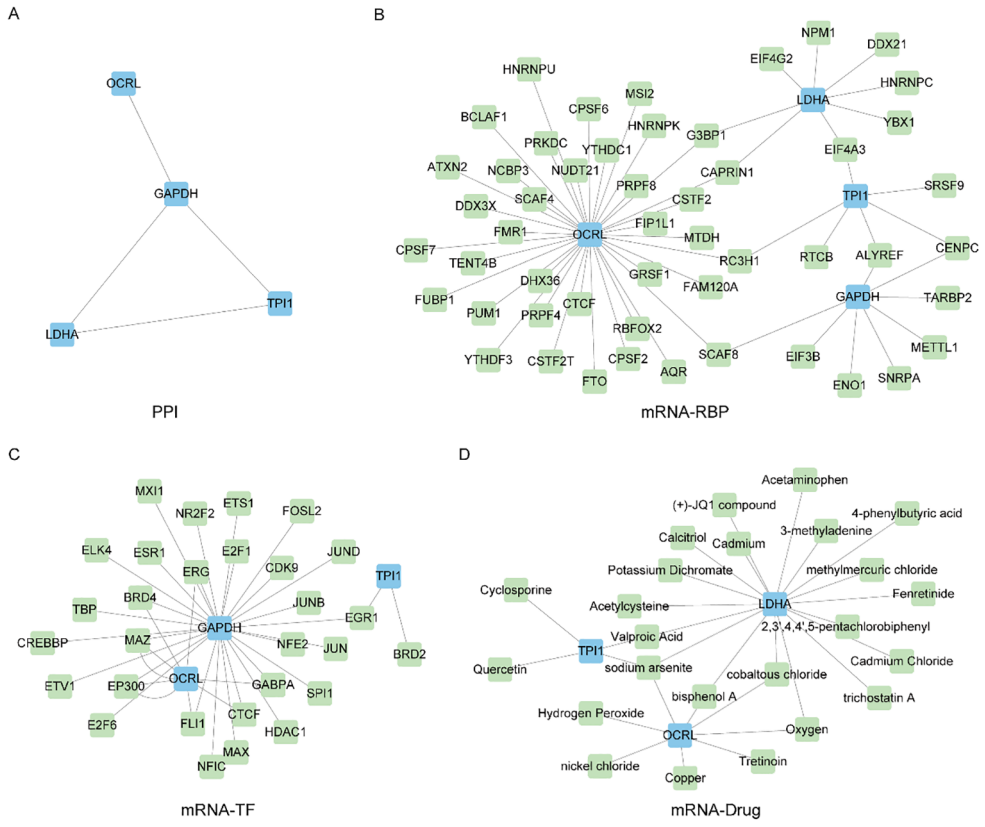

FIGURE 9
Construct PPI network and mRNA-RBP, mRNA-TF, mRNA-Drug interaction network. **(A)** Protein interaction network of Common MMRDEGs (PPI network). **(B)** mRNA-RBP network of Common MMRDEGs, blue quadrangle blocks are mRNA; Green quadrilateral blocks are RBP. **(C)** mRNA-TF network of Common MMRDEGs, and the blue quadrangle blocks in the mRNA-TF interaction network are mRNA; Green quadrangle-shaped blocks are TFs. **(D)** mRNA-Drug network of Common MMRDEGs, and the blue quadrangle blocks in the mRNA-Drug interaction network are mRNA; Green quadrangular blocks are drugs. PE, Preeclampsia; RBP, RNA binding protein; TFs, Transcription factors; Common MMRDEGs, Common Mitochondrial energy metabolism related differentially expressed genes.

development and progression of PE, with marked mitochondrial abnormalities being detected in PE patient (22, 60). The level of oxidative stress in patients with PE is significantly elevated. The excessive production of oxygen free radicals can induce damage to placental trophoblast cells (58, 61), while mitochondrial dysfunction further exacerbates oxidative stress, creating a vicious cycle that worsens the progression of PE (58). Mitochondria are the primary organelles responsible for cellular energy production. Impairment in mitochondrial function leads to a decrease in energy supply, which may contribute to elevated blood pressure, proteinuria, and multi-organ dysfunction among patients diagnosed with PE (62, 63). In addition, the immune response in patients with PE is markedly enhanced (8, 64). Another study suggests that immune system dysregulation may be closely associated with mitochondrial dysfunction (65), thus implying that immune dysregulation could contribute to the development of PE. Moreover, studies have further demonstrated that PE patients face a significantly elevated risk of developing hypertension and cardiovascular disease later in life (66, 67). PE can also result in FGRs, intrauterine distress, preterm delivery, and even intrauterine death due to its impact on maternal-fetal blood supply and oxygen delivery (68, 69). Therefore, the early diagnosis of PE is essential for enabling timely intervention and effectively reducing maternal and infant risks (70, 71). Currently, clinical screening primarily relies on the measurement of blood pressure and proteinuria (72), along with evaluations of edema, liver and kidney function (73, 74). However, these methods have limitations in terms of sensitivity and specificity.

Through integrative analysis of the GSE24129, GSE30186, and GSE54618 datasets, we identified 1,073 DEGs between PE cases and Control group. Subsequent comparative intersection analysis with MMRGs revealed 24 MMRDEGs. Notably, 16 of these MMRDEGs demonstrated significant differential expression patterns between PE cases and Control group. These DEGs may be associated with the development of PE, especially those MMRDEGs, which may affect cellular energy production and metabolic processes and play important roles in PE. Mitochondrial energy metabolism is a common metabolic pathway in tumor cells, and MMRDEGs may include key genes for hypoxia, oxidative stress and programmed cell death. Aberrant expression of these genes may lead to impaired chorionic trophoblast cell function, which in turn affects the development and prognosis of PE.

In this investigation, our findings revealed that *ATG7* expression was markedly decreased in PE cases. *ATG7* is an

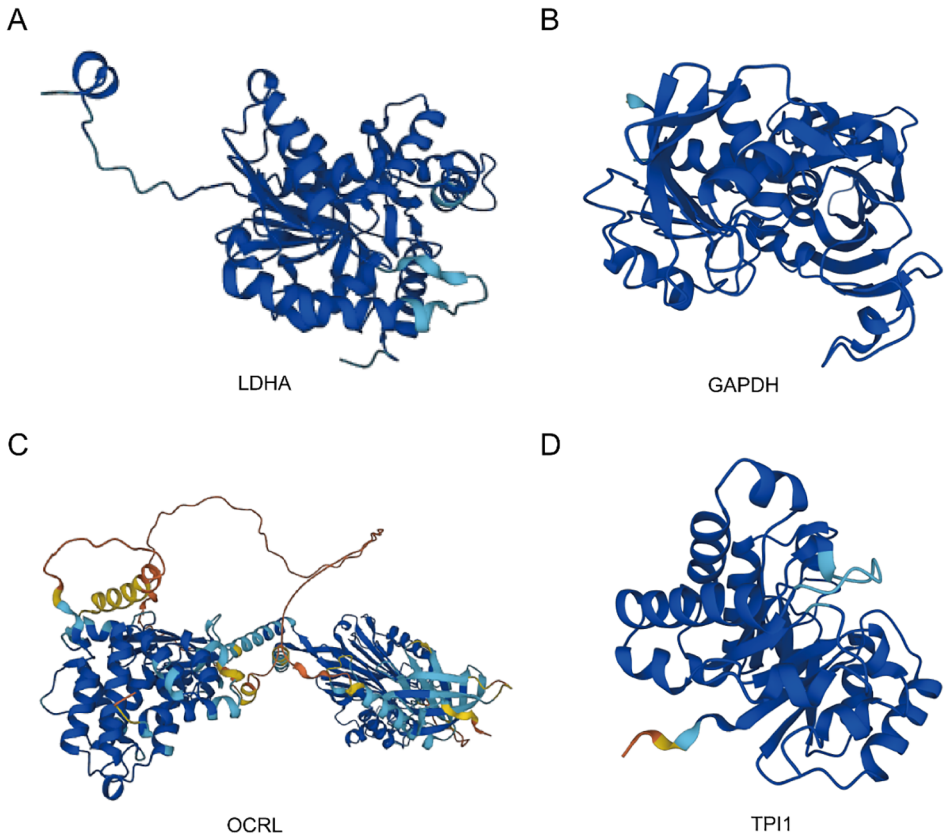

FIGURE 10
Protein structures of common MMRDEGs. The protein structures of LDHA **(A)**, GAPDH **(B)**, OCRL **(C)**, and TPI1 **(D)** are shown. The AlphaFold website produced a confidence score per residue (pLDDT) between 0 and 100. Some regions below 50 pLDDT may be isolated unstructured regions, and when pLDDT < 50 (red area), the model confidence is very low; When 50 < pLDDT < 70 (yellow area), the model confidence is low; When 70 < pLDDT < 90 (light blue area), the model confidence was normal. When 90 < pLDDT (blue area), the model confidence is very high. Common MMRDEGs, Common Mitochondrial energy metabolism related differentially expressed genes.

important component of early autophagy that encodes the E1 ubiquitin-activating enzyme, and its absence can lead to defective autophagy in the uterine vascular microenvironment, which in turn reduces uterine vascular permeability (75, 76). Decreased *ATG7* expression was found to inhibit primary cilia formation and trophoblast invasion, which in turn led to poor pregnancy outcomes (77). However, we must also acknowledge the dual role of autophagy in both physiological and pathological states, as excessive inhibition of autophagy may similarly have negative impacts on placental function. Alzubaidi et al. discovered that *ATG7* was elevated expressed in placental tissues of PE patients (78). This contradiction indicates that our current understanding of the relationship between *ATG7* and PE is potentially inadequate. Therefore, it is crucial to clarify the role of *ATG7* in various environments. Future research, particularly longitudinal studies, will be essential to elucidate the precise role of *ATG7* in the pathogenesis of PE. The main function of *SOD1* is to reduce free radical damage to cells through redox reactions. Studies showed that Oxidative stress inhibited SOD1 expression in placental tissue, which was significantly decreased in L-NAME-induced preeclamptic mice (79, 80) and it align closely with the conclusions drawn in our study. *FOXO1* is a member of the *FOXO* family and is intimately linked to cellular autophagy (81). It was confirmed that *FOXO1* was highly expressed in placental tissues of PE patients, which is consistent with our findings (78).

Functional correlation analysis was performed to explore the 16 MMRDEGs, we acquired a series of crucial insights regarding the PE pathogenesis. Firstly, GO analysis findings indicated that these 16 genes were primarily enriched in pyruvate metabolism, glycolysis, and ATP metabolism. Furthermore, KEGG analysis demonstrated that these genes are linked to processes such as glycolysis/glycolysis, HIF-1 signaling pathway, carbon metabolism, inositol phosphate metabolism, alanine, aspartate and glutamate metabolism. It has been established that placental mitochondrial dysfunction is prevalent in preeclampsia, while the inability to upregulate glycolysis is significantly correlated with increased disease severity (82). Pyruvate, a key product of glycolysis, plays an essential role in the production of reducing equivalents within mitochondria, ATP synthesis, and biosynthesis pathways such as glucose, fatty acids, and amino acids. Pyruvate metabolism is crucial for maintaining carbon homeostasis, and its dysregulation has been linked to various diseases, including diabetes, cancer, Embryogenesis, and cardiovascular disorders (83, 84). HK-2 exhibits phosphotransferase activity, alcohol-group receptor activity, and fructokinase activity. Relevant

pathways include glycolysis and GDP-glucose biosynthesis II. Studies demonstrated that HK-2 is involved in glycolytic flux and mitochondrial activity during maladaptive inflammation in brain diseases. Additionally, HK-2 may exert therapeutic effects in osteoarthritis by modulating glucose metabolism (85–87). PGK-1, a glycolytic enzyme, is associated with glycolysis and gluconeogenesis pathways. Studies have shown that PGK-1 plays a significant role in neurodegenerative diseases (88, 89). Various studies have investigated the pivotal role of hypoxia-inducible factor-1 (HIF-1) in metabolic reprogramming across multiple pathways, including glycolysis, glycogen synthesis, lipid metabolism, the electron transport chain (ETC), the tricarboxylic acid (TCA) cycle, glutamine and serine metabolism, ROS production, as well as mitochondrial biogenesis and autophagy (90, 91). Abnormal expression of DNA and histone proteins represents a key characteristic of tumor cells. Their nucleotide metabolism and epigenetic regulation rely on the one-carbon metabolic pathway to preserve genomic stability and integrity (92). Given the further potential regulatory functions of mitochondria in abnormal energy metabolism, it offers a novel perspective for investigating the mechanism of preeclampsia. Finally, GSEA and GSVA analyses demonstrated a significant enrichment of genes from different (PE/Control) groups in the Combined dataset, specifically in the vascular smooth muscle contraction pathway, IL9 signaling pathway, Notch signaling pathway, IL2 signaling pathway, IL6/7 signaling pathway, cell surface interactions at the vascular wall. These gene clusters are critically involved in hypertension pathogenesis, immune regulation, inflammatory responses, and redox homeostasis maintenance through interconnected molecular pathways (93–96). These findings offer valuable insights and directions for further exploration of the pathogenesis of PE.

In the study, we constructed a diagnostic model containing four Common MMRDEGs (*OCRL, GAPDH, TPI1*, *LDHA)*, and verified that the model had high accuracy (AUC = 0.970) by ROC curve. Additionally, an external validation dataset was employed to assess the applicability of the model, and the results showed that the model achieved satisfactory accuracy for diagnosing PE. These four Common MMRDEGs not only showed significant differential expression, but also functional similarity among them. *OCRL* encodes an inositol polyphosphate 5-phosphatase that acts on phosphoinositide, which is a minor component of cell membranes but is a key regulator of intracellular transport (97, 98). *OCRL* catalyzes the production of the second messenger inositol triphosphate (IP3) and diacylglycerol (DAG) via phosphatidylinositol metabolism, thereby activating calcium release from intracellular stores. Deficiency in *OCRL1* results in mitochondrial calcium overload, ultimately causing mitochondrial dysfunction and apoptosis in T cells (99). Study shows that DAG mediates diabetic hyperglycemia and its associated complications via the DAG-PKC signaling pathway (100). In addition, research has demonstrated that the uterine artery endothelium exhibits an adaptive increase in Ca2+/IP3 exchange during pregnancy, however, a capacity that is notably diminished in preeclampsia (101). Recent studies have shown that *OCRL* plays an important role in cell metabolism, oxidative stress and inflammatory response, which provides new perspectives for understanding its specific effects in PE (99, 102, 103). Drugs that regulate the expression or function of *OCRL* may help restore the normal metabolic state of the placenta and reduce oxidative stress and inflammation, thereby improving the prognosis of PE.

As a glycolytic enzyme, the main function of *GAPDH* is to catalyze the conversion of glyceraldehyde-3-phosphate to 1,3-bisphosphoglycerate, concomitantly generating ATP. Therefore, *GAPDH* is a critical energy source for cellular metabolism (104). In addition, *GAPDH* has a variety of non-glycolytic functions. For instance, regulation of RNA export, DNA repair, autophagy and cell death (105). Dimethyl fumarate exerts its anti-inflammatory effects by inhibiting glycolysis in immune cells through inhibit the catalytic activity of *GAPDH (*106). Further functional validation and mechanism research may provide new targets and help for the early diagnosis and treatment of PE. *TPI1* regulates the interconversion between glyceraldehyde-3-phosphate and dihydroxyacetone phosphate during glycolysis and gluconeogenesis, therefore, it is essential in the modulation of energy metabolism. *TPI1* can function as an inhibitor to modulate NK cytotoxicity via the SHP-1-ERK-STAT3 pathway (107). And the Erk signaling pathway has a direct impact on trophoblast proliferation (108). In addition, an increasing number of studies indicated that this gene influences glycolysis in target cells via different pathways, such as the METTL5/cMyc/TPI1 pathway, thereby affecting the onset and prognosis of various diseases, including lung cancer, liver cancer, and myopia (109–111). *LDHA* is widely present in the cytoplasm and can also be expressed in mitochondria and nucleus, which participate in and regulate cellular energy metabolism and have an important impact on cellular function (112). *LDHA* depletion leads to a reduction in ATP production, consequently diminishing PI3K-AKT-Foxo1 signaling and impairing the redox responses of effector T cells (113). Yang M et al. showed that glucose transporter 1 plays a critical role in glucose uptake and subsequent metabolic utilization. Knockdown of *GLUT1* reduced glucose uptake and suppressed lactate production by modulating the mRNA expression of *LDHA*, resulting in impairment of blastocyst implantation, trophoblast invasion, and placental development (114). Furthermore, we validated their expression in placental tissues using RT-qPCR assay. The before mentioned metabolic and immune disorders were found to be consistent with the impaired mitochondrial function, reduced ATP synthesis, and abnormal immune cell function observed in the placenta of patients with PE. These findings present a novel perspective on potential early diagnostic biomarkers for PE. The diagnostic model combined the expression levels of these genes and successfully differentiated between PE and Control group samples, suggesting their potential utility as diagnostic indicators for pregnancy-related hypertensive conditions.

GSEA and GSVA analyses revealed multiple pathways that exhibited marked differences among the Low and High-risk groups in the Combined dataset, encompassing various biological processes such as redox reactions, immune responses, and cell cycle regulation. Significantly enriched or altered genes in these pathways may have different impacts on Low and High-risk cohorts, leading to significant differences in immune status and cellular function between patients at

different risk levels. This provides new insights for understanding risk assessment in PE patients and potential targets for future therapeutic strategies. Additionally, it confirmed the biological validity of the MMRDEGs correlation diagnosis model.

Existing research indicates that PE is a complex pregnancy-related disease involving multiple pathological mechanisms, including abnormal immune system responses. There is an increase in biomarkers indicating activation of the terminal complement pathway (115, 116). Deer et al. emphasized that immune cells such as regulatory T cells, macrophages, natural killer cells, and neutrophils are known to play major causal roles in the pathology of preeclampsia in their review (117). Aneman et al. further explored the distinct manifestations of the innate immune system in early and late stages of PE, positing that understanding immune cells holds the key to unveiling the pathogenesis of PE (118). In addition, Nieves et al. explored the impact of autoimmune diseases and infections on PE, highlighting that these factors can significantly exacerbate the condition (119). Lastly, Luo et al. uncovered immune interference at the maternal-fetal interface in PE via single-cell analysis and discussed HLA-F-mediated immune tolerance (120). Our study employed the ssGSEA and CIBERSORT algorithms to analyze immune cell infiltration characteristics between High-Risk and Low-Risk groups. Our study suggests that differential expression of neutrophils and plasmacytoid dendritic cells between these two groups, with neutrophils showing a positive correlation with four common MMRDEGs in the Low-Risk group. And among the 22 types of immune cells with non-zero infiltration abundance, Mast cells and B memory cells exhibited the strongest correlation.

Neutrophils constitute a critical component of the innate immune system. They are recruited to sites of infection or damaged tissues via a series of coordinated processes, including rolling, adhesion, spreading, intravascular crawling, transepithelial migration, and chemotaxis-driven tissue infiltration. These functions depend on cytoskeletal reorganization and energy metabolism. Studies indicated that neutrophils possess the ability to adapt to various metabolic pathways, such as metabolic pathways involving glucose, lipids, and amino acids, during inflammation or in response to different disease states (121, 122). Notably, mitochondria serve as crucial sites for the metabolic processing of these nutrients. Neutrophil extracellular traps (NETs), induced by oxidative stress, represent a critical immune defense mechanism against external bacterial infections (123). Moreover, NETs enhance mitochondrial stability through the TLR4/PGC1α pathway (122). Elevated neutrophil levels have been documented in the peripheral blood and subcutaneous fat micro vessels of patients with PE (124, 125). Furthermore, studies have demonstrated that the activity of neutrophils is influenced by the alteration in the plasma expression levels of MMP-1 and PAF in patients with PE (124, 126). One experimental study indicated that neutrophils cultured in placental conditioned medium derived from women with PE exhibited significantly greater adherence to endothelial cells compared to those cultured in placental conditioned medium from controls, suggesting that factors influencing neutrophil quantity and function may originate from placental sources (124). These studies were consistent with the results of our study.

Dendritic cells (DCs) are professional antigen-presenting cells, and plasmacytoid dendritic cells (pDCs) are one subset of DCs. pDCs can secrete substantial amounts of IFN-α and IFN-β, as well as IL-6, IL-8, IL-12, and tumor necrosis factors (TNFs), via the activation of the Toll-like receptor (TLR) 7/9-MyD88-IRF7 pathway (127). During pregnancy, the primary role of DCs is to present paternal/fetal antigens to regulatory T cells, thereby maintaining immune tolerance at the maternal-fetal interface (128). Studies have demonstrated that the levels of pDCs in the serum of PE patients are significantly decreased compared to those of normal patients (129). In addition, research has shown that DCs display diminished responsiveness to stimulation by various TLRs ligands in PE patients compared to those in healthy pregnancy (130). Moreover, the expression level of TLR3 at the maternal-fetal interface in PE is significantly elevated (131). The upregulated expression of TLR3 may function as a protective mechanism to counteract the impaired responsiveness of DCs to the stimulation by various TLR ligands. These findings suggest that DC-mediated inflammation is involved in local regulation at the maternal-fetal interface and may plays a crucial role in the pathogenesis and progression of PE. Our immune infiltration analysis demonstrated a significant inverse correlation between neutrophils and pDCs within the low-risk group. Conversely, no such significant correlation was detected in the high-risk group. These results suggest that there is complex immune regulation mediated by neutrophils and pDCs in PE patients, which may play a critical role in its progression.

Immunological alterations constitute a critical component of the etiology of PE, characterized by the presence of autoantibodies, including agonistic autoantibodies against the angiotensin II type 1 receptor (AT1) and so on (132). Salby et al. identified the proportion of the B cell is elevated in PE patients, because of a significantly diminished expression of programmed cell death protein 1 (PD-1) on CD27+CD24hiCD38hi regulatory B cells (133). Experimental investigations have confirmed that B2 cells activated by placental ischemia can induce hypertension, activate circulating NK cells, and promote the production of AT1 agonistic autoantibodies in normally pregnant rats (132). Mast cells are typically activated in response to pathogen invasion, tissue injury, or infection firstly and can release cytokines to regulate the local inflammatory immune reaction (134). Previous studies have shown that mast cell-derived exosomal miR-181a-5p regulates the viability, migration, and invasion of HTR-8/SVneo cells through the YY1/MMP-9 pathway (135). And relevant studies have indicated that the average histamine concentration and mast cell density are higher in PE patients (136). Our analysis of the immune infiltration in non-zero abundance immune cells showed that Mast cells activated and B cells memory had the strongest correlation. Further supporting of the observation was that Mast cells regulate B cell function through secreted cytokines in diseases such as allergic rhinitis and pulmonary hypertension (137, 138). In addition, antibodies generated by the B cell lineage and cytokines such as interleukin-

10 (IL-10) can substantially modulate the function of mast cells. This modulation can, in turn, promote or restrict the development of regulatory B cells via multiple mechanisms (134). This finding unveils the connection between mitochondrial metabolism and immune cell function, presenting a novel research avenue for future immunotherapy and targeted interventions targeting PE, offering a fresh perspective for its early diagnosis and intervention.

Finally, as the four Common MMRDEGs are the most potentially valuable biomarkers screened by the model constructed and they may play key roles in the pathogenesis of PE, we constructed the PPI, mRNA-Drug, mRNA-RBP and mRNA-TF interaction networks with the four common genes. We identified 51 RBPs genes that could be therapeutic targets for PE by analyzing gene nodes in the network. Then, we utilized the CTD database to forecast potential therapeutic agents or small molecule compounds for PE treatment, identifying 24 drug molecules. Furthermore, we displayed the protein structures of four common MMRDEGs by leveraging the resources of AlphaFold. The results provided molecular basis for exploring the mechanism of PE. However, the potential mechanism and role required more investigation.

However, there are several important limitations to this study that should be considered when interpreting the results. Firstly, the relatively small sample size of the combined dataset (45 total: 19 preeclampsia cases and 26 controls) may limit the generalizability of transcriptomics and machine learning approaches. Therefore, we validated the mRNA-level expression differences of MMRDEGs using RT-qPCR and conducted the external validation of an independent dataset. Additionally, the significant difference in gestational weeks at delivery between the PE group and the Control group, while clinically relevant to PE management, could introduce confounding factors into gene expression analysis. Future studies should focus on large-scale, multi-center cohorts to enhance the robustness and reliability of the findings and their clinical applicability. Furthermore, protein-level validation of these biomarkers and functional investigations using cell lines and animal models are essential to confirm their roles in the pathogenesis of PE and assess their potential as therapeutic targets.

5 Conclusion

In this paper, we comprehensively explored the pathogenesis of preeclampsia, constructed a scoring model, analyzed the relationship between MMRDEGs and immune micro-infiltration, and predicted potential therapeutic targets and drug molecules for PE by GO, KEGG, GSEA, and GSVA. Nevertheless, the specific pathogenesis and molecular targets still need to be further verified.

Data availability statement

The raw data supporting the conclusions of this article will be made available by the authors, without undue reservation.

Ethics statement

The studies involving humans were approved by Ethics Committee of the Affiliated Hospital of Qingdao University (Approval No: QYFY WZLL 29434). The studies were conducted in accordance with the local legislation and institutional requirements. The participants provided their written informed consent to participate in this study.

Author contributions

CaL: Conceptualization, Data curation, Formal Analysis, Investigation, Methodology, Resources, Software, Supervision, Validation, Visualization, Writing – original draft, Writing – review & editing. FL: Formal Analysis, Data curation, Investigation, Software, Visualization, Writing – original draft. ChL: Methodology, Writing – review & editing. XZ: Methodology, Writing – review & editing. QL: Formal Analysis, Writing – review & editing. AJ: Resources, Writing – review & editing. SZ: Conceptualization, Formal Analysis, Methodology, Resources, Supervision, Writing – review & editing.

Funding

The author(s) declare that no financial support was received for the research and/or publication of this article.

Conflict of interest

The authors declare that the research was conducted in the absence of any commercial or financial relationships that could be construed as a potential conflict of interest.

Generative AI statement

The author(s) declare that no Generative AI was used in the creation of this manuscript.

Publisher's note

Supplementary material

The Supplementary Material for this article can be found online at: https://www.frontiersin.org/articles/10.3389/fimmu.2025.1595706/full#supplementary-material

References

1. Wu Y, Li M, Ying H, Gu Y, Zhu Y, Gu Y, et al. Mitochondrial quality control alterations and placenta-related disorders. *Front Physiol*. (2024) 15:1344951. doi: 10.3389/fphys.2024.1344951

2. Taglauer ES, Fernandez-Gonzalez A, Willis GR, Reis M, Yeung V, Liu X, et al. Antenatal mesenchymal stromal cell extracellular vesicle therapy prevents preeclamptic lung injury in mice. *Am J Respir Cell Mol Biol*. (2022) 66:86–95. doi: 10.1165/rcmb.2021-0307OC

3. Cipolla MJ, Biller J. Persistent brain injury after preeclampsia. *Neurology*. (2017) 88:1216–7. doi: 10.1212/WNL.0000000000003773

4. Duffy J, Cairns AE, Richards-Doran D, van 't Hooft J, Gale C, Brown M, et al. A core outcome set for pre-eclampsia research: an international consensus development study. *BJOG: an Int J obstetrics gynaecology*. (2020) 127:1516–26. doi: 10.1111/1471-0528.16319

5. Xu X, Zhu M, Zu Y, Wang G, Li X, Yan J. Nox2 inhibition reduces trophoblast ferroptosis in preeclampsia via the STAT3/GPX4 pathway. *Life Sci*. (2024) 343:122555. doi: 10.1016/j.lfs.2024.122555

6. Murugesan S, Hussey H, Saravanakumar L, Sinkey RG, Sturdivant AB, Powell MF, et al. Extracellular vesicles from women with severe preeclampsia impair vascular endothelial function. *Anesth analgesia*. (2022) 134:713–23. doi: 10.1213/ANE.0000000000005812

7. Hobson SR, Gurusinghe S, Lim R, Alers NO, Miller SL, Kingdom JC, et al. Melatonin improves endothelial function *in vitro* and prolongs pregnancy in women with early-onset preeclampsia. *J pineal Res*. (2018) 65:e12508. doi: 10.1111/jpi.2018.65.issue-3

8. Horvat Mercnik M, Schliefsteiner C, Sanchez-Duffhues G, Wadsack C. TGFβ signalling: a nexus between inflammation, placental health and preeclampsia throughout pregnancy. *Hum Reprod Update*. (2024) 30:442–471. doi: 10.1093/humupd/dmae007

9. Overton E, Tobes D, Lee A. Preeclampsia diagnosis and management. *Best Pract Res Clin anaesthesiology*. (2022) 36:107–21. doi: 10.1016/j.bpa.2022.02.003

10. Phipps EA, Thadhani R, Benzing T, Karumanchi SA. Pre-eclampsia: pathogenesis, novel diagnostics and therapies. *Nat Rev Nephrology*. (2019) 15:275–89. doi: 10.1038/s41581-019-0119-6

11. Xiong D, Yin Z, Huang M, Wang Y, Hardy M, Kalyanaraman B, et al. Mitochondria-targeted atovaquone promotes anti-lung cancer immunity by reshaping tumor microenvironment and enhancing energy metabolism of anti-tumor immune cells. *Cancer Commun (London England)*. (2024) 44:448–52. doi: 10.1002/cac2.12500

12. Zou B, Jia F, Ji L, Li X, Dai R. Effects of mitochondria on postmortem meat quality: characteristic, isolation, energy metabolism, apoptosis and oxygen consumption. *Crit Rev Food Sci Nutr*. (2023) 64:11239–62. doi: 10.1080/10408398.2023.2235435

13. Su L, Zhang J, Gomez H, Kellum JA, Peng Z. Mitochondria ROS and mitophagy in acute kidney injury. *Autophagy*. (2023) 19:401–14. doi: 10.1080/15548627.2022.2084862

14. Haridevamuthu B, Murugan R, Seenivasan B, Meenatchi R, Pachaiappan R, Almutairi BO, et al. Synthetic azo-dye, Tartrazine induces neurodevelopmental toxicity via mitochondria-mediated apoptosis in zebrafish embryos. *J hazardous materials*. (2024) 461:132524. doi: 10.1016/j.jhazmat.2023.132524

15. Yang L, Yao C, Su Z, Fang Y, Pandey NK, Amador E, et al. Combination of disulfiram and Copper-Cysteamine nanoparticles induces mitochondria damage and promotes apoptosis in endometrial cancer. *Bioactive materials*. (2024) 36:96–111. doi: 10.1016/j.bioactmat.2024.02.009

16. Ticiani E, Gingrich J, Pu Y, Vettathu M, Davis J, Martin D, et al. Bisphenol S and epidermal growth factor receptor signaling in human placental cytotrophoblasts. *Environ Health perspectives*. (2021) 129:27005. doi: 10.1289/EHP7297

17. Li J, Quan X, Zhang Y, Yu T, Lei S, Huang Z, et al. PPARγ Regulates triclosan induced placental dysfunction. *Cells*. (2021) 11:86. doi: 10.3390/cells11010086

18. Huang P, Song Y, Yang Y, Bai F, Li N, Liu D, et al. Identification and verification of diagnostic biomarkers based on mitochondria-related genes related to immune microenvironment for preeclampsia using machine learning algorithms. *Front Immunol*. (2023) 14:1304165. doi: 10.3389/fimmu.2023.1304165

19. Fisher JJ, Vanderpeet CL, Bartho LA, McKeating DR, Cuffe JSM, Holland OJ, et al. Mitochondrial dysfunction in placental trophoblast cells experiencing gestational diabetes mellitus. *J Physiol*. (2021) 599:1291–305. doi: 10.1113/tjp.v599.4

20. Juan-Reyes SS, Gómez-Oliván LM, Juan-Reyes NS, Islas-Flores H, Dublán-García O, Orozco-Hernández JM, et al. Women with preeclampsia exposed to air pollution during pregnancy: Relationship between oxidative stress and neonatal disease - Pilot study. *Sci total environment*. (2023) 871:161858. doi: 10.1016/j.scitotenv.2023.161858

21. Cipolla MJ, Tremble SM, DeLance N, Johnson AC. Worsened stroke outcome in a model of preeclampsia is associated with poor collateral flow and oxidative stress. *Stroke*. (2023) 54:354–63. doi: 10.1161/STROKEAHA.122.041637

22. Long J, Huang Y, Tang Z, Shan Y, Feng D, Wang W, et al. Mitochondria targeted antioxidant significantly alleviates preeclampsia caused by 11β-HSD2 dysfunction via OPA1 and mtDNA maintenance. *Antioxidants (Basel Switzerland)*. (2022) 11:1505. doi: 10.3390/antiox11081505

23. Pearce SF, Rebelo-Guiomar P, D'Souza AR, Powell CA, Haute LV, Minczuk M. Regulation of mammalian mitochondrial gene expression: recent advances. *Trends Biochem Sci*. (2017) 42:625–39. doi: 10.1016/j.tibs.2017.02.003

24. Ricci CA, Reid DM, Sun J, Santillan DA, Santillan MK, Phillips NR, et al. Maternal and fetal mitochondrial gene dysregulation in hypertensive disorders of pregnancy. *Physiol Genomics*. (2023) 55:275–85. doi: 10.1152/physiolgenomics.00005.2023

25. Pandey D, Yevale A, Naha R, Kuthethur R, Chakrabarty S, Satyamoorthy K. Mitochondrial DNA copy number variation - A potential biomarker for early onset preeclampsia. *Pregnancy hypertension*. (2021) 23:1–4. doi: 10.1016/j.preghy.2020.10.002

26. Deng YJ, Ren EH, Yuan WH, Zhang GZ, Wu ZL, Xie QQ. GRB10 and E2F3 as diagnostic markers of osteoarthritis and their correlation with immune infiltration. *Diagnostics (Basel)*. (2020) 10:171. doi: 10.3390/diagnostics10030171

27. Dunk CE, Bucher M, Zhang J, Hayder H, Geraghty DE, Lye SJ, et al. Human leukocyte antigen HLA-C, HLA-G, HLA-F, and HLA-E placental profiles are altered in early severe preeclampsia and preterm birth with chorioamnionitis. *Am J Obstetrics Gynecology*. (2022) 227:641.e641–641.e613. doi: 10.1016/j.ajog.2022.07.021

28. Zhao Y, Zhang X, Du N, Sun H, Chen L, Bao H, et al. Immune checkpoint molecules on T cell subsets of pregnancies with preeclampsia and gestational diabetes mellitus. *J Reprod Immunol*. (2020) 142:103208. doi: 10.1016/j.jri.2020.103208

29. Roberts JM. Preeclampsia epidemiology(ies) and pathophysiology(ies). *Best Pract Res Clin Obstetrics Gynaecology*. (2024) 94:102480. doi: 10.1016/j.bpobgyn.2024.102480

30. Duckitt K, Harrington D. Risk factors for pre-eclampsia at antenatal booking: systematic review of controlled studies. *Bmj*. (2005) 330:565. doi: 10.1136/bmj.38380.674340.E0

31. Nishizawa H, Ota S, Suzuki M, Kato T, Sekiya T, Kurahashi H, et al. Comparative gene expression profiling of placentas from patients with severe pre-eclampsia and unexplained fetal growth restriction. *Reprod Biol Endocrinol*. (2011) 9:107. doi: 10.1186/1477-7827-9-107

32. Meng T, Chen H, Sun M, Wang H, Zhao G, Wang X. Identification of differential gene expression profiles in placentas from preeclamptic pregnancies versus normal pregnancies by DNA microarrays. *Omics: J Integr Biol*. (2012) 16:301–11. doi: 10.1089/omi.2011.0066

33. Jebbink JM, Boot RG, Keijser R, Moerland PD, Aten J, Veenboer GJM, et al. Increased glucocerebrosidase expression and activity in preeclamptic placenta. *Placenta*. (2015) 36:160–9. doi: 10.1016/j.placenta.2014.12.001

34. Gibbs I, Leavey K, Benton SJ, Grynspan D, Bainbridge SA, Cox BJ. Placental transcriptional and histologic subtypes of normotensive fetal growth restriction are comparable to preeclampsia. *Am J Obstetrics Gynecology*. (2018) 220:110.e1–110.e21. doi: 10.1016/j.ajog.2018.10.003

35. Barrett T, Troup DB, Wilhite SE, Ledoux P, Rudnev D, Evangelista C, et al. NCBI GEO: mining tens of millions of expression profiles–database and tools update. *Nucleic Acids Res*. (2007) 35:D760–765. doi: 10.1093/nar/gkl887

36. Davis S, Meltzer PS. GEOquery: a bridge between the gene expression omnibus (GEO) and bioConductor. *Bioinf (Oxford England)*. (2007) 23:1846–7. doi: 10.1093/bioinformatics/btm254

37. Stelzer G, Rosen N, Plaschkes I, Zimmerman S, Twik M, Fishilevich S, et al. The geneCards suite: from gene data mining to disease genome sequence analyses. *Curr Protoc Bioinf*. (2016) 54:1.30.31–31.30.33. doi: 10.1002/0471250953.2016.54.issue-1

38. Ye Z, Zhang H, Kong F, Lan J, Yi S, Jia W, et al. Comprehensive analysis of alteration landscape and its clinical significance of mitochondrial energy metabolism pathway-related genes in lung cancers. *Oxid Med Cell Longev*. (2021) 2021:9259297. doi: 10.1155/2021/9259297

39. Leek JT, Johnson WE, Parker HS, Jaffe AE, Storey JD. The sva package for removing batch effects and other unwanted variation in high-throughput experiments. *Bioinformatics*. (2012) 28:882–3. doi: 10.1093/bioinformatics/bts034

40. Li S, Gao K, Yao D. Comprehensive Analysis of angiogenesis associated genes and tumor microenvironment infiltration characterization in cervical cancer. *Heliyon*. (2024) 10:e33277. doi: 10.1016/j.heliyon.2024.e33277

41. Yu G. Gene ontology semantic similarity analysis using GOSemSim. *Methods Mol Biol (Clifton NJ)*. (2020) 2117:207–15. doi: 10.1007/978-1-0716-0301-7_11

42. Kanehisa M, Goto S. KEGG: kyoto encyclopedia of genes and genomes. *Nucleic Acids Res*. (2000) 28:27–30. doi: 10.1093/nar/28.1.27

43. Yu G, Wang LG, Han Y, He QY. clusterProfiler: an R package for comparing biological themes among gene clusters. *Omics: J Integr Biol*. (2012) 16:284–7. doi: 10.1089/omi.2011.0118

44. Subramanian A, Tamayo P, Mootha VK, Mukherjee S, Ebert BL, Gillette MA, et al. Gene set enrichment analysis: a knowledge-based approach for interpreting genome-wide expression profiles. *Proc Natl Acad Sci United States America*. (2005) 102:15545–50. doi: 10.1073/pnas.0506580102

45. Liberzon A, Subramanian A, Pinchback R, Thorvaldsdóttir H, Tamayo P, Mesirov JP. Molecular signatures database (MSigDB) 3. *0 Bioinf*. (2011) 27:1739–40. doi: 10.1093/bioinformatics/btr260

46. Hänzelmann S, Castelo R, Guinney J. GSVA: gene set variation analysis for microarray and RNA-seq data. *BMC Bioinf*. (2013) 14:7. doi: 10.1186/1471-2105-14-7

47. Liu Y, Zhao H. Variable importance-weighted random forests. *Quantitative Biol (Beijing China)*. (2017) 5:338–51. doi: 10.1007/s40484-017-0121-6

48. Engebretsen S, Bohlin J. Statistical predictions with glmnet. *Clin epigenetics*. (2019) 11:123. doi: 10.1186/s13148-019-0730-1

49. Park SY. Nomogram: An analogue tool to deliver digital knowledge. *J Thorac Cardiovasc surgery*. (2018) 155:1793. doi: 10.1016/j.jtcvs.2017.12.107

50. Tataranni T, Piccoli C. Dichloroacetate (DCA) and cancer: an overview towards clinical applications. *Oxid Med Cell longevity*. (2019) 2019:8201079. doi: 10.1155/2019/8201079

51. Charoentong P, Finotello F, Angelova M, Mayer C, Efremova M, Rieder D, et al. Pan-cancer immunogenomic analyses reveal genotype-immunophenotype relationships and predictors of response to checkpoint blockade. *Cell Rep*. (2017) 18:248–62. doi: 10.1016/j.celrep.2016.12.019

52. Barbie DA, Tamayo P, Boehm JS, Kim SY, Moody SE, Dunn IF, et al. Systematic RNA interference reveals that oncogenic KRAS-driven cancers require TBK1. *Nature*. (2009) 462:108–12. doi: 10.1038/nature08460

53. Chen B, Khodadoust MS, Liu CL, Newman AM, Alizadeh AA. Profiling tumor infiltrating immune cells with CIBERSORT. *Methods Mol Biol (Clifton NJ)*. (2018) 1711:243–59. doi: 10.1007/978-1-4939-7493-1_12

54. von Mering C, Huynen M, Jaeggi D, Schmidt S, Bork P, Snel B. STRING: a database of predicted functional associations between proteins. *Nucleic Acids Res*. (2003) 31:258–61. doi: 10.1093/nar/gkg034

55. Li JH, Liu S, Zhou H, Qu LH, Yang JH. starBase v2.0: decoding miRNA-ceRNA, miRNA-ncRNA and protein-RNA interaction networks from large-scale CLIP-Seq data. *Nucleic Acids Res*. (2014) 42:D92–97. doi: 10.1093/nar/gkt1248

56. Zhang Q, Liu W, Zhang HM, Xie JY, Miao YR, Xia M, et al. hTFtarget: A comprehensive database for regulations of human transcription factors and their targets. *Genomics Proteomics Bioinf*. (2020) 18:120–8. doi: 10.1016/j.gpb.2019.09.006

57. Torbergsen T, øian P, Mathiesen E, Borud O. Pre-eclampsia-A mitochondrial disease? *Acta Obstetricia Gynecologica Scandinavica*. (1989) 68:145–8. doi: 10.3109/00016348909009902

58. Marín R, Chiarello DI, Abad C, Rojas D, Toledo F, Sobrevia L. Oxidative stress and mitochondrial dysfunction in early-onset and late-onset preeclampsia. *Biochim Biophys Acta Mol Basis Dis*. (2020) 1866:165961. doi: 10.1016/j.bbadis.2020.165961

59. Dimitriadis E, Rolnik DL, Zhou W, Estrada-Gutierrez J, Koga K, Francisco RPV, et al. Pre-eclampsia. *Nat Rev Dis primers*. (2023) 9:8. doi: 10.1038/s41572-023-00417-6

60. Yung HW, Colleoni F, Dommett E, Cindrova-Davies T, Kingdom J, Murray AJ, et al. Noncanonical mitochondrial unfolded protein response impairs placental oxidative phosphorylation in early-onset preeclampsia. *Proc Natl Acad Sci United States America*. (2019) 116:18109–18. doi: 10.1073/pnas.1907548116

61. Chiarello DI, Abad C, Rojas D, Toledo F, Vázquez CM, Mate A, et al. Oxidative stress: Normal pregnancy versus preeclampsia. *Biochim Biophys Acta Mol Basis Dis*. (2020) 1866:165354. doi: 10.1016/j.bbadis.2018.12.005

62. Hu XQ, Zhang L. Hypoxia and the integrated stress response promote pulmonary hypertension and preeclampsia: Implications in drug development. *Drug Discov Today*. (2021) 26:2754–73. doi: 10.1016/j.drudis.2021.07.011

63. Zhao Y, Zhao H, Xu H, An P, Ma B, Lu H, et al. Perfluorooctane sulfonate exposure induces preeclampsia-like syndromes by damaging trophoblast mitochondria in pregnant mice. *Ecotoxicology Environ safety*. (2022) 247:114256. doi: 10.1016/j.ecoenv.2022.114256

64. Li Y, Sang Y, Chang Y, Xu C, Lin Y, Zhang Y, et al. A galectin-9-driven CD11c (high) decidual macrophage subset suppresses uterine vascular remodeling in preeclampsia. *Circulation*. (2024) 149:1670–88. doi: 10.1161

65. Iborra-Pernichi M, Ruiz García J, Velasco de la Esperanza M, Estrada BS, Bovolenta ER, Cifuentes C, et al. Defective mitochondria remodelling in B cells leads to an aged immune response. *Nat Commun*. (2024) 15:2569. doi: 10.1038/s41467-024-46763-1

66. Olivera S, Graham D. Modelling pre-eclampsia and its cardiovascular effects. *Nat Rev Cardiol*. (2024) 21:281. doi: 10.1038/s41569-024-01006-0

67. Yang C, Baker PN, Granger JP, Davidge ST, Tong C. Long-term impacts of preeclampsia on the cardiovascular system of mother and offspring. *Hypertension*. (2023) 80:1821–33. doi: 10.1161/HYPERTENSIONAHA.123.21061

68. Stubert J, Hinz B, Berger R. The role of acetylsalicylic acid in the prevention of pre-eclampsia, fetal growth restriction, and preterm birth. *Deutsches Arzteblatt Int*. (2023) 120:617–26. doi: 10.3238/arztebl.m2023.0133

69. Cluver CA, Bergman L, Bergkvist J, Imberg H, Geerts L, Hall DR, et al. Impact of fetal growth restriction on pregnancy outcome in women undergoing expectant management for preterm pre-eclampsia. *Ultrasound obstetrics gynecology: Off J Int Soc Ultrasound Obstetrics Gynecology*. (2023) 62:660–7. doi: 10.1002/uog.26282

70. Benzing T. Hypertension: Testing for pre-eclampsia: paving the way to early diagnosis. *Nat Rev Nephrology*. (2016) 12:200–2. doi: 10.1038/nrneph.2016.21

71. Chaudhary RK, Madaboosi N, Satija J, Nandagopal B, Srinivasan R, Sai VVR. Polymeric optical fiber biosensor with PAMAM dendrimer-based surface modification and PlGF detection for pre-eclampsia diagnosis. *Biosensors bioelectronics*. (2024) 257:116312. doi: 10.1016/j.bios.2024.116312

72. Wright A, von Dadelszen P, Magee LA, Syngelaki A, Akolekar R, Wright D, et al. Effect of race on the measurement of angiogenic factors for prediction and diagnosis of pre-eclampsia. *BJOG: an Int J obstetrics gynaecology*. (2023) 130:78–87. doi: 10.1111/1471-0528.17296

73. Andronikidi PE, Orovou E, Mavrigiannaki E, Athanasiadou V, Tzitiridou-Chatzopoulou M, Iatrakis G, et al. Placental and renal pathways underlying pre-eclampsia. *Int J Mol Sci*. (2024) 25:2741. doi: 10.3390/ijms25052741

74. Ahmadian E, Rahbar Saadat Y, Hosseiniyan Khatibi SM, Nariman-Saleh-Fam Z, Bastami M, Zununi Vahed F, et al. Pre-Eclampsia: Microbiota possibly playing a role. *Pharmacol Res*. (2020) 155:104692. doi: 10.1016/j.phrs.2020.104692

75. Lee B, Shin H, Oh JE, Park J, Yang SC, Jun JH, et al. An autophagic deficit in the uterine vessel microenvironment provokes hyperpermeability through deregulated VEGFA, NOS1, and CTNNB1. *Autophagy*. (2021) 17:1649–66. doi: 10.1080/15548627.2020.1778292

76. Nakashima A, Cheng SB, Ikawa M, Yoshimori T, Huber J, Menon R, et al. Evidence for lysosomal biogenesis proteome defect and impaired autophagy in preeclampsia. *Autophagy*. (2020) 16:1771–85. doi: 10.1080/15548627.2019.1707494

77. Lin RC, Chao YY, Su MT, Tsai HL, Tsai PY, Wang CY. Upregulation of miR-20b-5p inhibits trophoblast invasion by blocking autophagy in recurrent miscarriage. *Cell signalling*. (2024) 113:110934. doi: 10.1016/j.cellsig.2023.110934

78. Alzubaidi KRK, Mahdavi M, Dolati S, Yousefi M. Observation of increased levels of autophagy-related genes and proteins in women with preeclampsia: a clinical study. *Mol Biol Rep*. (2023) 50:4831–40. doi: 10.1007/s11033-023-08385-6

79. Ye L, Huang Y, Liu X, Zhang X, Cao Y, Kong X, et al. Apelin/APJ system protects placental trophoblasts from hypoxia-induced oxidative stress through activating PI3K/Akt signaling pathway in preeclampsia. *Free Radical Biol Med*. (2023) 208:759–70. doi: 10.1016/j.freeradbiomed.2023.09.030

80. Martinez-Fierro ML, Garza-Veloz I, Castañeda-Lopez ME, Wasike D, la Rosa CCD, Rodriguez-Sanchez IP, et al. Evaluation of the effect of the fibroblast growth factor type 2 (FGF-2) administration on placental gene expression in a murine model of preeclampsia induced by L-NAME. *Int J Mol Sci*. (2022) 23:10129. doi: 10.3390/ijms231710129

81. Santos BF, Grenho I, Martel PJ, Ferreira BI, Link W. FOXO family isoforms. *Cell Death disease*. (2023) 14:702. doi: 10.1038/s41419-023-06177-1

82. Aye ILMH, Aiken CE, Charnock-Jones DS, Smith GCS. Placental energy metabolism in health and disease&x2014;significance of development and implications for preeclampsia. *Am J Obstetrics Gynecology*. (2022) 226:S928–44. doi: 10.1016/j.ajog.2020.11.005

83. Yiew NKH, Finck BN. The mitochondrial pyruvate carrier at the crossroads of intermediary metabolism. *Am J Physiol Endocrinol Metab*. (2022) 323:E33–e52. doi: 10.1152/ajpendo.00074.2022

84. Prochownik EV, Wang H. The metabolic fates of pyruvate in normal and neoplastic cells. *Cells*. (2021) 10:762. doi: 10.3390/cells10040762

85. Hu Y, Cao K, Wang F, Wu W, Mai W, Qiu L, et al. Dual roles of hexokinase 2 in shaping microglial function by gating glycolytic flux and mitochondrial activity. *Nat Metab*. (2022) 4:1756–74. doi: 10.1038/s42255-022-00707-5

86. Fang J, Luo S, Lu Z. HK2: Gatekeeping microglial activity by tuning glucose metabolism and mitochondrial functions. *Mol Cell*. (2023) 83:829–31. doi: 10.1016/j.molcel.2023.02.022

87. Bao C, Zhu S, Song K, He C. HK2: a potential regulator of osteoarthritis via glycolytic and non-glycolytic pathways. *Cell Commun Signal*. (2022) 20:132. doi: 10.1186/s12964-022-00943-y

88. Siddique AHH, Kale PP. Importance of glucose and its metabolism in neurodegenerative disorder, as well as the combination of multiple therapeutic strategies targeting α-synuclein and neuroprotection in the treatment of Parkinson's disease. *Rev Neurologique*. (2024) 180:736–53. doi: 10.1016/j.neurol.2023.08.011

89. Duncan L, Shay C, Teng Y. PGK1: an essential player in modulating tumor metabolism. *Methods Mol Biol (Clifton NJ)*. (2022) 2343:57–70. doi: 10.1007/978-1-0716-1558-4_4

90. Infantino V, Santarsiero A, Convertini P, Todisco S, Iacobazzi V. Cancer cell metabolism in hypoxia: role of HIF-1 as key regulator and therapeutic target. *Int J Mol Sci*. (2021) 22:5703. doi: 10.3390/ijms22115703

91. Zhao M, Wang S, Zuo A, Zhang J, Wen W, Jiang W, et al. HIF-1α/JMJD1A signaling regulates inflammation and oxidative stress following hyperglycemia and hypoxia-induced vascular cell injury. *Cell Mol Biol Lett*. (2021) 26:40. doi: 10.1186/s11658-021-00283-8

92. Islam A, Shaukat Z, Hussain R, Gregory SL. One-carbon and polyamine metabolism as cancer therapy targets. *Biomolecules*. (2022) 12:1902. doi: 10.3390/biom12121902

93. Le Floc'h A, Nagashima K, Birchard D, Scott G, Ben L-H, Ajithdoss D, et al. Blocking common γ chain cytokine signaling ameliorates T cell–mediated pathogenesis in disease models. *Sci Trans Med*. (2023) 15:eabo0205. doi: 10.1126/scitranslmed

94. Touyz RM, Alves-Lopes R, Rios FJ, Camargo LL, Anagnostopoulou A, Arner A, et al. Vascular smooth muscle contraction in hypertension. *Cardiovasc Res*. (2018) 114:529–39. doi: 10.1093/cvr/cvy023

95. Xiao L, Ma X, Ye L, Su P, Xiong W, Bi E, et al. IL-9/STAT3/fatty acid oxidation-mediated lipid peroxidation contributes to Tc9 cell longevity and enhanced antitumor activity. *J Clin Invest*. (2022) 132:e153247. doi: 10.1172/JCI153247

96. Yang S, Li F, Lu S, Ren L, Bian S, Liu M, et al. Ginseng root extract attenuates inflammation by inhibiting the MAPK/NF-κB signaling pathway and activating autophagy and p62-Nrf2-Keap1 signaling *in vitro* and *in vivo*. *J Ethnopharmacology*. (2022) 283:114739. doi: 10.1016/j.jep.2021.114739

97. Erdmann KS, Mao Y, McCrea HJ, Zoncu R, Lee S, Paradise S, et al. A role of the Lowe syndrome protein OCRL in early steps of the endocytic pathway. *Dev Cell*. (2007) 13:377–90. doi: 10.1016/j.devcel.2007.08.004

98. Hagemann N, Hou X, Goody RS, Itzen A, Erdmann KS. Crystal structure of the Rab binding domain of OCRL1 in complex with Rab8 and functional implications of the OCRL1/Rab8 module for Lowe syndrome. *Small Gtpases*. (2012) 3:107–10. doi: 10.4161/sgtp.19380

99. Chen H, Lu C, Tan Y, Weber-Boyvat M, Zheng J, Xu M, et al. Oculocerebrorenal syndrome of Lowe (OCRL) controls leukemic T-cell survival by preventing excessive PI (4,5)P(2) hydrolysis in the plasma membrane. *J Biol Chem*. (2023) 299:104812. doi: 10.1016/j.jbc.2023.104812

100. Liu Y, Wang X, Nawaz A, Kong Z, Hong Y, Wang C, et al. Wogonin ameliorates lipotoxicity-induced apoptosis of cultured vascular smooth muscle cells via interfering with DAG-PKC pathway. *Acta Pharmacologica Sinica*. (2011) 32:1475–82. doi: 10.1038/aps.2011.120

101. Ampey AC, Dahn RL, Grummer MA, Bird IM. Differential control of uterine artery endothelial monolayer integrity by TNF and VEGF is achieved through multiple mechanisms operating inside and outside the cell - Relevance to preeclampsia. *Mol Cell Endocrinol*. (2021) 534:111368. doi: 10.1016/j.mce.2021.111368

102. Li J, Jiang L, Kai H, Zhou Y, Cao J, Tang W. Identifying preeclampsia-associated key module and hub genes via weighted gene co-expression network analysis. *Sci Rep*. (2025) 15:1364. doi: 10.1038/s41598-025-85599-7

103. Lei C, Chen W, Wang Y, Zhao B, Liu P, Kong Z, et al. Prognostic prediction model for glioblastoma: A metabolic gene signature and independent external validation. *J Cancer*. (2021) 12:3796–808. doi: 10.7150/jca.53827

104. Liu S, Sun Y, Jiang M, Li Y, Tian Y, Xue W, et al. Glyceraldehyde-3-phosphate dehydrogenase promotes liver tumorigenesis by modulating phosphoglycerate dehydrogenase. *Hepatol (Baltimore Md)*. (2017) 66:631–45. doi: 10.1002/hep.29202

105. Sirover MA. The role of posttranslational modification in moonlighting glyceraldehyde-3-phosphate dehydrogenase structure and function. *Amino Acids*. (2021) 53:507–15. doi: 10.1007/s00726-021-02959-z

106. Kornberg MD, Bhargava P, Kim PM, Putluri V, Snowman AM, Putluri N, et al. Dimethyl fumarate targets GAPDH and aerobic glycolysis to modulate immunity. *Science*. (2018) 360:449–53. doi: 10.1126/science.aan4665

107. Teng R, Wang Y, Lv N, Zhang D, Williamson RA, Lei L, et al. Hypoxia impairs NK cell cytotoxicity through SHP-1-mediated attenuation of STAT3 and ERK signaling pathways. *J Immunol Res*. (2020) 2020:4598476. doi: 10.1155/2020/4598476

108. Pang H, Lei D, Huang J, Guo Y, Fan C. Elevated PGT promotes proliferation and inhibits cell apoptosis in preeclampsia by Erk signaling pathway. *Mol Cell Probes*. (2023) 67:101896. doi: 10.1016/j.mcp.2023.101896

109. Lin X, Lei Y, Pan M, Hu C, Xie B, Wu W, et al. Augmentation of scleral glycolysis promotes myopia through histone lactylation. *Cell Metab*. (2024) 36:511–525.e517. doi: 10.1016/j.cmet.2023.12.023

110. Liu P, Sun SJ, Ai YJ, Feng X, Zheng YM, Gao Y, et al. Elevated nuclear localization of glycolytic enzyme TPI1 promotes lung adenocarcinoma and enhances chemoresistance. *Cell Death Dis*. (2022) 13:205. doi: 10.1038/s41419-022-04655-6

111. Xia P, Zhang H, Lu H, Xu K, Jiang X, Jiang Y, et al. METTL5 stabilizes c-Myc by facilitating USP5 translation to reprogram glucose metabolism and promote hepatocellular carcinoma progression. *Cancer Commun (Lond)*. (2023) 43:338–64. doi: 10.1002/cac2.12403

112. Dai M, Wang L, Yang J, Chen J, Dou X, Chen R, et al. LDHA as a regulator of T cell fate and its mechanisms in disease. *Biomedicine pharmacotherapy = Biomedecine pharmacotherapie*. (2023) 158:114164. doi: 10.1016/j.biopha.2022.114164

113. Xu K, Yin N, Peng M, Stamatiades EG, Shyu A, Li P, et al. Glycolysis fuels phosphoinositide 3-kinase signaling to bolster T cell immunity. *Science*. (2021) 371:405–10. doi: 10.1126/science.abb2683

114. Yang M, Li H, Rong M, Zhang H, Hou L, Zhang C. Dysregulated GLUT1 may be involved in the pathogenesis of preeclampsia by impairing decidualization. *Mol Cell Endocrinology*. (2022) 540:111509. doi: 10.1016/j.mce.2021.111509

115. Burwick RM, Feinberg BB. Complement activation and regulation in preeclampsia and hemolysis, elevated liver enzymes, and low platelet count syndrome. *Am J obstetrics gynecology*. (2022) 226:S1059–s1070. doi: 10.1016/j.ajog.2020.09.038

116. Ho SJ, Chaput D, Sinkey RG, Garces AH, New EP, Okuka M, et al. Proteomic studies of VEGFR2 in human placentas reveal protein associations with preeclampsia, diabetes, gravidity, and labor. *Cell communication signaling: CCS*. (2024) 22:221. doi: 10.1186/s12964-024-01567-0

117. Deer E, Herrock O, Campbell N, Cornelius D, Fitzgerald S, Amaral LM, et al. The role of immune cells and mediators in preeclampsia. *Nat Rev Nephrol*. (2023) 19:257–70. doi: 10.1038/s41581-022-00670-0

118. Aneman I, Pienaar D, Suvakov S, Simic TP, Garovic VD, McClements L. Mechanisms of key innate immune cells in early- and late-onset preeclampsia. *Front Immunol*. (2020) 11:1864. doi: 10.3389/fimmu.2020.01864

119. Nieves C, Victoria da Costa Ghignatti P, Aji N, Bertagnolli M. Immune cells and infectious diseases in preeclampsia susceptibility. *Can J Cardiol*. (2024) 40:2340–55. doi: 10.1016/j.cjca.2024.09.012

120. Luo F, Liu F, Guo Y, Xu W, Li Y, Yi J, et al. Single-cell profiling reveals immune disturbances landscape and HLA-F-mediated immune tolerance at the maternal-fetal interface in preeclampsia. *Front Immunol*. (2023) 14:1234577. doi: 10.3389/fimmu.2023.1234577

121. Kumar S, Dikshit M. Metabolic insight of neutrophils in health and disease. *Front Immunol*. (2019) 10:2099. doi: 10.3389/fimmu.2019.02099

122. Yazdani HO, Roy E, Comerci AJ, van der Windt DJ, Zhang H, Huang H, et al. Neutrophil extracellular traps drive mitochondrial homeostasis in tumors to augment growth. *Cancer Res*. (2019) 79:5626–39. doi: 10.1158/0008-5472.CAN-19-0800

123. Dyhia M, Ahmad Haidar A, Patrice D. Neutrophil extracellular traps (NET): not only antimicrobial but also modulators of innate and adaptive immunities in inflammatory autoimmune diseases. *RMD Open*. (2023) 9:e003104. doi: 10.1136/rmdopen-2023-003104

124. Wang Y, Adair CD, Weeks JW, Lewis DF, Alexander JS. Increased neutrophil-endothelial adhesion induced by placental factors is mediated by platelet-activating factor in preeclampsia. *J Soc Gynecol Investig*. (1999) 6:136–41. doi: 10.1016/S1071-5576(99)00004-0

125. Hu Y, Li H, Yan Y, Wang C, Wang Y, Zhang C, et al. Increased neutrophil activation and plasma DNA levels in patients with pre-eclampsia. *Thromb Haemostasis*. (2018) 118:2064–2073. doi: 10.1055/s-0038-1675788

126. Walsh SW, Nugent WH, Al Dulaimi M, Washington SL, Dacha P, Strauss JF 3rd, et al. Proteases activate pregnancy neutrophils by a protease-activated receptor 1 pathway: epigenetic implications for preeclampsia. *Reprod Sci*. (2020) 27:2115–27. doi: 10.1007/s43032-020-00232-4

127. Jing Y, Shaheen E, Drake RR, Chen N, Gravenstein S, Deng Y, et al. Aging is associated with a numerical and functional decline in plasmacytoid dendritic cells, whereas myeloid dendritic cells are relatively unaltered in human peripheral blood. *Hum Immunol*. (2009) 70:777–84. doi: 10.1016/j.humimm.2009.07.005

128. Moldenhauer LM, Diener KR, Thring DM, Brown MP, Hayball JD, Robertson SA. Cross-presentation of male seminal fluid antigens elicits T cell activation to initiate the female immune response to pregnancy1. *J Immunol*. (2009) 182:8080–93. doi: 10.4049/jimmunol.0804018

129. Wang J, Tao YM, Cheng XY, Zhu TF, Chen ZF, Yao H, et al. Vascular endothelial growth factor affects dendritic cell activity in hypertensive disorders of pregnancy. *Mol Med Rep*. (2015) 12:3781–6. doi: 10.3892/mmr.2015.3783

130. Panda B, Panda A, Ueda I, Abrahams VM, Norwitz ER, Stanic AK, et al. Dendritic cells in the circulation of women with preeclampsia demonstrate a pro-inflammatory bias secondary to dysregulation of TLR receptors. *J Reprod Immunol*. (2012) 94:210–5. doi: 10.1016/j.jri.2012.01.008

131. Gierman LM, Silva GB, Pervaiz Z, Rakner JJ, Mundal SB, Thaning AJ, et al. TLR3 expression by maternal and fetal cells at the maternal-fetal interface in normal and preeclamptic pregnancies. *J Leukocyte Biol*. (2020) 109:173–83. doi: 10.1002/JLB.3MA0620-728RR

132. Herrock OT, Deer E, Amaral LM, Campbell N, Lemon J, Ingram N, et al. B2 cells contribute to hypertension and natural killer cell activation possibly via AT1-AA in response to placental ischemia. *Am J Physiol Renal Physiol*. (2023) 324:F179–f192. doi: 10.1152/ajprenal.00190.2022

133. Salby SB, Persson G, Pedersen NH, Turan G, Kimmerslev L, Finne KF, et al. Reduced expression of programmed cell death protein 1 on peripheral regulatory B cells in pre-eclampsia – Signs of impaired immune suppression. *J Reprod Immunol*. (2025) 168:104426. doi: 10.1016/j.jri.2025.104426

134. Palma AM, Hanes MR, Marshall JS. Mast cell modulation of B cell responses: an under-appreciated partnership in host defence. *Front Immunol*. (2021) 12:718499. doi: 10.3389/fimmu.2021.718499

135. Wang Y, Chen A. Mast cell-derived exosomal miR-181a-5p modulated trophoblast cell viability, migration, and invasion via YY1/MMP-9 axis. *J Clin Lab Anal*. (2022) 36:e24549. doi: 10.1002/jcla.24549

136. Szewczyk G, Pyzlak M, Klimkiewicz J, Smiertka W, Miedzińska-Maciejewska M, Szukiewicz D. Mast cells and histamine: do they influence placental vascular network and development in preeclampsia? *Mediators Inflammation*. (2012) 2012:307189. doi: 10.1155/2012/307189

137. Pawankar R, Okuda M, Yssel H, Okumura K, Ra C. Nasal mast cells in perennial allergic rhinitics exhibit increased expression of the Fc epsilonRI, CD40L, IL-4, and IL-13, and can induce IgE synthesis in B cells. *J Clin Invest*. (1997) 99:1492–9. doi: 10.1172/JCI119311

138. Breitling S, Hui Z, Zabini D, Hu Y, Hoffmann J, Goldenberg NM, et al. The mast cell–B cell axis in lung vascular remodeling and pulmonary hypertension. *Am J Physiology-Lung Cell Mol Physiol*. (2017) 312:L710–21. doi: 10.1152/ajplung.00311.2016

frontiers | Frontiers in Cell and Developmental Biology

TYPE Original Research
PUBLISHED 31 July 2025
DOI 10.3389/fcell.2025.1635878

OPEN ACCESS

EDITED BY
Rajesh Kumar Manne,
Duke University, United States

REVIEWED BY
Atar Singh Kushwah,
Icahn School of Medicine at Mount Sinai, United States
Hong Wu,
Sichuan Cancer Hospital, China

*CORRESPONDENCE
Olivia Holland,
o.holland@griffith.edu.au

RECEIVED 27 May 2025
ACCEPTED 15 July 2025
PUBLISHED 31 July 2025

CITATION
Han L, da Silva Costa F, Perkins A and Holland O (2025) Molecular signatures of preeclampsia subtypes determined through integrated weighted gene co-expression network analysis and differential gene expression analysis of placental transcriptomics.
Front. Cell Dev. Biol. 13:1635878.
doi: 10.3389/fcell.2025.1635878

Molecular signatures of preeclampsia subtypes determined through integrated weighted gene co-expression network analysis and differential gene expression analysis of placental transcriptomics

Luhao Han[1], Fabricio da Silva Costa[2,3], Anthony Perkins[1,4] and Olivia Holland[1,5]*

[1]School of Pharmacy and Medical Sciences, Griffith University, Gold Coast, QLD, Australia, [2]School of Medicine and Dentistry, Griffith University, Gold Coast, QLD, Australia, [3]Maternal Fetal Medicine Unit, Women-Newborn-Children Services, Gold Coast University Hospital, Gold Coast, QLD, Australia, [4]School of Health, University of the Sunshine Coast, Sunshine Coast, QLD, Australia, [5]Women-Newborn-Children-Services, Gold Coast University Hospital, Gold Coast Hospital and Health Services, Gold Coast, QLD, Australia

Background: Preeclampsia (PE) is a multisystemic pregnancy syndrome that presents in different clinical subtypes. While placental dysfunction is a critical feature of PE, its contribution to different PE subtypes remains unclear. This study aims to use integrated bioinformatics analysis of placental transcriptomics to investigate subtype-specific molecular mechanisms associated with PE.

Methods: A systematic search of the Gene Expression Omnibus (GEO) repository identified two datasets (GSE234729, n = 123; GSE75010, n = 157) for integrated Weighted Gene Co-expression Network Analysis (WGCNA) and differential gene expression analysis. We constructed co-expression networks and identified gene modules correlated with three PE subtypes (severe, early-onset and late-onset). Differential gene expression analysis was conducted using the "limma" R package. Differentially expressed genes (DEGs) overlapping with PE subtype-correlated WGCNA modules underwent Gene Ontology (GO) enrichment analysis. Consistently dysregulated genes were validated in an additional external dataset (GSE25906) and RT-PCR analysis of placental samples from 21 PE cases and 21 uncomplicated controls.

Results: We identified distinct molecular signatures associated with each PE subtype. The green gene module was positively correlated with severe PE (r = 0.63, p = 4e-15), containing 179 DEGs primarily involved in lipid metabolism and hypoxia response processes. Early-onset PE had two highly significant gene modules: the yellow module (r = 0.73, p = 4e-15) with 112 DEGs enriched in biological processes related to gonadotrophin secretion and lipid storage, and the black module (r = −0.55, p = 5e-08) with 47 DEGs

significantly enriched in chronic inflammation responses. Late-onset PE showed moderate correlation with the ivory module (r = 0.46, p = 5e-05), containing 23 DEGs enriched in p38MAPK stress-response signalling. Cross-subtype analysis identified 20 consistently dysregulated genes across three PE subtypes, with four upregulated genes (*LEP*, *FSTL3*, *HTRA4*, and *HK2*) confirmed in the external dataset GSE25906. However, RT-PCR validation showed only moderate upregulation without statistical significance.

Conclusion: Though placental dysfunction occurs across all subtypes with a core set of upregulated genes, variation exits in placental gene expression patterns among PE subtypes. Severe and early-onset PE exhibit large molecular perturbations, while late-onset PE presents more subtle alterations. Aberrant placental lipid storage may contribute to disease severity and early manifestation.

KEYWORDS

preeclampsia subtypes, pregnancy complications, hypertensive disorders of pregnancy, placental gene expression, transcriptomic analysis

1 Introduction

Preeclampsia (PE) poses a critical global health challenge, contributing substantially to maternal, fetal, and neonatal morbidity and mortality (Magee et al., 2022; Abalos et al., 2014). Affecting approximately 2%–8% of pregnancies worldwide, this complex multisystem disorder manifests through a diverse spectrum of clinical symptoms, ranging from mild hypertension to severe complications including eclampsia and HELLP syndrome (Hemolysis, Elevated Liver enzymes, Low Platelet count) (Gestational Hypertension and Preeclampsia: ACOG Practice Bulletin, 2020). PE can develop at various time points in pregnancy after 20 weeks of gestation and vary in severity. The condition is often classified into subtypes based on onset timing: early-onset (<34 gestational weeks) *versus* late-onset (≥34 weeks), or preterm (delivery <37 weeks) *versus* term (delivery ≥37 weeks). Additionally, PE can be further categorized as mild and severe depending on maternal symptom severity, or whether complicated with fetal growth restriction (FGR) (Dimitriadis et al., 2023).

Although PE subtypes present similar clinical symptoms, a common pathophysiological mechanism currently fails to explain the aetiology of all PE cases. Substantial evidence from clinical, epidemiologic, histologic and biological studies supports placental dysfunction as a central factor in PE pathophysiology (Dimitriadis et al., 2023). It has been proposed that dysfunctional placenta releases pathogenic factors into maternal circulation, triggering endothelial dysfunction and systemic inflammation responses, leading to clinical manifestation of PE (Pankiewicz et al., 2021; Michalczyk et al., 2020; Ngene and Moodley, 2018).

The cause and degree of placental dysfunction varies among preeclampsia subtypes, likely reflecting various pathophysiological processes. Early-onset PE is often associated with inadequate trophoblast invasion and poor remodelling of the uterine spiral arteries, leading to placental hypoxia and oxidative stress. This defective placentation is believed to be influenced by aberrant maternal immune responses to the feto-placental unit (Burton et al., 2019). Additionally, early-onset PE is characterized by more pronounced systemic inflammation and disruption of the angiogenic balance (Chuah et al., 2018; Pinheiro et al., 2014). Another potential aetiology is suboptimal maternal cardiovascular function secondary to uteroplacental malperfusion, which may contribute to placental dysfunction in certain PE cases (Melchiorre et al., 2022). Epidemiological evidence has revealed shared risk factors between PE and cardiovascular disease (Wu et al., 2017; Leon et al., 2019), and echocardiographic studies have found cardiac parameter abnormalities in women several weeks prior to the manifestation of clinical signs of both preterm and term PE (Thilaga and nathan, 2020; Castleman et al., 2016; Garcia-Gonzalez et al., 2020; Melchiorre et al., 2013).

Previous transcriptomic studies have provided valuable insights into the molecular differences between early-onset and late-onset PE, supporting the hypothesis that these subtypes may be driven by different pathogenic mechanisms. As early as 2007, Nishizawa et al. conducted a microarray analysis of placental samples from severe PE cases and identified 11 differentially expressed genes between early-onset and late-onset subtypes (Nishizawa et al., 2007). Later, Sitras et al. reported 168 differentially expressed gene between these two PE subtypes, with pathways related to oxidative stress, inflammation, and endothelin signalling involved in early-onset PE (Sitras et al., 2009). Similarly, Junus et al. found significant downregulation of angiogenesis-related genes specifically in early-onset type, suggesting its association with more severe placental vascular dysfunction (Junus et al., 2012). Subsequent transcriptomic investigations have consistently shown that late-onset PE exhibits fewer placental gene alterations compared to early type (Ren et al., 2021; Liang et al., 2016). Furthermore, dysregulation of the placental innate immune system has been identified as a feature specific to early-onset PE but not observed in the late-onset subtype (Broekhuizen et al., 2021). Most recently, a single-cell transcriptomics study of PE placentae reinforced this evidence, showing widespread cell-type–specific gene dysregulation in early-onset PE but fewer changes in late-onset (Admati et al., 2023).

The classical analytic method for those transcriptomic studies focuses on differential gene expression, examining individual genes

based on fold changes and statistical significance. However, this approach cannot fully capture the complex gene-gene interactions and regulatory networks underlying multifactorial diseases like PE. Advanced bioinformatics methods like weighted gene co-expression network analysis (WGCNA) can identify co-expression modules of functionally related genes that can be correlated with clinical phenotypes and disease pathophysiology (Langfelder and Horvath, 2008). Our study employs an integrated approach, combining WGCNA with differential expression analysis to systematically characterise molecular signatures across three PE subtypes. This investigation elucidates distinct molecular mechanisms underlying subtype-specific placental pathologies in PE.

2 Materials and methods

2.1 Selection of datasets

A systematic search was conducted from GEO website to identify transcriptomic datasets related to PE in placental tissue. The search terms included "placenta" and "preeclampsia." Key dataset information including GEO accession number, platform, sample type, processing methods, and sample numbers was extracted and summarized in Supplementary File S1. Dataset selection criteria included placental villous tissue samples collected at delivery, with a sample size over 60, representation of a multi-ethnic population, and contained information about PE subtypes. Based on these criteria, we selected two eligible datasets (GSE234729, GSE75010) for combined WGCNA and DEGs analysis. GSE234729 is RNA-seq data from 50 severe PE placentae and 73 normotensive controls (Aisagbonhi et al., 2023). Severe PE features were defined according to the original study, which was based on the American College of Obstetricians and Gynecologists (ACOG) guideline (Aisagbonhi et al., 2023). Although the classification of PE severity is not recommended for clinical use, this classification remains useful in research (Magee et al., 2022; Dimitriadis et al., 2023). GSE75010 is a microarray dataset from 80 PE cases and 77 normotensive controls with accompanying clinical data including maternal body mass index (BMI), gestational age, newborn weight, and placental weight (Leavey et al., 2016). For this study, cases from GSE75010 were divided into early-onset PE (delivery <34 weeks) and late-onset PE (delivery ≥34 weeks) groups to explore potential molecular mechanism differences between PE subtypes (Dimitriadis et al., 2023; Poon et al., 2019). Additionally, GSE25906 (n = 60), the third-largest available dataset, was included for external validation (Tsai et al., 2011). The overall analytical workflow is illustrated in Figure 1.

2.2 Data acquisition and Preprocessing

Gene expression datasets GSE75010, GSE234729, and GSE25906 with clinical information were retrieved from the GEO website or the "GEOquery" R package (Sean and Meltzer, 2007). All datasets were pre-processed using log2 transformation for normalization to stabilize variance and reduce skewness in expression values. Boxplots were generated after transformation to visualize sample distribution and identify potential outliers as part of quality control.

2.3 Weighted gene Co-expression network analysis (WGCNA)

We performed WGCNA analysis using the "WGCNA" R package, following the workflow recommended by the package developers (Langfelder and Horvath, 2008). First, a sample dendrogram was generated to visualize the hierarchical clustering of the samples based on overall gene expression profiles and clinical traits, which aided in the detection and removal of outlier samples to ensure robust network construction. Subsequently, we constructed the co-expression network by computing a co-expression similarity matrix based on Pearson correlation coefficients between all gene pairs. This matrix was then transformed into a dissimilarity matrix using the Topological Overlap Measure (TOM) by subtracting the TOM from 1. Hierarchical clustering was performed on this dissimilarity matrix to group genes with similar expression patterns. Gene modules were identified using the dynamic tree cut algorithm with a minimum module size set to 30 genes. Modules with highly similar expression profiles were merged if their correlation height was below 0.25, resulting in distinct modules with unique colour labels. For each module, eigengenes (MEs) were calculated as the first principal component of the module's gene expression data. These eigengenes serve as a summary of the expression pattern within the module and can be used in subsequent correlation analyses with clinical traits.

To identify gene expression significantly associated with clinical traits such as PE and maternal ethnicity, we calculated the correlations between MEs and the clinical traits. The relationships between modules and clinical traits were visualized using heatmaps to provide a clear overview of the associations. We defined significance thresholds where correlation coefficients greater than 0.5 indicated strong relationships, while coefficients between 0.3 and 0.5 suggested moderate relationships. Additionally, an adjusted p-value less than 0.05 was required to confirm a statistically significant relationship between a module's gene expression profile and the clinical trait. Furthermore, we conducted a comparative Gene Ontology (GO) analysis across different gene modules using the compareCluster function from the clusterProfiler R package (Yu et al., 2012). This analysis enabled systematic comparison of gene lists and identification of enriched GO terms across multiple modules simultaneously, revealing both unique and shared biological processes, molecular functions, and cellular components associated with each module.

2.4 Differential expression analysis

Gene expression differences were assessed for three PE subtypes (severe, early-onset, and late-onset), each compared to uncomplicated pregnant control groups individually within the same dataset. Differential expression analysis between PE

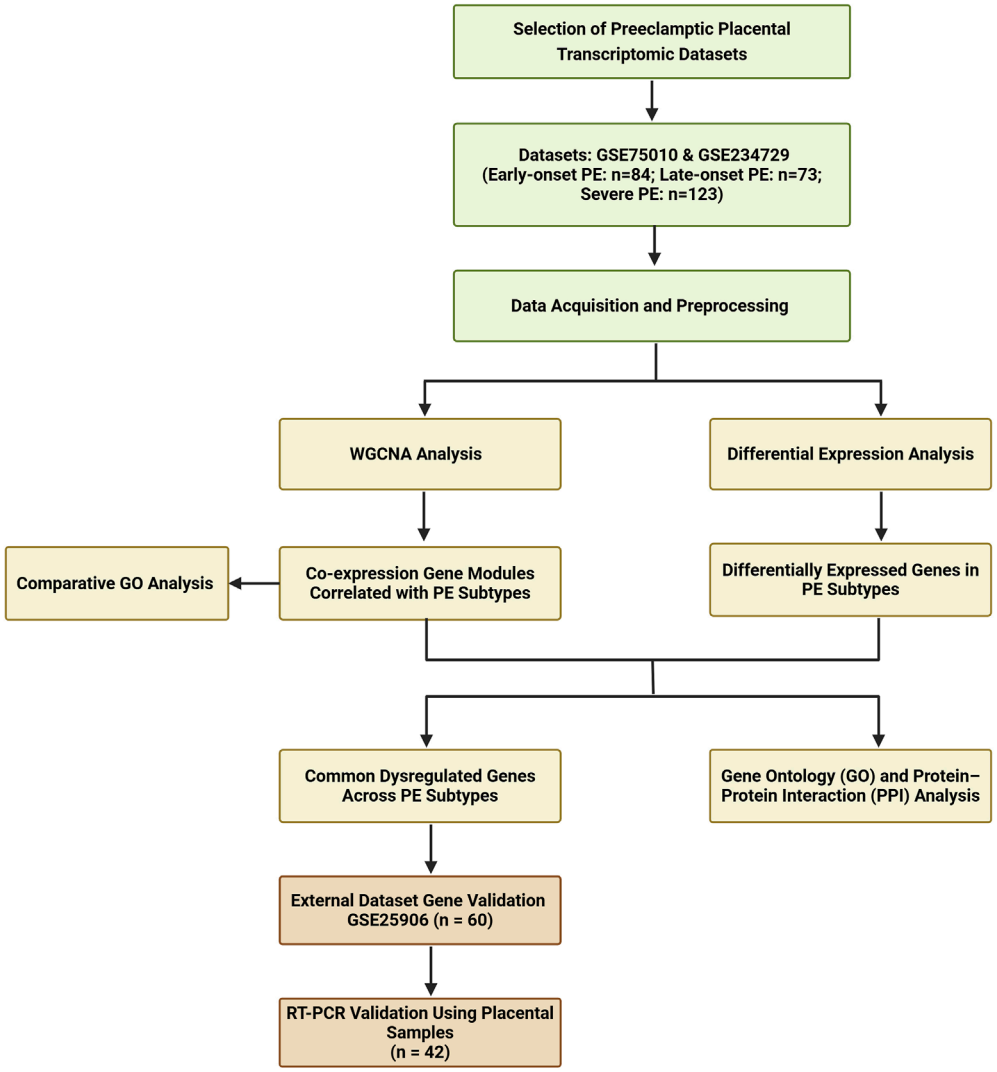

FIGURE 1
Flowchart of this study.

cases and uncomplicated controls was performed using the "limma" R package (Ritchie et al., 2015). Genes were considered differentially expressed based on the following criteria: an adjusted p-value <0.05, using the Benjamini–Hochberg method to control the false discovery rate, and an absolute log2 fold change >0.5.

2.5 Functional enrichment and interaction network analysis

Key dysregulated placental genes were defined as the intersection of genes within PE subtype correlated modules and DEGs, followed by functional GO enrichment analysis and protein-protein interaction (PPI) analysis. GO enrichment analysis was performed using the "clusterProfiler" R package to examine biological processes (Yu et al., 2012). GO terms with an adjusted p-value <0.05 were considered significantly enriched. PPI analysis was conducted using the STRING database and visualized by Cytoscape. The Maximal Clique Centrality (MCC) algorithm, implemented in the CytoHubba plugin, was employed to precisely identify highly interconnected and influential genes within the network (Shannon et al., 2003; Sz et al., 2019).

2.6 Validation and experimental confirmation

Gene validation was conducted using dataset GSE25906, which includes 37 PE cases and 23 controls. The diagnostic performance of genes was evaluated through Receiver Operating Characteristic (ROC) curve analysis using the "pROC" R package (Robin et al., 2011). The area under the curve (AUC) was calculated to assess the discriminatory power of these genes in distinguishing PE cases from controls.

Placental villous tissues from 21 PE cases and 21 controls matched by prepregnancy BMI, gestational age of delivery, and maternal age were collected at Gold Coast University Hospital. Ethical approval for this study was granted by the Royal Brisbane and Women's Hospital Human Research Ethics Committee (HREC/2020/QRBW/59479) and the Griffith University Human Research Ethics Committee (GU Ref No: 2020/049). Written informed consent was obtained from all participants. Placental samples were collected immediately post-delivery following the Stillbirth Centre for Research Excellence collection guideline, snap-frozen in liquid nitrogen, and stored at −80°C (Stillbirth CoRE, 2018). RNA was extracted using the RNeasy Mini Kit (Qiagen), and reverse transcription was performed with the QuantiTect Reverse Transcription Kit (Qiagen). Gene expression was quantified via quantitative PCR (qPCR) using SYBR Green Mix (Qiagen) with gene-specific primers. Expression levels were normalized to the housekeeping gene *YWHAZ*, known for its stability in placental tissue (Murthi et al., 2008). Relative gene expression was calculated using the delta-delta Ct method (Meller et al., 2005). Statistical analysis was performed using unpaired two-tailed t-test, and a p-value <0.05 was considered statistically significant. Plots were created with the "ggplot2" package in R (Wickham, 2016).

3 Results

3.1 Overview of placental transcriptomic studies in PE research

Through a comprehensive review of the GEO repository, we found 51 placental transcriptomic datasets focused on PE research (Supplementary File S1). The datasets were generated using three primary molecular profiling methods: 34 studies utilized microarray-based expression profiling, 16 employed high-throughput sequencing including one single-cell sequencing dataset, and one study used RT-PCR array. In addition, 36 studies focused on mRNA expression profiling, 11 targeted non-coding RNA profiling, and four studies conducted profiling for both mRNA and non-coding RNA. Sample collection timing varied across studies: 47 datasets used placental tissue collected after delivery, two used first-trimester chorionic villous sampling, and two datasets included placental tissue collected during both second trimester and at delivery.

3.2 Gene co-expression network analysis across PE subtypes

3.2.1 Co-expressed modules related to severe PE of GSE234729

WGCNA was performed for the GSE234729 dataset, encompassing 13,507 genes among 50 severe PE cases and 73 uncomplicated control samples. Sample clustering analysis and clinical trait associations are illustrated in Figure 2A. We constructed a scale-free co-expression network using a soft-threshold power of three, which achieved high scale independence (R^2 > 0.8) while maintaining robust gene connectivity (Figure 2B). The dynamic tree cutting algorithm identified eight distinct gene modules (Figure 2C), each assigned a unique colour and containing genes with highly correlated expression patterns. Module-trait relationship analysis examined correlations between each module and clinical characteristics (severe PE status, maternal ethnicity, and newborn gender). The correlation heatmap (Figure 2D) revealed that the green module demonstrated the strongest positive correlation with severe PE (r = 0.63, p = 4e-15).

We conducted comparative GO analysis to functionally annotate the WGCNA-identified gene modules, delineating their associated biological processes, molecular functions, and cellular components (Supplementary File S2; Supplementary Figure S1). The green module (which demonstrated the strongest correlation with severe PE; Figure 2D) showed predominant enrichment in biological processes related to responses to xenobiotic stimuli, lipid storage, epidermis development, and response to decreased oxygen levels.

3.2.2 Co-expressed modules related to early-onset and late-onset PE of GSE75010

For early-onset PE analysis of GSE75010, WGCNA was performed on 84 samples (49 early-onset PE cases and 35 uncomplicated cases delivered before 34 gestational weeks). The sample dendrogram (Figure 3A) illustrates hierarchical clustering based on gene expression patterns, alongside clinical traits (disease status, maternal BMI, ethnicity, HELLP syndrome, and FGR). Using a soft-threshold power of 10 to achieve scale-free topology (Figure 3B), we identified 23 co-expression modules (Figure 3C). Module-trait correlation analysis (Figure 3D) revealed that the yellow module demonstrated a strong correlation with clinical traits: positive correlations with early-onset PE (r = 0.73, p = 4e-15), HELLP syndrome (r = 0.44, p = 4e-05), FGR (r = 0.36, p = 0.001), and negative correlations with newborn weight (r = 0.59, p = 4e-09) and placental weight (r = −0.55, p = 7e-08). In contrast, the black and midnight-blue modules showed significant negative correlations with early-onset PE and positive correlations with newborn and placental weight. Comparative GO analysis (Supplementary File S2; Supplementary Figure S2) revealed that genes within yellow module were predominantly enriched in biological processes related to hypoxic responses while genes within black module were enriched in cellular division processes.

A similar analysis was conducted for late-onset PE from GSE75010 (Figure 4). The analysis identified 32 co-expression modules (Figure 4D). The bisque4 module showed the strongest negative correlation with late-onset PE (r = −0.56, p = 3e-07) and positive correlations with gestational age (r = 0.54, p = 1e-06), newborn weight (r = 0.52, p = 3e-06) and placental weight (r = 0.38, p = 0.001). The ivory module exhibited moderate positive correlation with late-onset PE (r = 0.46, p = 5e-05) and negative correlations with gestational age (r = −0.4, p = 5e-04), newborn weight (r = −0.44, p = 9e-05) and placental weight (r = −0.37, p = 0.001). Notably, the light-steel-blue1 module showed strong positive correlation with newborn weight (r = 0.6, p = 3e-08). Comparative GO analysis (Supplementary File S2; Supplementary Figure S3) revealed that the genes from ivory module was predominantly enriched in biological processes related to hypoxic response, cell-substrate adhesion and cellular response to external stimulus.

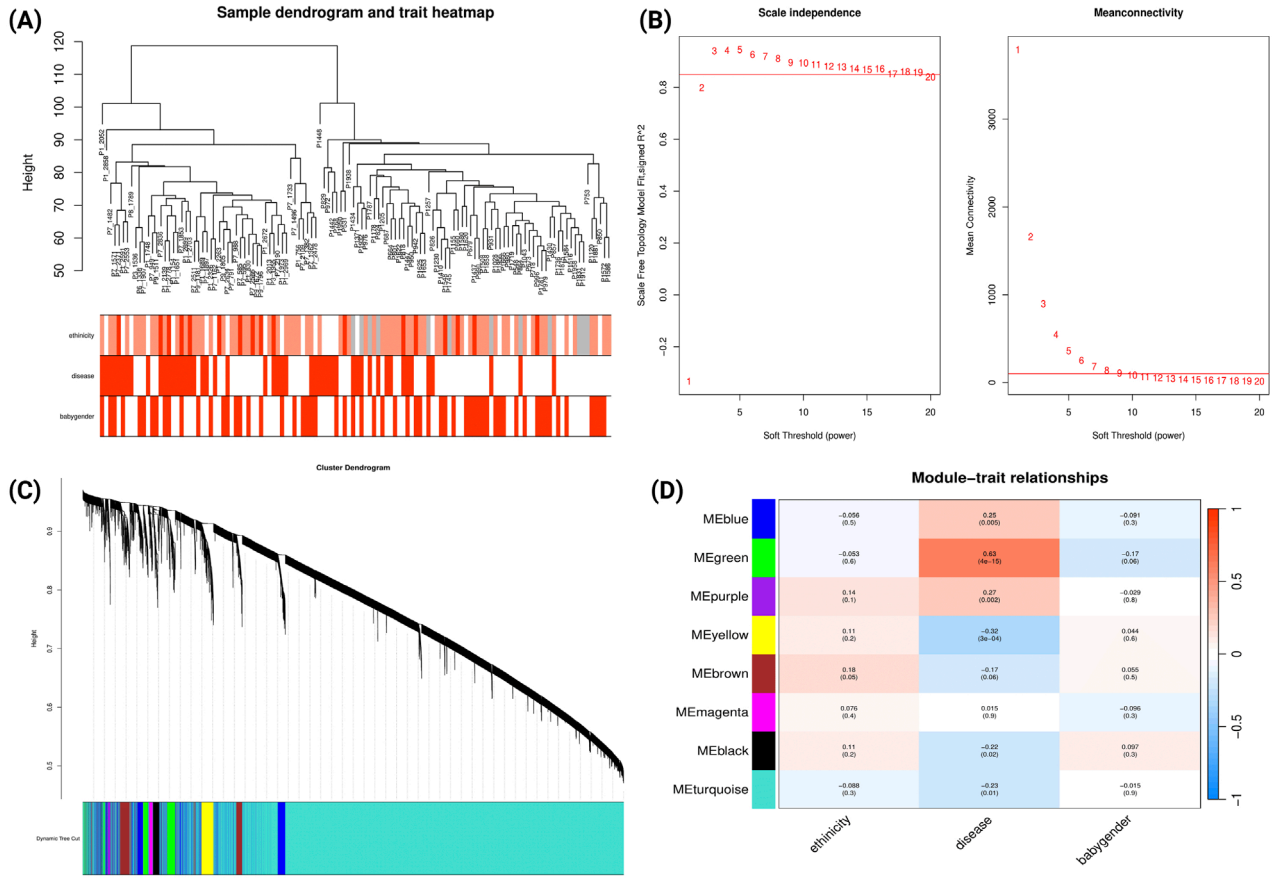

FIGURE 2
WGCNA Network Analysis of Severe Preeclampsia Dataset (GSE234729). **(A)** Sample dendrogram and clinical traits heatmap. The colour intensity below the dendrogram reflects the presence or magnitude of the clinical traits PE status, maternal ethnicity, and newborn gender. **(B)** Determination of soft-threshold power based on scale independence (left) and mean connectivity (right). **(C)** Gene cluster dendrogram showing module identification. Coloured bands below represent distinct co-expression modules identified through dynamic tree cutting. **(D)** Module-trait relationships heatmap. This heatmap displays correlations between module eigengenes (rows) and clinical traits (columns). Each cell contains the correlation coefficient (red indicating positive correlations, blue indicating negative correlations) and corresponding p-value.

3.3 Differential expression analysis and Integration of WGCNA

3.3.1 Identification of differentially expressed genes

We performed differential expression analysis for each dataset using criteria (|log2FC| > 0.5, FDR <0.05). In GSE234729 dataset, we identified 953 differentially expressed genes (DEGs) in severe PE, including 457 upregulated genes and 496 downregulated genes. Analysis of the GSE75010 dataset revealed 175 DEGs in early-onset PE (103 upregulated and 72 downregulated genes) and 34 DEGs in late-onset PE (26 upregulated and 8 downregulated genes).

3.3.2 Integration DEGs with PE-correlated gene modules

To identify key dysregulated genes potentially involved in PE subtype pathogenesis, we took the intersection between WGCNA gene modules and DEGs for each PE subtype, which are summarized in Table 1. For severe PE, the green module with the strongest positive correlation with disease status contains 179 DEGs. GO enrichment analysis of dysregulated genes from the green module (Figure 5A) revealed biological processes predominantly enriched in pathways related to lipid storage, epidermis development, and hypoxic response. PPI network analysis (Supplementary File S2; Supplementary Figure S4) identified the top ten hub genes using the Maximal Clique Centrality (MCC) algorithm that appear to play central roles in the network. These hub genes, ranked from highest to lowest MCC scores, are *SCARB1, LEP, ENG, SLC2A1, LPL, THY1, FLT1, MME, PLIN2,* and *P4HA1*. For early-onset PE, we identified 112 dysregulated genes in the positively correlated yellow module and 47 in the negatively correlated black module shown in Table 1. The yellow module DEGs were enriched in gonadotropin secretion regulation and lipid storage processes (Figure 5B). Similar PPI network analysis was performed and shown in Supplementary File S2; Supplementary Figure S5. Six hub genes (*SCARB1, LEP, PLIN2, LPL, ENG, P4HA1*) were common between the green module in severe PE and the yellow module in early-onset PE. The black module dysregulated genes (*IDO1, VNN1, S100A8*) of early-onset

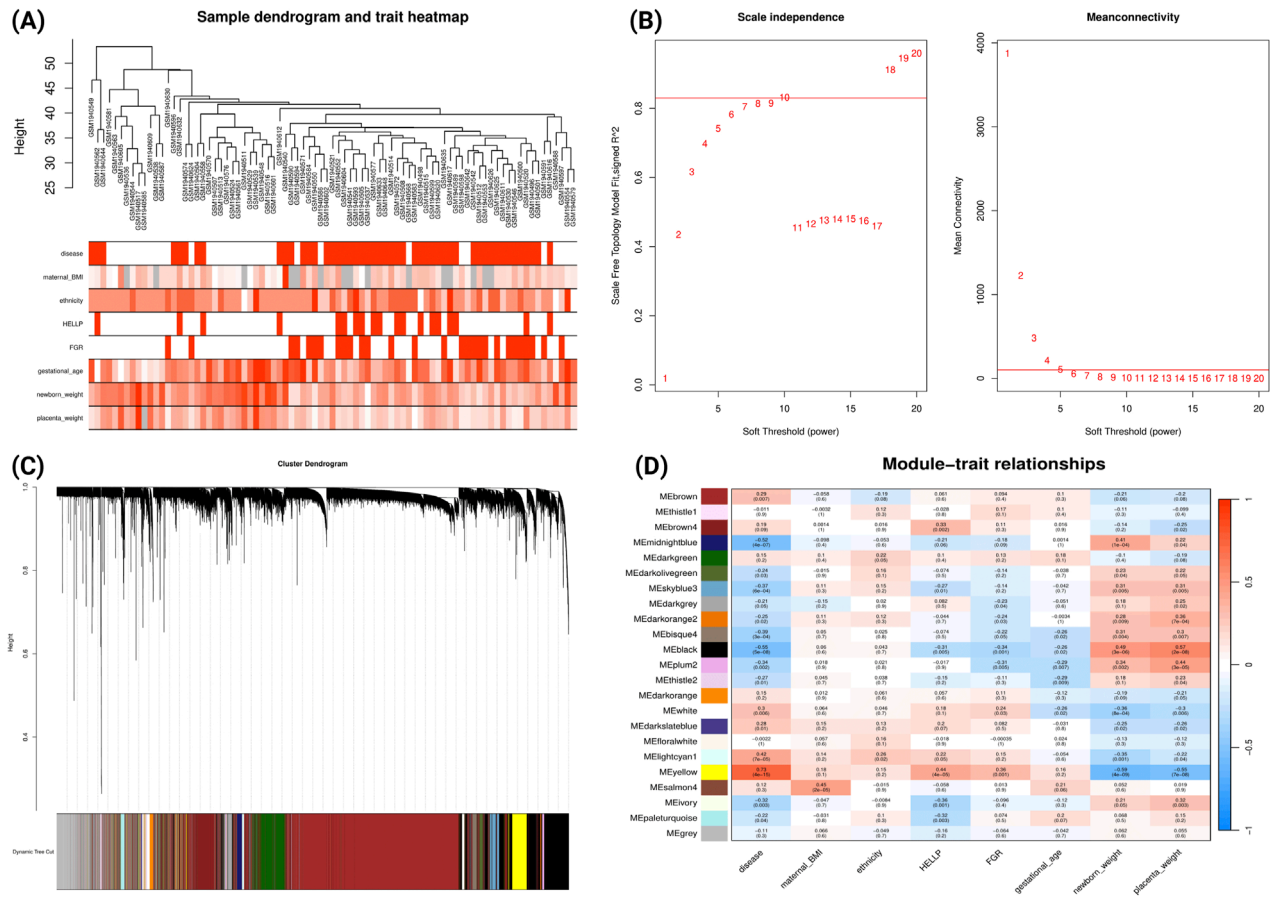

FIGURE 3
WGCNA Network Analysis of Early-onset Preeclampsia Dataset (GSE75010) **(A)** Sample dendrogram and clinical traits heatmap. Colour intensity represents the magnitude of clinical characteristics including PE status, maternal BMI, ethnicity, HELLP syndrome, FGR, gestational age, newborn weight, and placental weight. **(B)** Determination of soft-threshold power based on scale independence (left) and mean connectivity (right). **(C)** Gene cluster dendrogram with coloured bands representing distinct co-expression modules identified through dynamic tree cutting. **(D)** Module-trait relationship heatmap displaying correlations between module eigengenes (rows) and clinical traits (columns). Each cell contains the correlation coefficient (red indicating positive, blue indicating negative correlations) and corresponding p-value.

PE were significantly enriched in chronic inflammatory response (Figure 5C). The ivory module of late-onset PE contained 23 DEGs enriched in the p38 mitogen-activated protein kinase (p38MAPK) signalling pathway (Figure 5D). In this module, the top hub genes were *HTRA4, LEP, FLT1, BHLHE40, FSTL3, SASH1, SIGLEC6, FLNB, COL17A1, and ANKRD37* (Supplementary File S2; Supplementary Figure S6).

3.4 Identification and validation of potential biomarker candidates

We further performed a cross-analysis of DEGs from three modules showing positive correlation with PE subtypes to identify common dysregulated placental genes. There are 20 consistently dysregulated genes (*BHLHE40, SH3BP5, CORO2A, TMEM45A, QPCT, C12orf75, HK2, NRIP1, FSTL3, ANKRD37, FLNB, HTRA4, FLT1, COL17A1, NPNT, RASEF, SIGLEC6, HILPDA, SASH1, LEP*) overlapping among the green module (severe PE, GSE234729), yellow module (early-onset PE, GSE75010), and ivory module (late-onset PE, GSE75010), as illustrated in Figure 6. External validation using GSE25906 dataset confirmed differential expression of four genes: *FSTL3, HK2, HTRA4,* and *LEP*. Receiver Operating Characteristic (ROC) analysis of four validated genes in GSE25906 demonstrated their diagnostic potential (Supplementary File S2; Supplementary Figure S7), with LEP showing the highest discriminatory power (AUC = 0.84, 95% CI: 0.73–0.95). However, RT-PCR validation in our placental tissue cohort showed only modest upregulation of these genes, approximately 0.5 log2 fold change without statistical significance. The log2 fold change expression these genes in different datasets, RT-PCR results, and the area under the receiver operating characteristic curve (AUC) are summarized in Table 2.

4 Discussion

The exact aetiology of PE remains elusive, and its clinical management continues to be challenging due to its multifactorial

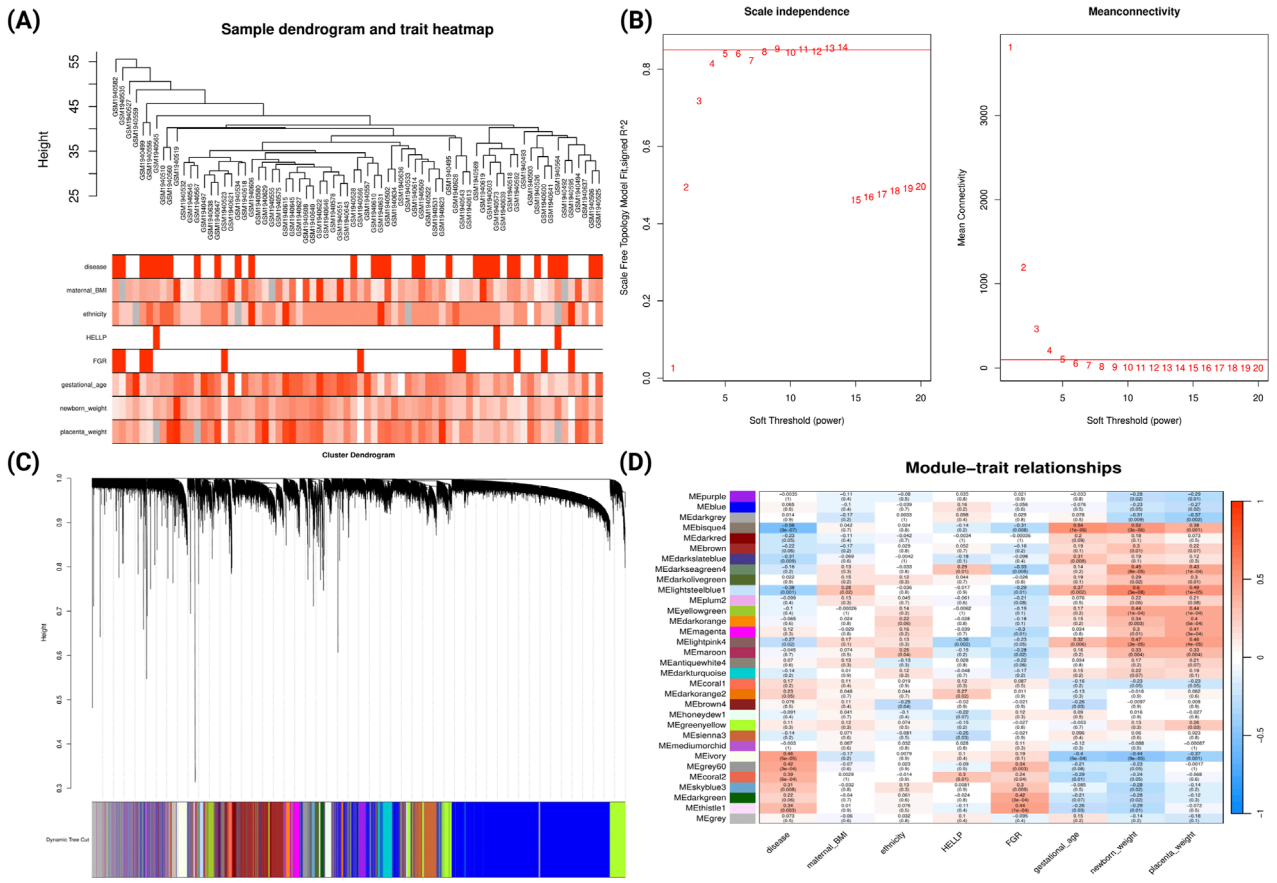

FIGURE 4
WGCNA Network Analysis of Late-onset Preeclampsia Dataset (GSE75010) **(A)** Sample dendrogram and clinical traits heatmap. Colour intensity represents the magnitude of clinical characteristics including PE status, maternal BMI, ethnicity, HELLP syndrome, FGR, gestational age, newborn weight, and placental weight. **(B)** Determination of soft-threshold power based on scale independence (left) and mean connectivity (right). **(C)** Gene cluster dendrogram with coloured bands representing distinct co-expression modules identified through dynamic tree cutting. **(D)** Module-trait relationship heatmap displaying correlations between module eigengenes (rows) and clinical traits (columns). Each cell contains the correlation coefficient (red indicating positive, blue indicating negative correlations) and corresponding p-value.

and heterogenous nature. Through integrated analysis of placental transcriptomics, we have identified both subtype-specific molecular signatures and overlapped biological processes with a core placental dysregulation signature underlying the three PE subtypes (severe, early-onset, and late-onset). Co-expression gene modules showed stronger association with severe and early-onset PE and these subtypes also have a greater number of differentially expressed genes. In contrast, late-onset PE presents modest correlation with WGCNA gene modules and fewer dysregulated genes. This may indicate that placental dysfunction is closely related to disease severity and early manifestation. We also identified 20 commonly dysregulated placental genes across PE-related modules in all PE subtypes, with four upregulated genes (*LEP*, *FSTL3*, *HTRA4*, and *HK2*) validated in the external dataset, suggesting a potential shared pathogenic feature despite the clinical and molecular heterogeneity among subtypes.

In this study, we found a robust association between severe PE and the WGCNA green module. GO functional annotation of dysregulated genes in this module revealed enrichment of several biological processes, including lipid storage, epidermis development, and response to decreased oxygen levels. These dysregulated pathways, particularly abnormal lipid metabolism and hypoxia response, appear to be key features of severe PE placental pathology. Previous research found increased levels of phospholipids, total cholesterol and lipid peroxides in preeclamptic decidua basalis tissue (Staff et al., 1999). Subsequent lipidomic studies also confirmed significantly higher lipid content in preeclamptic placental tissue (Zhang et al., 2022; Brown et al., 2016). In addition, maternal blood lipidomic profiling study has identified a significant correlation between oxidized phospholipids (OxPLs) and PE. They also found specific lipid species are uniquely associated with severe PE (He et al., 2021). Additionally, a study found that hypoxia promotes accumulation of lipid droplets in primary human trophoblast, and that perilipin (*PLIN*) proteins play key roles in the process (Bildirici et al., 2018). This evidence suggests there may be a potential link between placental hypoxia and altered lipid metabolism. Despite established research for both placental hypoxia and dysregulated lipid metabolism in PE, the relationship between these processes and how hypoxia-induced alterations in placental lipid metabolism may drive PE development and progression remains unclear.

10.3389/fcell.2025.1635878

TABLE 1 Summary of gene modules and differentially expressed genes across PE subtypes.

Dataset	Module colour	Total genes in module	Number of DEGs
GSE234729 (Severe PE)	Blue	928	35
	Green	390	179
	Purple	62	20
	Yellow	322	36
	Brown	613	22
	Magenta	86	1
	Black	175	2
	Turquoise	10,931	658
GSE75010 (Early-onset PE)	Yellow	724	112
	Black	2927	47
	Midnightblue	218	7
	White	147	5
	Brown	7815	1
	Brown4	1300	1
	Paleturquoise	134	1
	Salmon4	35	1
GSE75010 (Late-onset PE)	Ivory	562	23
	Grey60	187	3
	Bisque4	218	2
	Coral2	39	1
	Lightpink4	49	1
	Lightsteelblue1	153	1
	Grey	1188	1
	Sienna3	1409	1
	Skyblue3	225	1

The enrichment of lipid storage pathways was also observed in early-onset PE within the yellow module. Four genes involved in lipid metabolism (*SCARB1, LEP, PLIN2, LPL*) are upregulated in both severe and early-onset subtypes: *SCARB1* mediating cholesterol uptake (West et al., 2009), *LEP* encoding leptin, a hormone regulating energy consumption and adiposity (LeDuc et al., 2021), *PLIN2* facilitating lipid storage droplets formation (Itabe et al., 2017), and *LPL* hydrolysing triglycerides (Mead et al., 2002). These molecular alterations in placental lipid processing may contribute to both PE severity and early-onset manifestation. Moreover, DEGs genes (*LEP*, *INHBA*, *INHA* and *CRH*) in the yellow module are enriched endocrine hormone secretion pathways. This molecular signature suggests that disruption of endocrine and gonadotropin secretion processes may be a pathogenic mechanism in early-onset PE. *INHA* and *INHBA* encode inhibin A and activin A, modulating placental hormone synthesis. Elevated levels of activin A and inhibin A have been previously reported in placenta and maternal circulation as potential endocrine markers for PE (Florio et al., 2002; Muttukrishna et al., 2000; Spencer et al., 2008). Furthermore, dysregulated genes in the black module are mostly downregulated. We found *IDO1, VNN1, S100A8* are enriched in chronic inflammatory and immune response

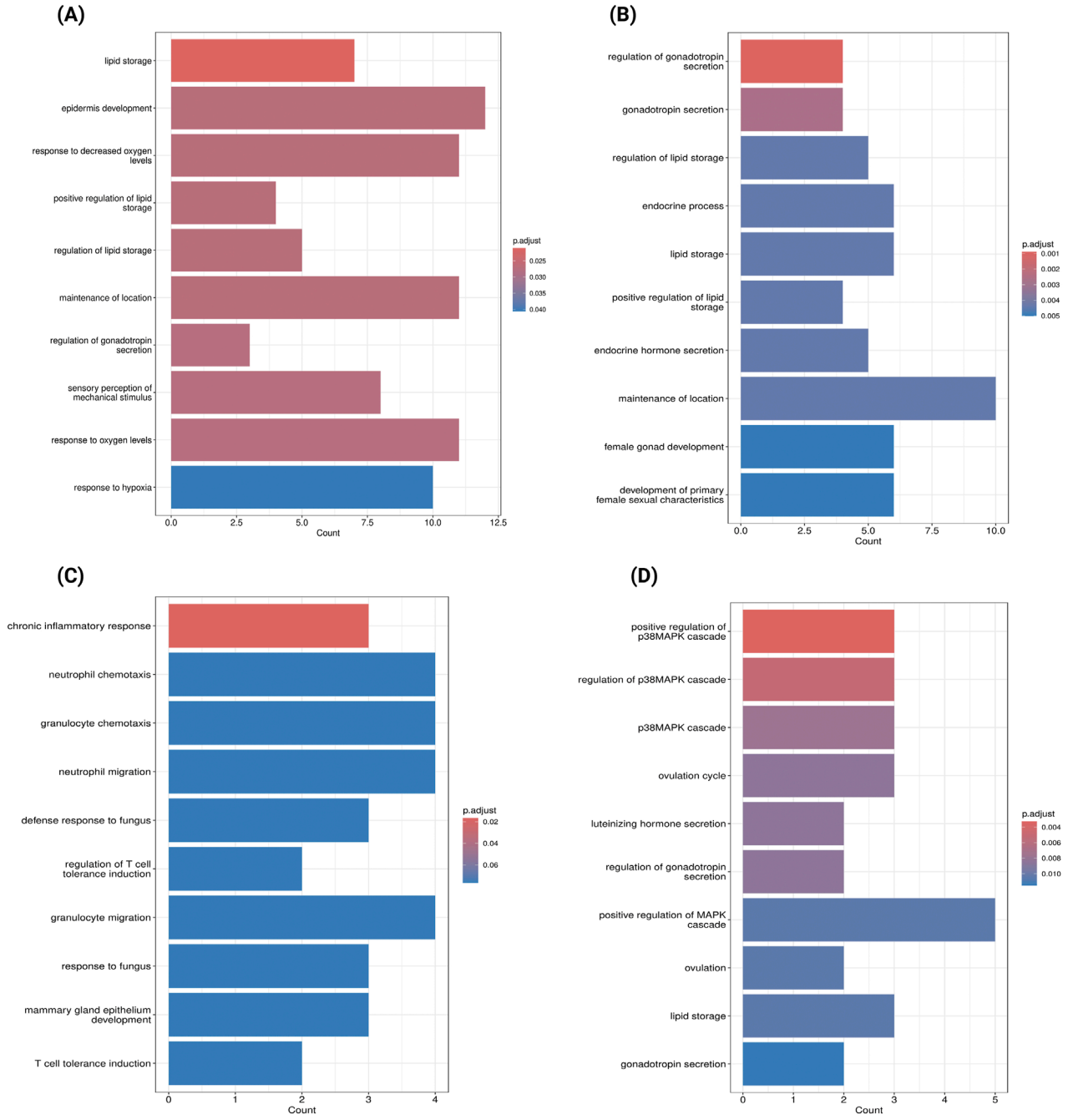

FIGURE 5
Gene Ontology Enrichment Analysis of Key Dysregulated Genes in Preeclampsia Subtypes **(A)** GO enrichment analysis of genes overlapping between the green module and DEGs in severe Preeclampsia (GSE234729). **(B)** GO enrichment analysis of genes overlapping between the yellow module and DEGs in early-onset Preeclampsia (GSE75010). **(C)** GO enrichment analysis of genes overlapping between the black module and DEGs in early-onset Preeclampsia (GSE75010). **(D)** GO enrichment analysis of genes overlapping between the ivory module and DEGs in late-onset Preeclampsia (GSE75010). Bar length represents the number of genes associated with each biological process, and colour intensity indicates statistical significance (darker blue represents lower adjusted p-values).

processes, indicating possible altered inflammatory or immune regulation in early-onset PE. *IDO1* is an interesting gene encoding indoleamine 2,3-dioxygenase (IDO), with functions involved in chronic inflammatory response, T cell tolerance induction, and L-tryptophan catabolism (Seo and Kwon, 2023). Reduced expression and activity of IDO1 have been reported in preeclamptic placentae (Kudo et al., 2003; Iwahashi et al., 2017), with one study suggesting this downregulation only occurs in early-onset PE but not in late-onset PE (Broekhuizen et al., 2021). Overall, these findings provide molecular evidence of complex interactions among metabolic, endocrine, and immune-inflammatory pathways in the pathogenesis of early-onset PE.

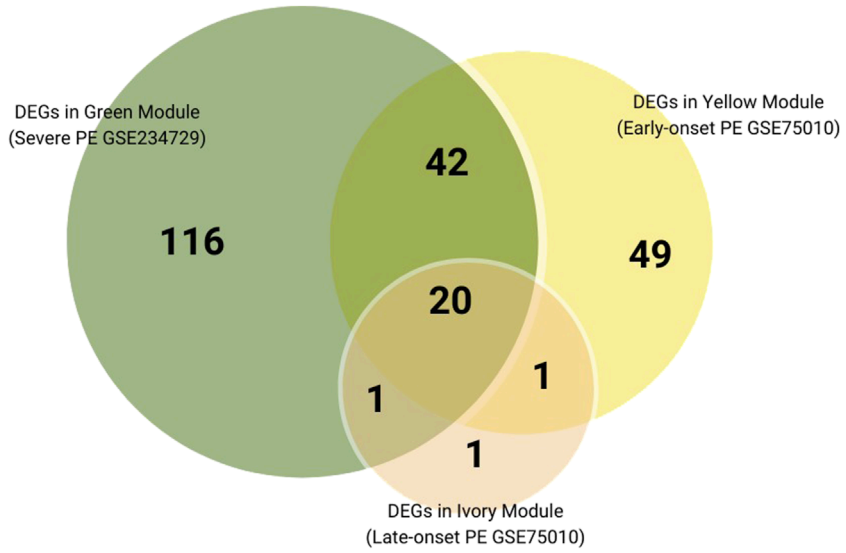

FIGURE 6
Venn diagram of DEGs overlaps among positively correlated Preeclampsia-related modules across subtypes.

TABLE 2 Log2 fold change expression of four validated genes across datasets.

Gene	Change	GSE234729 (severe PE)	GSE75010 (early-onset PE)	GSE75010 (late-onset PE)	GSE25906 (no subtype indicated)	GSE25906 (AUC)	RT-PCR results
LEP	Upregulated	4.39*	2.67*	1.39*	2.26*	0.84 (95%CI 0.73–0.95)	0.32ns
FSTL3	Upregulated	2.53*	1.54*	1.02*	1.28*	0.77 (95%CI 0.63–0.90)	0.51 ns
HK2	Upregulated	1.76*	1.29*	0.75*	0.79*	0.75 (95%CI 0.61–0.88)	0.51 ns
HTRA4	Upregulated	2.67*	1.58*	0.72*	0.84*	0.74 (95%CI 0.59–0.88)	0.47 ns

*indicates statistical significance (adjusted $p < 0.05$) and ns indicates not statistically significant.

Previous research suggests that late-onset PE is less associated with placental dysfunction than severe and/or early-onset forms (Ren et al., 2021). These differences likely reflect distinct underlying pathophysiological mechanism. Early-onset PE is primarily characterised by defective placentation in early gestation, resulting in widespread transcriptomic and histopathological disruption. In contrast, late-onset PE is believed to being predominantly driven by maternal factors, such as preexisting cardiovascular and metabolic conditions, with placental stress and aging emerging as secondary contributors in later gestation (Melchiorre et al., 2022; Redman et al., 2022; Robillard et al., 2022; Staff, 2019; Khodzhaeva et al., 2016). This is further supported by clinical evidence demonstrating higher frequencies of fetal growth restriction in early-onset PE compared to late-onset PE, as well as placental pathology analyses reporting a higher rate of maternal vascular malperfusion lesions in early-onset cases (Freedman et al., 2023; Ogge et al., 2011; Gilgannon et al., 2023; Hung et al., 2018). Consistent with these established findings, our analysis found that late-onset PE exhibited fewer differentially expressed genes and only modest correlations with WGCNA gene modules, which may indicate more subtle placental transcriptomic alterations in the late subtype. The ivory module has a moderate correlation with disease status, with DEGs primarily enriched in the p38MAPK signalling pathway (SASH1/FLT1/NPNT/LEP/OPRK1). This pathway plays a critical role in stress response and inflammatory signalling (Cuenda and Rousseau, 2007). The enrichment of p38MAPK signalling in late-onset PE placenta may reflect activation of stress-response mechanisms proximal to term.

We externally validated twenty placental genes that are consistently dysregulated across PE subtypes and confirmed that four genes (*LEP, FSTL3, HTRA4, HK2*) were significantly upregulated. However, clinical validation by RT-PCR only presented moderate upregulation, which may be attributed to the predominance of term PE cases (19/22) in our validation cohort, all of which developed and delivered at or beyond 37 weeks of gestation. Previous studies support the clinical utility of three of these candidates as maternal biomarkers. *LEP* plays a multifunctional role in the placenta such as regulating endocrine

processes, angiogenesis, and inflammatory responses (Zeng et al., 2023). Maternal serum and plasma leptin levels have been found to differ between preeclamptic women and normotensive pregnant women, with higher concentrations in severe and early-onset cases (Taylor et al., 2015; Hao et al., 2020; El et al., 2013; Salimi et al., 2014). Similarly, increased follistatin-like 3 (FSTL-3) levels is reported with increased likelihood of developing PE (Found et al., 2015; Han et al., 2014), although another study found that FSTL-3 did not alter in early-onset PE (Nevalainen et al., 2017). Elevated serum HtrA4 levels were also higher in the PE group compared to the control group, and this biomarker showed predictive value when combined with first-trimester uterine artery Doppler measurements (Siricharoenthai and Phupong, 2023). *HK2* encodes hexokinase 2, a key glycolytic enzyme that is upregulated in preeclamptic and FGR placentas (Wong et al., 2024). Currently, no studies have investigated whether hexokinase 2 levels are elevated in the maternal circulation in PE cases.

Our study identified subtype-specific mechanisms and key dysregulated genes associated with PE. Future research should validate key dysregulated placental genes through functional experiments such as placenta organoid models to define their roles in placental dysfunction. Moreover, determining whether candidate genes such as *LEP*, *FSTL3*, *HTRA4*, and *HK2*, or their protein products, can be reliably detected and quantified in maternal circulation is essential for translating these findings into clinical applications as potential biomarkers. Several limitations should be considered when interpreting these results. First, heterogeneity in sample sources and transcriptomic platforms may impact reproducibility. Datasets GSE75010 and GSE25906 were generated using microarray technology, whereas dataset GSE234729 utilized RNA-sequencing. Such technique and platform differences introduce technical variations that may affect gene expression comparison across datasets. For the current analysis, we also selected only studies with greater than 60 samples; this was done to provide a good level of statistical power, but may have introduced selection bias by excluding smaller studied. Additionally, potential confounding factors like maternal clinical characteristics may also influence placental gene expression patterns. Second, although PE cases and controls were matched for key maternal variables in RT-PCR validation, several factors are likely to have limited our capacity to detect gene expression with significant differences, including the modest sample size, the predominance of term PE cases (19/22 delivering ≥37 weeks gestation), and potential RNA degradation during sample processing. Third, the computational methodologies employed generate preliminary findings that require experimental validation. While WGCNA is a powerful tool for identifying gene co-expression modules, this approach is susceptible to various sources of bias, including technical artifacts, suboptimal experimental design, and analytical decisions (e.g., sample clustering, module selection). Similarly, predicted PPI networks need experimental confirmation at the protein level to establish biological relevance and functional significance. These methodological limitations collectively affect the reproducibility and clinical interpretation of our results, indicating that further experimental validation is required.

In conclusion, this study presents a detailed analysis of placental transcriptomic data across different PE subtypes, revealing both distinct molecular signatures and shared potential pathogenic mechanisms. Severe and early-onset PE are characterized by significant molecular dysregulation in placenta, while late-onset PE shows more modest alterations. There is evidence that disrupted lipid storage pathways are a common molecular feature in both early-onset and severe PE, suggesting that altered placental lipid homeostasis may be a critical determinant of disease severity and early manifestation. Whilst these findings provide evidence of placental transcriptomic changes associated with PE, they are preliminary and require further experimental confirmation in additional cohorts to determine the potential translation of evidence into clinical care.

Data availability statement

The original contributions presented in the study are included in the article/Supplementary Material, further inquiries can be directed to the corresponding author.

Ethics statement

The studies involving humans were approved by Royal Brisbane and Women's Hospital Human Research Ethics Committee (HREC/2020/QRBW/59479) and Griffith University Human Research Ethics Committee (GU Ref No: 2020/049). The studies were conducted in accordance with the local legislation and institutional requirements. The participants provided their written informed consent to participate in this study.

Author contributions

LH: Validation, Formal Analysis, Writing – original draft, Project administration, Visualization, Conceptualization, Software, Methodology, Investigation, Data curation. FS: Writing – review and editing, Supervision, Funding acquisition, Resources. AP: Supervision, Funding acquisition, Resources, Writing – review and editing. OH: Resources, Project administration, Funding acquisition, Writing – review and editing, Supervision.

Funding

The author(s) declare that no financial support was received for the research and/or publication of this article.

Conflict of interest

The authors declare that the research was conducted in the absence of any commercial or financial relationships that could be construed as a potential conflict of interest.

Generative AI statement

The author(s) declare that Generative AI was used in the creation of this manuscript to assist with language editing, grammar correction, and troubleshooting code during data analysis in R Studio. No AI-generated content contributed to the interpretation

of results or the formulation of scientific conclusions. All analytical decisions, interpretations, and intellectual contributions are those of the author(s).

Publisher's note

All claims expressed in this article are solely those of the authors and do not necessarily represent those of their affiliated organizations, or those of the publisher, the editors and the reviewers. Any product that may be evaluated in this article, or claim that may be made by its manufacturer, is not guaranteed or endorsed by the publisher.

Supplementary material

The Supplementary Material for this article can be found online at: https://www.frontiersin.org/articles/10.3389/fcell.2025.1635878/full#supplementary-material

References

Abalos, E., Cuesta, C., Carroli, G., Qureshi, Z., Widmer, M., Vogel, J. P., et al. (2014). Pre-eclampsia, eclampsia and adverse maternal and perinatal outcomes: a secondary analysis of the world health organization multicountry survey on maternal and newborn health. *Bjog* 121 (Suppl. 1), 14–24. doi:10.1111/1471-0528.12629

Admati, I., Skarbianskis, N., Hochgerner, H., Ophir, O., Weiner, Z., Yagel, S., et al. (2023). Two distinct molecular faces of preeclampsia revealed by single-cell transcriptomics. *Med* 4 (10), 687–709 e7. doi:10.1016/j.medj.2023.07.005

Aisagbonhi, O., Bui, T., Nasamran, C. A., St Louis, H., Pizzo, D., Meads, M., et al. (2023). High placental expression of FLT1, LEP, PHYHIP and IL3RA - in persons of African ancestry with severe preeclampsia. *Placenta* 144, 13–22. doi:10.1016/j.placenta.2023.10.008

Bildirici, I., Schaiff, W. T., Chen, B., Morizane, M., Oh, S. Y., O'Brien, M., et al. (2018). PLIN2 is essential for trophoblastic lipid droplet accumulation and cell survival during hypoxia. *Endocrinology* 159 (12), 3937–3949. doi:10.1210/en.2018-00752

Broekhuizen, M., Hitzerd, E., van den Bosch, T. P. P., Dumas, J., Verdijk, R. M., van Rijn, B. B., et al. (2021). The placental innate immune system is altered in early-onset preeclampsia, but not in late-onset preeclampsia. *Front. Immunol.* 12, 780043. doi:10.3389/fimmu.2021.780043

Brown, S. H., Eather, S. R., Freeman, D. J., Meyer, B. J., and Mitchell, T. W. (2016). A lipidomic analysis of placenta in preeclampsia: evidence for lipid storage. *PLoS One* 11 (9), e0163972. doi:10.1371/journal.pone.0163972

Burton, G. J., Redman, C. W., Roberts, J. M., and Moffett, A. (2019). Pre-eclampsia: pathophysiology and clinical implications. *BMJ* 366, l2381. doi:10.1136/bmj.l2381

Castleman, J. S., Ganapathy, R., Taki, F., Lip, G. Y., Steeds, R. P., and Kotecha, D. (2016). Echocardiographic structure and function in hypertensive disorders of pregnancy: a systematic review. *Circ. Cardiovasc Imaging* 9 (9), e004888. doi:10.1161/CIRCIMAGING.116.004888

Chuah, T. T., Tey, W. S., Ng, M. J., Tan, E. T. H., Chern, B., and Tan, K. H. (2018). Serum sFlt-1/PlGF ratio has better diagnostic ability in early-compared to late-onset pre-eclampsia. *J. Perinat. Med.* 47 (1), 35–40. doi:10.1515/jpm-2017-0288

Cuenda, A., and Rousseau, S. (2007). p38 MAP-Kinases pathway regulation, function and role in human diseases. *Biochim. Biophys. Acta* 1773 (8), 1358–1375. doi:10.1016/j.bbamcr.2007.03.010

Dimitriadis, E., Rolnik, D. L., Zhou, W., Estrada-Gutierrez, G., Koga, K., Francisco, R. P. V., et al. (2023). Pre-eclampsia. *Nat. Rev. Dis. Prim.* 9 (1), 8. doi:10.1038/s41572-023-00417-6

El, S. A. M., Ahmed, A. B., Ahmed, M. R., and Mohamed, H. S. (2013). Maternal serum leptin as a marker of preeclampsia. *Arch. Gynecol. Obstet.* 288 (6), 1317–1322. doi:10.1007/s00404-013-2915-8

Florio, P., Ciarmela, P., Luisi, S., Palumbo, M. A., Lambert-Messerlian, G., Severi, F. M., et al. (2002). Pre-eclampsia with fetal growth restriction: placental and serum activin A and inhibin A levels. *Gynecol. Endocrinol.* 16 (5), 365–372. doi:10.1080/gye.16.5.365.372

Founds, S. A., Ren, D., Roberts, J. M., Jeyabalan, A., and Powers, R. W. (2015). Follistatin-like 3 across gestation in preeclampsia and uncomplicated pregnancies among lean and Obese women. *Reprod. Sci.* 22 (4), 402–409. doi:10.1177/1933719114529372

Freedman, A. A., Suresh, S., and Ernst, L. M. (2023). Patterns of placental pathology associated with preeclampsia. *Placenta* 139, 85–91. doi:10.1016/j.placenta.2023.06.007

Garcia-Gonzalez, C., Georgiopoulos, G., Azim, S. A., Macaya, F., Kametas, N., Nihoyannopoulos, P., et al. (2020). Maternal cardiac assessment at 35 to 37 weeks improves prediction of development of preeclampsia. *Hypertension* 76 (2), 514–522. doi:10.1161/HYPERTENSIONAHA.120.14643

Gestational Hypertension and Preeclampsia: ACOG Practice Bulletin (2020). Number 222. *Obstet. Gynecol.* 135 (6), e237–e260. doi:10.1097/AOG.0000000000003891

Gilgannon, L., Martins, J. G., Srinivas, R. S., Gupta, N., Long, D., King, K., et al. (2023). Adverse maternal outcomes of patients with preeclampsia complicated by fetal growth restriction. *Am. J. Obstetrics and Gynecol.* 228 (1), S515–S516. doi:10.1016/j.ajog.2022.11.883

Han, X., He, J., Wang, A., and Dong, M. (2014). Serum Follistatin-like-3 was elevated in second trimester of pregnant women who subsequently developed preeclampsia. *Hypertens. Pregnancy* 33 (3), 277–282. doi:10.3109/10641955.2013.874439

Hao, S., You, J., Chen, L., Zhao, H., Huang, Y., Zheng, L., et al. (2020). Changes in pregnancy-related serum biomarkers early in gestation are associated with later development of preeclampsia. *PLoS One* 15 (3), e0230000. doi:10.1371/journal.pone.0230000

He, B., Liu, Y., Maurya, M. R., Benny, P., Lassiter, C., Li, H., et al. (2021). The maternal blood lipidome is indicative of the pathogenesis of severe preeclampsia. *J. Lipid Res.* 62, 100118. doi:10.1016/j.jlr.2021.100118

Hung, T. H., Hsieh, T. T., and Chen, S. F. (2018). Risk of abnormal fetal growth in women with early- and late-onset preeclampsia. *Pregnancy Hypertens.* 12, 201–206. doi:10.1016/j.preghy.2017.09.003

Itabe, H., Yamaguchi, T., Nimura, S., and Sasabe, N. (2017). Perilipins: a diversity of intracellular lipid droplet proteins. *Lipids Health Dis.* 16 (1), 83. doi:10.1186/s12944-017-0473-y

Iwahashi, N., Yamamoto, M., Nanjo, S., Toujima, S., Minami, S., and Ino, K. (2017). Downregulation of indoleamine 2, 3-dioxygenase expression in the villous stromal endothelial cells of placentas with preeclampsia. *J. Reprod. Immunol.* 119, 54–60. doi:10.1016/j.jri.2017.01.003

Junus, K., Centlow, M., Wikstrom, A. K., Larsson, I., Hansson, S. R., and Olovsson, M. (2012). Gene expression profiling of placentae from women with early- and late-onset pre-eclampsia: down-regulation of the angiogenesis-related genes ACVRL1 and EGFL7 in early-onset disease. *Mol. Hum. Reprod.* 18 (3), 146–155. doi:10.1093/molehr/gar067

Khodzhaeva, Z. S., Kogan, Y. A., Shmakov, R. G., Klimenchenko, N. I., Akatyeva, A. S., Vavina, O. V., et al. (2016). Clinical and pathogenetic features of early- and late-onset pre-eclampsia. *J. Matern. Fetal Neonatal Med.* 29 (18), 2980–2986. doi:10.3109/14767058.2015.1111332

Kudo, Y., Boyd, C. A., Sargent, I. L., and Redman, C. W. (2003). Decreased tryptophan catabolism by placental indoleamine 2,3-dioxygenase in preeclampsia. *Am. J. Obstet. Gynecol.* 188 (3), 719–726. doi:10.1067/mob.2003.156

Langfelder, P., and Horvath, S. (2008). WGCNA: an R package for weighted correlation network analysis. *Bmc Bioinforma.* 9, 559. doi:10.1186/1471-2105-9-559

Leavey, K., Benton, S. J., Grynspan, D., Kingdom, J. C., Bainbridge, S. A., and Cox, B. J. (2016). Unsupervised placental gene expression profiling identifies clinically relevant subclasses of human preeclampsia. *Hypertension* 68 (1), 137–147. doi:10.1161/HYPERTENSIONAHA.116.07293

LeDuc, C. A., Skowronski, A. A., and Rosenbaum, M. (2021). The role of leptin in the development of energy homeostatic systems and the maintenance of body weight. *Front. Physiol.* 12, 789519. doi:10.3389/fphys.2021.789519

Leon, L. J., McCarthy, F. P., Direk, K., Gonzalez-Izquierdo, A., Prieto-Merino, D., Casas, J. P., et al. (2019). Preeclampsia and cardiovascular disease in a large UK pregnancy cohort of linked electronic health records: a CALIBER study. *Circulation* 140 (13), 1050–1060. doi:10.1161/CIRCULATIONAHA.118.038080

Liang, M., Niu, J., Zhang, L., Deng, H., Ma, J., Zhou, W., et al. (2016). Gene expression profiling reveals different molecular patterns in G-protein coupled receptor signaling pathways between early- and late-onset preeclampsia. *Placenta* 40, 52–59. doi:10.1016/j.placenta.2016.02.015

Magee, L. A., Brown, M. A., Hall, D. R., Gupte, S., Hennessy, A., Karumanchi, S. A., et al. (2022). The 2021 international society for the study of hypertension in pregnancy classification, diagnosis and management recommendations for international practice. *Pregnancy Hypertens.* 27, 148–169. doi:10.1016/j.preghy.2021.09.008

Mead, J. R., Irvine, S. A., and Ramji, D. P. (2002). Lipoprotein lipase: structure, function, regulation, and role in disease. *J. Mol. Med. Berl.* 80 (12), 753–769. doi:10.1007/s00109-002-0384-9

Melchiorre, K., Giorgione, V., and Thilaganathan, B. (2022). The placenta and preeclampsia: villain or victim? *Am. J. Obstet. Gynecol.* 226 (2S), S954–S962. doi:10.1016/j.ajog.2020.10.024

Melchiorre, K., Sutherland, G., Sharma, R., Nanni, M., and Thilaganathan, B. (2013). Mid-gestational maternal cardiovascular profile in preterm and term pre-eclampsia: a prospective study. *BJOG* 120 (4), 496–504. doi:10.1111/1471-0528.12068

Meller, M., Vadachkoria, S., Luthy, D. A., and Williams, M. A. (2005). Evaluation of housekeeping genes in placental comparative expression studies. *Placenta* 26 (8-9), 601–607. doi:10.1016/j.placenta.2004.09.009

Michalczyk, M., Celewicz, A., Celewicz, M., Woźniakowska-Gondek, P., and Rzepka, R. (2020). The role of inflammation in the pathogenesis of preeclampsia. *Mediat. Inflamm.* 2020, 3864941. doi:10.1155/2020/3864941

Murthi, P., Fitzpatrick, E., Borg, A. J., Donath, S., Brennecke, S. P., and Kalionis, B. (2008). GAPDH, 18S rRNA and YWHAZ are suitable endogenous reference genes for relative gene expression studies in placental tissues from human idiopathic fetal growth restriction. *Placenta* 29 (9), 798–801. doi:10.1016/j.placenta.2008.06.007

Muttukrishna, S., North, R. A., Morris, J., Schellenberg, J. C., Taylor, R. S., Asselin, J., et al. (2000). Serum inhibin A and activin A are elevated prior to the onset of pre-eclampsia. *Hum. Reprod.* 15 (7), 1640–1645. doi:10.1093/humrep/15.7.1640

Nevalainen, J., Korpimaki, T., Kouru, H., Sairanen, M., and Ryynanen, M. (2017). Performance of first trimester biochemical markers and mean arterial pressure in prediction of early-onset pre-eclampsia. *Metabolism* 75, 6–15. doi:10.1016/j.metabol.2017.07.004

Ngene, N. C., and Moodley, J. (2018). Role of angiogenic factors in the pathogenesis and management of pre-eclampsia. *Int. J. Gynaecol. Obstet.* 141 (1), 5–13. doi:10.1002/ijgo.12424

Nishizawa, H., Pryor-Koishi, K., Kato, T., Kowa, H., Kurahashi, H., and Udagawa, Y. (2007). Microarray analysis of differentially expressed fetal genes in placental tissue derived from early and late onset severe pre-eclampsia. *Placenta* 28 (5-6), 487–497. doi:10.1016/j.placenta.2006.05.010

Ogge, G., Chaiworapongsa, T., Romero, R., Hussein, Y., Kusanovic, J. P., Yeo, L., et al. (2011). Placental lesions associated with maternal underperfusion are more frequent in early-onset than in late-onset preeclampsia. *J. Perinat. Med.* 39 (6), 641–652. doi:10.1515/jpm.2011.098

Pankiewicz, K., Fijałkowska, A., Issat, T., and Maciejewski, T. M. (2021). Insight into the key points of preeclampsia pathophysiology: uterine artery remodeling and the role of MicroRNAs. *Int. J. Mol. Sci.* 22 (6), 3132. doi:10.3390/ijms22063132

Pinheiro, C. C., Rayol, P., Gozzani, L., Reis, L. M., Zampieri, G., Dias, C. B., et al. (2014). The relationship of angiogenic factors to maternal and neonatal manifestations of early-onset and late-onset preeclampsia. *Prenat. Diagn* 34 (11), 1084–1092. doi:10.1002/pd.4432

Poon, L. C., Shennan, A., Hyett, J. A., Kapur, A., Hadar, E., Divakar, H., et al. (2019). The international Federation of gynecology and obstetrics (FIGO) initiative on pre-eclampsia: a pragmatic guide for first-trimester screening and prevention. *Int. J. Gynaecol. Obstet.* 145 (1), 1–33. doi:10.1002/ijgo.12802

Redman, C. W. G., Staff, A. C., and Roberts, J. M. (2022). Syncytiotrophoblast stress in preeclampsia: the convergence point for multiple pathways. *Am. J. Obstet. Gynecol.* 226 (2S), S907–S927. doi:10.1016/j.ajog.2020.09.047

Ren, Z., Gao, Y., Gao, Y., Liang, G., Chen, Q., Jiang, S., et al. (2021). Distinct placental molecular processes associated with early-onset and late-onset preeclampsia. *Theranostics* 11 (10), 5028–5044. doi:10.7150/thno.56141

Ritchie, M. E., Phipson, B., Wu, D., Hu, Y. F., Law, C. W., Shi, W., et al. (2015). Limma powers differential expression analyses for RNA-Sequencing and microarray studies. *Nucleic Acids Res.* 43 (7), e47. doi:10.1093/nar/gkv007

Robillard, P. Y., Dekker, G., Scioscia, M., and Saito, S. (2022). Progress in the understanding of the pathophysiology of immunologic maladaptation related to early-onset preeclampsia and metabolic syndrome related to late-onset preeclampsia. *Am. J. Obstet. Gynecol.* 226 (2S), S867–S875. doi:10.1016/j.ajog.2021.11.019

Robin, X., Turck, N., Hainard, A., Tiberti, N., Lisacek, F., Sanchez, J. C., et al. (2011). pROC: an open-source package for R and S+ to analyze and compare ROC curves. *BMC Bioinforma.* 12, 77. doi:10.1186/1471-2105-12-77

Salimi, S., Farajian-Mashhadi, F., Naghavi, A., Mokhtari, M., Shahrakipour, M., Saravani, M., et al. (2014). Different profile of serum leptin between early onset and late onset preeclampsia. *Dis. Markers* 2014, 628476. doi:10.1155/2014/628476

Sean, D., and Meltzer, P. S. (2007). GEOquery: a bridge between the gene expression omnibus (GEO) and BioConductor. *Bioinformatics* 23 (14), 1846–1847. doi:10.1093/bioinformatics/btm254

Seo, S. K., and Kwon, B. (2023). Immune regulation through tryptophan metabolism. *Exp. Mol. Med.* 55 (7), 1371–1379. doi:10.1038/s12276-023-01028-7

Shannon, P., Markiel, A., Ozier, O., Baliga, N. S., Wang, J. T., Ramage, D., et al. (2003). Cytoscape: a software environment for integrated models of biomolecular interaction networks. *Genome Res.* 13 (11), 2498–2504. doi:10.1101/gr.1239303

Siricharoenthai, P., and Phupong, V. (2023). The first-trimester serum high-temperature requirement protease A4 and uterine artery doppler for the prediction of preeclampsia. *Sci. Rep.* 13 (1), 8295. doi:10.1038/s41598-023-35243-z

Sitras, V., Paulssen, R. H., Gronaas, H., Leirvik, J., Hanssen, T. A., Vartun, A., et al. (2009). Differential placental gene expression in severe preeclampsia. *Placenta* 30 (5), 424–433. doi:10.1016/j.placenta.2009.01.012

Spencer, K., Cowans, N. J., and Nicolaides, K. H. (2008). Maternal serum inhibin-A and activin-A levels in the first trimester of pregnancies developing pre-eclampsia. *Ultrasound Obstet. Gynecol.* 32 (5), 622–626. doi:10.1002/uog.6212

Staff, A. C. (2019). The two-stage placental model of preeclampsia: an update. *J. Reprod. Immunol.* 134-135, 1–10. doi:10.1016/j.jri.2019.07.004

Staff, A. C., Ranheim, T., Khoury, J., and Henriksen, T. (1999). Increased contents of phospholipids, cholesterol, and lipid peroxides in decidua basalis in women with preeclampsia. *Am. J. Obstet. Gynecol.* 180 (3 Pt 1), 587–592. doi:10.1016/s0002-9378(99)70259-0

Stillbirth CoRE. Protocol: human placental tissue collection (1999).

Szklarczyk, D., Gable, A. L., Lyon, D., Junge, A., Wyder, S., Huerta-Cepas, J., et al. (2019). STRING v11: protein-protein association networks with increased coverage, supporting functional discovery in genome-wide experimental datasets. *Nucleic Acids Res.* 47 (D1), D607–D613. doi:10.1093/nar/gky1131

Taylor, B. D., Ness, R. B., Olsen, J., Hougaard, D. M., Skogstrand, K., Roberts, J. M., et al. (2015). Serum leptin measured in early pregnancy is higher in women with preeclampsia compared with normotensive pregnant women. *Hypertension* 65 (3), 594–599. doi:10.1161/HYPERTENSIONAHA.114.03979

Thilaganathan, B. (2020). Maternal cardiac dysfunction precedes development of preeclampsia. *Hypertension* 76 (2), 321–322. doi:10.1161/HYPERTENSIONAHA.120.15281

Tsai, S., Hardison, N. E., James, A. H., Motsinger-Reif, A. A., Bischoff, S. R., Thames, B. H., et al. (2011). Transcriptional profiling of human placentas from pregnancies complicated by preeclampsia reveals disregulation of sialic acid acetylesterase and immune signalling pathways. *Placenta* 32 (2), 175–182. doi:10.1016/j.placenta.2010.11.014

West, M., Greason, E., Kolmakova, A., Jahangiri, A., Asztalos, B., Pollin, T. I., et al. (2009). Scavenger receptor class B type I protein as an independent predictor of high-density lipoprotein cholesterol levels in subjects with hyperalphalipoproteinemia. *J. Clin. Endocrinol. Metab.* 94 (4), 1451–1457. doi:10.1210/jc.2008-1223

Wickham, H. (2016). *Ggplot2: elegant graphics for data analysis*. 2 ed. Springer International Publishing.

Wong, G. P., Hartmann, S., Simmons, D. G., Ellis, S., Nonn, O., Cannon, P., et al. (2024). Trophoblast side-population markers are dysregulated in preeclampsia and fetal growth restriction. *Stem Cell. Rev. Rep.* 20 (7), 1954–1970. doi:10.1007/s12015-024-10764-w

Wu, P., Haththotuwa, R., Kwok, C. S., Babu, A., Kotronias, R. A., Rushton, C., et al. (2017). Preeclampsia and future cardiovascular health: a systematic review and meta-analysis. *Circ. Cardiovasc Qual. Outcomes* 10 (2), e003497. doi:10.1161/CIRCOUTCOMES.116.003497

Yu, G., Wang, L. G., Han, Y., and He, Q. Y. (2012). clusterProfiler: an R package for comparing biological themes among gene clusters. *OMICS* 16 (5), 284–287. doi:10.1089/omi.2011.0118

Zeng, S., Liu, Y., Fan, P., Yang, L., and Liu, X. (2023). Role of leptin in the pathophysiology of preeclampsia. *Placenta* 142, 128–134. doi:10.1016/j.placenta.2023.09.005

Zhang, L., Bi, S., Liang, Y., Huang, L., Li, Y., Huang, M., et al. (2022). Integrated metabolomic and lipidomic analysis in the placenta of preeclampsia. *Front. Physiol.* 13, 807583. doi:10.3389/fphys.2022.807583

frontiers | Frontiers in Cell and Developmental Biology

TYPE Original Research
PUBLISHED 29 August 2025
DOI 10.3389/fcell.2025.1608647

OPEN ACCESS

EDITED BY
Subhradip Karmakar,
All India Institute of Medical Sciences, India

REVIEWED BY
Ananya Datta Mitra,
UC Davis Health, United States
Narasaiah Kovuru,
University of Pennsylvania, United States

*CORRESPONDENCE
Feng Guo,
fguo@sj-hospital.org
Xiuhua Yang,
xhyang@cmu.edu.cn

RECEIVED 09 April 2025
ACCEPTED 04 August 2025
PUBLISHED 29 August 2025

CITATION
Ibeh CO-A, Guo F and Yang X (2025) Maternal and fetal outcomes in 151 cases of thrombocytopenia in pregnancy.
Front. Cell Dev. Biol. 13:1608647.
doi: 10.3389/fcell.2025.1608647

Maternal and fetal outcomes in 151 cases of thrombocytopenia in pregnancy

Chinwe Oluchi-Amaka Ibeh[1], Feng Guo[2]* and Xiuhua Yang[1]*

[1]Department of Obstetrics, The First Hospital of China Medical University, Shenyang, China,
[2]Department of Emergency Medicine, Shengjing Hospital of China Medical University, Shenyang, China

Introduction: Thrombocytopenia during pregnancy is one of the important causes of maternal and perinatal mortality. This study aims to retrospectively analyze the clinical data of 151 pregnant patients with thrombocytopenia, in order to help obstetricians better understand the etiology, related risk factors and maternal and fetal outcomes of this disease.

Methods: A total of 151 cases of pregnant women with thrombocytopenia were collected. According to the cause of thrombocytopenia, patients were divided into gestational thrombocytopenia (GT) group, hypertensive disorders in pregnancy (HDP) group, immune thrombocytopenia (ITP) group and the other group. According to the degree of thrombocytopenia, patients were divided into mild group, moderate group and severe group. According to different grouping criteria, the clinical characteristics, delivery outcomes and delivery modes, maternal treatments during pregnancy, maternal laboratory indexes, and neonatal birth conditions were compared.

Results: Among the 151 patients, the GT group had the largest proportion. Moreover, the ITP group had a higher proportion of skin and mucous membrane bleeding during pregnancy, the smallest gestational age at first diagnosis and the lowest platelet count at first diagnosis. The treatment effect of glucocorticoids alone in the ITP group was not good. The HDP group had a higher neonatal intensive care unit (NICU) transfer rate and the lowest birth weight in newborns. In terms of severity, majority of the patients were in the mild group. The parameters of thromboelastography (TEG) were related to the pre-delivery platelet count of patients in the moderate and severe groups, but not in the mild group.

Conclusion: In conclusion, ITP is associated with more severe thrombocytopenia and bleeding, often presenting in the early stage of pregnancy. In the treatment of ITP, the combined use of glucocorticoids and platelet transfusion is recommended. TEG parameter analysis suggests that patients in the moderate and severe groups may have changes in the blood coagulation and fibrinolysis systems. More attention should be paid to the monitoring of the newborns delivered by HDP patients.

KEYWORDS

pregnancy, thrombocytopenia, hypertensive disorders in pregnancy, immune thrombocytopenia, postpartum hemorrhage

1 Introduction

Thrombocytopenia during pregnancy is a relatively common disease in the gestational period, involving about 8%–10% of low-risk pregnant women (Townsley, 2013). Generally, thrombocytopenia is considered to be the case where the platelet count is less than 150 × 10^9/L (Kam et al., 2004; Smock and Perkins, 2014; Veneri et al., 2009). However, only platelet counts below 100 × 10^9/L are considered clinical significant (Smock and Perkins, 2014; Veneri et al., 2009). Thrombocytopenia is caused by increased destruction or reduced production of platelets (Kam et al., 2004). During pregnancy, the physiological system of pregnant women undergoes changes that alters the concentration of plasma coagulation factors and blood system components (Bar et al., 2025; Wang et al., 2021). Some secondary physiological changes specific to pregnancy, such as increased blood volume, abnormal platelet activation and increased platelet clearance rate, may eventually cause thrombocytopenia (Townsley, 2013). Patients with thrombocytopenia during pregnancy may show bleeding symptoms during physical examination such as bruising, petechiae, purpura, oral mucosal blood blisters and conjunctival hemorrhages (Fogerty and Kuter, 2024).

According to the severity of the disease, some scholars believe that platelet count of 100–150 × 10^9/L is mild thrombocytopenia, 50–100 × 10^9/L is moderate thrombocytopenia, and less than 50 × 10^9/L is severe thrombocytopenia (Kam et al., 2004). In severe thrombocytopenia, life-threatening bleeding may occur, which is manifested by pulmonary bleeding, gastrointestinal bleeding and rare intracranial hemorrhage (Connors and Fein, 2023; Mithoowani et al., 2020). Thrombocytopenia in pregnancy is also related to the occurrence of premature birth (Parnas et al., 2006). Patients with platelet count <20 × 10^9/L have the risk of spontaneous intracranial hemorrhage, postpartum hemorrhage and placental abruption. In severe cases, disseminated intravascular coagulation (DIC) may occur and cause serious impact on the health of mothers and fetuses (Kelton, 2002).

The etiology of thrombocytopenia in pregnancy can be classified according to "pregnancy specific" etiology and "general etiology." The etiology of thrombocytopenia in pregnancy may include gestational thrombocytopenia (GT), pre-eclampsia (PE) and hypertensive disorders in pregnancy (HDP) associated thrombocytopenia caused by HELLP syndrome (hemolysis, elevated liver enzymes and thrombocytopenia), immune thrombocytopenia (ITP), hereditary thrombocytopenia Type 2B von Willebrand disease, drug-induced thrombocytopenia, infection, liver cirrhosis, splenomegaly, bone marrow diseases (such as aplastic anemia, myelodysplastic syndrome, leukemia, and lymphoma), paroxysmal nocturnal hemoglobinuria, complement mediated thrombotic microangiopathy, thrombotic thrombocytopenic purpura (TTP), and autoimmune diseases (such as lupus erythematosus, antiphospholipid syndrome (APS)) (Pishko and Marshall, 2022).

The most common cause of thrombocytopenia in pregnancy is GT (Yan et al., 2016; Park, 2022; Fogerty, 2018), accounting for about 75% of all thrombocytopenia in pregnancies (Parnas et al., 2006; Fogerty, 2018; Yuce et al., 2014) and 5%–11% of all pregnancies (Cines and Levine, 2017a). Its symptoms are usually relatively mild, rarely posing a serious threat to the safety of the mother and fetus (Townsley, 2013; Fogerty and Kuter, 2024; Rottenstreich et al., 2018), and often occurring in the third trimester of pregnancy (Fogerty and Kuter, 2024; Cines and Levine, 2017b; Reese et al., 2018). It is worth noting that few cases of moderate to severe thrombocytopenia could be caused by GT, therefore, before making a diagnosis of GT in these cases, a comprehensive clinical evaluation should be conducted, and other potential causes should be examined (Cines and Levine, 2017a). Mild thrombocytopenia, especially when the platelet count ≥70 × 10^9/L, strongly suggests the diagnosis of GT. For GT patients with platelet count <80 × 10^9/L, platelet count examination should be performed on the first and fourth day after birth (Gernsheimer et al., 2013).

HDP caused by PE and HELLP syndrome is also a common cause of thrombocytopenia in the second and third trimester of pregnancy, accounting for about 21% (Kam et al., 2004; Parnas et al., 2006; Yuce et al., 2014). Platelet <100 × 10^9/L is one of the diagnostic criteria for severe PE (Mol et al., 2016). HELLP syndrome is a slightly different PE, characterized by more severe thrombocytopenia (Cines and Levine, 2017b) and higher maternal and neonatal mortality (Young et al., 2010). Patients with HELLP syndrome have a higher rate of cesarean section, and may also have placental abruption and DIC, which may require blood transfusion, and prolong the length of hospital stay (Young et al., 2010). When patients with hypertensive disorders in pregnancy have progressive thrombocytopenia, the diagnosis of HELLP syndrome should be considered. DIC occurs in 20% of HELLP syndrome, which can lead to uncontrollable massive bleeding (Cines and Levine, 2017b; Brown et al., 2018; Fitzpatrick et al., 2014; Thomas et al., 2016).

ITP is another cause of thrombocytopenia in pregnancy, which can occur in any of the different trimesters of pregnancy (Fogerty and Kuter, 2024; Pishko and Marshall, 2022; Park, 2022) and even postpartum (Fogerty and Kuter, 2024), accounting for 3%–10% of thrombocytopenia during pregnancy (Fogerty and Kuter, 2024; Parnas et al., 2006; Yuce et al., 2014). The platelet count of ITP is significantly lower than that of GT. However, there is still no gold standard method to distinguish GT and ITP (Fogerty and Kuter, 2024; Cines and Levine, 2017a). If the platelet count drops below 80 × 10^9/L during pregnancy, the possibility of ITP should be considered (Townsley, 2013; Cines and Levine, 2017b). A guideline on ITP points out that if the platelet count is 20–30 × 10^9/L and there is no active bleeding, most pregnancies are safe, and it is safer to have the platelet count ≥50 × 10^9/L during delivery (Provan et al., 2019).

TTP is a rare life-threatening hematological disease (Thomas et al., 2016; Joly et al., 2017), characterized by widespread blood vessel clotting and bleeding (Xu et al., 2024), microangiopathic hemolytic anemia, severe thrombocytopenia, and organ ischemia linked to disseminated microvascular platelet rich-thrombi (Joly et al., 2017). It presents in any trimester or postpartum (Fogerty and Kuter, 2024; Martin et al., 2008) and in about 5%–25% of TTP cases, pregnancy may be a pathogenic factor (Gerth et al., 2009). The symptoms of TTP are like those of thrombocytopenia associated with severe PE and HELLP syndrome and hemolytic uremic syndrome, so it needs to be differentiated (Xu et al., 2024). When pregnant women with thrombotic micro angiopathies do not meet the diagnostic criteria for severe PE or HELLP syndrome, if the platelet count drops below 20 × 10^9/L, or if neurological symptoms occur, such as numbness, aphasia, etc., the possibility of TTP should be considered (Martin et al., 2008; George et al., 2015). In late diagnosis and untreated TTP, the mortality rate can go as

high as 90% (Xu et al., 2024; Zhou et al., 2017) and microvascular thrombosis leading to fetal growth restriction and/or fetal death, may develop due to impaired placental circulation (Ferrari and Peyvandi, 2020). If the maternal platelet count does not recover to more than 100×10^9/L within 48–72 h after delivery, and the clinical signs and symptoms are not relieved, then the diagnosis of TTP should be considered (George et al., 2015).

APS is an autoimmune disease characterized by arterial or venous thrombosis and/or pregnancy complications (Jin et al., 2022). Thrombocytopenia is a common blood system manifestation in patients with APS, with an incidence of 16%–53% (Cervera et al., 2011), and its mechanism may be due to platelet consumption and/or destruction mediated by antiphospholipid antibodies (Vreede et al., 2019). APS is associated with the increased incidence of unexplained recurrent abortion, fetal growth restriction, premature birth, stillbirth, neonatal death, early-onset PE and severe PE (Park, 2022; De Carolis et al., 2018; Liu and Sun, 2019).

Therefore, thrombocytopenia in pregnancy is an important reason for the increase of maternal and perinatal mortality (Huang et al., 2020). Maternal thrombocytopenia may cause severe postpartum hemorrhage and even require hysterectomy. For pregnant women whose platelet count is lower than 50×10^9/L, these patients may occasionally require intravenous immunoglobulin (IVIg) to maintain safe platelet counts throughout pregnancy or especially in preparation for delivery when a rapid platelet increase is required, as platelet count greater than 50×10^9/L is preferred for delivery (Provan et al., 2019). The newborns of pregnant women with thrombocytopenia may have adverse consequences such as premature delivery, neonatal thrombocytopenia (Guillet et al., 2023; van der Lugt et al., 2013), neonatal asphyxia (McCrae, 2010; Wang et al., 2017) and intracranial hemorrhage (Cines and Levine, 2017b; Li et al., 2022). Some independent predictors of thrombocytopenia include poor economic conditions, elderly mothers, alcohol consumption and human immunodeficiency virus (HIV) infection (Haile et al., 2022).

In this study, we retrospectively analyzed the clinical data of 151 cases of pregnancy with thrombocytopenia. According to the etiological classification and disease severity, patients were divided into different groups, and the clinical characteristics, delivery outcomes and delivery modes, maternal treatments during pregnancy, maternal laboratory indexes, and neonatal birth conditions of each group were compared. The objective of this manuscript is to help obstetricians better understand the etiology, related risk factors and maternal and fetal outcomes of this disease and improve the prognosis by increasing related monitoring.

2 Materials and methods

2.1 Study population

A total of 151 pregnant women diagnosed with thrombocytopenia aged 18–40 years old, who gave birth in our obstetric department from December 2010 to July 2024 were collected. Two or more occurrences of platelet count less than 100×10^9/L during pregnancy are considered thrombocytopenia. Patients with twin or triple pregnancies, thrombocytopenia caused by medication or viral infections, and congenital coagulation disorders were excluded. Our study was approved by the Medical Science Research Ethics Committee of the First Hospital of China Medical University (Approval No. 2021-108).

According to the cause of thrombocytopenia, patients were divided into gestational thrombocytopenia (GT) group, hypertensive disorders in pregnancy (HDP) group, immune thrombocytopenia (ITP) group and the other group. The GT group includes cases where thrombocytopenia first occurs during pregnancy without history of thrombocytopenia before pregnancy, and platelet counts typically recover spontaneously after delivery, usually without causing significant maternal or fetal complications. When diagnosing GT, it is necessary to exclude other diseases that cause thrombocytopenia. The HDP group comprises pregnant women with thrombocytopenia associated with gestational hypertension, particularly those with PE or HELLP syndrome. The ITP group involves pregnant women with evident bleeding symptoms, such as bleeding points and bruising on the skin and mucous membranes, or symptoms of visceral bleeding, with a significant decrease in platelet counts. Bone marrow examination in ITP cases shows normal or increased megakaryocytes with maturation disorders. The other group includes thrombocytopenia during pregnancy caused by other conditions, such as TTP, aplastic anemia, systemic lupus erythematosus, APS, Sjögren's syndrome, undifferentiated connective tissue disease, myelodysplastic syndrome, or hereditary thrombocytopenia.

According to the degree of thrombocytopenia (Veneri et al., 2009), patients were divided into mild group (platelet: $50–100 \times 10^9$/L), moderate group (platelet: $30–50 \times 10^9$/L) and severe group (platelet: $<30 \times 10^9$/L).

2.2 Observed indicators

Clinical records were reviewed to collect the following information: the clinical characteristics of each group of patients (age, skin and mucosa bleeding during pregnancy, gestational age at first diagnosis, platelet count at first diagnosis, lowest platelet count during pregnancy, and platelet count on the third day after delivery), whether the patient was transferred to intensive care unit (ICU), length of hospital stay, gestational age at delivery, and the occurrence of postpartum hemorrhage), and delivery mode. Postpartum hemorrhage was defined as the loss of 500 mL or more of blood with a vaginal delivery or 1,000 mL or more with a caesarean section. Maternal treatments for thrombocytopenia during pregnancy included the use of glucocorticoids, platelet transfusions, or IVIg. The criteria for determining the effectiveness of treatment are platelet count $\geq 5 \times 10^9$/L within 24–96 h after treatment, otherwise it is considered ineffective (Provan et al., 2019; Bauer et al., 2021; Estcourt et al., 2017).

We collected the results of blood routine test within 1 week before delivery and on the third day after delivery at our hospital. Blood routine indicators included platelets, hemoglobin (Hb), platelet distribution width (PDW), mean platelet volume (MPV), mean platelet count (PCT), and platelet large cell ratio (P-LCR). Coagulation function indicators included prothrombin time (PT), activated partial thromboplastin time (APTT), D-dimer,

international normalized ratio (INR), coagulation time (TT), and plasma fibrinogen (Fg). Thromboelastography (TEG) parameters included reaction time (R), kinetics (K), rate of blood clot formation (Angle), maximum amplitude (MA), clot lysis at 30 min (LY30), estimated percent lysis (EPL), and coagulation index (CI). Immune indicators included anti-nuclear antibody (ANA), anti-double stranded DNA antibody (dsDNA Ab), anti-SSA antibody (SSA Ab), anti-SSB antibody (SSB Ab), anti-Pm Scl antibody (Pm-Scl Ab), anti-cardiolipin antibody (ACA Ab), and standardized ratio of lupus anticoagulant dRVVT.

Information collected on the birth status of newborns included presence of thrombocytopenia at birth, preterm birth rate, neonatal asphyxia rate, admission to neonatal intensive care unit (NICU), low birth weight infants, 1-min and 5-min Apgar scores, and birth weight.

2.3 Statistical analysis

We used IBM SPSS Statistics v27.0 software for statistical analysis. Normal distribution continuous data are represented as mean ± SD. For multiple sample means, one-way analysis of variance was used. If there were significant inter group differences in the results, Tukey's test was used for pairwise comparison; for the mean of two paired samples, paired *t*-test was used. If the data did not follow a normal distribution, we used the median (interquartile range) to represent it. For comparing multiple sets of samples, we used Kruskal Wallis test. If there was a significant difference in the results, we used Mann Whitney U test for pairwise comparison; for the comparison of two paired samples, Wilcoxon signed rank test was used. The categorical data is represented as (%) and analyzed using chi square test. For categorical data that did not meet the chi square test hypothesis, Fisher exact test was used. To correct type I errors in pairwise comparisons, Bonferroni correction was used. We used Pearson correlation analysis to calculate the relationship between TEG parameters and prenatal platelets. $P < 0.05$ was considered statistically significant.

3 Results

3.1 Distribution of causes and severity of thrombocytopenia in pregnancy

According to the etiology of thrombocytopenia, a total of 67 cases (44.40%) were in the GT group, 24 cases (15.90%) in the HDP group, 44 cases (29.10%) in the ITP group, and 16 cases (10.60%) in the other group (Figure 1). According to the severity of thrombocytopenia, there were 107 cases (70.90%) in the mild group, 23 cases (15.20%) in the moderate group, and 21 cases (13.90%) in the severe group (Figure 2).

3.2 Comparison of clinical characteristics

Grouping according to the etiology of thrombocytopenia, pairwise comparisons between groups showed that patients in the

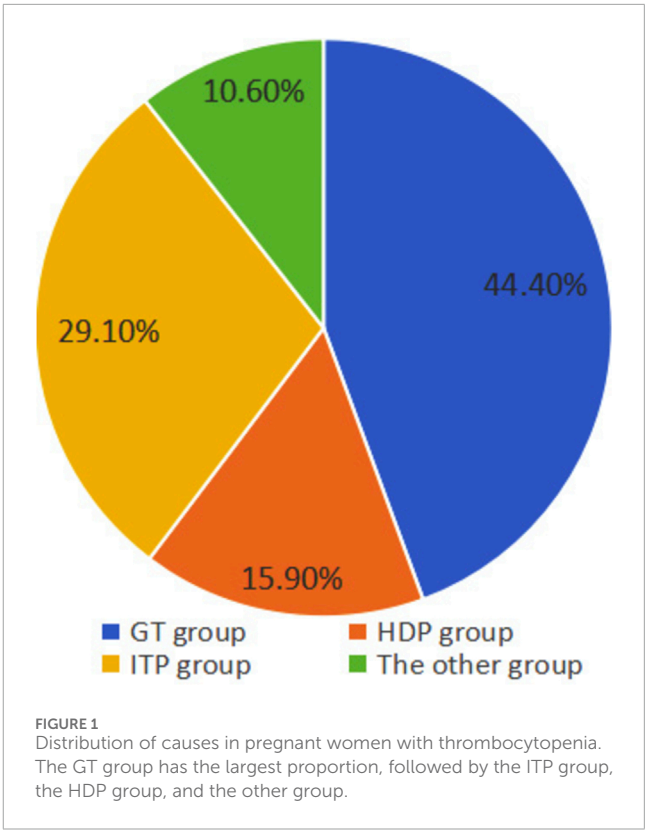

FIGURE 1
Distribution of causes in pregnant women with thrombocytopenia. The GT group has the largest proportion, followed by the ITP group, the HDP group, and the other group.

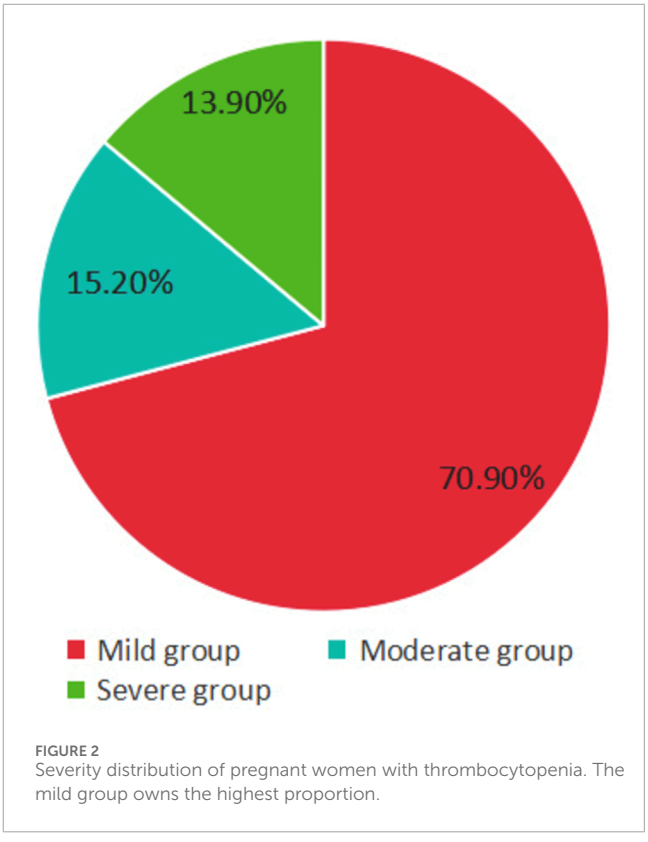

FIGURE 2
Severity distribution of pregnant women with thrombocytopenia. The mild group owns the highest proportion.

10.3389/fcell.2025.1608647

TABLE 1 Comparison of clinical characteristics of patients.

Groups	Age (years)	Skin and mucosa bleeding during pregnancy (%)	Gestational age at first diagnosis (week)	Platelet count at first diagnosis ($\times10^9$/L)	Lowest platelet count during pregnancy ($\times10^9$/L)	Platelet count on the third day after delivery ($\times10^9$/L)
Grouping according to etiology						
GT group (n = 67)	30.00 (27.00–34.00)	12 (17.91)	36.00 (31.00–39.00)	88.00 (80.00–93.50)	83.00 (76.50–89.50)	108.00 (91.00–121.00)
HDP group (n = 24)	29.00 (27.00–32.00)	4 (16.67)	35.00 (33.50–37.00)	78.50 (67.00–89.50)[1]	76.50 (57.50–81.00)[1]	108.00 (96.50–123.50)
ITP group (n = 44)	28.00 (26.00–31.00)[1]	19 (43.18)[1]	24.00 (12.00–34.00)[1,2]	53.00 (35.00–74.00)[1,2]	36.00 (22.50–50.00)[1,2]	66.00 (46.50–96.50)[1,2]
The other group (n = 16)	30.50 (28.50–33.00)[3]	2 (12.50)	24.00 (12.00–34.00)[1]	86.00 (50.50–92.50)[1,3]	56.50 (34.00–88.50)[3]	86.00 (61.00–106.00)[1]
H/χ^2	10.89	11.92	35.05	57.32	76.11	30.00
P	0.012*	0.008*	<0.001*	<0.001*	<0.001*	<0.001*
Grouping according to severity						
Mild group (n = 107)	30.00 (28.00–34.00)	16 (14.95)	36.00 (31.00–39.00)	86.00 (76.00–93.00)	-	106.00 (91.00–119.00)
Moderate group (n = 23)	27.00 (25.50–30.00)[4]	9 (39.13)[4]	16.00 (12.00–28.00)[4]	59.00 (46.00–76.00)[4]	-	63.00 (51.00–82.00)[4]
Severe group (n = 21)	29.00 (27.00–29.00)	12 (57.14)[4]	24.00 (16.00–32.00)[4]	30.00 (21.00–41.50)[4,5]	-	47.00 (39.00–107.00)[4]
H/χ^2	9.66	20.03	37.50	58.50	-	33.66
P	0.008*	<0.001*	<0.001*	<0.001*	-	<0.001*

*$P < 0.05$.
[1]Compared with the GT, group.
[2]Compared with the HDP, group.
[3]Compared with the ITP, group.
[4]Compared with the mild group.
[5]Compared with the moderate group.

ITP group were significantly younger than those in the GT group and the other group. The ITP group had a higher proportion of skin and mucosal bleeding during pregnancy (43.18%), the smallest gestational age at the first diagnosis, the lowest platelet count at the time of the first diagnosis, during pregnancy and on the third day postpartum. The lowest platelet count during pregnancy was ranked from low to high: ITP group < the other group < HDP group < GT group, and the difference was statistically significant ($P < 0.05$) (Table 1).

Grouping according to the severity of thrombocytopenia, pairwise comparisons between groups showed that the age of the mild group was significantly higher than that of the moderate group; the mild group had the highest platelet count at the first diagnosis of gestational age, and the highest platelet count on the third day after delivery, with statistical significance ($P < 0.05$) (Table 1).

3.3 Comparison of delivery outcomes and delivery methods

According to the etiological grouping, there was no statistically significant difference in the ICU transfer rate and postpartum hemorrhage between the groups. However, there were significant differences in the length of hospital stay, gestational age, and delivery mode. The pairwise comparison showed that the length of hospital stay in the GT group was significantly lower than those in the HDP and ITP groups. Patients in the GT group had the largest gestational age during delivery, and the proportion of cesarean section in the GT group was significantly higher than that in the HDP group ($P < 0.05$) (Table 2).

According to the severity of thrombocytopenia, there were no statistically significant differences in the ICU transfer rate, postpartum hemorrhage, and delivery mode among the groups. Comparison between groups showed that the hospitalization days

10.3389/fcell.2025.1608647

TABLE 2 Comparison of delivery outcomes and delivery modes of pregnant women.

Groups	ICU transfer (%)	Hospital length of stay (days)	Gestational age at delivery (week)	Postpartum hemorrhage (%)	Delivery mode (%)	
					Vaginal delivery	Cesarean section
Grouping according to etiology						
GT group (n = 67)	0 (0.00)	5.00 (4.00–6.00)	39.00 (39.00–40.00)	2 (3.00)	18 (26.90)	49 (73.10)
HDP group (n = 24)	2 (8.30)	7.00 (5.00–7.50)[1]	37.00 (35.00–38.50)[1]	1 (4.20)	0 (0.00)[1]	24 (100.00)[1]
ITP group (n = 44)	1 (2.30)	7.00 (4.50–8.00)[1]	38.00 (37.00–39.00)[1]	1 (2.30)	5 (11.40)	39 (88.60)
The other group (n = 16)	0 (0.00)	5.00 (4.00–8.50)	37.50 (37.00–39.00)[1]	0 (0.00)	1 (6.30)	15 (93.80)
H/Fisher	5.05	14.35	36.44	0.91	12.36	
P	0.063	0.002*	<0.001*	1.000	0.006*	
Grouping according to severity						
Mild group (n = 107)	1 (0.90)	5.00 (4.0–6.0)	39.00 (38.00–40.00)	3 (2.80)	21 (19.60)	86 (80.40)
Moderate group (n = 23)	1 (4.30)	7.00 (4.50–8.00)	37.00 (37.00–39.00)[2]	0 (0.00)	3 (13.00)	20 (87.00)
Severe group (n = 21)	1 (4.80)	7.00 (6.00–10.0)[2]	37.00 (35.00–39.00)[2]	1 (4.80)	0 (0.00)	21 (100.00)
H/Fisher	3.14	14.80	19.45	1.02	5.66	
P	0.204	<0.001*	<0.001*	0.533	0.055	

*$P < 0.05$.
[1]Compared with the GT, group.
[2]Compared with the mild group.

of patients in the mild group were significantly lower than those in the severe group, and the mild group had the largest gestational age at delivery, with statistical significance ($P < 0.05$) (Table 2).

3.4 Comparison of the effectiveness of diverse treatments of thrombocytopenia

Among the 151 study subjects, 140 pregnant women received thrombocytopenia related treatments during pregnancy. According to the etiology, only patients in the ITP group were treated with IVIg. After treatments with glucocorticoids and glucocorticoids plus platelet transfusion, both the GT group and the HDP group patients showed a significant increase in platelet counts, indicating a significant therapeutic effect. The ITP group also achieved good therapeutic effects after treatments with glucocorticoids and platelet transfusion, and the difference was statistically significant ($P < 0.05$). However, the treatment of ITP with glucocorticoids alone was not effective, as shown in Table 3.

According to the severity of thrombocytopenia, only patients in the severe group were treated with IVIg. In comparison among the groups, the mild group received significant effects of glucocorticoid or glucocorticoid plus platelet transfusion therapy. After treatments with glucocorticoids plus platelet transfusion, the platelet count significantly increased in the moderate and severe groups, and the therapeutic effect was statistically significant ($P < 0.05$). However, for patients in the moderate and severe groups, the use of glucocorticoids alone or platelet transfusion alone did not achieve satisfactory therapeutic effects (Table 3).

3.5 Comparison of laboratory indexes

3.5.1 Comparison of blood routine and coagulation function

Grouped by etiology, postpartum platelet counts and Fg levels in each group were significantly higher than those before delivery. In the ITP group and the other group, postpartum PT and INR values were significantly higher than their prenatal values. For the GT group and the ITP group, APTT values after delivery were significantly higher than those before delivery. The postpartum TT values in the other group were significantly lower compared to the prenatal numbers ($P < 0.05$). In addition, postpartum Hb concentrations in the GT group, ITP group, and the other group were

10.3389/fcell.2025.1608647

TABLE 3 Comparison of clinical effects of different treatments.

Groups	Number of effective cases (%)	Number of non-effective cases (%)	Platelet count before treatment ($\times10^9$/L)	Platelet count after treatment ($\times10^9$/L)	*t*	*P*
Grouping according to etiology						
GT group (*n* = 61)						
Glucocorticoids (*n* = 54)	36 (66.70)	18 (33.30)	89.33 ± 16.68	103.51 ± 20.54	5.60	<0.001*
Glucocorticoids + platelet transfusion (*n* = 7)	7 (100.00)	0 (0.00)	80.17 ± 9.33	107.50 ± 17.59	4.15	0.009*
Total	43	18				
HDP group (*n* = 23)						
Glucocorticoids (*n* = 13)	12 (72.30)	1 (7.70)	81.00 (77.00–94.00)	109.00 (94.50–121.00)	2.76[a]	0.006*
Platelet transfusion (*n* = 1)	1 (100.00)	0 (0.00)	-	-	-	-
Glucocorticoids + platelet transfusion (*n* = 9)	7 (79.80)	2 (22.80)	58.00 ± 29.00	79.13 ± 44.78	2.41	0.047*
Total	20	3				
ITP group (*n* = 42)						
Glucocorticoids (*n* = 14)	8 (57.10)	6 (42.90)	62.50 (57.00–91.00)	70.00 (57.00–92.00)	1.08[a]	0.279
IVIg (*n* = 1)	1 (100.00)	0 (0.00)	-	-	-	-
Platelet transfusion (*n* = 7)	6 (85.70)	1 (14.30)	375.43 ± 10.50	51.71 ± 11.66	2.06	0.086
Glucocorticoids + platelet transfusion (*n* = 20)	17 (85.00)	3 (15.00)	35.50 (21.00–56.50)	65.00 (45.50–95.00)	3.87[a]	<0.001*
Total	32	10				
The other group (*n* = 14)						
Glucocorticoids (*n* = 10)	4 (40.00)	6 (60.00)	78.30 ± 23.74	81.20 ± 17.94	0.43	0.678
Platelet transfusion (*n* = 1)	1 (100.00)	0 (0.00)	-	-	-	0.288
Glucocorticoids + platelet transfusion (*n* = 3)	3 (100.00)	0 (0.00)	43.00 (37.00–57.50)	112.00 (83.50–16.50)	1.60[a]	0.109
Total	8	6				
Grouping according to severity						
Mild group (*n* = 98)						
Glucocorticoids (*n* = 79)	52 (65.80)	27 (34.20)	88.01 ± 16.87	101.89 ± 23.44	5.98	<0.001*
Platelet transfusion (*n* = 1)	1 (100.00)	0 (0.00)	-	-	-	-
Glucocorticoids + platelet transfusion (*n* = 18)	17 (94.40)	1 (5.60)	75.00 (66.00–82.00)	103.00 (93.00–114.00)	3.68[a]	<0.001*
Total	70	28				
Moderate group (*n* = 21)						
Glucocorticoids (*n* = 9)	5 (55.60)	4 (44.40)	61.00 ± 21.47	66.78 ± 17.33	0.77	0.461

(Continued on the following page)

TABLE 3 (*Continued*) Comparison of clinical effects of different treatments.

Groups	Number of effective cases (%)	Number of non-effective cases (%)	Platelet count before treatment ($\times 10^9$/L)	Platelet count after treatment ($\times 10^9$/L)	*t*	*P*
Platelet transfusion ($n = 4$)	4 (100.00)	0 (0.00)	37.00 (33.00–42.50)	51.00 (47.00–58.50)	1.83[a]	0.068
Glucocorticoids + platelet transfusion ($n = 8$)	7 (87.50)	1 (12.50)	42.50 (39.00–53.00)	67.00 (53.50–87.50)	2.52[a]	0.012*
Total	16	5				
Severe group ($n = 21$)						
Glucocorticoids ($n = 3$)	3 (100.00)	0 (0.00)	47.00 (43.50–72.50)	135.00 (97.00–135.50)	1.60[a]	0.109
IVIg ($n = 1$)	1 (100.00)	0 (0.00)	-	-		-
Platelet transfusion ($n = 4$)	3 (75.00)	1 (25.00)	30.00 (24.00–39.50)	40.50 (37.00–59.5)	1.10[a]	0.273
Glucocorticoids + platelet transfusion ($n = 13$)	10 (76.90)	3 (23.10)	21.00 (19.00–24.00)	46.00 (39.00–67.00)	2.97[a]	0.003*
Total	17	4				

*$P < 0.05$.
[a]Nonparametric Wilcoxon signed rank test was used.

significantly lower than those before delivery. Postpartum PDW and MPV counts were significantly lower than the prenatal counts before delivery among the three groups. Postpartum PCT counts in the GT group, HDP group and ITP group were significantly higher than the prenatal counts. In the GT group and ITP group, postpartum P-LCR values were significantly lower than the prenatal values (Table 4).

According to the severity of thrombocytopenia, postpartum platelet and PCT counts in each group were significantly higher than the prenatal counts. The postpartum PT value in the severe group was significantly higher compared to the prenatal value. In the mild and moderate groups, APTT values after delivery were significantly higher than those of before delivery. In addition, the postpartum D-dimer value of the mild group was significantly lower than that of the prenatal value. Postpartum Fg levels in the mild group and the severe group were significantly higher compared to the prenatal levels. The postpartum Hb counts and P-LCR values in the mild group and the moderate group were significantly lower than those before delivery. The postpartum PDW and MPV counts of each group were significantly lower than the prenatal counts ($P < 0.05$) (Table 4).

3.5.2 Correlation between platelet count and TEG parameters

We collected platelet count and TEG parameters which were both tested in our hospital within 1 week before delivery. R value, angle, Ma value and CI value were positively correlated with platelet count in the other group, while K value was negatively correlated with platelet count in the other group. There was no correlation between platelet count and TEG parameters in the GT group, HDP group and ITP group (Table 5).

Grouped by severity, R value and K value were negatively correlated with the platelet count in the moderate and severe groups, while angle, Ma value and CI value were positively correlated with the platelet count in the moderate and severe groups. TEG parameters were not correlated with the platelet count in the mild group (Table 5).

3.5.3 Comparison of immune indexes

There was no significant difference in the immune indexes of ANA, dsDNA Ab, SSA Ab, SSB Ab, Pm-Scl Ab, ACA Ab and dRVVT among all groups, regardless of grouping based on the etiology or the severity of thrombocytopenia (Table 6).

3.6 Comparison of newborn birth conditions

Grouping based on the etiology of thrombocytopenia, there were no significant differences in the rate of thrombocytopenia at birth, the rate of premature birth, the rate of asphyxia, and the Apgar scores at 1 min and 5 min among the groups. In pairwise comparison, the NICU transfer rate and the incidence of low birth weight infants in the HDP group were significantly higher than those in the GT group, and the neonatal birth weight in the HDP group was significantly lower than those in the GT group and the ITP group ($P < 0.05$) (Table 7).

Grouping according to the severity of thrombocytopenia, there were no significant differences in the rates of neonatal thrombocytopenia, premature birth, asphyxia, NICU transfer, and 5-min Apgar score among the groups. The 1-min Apgar score of newborns in the mild group was significantly higher than that in the moderate group, and the birth weight of newborns in the severe group was significantly lower than that in the mild group (Table 7).

10.3389/fcell.2025.1608647

TABLE 4 Comparison of blood routine and coagulation function in the first week before delivery and the third day after delivery.

Grouping according to etiology		
Groups	Prenatal count	Postnatal count
	Platelet	
GT group	89.00 (80.00–97.00)	108.00 (91.00–121.00)[1]
HDP group	80.00 (66.00–87.50)	108.00 (96.50–123.50)[1]
ITP group	46.50 (31.00–64.00)	66.00 (46.50–96.50)[1]
The other group	69.00 (44.50–90.00)	86.00 (61.00–106.00)[1]
P	<0.001*	<0.001*
Hb		
GT group	119.00 (111.00–126.50)	106.52 ± 18.48[1]
HDP group	114.50 (107.00–123.00)	104.00 ± 20.43
ITP group	107.00 (95.00–118.50)	98.23 ± 17.32[1]
The other group	120.00 (107.50–128.50)	104.13 ± 14.64[1]
P	0.006*	0.138
PDW		
GT group	17.06 ± 3.73	15.30 (12.70–18.70)[1]
HDP group	17.12 ± 3.77	14.95 (13.30–17.20)[1]
ITP group	16.00 ± 4.00	13.50 (11.60–14.90)[1]
The other group	14.86 ± 2.06	14.00 (11.60–15.65)[1]
P	0.16	0.042*
MPV		
GT group	12.35 ± 1.20	11.90 (11.10–13.05)[1]
HDP group	12.41 ± 1.04	11.80 (10.90–12.50)[1]
ITP group	12.20 ± 1.48	11.30 (10.60–12.00)[1]
The other group	11.94 ± 0.93	11.30 (10.65–11.80)[1]
P	0.679	0.041*
PCT		
GT group	0.10 (0.10–0.12)	0.10 (0.10–0.15)[1]
HDP group	0.10 (0.08–0.10)	0.10 (0.10–0.14)[1]
ITP group	0.06 (0.00–0.10)	0.10 (0.08–0.10)[1]
The other group	0.09 (0.07–0.10)	0.10 (0.10–0.10)
P	<0.001*	<0.001*
P-LCR		
GT group	41.20 (33.10–50.65)	39.30 (33.15–46.50)[1]

(Continued on the following page)

TABLE 4 (*Continued*) Comparison of blood routine and coagulation function in the first week before delivery and the third day after delivery.

Grouping according to etiology		
Groups	Prenatal count	Postnatal count
	Platelet	
HDP group	39.65 (28.75–49.40)	40.20 (31.80–41.80)
ITP group	38.50 (24.90–47.50)	34.00 (27.10–39.20)[1]
The other group	37.70 (32.40–43.55)	34.95 (29.20–39.20)
P	0.374	0.025*
PT		
GT group	12.40 (12.00–12.90)	12.65 (12.10–12.90)
HDP group	12.10 (11.70–12.60)	12.30 (11.40–12.50)
ITP group	12.50 (12.10–12.90)	12.90 (12.30–13.20)[1]
The other group	11.95 (11.70–12.20)	12.50 (11.95–12.85)[1]
P	0.294	0.012*
APTT		
GT group	32.68 ± 2.34	33.64 ± 3.52[1]
HDP group	33.58 ± 4.05	33.28 ± 5.33
ITP group	32.66 ± 2.76	34.22 ± 3.48[1]
The other group	32.22 ± 3.29	33.25 ± 4.08
P	0.475	0.837
D-dimer		
GT group	1.44 (1.17–2.13)	1.36 (1.00–1.82)
HDP group	1.68 (0.89–2.55)	1.42 (0.86–2.20)
ITP group	1.85 (1.07–2.55)	1.69 (1.21–2.45)
The other group	1.34 (0.95–1.87)	1.29 (0.96–1.75)
P	0.36	0.125
INR		
GT group	1.00 (0.90–1.00)	0.97 (0.93–1.00)
HDP group	1.00 (0.94–1.00)	1.00 (0.96–1.00)
ITP group	1.00 (0.96–1.00)	1.00 (1.00–1.00)[1]
The other group	0.99 (0.89–1.00)	1.00 (0.93–1.00)[1]
P	0.182	0.058
TT		
GT group	15.50 (14.75–16.00)	15.40 (15.00–16.00)
HDP group	16.40 (15.85–17.20)	15.95 (15.55–16.50)

(Continued on the following page)

TABLE 4 (*Continued*) Comparison of blood routine and coagulation function in the first week before delivery and the third day after delivery.

Grouping according to etiology		
Groups	Prenatal count	Postnatal count
	Platelet	
ITP group	15.50 (15.20–15.85)	15.55 (14.80–15.90)
The other group	15.70 (15.35–16.45)	15.40 (14.70–15.80)[1]
P	0.004*	0.165
Fg		
GT group	4.35 (3.84–4.83)	4.87 (3.83–5.35)[1]
HDP group	4.17 (3.30–4.47)	4.76 (4.11–5.15)[1]
ITP group	4.18 (3.61–5.00)	4.48 (4.08–5.11)[1]
Grouping according to severity		
The other group	4.42 (3.86–4.91)	5.03 (4.43–5.77)[1]
P	0.373	0.472
Platelet		
Mild group	87.00 (73.00–94.00)	106.00 (91.00–119.00)[1]
Moderate group	46.00 (39.50–61.00)	63.00 (51.00–82.00)[1]
Severe group	26.00 (20.00–40.00)	47.00 (39.00–107.00)[1)]
P	<0.001*	<0.001*
Hb		
Mild group	118.00 (109.00–126.00)	105.94 ± 18.19[1)]
Moderate group	111.00 (104.50–124.00)	101.70 ± 15.33[1]
Severe group	103.00 (86.50–110.50)	92.05 ± 17.93
P	<0.001*	0.006*
PDW		
Mild group	15.80 (14.40–20.00)	15.00 (12.90–18.40)[1]
Moderate group	16.20 (14.50–16.90)	13.75 (12.80–15.40)[1]
Severe group	14.65 (12.15–17.00)	12.10 (11.10–14.30)[1]
P	0.252	0.001*
MPV		
Mild group	12.32 ± 1.20	11.80 (11.05–12.85)[1]
Moderate group	12.15 ± 1.30	11.55 (10.90–12.00)[1]
Severe group	12.08 ± 1.35	10.95 (10.10–11.50)[1]
P	0.772	0.003*

(Continued on the following page)

TABLE 4 (*Continued*) Comparison of blood routine and coagulation function in the first week before delivery and the third day after delivery.

Grouping according to severity		
PCT		
Mild group	0.10 (0.09–0.11)	0.10 (0.10–0.13)[1]
Moderate group	0.08 (0.04–0.10)	0.10 (0.10–0.10)[1]
Severe group	0.00 (0.00–0.03)	0.10 (0.00–0.10)[1]
P	<0.001*	<0.001*
P-LCR		
Mild group	40.45 (32.20–49.50)	39.30 (32.10–46.45)[1]
Moderate group	40.25 (35.80–47.00)	34.20 (30.30–38.30)[1]
Severe group	0.00 (0.00–41.70)	31.80 (25.35–37.35)
P	0.038*	0.002*
PT		
Mild group	12.30 (11.90–12.80)	12.50 (11.95–12.85)
Moderate group	12.40 (12.10–12.75)	12.90 (12.30–13.20)
Severe group	12.20 (11.95–12.80)	12.60 (12.20–13.20)[1]
P	0.83	0.151
APTT		
Mild group	32.90 (31.30–34.20)	33.45 (31.45–36.30)[1]
Moderate group	32.80 (30.45–33.85)	35.10 (32.20–35.70)[1]
Severe group	31.00 (29.90–34.85)	33.20 (31.10–34.30)
P	0.247	0.679
D-dimer		
Mild group	1.48 (1.12–2.26)	1.36 (1.01–1.85)[1]
Moderate group	1.34 (0.99–2.71)	1.29 (0.94–1.92)
Severe group	1.82 (1.36–2.20)	1.95 (1.52–2.64)
P	0.731	0.003*
INR		
Mild group	1.00 (0.92–1.00)	0.98 (0.94–1.00)
Moderate group	1.00 (0.99–1.00)	1.00 (1.00–1.02)
Severe group	0.98 (0.90–1.00)	1.00 (1.00–1.00)
P	0.302	0.015*
TT		
Mild group	15.70 (15.35–16.10)	15.77 ± 0.93

(Continued on the following page)

TABLE 4 (*Continued*) Comparison of blood routine and coagulation function in the first week before delivery and the third day after delivery.

Grouping according to severity		
Moderate group	15.50 (14.90–16.00)	15.39 ± 0.66
Severe group	15.50 (15.30–15.70)	15.09 ± 0.75
P	0.569	0.085
Fg		
Mild group	4.29 (3.80–4.87)	4.71 ± 0.93[1]
Moderate group	4.14 (3.51–4.82)	4.61 ± 0.50
Severe group	4.20 (3.78–4.93)	4.66 ± 1.12[1]
P	0.727	0.905

*$P < 0.05$.
[1]Comparison with the same index before delivery.

TABLE 5 The correlation between prenatal platelet count and TEG parameters.

Indicators	GT group (*n* = 39)		HDP group (*n* = 13)		ITP group (*n* = 13)		The other group (*n* = 12)	
	r	*P*	r	*P*	r	*P*	r	*P*
Grouping according to etiology								
R (mins)	−0.47	0.207	−0.26	0.830	−0.73	0.479	1.00	
K (mins)	−0.39	0.307	−0.99	0.099	−0.92	0.252	−1.00	
Angle (°)	0.04	0.928	0.96	0.180	0.89	0.304	1.00	
MA (mm)	0.42	0.262	0.83	0.377	0.99	0.085	1.00	
LY30 (%)	−0.19	0.744	0.00	1.000	N/A	N/A	N/A	N/A
EPL (%)	−0.13	0.744	0.00	1.000	N/A	N/A	N/A	N/A
CI	0.20	0.600	0.95	0.200	0.90	0.282	1.00	

Indicators	Mild group (*n* = 53)		Moderate group (*n* = 12)		Severe group (*n* = 12)	
	r	*P*	r	*P*	r	*P*
Grouping according to severity						
R (mins)	−0.27	0.365	−1.00		−1.00	
K (mins)	−0.54	0.058	−1.00		−1.00	
Angle (°)	0.55	0.051	1.00		1.00	
MA (mm)	0.44	0.137	1.00		1.00	
LY30 (%)	−0.19	0.533	N/A	N/A	N/A	N/A
EPL (%)	−0.19	0.533	N/A	N/A	N/A	N/A
CI	0.55	0.054	1.00		1.00	

Note: "." due to the existence of complete correlation, significance was not calculated; N/A, not applicable.

TABLE 6 Comparison of positive immune antibodies of pregnant women.

Indicators	GT group (%) (*n* = 16)	HDP group (%) (*n* = 8)	ITP group (%) (*n* = 14)	The other group (%) (*n* = 10)	*P*
Grouping according to etiology					
ANA>1:80	2 (12.50)	0 (0.00)	0 (0.00)	2 (20.00)	0.262
dsDNA Ab	0 (0.00)	0 (0.00)	0 (0.00)	1 (10.00)	0.375
SSA Ab	0 (0.00)	0 (0.00)	1 (7.69)	0 (0.00)	0.667
SSB Ab	0 (0.00)	0 (0.00)	0 (0.00)	0 (0.00)	N/A
Pm-Scl Ab	0 (0.00)	1 (12.50)	0 (0.00)	0 (0.00)	0.167
ACA Ab	0 (0.00)	0 (0.00)	0 (0.00)	1 (10.00)	0.658
dRVVT>1.20	0 (0.00)	0 (0.00)	0 (0.00)	1 (10.00)	0.286

Indicators	Mild group (%) (*n* = 28)	Moderate group (%) (*n* = 9)	Severe group (%) (*n* = 11)	*P*
Grouping according to severity				
ANA>1:80	3 (10.71)	1 (11.11)	0 (0.00)	0.622
dsDNA Ab	0 (0.00)	0 (0.00)	1 (9.09)	0.417
SSA Ab	0 (0.00)	1 (11.11)	0 (0.00)	0.208
SSB Ab	0 (0.00)	0 (0.00)	0 (0.00)	N/A
Pm-Scl Ab	1 (3.57)	0 (0.00)	0 (0.00)	1.000
ACA Ab	0 (0.00)	0 (0.00)	1 (9.09)	0.421
dRVVT>1.20	0 (0.00)	1 (11.11)	0 (0.00)	0.143

Note: Fisher test was used; N/A, not applicable.

4 Discussion

Thrombocytopenia in pregnancy can cause serious adverse consequences, leading to postpartum hemorrhage, hemorrhagic shock, and neonatal intracranial hemorrhage. In this study, GT group accounted for the largest proportion, followed by the ITP group, the HDP group and the other group. Grouped by the severity of thrombocytopenia, 70.90% of patients belong to the mild group, 15.20% in the moderate group, and only 13.90% in the severe group. In terms of clinical manifestations, the ITP group had a higher proportion of skin and mucous membrane bleeding during pregnancy (43.18%), the smallest gestational age at first diagnosis and the lowest platelet count at first diagnosis. In terms of delivery outcomes, the length of hospital stay in the GT group was significantly lower than that in the HDP group and the ITP group, and the gestational age of delivery was the largest, suggesting that the condition of GT group might be mild. Regarding the treatments of thrombocytopenia in pregnancy, the platelet counts of the GT group and the HDP group increased significantly after the treatment of glucocorticoid alone or glucocorticoid plus platelet infusion. However, the effect of glucocorticoid alone in the ITP group was not good, thus the combination therapy was needed to achieve better effect. In addition, postpartum Hb counts in the GT group, the ITP group and the other group were significantly lower than those in prenatal, suggesting that thrombocytopenia could aggravate the loss of Hb for these patients. TEG parameters were correlated with the prenatal platelet count of patients in the moderate and the severe groups, but not with the mild group, indicating that only patients in the moderate and severe groups could cause changes in blood coagulation and fibrinolysis system. For the newborns, the NICU transfer rate and the incidence of low birth weight infants in the HDP group were significantly higher than those in the GT group, and the birth weight of newborns delivered by pregnant women in the HDP group was lower, indicating that HDP had a greater impact on newborns, which needed special attention.

As for the etiology of thrombocytopenia in pregnancy, our results are slightly different from other reports (Parnas et al., 2006; Yuce et al., 2014). They believed that the incidence of HDP was higher than that of ITP, but we found that the incidence of HDP was lower than that of ITP. The difference may be related to the different research subjects. The unified viewpoint is that GT is still the most common cause of thrombocytopenia in pregnancy (Yan et al., 2016; Park, 2022; Fogerty, 2018). In the present study, 70.90% of cases

TABLE 7 Comparison of birth conditions of newborns.

Groups	Thrombocytopenia at birth (%)	Preterm birth rate (%)		Asphyxia rate (%)	NICU transfer (%)	Low birth weight (%)	Apgar score		Weight (grams)
		<34 weeks					1 min	5 min	
Grouping according to etiology									
GT group (n = 67)	1 (5.30)	1 (25.00)	3 (75.00)	1 (1.50)	5 (7.50)	1 (1.50)	10.00 (10.00–10.00)	10.00 (10.00–10.00)	3335.00 (3140.00–3660.00)
HDP group (n = 24)	0 (0.00)	2 (28.60)	5 (71.40)	0 (0.00)	8 (33.30)[1]	9 (37.50)[1]	10.00 (9.50–10.00)	10.00 (10.00–10.00)	2720.00 (2210.00–3125.00)[1]
ITP group (n = 44)	2 (20.00)	7 (77.70)	2 (22.20)	1 (2.30)	7 (15.90)	5 (11.40)	10.00 (10.00–10.00)	10.00 (10.00–10.00)	3165.00 (2740.00–3535.00)[2]
The other group (n = 16)	1 (25.00)	3 (100.00)	0 (0.00)	0 (0.00)	4 (25.00)	3 (18.80)	10.00 (10.00–10.00)	10.00 (10.00–10.00)	3135.00 (2690.00–3520.00)
H/Fisher	3.11	7.07		1.27	9.88	21.02	5.42	4.92	25.20
P	0.276	0.071		1.000	0.015*	<0.001*	0.144	0.178	<0.001*
Grouping according to severity									
Mild group (n = 107)	3 (10.00)	3 (33.30)	6 (66.70)	1 (0.90)	14 (13.10)	8 (7.50)	10.00 (10.00–10.00)	10.00 (10.00–10.00)	3330.00 (2995.00–3565.00)
Moderate group (n = 23)	1 (16.70)	4 (66.70)	2 (33.30)	0 (0.00)	4 (17.40)	2 (8.70)	10.00 (8.50–10.00)[3]	10.00 (10.00–10.00)	3110.00 (2820.00–3250.00)
Severe group (n = 21)	0 (0.00)	6 (75.00)	2 (25.00)	1 (4.80)	6 (28.60)	8 (38.10)[3]	10.00 (10.00–10.00)	10.00 (10.00–10.00)	2580.00 (2390.00–3160.00)[3]
H/Fisher	1.02	3.16		2.40	3.25	12.18	7.03	0.45	14.04
P	0.629	0.183		0.282	0.188	<0.001*	0.030*	0.800	<0.001*

*$P < 0.05$.
[1]Compared with the GT, group.
[2]Compared with the HDP, group.
[3]Compared with the mild group.

10.3389/fcell.2025.1608647

belong to the mild group, which is consistent with other studies (Gernsheimer et al., 2013; Govindappagari et al., 2020).

In this paper, the platelet count of ITP group during pregnancy and the third day after delivery is the lowest, which is consistent with the nature of ITP. ITP is a disease caused by immune-mediated platelet destruction (Fogerty, 2018) or decreased platelet production (Fogerty, 2024), which is usually associated with more severe thrombocytopenia and bleeding. The research of Rodeghiero et al. (2009) provided a comprehensive analysis for the classification and severity of ITP, emphasizing that the increased risk of bleeding is the main clinical problem of ITP, which depends on the degree of thrombocytopenia. In addition, the number of gestational weeks at the first diagnosis of ITP group was the lowest, which showed that compared with other groups, ITP often appeared in the early pregnancy. This is of great clinical significance because it emphasizes the necessity of early screening and management of suspected ITP cases. In contrast to ITP group, the GT group had fewer symptoms of skin mucosal bleeding during pregnancy, and maintained higher platelet counts in pregnancy and postpartum. GT may be due to hemodilution caused by the increase of plasma volume during pregnancy (Pishko et al., 2020), which is different from ITP. Additionally, the hospital stay of patients in the GT group was shorter than that in the HDP group and the ITP group, which showed that although thrombocytopenia existed, the complexity of GT was relatively low. Moreover, the gestational week of delivery in the GT group was higher, suggesting that GT did not seem to increase the risk of adverse pregnancy outcomes (Cines and Levine, 2017a).

Regarding the mode of delivery, women undergoing elective cesarean section have been associated with an increased risk of blood loss and blood transfusion (Attali et al., 2021), hence, the indications of cesarean section should be determined according to the obstetric situation. Researchers believe that cesarean section is safe and feasible when the platelet count reaches is more than 50×10^9/L (Provan et al., 2019). At present, it is generally believed that cesarean section can be considered for full-term pregnancy with platelet count less than 50×10^9/L and bleeding tendency (Myers, 2012). For full-term pregnancy with platelet count more than 50×10^9/L, if there is no indication of obstetric cesarean section, vaginal natural delivery can be considered (Myers, 2012). The reason for the increase of cesarean section rate in the GT group in our study may be due to the patients' fear of fetal intracranial hemorrhage. In the future, it is necessary to encourage these mild GT patients to have vaginal delivery if the condition allows.

In the treatment of thrombocytopenia, the efficacy of platelet transfusion has been fully affirmed (Kaufman et al., 2015), and the transfusion of a therapeutic amount of platelet will increase the platelet count by about $5–10 \times 10^9$/L (Bauer et al., 2021). However, for massive hemorrhage (platelet count $<10 \times 10^9$/L), platelet transfusion has no significant effect on reducing mortality (Stanworth and Shah, 2022). Platelet transfusion is suitable for patients with impaired platelet formation or increased platelet destruction, but platelet transfusion may be harmful to patients with increased intravascular platelet activation (Greinacher and Selleng, 2016). At present, general supportive care with a combination of treatments, including corticosteroids, IVIg, and platelet transfusion has been recommended for a more effective and rapid increase of platelet count for treatment of life-threatening hemorrhage due to ITP, and in the absence of significant response, the early addition of a thrombopoietin receptor agonists (TPO-Ras) should also be considered (Provan et al., 2019). A recent systematic review suggested that pregnant women with ITP might be suitable for TPO-Ras treatment, although it was off-label (Snow et al., 2023). In our study, patients in the ITP group benefited from the combined treatment of glucocorticoid and platelet transfusion. If only glucocorticoid was used, the effect was not good. It has been reported that patients with moderate and severe thrombocytopenia should be treated with glucocorticoid and platelet transfusion before cesarean section, in order to quickly stabilize the platelet level and reduce intraoperative bleeding (Gernsheimer et al., 2013). The American Society of Hematology (ASH) 2019 guidelines also recommend that pregnant women with ITP receive corticosteroids or IVIg, and the mode of delivery should be determined based on obstetric indications (Neunert et al., 2019). Moreover, we found that the platelet counts in the GT group and the HDP group treated with glucocorticoids alone increased significantly after treatment, which was consistent with another report (Woudstra et al., 2010). This indicates that monotherapy may be enough to treat mild thrombocytopenia.

Postpartum platelet counts in each group of patients are higher than those before delivery, which reflects the recovery of postpartum platelet production, because the physiological demand for platelet after delivery is reduced. For patients with thrombocytopenia in pregnancy, platelet consumption decreases after delivery, resulting in a significant increase in postpartum platelet count (Ushida et al., 2021). Moreover, PCT refers to the volume percentage of platelets in the blood (Budak et al., 2016). Monitoring PCT can help track the body's response to platelet turnover/production, especially in severe cases. If PCT is reduced, a higher level of platelet production may be required to make up for the reduced platelets. The postpartum PCT level of patients in each group (except the other group) was significantly higher than that in prenatal, representing the recovery of postpartum platelet consumption. In addition, PDW is a marker of platelet size variability (Budak et al., 2016), and can predict coagulation activation (Liu et al., 2019). Therefore, the decrease of PDW may indicate stable platelet formation and turnover. MPV is a marker of platelet activation (Budak et al., 2016) and can also be considered an indicator of platelet function (Vizioli et al., 2009). The increase of MPV reflects the increase of platelet clearance or destruction (Cines and Levine, 2017a). The decrease of postpartum MPV in this study may represent the improvement of postpartum platelet count. Researchers proposed that MPV can be used to discriminate ITP from thrombocytopenia caused by decreased platelet production (i.e., hypo-productive thrombocytopenia) (Walle et al., 2023). Large platelets are mostly young platelets, and P-LCR refers to the presence of large platelets in the blood and is used to monitor platelet activity (Budak et al., 2016). In our study, the postpartum P-LCR levels in the GT group and the ITP group decreased significantly. Since the overall change trend of platelet count showed an increase after delivery, the decrease of postpartum P-LCR might indicate that platelet production was gradually recovering, and platelets were more mature and smaller in size.

Xie et al. (2021) established the reference interval of TEG parameters including R, K, Ma and α-angle of healthy pregnant women in the third trimester of pregnancy. They

found that compared with normal women without pregnancy, R value decreased (without statistical significance), Ma increased significantly, which was consistent with the hypercoagulable state during pregnancy. TEG can help to detect and quantify platelet function, and it is useful to assist physicians in providing targeted medical interventions earlier (Dias et al., 2020). In general, a prolonged R value indicates a deficiency of coagulation factors, a prolonged K value shows a deficiency of fibrinogen, a decrease in MA value indicates either a reduction in platelets or abnormal platelet function, and a decreased CI value indicates a decrease in coagulation factors, a decrease in platelets, or an overactivity of the fibrinolytic system. The correlation between prenatal platelet count and TEG parameters in the HDP group was not significant, which indicated that for HDP patients, in addition to platelet count, there might be other factors that affect the coagulation process (Andersson et al., 2024; Davies et al., 2007; Spiezia et al., 2015). However, platelet counts in the moderate group and severe group were negatively correlated with R value and K value, indicating that lower platelet count resulted in delayed clot formation and weakened coagulation strength. Therefore, it is necessary to perform the TEG test for patients with moderate and severe thrombocytopenia, as these patients have a higher likelihood of blood transfusions. Changes in the R and K values can assist obstetricians in determining the type of blood product that needs to be transfused. Moreover, the traditional view is that cesarean section will aggravate the postpartum hypercoagulable state, because the R, K and α-angle after cesarean section are significantly shortened (Boyce et al., 2011). However, a few studies have revealed that the TEG parameters before and immediately after cesarean section are similar (Macafee et al., 2012; Sharma and Philip, 1997), which does not support the above view. A prospective study measured the changes of TEG parameters during the postnatal period up to 6 weeks after delivery and found that there was still a hypercoagulable state in the maternal body within 3 weeks after delivery (Saha et al., 2009). Compared with vaginal delivery, the thrombus parameters after cesarean section did not increase significantly (Saha et al., 2009). We did not test TEG after delivery, therefore, we were unable to analyze the relationship between postpartum platelet count and TEG parameters.

In clinical, thrombocytopenia not only occurs in ITP, but also in some secondary autoimmune diseases, such as systemic lupus erythematosus, APS, Sjögren's syndrome, or rheumatoid arthritis. Therefore, we analyzed whether there was a correlation between immune indicators and the types of thrombocytopenia. In our study, there was no statistical difference in the autoimmune antibodies of patients in each group. It seems that immunity has no effect on thrombocytopenia in pregnancy. However, the number of patients undergoing autoimmune antibody testing is relatively small, thus this conclusion needs to be further confirmed by expanding the sample size.

We found that the incidence of low birth weight infants was the highest in the HDP group. This may be due to the impaired placentation caused by HDP, which increases the likelihood of fetal growth restriction (Di Martino et al., 2022). Similarly, the birth weight of newborns in the GT group was the highest, which was significantly higher than that in the HDP group and the ITP group. This is consistent with the mild systemic effects of GT, which is usually transient and self-limiting, and may have the least impact on fetal growth. Grouping according to the severity of thrombocytopenia, the incidence of low birth weight was higher in the severe group compared with the mild group, indicating that severe thrombocytopenia may affect the growth and development of newborns.

This study has some limitations. First, the sample size is limited, and larger sample size research is needed to further verify our results. Second, there may be a potential selection bias in our study. Third, we did not conduct long-term follow-up on the prognosis of newborns. In the future, we can collaborate with pediatricians to perform follow-up on neonates for a longer period, so as to provide more information for clinical practice.

5 Conclusion

In conclusion, ITP is associated with more severe thrombocytopenia and bleeding, often presenting in the early stage of pregnancy. Therefore, early screening and management should be carried out for suspected ITP cases. In the treatment of ITP, the combined use of glucocorticoids and platelet transfusion is recommended. GT patients have relatively mild clinical symptoms and less clinical harm, and do not seem to increase the risk of adverse pregnancy outcomes. For most patients with thrombocytopenia during pregnancy, postpartum Hb is significantly lower than that before delivery, suggesting that thrombocytopenia may have aggravated the loss of Hb in these patients. Obstetricians need to pay more attention to the prevention and treatment of postpartum hemorrhage. TEG parameter analysis suggests that patients in the moderate and severe groups may have changes in the blood coagulation and fibrinolysis systems, and changes in the coagulation function of these patients need to be monitored. Newborns delivered by HDP patients are more likely to be transferred to the NICU, and the probability of delivering low birth weight infants is increased. Therefore, more attention should be paid to the monitoring of these newborns. Our study provides new insights into the pregnancy outcomes of pregnant women with thrombocytopenia and lays a foundation for the development of targeted treatment strategies for these patients.

Data availability statement

The raw data supporting the conclusions of this article will be made available by the authors, without undue reservation.

Ethics statement

The studies involving humans were approved by the Medical Science and Research Ethics Committee of The First Hospital of China Medical University. The studies were conducted in accordance with the local legislation and institutional requirements. The ethics committee/institutional review board waived the requirement of written informed consent for participation from the participants or the participants' legal guardians/next of kin because it was a retrospective study and written informed consent was impossible.

Author contributions

CI: Investigation, Data curation, Formal Analysis, Methodology, Writing – original draft. FG: Validation, Writing – review and editing. XY: Conceptualization, Supervision, Validation, Writing – review and editing.

Funding

The author(s) declare that no financial support was received for the research and/or publication of this article.

Conflict of interest

The authors declare that the research was conducted in the absence of any commercial or financial relationships that could be construed as a potential conflict of interest.

Generative AI statement

The author(s) declare that no Generative AI was used in the creation of this manuscript.

Any alternative text (alt text) provided alongside figures in this article has been generated by Frontiers with the support of artificial intelligence and reasonable efforts have been made to ensure accuracy, including review by the authors wherever possible. If you identify any issues, please contact us.

Publisher's note

All claims expressed in this article are solely those of the authors and do not necessarily represent those of their affiliated organizations, or those of the publisher, the editors and the reviewers. Any product that may be evaluated in this article, or claim that may be made by its manufacturer, is not guaranteed or endorsed by the publisher.

References

Andersson, M., Bengtsson, P., Karlsson, O., Thörn, S. E., Thorgeirsdottir, L., Bergman, L., et al. (2024). Platelet aggregation and thromboelastometry monitoring in women with preeclampsia: a prospective observational study. *Int. J. Obstet. Anesth.* 61, 104297. doi:10.1016/j.ijoa.2024.104297

Attali, E., Epstein, D., Reicher, L., Lavie, M., Yogev, Y., and Hiersch, L. (2021). Mild thrombocytopenia prior to elective cesarean section is an independent risk factor for blood transfusion. *Arch. Gynecol. Obstet.* 304 (3), 627–632. doi:10.1007/s00404-021-05988-x

Bar, A., Moran, R., Mendelsohn-Cohen, N., Korem Kohanim, Y., Mayo, A., Toledano, Y., et al. (2025). Pregnancy and postpartum dynamics revealed by millions of lab tests. *Sci. Adv.* 11 (13), eadr7922. doi:10.1126/sciadv.adr7922

Bauer, M. E., Arendt, K., Beilin, Y., Gernsheimer, T., Perez Botero, J., James, A. H., et al. (2021). The society for obstetric Anesthesia and perinatology interdisciplinary consensus statement on neuraxial procedures in obstetric patients with thrombocytopenia. *Anesth. Analg.* 132 (6), 1531–1544. doi:10.1213/ANE.0000000000005355

Boyce, H., Hume-Smith, H., Ng, J., Columb, M. O., and Stocks, G. M. (2011). Use of thromboelastography to guide thromboprophylaxis after caesarean section. *Int. J. Obstet. Anesth.* 20 (3), 213–218. doi:10.1016/j.ijoa.2011.03.006

Brown, M. A., Magee, L. A., Kenny, L. C., Karumanchi, S. A., McCarthy, F. P., Saito, S., et al. (2018). Hypertensive disorders of pregnancy: ISSHP classification, diagnosis, and management recommendations for international practice. *Hypertension* 72 (1), 24–43. doi:10.1161/HYPERTENSIONAHA.117.10803

Budak, Y. U., Polat, M., and Huysal, K. (2016). The use of platelet indices, plateletcrit, mean platelet volume and platelet distribution width in emergency non-traumatic abdominal surgery: a systematic review. *Biochem. Med. Zagreb.* 26 (2), 178–193. doi:10.11613/BM.2016.020

Cervera, R., Tektonidou, M. G., Espinosa, G., Cabral, A. R., González, E. B., Erkan, D., et al. (2011). Task Force on Catastrophic Antiphospholipid Syndrome (APS) and Non-criteria APS Manifestations (II): thrombocytopenia and skin manifestations. *Lupus.* 20 (2), 174–181. doi:10.1177/0961203310395052

Cines, D. B., and Levine, L. D. (2017a). Thrombocytopenia in pregnancy. *Blood* 130 (21), 2271–2277. doi:10.1182/blood-2017-05-781971

Cines, D. B., and Levine, L. D. (2017b). Thrombocytopenia in pregnancy. *Hematol. Am. Soc. Hematol. Educ. Program* 2017 (1), 144–151. doi:10.1182/asheducation-2017.1.144

Connors, J. M., and Fein, S. (2023). How to manage ITP with life-threatening bleeding. *Hematol. Am. Soc. Hematol. Educ. Program* 2023 (1), 254–258. doi:10.1182/hematology.2023000478

Davies, J. R., Fernando, R., and Hallworth, S. P. (2007). Hemostatic function in healthy pregnant and preeclamptic women: an assessment using the platelet function analyzer (PFA-100) and thromboelastograph. *Anesth. Analg.* 104 (2), 416–420. doi:10.1213/01.ane.0000253510.00213.05

De Carolis, S., Tabacco, S., Rizzo, F., Giannini, A., Botta, A., Salvi, S., et al. (2018). Antiphospholipid syndrome: an update on risk factors for pregnancy outcome. *Autoimmun. Rev.* 17 (10), 956–966. doi:10.1016/j.autrev.2018.03.018

Di Martino, D. D., Avagliano, L., Ferrazzi, E., Fusè, F., Sterpi, V., Parasiliti, M., et al. (2022). Hypertensive disorders of pregnancy and fetal growth restriction: clinical characteristics and placental lesions and possible preventive nutritional targets. *Nutrients* 14 (16), 3276. doi:10.3390/nu14163276

Dias, J. D., Lopez-Espina, C. G., Bliden, K., Gurbel, P., Hartmann, J., and Achneck, H. E. (2020). TEG® 6s system measures the contributions of both platelet count and platelet function to clot formation at the site-of-care. *Platelets* 31 (7), 932–938. doi:10.1080/09537104.2019.1704713

Estcourt, L. J., Birchall, J., Allard, S., Bassey, S. J., Hersey, P., Kerr, J. P., et al. (2017). Guidelines for the use of platelet transfusions. *Br. J. Haematol.* 176 (3), 365–394. doi:10.1111/bjh.14423

Ferrari, B., and Peyvandi, F. (2020). How I treat thrombotic thrombocytopenic purpura in pregnancy. *Blood* 136 (19), 2125–2132. doi:10.1182/blood.2019000962

Fitzpatrick, K. E., Hinshaw, K., Kurinczuk, J. J., and Knight, M. (2014). Risk factors, management, and outcomes of hemolysis, elevated liver enzymes, and low platelets syndrome and elevated liver enzymes, low platelets syndrome. *Obstet. Gynecol.* 123 (3), 618–627. doi:10.1097/AOG.0000000000000140

Fogerty, A. E. (2018). Thrombocytopenia in pregnancy: mechanisms and management. *Transfus. Med. Rev.* 32 (4), 225–229. doi:10.1016/j.tmrv.2018.08.004

Fogerty, A. E. (2024). ITP in pregnancy: diagnostics and therapeutics in 2024. *Hematol. Am. Soc. Hematol. Educ. Program* 2024 (1), 685–691. doi:10.1182/hematology.2024000595

Fogerty, A. E., and Kuter, D. J. (2024). How I treat thrombocytopenia in pregnancy. *Blood* 143 (9), 747–756. doi:10.1182/blood.2023020726

George, J. N., Nester, C. M., and McIntosh, J. J. (2015). Syndromes of thrombotic microangiopathy associated with pregnancy. *Hematol. Am. Soc. Hematol. Educ. Program* 2015, 644–648. doi:10.1182/asheducation-2015.1.644

Gernsheimer, T., James, A. H., and Stasi, R. (2013). How I treat thrombocytopenia in pregnancy. *Blood* 121 (1), 38–47. doi:10.1182/blood-2012-08-448944

Gerth, J., Schleussner, E., Kentouche, K., Busch, M., Seifert, M., and Wolf, G. (2009). Pregnancy-associated thrombotic thrombocytopenic purpura. *Thromb. Haemost.* 101 (2), 248–251. doi:10.1160/th07-12-0739

Govindappagari, S., Moyle, K., and Burwick, R. M. (2020). Mild thrombocytopenia and postpartum hemorrhage in nulliparous women with term, singleton, vertex deliveries. *Obstet. Gynecol.* 135 (6), 1338–1344. doi:10.1097/AOG.0000000000003861

Greinacher, A., and Selleng, S. (2016). How I evaluate and treat thrombocytopenia in the intensive care unit patient. *Blood* 128 (26), 3032–3042. doi:10.1182/blood-2016-09-693655

Guillet, S., Loustau, V., Boutin, E., Zarour, A., Comont, T., Souchaud-Debouverie, O., et al. (2023). Immune thrombocytopenia and pregnancy: an exposed/nonexposed cohort study. *Blood* 141 (1), 11–21. doi:10.1182/blood.2022017277

Haile, K., Kebede, S., Abera, T., Timerga, A., and Mose, A. (2022). Thrombocytopenia among pregnant women in Southwest Ethiopia: burden, severity, and predictors. *J. Blood Med.* 13, 275–282. doi:10.2147/JBM.S365812

Huang, J., Zeng, B., Li, X., Huang, M., and Zhan, R. (2020). Comparative Study of the clinical application of 2 bleeding grading systems for pregnant women with immune thrombocytopenia. *Clin. Appl. Thromb. Hemost.* 26, 1076029620910790. doi:10.1177/1076029620910790

Jin, J., Xu, X., Hou, L., Hou, Y., Li, J., Liang, M., et al. (2022). Thrombocytopenia in the first trimester predicts adverse pregnancy outcomes in obstetric antiphospholipid syndrome. *Front. Immunol.* 13, 971005. doi:10.3389/fimmu.2022.971005

Joly, B. S., Coppo, P., and Veyradier, A. (2017). Thrombotic thrombocytopenic purpura. *Blood* 129 (21), 2836–2846. doi:10.1182/blood-2016-10-709857

Kam, P. C., Thompson, S. A., and Liew, A. C. (2004). Thrombocytopenia in the parturient. *Anaesthesia* 59 (3), 255–264. doi:10.1111/j.1365-2044.2004.03576.x

Kaufman, R. M., Djulbegovic, B., Gernsheimer, T., Kleinman, S., Tinmouth, A. T., Capocelli, K. E., et al. (2015). Platelet transfusion: a clinical practice guideline from the AABB. *Ann. Intern Med.* 162 (3), 205–213. doi:10.7326/M14-1589

Kelton, J. G. (2002). Idiopathic thrombocytopenic purpura complicating pregnancy. *Blood Rev.* 16 (1), 43–46. doi:10.1054/blre.2001.0181

Li, J., Gao, Y. H., Su, J., Zhang, L., Sun, Y., and Li, Z. Y. (2022). Diagnostic ideas and management strategies for thrombocytopenia of unknown causes in pregnancy. *Front. Surg.* 9, 799826. doi:10.3389/fsurg.2022.799826

Liu, L., and Sun, D. (2019). Pregnancy outcomes in patients with primary antiphospholipid syndrome: a systematic review and meta-analysis. *Med. Baltim.* 98 (20), e15733. doi:10.1097/MD.0000000000015733

Liu, X., Wang, H., Huang, C., Meng, Z., Zhang, W., Li, Y., et al. (2019). Association between platelet distribution width and serum uric acid in Chinese population. *Biofactors* 45 (3), 326–334. doi:10.1002/biof.1491

Macafee, B., Campbell, J. P., Ashpole, K., Cox, M., Matthey, F., Acton, L., et al. (2012). Reference ranges for thromboelastography (TEG®) and traditional coagulation tests in term parturients undergoing caesarean section under spinal anaesthesia. *Anaesthesia* 67 (7), 741–747. doi:10.1111/j.1365-2044.2012.07101.x

Martin, J. N., Jr., Bailey, A. P., Rehberg, J. F., Owens, M. T., Keiser, S. D., and May, W. L. (2008). Thrombotic thrombocytopenic purpura in 166 pregnancies: 1955-2006. *Am. J. Obstet. Gynecol.* 199 (2), 98–104. doi:10.1016/j.ajog.2008.03.011

McCrae, K. R. (2010). Thrombocytopenia in pregnancy. *Hematol. Am. Soc. Hematol. Educ. Program* 2010, 397–402. doi:10.1182/asheducation-2010.1.397

Mithoowani, S., Cervi, A., Shah, N., Ejaz, R., Sirotich, E., Barty, R., et al. (2020). Management of major bleeds in patients with immune thrombocytopenia. *J. Thromb. Haemost.* 18 (7), 1783–1790. doi:10.1111/jth.14809

Mol, B. W. J., Roberts, C. T., Thangaratinam, S., Magee, L. A., de Groot, C. J. M., and Hofmeyr, G. J. (2016). Pre-eclampsia. *Lancet* 387 (10022), 999–1011. doi:10.1016/S0140-6736(15)00070-7

Myers, B. (2012). Diagnosis and management of maternal thrombocytopenia in pregnancy. *Br. J. Haematol.* 158 (1), 3–15. doi:10.1111/j.1365-2141.2012.09135.x

Neunert, C., Terrell, D. R., Arnold, D. M., Buchanan, G., Cines, D. B., Cooper, N., et al. (2019). American society of hematology 2019 guidelines for immune thrombocytopenia. *Blood Adv.* 3 (23), 3829–3866. doi:10.1182/bloodadvances.2019000966

Park, Y. H. (2022). Diagnosis and management of thrombocytopenia in pregnancy. *Blood Res.* 57 (S1), 79–85. doi:10.5045/br.2022.2022068

Parnas, M., Sheiner, E., Shoham-Vardi, I., Burstein, E., Yermiahu, T., Levi, I., et al. (2006). Moderate to severe thrombocytopenia during pregnancy. *Eur. J. Obstet. Gynecol. Reprod. Biol.* 128 (1-2), 163–168. doi:10.1016/j.ejogrb.2005.12.031

Pishko, A. M., and Marshall, A. L. (2022). Thrombocytopenia in pregnancy. *Hematol. Am. Soc. Hematol. Educ. Program* 2022 (1), 303–311. doi:10.1182/hematology.2022000375

Pishko, A. M., Levine, L. D., and Cines, D. B. (2020). Thrombocytopenia in pregnancy: diagnosis and approach to management. *Blood Rev.* 40, 100638. doi:10.1016/j.blre.2019.100638

Provan, D., Arnold, D. M., Bussel, J. B., Chong, B. H., Cooper, N., Gernsheimer, T., et al. (2019). Updated international consensus report on the investigation and management of primary immune thrombocytopenia. *Blood Adv.* 3 (22), 3780–3817. doi:10.1182/bloodadvances.2019000812

Reese, J. A., Peck, J. D., Deschamps, D. R., McIntosh, J. J., Knudtson, E. J., Terrell, D. R., et al. (2018). Platelet counts during pregnancy. *N. Engl. J. Med.* 379 (1), 32–43. doi:10.1056/NEJMoa1802897

Rodeghiero, F., Stasi, R., Gernsheimer, T., Michel, M., Provan, D., Arnold, D. M., et al. (2009). Standardization of terminology, definitions and outcome criteria in immune thrombocytopenic purpura of adults and children: report from an international working group. *Blood* 113 (11), 2386–2393. doi:10.1182/blood-2008-07-162503

Rottenstreich, A., Israeli, N., Levin, G., Rottenstreich, M., Elchalal, U., and Kalish, Y. (2018). Clinical characteristics, neonatal risk and recurrence rate of gestational thrombocytopenia with platelet count <100 × 10(9)/L. *Eur. J. Obstet. Gynecol. Reprod. Biol.* 231, 75–79. doi:10.1016/j.ejogrb.2018.10.026

Saha, P., Stott, D., and Atalla, R. (2009). Haemostatic changes in the puerperium '6 weeks postpartum' (HIP Study) - implication for maternal thromboembolism. *Bjog* 116 (12), 1602–1612. doi:10.1111/j.1471-0528.2009.02295.x

Sharma, S. K., and Philip, J. (1997). The effect of anesthetic techniques on blood coagulability in parturients as measured by thromboelastography. *Anesth. Analg.* 85 (1), 82–86. doi:10.1097/00000539-199707000-00015

Smock, K. J., and Perkins, S. L. (2014). Thrombocytopenia: an update. *Int. J. Lab. Hematol.* 36 (3), 269–278. doi:10.1111/ijlh.12214

Snow, L., Knapp, G., Llaneza, A. J., Sowdagar, S., Khawandanah, M. O., Vesely, S., et al. (2023). Current management of pregnant persons with ITP: Systematic literature review. *Blood* 142 (Suppl. 1), 3957. doi:10.1182/blood-2023-191326

Spiezia, L., Bogana, G., Campello, E., Maggiolo, S., Pelizzaro, E., Carbonare, C. D., et al. (2015). Whole blood thromboelastometry profiles in women with preeclampsia. *Clin. Chem. Lab. Med.* 53 (11), 1793–1798. doi:10.1515/cclm-2014-1128

Stanworth, S. J., and Shah, A. (2022). How I use platelet transfusions. *Blood* 140 (18), 1925–1936. doi:10.1182/blood.2022016558

Thomas, M. R., Robinson, S., and Scully, M. A. (2016). How we manage thrombotic microangiopathies in pregnancy. *Br. J. Haematol.* 173 (6), 821–830. doi:10.1111/bjh.14045

Townsley, D. M. (2013). Hematologic complications of pregnancy. *Semin. Hematol.* 50 (3), 222–231. doi:10.1053/j.seminhematol.2013.06.004

Ushida, T., Kotani, T., Moriyama, Y., Imai, K., Nakano-Kobayashi, T., Kinoshita, F., et al. (2021). Platelet counts during normal pregnancies and pregnancies complicated with hypertensive disorders. *Pregnancy Hypertens.* 24, 73–78. doi:10.1016/j.preghy.2021.02.013

van der Lugt, N. M., van Kampen, A., Walther, F. J., Brand, A., and Lopriore, E. (2013). Outcome and management in neonatal thrombocytopenia due to maternal idiopathic thrombocytopenic purpura. *Vox Sang.* 105 (3), 236–243. doi:10.1111/vox.12036

Veneri, D., Franchini, M., Randon, F., Nichele, I., Pizzolo, G., and Ambrosetti, A. (2009). Thrombocytopenias: a clinical point of view. *Blood Transfus.* 7 (2), 75–85. doi:10.2450/2008.0012-08

Vizioli, L., Muscari, S., and Muscari, A. (2009). The relationship of mean platelet volume with the risk and prognosis of cardiovascular diseases. *Int. J. Clin. Pract.* 63 (10), 1509–1515. doi:10.1111/j.1742-1241.2009.02070.x

Vreede, A. P., Bockenstedt, P. L., McCune, W. J., and Knight, J. S. (2019). Cryptic conspirators: a conversation about thrombocytopenia and antiphospholipid syndrome. *Curr. Opin. Rheumatol.* 31 (3), 231–240. doi:10.1097/BOR.0000000000000595

Walle, M., Arkew, M., Asmerom, H., Tesfaye, A., and Getu, F. (2023). The diagnostic accuracy of mean platelet volume in differentiating immune thrombocytopenic purpura from hypo-productive thrombocytopenia: a systematic review and meta-analysis. *PLoS One* 18 (11), e0295011. doi:10.1371/journal.pone.0295011

Wang, X., Xu, Y., Luo, W., Feng, H., Luo, Y., Wang, Y., et al. (2017). Thrombocytopenia in pregnancy with different diagnoses: differential clinical features, treatments, and outcomes. *Med. Baltim.* 96 (29), e7561. doi:10.1097/MD.0000000000007561

Wang, W., Long, K., Deng, F., Ye, W., Zhang, P., Chen, X., et al. (2021). Changes in levels of coagulation parameters in different trimesters among Chinese pregnant women. *J. Clin. Lab. Anal.* 35 (4), e23724. doi:10.1002/jcla.23724

Woudstra, D. M., Chandra, S., Hofmeyr, G. J., and Dowswell, T. (2010). Corticosteroids for HELLP (hemolysis, elevated liver enzymes, low platelets) syndrome in pregnancy. *Cochrane Database Syst. Rev.* (9), Cd008148. doi:10.1002/14651858.CD008148.pub2

Xie, X., Wang, M., Lu, Y., Zeng, J., Wang, J., Zhang, C., et al. (2021). Thromboelastography (TEG) in normal pregnancy and its diagnostic efficacy in patients with gestational hypertension, gestational diabetes mellitus, or preeclampsia. *J. Clin. Lab. Anal.* 35 (2), e23623. doi:10.1002/jcla.23623

Xu, J., Tan, L. N., Li, L. X., and Qiao, G. Y. (2024). Case report of thrombotic thrombocytopenic purpura during pregnancy with a review of the relevant research. *Med. Baltim.* 103 (20), e38112. doi:10.1097/MD.0000000000038112

Yan, M., Malinowski, A. K., and Shehata, N. (2016). Thrombocytopenic syndromes in pregnancy. *Obstet. Med.* 9 (1), 15–20. doi:10.1177/1753495X15601937

Young, B., Levine, R. J., Salahuddin, S., Qian, C., Lim, K. H., Karumanchi, S. A., et al. (2010). The use of angiogenic biomarkers to differentiate non-HELLP related thrombocytopenia from HELLP syndrome. *J. Matern. Fetal Neonatal Med.* 23 (5), 366–370. doi:10.1080/14767050903184207

Yuce, T., Acar, D., Kalafat, E., Alkilic, A., Cetindag, E., and Soylemez, F. (2014). Thrombocytopenia in pregnancy: do the time of diagnosis and delivery route affect pregnancy outcome in parturients with idiopathic thrombocytopenic purpura? *Int. J. Hematol.* 100 (6), 540–544. doi:10.1007/s12185-014-1688-6

Zhou, Y., Reilly, S. D., Gangaraju, R., Reddy, V. V. B., and Marques, M. B. (2017). An unusual presentation of thrombotic thrombocytopenic purpura. *Am. J. Med.* 130 (8), e323–e326. doi:10.1016/j.amjmed.2017.04.022

frontiers | Frontiers in Medicine

TYPE Review
PUBLISHED 19 September 2025
DOI 10.3389/fmed.2025.1539651

OPEN ACCESS

EDITED BY
Bramanandam Manavathi,
University of Hyderabad, India

REVIEWED BY
Xin Kang,
University Hospital Brugmann, Belgium
Annalisa Vidiri,
Cannizzaro Hospital, Italy

*CORRESPONDENCE
Li Wang
✉ liwang80@njmu.edu.cn

†These authors have contributed equally to this work

RECEIVED 04 December 2024
ACCEPTED 02 September 2025
PUBLISHED 19 September 2025

CITATION
Guo Z, Zhang B, Yang D and Wang L (2025) Multidimensional roles of cfDNA fragmentomics in preeclampsia: from placental hypoxia and TLR9 inflammation to clinical risk stratification.
Front. Med. 12:1539651.
doi: 10.3389/fmed.2025.1539651

Multidimensional roles of cfDNA fragmentomics in preeclampsia: from placental hypoxia and TLR9 inflammation to clinical risk stratification

Ziyi Guo†, Bin Zhang†, Di Yang and Li Wang*

Changzhou Maternal and Child Health Care Hospital, Changzhou Medical Center, Nanjing Medical University (Changzhou Maternal and Child Health Care Hospital), Changzhou, China

Cell-free DNA (cfDNA) has emerged as a pivotal biomarker for predicting preeclampsia (PE), a multisystem syndrome characterized by placental hypoperfusion and systemic inflammation. This review synthesizes critical advances in the field, highlighting quantitative alterations in cfDNA, fragmentomic profiles, and placenta-specific methylation patterns (e.g., RASSF1A) that demonstrate significant value for early prediction and severity stratification of PE. Mechanistically, placental hypoxia-induced trophoblast apoptosis (releasing cfDNA), epigenetic dysregulation activating TLR9/NF-κB inflammatory pathways, and oxidative stress-mediated mitochondrial cfDNA fragmentation collectively drive disease progression. In clinical translation, integrating cfDNA with complementary biomarkers enhances predictive performance, though limitations persist regarding preanalytical variability and dynamic gestational changes. Future efforts must advance fragmentomics-integrated multi-omics frameworks for precision prediction, where assay standardization constitutes the fundamental translational bottleneck.

KEYWORDS

cell-free DNA, preeclampsia, placenta, fragmentomics, methylation

1 Introduction

Preeclampsia (PE) is an autoimmune disorder characterized by hypertension during pregnancy (1), with an incidence ranging from 3% to 7% in primiparous women and 1% to 3% in multiparous women. Elevated levels of fetal DNA and RNA derived from the placenta have been observed in pregnant women with PE, indicating placental dysfunction, which likely plays a central role in the pathophysiology of the disease. Common pathological findings in preeclamptic placentas include arteriosclerosis, hypertensive narrowing of arteries and small arterioles, fibrin deposition, and infarction, all of which are consistent with inadequate placental perfusion and ischemia and seem to correlate with the severity of PE. In mothers, PE may lead to premature cardiovascular disease in later life, while children born from preeclamptic pregnancies tend to be relatively small at birth, with an increased risk of stroke, coronary heart disease, and metabolic syndrome in adulthood (2). The development of clinical symptoms of PE is thought to result from impaired trophoblastic invasion of maternal spiral arteries, leading to

placental hypoxia and the release of inflammatory cytokines, which alter maternal systemic endothelial function, causing widespread endothelial cell dysfunction (3).

Circulating cell-free DNA (cfDNA) refers to trace amounts of endogenous and exogenous DNA fragments present in the bloodstream, existing outside of cells. Apoptosis is generally considered the primary source of cfDNA in serum or plasma, as dead cells are phagocytized by macrophages, releasing digested DNA into circulation to form cfDNA. Gel electrophoresis analysis of cfDNA typically shows a predominant band around 180 bp, with another distribution near 360 bp, which corresponds to the lengths of DNA wrapped around mononucleosomes and dinucleosomes, further indicating that cfDNA originates from apoptosis (4). In contrast, DNA released from necrotic cells tends to be larger, ~10,000 bp, due to incomplete and non-specific digestion. Additionally, the observed increase in plasma cfDNA during hepatocyte apoptosis in mice supports the notion that apoptosis is a source of cfDNA. Notably, the concentration and composition of cfDNA is a dynamic process; cfDNA is protein-bound with a relatively short half-life, with reported half-lives ranging from a few minutes to 2 h (5).

Recent breakthroughs in cfDNA detection technologies—particularly high-throughput sequencing (NGS) and epigenetic marker analyses (e.g., methylation profiling, fragmentomics)—have substantially expanded their applications in non-invasive prenatal testing (NIPT) and early cancer screening (6). Nevertheless, within the preeclampsia (PE) field, although cfDNA's biological features (such as placenta-specific methylation patterns and fragment size distributions) have been robustly associated with placental pathology, their translational potential for early clinical prediction remains systematically underexplored. Current clinical practice relies on maternal risk factors (e.g., hypertension history, BMI) combined with uterine artery Doppler ultrasonography for PE risk assessment; however, these methods exhibit limited sensitivity/specificity and demonstrate inadequate reliability for identifying high-risk populations during early gestation. While established biochemical markers (e.g., PlGF, sFlt-1) provide diagnostic value, their late detection window (typically post-second trimester) fails to meet the critical time requirement for early intervention.

This review synthesizes cutting-edge advances in cfDNA research to systematically evaluate its potential as a non-invasive biomarker for early PE detection through three dimensions: Elucidating molecular mechanisms governing placental cfDNA release and its pathophysiological links to PE; Critically assessing innovative cfDNA detection technologies for enhancing early diagnostic accuracy; Analyzing current translational research bottlenecks (e.g., sample heterogeneity, standardization gaps) and multi-omics integration strategies. By defining the pivotal role of cfDNA in PE predictive modeling, this work will establish a theoretical foundation for developing highly sensitive, first-trimester-compatible non-invasive screening tools. Such advancements are positioned to address critical voids in existing clinical surveillance systems, ultimately improving long-term maternal and neonatal outcomes.

2 Relationship between cfDNA and the severity of preeclampsia

2.1 Molecular characteristics of cfDNA relevant to preeclampsia prediction

In 1997, Lo et al. first discovered the presence of cfDNA in maternal plasma and serum, introducing the unique possibility of using non-invasive methods (i.e., routine blood tests) to obtain fetal material. Since then, numerous studies have focused on identifying the source, characteristics, and predictive potential of cfDNA, with particular emphasis on predicting pregnancy-related complications and prenatal diagnosis or screening of genetic fetal disorders. To date, cfDNA has been widely used in prenatal screening for aneuploidy, single-gene disorders, chromosomal abnormalities, placenta-associated diseases, and Rh factor assessment (7, 8). Some studies have found elevated levels of cfDNA in the blood of women with preeclampsia (9, 10), but the role of cfDNA as a reliable predictor of preeclampsia remains controversial (11). As such, the predictive value of cfDNA in preeclampsia is still under investigation. In addition to the well-established parameters such as fetal fraction and total cfDNA concentration, increasing attention has been directed toward cfDNA-associated mutational and fragmentation patterns. Mutations refer to specific genetic alterations present in fetal or maternal DNA. For instance, if DNA released from the placenta harbors mutations in certain genes, this may indicate placental dysfunction and has been associated with preeclampsia (PE). Some studies have reported that epigenetic markers, such as DNA methylation, can be utilized to differentiate fetal from maternal cfDNA or to detect alterations in specific methylation patterns. Placental dysfunction in preeclampsia has been linked to aberrant methylation in genes such as RASSF1A, HLTF, and TIMP3. Therefore, assessing methylation levels of placenta-derived cfDNA in maternal plasma may serve as an indirect indicator of placental health (12). Furthermore, the presence of other genetic variations, such as single nucleotide polymorphisms (SNPs) or copy number variations (CNVs), may also be associated with an increased risk of preeclampsia. Certain SNPs have been implicated in elevated PE susceptibility, and the detection of these variants via cfDNA analysis could aid in early risk prediction.

Fragmentation patterns, particularly the size distribution of cfDNA fragments, are another area of growing interest. In healthy pregnancies, fetal cfDNA fragments are typically shorter than maternal fragments, with a predominant size around 166 base pairs (bp). Preeclampsia may result in altered placental DNA release, leading to shifts in cfDNA fragment size distributions, such as an increased proportion of shorter fragments (<150 bp) (13). This phenomenon is potentially linked to shifts in apoptotic or necrotic processes due to placental ischemia. Moreover, nucleosome positioning patterns may also be disrupted. Aberrant apoptosis in the preeclamptic placenta can modify nucleosome occupancy, leading to specific fragment end preferences, such as an increased presence of fragment ends in open chromatin or gene regulatory regions. These alterations are potentially associated with altered nuclease activity, particularly that of enzymes like DNASE1L3

(14). Additionally, genomic instability, including microdeletions or duplications in certain chromosomal regions, may be more prevalent in preeclampsia and can be detected through cfDNA sequencing. Finally, analysis of cfDNA end motifs—the specific nucleotide sequences at the fragment ends—may reveal disease-specific patterns. Differences in end motif distributions in PE patients could reflect alterations in nuclease activity or underlying cell death mechanisms.

Researchers have measured circulating DNA levels in samples from women with preeclampsia and those with normal pregnancies using real-time polymerase chain reaction (PCR), and the results suggest that elevated fetal DNA levels are associated with preeclampsia (9). Another study reported a fivefold increase in fetal cfDNA levels in symptomatic preeclamptic women compared to asymptomatic preeclamptic women (15). Similarly, it has been reported that fetal DNA levels rise in women who eventually develop preeclampsia, with the important finding that cfDNA levels increase prior to the onset of clinical symptoms (16).

2.2 Dynamics of cffDNA and its contribution to overall cfDNA concentration

Circulating cell-free DNA (cfDNA) refers to fragmented DNA molecules present in the bloodstream, with the fetal-derived fraction known as cell-free fetal DNA (cffDNA), which predominantly circulates in the maternal peripheral blood. cffDNA primarily originates from the programmed cell death (apoptosis) or necrosis of placental syncytiotrophoblasts and exhibits placental specificity. Its levels are closely associated with placental function, and significant elevations have been observed in pathological conditions such as placental abruption and preeclampsia (17). During its release, cffDNA exhibits characteristic fragmentation, with an average fragment size of ∼143 base pairs (bp), which is markedly shorter than that of maternal cfDNA (∼166 bp). This size difference may be attributed to placenta-specific nuclease activity. The release rate of cffDNA is influenced by changes in placental metabolism, and increased release is observed with placental aging during late pregnancy. cffDNA has a very short half-life in maternal circulation, ranging from ∼15 min to 2 h, and is rapidly cleared through renal filtration, hepatic and splenic uptake, and nuclease-mediated degradation. This rapid turnover allows cffDNA levels to reflect the real-time status of the placenta; however, it also necessitates prompt sample processing after collection to ensure the accuracy of downstream analyses.

The proportion of cffDNA within the total cfDNA varies significantly with gestational age. In early pregnancy (10–20 weeks of gestation), cffDNA accounts for ∼10%−15% of maternal plasma cfDNA, during which the total maternal cfDNA concentration is relatively low (around 50–100 ng/ml of plasma). During the mid-gestation period (20–30 weeks), the proportion of cffDNA increases to 15%−30%, accompanied by a slight rise in total maternal cfDNA due to increased blood volume (18). In late pregnancy (>30 weeks), the cffDNA fraction can exceed 30%, although substantial interindividual variability exists, influenced by factors such as maternal body mass index (BMI) and placental function. For example, in obese pregnant women, expanded blood volume may lead to a relative reduction in the proportion of cffDNA. In pathological conditions such as preeclampsia and placenta accreta, cffDNA levels can be abnormally elevated. Additionally, fetal chromosomal abnormalities, such as trisomy 21, may also result in increased cffDNA release.

2.3 The potential of cfDNA as a biomarker for preeclampsia severity

In preeclampsia, the increase in circulating cell-free DNA (cfDNA) levels is associated with markers of disease severity, including preterm birth and worsening systolic blood pressure—two recognized key indicators of disease severity (19). These findings may suggest an increase in cfDNA release following maternal tissue injury (20). Given the close correlation between total cfDNA concentration and preeclampsia, one study analyzed the relationship between total cfDNA levels in preeclamptic patients and surrogate markers of disease severity. The results indicated that cfDNA concentration was negatively correlated with gestational age at delivery and moderately positively correlated with maximum systolic blood pressure (21). Furthermore, the study found that the fraction of placental-derived cfDNA was moderately negatively correlated with maximum systolic blood pressure, but showed no association with maximum diastolic blood pressure.

Fetal sex is considered an important risk factor for preeclampsia, with growing speculation that placental formation and maternal adaptation to pregnancy may be influenced by fetal sex. Therefore, it is essential to characterize fetal sex when studying the pathophysiological processes at the maternal-fetal interface (22, 23). Previous studies have indicated that the amount of placental-derived cfDNA in maternal plasma is higher in cases of preeclampsia; however, these studies were limited to male fetuses and employed alternative methods (such as PCR for Y-chromosome material), making it difficult to ascertain the specific contributions. In healthy non-pregnant individuals, cfDNA primarily originates from hematopoietic lineages, with smaller contributions from endothelial cells, neurons, and hepatocytes. Understanding the exact sources of maternal cfDNA can enhance insights into the pathophysiology of preeclampsia and determine whether cfDNA sources are related to disease phenotypes, given the particularly heterogeneous manifestations of preeclampsia (21). In addition to increased production, cfDNA levels are also influenced by clearance mechanisms found in the liver, spleen, and kidneys. It has been proposed that placental cfDNA increases 3 weeks prior to the clinical manifestations of preeclampsia, a rise attributed to accelerated apoptosis of trophoblasts.

In a large multicenter study involving 44 women with preeclampsia and 53 controls, it was concluded that not only are fetal cfDNA levels elevated in preeclampsia, but maternal cfDNA levels also exhibit a similar increase, both showing a tenfold rise compared to the control group. Moreover, this study's population was significantly larger than those previously described, allowing for stratification of preeclampsia cases based on the severity of symptoms. The analysis included three cases

of HELLP syndrome (hemolysis, elevated liver enzymes, low platelet count) and four cases of eclampsia, revealing that the increases in cell-free fetal and maternal cfDNA corresponded with disease severity. Notably, cfDNA levels in women with severe preeclampsia increased by 3.5 times compared to those with mild preeclampsia, and were tenfold higher than in the control group. Furthermore, it was demonstrated that the levels of these two types of cfDNA are correlated in pregnancies affected by preeclampsia, unlike in normal pregnancies. Recent observational reports on cell-free fetal DNA and maternal DNA levels in pregnancies with preeclampsia and subsequent HELLP syndrome have yielded similar findings. These authors also noted that, compared to women with mild preeclampsia, levels of cell-free fetal and maternal DNA in pregnancies complicated by HELLP syndrome nearly quadrupled (24). Maternal cfDNA levels were similarly elevated. In summary, the increase in disease severity is associated with enhanced release of cell-free fetal and maternal DNA into the maternal circulation. These studies collectively suggest that quantitative and fragmentomic profiles of cfDNA are significantly associated with the clinical stratification of preeclampsia. Taken together, these findings indicate that cfDNA levels, particularly the placental-derived fraction, are closely associated with the severity of PE. This suggests that cfDNA may not only serve as a biomarker of disease severity but could also potentially participate directly in the pathophysiology of PE by mediating immune-inflammatory responses. Key evidence and correlations are summarized in Table 1.

3 The central role of cfDNA in the pathogenesis of preeclampsia: bridging immune activation and metabolic dysregulation

The core pathophysiology of preeclampsia involves systemic maternal inflammation and endothelial damage triggered by placental dysfunction. Recent studies indicate that circulating cell-free DNA (cfDNA), particularly placental-derived fetal cfDNA (cffDNA), not merely serves as a biomarker of disease severity but functions as a culprit damage-associated molecular pattern (DAMP) molecule that drives the immunoinflammatory cascade and metabolic dysregulation.

3.1 Mechanisms and biomolecular features of cfDNA as a DAMP

Placentas in preeclampsia commonly exhibit inadequate perfusion and ischemia-hypoxia, leading to exacerbated trophoblast cell apoptosis and/or necrosis. This process releases substantial amounts of cfDNA/cffDNA exhibiting DAMP properties. Fragmentation profile: placenta-derived cfDNA in PE patients shows significantly shortened fragments (typically < 150 bp), resembling DNA released from apoptotic bodies and facilitating immune recognition. Hypomethylation status: in preeclampsia, the free circulating cell-free fetal DNA in maternal blood is hypomethylated, indicating that methyl groups are added to cytosine-guanine (CpG) residues in the DNA molecule. Hypomethylated CpG motifs structurally mimic bacterial DNA. Mitochondrial DNA (mtDNA) enrichment: in preeclamptic placentas associated with pregnancy, there is an increased apoptosis of trophoblasts, resulting in the release of circulating fetal DNA containing mitochondrial DNA (mtDNA) (25). MtDNA similarly contains abundant unmethylated CpG islands and demonstrates striking structural similarity to bacterial DNA.

3.2 DAMP recognition receptor-mediated immune-inflammatory pathway activation

Elevated levels of cfDNA/cffDNA/mtDNA in maternal circulation act as DAMPs, sensed by pattern recognition receptors (PRRs) that trigger a robust sterile inflammatory response—a hallmark of PE pathophysiology. The Toll-like receptor 9 (TLR9) pathway plays a central role: as the key receptor for unmethylated CpG DNA motifs, TLR9 demonstrates significantly upregulated expression in placental tissue and peripheral blood monocytes from preeclampsia patients. Serological analysis revealed that phosphorylation levels of MyD88 and NF-κB, key downstream molecules of the TLR9 signaling pathway, were significantly elevated in peripheral blood mononuclear cells (PBMCs) from preeclamptic patients (26). Activated NF-κB translocates to the nucleus, driving the transcription and expression of multiple pro-inflammatory cytokines (e.g., TNF-α, IL-6, IL-8) and type I interferons (e.g., IFN-β). In addition, the number of extracellular vesicles (EVs) in the placentas of preeclamptic patients was approximately twofold higher than that in normal pregnancies. These EVs were enriched in mitochondrial DNA (mtDNA) and nucleosomal fragments, and may exacerbate local placental inflammation via the TLR9/NF-κB axis (27). Key experimental evidence supports this mechanism that trophoblast cells treated with preeclamptic serum exhibited significantly increased mRNA expression of TLR9 and IFN-β (28). Treatment with genomic DNA removal agents significantly inhibited the secretion of IL-6 and IL-8 induced by both normal and preeclamptic serum. Beck et al. (29) proposed that cfDNA has pro-inflammatory effects, cfDNA injection provokes IL-6 production in mice via TLR9. When both cfDNA and the TLR9 inhibitor chloroquine were administered to mice, the pregnancy outcomes improved (30).

Cytosolic DNA-Sensing Receptors Pathway (AIM2/IFI16): at the placental level, protein expression of AIM2 and IFI16 is significantly elevated in placentas from preeclamptic patients (31). This recognition triggers inflammasome assembly, activating caspase-1. Active caspase-1 then cleaves pro-IL-1β and pro-IL-18 into their mature, highly pro-inflammatory forms, while concurrently suppressing pro-angiogenic factors like PlGF, thereby exacerbating PE symptoms.

3.3 Pathological effects of the immunoinflammatory cascade

CfDNA activates both TLR9 and cytosolic DNA-sensing pathways, collectively driving exaggerated inflammatory responses

TABLE 1 Summary of the relationship between cfDNA and the severity of preeclampsia*.

Study/Author (year)	Sample size	Detection method	Main findings	Conclusions
Teodora et al. (2021)	20PE/22 healthy pregnant women	Total cfDNA (Qubit fluorometric assay)	Total cfDNA in the PE group was >10 times higher than controls (1,235 vs. 106.5 pg/μl, $P < 0.001$)	Total cfDNA levels correlate positively with PE severity (19).
Lorena et al. (2021)	88GH/91PE/98 healthy pregnant women	Total cfDNA (Quant-iT^{TM} PicoGreen dsDNA assay)	Total cfDNA levels in GH and PE (197.0 and 174.2 ng/mL, respectively) were higher than in healthy pregnancies (140.5 ng/ml; all $P < 0.0001$)	Total cfDNA is elevated in HDP pregnancies (both male and female fetuses), with higher levels in severe cases (15).
Marie et al. (2023)	166PE/332 healthy pregnant women	cfDNA methylation analysis	A methylation-based model identified 72% of early-onset PE cases with 80% specificity.	cfDNA methylation analysis is a promising tool for pre-symptomatic PE risk assessment (9).
Marialuigia et al. (2023)	25PE/422 healthy pregnant women	Whole-genome bisulfite sequencing	Women with HDP showed similar cfDNA methylation patterns in the first trimester (11–14 weeks).	Maternal cardiovascular susceptibility to HDP may be detectable early via cfDNA methylation, enabling personalized screening (10).

*Data sources from references (8, 9, 14, 18).

locally (placenta) and systemically. The resulting proinflammatory cytokine storm: Characterized by massive release of TNF-α, IL-6, IL-8, IL-1β, IL-18, IFN-β, etc.—inflicts direct cytotoxic effects on placental trophoblast cells and maternal vascular endothelial cells. Release of Anti-angiogenic Factors: at the RNA level, the mRNA expression of IL-6 and IL-8 is significantly elevated in trophoblast cells treated with preeclamptic serum compared to those treated with serum from normal pregnancies. However, there is no significant difference in mRNA expression of Eng and Flt1 between the two groups. At the protein level, trophoblast cells stimulated with preeclamptic serum exhibit significantly increased secretion of soluble endoglin (sEng) and soluble fms-like tyrosine kinase-1 (sFlt-1) (32, 33). However, the protein levels of IL-6 and IL-8 remained below the detection threshold in both preeclamptic and normal serum-treated groups. Notably, no significant differences were observed in the expression of Eng and Flt1 genes in placental tissues from preeclamptic patients compared to controls, despite markedly elevated serum levels of sEng and sFlt-1 (34, 35). These findings suggest that preeclamptic serum exacerbates placental dysfunction primarily by enhancing the secretion of anti-angiogenic factors (sEng and sFlt-1) from trophoblast cells, rather than by upregulating their gene expression. Endothelial Injury and Systemic Inflammation: proinflammatory cytokines and anti-angiogenic factors act synergistically to damage maternal vascular endothelium, leading to systemic vasoconstriction, hypertension, coagulation activation, and multi-organ hypoperfusion—the cardinal clinical manifestations of preeclampsia.

Research has reported that inflammatory cells in preeclamptic patients, including neutrophils and monocytes, are activated and secrete large amounts of inflammatory cytokines. Even in the absence of microbial infection, inflammation associated with preeclampsia occurs, representing a form of sterile inflammation. In preeclamptic patients, the number of trophoblast-derived extracellular vesicles entering the maternal bloodstream significantly increases. These extracellular vesicles contain various factors, including DNA, RNA, lipids, and proteins, acting as damage-associated molecular patterns (DAMPs). In fact, extracellular vesicles can induce sterile inflammation and preeclampsia-like features in mouse placentas. Recent studies indicate that cfDNA, considered a product of apoptosis and/or necrosis, functions as a DAMP and is associated with various inflammatory diseases (27). During pregnancy, the total amount of cfDNA in maternal blood significantly increases, and elevated cfDNA levels are significantly correlated with pregnancy complications. Empirical findings are detailed in Table 2.

3.4 Association between cfDNA and metabolic dysregulation

The pathogenesis of preeclampsia further involves aberrations in metabolic pathways, in which the release and sensing of cfDNA may play interrelated roles: mitochondrial dysfunction and the release of mtDNA contribute to this process: placental ischemia and hypoxia not only promote cell death, leading to the release of cfDNA and mtDNA, but also reflect an underlying disruption in mitochondrial bioenergetics. Circulating cell-free mitochondrial DNA (ccf-mtDNA) is considered a DAMP molecule that triggers immune responses by activating the pattern recognition receptor Toll-like receptor 9 (TLR9). Compared to gestational age–matched healthy pregnant individuals, those with preeclampsia exhibit aberrations in circulating DNA dynamics, including elevated levels of ccf-mtDNA and compromised DNA clearance mechanisms (36).

Notably, this mechanism of immune activation mediated by mtDNA is not unique to PE. In sepsis, a systemic inflammatory response syndrome secondary to bacterial infection, mitochondrial dysfunction and the subsequent release of mtDNA are also established as central to its pathogenesis (37). Here, reactive oxygen species (ROS) and reactive nitrogen species can induce functional impairment in multiple organelles, including mitochondria, thereby amplifying the inflammatory cascade. Furthermore, studies suggest that variations in mitochondrial DNA haplogroups may influence the severity and progression of sepsis. This analogy provides strong supportive evidence for understanding the similar role of mtDNA in amplifying inflammation in preeclampsia.

Aberrant Expression of Metabolism-Associated Genes: canonical preeclampsia-associated genes—previously implicated in metabolic regulation, hypoxia, and angiogenesis—include LEP,

TABLE 2 Summary of the immune relationship between cfDNA and preeclampsia*.

Study/Author (year)	Sample size	Detection method	Immune-related markers	Main findings	Conclusions
Ane Cecilie et al. (2024)	75PE/37 healthy pregnant women	SomaScan assay	sFlt-1, Endothelin, PlGF	Higher levels of sFlt-1 and endothelin-1 in PE, especially in early-onset cases.	Maternal sFlt-1 and endothelin-1 levels increase in PE, with the highest levels in early-onset cases (34).
Ruby et al. (2023)	194 PE/194 healthy pregnant women	Immunohistochemistry	TLR-4, HMGB1, NF-κB, IκBα	Upregulation of TLR pathway (TLR-4, HMGB1, NF-κB, IκBα) and hypoxia markers in PE placentas.	In preeclampsia, the placenta exhibits aberrant activation of both the TLR pathway (pro-inflammatory) and the hypoxia pathway (hypoxic stress). These two pathways are interconnected and form a positive feedback loop, exacerbating placental injury (28).
Dorota et al. (2022)	35PE/45 healthy pregnant women	Immunoenzymatic assay	IL-17, PlGF, sENG	Preeclampsia patients showed markedly higher sENG levels than healthy third-trimester controls (11.47 ± 4.65 vs. 5.68 ± 2.78 ng/ml, $P < 0.01$).	sENG is elevated in PE pregnancies (33).
Jiang et al. (2022)	14PE/7 rats	Immunohistochemistry, Western blot, transcriptomics	NF-κB, LPS, Bax/Bcl-2	Transcriptomics revealed NF-κB downregulation in LPS + ghrelin-treated groups.	Ghrelin ameliorates placental trophoblast migration and apoptosis by downregulating the NF-κB signaling pathway (26).

*Data sources from references (25, 26, 29, 35).

HK2, FSTL3, FLT1, ENG, TMEM45A, ARHGEF4, and HTRA1. These genes have consistently been shown to be upregulated in preeclamptic placentas compared with normotensive controls across diverse ancestral backgrounds. In the present study, RNA sequencing of placental tissue from patients with severe PE (sPE) of African, Asian, and European ancestry confirmed the sustained upregulation of these canonical genes across all cohorts. Among them, HK2, FSTL3, LEP, and FLT1 exhibited the most pronounced increases. Hexokinase 2 (HK2), which plays a critical role in glucose metabolism, has been frequently reported to be dysregulated in PE (38). Leptin (LEP), a secreted adipokine, systemically regulates energy homeostasis, neuroendocrine signaling, and cytoplasmic metabolic processes. Elevated early-pregnancy leptin levels are a recurrent observation in PE patients, and exogenous leptin administration in murine models recapitulates key clinical features of preeclampsia (39).

The potential role of the cGAS-STING pathway: cytosolic DNA (including cfDNA/mtDNA) is recognized by cyclic GMP-AMP synthase (cGAS), catalyzing the production of the second messenger cyclic GMP-AMP (cGAMP). In pregnancies complicated by PE, increased cGAMP levels are associated with elevated circulating natriuretic peptides. Transfected cytosolic DNA triggers cGAMP production, which binds to the endoplasmic reticulum-resident protein STING and subsequently activates interferon regulatory factor 3 (IRF3) and interferon-beta (IFN-β). As a nucleotide second messenger belonging to the family of cyclic dinucleotides, cGAMP is capable of forming unique2′5′ phosphodiester linkages. Taken together, it is plausible that circulating fetal DNA in PE behaves in a manner similar to bacterial or mitochondrial DNA, potentially activating the cGAS–STING pathway and inducing inflammation (40). This process represents another potential pathway through which cfDNA drives inflammation, meriting further research. The interplay mechanisms between cfDNA and placental metabolic perturbations, including bioenergetic failure and oxidative stress, along with their clinical implications, are systematically collated in Table 3.

4 Ntegrated mechanistic model of preeclampsia pathogenesis

Placental ischemia-hypoxia initiates a cascade beginning with increased trophoblast apoptosis and necrosis. This triggers the release of cfDNA/cffDNA exhibiting hallmark damage-associated molecular patterns (DAMPs), including hypomethylated CpG, short fragments, and mitochondrial DNA enrichment. Such DNA fragments are recognized by pattern recognition receptors (PRRs) such as TLR9, AIM2, IFI16, and potentially cGAS. Subsequent activation of downstream signaling pathways—including MyD88/NF-κB, inflammasomes, and STING—induces pro-inflammatory cytokine storms (TNF-α, IL-6, IL-8, IL-1β, IL-18, IFN-β) and promotes the release of anti-angiogenic factors (sFlt-1, sEng). These events collectively damage placental trophoblasts and maternal vascular endothelium, ultimately manifesting as hypertension, proteinuria, and multi-system injury characteristic of preeclampsia.

Concurrently, hypoxic and inflammatory microenvironments feedback to dysregulate placental metabolic gene expression (e.g., LEP, HK2), exacerbating metabolic imbalance. Critically, cfDNA serves as a linchpin molecule integrating four key pathological axes: placental injury, immune-inflammatory

TABLE 3 Summary of the metabolic relationship between cfDNA and preeclampsia*.

Study/Author (year)	Sample size	Detection method	Metabolic markers	Main findings	Conclusions
SpencerC et al. (2022)	19PE/19 healthy pregnant women	ccfDNA (qPCR), ELISA	ccf-mtDNA, cf-nDNA, DNase I, TLR9	Lower ccf-mtDNA in PE ($P \leq 0.02$), but no difference in PBMC mtDNA copy number ($P > 0.05$).	PE is associated with abnormal cfDNA dynamics, including reduced ccf-mtDNA and impaired DNA clearance (36).
Deeksha et al. (2021)	17PE/15 healthy pregnant women	qRT-PCR	MT-ND1, NADH dehydrogenase 1	Higher mtDNA copies in PE (median: 24.32 vs. 20.32), especially in early-onset cases (28.06).	Early-onset PE may involve severe mitochondrial damage, elevating mtDNA copies as a compensatory response (25).
Omonigho et al. (2023)	50PE/73 healthy pregnant women	RNA sequencing	LEP, HK2, FSTL3, FLT1, ENG, HTRA1	Upregulated HK2 ($P<0.01$) and elevated placental cfDNA in severe PE, suggesting enhanced glycolysis.	Classic PE genes (e.g., LEP, FSTL3, HK2, FLT1) are highly upregulated in PE (38).
Huang et al. (2021)	78PE/95 healthy pregnant women	ELISA	LEP, Cer	Lep levels were higher in PE compared with non-PE placentas ($P < 0.05$)	PE placentas exhibit significantly elevated Lep expression (39).

*Data sources from references (36, 37, 39, 40).

activation, endothelial dysfunction, and metabolic dysregulation, thereby constituting a core pathophysiological mechanism in preeclampsia. The integrated mechanisms underlying the pathogenesis of preeclampsia are shown in Figure 1.

5 Clinical feasibility and validation status of multi-omics integrated predictive models

Integrated multi-omics models combining cfDNA fragmentomics, proteomics, and metabolomics significantly enhance early preeclampsia (PE) risk stratification by concurrently capturing multidimensional signals of placental hypoxia, inflammatory activation, and metabolic dysregulation. Technically, a single maternal plasma sample enables compatible analysis of cfDNA fragmentation, proteins (e.g., sFlt-1/PlGF), and metabolites (e.g., leucine), with standardized workflows for next-generation sequencing (NGS) and liquid chromatography–tandem mass spectrometry (LC-MS/MS) validated in large cohorts (e.g., SPREE study). Retrospective studies demonstrate superior predictive performance of cfDNA methylation combined with proteomics for early-onset PE (9), while the prospective PREMOM trial further reveals that integrating cfDNA fragmentomics and metabolomics increases the positive predictive value (PPV) at 16 gestational weeks from 42% (conventional models) to 67% (21). Nevertheless, real-world implementation faces critical challenges: population-specific calibration algorithms are required to address baseline omics heterogeneity induced by maternal ethnicity and comorbidities (e.g., chronic hypertension); low cfDNA abundance in early gestation (<12 weeks) compromises dynamic monitoring accuracy, necessitating compensation via ultrasound biomarkers; additionally, although multi-omics screening reduced preterm birth by 24% in the NHS Scotland trial, its 30% cost increase and lack of long-term health economic evaluations hinder widespread adoption. Future translation should prioritize: developing microfluidic point-of-care systems for ≤4-h reporting; establishing international multi-omics data registries (e.g., IPD Meta-analysis Consortium) to accelerate model refinement; and defining cost-containment targets for resource-limited settings.

6 Conclusion

The advancement of cfDNA analysis is reshaping prenatal medicine practice. This review highlights that plasma cfDNA concentration is significantly elevated (3–5 fold) in preeclampsia (PE) patients and is strongly associated with placental hypoxia-induced trophoblast apoptosis, underscoring its considerable potential as a pathological biomarker for PE. Multi-parameter models based on cfDNA—integrating fetal fraction, fragmentomics, and placenta-specific methylation markers—outperform traditional serological biomarkers (e.g., PlGF and sFlt-1) in enhancing early PE prediction accuracy. The non-invasive nature of cfDNA analysis makes it particularly suitable for large-scale screening; however, clinical translation requires defining the optimal gestational window. Existing evidence suggests the second trimester (16–20 weeks) is a feasible and effective window for cfDNA-based risk stratification, while its first-trimester (12–14 weeks) potential hinges on further validation of ultra-sensitive technologies, such as targeted methylation sequencing—a key focus for future prospective multicenter studies.

It is essential to recognize that key scientific bottlenecks still exist in current research. First, the short half-life of cfDNA has yet to establish a standardized optimal detection window, which contrasts with the methodological differences seen in long half-life protein biomarkers. Second, there is a lack of uniform quality control standards for comparing results across different detection platforms, which may affect the reproducibility of multi-center studies. More importantly, the causal relationship between elevated cfDNA levels and preeclampsia remains unclear: whether it is passive release due to placental ischemia or active secretion triggered by maternal inflammation. This ongoing debate regarding

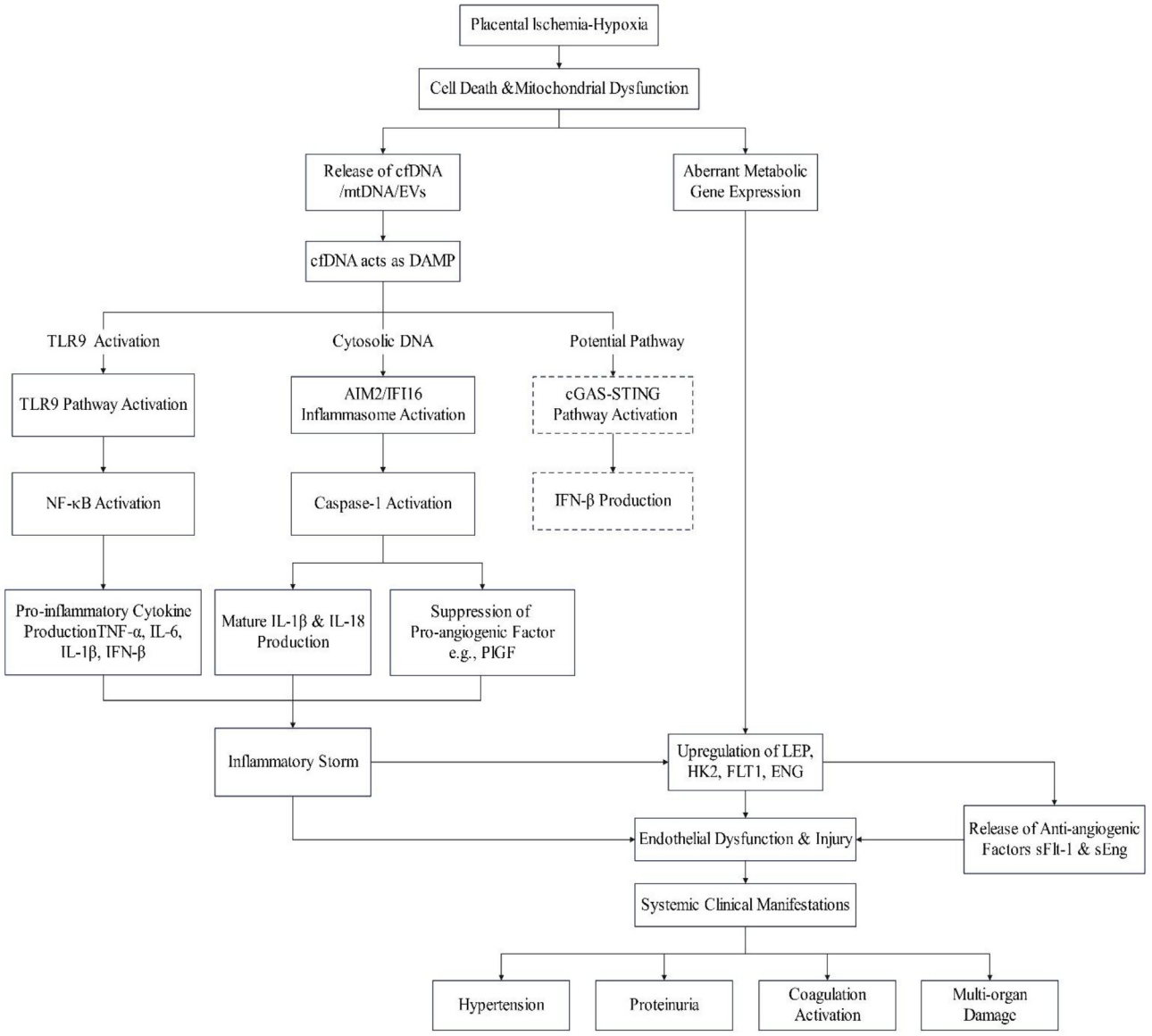

FIGURE 1
The central role of cfDNA in driving inflammation and endothelial dysfunction in preeclampsia.

the underlying mechanism directly impacts the choice of intervention strategies.

Future clinical research should focus on: developing integrated models that combine cfDNA with other clinical parameters (e.g., uterine artery Doppler) to improve first-trimester predictive performance; conducting large-scale, multi-ethnic prospective cohorts to rigorously validate screening efficacy and cost-effectiveness across early and mid-pregnancy; and establishing clinical pathways for managing incidental findings, such as maternal malignancy. Ultimately, translating cfDNA from a research tool into routine clinical screening will be pivotal for enabling early PE identification and personalized intervention, profoundly transforming prenatal care practice.

Author contributions

ZG: Writing – original draft. BZ: Writing – review & editing. DY: Writing – review & editing. LW: Supervision, Writing – review & editing.

Funding

The author(s) declare that financial support was received for the research and/or publication of this article. This study was funded by grants from Clinical Research Project of Changzhou Medical Center, Nanjing Medical University (CMCC202315), Changzhou City's "14th Five Year Plan" High Level Health

Talent Training Project-Top Talents (2022CZBJ087), and Major Science and Technology Project of Changzhou Municipal Health Commission (ZD202418).

Conflict of interest

The authors declare that the research was conducted in the absence of any commercial or financial relationships that could be construed as a potential conflict of interest.

Generative AI statement

The author(s) declare that no Gen AI was used in the creation of this manuscript.

Any alternative text (alt text) provided alongside figures in this article has been generated by Frontiers with the support of artificial intelligence and reasonable efforts have been made to ensure accuracy, including review by the authors wherever possible. If you identify any issues, please contact us.

Publisher's note

References

1. Dimitriadis E, Rolnik DL, Zhou W, Estrada-Gutierrez G, Koga K, Francisco RPV, et al. Pre-eclampsia. *Nat Rev Dis Primers.* (2023) 9:8. doi: 10.1038/s41572-023-00417-6

2. Chappell LC, Cluver CA, Kingdom J, Tong S. Pre-eclampsia. *Lancet.* (2021) 398:341–54. doi: 10.1016/S0140-6736(20)32335-7

3. Qi J, Wu B, Chen X, Wei W, Yao X. Diagnostic biomolecules and combination therapy for pre-eclampsia. *Reprod Biol Endocrinol.* (2022) 20:136. doi: 10.1186/s12958-022-01003-3

4. Hu Z, Chen H, Long Y, Li P, Gu Y. The main sources of circulating cell-free DNA: apoptosis, necrosis and active secretion. *Crit Rev Oncol Hematol.* (2021) 157:103166. doi: 10.1016/j.critrevonc.2020.103166

5. Oellerich M, Sherwood K, Keown P, Schütz E, Beck J, Stegbauer J, et al. Liquid biopsies: donor-derived cell-free DNA for the detection of kidney allograft injury. *Nat Rev Nephrol.* (2021) 17:591–603. doi: 10.1038/s41581-021-00428-0

6. Yuen N, Lemaire M, Wilson SL. Cell-free placental DNA: what do we really know? *PLoS Genet.* (2024) 20:e1011484. doi: 10.1371/journal.pgen.1011484

7. Moufarrej MN, Bianchi DW, Shaw GM, Stevenson DK, Quake SR. Noninvasive prenatal testing using circulating DNA and RNA: advances, challenges, and possibilities. *Annu Rev Biomed Data Sci.* (2023) 6:397–418. doi: 10.1146/annurev-biodatasci-020722-094144

8. Norton ME, MacPherson C, Demko Z, Egbert M, Malone F, Wapner RJ, et al. Obstetrical, perinatal, and genetic outcomes associated with nonreportable prenatal cell-free DNA screening results. *Am J Obstet Gynecol.* (2023) 229:300.e1–e9. doi: 10.1016/j.ajog.2023.03.026

9. De Borre M, Che H, Yu Q, Lannoo L, De Ridder K, Vancoillie L, et al. Cell-free DNA methylome analysis for early preeclampsia prediction. *Nat Med.* (2023) 29:2206–15. doi: 10.1038/s41591-023-02510-5

10. Spinelli M, Zdanowicz JA, Keller I, Nicholson P, Raio L, Amylidi-Mohr S, et al. Hypertensive disorders of pregnancy share common cfDNA methylation profiles. *Sci Rep.* (2022) 12:19837. doi: 10.1038/s41598-022-24348-6

11. Bokuda K, Ichihara A. Preeclampsia up to date—What's going on? *Hypertens Res.* (2023) 46:1900–7. doi: 10.1038/s41440-023-01323-w

12. Meng Y, Meng Y, Li L, Li Y, He J, Shan Y. The role of DNA methylation in placental development and its implications for preeclampsia. *Front Cell Dev Biol.* (2024) 12:1494072. doi: 10.3389/fcell.2024.1494072

13. Jia R, Zhu J, Zhang F, Sun Y, Zhang B, Du Y, et al. Exploration of cfDNA landscape in NIPT and clinical utilities of cfDNA based gene expression inference in prenatal diagnostics. *Front Genet.* (2025) 16:1527884. doi: 10.3389/fgene.2025.1527884

14. Zhou Z, Ma ML, Chan RWY, Lam WKJ, Peng W, Gai W, et al. Fragmentation landscape of cell-free DNA revealed by deconvolutional analysis of end motifs. *Proc Natl Acad Sci U S A.* (2023) 120:e2220982120. doi: 10.1073/pnas.2220982120

15. Amaral LM, Sandrim VC, Kutcher ME, Spradley FT, Cavalli RC, Tanus-Santos JE, et al. Circulating total cell-free DNA levels are increased in hypertensive disorders of pregnancy and associated with prohypertensive factors and adverse clinical outcomes. *Int J Mol Sci.* (2021) 22:564. doi: 10.3390/ijms22020564

16. Del Vecchio G, Li Q, Li W, Thamotharan S, Tosevska A, Morselli M, et al. Cell-free DNA methylation and transcriptomic signature prediction of pregnancies with adverse outcomes. *Epigenetics.* (2021) 16:642–61. doi: 10.1080/15592294.2020.1816774

17. Zaki-Dizaji M, Shafiee A, Kohandel Gargari O, Fathi H, Heidary Z. Maternal and fetal factors affecting cell-free fetal DNA (cffDNA) fraction: a systematic review. *J Reprod Infertil.* (2023) 24:219–31. doi: 10.18502/jri.v24i4.14149

18. Jayashankar SS, Nasaruddin ML, Hassan MF, Dasrilsyah RA, Shafiee MN, Ismail NAS, et al. Non-invasive prenatal testing (NIPT): reliability, challenges, and future directions. *Diagnostics.* (2023) 13:2570. doi: 10.3390/diagnostics13152570

19. Kolarova TR, Gammill HS, Nelson JL, Lockwood CM, Shree R. At preeclampsia diagnosis, total cell-free DNA concentration is elevated and correlates with disease severity. *J Am Heart Assoc.* (2021) 10:e021477. doi: 10.1161/JAHA.121.021477

20. Tarca AL, Taran A, Romero R, Jung E, Paredes C, Bhatti G, et al. Prediction of preeclampsia throughout gestation with maternal characteristics and biophysical and biochemical markers: a longitudinal study. *Am J Obstet Gynecol.* (2022) 226:126.e1–e22. doi: 10.1016/j.ajog.2021.01.020

21. MacDonald TM, Walker SP, Hannan NJ, Tong S, Kaitu'u-Lino TJ. Clinical tools and biomarkers to predict preeclampsia. *EBioMedicine.* (2022) 75:103780. doi: 10.1016/j.ebiom.2021.103780

22. Martin K, Dar P, MacPherson C, Egbert M, Demko Z, Parmar S, et al. Performance of prenatal cfDNA screening for sex chromosomes. *Genet Med.* (2023) 25:100879. doi: 10.1016/j.gim.2023.100879

23. Shear MA, Swanson K, Garg R, Jelin AC, Boscardin J, Norton ME, et al. A systematic review and meta-analysis of cell-free DNA testing for detection of fetal sex chromosome aneuploidy. *Prenat Diagn.* (2023) 43:133–43. doi: 10.1002/pd.6298

24. Iannaccone A, Reisch B, Mavarani L, Darkwah Oppong M, Kimmig R, Mach P, et al. Soluble endoglin versus sFlt-1/PlGF ratio: detection of preeclampsia, HELLP syndrome, and FGR in a high-risk cohort. *Hypertens Pregnancy.* (2022) 41:159–72. doi: 10.1080/10641955.2022.2066119

25. Pandey D, Yevale A, Naha R, Kuthethur R, Chakrabarty S, Satyamoorthy K. Mitochondrial DNA copy number variation - a potential biomarker for early onset preeclampsia. *Pregnancy Hypertens.* (2021) 23:1–4. doi: 10.1016/j.preghy.2020.10.002

26. Shen J, Hu N, Wang Z, Yang L, Chen R, Zhang L, et al. Ghrelin alleviates placental dysfunction by down-regulating NF-κB phosphorylation in LPS-induced rat model of preeclampsia. *Eur J Pharmacol.* (2024) 972:176569. doi: 10.1016/j.ejphar.2024.176569

27. Roh JS, Sohn DH. Damage-associated molecular patterns in inflammatory diseases. *Immune Netw.* (2018) 18:e27. doi: 10.4110/in.2018.18.e27

28. Aggarwal R, Jain AK, Mehta V, Rath G. Amalgamation of toll-like receptor and hypoxic signaling in etiology of preeclampsia. *Appl Immunohistochem Mol Morphol.* (2023) 31:429–37. doi: 10.1097/PAI.0000000000001129

29. Beck S, Buhimschi IA, Summerfield TL, Ackerman WE, Guzeloglu-Kayisli O, Kayisli UA, et al. Toll-like receptor 9, maternal cell-free DNA and myometrial cell response to CpG oligodeoxynucleotide stimulation. *Am J Reprod Immunol.* (2019) 81:e13100. doi: 10.1111/aji.13100

30. Choi M, Hwang JR, Sung JH, Byun N, Seok YS, Cho GJ, et al. Hydroxychloroquine reduces hypertension and soluble fms-like kinase-1 in a Nω-nitro-l-arginine methyl ester-induced preeclampsia rat model. *J Hypertens.* (2022) 40:2459–68. doi: 10.1097/HJH.0000000000003279

31. Fan Z, Chen R, Yin W, Xie X, Wang S, Hao C. Effects of AIM2 and IFI16 on infectious diseases and inflammation. *Viral Immunol.* (2023) 36:438–48. doi: 10.1089/vim.2023.0044

32. Garrido-Giménez C, Cruz-Lemini M, Álvarez FV, Nan MN, Carretero F, Fernández-Oliva A, et al. Predictive model for preeclampsia combining sFlt-1, PlGF, NT-proBNP, and uric acid as biomarkers. *J Clin Med.* (2023) 12:431. doi: 10.3390/jcm12020431

33. Darmochwal-Kolarz D, Chara A. The association of IL-17 and PlGF/sENG ratio in pre-eclampsia and adverse pregnancy outcomes. *Int J Environ Res Public Health.* (2022) 20:768. doi: 10.3390/ijerph20010768

34. Westerberg AC, Degnes ML, Andresen IJ, Roland MCP, Michelsen TM. Angiogenic and vasoactive proteins in the maternal-fetal interface in healthy pregnancies and preeclampsia. *Am J Obstet Gynecol.* (2024) 231:550.e1–e22. doi: 10.1016/j.ajog.2024.03.012

35. Mitranovici MI, Chiorean DM, Moraru R, Moraru L, Caravia L, Tiron AT, et al. Understanding the pathophysiology of preeclampsia: exploring the role of antiphospholipid antibodies and future directions. *J Clin Med.* (2024) 13:2668. doi: 10.3390/jcm13092668

36. Cushen SC, Ricci CA, Bradshaw JL, Silzer T, Blessing A, Sun J, et al. Reduced maternal circulating cell-free mitochondrial DNA is associated with the development of preeclampsia. *J Am Heart Assoc.* (2022) 11:e021726. doi: 10.1161/JAHA.121.021726

37. Filetici N, Van de Velde M, Roofthooft E, Devroe S. Maternal sepsis. *Best Pract Res Clin anaesthesiol.* (2022) 36:165–77. doi: 10.1016/j.bpa.2022.03.003

38. Aisagbonhi O, Bui T, Nasamran CA, St Louis H, Pizzo D, Meads M, et al. High placental expression of FLT1, LEP, PHYHIP and IL3RA - in persons of African ancestry with severe preeclampsia. *Placenta.* (2023) 144:13–22. doi: 10.1016/j.placenta.2023.10.008

39. Huang Q, Hao S, You J, Yao X, Li Z, Schilling J, et al. Early-pregnancy prediction of risk for pre-eclampsia using maternal blood leptin/ceramide ratio: discovery and confirmation. *BMJ Open.* (2021) 11:e050963. doi: 10.1136/bmjopen-2021-050963

40. Tsuji N, Agbor-Enoh S. Cell-free DNA beyond a biomarker for rejection: biological trigger of tissue injury and potential therapeutics. *J Heart Lung Transpl.* (2021) 40:405–13. doi: 10.1016/j.healun.2021.03.007

Frontiers in
Cell and Developmental Biology

Explores the fundamental biological processes of life, covering intracellular and extracellular dynamics.

The world's most cited developmental biology journal, advancing our understanding of the fundamental processes of life. It explores a wide spectrum of cell and developmental biology, covering intracellular and extracellular dynamics.

Discover the latest Research Topics

See more →

Frontiers

Avenue du Tribunal-Fédéral 34
1005 Lausanne, Switzerland
frontiersin.org

Contact us

+41 (0)21 510 17 00
frontiersin.org/about/contact